Synthesis and Properties of Donor Acceptor Molecular Dyads

A PhD Thesis submitted to:

The University of Newcastle upon Tyne

Xiaoyan He

December 2013

Abstract

This thesis is concerned with the design, preparation and structural characterisation of several molecular dyads. The molecular dyads were synthesized for the study of energy/electron/charge transfer processes to advance our understanding of artificial photosynthesis. We were hoping to enhance our ability in mimicking natural photosynthesis through our discoveries.

Chapter 1 introduces the field of artificial photosynthesis. The working principles and the highest efficiency dye sensitized solar cells (DSSCs) to date are highlighted. Molecular units working as photo-active switches for fabrication of light-driven molecular scale machines are emphasized. Finally, previous work on the acridinium-, naphthalimde-, viologen- and 1,1'-bi-2-naphthol-based derivatives are reviewed.

Chapter 2 is the experimental section, it describes the techniques used for characterisation, and details of synthetic procedures used to obtain molecular dyads discussed in chapters 3 to 6.

Chapter 3 discusses the synthesis and properties of expanded acridinium dyads, and their application as sensitizers for DSSCs. Coupling of *N,N*-dimethylaniline and an expanded acridinium unit afforded a purple dyad, **DMA**. The charge transfer property of **DMA** was studied by solvent polarity dependent UV-Visible absorption spectroscopy. The fluorescence of **DMA** was almost totally quenched by the charge transfer state. The quenching of fluorescence was also found in **BODAC**, which couples a bodipy unit with the expanded acridinium unit through an acetylene bridge. No long-lived species were found from a transient absorption study of **DMA** and a decay model was proposed to explain the relaxation process. We demonstrated for the first time that acridinium based dyads can be used as sensitizers for DSSCs by testing results of two dyads on p- and/or n-type semiconductors.

Chapter 4 demonstrates the synthesis of donor-acceptor systems based on naphthalimide and phthalimide derivatives for a solid state charge transfer fluorescence study. The fluorescence images of the dyads were obtained through confocal microscopy. UV-Vis absorption spectra also revealed their charge transfer properties. X-ray crystal structures of several compounds were obtained. The existence of two polymorphs of one dyad enabled us to compare their solid state fluorescence properties more closely. The polymorphs displayed different properties such as colours, melting points and the emission lifetimes.

Chapter 5 concerns the synthesis of a disulfide-strapped methyl viologen derivative **DSV**, which can work as a molecular switch. The viologen derivative is capable of storing up to four electrons as revealed by reversible reduction peaks for a cyclic voltammogram. **DSV** is one of the easiest to reduce viologen derivatives to date. Molecular orbital calculations were used to model the "spring opening" of the disulfide-strapped six membered ring.

Chapter 6 continues our further work into bridging units for donor acceptor assemblies and focuses on the synthesis of 1,1'-bi-2-naphthol based molecular dyads. The length of alkyl chain to link the diol group was varied to control the conformation of the chiral bridges. The aim was to study chirality effects on energy/electron transfer processes. Different synthetic routes were tried to achieve the target molecular dyads. Primary photophysical properties and results on attaching the dyad to fullerene are presented.

Acknowledgements

Firstly, I want to thank my supervisors Prof. Andrew C. Benniston and Prof. Anthony Harriman for their guidance, encouragement and overwhelming support during the past three years. Enjoyable discussion on both theoretical and practical work, and invaluable advice have brought me through this challenging but fruitful journey.

I want to acknowledge support of all the members of the Molecular Photonics Laboratory. Thanks to their help with the technical aspects and humours in the lab. This includes Dr Songjie Yang, Dr Sophie Clift, Dr Pau Farras, Effat Bahaidarah, Tommy Winstanley and Dan Bai.

I want to thank the group members of making dye-sensitised solar cells in Nottingham University including Dr Libby Gibson, Sean Baxter and Christopher Wood for their help with making the solar cells and enjoyable discussions. Noor Aniza Harun and Jonathan Pate in Nanochemistry Laboratory are also acknowledged for help with confocal microscopy and crystal conductivity measurements, respectively. I want to acknowledge Professor William MacFarlane and Dr Corrine Wills for their kind help with NMR experiments and NMR simulation. I want to thank Prof. Nikolai V. Tkachenko's group for charge transfer process analysis and transient absorption measurements. I also want to thank Dr Ross Harrington for recording the X-ray crystal data of my compounds. Dr Jerry Hagon is acknowledged for molecular orbital calculations. Thanks to Prof. Andrew C. Benniston for fluorescence spectra measurements and molecular orbital calculations.

I want to thank former supervisor and lecturers from University of the West of Scotland Professor Sabbir Ahmed, Dr Andrew McLean and Dr Ciaran Ewins who helped me going through a very special year when I came to this country first time and encouraged me to start my PhD study.

Finally, special thanks to my amazing family for supporting me from all aspects, especially my mum and my dad who have been working so hard to support me and encourage me to getting through my study from the beginning until now. Without their love, care and generosity, all the work described here is impossible.

List of publications

1. A. C. Benniston, **X. He**, H. Lemmetyinen and N. V. Tkachenko, Charge transfer properties of a donor-acceptor dyad based on an expanded acridinium cation, *RSC Adv.,* 2013, **3**, 4995.

2. A. C. Benniston, J. Hagon, **X. He**, H. Lemmetyinen, N. V. Tkachenko, W. Clegg and R. W. Harrington, Photoinduced charge shift and charge recombination through an alkynyl spacer for an expanded acridinium-based dyad, *Phys. Chem. Chem. Phys.*, 2012, **14**, 3194.

3. A. C. Benniston, J. Hagon, **X. He**, S. Yang, R. W. Harrington, Spring open Two-plus-Two electron storage in a disulfide-strapped methyl viologen derivative, *Org. Lett.*, 2012, **14**, 506.

Abbreviations

A	Acceptor
B	Bridge
D	Donor
DSSC	Dye-Sensitized Solar Cell
EE	Electron Exchange
Lc	Lucigenin
NMA	*N*-methylacridone
DMB	Dimethylbiacridene
THF	Tetrahydrofuran
DCM	Dichloromethane
NMP	*N*-Methyl-2-pyrrolidone
DMF	*N,N*-Dimethylformamide
TMEDA	Tetramethylethylenediamine
TBATFB	*N*-tetrabutylammonium Tetrafluoroborate
Bodipy	Boron Dipyrromethene
DCE	1,2-Dichloroethane
RT	Room Temperature
CV	Cyclic Voltammogram
CS	Charge Shift
CR	Charge Recombination
CT	Charge Transfer
FWHM	Full Width at Half Maximum
HOMO	Highest Occupied Molecular Orbital
SOMO	Single Occupied Molecular Orbital
LUMO	Lowest Unoccupied Molecular Orbital
OTFTs	Organic Thin-Film Transistors
COSY	Correlation Spectroscopy

Table of Contents

Chapter 1

Introduction

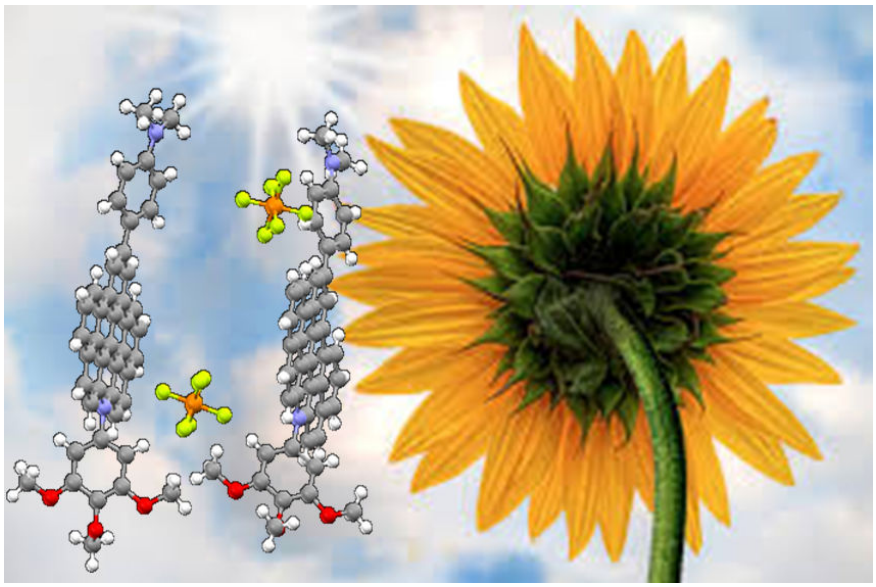

1.1 An overview

The work in this thesis is split into two parts but overall is based on the design, synthesis and fundamental study of molecular dyads. Chapter 3 and Chapter 4 address the study of charge transfer in donor-acceptor molecular dyads. Chapter 5 and Chapter 6 emphasise the understanding of bridging units in molecular dyads. Charge transfer studies were carried out on newly designed acridinium dyes in Chapter 3. We developed a new synthetic route to achieve acridinium-based ionic molecular dyads and one of them exhibits charge transfer properties in solution. The potential of the dyads as sensitizers for dye-sensitised solar cells (DSSCs) was tested on both p- and n-type semiconductors. In Chapter 4, we move away from charge transfer in solution and study the effect in the solid state using naphthalimide/phthalimide derivatives. Strong charge transfer fluorescence character was found for some of the crystalline naphthalimide/phthalimide derivatives, and the existence of polymorphs enables us to compare their charge transfer properties in the solid state more closely. Multi-electron storage in a synthesised viologen-based bridge is described in Chapter 5. Incorporation of a disulfide with viologen afforded a unit capable of four electron storage. Finally, efforts of trying to synthesis binaphthol bridging molecular dyads were carried out in Chapter 6. The aim of the work was to develop a method to obtain molecular dyads with binaphthol spacer groups and to study the effects of chirality on energy transfer processes. The work in this whole thesis is served to advance our understanding on molecular devices and artificial photosynthesis from theoretical to practical applications.

The design, construction and practical application of artificial molecular machines are still profound topics, while the concept of a molecular-level machine is not unfamiliar to us [1]. The functions of molecular machines are not hard to find, for example, photosynthesis of plants and bacteria, metabolism, and self-repair of damaged tissue.

However, the artificial construction of a molecular machine was not considered seriously until 1960 when Richard Feynman[2] defined that a molecular machine consists of different molecular level components and can function as a macro-machine under the stimulation of appropriate "energy" sources. Photons and electrons have been considered as the best energy sources since the consumption of these types of energy will not cause the accumulation of by-products. There are a variety of possible applications of artificial molecular machines such as artificial photosynthesis[3], data storage systems[4], sensors[5] and drug delivery[6].

1.2 Artificial photosynthesis

As a result of the consumption of fossil fuels, the energy crises as well as global warming are two serious issues that we need to consider now. Nuclear energy, one of the most powerful alternative energy to fossil fuels, has been widely used all over the world; however, the leaking of radioactive waste is always a problem. Renewable and clean energy is no doubt one of the solutions for these problems.

Nature has known how to harvest photons and utilise the free solar energy for billions of years, such as photosynthesis of purple bacteria (*Figure 1*)[7]. To complete the photosynthesis process, the photon-capture centres as well as reaction centres are essential[3]. The light-harvesting centre captures photons forming an excited state, with the energy finally transferred via energy transfer to the reaction centre. There are two types of mechanism of excitation energy transfer (explained later): Förster energy transfer (through space) and Dexter energy transfer (through bond). Nature utilises the former type of energy transfer in the highly ordered chlorophyll. For example, in the photon capture centre of purple bacteria (*Figure 2*)[8], the energy is transferred through space with the assistance of pigments (α and β–apoproteins).

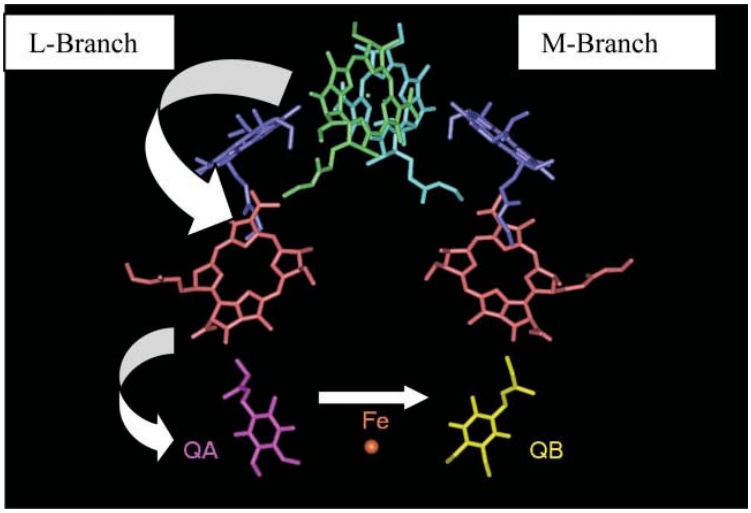

Figure 1. Photosynthetic reaction centre of the purple bacteria Rhodopseudomonas viridis. The electron transfer undergoes preferentially along the L-Branch even though the two branches are almost identical[7].

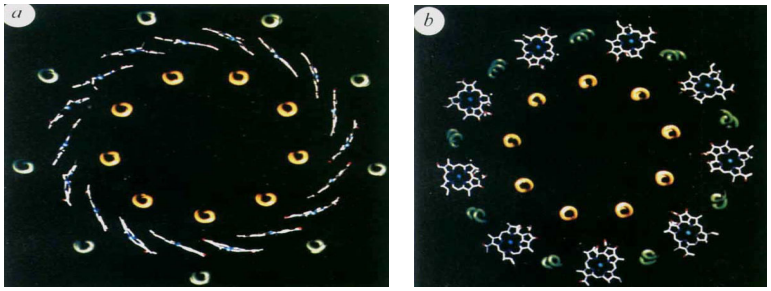

Figure 2. Illustration of bacterial photon capture centre, (a) ring of 18 B850 bacteriochlorophyll, (b) B800 bacteriochlorophyll. β–Apoproteins (green) in the outer ring and α–apoproteins (yellow) in the inter cylindrical. The energy is transferred through space (Förster mechanism) within the system through different chlorophylls [8].

To mimic natural photosynthesis, various artificial photosynthesis systems have been developed. Generally, artificial light harvesting systems consist of donors and acceptors; the light harvesting systems are connected to reaction centres via bridges. Porphyrin-based[9] and bodipy-based[10], arrays, dendrimers and polymers have been reported to be efficient light harvesting systems with fast energy transfer rates. For example, the incorporation of porphyrin dimers (**PorD**, *Figure 3*) within a dye-sensitized solar cell, a 70% of absorbed photon-to-current conversion efficiency has been shown[9]. Dye-loaded zeolites have been used to direct the energy transfer along a pre-designed route[11]. The energy captured by the collectors was transferred to the reaction centre to drive the electron transfer leading to formation of a charge-separated state. The main

problem here is the competing process, i.e., charge recombination, which decreases the conversion efficiency. To overcome this problem, triads, tetrads, etc have been synthesised based on the discovery that electron transfer rates decrease with the increasing separation between the donors and acceptors[12]. These designs do help to decrease the charge recombination rate to some extent, but this is not the ultimate solution and the coupling of the collector and reaction centre is another issue.

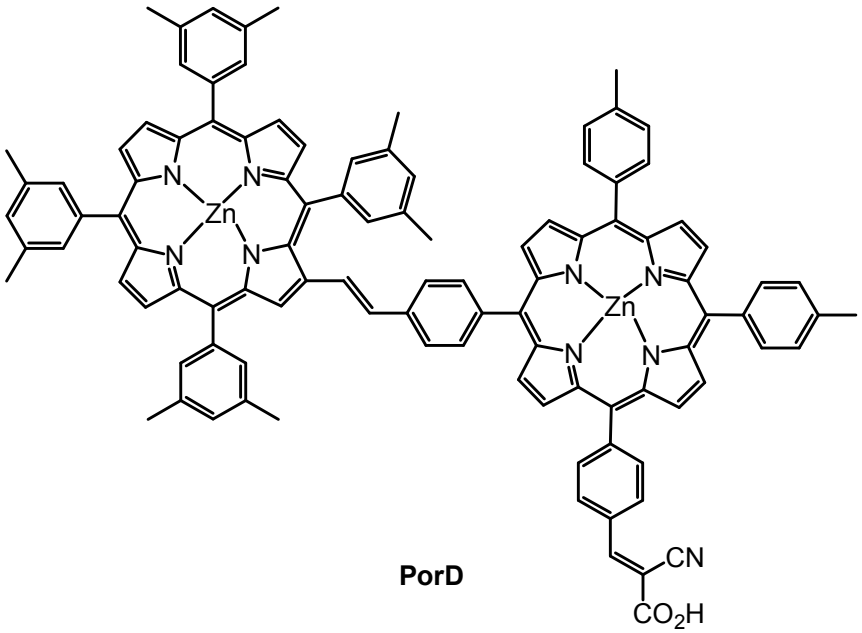

PorD

Figure 3. A selected example of a porphyrin-based light-harvesting complex, ***PorD****.*

Energy transfer

The two main photo-induced energy transfer mechanisms are Förster theory mechanism and Dexter mechanism. The Föster mechanism [13] (also known as Coulombic mechanism, *Figure 4*) does not require physical contacts of donors and acceptor, the energy is transferred trough space. The dipole-dipole term is the most important factor. In addition, the donor and acceptor molecules must be in close proximity (typically between 1 - 10 nm), and the donor emission spectrum needs to overlap with the acceptor absorption spectrum. The Dexter mechanism[14] (also known as Exchange mechanism, *Figure 5*) relies on electron coupling between donors and acceptors for the exchange mechanism to take place. There is a simultaneous electron transfer between donor and acceptor. The electron transfers from the LUMO of the donor to the LUMO of the acceptor and at the same time one electron transfer from the HOMO of the

acceptor to the HOMO of the donor. This is different from the Förster-type mechanism.

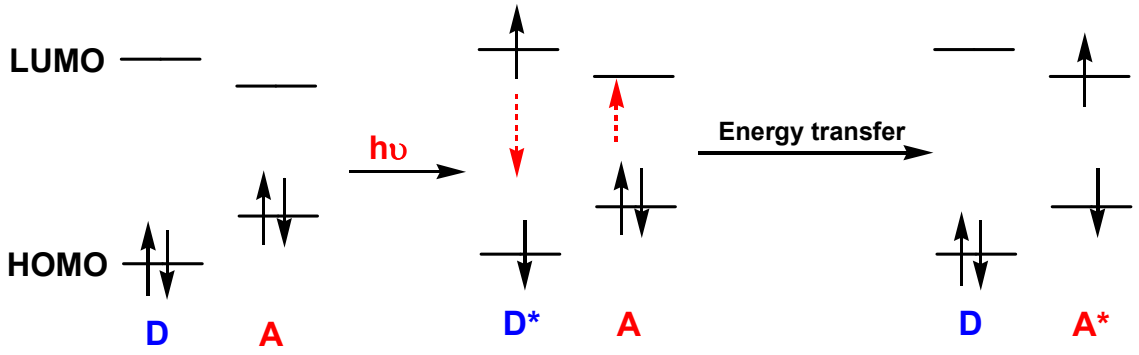

Figure 4. Förster mechanism of photo-induced energy transfer, D = Donor and A = Acceptor, HOMO = Highest occupied molecular orbital and LUMO = lowest unoccupied molecular orbital.

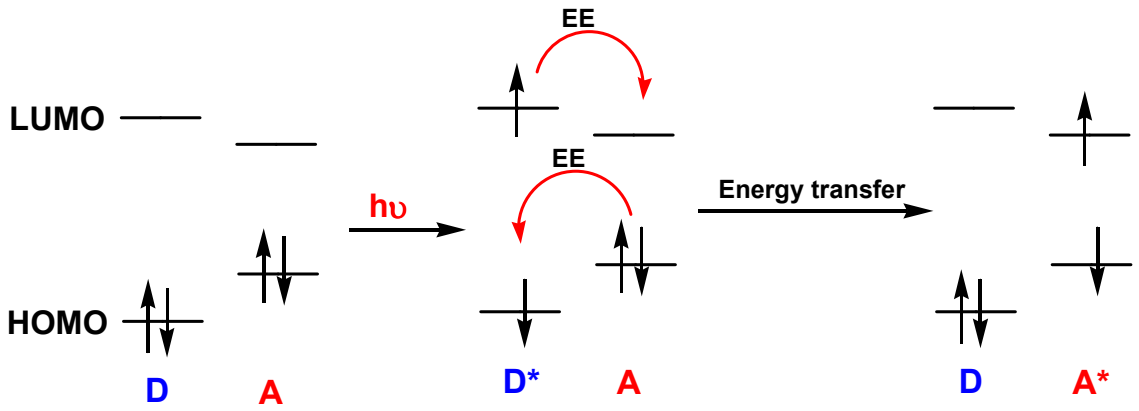

Figure 5. Dexter mechanism of photo-induced energy transfer, D = Donor, A = Acceptor and EE = electron exchange.

Electron transfer

There are two types of electron transfer process: electron transfer and hole transfer (both are referred to the donor). As pictorially presented in *Figure 6*, during the electron transfer process, an electron was transferred from the SOMO of donor to the LUMO of the acceptor. As a result, the SOMO of the donor and the LUMO of the acceptor became the LUMO and the SOMO, respectively. Whilst for the hole transfer process (*Figure 7*), a hole was transferred from the SOMO of the donor to the HOMO of the acceptor (the electron was transferred from the HOMO of the acceptor to the SOMO of the donor).

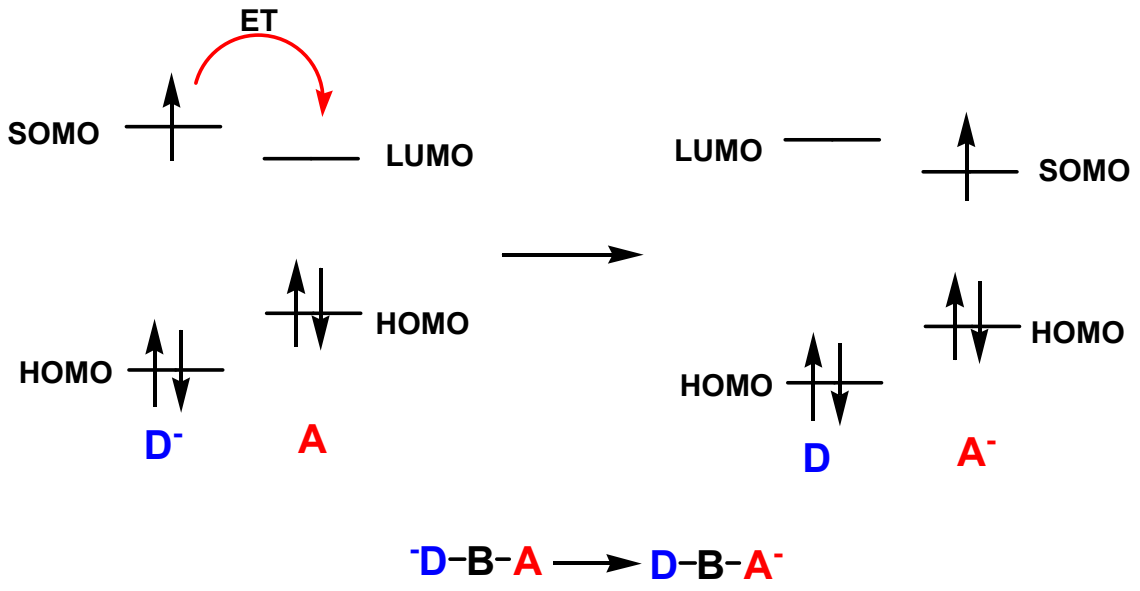

Figure 6.Electron transfer, D = Donor, A = Acceptor, B = Bridge, ET = Electron transfer, HOMO = Highest occupied molecular orbital, SOMO = single electron occupied molecular orbital, LUMO = lowest unoccupied molecular orbital.

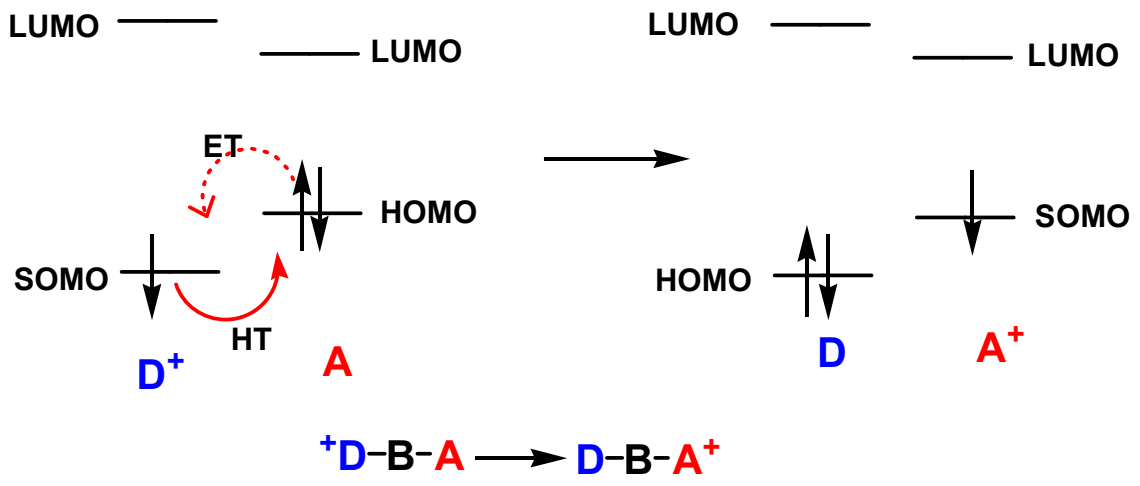

Figure 7. Hole transfer, D = Donor, A = Acceptor, B = Bridge, ET = Electron transfer, HT = Hole transfer, HOMO = Highest occupied molecular orbital, SOMO = single electron occupied molecular orbital and LUMO = lowest unoccupied molecular orbital.

1.3 Dye-sensitized solar cells

Since the first discovery of DSSCs by O'Regan and Grätzel[15], research into this area has expanded dramatically. In comparison to photovoltaic devices, organic dyes are introduced into the cell as light-absorbing materials attaching on nanocrystalline

semiconductor surfaces. Operation principle of n-type DSSC is shown in *Figure 8*. The TiO_2 semiconductor, other oxides such as ZnO[16] and Nb_2O_5[17] have also been studied, was coated on the conducting FTO glass surface. Then the dye molecules working as sensitizers were attached to the semiconductor surface through anchoring groups. The most widely used anchoring units are carboxylic acid and phosphonic acid[18], which are able to firmly graft the sensitizer to the semiconductor oxide surface. The electrolyte is an organic solution of redox systems such as the I^-/I_3^- couple. The cathode, counter electrode, is usually a platinum-coated conducting glass. Upon photo-excitation of the sensitizer (S) the excited state molecule (S*) is generated, and electrons are injected (10^{-9} s) into the conduction band of the semiconductor from the dye. Then electrons are supplemented back to the sensitizer through transferring of electrons from the redox couple (10^{-6} s), and this process helps to reduce the possibility of recapture of an electron from the conduction band (10^{-4} s). Electrons migrate from external load passing through counter electrode to reduce I_3^- back to I^- to complete a whole circuit. If the charge recombination, S* decay back to S, is faster than the injection of electron into the conduction band then the injection efficiency will be low.

In order to achieve high efficiency and low cost cells, the requirement of each component has to be considered. The FTO glass and TiO_2 semiconductor are relatively cheap and unquestionably robust, therefore, attention has been paid to the other components. An ideal sensitizer needs to absorb all light below 920 nm, to attach firmly to the semiconductor and to inject electrons into the valence band with unity quantum yield. The energy level of the dye needs to match with conduction band energy level and redox potential of redox couples. Finally, the organic dye should be stable enough to last for about 20 years, ~10^8 turnovers, on exposure to natural sunlight. Criteria for appropriate electrolyte redox couples are that they need to be stable enough, the energy level must match with the dye and the injection of electron into the excited sensitizer is fast enough to compete with charge recombination or injection of an electron from the semiconductor. The counter electrode also needs to be cheap and stable enough but

platinum is expensive and is used in coating the conducting glass at the moment.

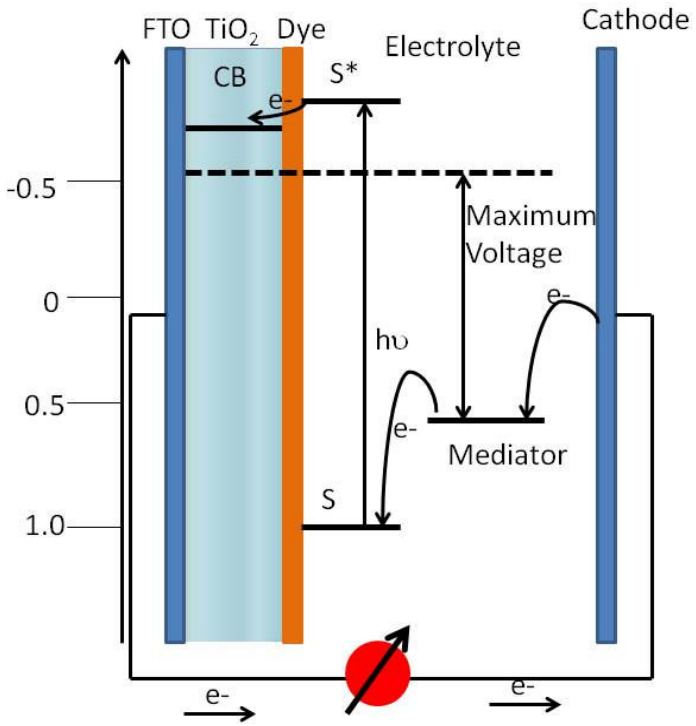

Figure 8. Illustration of working principle of a n-type DSSCs. FTO: Fluorine doped tin oxide conducting glass; CB: conduction band of semiconductor; S: ground state dye; S: excited state dye.*

The overall solar to energy efficiency, η, of the cell is calculated by *Equation 1*[19].

$$\eta = \frac{J_{SC}\, V_{OC}\, FF}{P_{in}} \qquad \text{Equation 1}$$

Where J_{SC} is the short circuit current, Voc is the open circuit voltage, FF is the fill factor, and P_{in} is the incident light intensity. An overall efficiency of over 12%[20] has been reported using **YD2-*O*-C8** (*Figure 9*) as a sensitizer, and the electrolyte solution consists of $Co^{(II/III)}$tris(bipyridyl)tetracyanoborate complexes as the redox couple and tert-butyl pyridine (TBP) and $LiClO_4$ as additives. Efficiency of cells can be improved to 17% in theory through proper combination of different components[21].

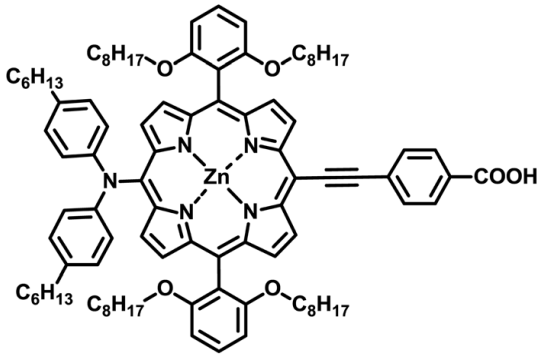

Figure 9. Molecular structure of ***YD2-O-C8****.*

Another factor to evaluate the performance of the cell is incident photon-to-current conversion efficiency (IPCE), IPCE = LHE x Φ_{inj} x η_{col}, where LHE is light harvesting efficiency, Φ_{inj} is the electron injection efficiency from the excited sensitizer into the TiO_2 conduction band, and η_{col} is the charge collection efficiency of the photo-generated charge carriers (determined by time constant for transport (τ_{trans}) and recombination (τ_{rec}) of the conduction band electrons injected into the nanocrystalline TiO_2 film, $\eta_{col} = 1/(1 + \tau_{trans}/\tau_{rec})$[22]). The best DSSC has almost unity Φ_{inj} and η_{col}, therefore to broaden light harvesting spectral range is the best way to improve IPCE.

In addition to n-type DSSCs, the research into p-type DSSCs (base on p-type inorganic semiconductors such as NiO, $CuAlO_2$ and $CuGaO_2$)[23] has started to increase. The working principle is based on hole injection from the photo-excited sensitizer to the valence band of the p-type semiconductor, i.e., the injection of electrons is in opposite direction in comparison to a n-type cell. A major performance limitation of p-type DSSCs is low Voc, which is defined by the difference of the quasi-Femi-level in the p-type semiconductor and the redox potential of the electrolyte. There are two possible ways to improve Voc; either to find a semiconductor with a higher ionization potential or find a redox mediator that is more easily oxidized relative to I^-/I_3^-. In particular, cobalt(II/III) complexes have been found to be good alternatives, such as $[Co(ttb\text{-}tpy)_2]^{2+/3+}$, $[Co(dMeO\text{-}bpy)_3]^{2+/3+}$, $[Co(dtb\text{-}bpy)_3]^{2+/3+}$, $[Co(dm\text{-}bpy)_3]^{2+/3+}$, and $[Co(en)_3]^{2+/3+}$, (ttb-tpy = 4,4’4’’-tri-tert-butyl tripyridine, dMeO-bpy = 4,4’-dimethoxyl

bipyridine, dtb-bpy = 4,4'-ditert-butyl bipyridine, and dm-bpy = 4,4'4''-dimethyl bipyridine, en = 1,2-diaminoethane)[24]. The record efficiency of p-DSSCs, η = 1.3% and Voc = 709 mV, was achieved using $[Co(en)_3]^{2+/3+}$ as electrolyte and **PMI-6T-TPA** (*Figure 10*) as a sensitizer.

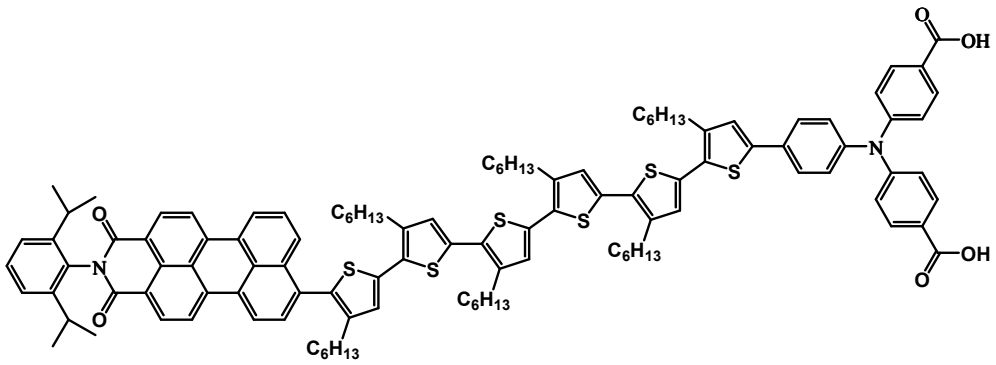

*Figure 10. Molecular structure of **PMI-6T-TPA**.*

Following the development in p-DSSCs, tandem cells have started to appear which consist of a TiO_2 photosensitized anode and a photosensitized p-type semiconductor as a cathode. The advantages of a tandem cell are that the Voc is independent of redox couple in the electrolyte (depends only on the difference between the potentials of the valence band of the p-semiconductor and the conduction band of the n-semiconductor), and two different sensitizers (one on each electrode) can enhance the absorption region of the cell. Higher Voc in tandem cells has been achieved in comparison to single semiconductor DSSCs[24, 25]. The best performance cell (η = 2.42%, Jsc = 4.07 mA/cm^2 and Voc = 958 mV) is achieved by using **PMI-6T-TPA** as a sensitizer on a NiO cathode and **N719** (*Figure 11*) as a sensitizer on a TiO_2 anode. The advance of p-type DSSCs is vital for development of tandem cells, as it is a limiting factor for improvement of the tandem cells' overall efficiency.

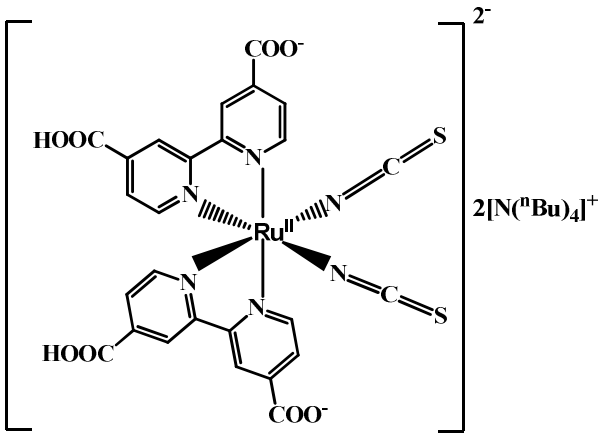

*Figure 11. Molecular structure of **N719**.*

1.4 Molecular switches and molecular machines

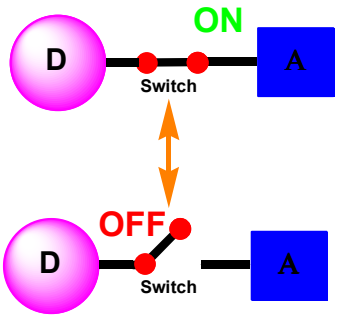

Figure 12. A pictorial representation of a one-dimensional molecular switch. Upon photochemical or electrochemical or chemical stimulation the switch can be turned ON and OFF reversibly.

In order to control properly the function of a molecular machine, switches are an essential part of the overall structure. Upon photochemical (UV/Vis), chemical (protonation/deprotonation) or electrochemical (oxidation/reduction) stimulation, reversible changes of optical and electronic properties of molecules can be achieved; i.e., ON and OFF states can be obtained upon the changes of conditions (*Figure 12*). In our work we try to discover molecular bridges which are able to direct energy/electron transfer in molecular dyads. In chapter 5, a four electron storage bridge was synthesized and in Chapter 6 we tried to develop methods to incorporate a chiral bridge in a molecular dyad to study the affect of chirality on the energy or electron transfer processes.

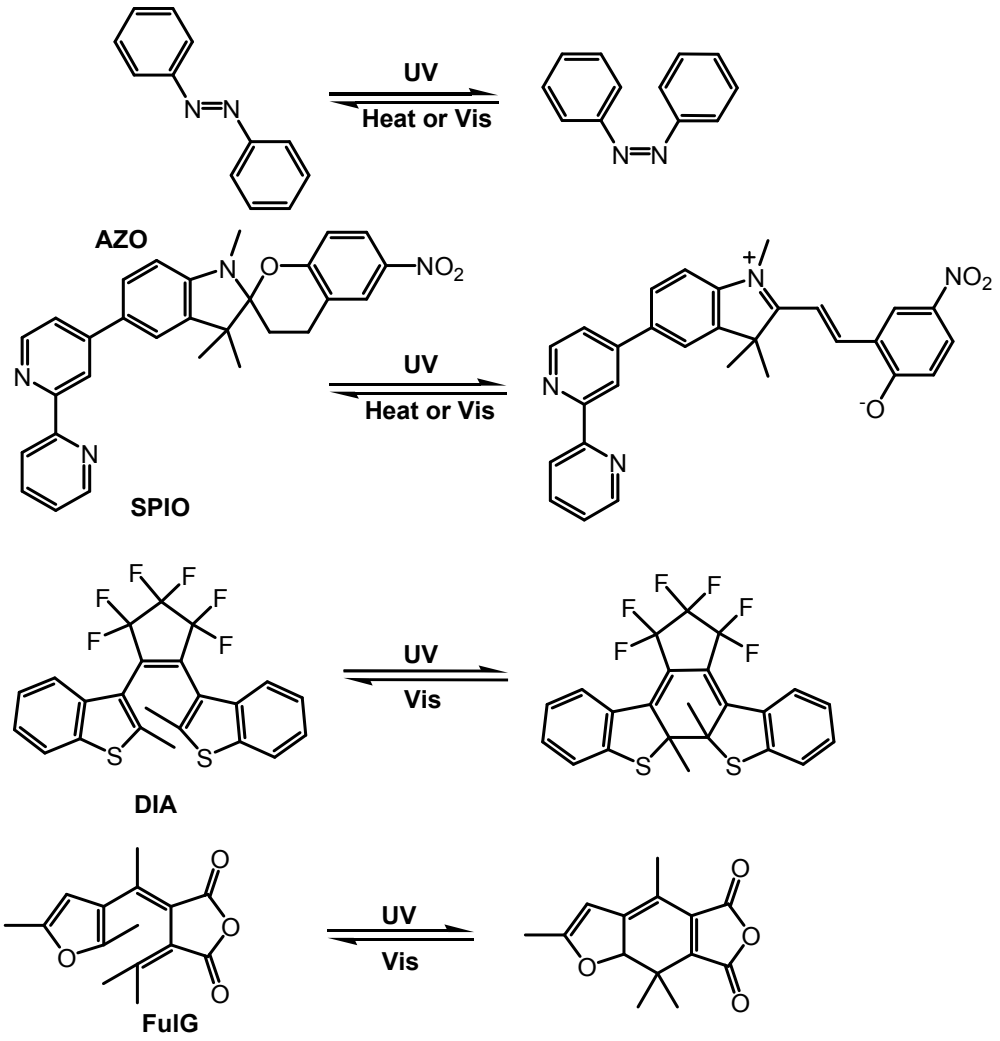

Figure 13. Some examples of photochromic molecules (from top to bottom shows azobenzene-, spiropyran-, diarylethene- and fulgide-based molecular switches)[26].

Chemically powered systems need input reactants and output waste products; therefore, it is not always a green and favourable prototype. On the other hand, photons are cheap, clean and an abundant primary energy source. Large numbers of photon-induced molecular switch prototypes (also known as photochromic molecules) have been reported, including azobenzene-, spiropyran- diarylethene- and fulgide-based molecules. The irradiation of photochromic materials with different wavelengths of light lead to changes of the electronic structures and geometries (showing up as the changes of the colours) which turn ON or OFF the switch (*Figure 13*)[26]. Azobenzene isomerises from *trans to cis* under UV irradiation and reverses back under visible light or heat conditions. Fluorescence of spiropyran- diarylethene- and fulgide-based compounds can be turned ON/OFF by ring opening/ ring closure. Molecular switches have been incorporated into

different donors and acceptors through supramolecular construction, showing some interesting properties. Some selected examples of molecular machines containing photochromic switches will be discussed briefly.

Azobenzene incorporating a crown ether (**AzoCrE**, *Figure 14*) has been shown to be a potential candidate for ion transportation[27]. By isomerisation of the *trans* azobenzene to the *cis* form, the ammonium tail can "bite" the crown ether "head" and so functions as a K^+ transportation system (when the concentration of K^+ is low). Under higher ion concentration conditions, the ion-transportation can also be achieved but through intermolecular complexation instead of isomerisation of the azobenzene and "biting of the tail to the head".

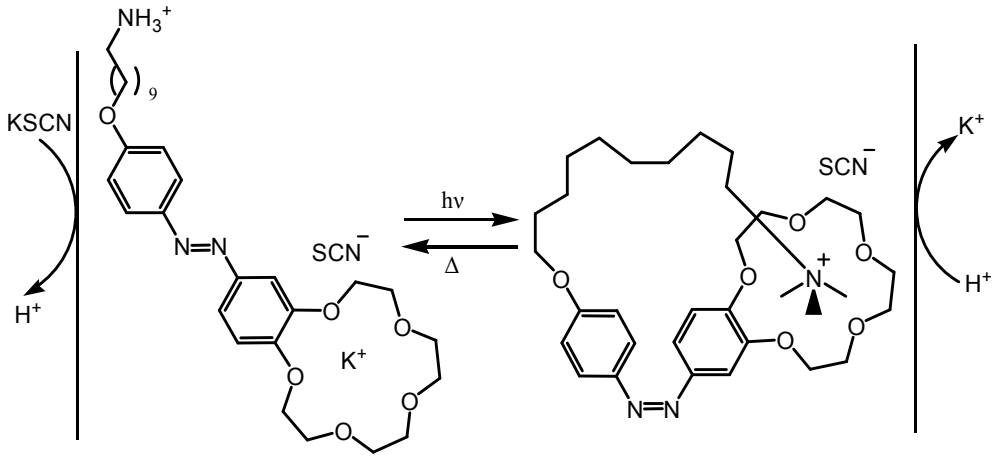

Figure 14. Transportation of K^+ through the isomerisation of azobenzene.

The first photoswitchable saccharide receptor containing a diarylethene unit as a switch was reported by Takeshita *et al.*[28]. As shown in *Figure 15*, the open-ring form has two both anti-parallel and parallel conformations which can exchange with each other at room temperature. The complexation of saccharides with the diarylethene containing boronic acid groups was achieved by formation of esters, because of the presence of the hydroxyl groups on the saccharides. The anti-parallel conformation of the ring opened form can be isomerised to the ring closed form, while the parallel conformation cannot be isomerised under UV radiation. Therefore, the recognition of saccharides can be controlled by irradiation of different wavelengths of light.

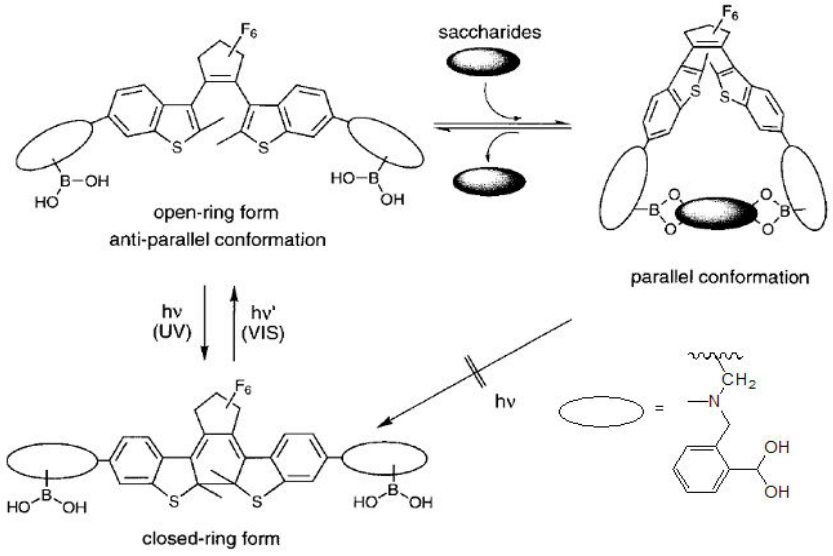

Figure 15. Photo-switchable recognition of saccharides by diarylethene based photochromic complex[28].

1.5 Molecular systems involved in this thesis

A brief review of some research published in the literature of acridinium derivatives, naphthalimide based molecular systems, viologen based complexes and binaphthol derivatives are discussed as follows.

1.5.1 Acridinium fluorophores

Acridinium derivatives have found wide application in different aspects such as biological sensors (especially dimethyl acridinium ion for superoxide sensing in vascular cell or tissue)[29], molecular switches[30] and photocatalysts[31]. Dimethyl acridinium ion was known as lucigenin (**Lc**, *Figure 16*) and its green or blue (depending on reaction conditions) chemiluminescence (CL) properties in basic hydrogen peroxide solution were first reported by Gleu and co-workers[32]. **Lc** is one of the most popular solution CL reagents, however, there is still no conclusive agreement on the mechanism involved in the CL process. There is some agreement that the CL process involved a redox reaction, the primary reaction products were N-methylacridone (**NMA**) and dimethylbiacridene (**DMB**), and the blue CL arises primarily from N-methylacridone

(*Figure 16*)[33]. A study of electrochemically generated chemiluminescence of **Lc** was carried out by Legg and co-authors[34] to identify the intermediates generated in the redox process. They proposed that the longer wavelength emission is assigned to either **NMA** or **DMB**. Excited **NMA** transfers energy to **DMB** and/or **Lc** through singlet-singlet energy transfer. Amiet[35] proposed that the fluorescence is due to the presence of **NMA** (blue) and **Lc** (green) under basic conditions. To summarize, the possible conversion route between **DMB** and **NMA** is illustrated in *Figure 16*.

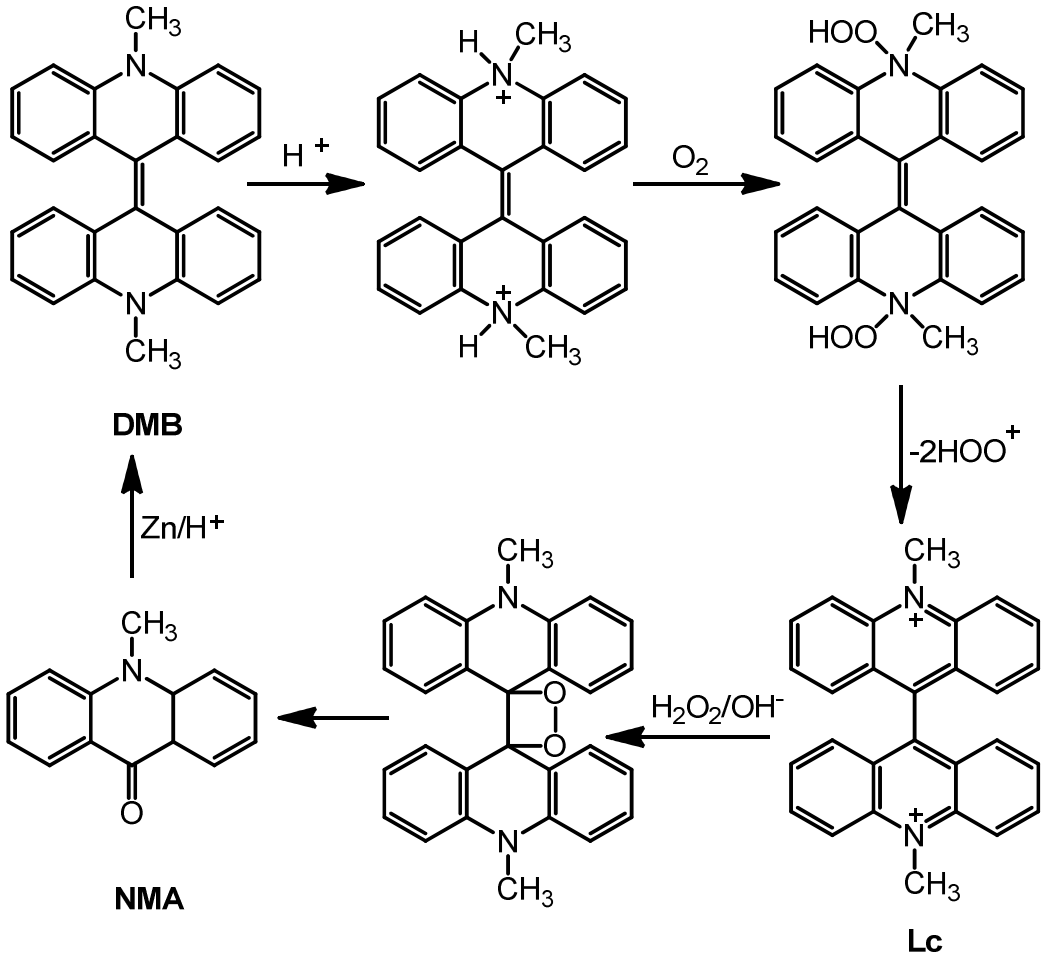

*Figure 16. Conversion between **DMB** and **NMA**.*

More recently, chemiluminescent acridinium dimethylphenyl esters with different charges were synthesized to study the charge effect on immunoassays applications. It was suggested that an acridinium ester with a hydrophilic and neutral N-alkyl group (**AcEs1**, *Figure 17*) performed better than the analogue with an anionic N-alkyl group (**AcEs2**, *Figure 17*) in terms of selectivity, stability and speed of light emission[36].

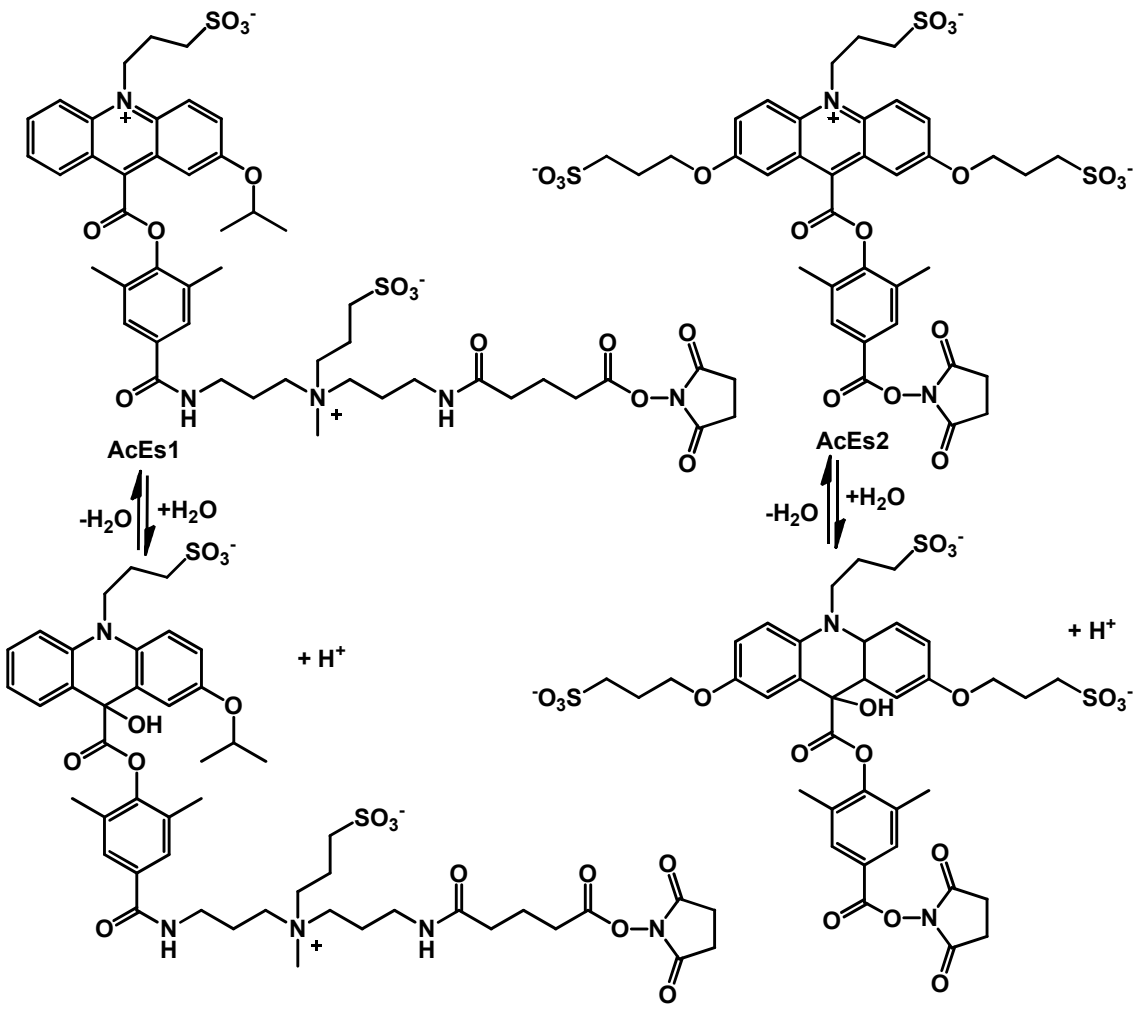

*Figure 17. Structure of **AcEs1** and **AcEs2** and their pseudobases*[36].

Furthermore, acridinium was used as photoactive moiety in photochemical/thermal switchable molecular devices[37,38]. Abraham and co-workers[38] carried out a study to examine the response of the acridinium moiety by attaching it on gold nanoparticles (GNPs). A photo/thermal reversible molecular switch (**AcMeGNP**) was found (*Figure 18*). This indicates that it is possible to use an acridinium derivative as a photoactive component for photophysical studies carried out on a nanoparticle surface, and it could have an interesting application in plasmon resonance energy transfer between molecular dyads and nanoparticles. Another application of acridinium derivatives (e.g., 9-mesityl-10-methyl-acridinium ion[39]) is to function as a photocatalyst for chemical reactions under visible light irradiation. However, to the best of our knowledge, there are no examples of acridinium derivatives working as sensitizers for DSSCs. In our work, discussed in Chapter 3, we demonstrate that it is possible to modify the structure

and apply them as sensitizers for DSSCs.

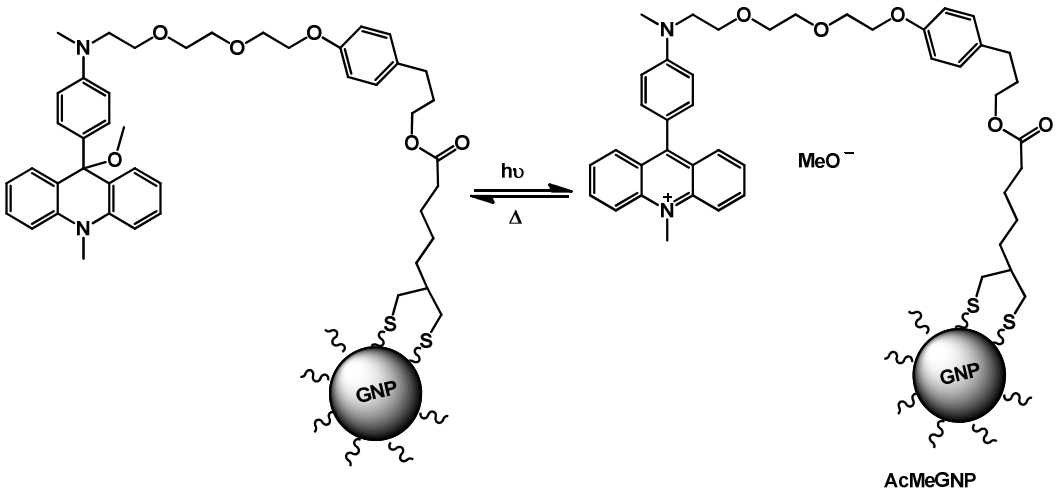

*Figure 18. Molecular switch of **AcMeGNP**[38].*

1.5.2 Naphthalimide based molecular systems

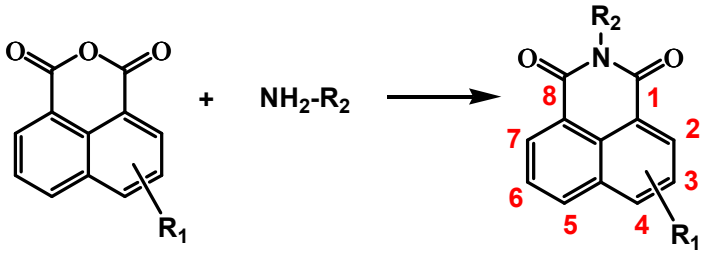

Figure 19. General synthetic route to 1,8-naphthalimide derivatives.

Basic naphthalimides can be conveniently synthesized from 1,8-naphthalic anhydrides and amines (*Figure 19*)[40]. The properties can be tuned by variation of the amines and the substituent in the naphthalene ring. Majority of these complexes are strongly fluorescent with a considerable Stokes shift[41]. Emission was found between green to red part of visible light depending on the substituent. Based on these findings naphthalimide derivatives have been considered as promising candidates for practical applications, most significant as n-channel semiconductors for organic thin-film transistors[42] and imaging agents (some of them are also potential anticancer drugs)[43]. A core-extended naphthalene diimide p-channel semiconductor was also reported by Würthner and co-workers[44]. Beyond these they have also been used as fluorescence probes[45], sensitizers for DSSCs[46], energy storage materials[47] and laser dyes[48]. The ease of

synthesis on large scale and high purity further enhance their roles in these practical fields.

Even simple 1,8-naphthalimide derivatives have been found as potent anticancer agents, the well known **Amonafide** and **Mitonafide** (*Figure 20*) have already entered phase II clinical trials[49]. They have been shown to be able to enhance thermal stability of DNA double strands[50]. **Amonafide** and **Mitonafide** can intercalate with DNA to break down DNA double strands and unwinding closed circular DNA, respectively in mammalian cells[51]. Naphthalimide derivatives have also been coordinated with metals for developing chemotherapeutic agents. **BisNAPPt1** and **BisNAPPt1** have been synthesized to overcome cell resistance for cis-platin based chemotherapeutics[52].

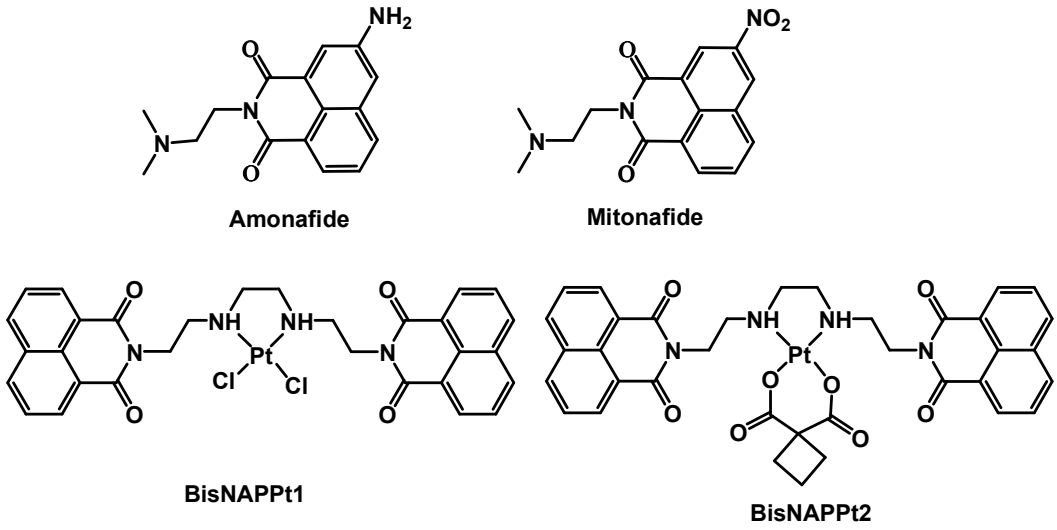

*Figure 20. Molecular structures of anticancer agents **Amonafide**, **Mitonafide**, **BisNAPPt1** and **BisNAPPt2**.*

Application of n-channel semiconductors for organic thin-film transistors (**OTFTs**) is a promising area of interest for naphthalimide derivatives. It was only over the last decade that the development of n-channel semiconductors started to became mature, and it has lagged behind the counterpart p-channel ones. Naphthalene/perylene diimides (**NDI**/**PDI**) have already been found to exhibit comparable properties with that of p-channel ones, since the first demonstration of their application in **OTFTs** by Dodabalapur *et al.*[53] and Horowitz *et al.*[54] in 1995. Recently, a chlorinated naphthalene

diimide derivative, **NDI1**, (*Figure 21*) was reported by Würthner and co-workers[55] which shows ambient stable electron mobility of 0.95 cm^2 V^{-1} s^{-1}. The performance can be further increased to 4.26 cm^2 V^{-1} s^{-1} under bias stress. The discovery of naphthalimide derivatives' prominent n-type semiconductor properties has also enabled them to be the focus of developing p-n-heterojunction tandem DSSCs, such as **PMI-6T-TPA** (*Figure 10*). As a sensitizer the best performance tandem cell (see 1.2.2 dye-sensitized solar cells) to the best of our knowledge was produced.

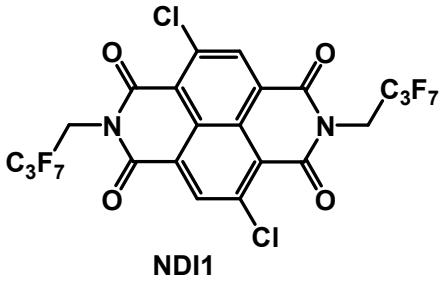

Figure 21 . Molecular structures of core chlorinated naphthalene diimide derivative, ***NDI1****.*

In order to achieve best performance practical devices, the understanding of the organic semiconductor solid state properties is of fundamental importance. We aimed to synthesize crystalline naphthalimide derivatives for study of their solid state photophysical properties as discussed in Chapter 4.

1.5.3 Viologen-based molecular dyads

N,N'-dialkyl-4,4'-bipyridinium cationic compounds (known as viologens), possessing low redox potentials, were originally developed as herbicides[56]. Later on they were developed as electron mediators in the catalytic cycle of artificial photosynthesis systems. More recently, by incorporation into rotaxanes, pseudorotaxanes, catenanes and cyclophanes, their applications in supramolecular construction of artificial molecular machines were widely studied[57].

Balzani *et al.*[58] reported a rotaxane (**VioRot1**, *Figure 22*) which can act as a nanomotor under the stimulation of sunlight or in the presence of a suitable electron relay. The motor

comprises a photosensitiser ($\mathbf{P}^{2+}$, also acting as a stopper), a spacer (**S**), two electron acceptors ($\mathbf{EA_1}^{2+}$ and $\mathbf{EA_2}^{2+}$), a crown ether derivative ring (**R**) and a secondary stopper (**T**). The stable form of **VioRot1** has the ring **R** located on $\mathbf{EA_1}^{2+}$ which is a better electron acceptor in comparison to $\mathbf{EA_2}^{2+}$. The ring **R** shuttled to $\mathbf{EA_2}^{2+}$ upon the reduction of $\mathbf{EA_1}^{2+}$ to $\mathbf{EA_1}^{1+}$. The shuttling back of **R** can be achieved by the oxidation of $\mathbf{EA_1}^{1+}$. The photon stimulated motion occurred through either intramolecular mechanism or intermolecular mechanism (with the assistance of phenothiazine as electron relay an auto-motion was reported)[58]. The intramolecular mechanism shows promising properties in the construction of a single-molecule level machine. In our work described in Chapter 5, a disulfide strapped methyl viologen derivative was synthesized, which is cable of storing up to four electrons (two-plus-two)[59].

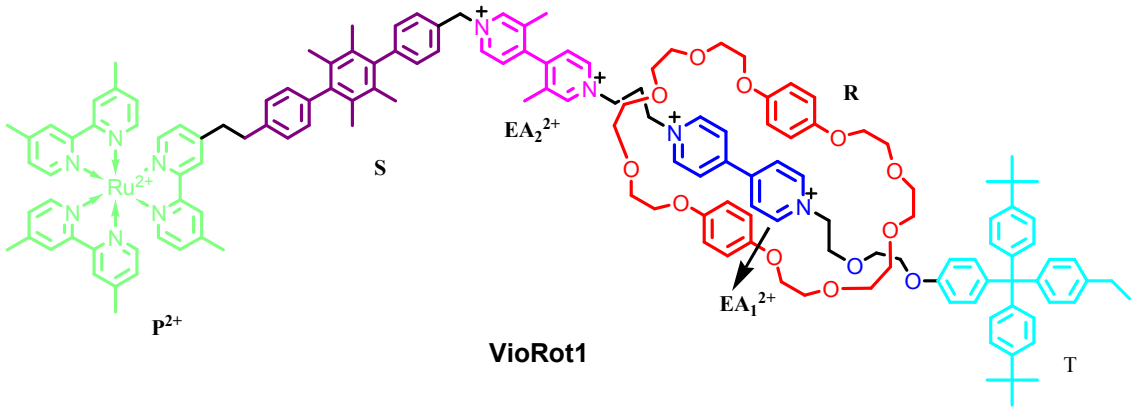

Figure 22. An example of viologen-based rotaxane reported by Balzani et al[58].

Viologen derivatives have been used as electron mediators in photocatalytic hydrogen evolution systems to increase the lifetime of the charge-separated state. As shown in *Figure 23*[60], under the stimulation of sunlight, the excited state of the sensitizer was generated then the excited state energy was transferred to the electron relay through the reduction of MV^{2+} (methylviologen dication) to MV^{+}. Platinum (Pt) acts as a catalyst in the reduction of H^{+} to H_2 and at the same time the reduced form of methyl-viologen MV^{+} was oxidised back to MV^{2+}. The fully reversible oxidation and reduction properties of viologen enable the repeating of the hydrogen evolution cycle. The drawback of this system is the low efficiency of hydrogen generation; however this system does provide a prototype for the future development of practical hydrogen evolution systems. Many

efforts have been devoted to the discovery of a better photo-sensitizer, cheaper catalyst (in comparison to platinum) and a higher efficiency electron mediator. The incorporation of different components is another issue which researchers need to take into consideration. To achieve a final practical hydrogen evolution system, elaborately designed and careful studies into the basic chemistry of different components needs to be done.

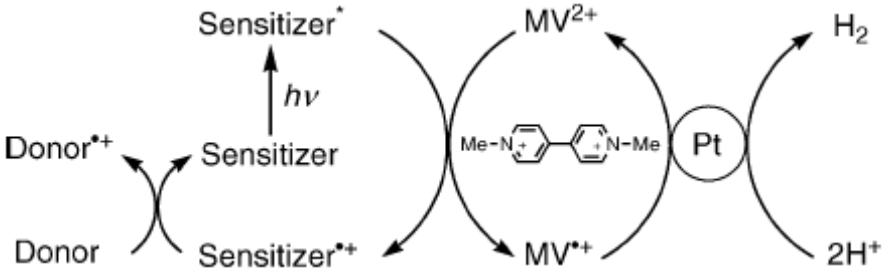

Figure 23. Example where methyl viologen acts as a mediator for hydrogen production.

1.5.4 Binaphthol derivatives

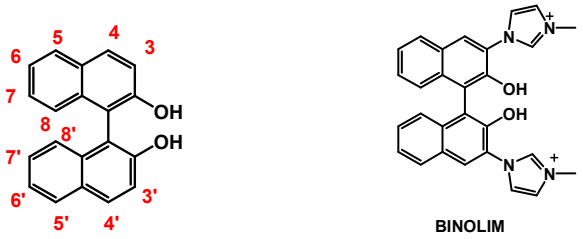

*Figure 24. Left: numbering of BINOL molecule; right: molecular structure of **BINOLIM**.*

Chiral 1,1'-bi-2-naphthol (BINOL, *Figure 24*) is a key building block for the synthesis of chiral optical molecular devices[61] and asymmetric catalysts[62] due to their stable chiral conformation and possible substitution in different positions. Substitution reactions can take place on the diol groups, 3 (3')-, 6 (6')- and 4 (4')- positions.

Hu *et al.*[63] reported a chiral anion recognition fluorescence sensor, **BINOLIM** (*Figure 24*), through incorporation of imidazolium units into BINOL on the 3,3'-positions. **BINOLIM** displays different fluorescence responses upon the addition of fluoride and acetate ions, which can be distinguished by naked eye. They reasoned the variation in fluorescence is due to the rapid charge transfer emission response induced by F^-. Pu and

co-workers[64] incorporated a BINOL based molecular system into a nanowire device through self-assembly on a gold surface. An electrically driven chiroptical macrocyclic switching, **BINOLVIO** (*Figure 25*) was constructed based on optically active BINOL and redox-active viologen units[65]. When the viologen units were electrochemically reduced absorption and circular dichroism spectra exhibit significant changes. The electrochemical reduction of **BINOLVIO** is reversible. Enhancement of BINOL fluorescence was found in a dendrimer derivative ((S)-**BINOLDEM1**, *Figure 26*) explored by Pu *et al.*[66] as a chiral fluorescence sensor for the detection of chiral amino alcohols. The fluorescence of (S)-**BINOLDEM1** is over 170 times stronger than the basic (S)-BINOL (compared with same concentration). A sensing mechanism was proposed that in the presence of amino alcohols there is a hydrogen-bonded complex formed between (S)-**BINOLDEM1** and amino alcohols. The proton-transfer complex is poorly emissive because of efficient quenching of fluorescence. The collection of energy from dendrons to the centre BINOL and further to the amino alcohol also indicated a directional energy transfer, which might also have potential application as an antenna in DSSCs. Lee and Lin[67] also reported an interesting BINOL based macrocyclic metal complex (*Figure 27*) for enantioseletive amino alcohol sensing. A thermally responsive BINOL based metal complex, **TpyBINOL**, was studied by Yam and co-workers[68]. As illustrated in *Figure 28*, upon the modulation of temperature both R and S enantiomers exhibit conformation changes between coils (low temperature) and helical strands (high temperature). The modulation of the metal-metal and π-π interactions account for the reversible thermal conformation transitions.

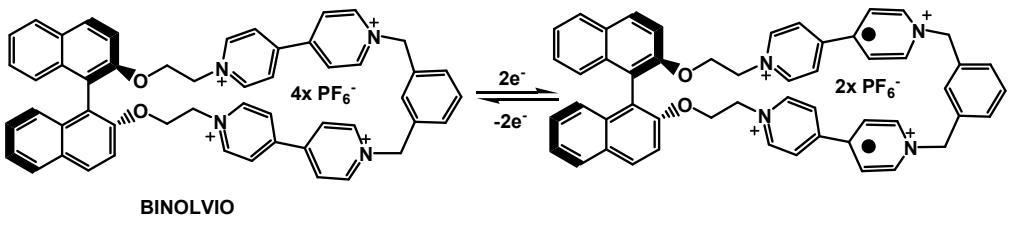

*Figure 25. Reversible electrochemical reduction of **BINOLVIO**[64].*

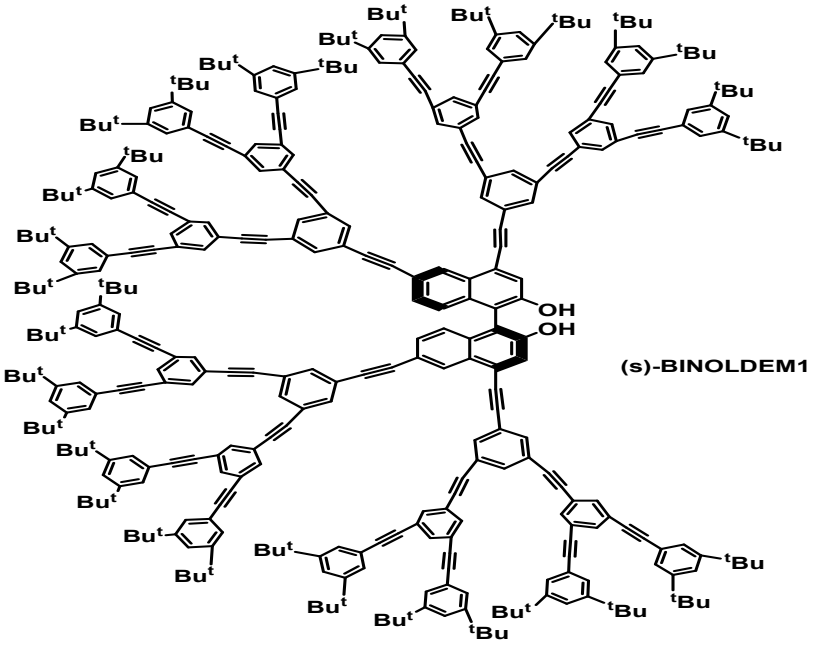

*Figure 26. Molecular structures of BINOL based dendrimer derivatives (S)-**BINOLDEM1**.*

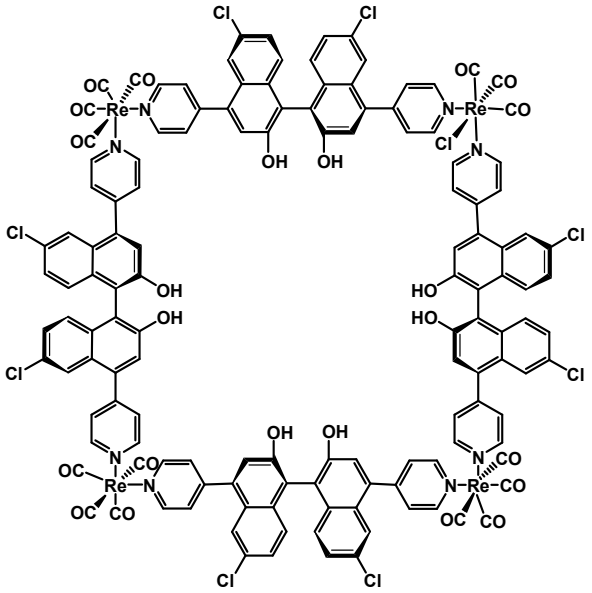

Figure 27. Molecular structures of BINOL based metallocyclic derivatives reported by Lee and Lin for enantioselective luminescence sensing.

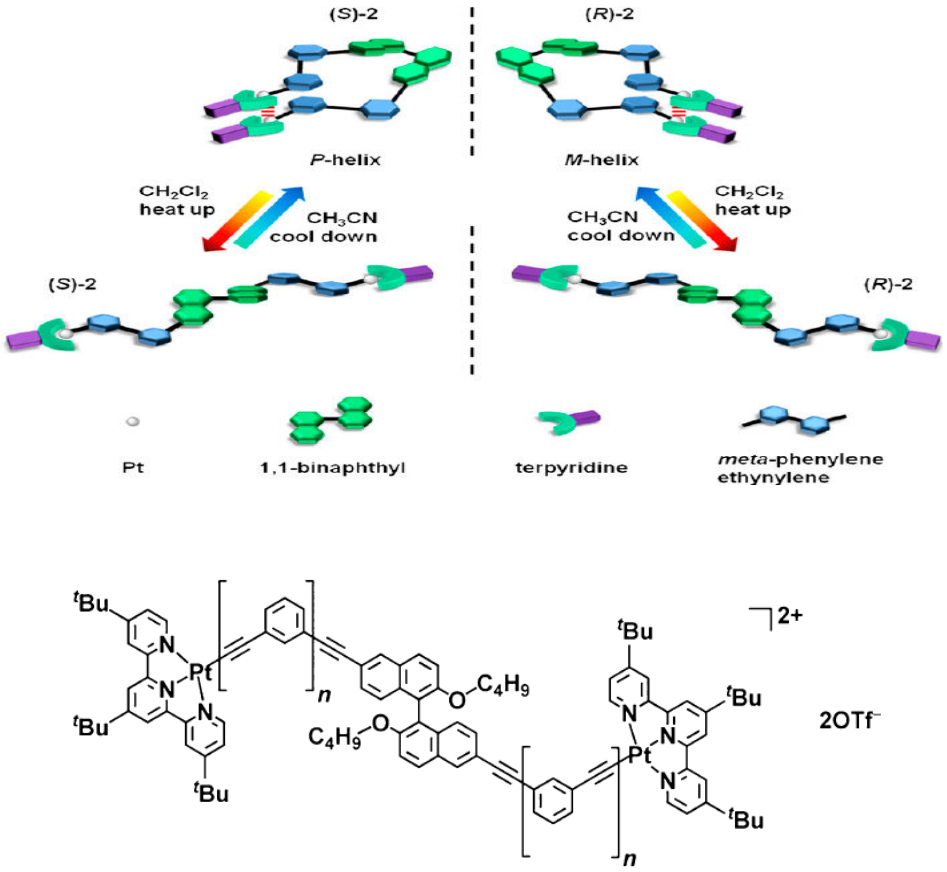

Figure 28. Pictorial representation of thermal responsive ***TpyBINOL*** *(Top) and the molecular structure of* ***TpyBINOL*** *where n =2 (bottom)*[68].

Beside the interesting applications in optical devices and fluorescence sensing, BINOL derivatives are also promising chiral ligands for asymmetric catalysis. Chiral phosphoramidites (*Figure 29*) have been discovered as efficient ligands for Cu-catalyzed 1,4-addition of diethylzinc to cyclic/acyclic enones[69]. When the ring size of the enone is large (e.g., cyclopentenone), the bisphosphoramidite is essential in order to improve the selectivity[70]. Pu and co-workers[71] found that through the incorporation of two monomer catalyst units into a rigid copolymer ((*R,R*)-**BINOLCoCat**, *Figure 30*), the catalyst activity can be retained. The replacement of the monomer catalyst with copolymer also exhibit advantages of easy recovery and simpler reaction mixture separation procedures. The co-polymer showed reactivity in both individual and tandem reactions. The results demonstrated a new way of finding catalysts for multi-step asymmetric reactions.

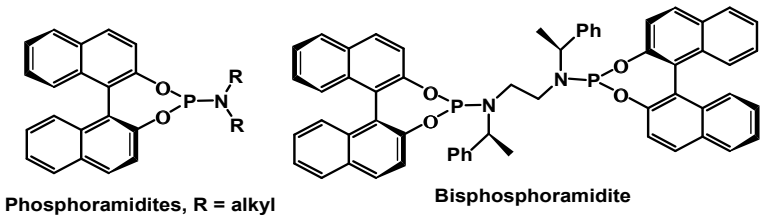

Figure 29. Molecular structures of BINOL based phosphoramidite ligands for asymmetric catalysis.

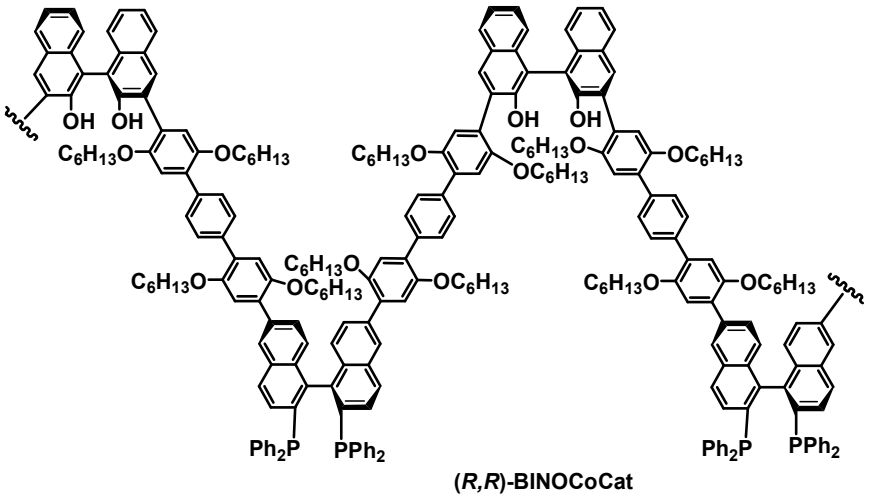

Figure 30. Repeating unit structure of a copolymer ***(R,R)-BINOCoCat****.*

In the following work discussed in Chapter 6, the BINOL unit was used as a chiral bridge for the study of energy/electron transfer from donor to acceptor. The synthesis of the donor-BINOL-acceptor type system required us to find a way to unsymmetrically functionalized the 4,4' positions.

1.6 Conclusions

In summary, it can be seen from the above discussion that enormous efforts have been make to advance our understanding of energy/electron/charge transfer processes in artificial molecular devices. Improvement in theoretical aspects has enabled us to get closer to the manufacture of practical devices such as DSSCs and OLED devices. DSSC is one of the most promising and fastest developing aspects of artificial photosynthesis. The development of p-type cells, n-type cells and to tandem cells seems to indicate that we will be able to use them of renewable and clean solar energy usage in our daily life. OLED devices are already found in small devices and the efforts to explore cheap and

full colour photo-/electro-active materials will bring us into a totally new technology world. Multi-electron mediators for water splitting are another exciting area. Upon the addressing of these problems, the shortage of energy and the pollution caused by the usage of fossil fuel will be solved. We endeavour to focus on some of these problems in this thesis, and to advance our understanding in some of the key issues. We believe that small advances will make a difference in the future of these exciting areas of science.

1.7 References

[1] V. Balzani, A. Credi, F. M. Raymo and J. F. Stoddart, *Angew. Chem. Int. Ed.*, 2000, **39**, 3348.

[2] R. P. Feynman, *Eng. Sci.* 1960, **23**, 22.

[3] A. C. Benniston and A. Harriman, *Mater. Today*, 2008, **11**, 26.

[4] H. Mustroph, M. Stollenwerk and V. Bressau, *Angew. Chem. Int. Ed.*, 2006, **45**, 2016.

[5] K. Rurack, *Spectrochimica Acta Part A*, 2001, **57**, 2161.

[6] C. McCusker, J. B. Carroll and V. M. Rotello, *Chem. Commun.*, 2005, **8**, 996.

[7] A. C. Benniston, *Chem. Soc. Rev.*, 2004, **33**, 573.

[8] G. McDermott, S. M. Prince, A. A. Freer, A. M. H. Lawless, M. Z. Papiz, R. J. Cogdell and N.W. Isaacs, *Nature*, 1995, **374**, 517.

[9] (i) O. Gonen and H. Levanon, *J. Chem. Phys*., 1986, **84**, 4132; (ii) D. Kim and A. Osuka, *J. Phys. Chem. A*, 2003, **107**, 8791; (iii) Y. Nakamura, N. Aratani and A. Osuka, *Chem. Soc. Rev.*, 2007, **36**, 831; (iv) A. J. Mozer, M. J. Griffith, G. Tsekouras, P. Wagner, G. G. Wallace, S. Mori, K. Sunahara, M. Miyashita, J. C. Earles, K. C. Gordon, L. Du, R. Katoh, A. Furube and D. L. Officer, *J. Am. Chem. Soc.*, 2009, **131**, 15621.

[10] (i) A. Harriman, L. J. Mallon, S. Goeb, G. Ulrich and R. Ziessel, *Chem. Eur. J.* 2009, **15**, 4553; (ii) G. Ulrich, R. Ziessel and A. Harriman, *Angew. Chem. Int. Ed.*, 2008, **47**, 1184; (iii) J. Iehl, J. F. Nierengarten, A. Harriman, T. Bura and R. Ziessel, *J. Am. Chem. Soc.*, 2012, **134**, 988.

[11] (i) N. Gfeller, S. Megelski and G. Calzaferri, *J. Phys. Chem. B*, 1998, **102**, 2433; (ii) G. Calzaferri and K. Lutkouskaya, *Photochem. Photobiol. Sci.,* 2008, **7**, 879.

[12] D. Gust, T. A. Moore and A. L. Moore, *Acc. Chem. Res.*, 1993, **26**, 198.

[13] T. Förster, *Discuss. Faraday Soc.*, 1959, **27**, 7.

[14] D. L. Dexter, *J. Chem. Phys.*, 1953, **21**, 836.

[15] B. O'Regan and M. Grätzel, *Nature*, 1991, **353**, 737.

[16] K. Tennakone, G. R. R. Kumara, I. R. M. Kottegoda and V. S. P. Perera, *Chem. Commun.*, 1999, **35**, 15.

[17] K. Sayama, H. Suguhara and H. Arakawa, *Chem. Mater.*, 1998, **10**, 3825.

[18] (i) V. Thavasi, V. Renugopalakrishnan, R. Jose and S. Ramakrishna, *Mater. Sci. Eng.*, 2009, **63**, 81; (ii) E. Baranoff, J. H. Yum, M. Gräetzel and M. K. Nazeeruddin, *J. Organomet. Chem.*, 2009, **694**, 2661; (iii) M. Grätzel, *Acc. Chem. Res.*, 2009, **42**, 1788; (iv) M. K. Nazeeruddin, E. Baranoff and M. Grätzel, *Sol. Energy*, 2011, **85**, 1172; (v) A. Hagfeldt, G. Boschloo, L. Sun, L. Kloo and H. Pettersson, *Chem. Rev.*, 2010, **110***,* 6595; (vi) F. Odobela, L. Pleux, Y. Pellegrin and E. Blart, *Acc. Chem. Res.*, 2010, **43**, 1063; (vii) M. Liang and J. Chen, *Chem. Soc. Rev.*, 2013, **42**, 3453; (viii) J. R. Swierk and T. E. Mallouk, *Chem. Soc. Rev.*, 2013, **42**, 2357; (ix) Y. Pellegrin, L. L. Pleuxa , E. Blart, A. Renaud, B. Chavillon, N. Szuwarski, M. Boujtita, L. Cario, S. Jobic, D. Jacquemina and F. Odobela, *J. Photochem. Photobiol. A*, 2011, **219**, 235.

[19] M. Grätzel, *J. Photoch. Photobio. C*, 1991, **335**, 737.

[20] A. Yella, H. W. Lee, H. N. Tsao, C. Y. Yi, A. K. Chandiran, M. K. Nazeeruddin, E. W. G. Diau, C. Y. Yeh, S. M. Zakeeruddin, and M. Grätzel, *Science*, 2011, **334**, 629.

[21] T. W. Hamann, R. A. Jensen, A. B. F. Martinson, H. Van Ryswyk, and J. T. Hupp, *Energy Environ. Sci.*, 2008, **1**, 66.

[22] A. Hagfeldt, M. Grätzel, *Chem. Rev.*, 1995. **95**, 49.

[23] (i) X. L. Zhang, F. Z. Huang, A. Nattestad, K.Wang, D. C. Fu, A. Mishra, P. Buerle, U. Bach and Y. B. Cheng, *Chem. Commun.*, 2011, **47**, 4808; (ii) A. Nattestad, X. Zhang, U. Bach and Y. B. Cheng, *J. Photonics Energy*, 2011, **1**, 011103; (iii) M. Yu, G. Natu, Z. Ji and Y. Wu, *J. Phys. Chem. Lett.*, 2012, **3**, 1074.

[24] (i) E. A. Gibson, A. L. Smeigh, L. Le Pleux, L. Hammarstrom, F. Odobel, G. Boschloo, A. Hagfeldt, *J. Phys. Chem. C*, 2011, **115**, 9772; (ii) E. A. Gibson, A. L. Smeigh, L. L. Pleux, J. Fortage, G. Boschloo, E. Blart, Y. Pellegrin, F. Odobel, A. Hagfeldt, L. Hammarstrom, *Angew. Chem. Int. Ed.*, 2009, **48**, 4402; (iii) S. Powar, T. Daeneke, M. T. Ma, D. Fu, N. W. Duffy, G. Gotz, M. Weidelener, A. Mishra, P. Bauerle, L. Spiccia and U. Bach, *Angew. Chem. Int. Ed.*, 2013, **52**, 602.

[25] A. Nattestad, A. J. Mozer, M. K. R. Fischer, Y. B. Cheng, A. Mishra, P. Bauerle and U. Bach, Nat. Mater., 2010, **9**, 31.

[26] (i) P. Belser, L. D. Cola, F. Hartl, V. Adamo, B. Bozic, Y. Chriqui, V. M. Iyer, R. T. F. Jukes, J. Kühni, M. Querol, S. Roma and N. Salluce, *Adv. Funct. Mater.*, 2006, **16**, 195; (ii) M. Irie, *Photochem. Photobiol. Sci.*, 2010, **9**, 1535; (iii) C. C. Corredor, Z. Huang and K. D. Belfield, *Adv. Mater.*, 2006, **18**, 2910.

[27] S. Shinkai, M. Khihara, K. Ueda and O. Manabe, *J. Chem. Soc. Perkin Trans.II*, 1985, 511.

[28] M. Takeshita, K. Uchida and M. Irie, *Chem. Commun.,* 1996, **15**, 1807.

[29] (i) A. Natrajan, D. Sharpe, J. Costello and Q. Jiang, *Anal. Biochem.*, 2010, **406**, 204. (ii) A. Natrajan, D. Sharpe and D. Wen, *Org. Biomol. Chem.*, 2012, **10**, 1883.

[30] (i) W. Abraham, K. Buck, M. Orda-Zgadzaj, S. Schmidt-Schaffer and U. W. Grummt, *Chem. Commun.*, 2007, **29**, 3094; (ii) W. Abraham, A. Wlosnewski, K. Buck and S. Jacob, *Org. Biomol. Chem.*, 2009, **7**, 142; (iii) Y. Duo, S. Jacob and W. Abraham, *Org. Biomol. Chem.*, 2011, **9**, 3549.

[31] K. Ohkubo, K. Mizushima, R. Iwata and S. Fukuzumi, *Chem. Sci.*, 2011, **2**, 715.

[32] K. Gleu and W. Petsch, *Angew. Chem.*, 1935, **48**, 57.

[33] A. Spruit-Van Der Burg, *Recueil*, 1950, **69**, 1525.

[34] K. D. Legg and D. M. Hercules, *J. Am. Chem. Soc.*, 1969, **91**, 1902,

[35] R. G. Amiet, *J. Chem. Educ.*, 1982, **59**, 163.

[36] A. Natrajan and D. Sharpe, *Org. Biomol. Chem.*, 2013, **11**, 1026.

[37] (i)W. Abraham, K. Buck, M. Orda-Zgadzaj, S. Schmidt-Schaffer and U.-W. Grummt, *Chem. Commun.*, 2007, **29**, 3094; (ii) W. Abraham, A. Wlosnewski, K. Buck and S. Jacob, *Org. Biomol. Chem.*, 2009, **7**, 142.

[38] Y. Duo, S. Jacob and W. Abraham, *Org. Biomol. Chem.*, 2011, **9**, 3549.

[39] K. Ohkubo, K. Mizushima, R. Iwat and S. Fukuzumi, *Chem. Sci.*, 2011, **2**, 715.

[40] M. Palucki, D. L Hughes, N. Yasuda, C. Yang and P. J Reider, *Tetrahedron Lett.*, 2001, **42**, 6811.

[41] (i) R. M. Duke, E. B. Veale, F. M. Pfeffer, P. E. Kruger and T. Gunnlaugsson, *Chem. Soc. Rev.*, 2010, **39**, 3936; (ii) T. Gunnlaugsson, M. Glynn, G. M. Tocci, P. E. Kruger and F. M. Pfeffer, *Coord. Chem. Rev.*, 2006, **250**, 3094; (iii) E. B. Veale, G. M. Tocci, F. M. Pfeffer, P. E.

Kruger and T. Gunnlaugsson, *Org. Biomol. Chem.*, 2009, **7**, 3447; (iv) E. B. Veale and T. Gunnlaugsson, *J. Org. Chem.*, 2008, **73**, 8073; (v) R. M. Duke and T. Gunnlaugsson, *Tetrahedron Lett.*, 2007, **48**, 8043; (vi) H. D. P. Ali, P. E. Kruger and T. Gunnlaugsson, *New J. Chem.*, 2008, **32**, 1153; (vii) Y. Li, L. Cao and H. Tian, *J. Org. Chem.*, 2006, **71**, 8279; (viii) E. Tamanini, A. Katewa, L. M. Sedger, M. H. Todd and M. Watkinson, *Inorg. Chem.*, 2009, **48**, 319; (ix) E. Tamanini, K. Flavin, M. Motevalli, S. Piperno, L. A. Gheber, M. H. Todd and M. Watkinson, *Inorg. Chem.*, 2010, **49**, 3789; (x) A. P. de Silva, H. Q. N. Gunaratne, J. L. Habib-Jiwan, C. P. McCoy, T. E. Rice and J. P. Soumillion, *Angew. Chem., Int. Ed.*, 1995, **34**, 1728; (xi) Z. Xu, X. Qian and J. Cui, *Org. Lett.*, 2005, **7**, 3029; (xii) Z. Xu, K. H. Baek, H. N. Kim, J. Cui, X. Qian, D. R. Spring, I. Shin and J. Yoon, *J. Am. Chem. Soc.*, 2009, **132**, 601.

[42] (i) X. Kong, Z. He, Y. Zhang, L. Mu, C. Liang, B. Chen, X. Jing and A. N. Cammidge, *Org. Lett.*, 2011, **13**, 764; (ii) H. Kar, M. R. Molla and S. Ghosh, *Chem. Commun.*, 2013, **49**, 4220; (iii) F. Würthner and M. Stolte, *Chem. Commun.*, 2011, **47**, 5109; (iv) J. Chang, Q. Ye, K. W. Huang, J. Zhang, Z. K. Chen, J. Wu and C. Chi, *Org. Lett.*, 2012, **14**, 2964; (v) M. Stolte, M. Gsanger, R. Hofmockel, S.-L. Suraru and F. Würthner, *Phys. Chem. Chem. Phys.*, 2012, **14**, 14181; (vi) X. Guo, Felix S. Kim, S. A. Jenekhe and M. D. Watson, *J. Am. Chem. Soc.*, 2009, **131**, 7206.

[43] (i) S. U. Hossain, S. Sengupta and S. Bhattacharya, *Bioorg. Med. Chem.*, 2005, **13**, 5750; (ii) S. Banerjee, E. B. Veale, C. M. Phelan, S. A. Murphy, G. M. Tocci, L. J. Gillespie, D. O. Frimannsson, J. M. Kelly and T. Gunnlaugsson, *Chem. Soc. Rev.*, 2013, **42**, 1601; (iii) C. M. Yang, I. W. Lee, T. L. Chen, W. L. Chien and J. L. Hong, *J. Mater. Chem. C*, 2013, **1**, 2842; (iv) M. E. Vázquez, J. B. Blanco, S. Salvadori, C. Trapella, R. Argazzi, S. D. Bryant, Y. Jinsmaa, L. H. Lazarus, L. Negri, E. Giannini, R. Lattanzi, M. Colucci and G. Balboni, *J. Med. Chem*., 2006, **49**, 3653; (v) R. M. Duke, E. B. Veale, F. M. Pfeffer, P. E. Kruger and T. Gunnlaugsson, *Chem. Soc. Rev.,* 2010, **39**, 3936.

[44] F. Würthner and M. Stolte, *Chem. Commun.*, 2011, **47**, 11504.

[45] K. D. Krishna, K. S. Ramendra and K. Misre, *Indian J. Chem. Sect. B*, 1995, **34**, 876.

[46] (i) X. Qian, Z. Zhu and K. Chen, *Dyes Pigm.*, 1989, **11**, 13; (ii) X. Qian, A. Zhu, K. Chen, Q.

Yin and G. Zhu, *Mater. Chem. Phys.*, 1989, **23**, 335.

[47] Z. Song, H. Zhan and Y. Zhou, *Angew. Chem. Int. Ed.*, 2010, **49**, 8444.

[48] (i) A. Pardo, J. M. L. Poyato, J. J. Camacho, M. F. Brana and J. M. Castellano, *J. Photochem.*, 1986, **36**, 323; (ii) A. Pardo, E. Martin, J. M. L. Poyato, J. J. Camacho, M. F. Brana and J. M. Castellano, *J. Photochem. Photobiol. A*, 1989, **48**, 259.

[49] (i) M. F. Brana and A. Ramos, *Curr. Med. Chem.: Anti-Cancer Agents*, 2001, **1**, 237; (ii) M. F. Brana, J. M. Castellano, C. M. Roldan, A. Santos, D. Va′zquez and A. Jimenez, *Cancer Chemother. Pharmacol.*, 1980, **4**, 61.

[50] M. F. Brana, A. M. Sanz, J. M. Castellano, C. M. Roldan and C. Roldan, *Eur. J. Med. Chem.*, 1981, **16**, 207.

[51] (i) B. S. Andersson, M. Beran, M. Bakic, L. E. Silberman, R. A. Newman and L. A. Zwelling, *Cancer Res.*, 1987, **47**, 1040; (ii) G. H. Su, T. A. Sohn, B. Ryu and S. E. Kern, *Cancer Res.*, 2000, **60**, 3137; (iii) J. Keen, L. Yan, K. Mack, C. Pettit, D. Smith, D. Sharma and N. Davidson, *Breast Cancer Res. Treat.*, 2003, **81**, 177; (iv) M. J. Waring, A. Gonzalez, A. Jimenez and D. Vazquez, *Nucleic Acids Res.*, 1979, **7**, 217.

[52] J. M. Perez, I. Lopez-Solera, E. I. Montero, M. F. Brana, C. Alonso, S. P. Robinson and C. Navarro-Ranninger, *J. Med. Chem.*, 1999, **42**, 5482.

[53] A. Dodabalapur, H. E. Katz, L. Torsi and R. C. Haddon, *Science*, 1995, **269**, 1560.

[54] G. Horowitz, F. Kouki, P. Spearman, D. Fichou, C. Nogues, X. Pan and F. Garnier, *Adv. Mater.*, 1996, **8**, 242.

[55] M. Stolte, M. Gsanger, R. Hofmockel, S. L. Suraru and F. Würthner, *Phys. Chem. Chem. Phys.*, 2012, **14**, 14181.

[56] (i) J. Volke, *Collect. Czech. Chem. Commun.*, 1968, **33**, 3044; (ii) L. A. Summers, *The Bipyridinium Herbicides*, Academic Press, London, **1980**.

[57] (i) Y. Liu, A. H. Flood, P. A. Bonvallett, S. A. Vignon, B. H. Northrop, H. R. Tseng, J. O. Jeppesen, T. J. Huang, B. Brough, M. Baller, S. Magonov, S. D. Solares, W. A. Goddard, C. M. Ho and J. F. Stoddart, *J. Am. Chem. Soc*., 2005, **127**, 9745; (ii) S. A. Vignon and J. F. Stoddart, *Collect. Czech. Chem. Commun,* 2005, **70**, 1493; (iii) A. C. Benniston and A. Harriman, *J. Am.*

Chem. Soc., 1994, **116**, 11531; (iv) F. M. Raymo and J. F. Stoddart, *Pure Appl. Chem.,* 1996, **68**, 313; (v) M. J. Frampton and H. L. Anderson, *Angew. Chem. Int. Ed.*, 2007, **46**, 1028; (vi) P. Ceroni, A. Credi, M. Venturi and V. Balzani, *Photochem. Photobiol. Sci.*, 2010, **9**, 1561; (vii) V. Balzani, A. Credi, F. M. Raymo and J. F. Stoddart, *Angew. Chem. Int. Ed.*, 2000, **39**, 3348.

[58] V. Balzani, M. C. Leo, A. Credi, B. Ferrer, M. Venturi, A. H. Flood and J. F. Stoddart, *PNAS*, 2006, **103**, 1178.

[59] A. C. Benniston, J. Hagon, X. He, S. Yang and R. W. Harrington, *Org. Lett.*, 2012, **14**, 506.

[60] S. Fukuzumi, *Eur. J. Inorg. Chem.,* 2008, **39**, 135.

[61] (i) C. Hu, Y. He, Z. Chen and X. Huang, *Tetrahedron: Asymmetry*, 2009, **20**, 104; (ii) Q. S.. Lu, L. Dong, J. Zhang, J. Li, L. Jiang, Y. Huang, S. Qin, C. W. Hu and X. Q. Yu, *Org. Lett.,* 2009, **11**, 669; (iii) M. Nishijima, J. W. Chang, C. Yang, G. Fukuhara, T. Mori and Y. Inoue, *Res. Chem. Intermed*, 2013, **39**, 371; (iv) K. Kano, Y. Kato and M. Kodera, *J. Chem. Soc. Perkin Trans. 2*, 1996, 1211; (v) K. Takaishi and M. Kawamoto, *Molecules,* 2011, **16**, 1603; (vi) Z. B. Li, J. Lin and L. Pu, *Angew. Chem. Int. Ed.*, 2005, **44**, 1690; (vii) L. Pu, *Chem. Rev.*, 2004, **104***,* 1687.

[62] (i) L. He, X. H. Chen, D. N. Wang, Sh. W. Luo, W. Q. Zhang, J. Yu, L. Ren and L. Z. Gong, *J. Am. Chem. Soc.*, 2011, **133**, 13504; (ii) H. Brunner, M. Weber and M. Zabel, *Asymmetric Catalysis*, 2003, **154**, 821; (iii) W. S. Huang, Q. S. Hu, X. F. Zheng, J. Anderson, and L. Pu, *J. Am. Chem. Soc.*, 1997, **119**, 4313; (iv) S. J. Lee, A. Hu, and W. Lin, *J. Am. Chem. Soc.*, 2002, **124**, 12948; (v) M. Terada, *Chem. Commun.*, 2008, **35**, 4097; (vi) P. Arya and H. Qin, *Tetrahedron*, 2000, **56**, 917; (vii) Q. H. Xia, H. Q. Ge, C. P. Ye, Z. M. Liu and K. X. Su, *Chem. Rev.*, 2005, **105***,* 1603.

[63] (i) Q. S. Hu, L. Dong, J. Zhang, J. Li, L. Jiang, Y. Huang, S. Qin, C. W. Hu and X. Q. Yu, *Org. Lett.,* 2009, **11**, 669; (ii) Q. S. Hu, V. Pugh, M. Sabat and L. Pu, *J. Org. Chem.*, 1999, **64***,* 7528.

[64] Y. Zhu, N. Gergel, N. Majumdar, L. R. Harriott, J. C. Bean and L. Pu, *Org. Lett.*, 2006, **8**, 355.

[65] J. Deng, N. Song, Q. Zhou and Z. Su, *Org. Lett.*, 2007, **9**, 5393.

[66] V. J. Pugh, Q. S. Hu and L. Pu, *Angew. Chem. Int. Ed.*, 2000, **39**, 3638.

[67] S. J. Lee and W. Lin, *J. Am. Chem. Soc.*, 2002, **124**, 4554.

[68] S. Y. L. Leung, W. H. Lam and V. W. W. Yam, *PNAS*, 2013, **110**, 7986.

[69] A. H. M. De Vries, A. Meetsma and B. L. Feringa, *Angew. Chem., Int. Ed. Engl.*, 1996, **35**, 2374.

[70] B. L. Feringa, *Acc. Chem. Res.*, 2000, **33**, 346.

[71] H. B. Yu, Q. S. Hu and L. Pu, *J. Am. Chem. Soc.*, 2000, **122**, 6500.

Chapter 2

General Experimental

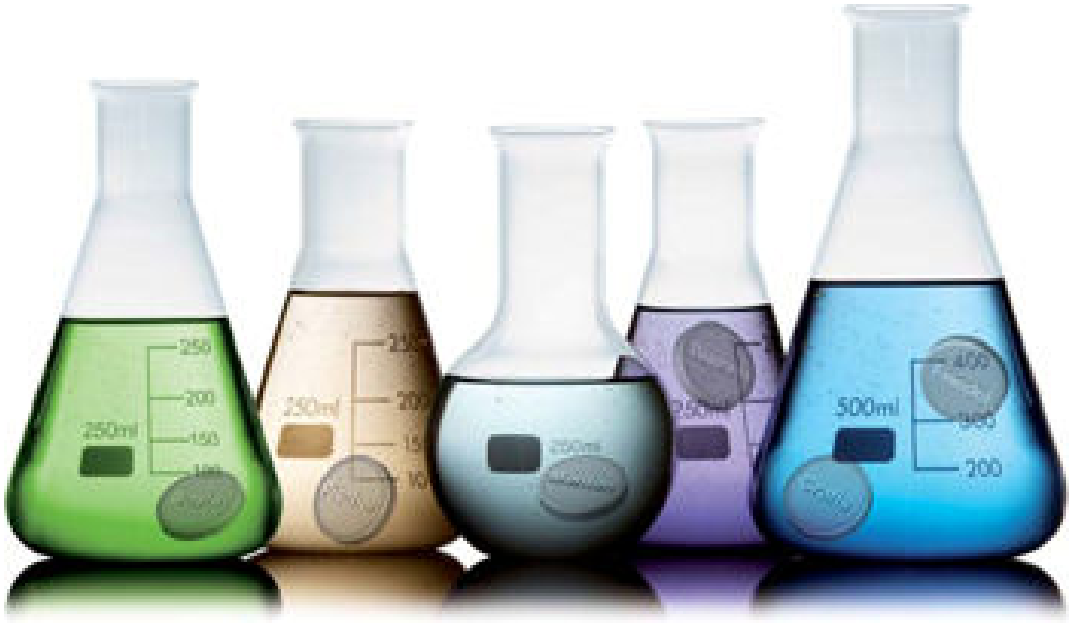

2.1 Instrumentation

2.1.1 Nuclear magnetic resonance

All ^{1}H-, ^{13}C-, ^{11}B-, ^{31}P- and ^{19}F-NMR spectra were recorded on a Bruker AVANCE 300MHz or a JEOL 400MHz spectrometer or a JEOL Lambda 500MHz spectrometer. All COSY, NOSEY, HMBC, HMQC spectra were recorded on either a JEOL 400 MHz spectrometer or a JEOL Lambda 500MHz spectrometer. Chemical shifts for ^{1}H- and ^{13}C-NMR spectra are referenced relative to the residual protiated solvent. $BF_3.Et_2O$ (δ = 0 ppm) and $CFCl_3$ (δ = 0 ppm) were used as references for the ^{11}B NMR and ^{19}F NMR chemical shifts, respectively.

2.1.2 Mass spectrometry

Mass Spectra were obtained from the EPSRC Mass Spectrometry service centre at Swansea or MEDAC LTD. A Thermofisher LTQ Orbitrap XL spectrometer was used to collect FT-MS spectra at Swansea University. EI-, CI-, ESI-, APCI-MS spectra were obtained from either a Thermofisher DSQ-II, a Finnigan MAT 95 XP or an Agilent 5975C Inert XL GC/MSD spectrometer.

2.1.3 Elemental analysis

Elemental analysis was carried out by MEDAC LTD with either a Thermo EA1108 or a FlashEA1112 series elemental analyser.

2.1.4 Absorption spectra

Absorption spectra were recorded in spectroscopic grade solvent with a cuvette of 1 cm path length using a Hitachi U3310 spectrophotometer. A baseline was corrected prior to the measurement. Spectroscopic grade solvents were used in all experiments.

2.1.5 Emission spectra

Emission spectra were obtained from a Hitachi F-4500 spectrometer. The solutions were purged with nitrogen prior to measurements.

2.1.6 Infrared spectra

Infrared spectra were obtained on an Avatar 370 DGTS spectrometer. The spectra were recorded by dispersing the solid phase sample on a diamond tip.

2.1.7 Time-resolved spectroscopy and data analysis[1]

Femto- to pico-second time-resolved absorption spectra were collected using a pump–probe technique described previously[2]. The femtosecond pulses of a Ti-sapphire generator were amplified using a multipass amplifier (CDP-Avesta, Moscow, Russia) pumped by a second harmonic of the Nd:YAG Q-switched laser (model LF114, Solar TII, Minsk, Belorussia). The amplified pulses were used to generate second harmonic (400 nm) for sample excitation (pump beam) and the white light continuum for a time-resolved spectrum detection (probe beam). The samples were placed in 1 mm rotating cuvettes, and averaging of 100 pulses at a 10 Hz repetition rate was used to improve the signal-to-noise ratio. The typical response time of the instrument was 150 fs (fwhm). Absorption spectra were recorded prior to and after all experiments to check for compound degradation.

Time-resolved transient absorption data were manipulated using the freely available software package, Decfit. In a typical analysis the whole collection of differential absorption spectra was inspected over the full timescale, and decay kinetics were

---

[1] A. C. Benniston, X. He, H. Lemmetyinenb and Nikolai V. Tkachenko, *RSC Adv.*, 2013, **3**, 4995.

[2] N. V. Tkachenko, L. Rantala, A. Y. Tuaber, J. Helaja, P. H. Hynninen and H. Lemmetyinen, *J. Am. Chem. Soc.*, 1999, **121**, 9378.

obtained at two specifically chosen wavelengths using an appropriate number of exponentials and instrument response function. Lifetimes obtained by a least-squares fit to the kinetic model were also checked by a global analysis at several different wavelengths. Up-conversion fluorescence lifetimes were obtained by fitting the single-photon-counting data to different kinetic models using a variable Gaussian instrument response function. Analysis was attempted using mono- to triexponentials and the stretched exponential function. Best fits were judged by the usual methods of remaining residuals and sigma value.

2.1.8 Cyclic voltammetry

Cyclic voltammograms were obtained from a fully automated HCH Instruments Electrochemical Analyzer and with a three-electrode set-up consisting of a platinum working electrode/carbon working electrode/gold working electrode, a platinum wire counter electrode and a Ag/AgCl reference electrode. Cyclic voltammograms were recorded in a solution containing the compound (1 mM) and *N*-tetrabutylammonium tetrafluoroborate (TBATFB, 0.2 M) as background electrolyte. The solution was deoxygenated before the measurement and kept under nitrogen during the whole experiment. The same concentration (1 mM) of ferrocene was added as internal reference.

2.1.9 X-Ray crystallography

X-Ray crystallography made use of either the Agilent dual-source single-crystal diffractometer with a CCD detector in Newcastle University or synchrotron radiation at SRS station 9.8, Daresbury Laboratory, UK, with a Bruker APEX2 CCD diffractometer. Software was standard Bruker APEX2 for data collection and processing, and SHELXTL for structure solution and refinement[3].

[3] G. M. Sheldrick, *Acta Crystallogr., Sect. A: Found. Crystallogr.*, 2008, **64**, 112.

2.2 Chemicals used

All chemicals used in preparative work, together with their supplier and stated purity, are summerised in *Table 1*.

Table 1. Commercially available chemicals used in the preparative work.

Chemicals	Suppliers	Purity
3-Hydroxypyridine	Sigma-Aldrich	98%
Triethylamine	Fluka	99.5%
Diethylcarbamyl chloride	Sigma-Aldrich	97%
N,N,N′,N′-Tetramethylethylenediamine	Sigma-Aldrich	99%
tert-Butyllithium solution	Sigma-Aldrich	1.7 M in pentane
Iodine	Sigma-Aldrich	≥99.8%
Sodium metabisulfite	Sigma-Aldrich	≥95%
Magnesium sulfate	Sigma-Aldrich	≥99.5%
Triisopropyl borate	Sigma-Aldrich	≥98%
Butyllithium solution	Sigma-Aldrich	1.6 M in hexane
Tetrakis-(triphenylphosphine) palladium(0),	Sigma-Aldrich	99%
Sodium carbonate	Sigma-Aldrich	≥99.5%
Sodium hydroxide	Sigma-Aldrich	≥98%
Dimethylthiocarbamoyl chloride	Sigma-Aldrich	97%
4-Dimethylaminopyridine	Sigma-Aldrich	≥99 %
Tetradecane	Sigma-Aldrich	≥99 %
Potassium hydroxide	Riedel-de Haen	≥85%
Phosphorous tribromide	Sigma-Aldrich	99%

4-Methylbenzyl alcohol	Sigma-Aldrich	98%
Iodomethane	Sigma-Aldrich	99%
Lithium diisopropylamide	Sigma-Aldrich	97%
Phthalic anhydride	Sigma-Aldrich	99%
3,4,5-Trimethoxyaniline	Sigma-Aldrich	97%
N,N-Dimethyl-*p*-phenylenediamine	Sigma-Aldrich	97%
Tetrachlorophthalic anhydride	Sigma-Aldrich	96%
2,4,6-Trimethylaniline	Sigma-Aldrich	98%
1,8-Naphthalic anhydride	Sigma-Aldrich	Not stated
Aniline	Sigma-Aldrich	99%
4-Chloro-1,8-naphthalic anhydride	Sigma-Aldrich	≥95%
4-Bromo-1,8-naphthalic anhydride	Sigma-Aldrich	95%
2-Napthol	Sigma-Aldrich	98%
Terephthalaldehyde	Sigma-Aldrich	99%
2,4-Dimethyl-3-ethylpyrrole	Sigma-Aldrich	97%
Trifluoroacetic acid	Sigma-Aldrich	≥99%
2,3-Dichloro-5,6-dicyano-*p*-benzoquinone	Sigma-Aldrich	98%
N,N-Diisopropylethylamine	Sigma-Aldrich	≥99%
Boron trifluoride diethyl etherate	Sigma-Aldrich	Purified by redistillation
4-Bromobenzaldehyde	Sigma-Aldrich	99%
Acetic acid	Sigma-Aldrich	≥99.7%
Hydrochloric acid	Sigma-Aldrich	37%
Lead dioxide	Sigma-Aldrich	≥97%
Tetrafluoroboric acid solution	Sigma-Aldrich	48% wt. in H_2O
Manganese(IV) oxide	Sigma-Aldrich	≥99%
Acetic anhydride	Sigma-Aldrich	≥99%

Potassium hexafluorophosphate	Sigma-Aldrich	99.5%
4-(Dimethylamino)phenylboronic acid	Sigma-Aldrich	≥95.0%
1,2-Dimethoxyethane	Sigma-Aldrich	99.5%
Copper(I) iodide	Sigma-Aldrich	≥99.5%
Boron tribromide	Sigma-Aldrich	≥99%
1,1-Bi-2-napthol	Sigma-Aldrich	99%
Bromine	Sigma-Aldrich	≥99.5%
Sodium iodide	Sigma-Aldrich	≥99%
Bis(triphenylphosphine)palladium(II) dichloride	Sigma-Aldrich	≥99.99%
4,4,5,5-Tetramethyl-1,3,2-dioxaborolane	Sigma-Aldrich	97%
Potassium carbonate	Sigma-Aldrich	≥99%
Bromoethane	Sigma-Aldrich	98%
n-Butyllithium solution	Sigma-Aldrich	2.6 M in hexane
Hexachloroethane	Sigma-Aldrich	99%
1,2-Dimethoxyethane	Sigma-Aldrich	≥99%
Potassium acetate	Sigma-Aldrich	≥99%
Fullerene-C_{60}	Sigma-Aldrich	98%
Sarcosine	Sigma-Aldrich	98%
Diiodomethane	Sigma-Aldrich	99%
Bis(pinacolato)diboron	Sigma-Aldrich	99%
Sodium sulfide nonahydrate	Alfa Aesar	98%
5-Formylfuran-2-boronic acid	Alfa Aesar	97%
Acetone-d_6	Cambridge Laboratory Supplies	99.9% atom D
Acetonitrile-d_3	Sigma-Aldrich	99.8% atom D

Toluene-d_8	Cambridge Laboratory Supplies	99.94% atom D
Chloroform-d_3	Sigma-Aldrich	99.8% atom D
Methylene chloride-d_2	Cambridge Laboratory Supplies	99.96% atom D

2.3 Solvents used

All solvents used in the preparative work and their purification methods are listed in *Table 2*.

Table 2. Lists of solvents used in the preparative work and the purification method.

Solvents	Purification methods
Tetrahydrofuran	Distilled from sodium/benzophenone under nitrogen
Triethylamine	Distilled from potassium hydroxide under nitrogen
Acetonitrile	Distilled from calcium hydride under nitrogen
Dichloromethane	Distilled from calcium hydride under nitrogen
Diethyl ether	Distilled from sodium under nitrogen
Toluene	Distilled from sodium under nitrogen
N,N'-Dimethylformamide	Dried over molecular sieves and distilled under reduced pressure
Tetramethylethylenediamine	Dried over molecular sieves and distilled under nitrogen
Ethyl acetate	
Methanol	
Ethanol	
Hexane	
Petroleum ether	
N-Methyl-2-pyrrolidone	

2.4 Synthetic protocols

2.4.1 Compounds discussed in chapter 3

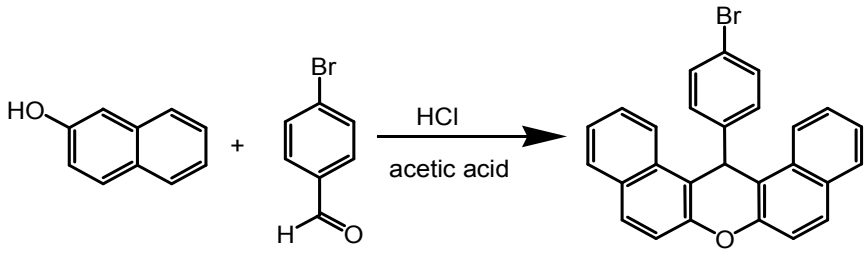

ACR1

4-Bromobenzaldehyde (2.97 g, 16.05 mmol) and 2-naphthol (5.21 g, 36.92 mmol, 15% excess) were added to acetic acid (80 mL) followed by the addition of concentrated (37%) hydrochloric acid (3.2 mL). The light yellow mixture was stirred and refluxed for 36 hours. After cooling to room temperature, the white solid was filtered off and washed with diethyl ether and dried under vacuum. The product was used for next step without further purification. Yield, 5.5 g, 12.58 mmol, 78%.

^{1}H NMR (400 MHz, $CDCl_3$): δ = 8.31 (d, *J* = 8.8 Hz, 2H; H of Ar), 7.84 (d, *J* = 8.4 Hz, 2H; H of Ar), 7.80 (d, *J* = 8.8Hz, 2H; H of Ar), 7.58 (apparent td, *J* = 1.2, 7.7 Hz, 2H; H of Ar), 7.47 (d, *J* = 8.8 Hz, 2H; H of Ar), 7.44 - 7.38 (m, 4H; H of Ar), 7.25 (d, *J* = 8.8 Hz, 2H; H of Ar), 6.46 (s, 1H; H of CH). ^{13}C NMR (101 MHz, $CDCl_3$): δ = 148.82, 144.11, 131.71, 131.38, 131.19, 130.00, 129.24, 129.04, 127.05, 124.51, 122.52, 120.34, 118.14, 116.79, 37.59 ppm.

All chemical shifts values were consistent with those stated in the literature[4].

[4] D. Wu , W. Pisula, M. C. Haberecht, X. Feng and K. Müllen, *Org. Lett.*, 2009, **11**, 5686.

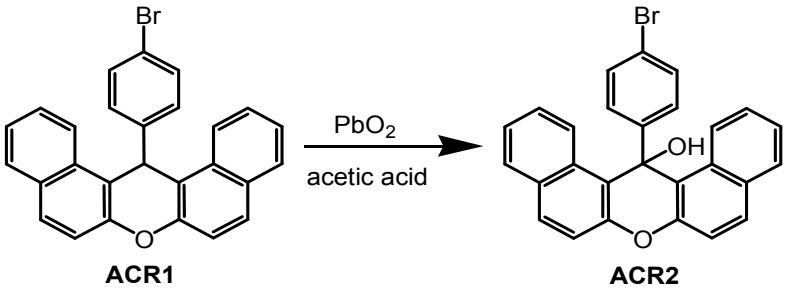

ACR1 ACR2

ACR1 (2.0 g, 4.57 mmol) and lead dioxide (1.86 g, 7.77 mmol, 70% excess) were added to acetic acid (50 mL). The mixture was stirred and refluxed for 6.5 hours. The solution was filtered to collect the first part of the biege solid. The rest of the solution was poured into 500 mL of distilled water to afford a beige solid. The solids were combined and purified by column chromatography (silica gel) eluting with petroleum ether / DCM = 3 / 1 to afford a white solid. Yield, 1.59 g, 3.51 mmol, 77%.

^{1}H NMR (400 MHz, $CDCl_3$): δ = 8.86 (d, *J* = 8.8 Hz, 2H; H of Ar), 7.81 (d, *J* = 8.8 Hz, 2H; H of Ar), 7.75 (d, *J* = 8.0 Hz, 2H; H of Ar), 7.62 (d, *J* = 8.0 Hz, 2H; H of Ar), 7.44 - 7.38 (m, 4H; H of Ar), 7.34 (apparent t, *J* = 8.0 Hz, 2H; H of Ar), 7.29 (d, *J* = 8.0 Hz, 2H; H of Ar), 3.25 (s, 1H; H of OH). ^{13}C NMR (101 MHz, $CDCl_3$): δ = 146.38, 131.92, 131.33, 131.05, 130.50, 129.88, 128.98, 128.86, 126.92, 126.58, 124.39, 117.99, 117.67, 62.63 ppm. EI-MS: m/z calcd for $[M]^+$: 452.0; found: 452.0.

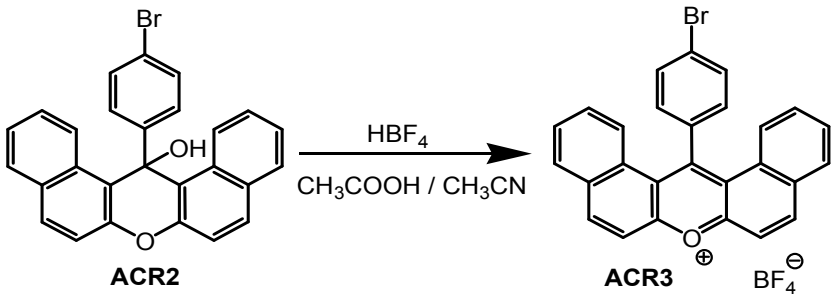

ACR2 (700 mg, 1.54 mmol) was dissolved in a mixture of acetic acid (10 mL) and acetonitrile (20 mL), and was followed by the addition of tetrafluoroboric acid solution (48% wt., 2.0 mL) in a dropwise manner. The reaction was protected from light and stirred at room temperature for 24 hours. The solvent volume was reduced under vacuum to about 3 mL, then filtered and removed completely to afford a dark red solid. The dark red solid was washed by dry diethyl ether and dried under vacuum. Yield, 753 mg, 1.44 mmol, 93%.

^{1}H NMR (400 MHz, CD_3CN): δ = 8.90 (d, *J* = 8.8 Hz, 2H; H of Ar), 8.30 (d, *J* = 8.0 Hz, 2H; H of Ar), 8.28 (d, *J* = 8.0 Hz, 2H; H of Ar), 8.09 (d, *J* = 8.0 Hz, 2H; H of Ar), 7.84 (apparent td, *J* = 1.6 Hz, 8.0 Hz, 2H; H of Ar), 7.56 (apparent td, *J* = 1.6 Hz, 8.4 Hz, 2H; H of Ar), 7.49 (d, *J* = 8.4 Hz, 2H; H of Ar), 7.29 (d, *J* = 8.8 Hz, 2H; H of Ar). ^{13}C NMR (101 MHz, CD_3CN): δ = 166.37, 160.68, 147.93, 138.43, 136.32, 133.70, 132.63, 131.17, 130.50, 129.75, 129.63, 128.85, 126.85, 123.17 ppm. FTMS: m/z calcd for $[M\text{-}BF_4]^+$: 435.0379; found: 435.0376.

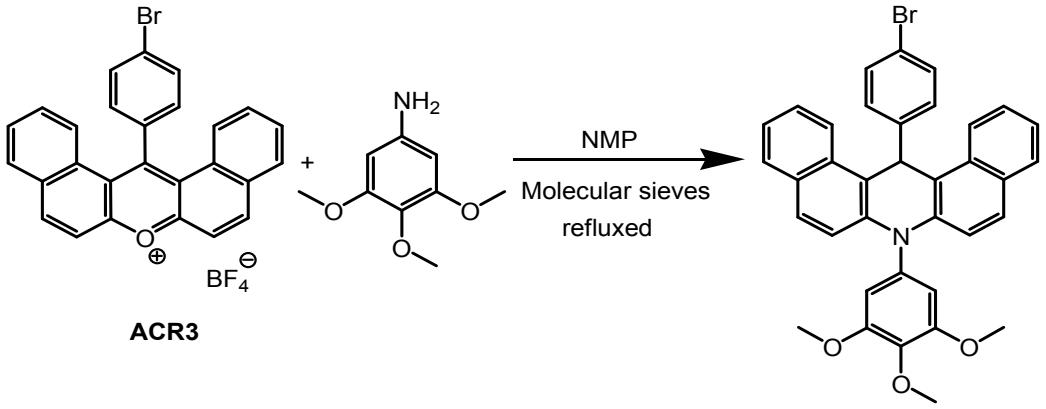

1-Methyl-2-pyrrolidinoneacetonitrile (NMP) (15 mL) was added to a mixture of **ACR3** (250 mg, 0.48 mmol), 3,4,6-trimethoxyaniline (1.70 g, 9.0 mmol) and molecular sieves (1.50 g). The mixture was stirred and refluxed under the protection of nitrogen for 8 hours. The dark brown solution was filtered to remove the molecular sieves and some insoluble black solid which was washed with dichloromethane. The dark brown solution was poured into distilled water and extracted with dichloromethane. The combined organic layers were dried over magnesium sulphate and the solvent was removed under vacuum to afford a brown oil. The brown oil was purified by column chromatography (silica gel) eluting with acetone / petroleum ether = 1 / 4. Yield, 110 mg, 0.18 mmol, 38%.

^{1}H NMR (400 MHz, $CDCl_3$): δ = 8.44 (d, *J* = 8.4 Hz, 2H; H of Ar), 7.77 (d, *J* = 8.4 Hz, 2H; H of Ar), 7.60 (apparent t, *J* = 9.2 Hz, 4H; H of Ar), 7.36 (apparent t, *J* = 7.2 Hz, 2H; H of Ar), 7.31 (d, *J* = 8.4 Hz, 2H; H of Ar), 7.22 (d, *J* = 7.2 Hz, 2H; H of Ar), 6.91 (d, *J* = 9.2 Hz, 2H; H of Ar), 6.91 (s, 1H; H of CH), 6.61 (s, 2H; H of Ar), 4.02 (s, 3H; H of OCH_3), 3.85 (s, 6H; H of OCH_3). ^{13}C NMR (101 MHz, $CDCl_3$) δ = 155.11, 144.91, 138.58, 138.24, 136.81, 131.75, 131.48, 130.07, 129.46, 128.83, 127.92, 127.11, 123.53, 122.05, 120.02, 116.87, 115.07, 107.95, 61.33, 56.47, 37.59 ppm. EI-MS: m/z calcd for $[M+H]^+$: 602.1328; found: 602.1325.

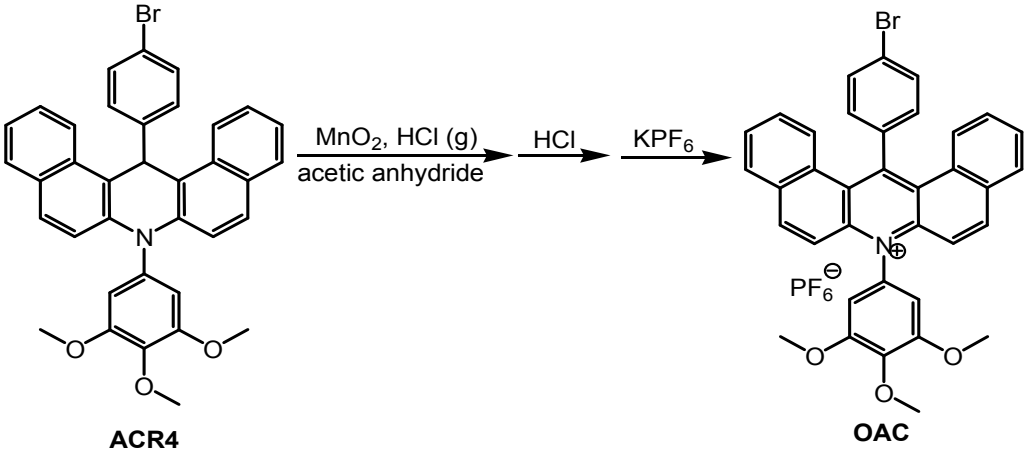

To a solution of **ACR4** (688 mg, 1.14 mmol) dissolved in acetic anhydride (60 mL) was added manganese(IV) oxide (297 mg, 3.42 mmol). The mixture was protected from light, bubbled with hydrochloric acid gas and refluxed. After 1 hour, manganese(IV) oxide was filtered off and diethyl ether was added to help the precipitation of a yellow solid. The solvent was removed to afford yellow solid. The yellow solid was dried under vacuum before being dissolved in acetic acid (30 mL). To the solution 12 drops of hydrochloric acid (37%) was added and the mixture was stirred at room temperature for 15 minutes. Then diethyl ether was added to aid the precipitation of a yellow solid. The solvent was removed and the yellow solid was dissolved in hot water. Saturated potassium hexafluorophosphate solution was added in a dropwise manner to obtain yellow solid. The crude product was recrystallised from acetonitrile and diethyl ether. Yield, 558 mg, 0.75 mmol, 66%.

^{1}H NMR (400 MHz, CD_3CN): δ = 8.35 (d, *J* = 9.2 Hz, 2H; H of Ar), 8.11 (d, *J* = 8.0 Hz, 2H; H of Ar), 7.92 (d, *J* = 8.0 Hz, 2H; H of Ar), 7.71 (apparent t, *J* = 8.0 Hz, 2H; H of Ar), 7.53 (d, *J* = 9.2 Hz, 2H; H of Ar), 7.43 (d, *J* = 8.0 Hz, 2H; H of Ar), 7.37 - 7.31 (m, 4H; H of Ar), 6.92 (s, 2H; H of Ar), 3.93 (s, 3H; H of OCH_3), 3.78 (s, 6H; H of OCH_3). ^{13}C NMR (101 MHz, CD_3CN): δ = 156.10, 154.97, 143.96, 140.91, 140.49, 135.64, 134.48, 133.60, 132.35, 130.93, 130.06, 129.80, 129.66, 128.87, 125.83, 125.65, 125.52, 118.77, 106.85, 61.32, 57.32 ppm. FTMS: m/z calcd for $[M\text{-}PF_6]^+$: 600.1169; found: 600.1159

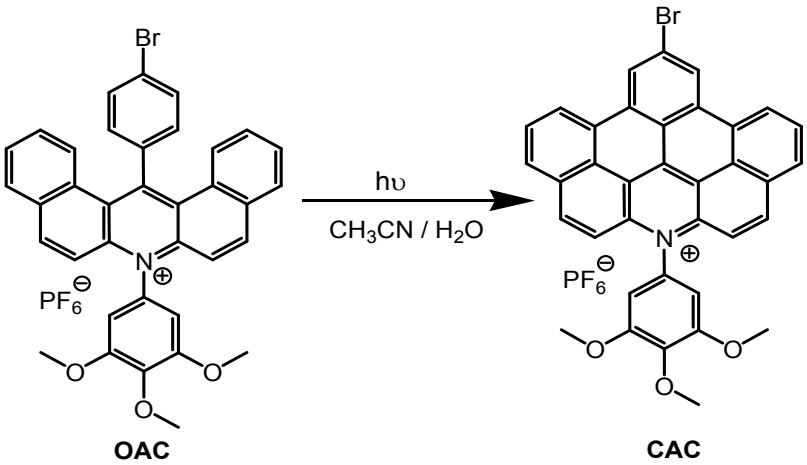

OAC **CAC**

Salt **OAC** (187 mg, 0.25 mmol) was dissolved in a mixture of acetonitrile and water (1:1, 80 mL). The solution was exposed to sunlight and the reaction was monitored by ^{1}H-NMR spectroscopy until all the starting material was consumed. During the process an orange solid precipitated out of the solution, and the colour of the solution changed from yellow to reddish orange. The solvents were removed under vacuum to afford an orange solid. Yield, 170 mg, 0.23 mmol, 91%.

^{1}H NMR (300 MHz, CD_3CN): δ = 9.24 (d, *J* = 8.1 Hz, 2H; H of Ar), 9.18 (s, 2H; H of Ar), 8.82 (d, *J* = 9.6 Hz, 2H; H of Ar), 8.69 (d, *J* = 8.1 Hz, 2H; H of Ar), 8.34 (apparent t, *J* = 7.8 Hz, 2H; H of Ar), 8.08 (d, *J* = 9.6 Hz, 2H; H of Ar), 7.14 (s, 2H; H of Ar), 4.04 (s, 3H; H of OCH_3), 3.90 (s, 6H; H of OCH_3) ppm. FT-MS: m/z calcd for $[M\text{-}PF_6]^+$: 596.0856; found: 596.0858.

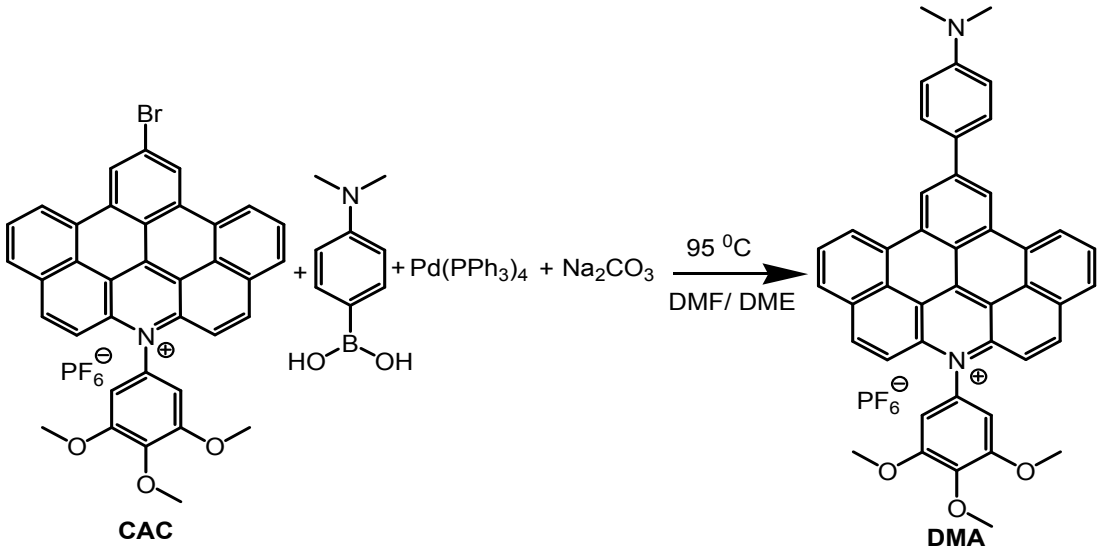

CAC (50 mg, 0.067 mmol), tetrakis-(triphenylphosphine) palladium(0), ($Pd(PPh_3)_4$) (8 mg, 1%), *N,N*-dimethylphenyl-boronic acid (24 mg, 00135 mmol), aqueous sodium carbonate (1M, 0.34 mL), 1,2-dimethoxyethane (DME) (5 mL) and dimethylformamide (DMF) (8 mL) were added to a two-necked round-bottomed flask. The mixture was bubbled with nitrogen for 15 minutes before heating and stirring for 24 hours at 95 ^{O}C. The solvents were removed under vacuum and the residue was dissolved in dichloromethane and washed with water. The combined organic layers were dried over magnesium sulphate, and the solvent was removed under vacuum to afford a dark brown solid. The crude product was purified by column chromatography (aluminium oxide, basic activated) eluting with DCM / petroleum ether = 1 / 1, DCM, DCM / acetone = 10 / 1 and gradually increasing the polarity to 7 / 1 to afford a dark purple solid. Yield, 16 mg, 0.02 mmol, 30%.

^{1}H NMR (400 MHz, CD_3CN): δ = 9.25 (d, *J* = 7.6 Hz, 2H; H of Ar), 9.05 (s, 2H; H of Ar), 8.65 (d, *J* = 9.6 Hz, 2H; H of Ar), 8.49 (d, *J* = 7.6 Hz, 2H; H of Ar), 8.19 (apparent t, *J* = 7.6 Hz, 2H; H of Ar), 7.92 (d, *J* = 9.6 Hz, 2H; H of Ar), 7.79 (d, *J* = 8.8 Hz, 2H; H of Ar), 7.05 (s, 2H; H of Ar), 6.86 (d, *J* = 8.8 Hz, 2H; H of Ar), 4.02 (s, 3H; H of OCH_3), 3.88 (s, 6H; H of OCH_3), 3.10 (s, 6H; H of NCH_3) ppm. ^{19}F NMR (CD_3CN, 367 MHz): δ (ppm) = -72.87 (d, $J_{P\text{-}F}$ = 686 Hz). ^{31}P NMR (CD_3CN, 162 MHz): δ (ppm) = -144.02 (sep, $J_{P\text{-}F}$ = 707 Hz). FT-MS: m/z calcd for $[M\text{-}PF_6]^+$: 637.2486; found: 637.2476.

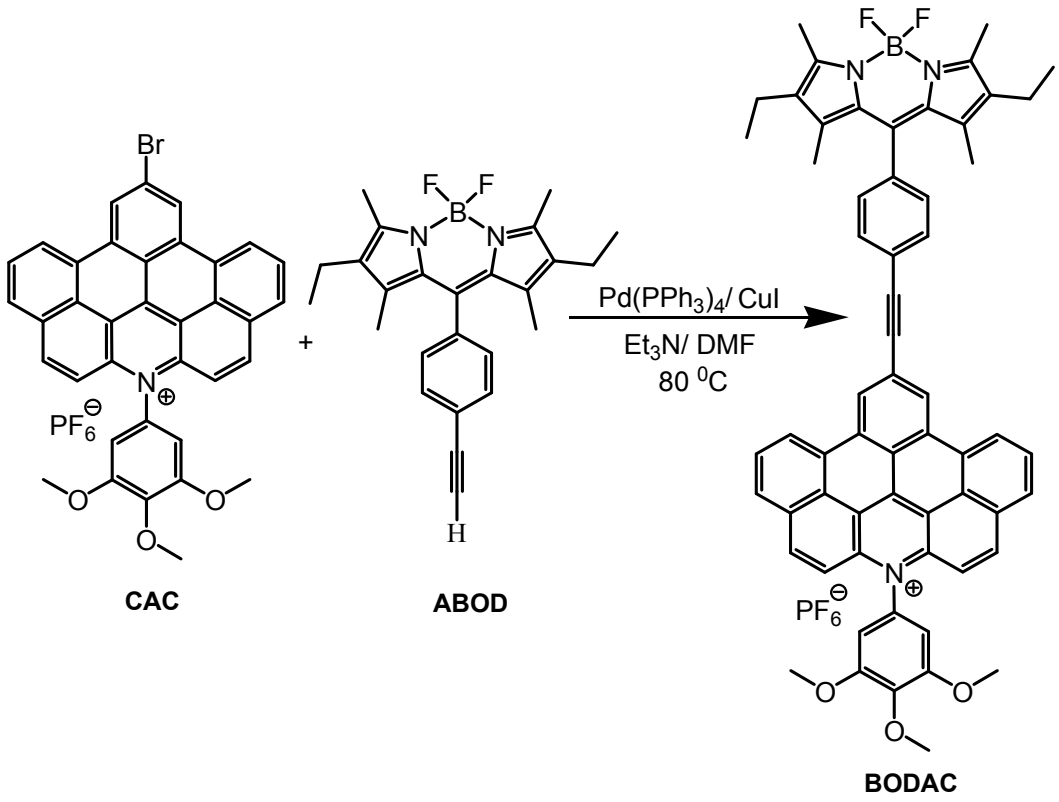

CAC **ABOD** **BODAC**

CAC (30 mg, 0.040 mmol) and bodipy **ABOD** (16.3 mg, 0.040 mmol) were dissolved in DMF (6 mL) followed by the addition of triethylamine (3 mL). The mixture was bubbled with nitrogen for 15 minutes before being heated to 80 ^{O}C. Then tetrakis-(triphenylphosphine) palladium(0), $Pd(PPh_3)_4$, (4 mg, 9%) and copper(I) iodide (0.7 mg, 9%) were added, and the resulting mixture was further heated and stirred under N_2 overnight (20 hours). Another portion of catalyst (i.e., $Pd(PPh_3)_4$ (4 mg, 9%) and copper(I) iodide (0.7 mg, 9%)) was added and the reaction was left for another 10 hours. After cooling to room temperature distilled water was added to the mixture to help the precipitation of the product. The solvent was removed and the residue was dissolved in dichloromethane, washed by water, dried over magnesium sulphate and the solvent was removed under vacuum to afford a dark red crude product. The crude product was purified by column chromatography (aluminium oxide, basic activated) eluting with DCM / petroleum ether = 1 / 1, DCM, DCM / acetone = 20 / 1, 10 / 1 and gradually increasing the ratio to 7 / 1. Yield, 8 mg, 0.0075 mmol, 19%.

^{1}H NMR (400 MHz, CD_3CN): δ = 8.92 (d, J = 8.0 Hz, 2H; H of Ar), 8.67 (d, J = 9.2 Hz,

2H; H of Ar), 8.63 (s, 2H; H of Ar), 8.50 (d, J = 8.0 Hz, 2H; H of Ar), 8.19 (apparent t, J = 8.0 Hz, 2H; H of Ar), 8.02 (d, J = 9.2 Hz, 2H; H of Ar), 7.80 (d, J = 8.0 Hz, 2H; H of Ar), 7.41 (d, J = 8.0 Hz, 2H; H of Ar), 7.17 (s, 2H; H of Ar), 4.03 (s, 3H; H of OCH_3), 3.95 (s, 6H; H of OCH_3), 2.27 (s, 6H; H of CH_3), 2.20 (q, J = 7.6 Hz, 4H; H of CH_2), 1.34 (s, 6H; H of CH_3), 0.93 (t, J = 7.6 Hz, 6H; H of CH_3) ppm. ^{11}B NMR (CD_3CN, 128 MHz): δ = -0.58 (t, J_{av} = 32 Hz) ppm. ^{19}F NMR (CD_3CN, 367 MHz): δ = -72.67 (d, $J_{P\text{-}F}$ = 690 Hz), -145.12 (q, $J_{F\text{-}B}$ = 32 Hz) ppm. ^{31}P NMR (CD_3CN, 162 MHz): δ = -144.04 (sep, $J_{P\text{-}F}$ = 707 Hz) ppm. MALDI: m/z calcd for $[M\text{-}PF_6]^+$: 919.4; found: 919.4.

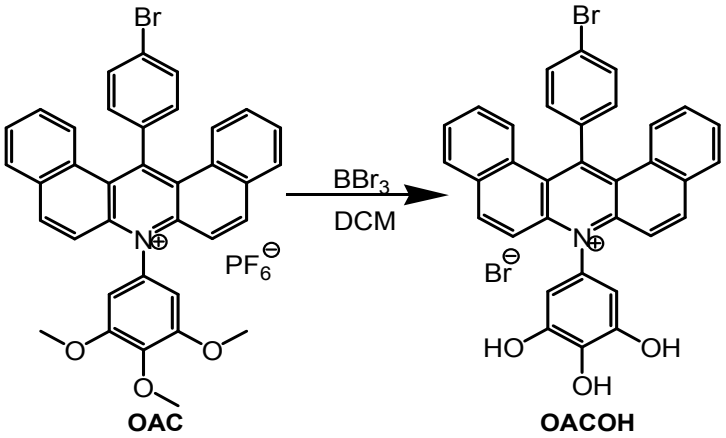

A solution of compound **OAC** (80 mg, 0.01 mmol) dissolved in freshly distilled DCM (3 mL) was cooled in an ice bath and boron tribromide (1M in DCM) was added dropwise. The ice bath was removed and the resulting solution was stirred overnight. Distilled water was added to quench the reaction. The organic phase was separated and the aqueous layer was extracted with dichloromethane. The combined organic layers were dried over magnesium sulphate, and the solvent was removed under vacuum. Recrystalisation from acetonitrile and diethyl ether afforded a yellow solid. Yield, 40 mg, 0.063 mmol, 63%.

^{1}H NMR (400 MHz, CD_3CN): δ = 8.35 (d, *J* = 9.2 Hz, 2H; H of Ar), 8.11 (d, *J* = 7.6 Hz, 2H; H of Ar), 7.92 (d, *J* = 8.4 Hz, 2H; H of Ar), 7.72 - 7.69 (m, 2H; H of Ar), 7.63 (d, *J* = 9.6 Hz, 2H; H of Ar), 7.43 (d, *J* = 8.4 Hz, 2H; H of Ar), 7.37 - 7.31 (m, 4H; H of Ar), 6.71 (s, 2H; H of Ar) ppm.

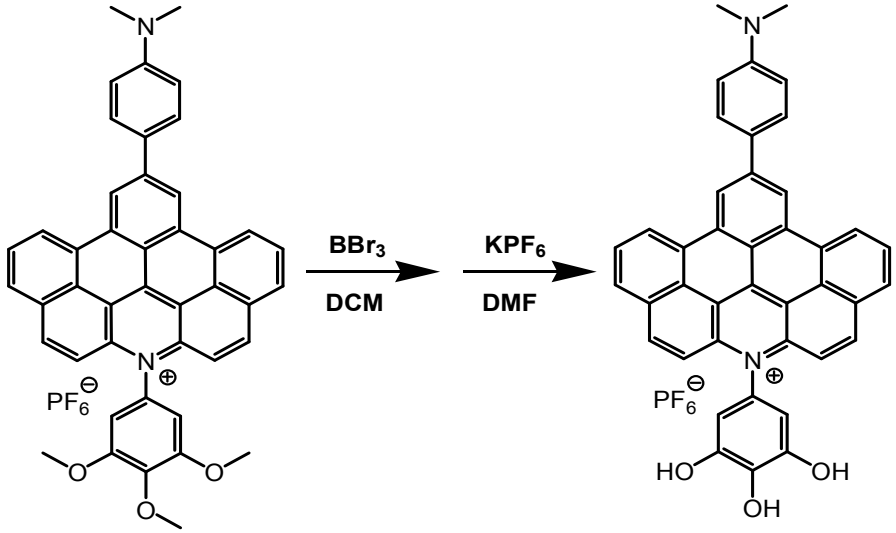

DMA **DMAOH**

A solution of compound **DMA** (8 mg, 0.01 mmol) dissolved in freshly distilled DCM (30 mL) was cooled to -78 ^{O}C before boron tribromide (0.77 mL, 1M in DCM) was added dropwise. The mixture was stirred under this temperature for 1.5 hours before warmed gradually to room temperature and stirred overnight. The reaction was quenched with distllled water. Upon the addition of water, the organic product precipitated out of the solution, which was filtrated off and dried. The dark red solid was dissolved in DMF and a saturated potassium hexafluorophosphate solution was added in a dropwise manner while stirring to obtain a dark red solid. The solvent was filtrated off to afford a dark red solid. Yield, 6 mg, 0.008 mmol, 80%.

^{1}H NMR (400 MHz, CD_3CN): δ = 8.71 (bs, 2H; H of Ar), 8.46 (d, *J* = 8.4 Hz, 2H; H of Ar), 7.94 - 7.90 (m, 2H; H of Ar), 7.80 (d, *J* = 8.4 Hz, 2H; H of Ar), 7.38 - 7.33 (m, 2H; H of Ar), 6.71 (bs, 4H; H of Ar), 3.13 (s, 6H; H of NCH_3) ppm. MALDI: m/z calcd for $[M\text{-}PF_6]^+$: 595.2; found: 595.2.

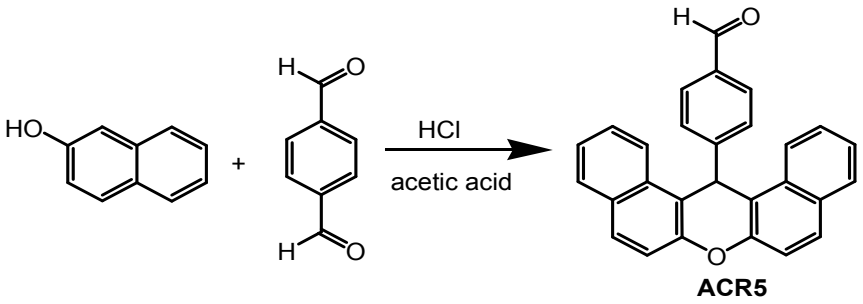

ACR5

2-Naphthol (2.07 g, 14.4 mmol) and terephthalaldehyde (804 mg, 6 mmol) were added to acetic acid (100 mL) following by the addition of concentrated (37%) hydrochloric acid (1.0 mL). The light yellow mixture was stirred and refluxed for 22 hours. After cooling to room temperature, the light pink solid was filtered, washed with diethyl ether and dried under vacuum. The product was used in the next step without further purification. Yield, 1.90 g, 4.92 mmol, 82%.

^{1}H NMR (400 MHz, $CDCl_3$): δ = 9.79 (s, 1H; H of CHO), 8.33 (d, *J* = 8.8 Hz, 2H; H of Ar), 7.83 (apparent t, *J* = 8.4 Hz, 4H; H of Ar), 7.69 (d, *J* = 8.4 Hz, 4H; H of Ar), 7.57 - 7.61 (m, 2H; H of Ar), 7.51 (d, *J* = 8.8 Hz, 2H; H of Ar), 7.41 - 7.45 (m, 2H; H of Ar), 6.58 (s, 1H; H of CH); ^{13}C NMR (101 MHz, $CDCl_3$): δ = 191.67, 148.90, 131.37, 131.19, 130.21, 129.50, 129.10, 129.03, 127.18, 124.60, 122.41, 119.45, 118.19, 116.35, 108.63, 38.38 ppm. EI-MS: m/z calcd for $[M]^+$: 386.1; found: 386.1. IR $\upsilon_{(max)}$ (film) cm^{-1}: 1685.7(υ C=O).

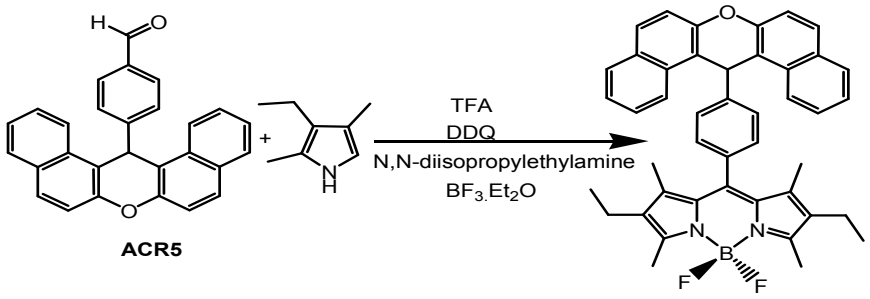

Aldehyde **ACR5** (773 mg, 2.00 mmol) was dissolved in dichloromethane (250 mL), followed by the addition of 2,4-dimethyl-3-ethylpyrrole (0.56 mL, 4 mmol) and 5 drops (plus 6 drops later on) of trifluoroacetic acid. The mixture was stirred at room temperature and the reaction was monitored by TLC until all of the aldehyde was consumed. After 2 days, dichlorodicyanobenzo quinone (463 mg, 2 mmol) was added. The mixture was stirred overnight, then *N,N*-diisopropylethylamine (4 mL, 22.8 mmol) and borontrifluoride diethyl etherate ($BF_3.Et_2O$) were added to the mixture which was stirred for a further 2 days at room temperature. Some black insoluble solid was filtered off to afford a dark brown solution. The solution was washed with brine and the combined organic layers were dried over magnesium sulphate and the solvent was removed under vacuum. The crude product was purified by column chromatography using dichloromethane / petroleum ether = 1 / 1 as eluent to afford a reddish orange product. Yield, 303 mg, 0.46 mmol, 23%.

^{1}H NMR (400 MHz, $CDCl_3$): δ = 8.37 (d, *J* = 8.8 Hz, 2H; H of Ar), 7.85 (d, *J* = 8.4 Hz, 2H; H of Ar), 7.83 (d, *J* = 8.8 Hz, 2H; H of Ar), 7.62 (d, *J* = 8.4 Hz, 2H; H of Ar), 7.58 (apparent td, *J* = 0.8, *J* = 8.4 Hz, 2H; H of Ar), 7.49 (d, *J* = 8.8 Hz, 2H; H of Ar), 7.43 (apparent td, *J* = 0.8, *J* = 8.8 Hz, 2H; H of Ar), 7.05 (d, *J* = 8.4 Hz, 2H; H of Ar), 6.55 (s, 1H; H of CH), 2.46 (s, 6H; H of CH_3), 2.16 (q, *J* = 7.6 Hz, 4H; H of CH_2), 0.86 (t, *J* = 7.6 Hz, 6H; H of CH_3), 0.83 (s, 6H; H of CH_3). ^{13}C NMR (101 MHz, $CDCl_3$): δ = 153.58, 148.67, 146.08, 139.90, 138.53, 133.78, 132.69, 131.47, 131.15, 130.76, 129.26, 128.91, 128.29, 126.77, 124.39, 122.80, 118.12, 116.72, 53.57, 38.33, 17.06, 14.67, 12.55, 11.38 ppm. ^{11}B NMR (128 MHz, $CDCl_3$): δ = 0.26 (t, J_{av} = 33.28 Hz) ppm. ^{19}F NMR (376 MHz, $CDCl_3$) δ = -145.69 (q, $J_{B\text{-}F}$ = 32.40 Hz) ppm. FT-MS: m/z calcd for $[M + H]^+$: 660.3233; found: 660.3232.

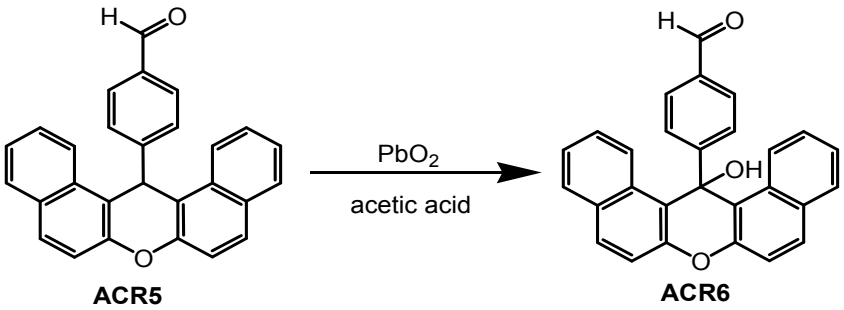

ACR5 **ACR6**

14-(4-benzaldehyde)-14*H*-dibenzo[*a,j*]xanthene (**ACR5**) (1.00 g, 2.59 mmol) and lead dioxide (0.93 g, 7.77 mmol, 50% excess) were added to acetic acid (130 mL). The mixture was stirred and heated to reflux for 4.5 hours. The solution was filtered to remove an insoluble solid. The brown solution was poured into distilled water (500 mL) to afford a light pink solid. The solid was collected and dissolved in ethyl acetate. The ethyl acetate was washed 3 times with water, dried over magnesium sulphate and the solvent was removed under vacuum. The crude product was purified by column chromatography (silica gel) eluting with petroleum ether / diethyl ether = 5 / 2 to afford a white solid. Yield, 728 mg, 1.81 mmol, 70%.

^{1}H NMR (400 MHz, $CDCl_3$): δ = 9.81 (s, 1H; H of CHO), 8.85 (d, *J* = 8.4 Hz, 2H; H of Ar), 7.92 (d, *J* = 8.0 Hz, 2H; H of Ar), 7.82 (d, *J* = 9.2 Hz, 2H; H of Ar), 7.73 (d, *J* = 8.0 Hz, 2H; H of Ar), 7.68 (d, *J* = 8.4 Hz, 2H; H of Ar), 7.42 - 7.38 (m, 4H; H of Ar), 7.33 - 7.29 (m, 2H; H of Ar), 3.33 (s, 1H; H of OH); ^{13}C NMR (101 MHz, $CDCl_3$): δ = 191.85, 153.79, 146.42, 134.35, 131.87, 131.50, 130.96, 129.00, 128.95, 127.77, 126.65, 124.43, 117.69, 117.63, 73.92 ppm. EI-MS: m/z calcd for $[M]^+$: 402.1; found: 402.1. IR $\upsilon_{(max)}$ (film) cm^{-1}: 3554 (υ O-H), 1701 (υ C=O); 1597, 1509, 1458 (υ C=C of Ar).

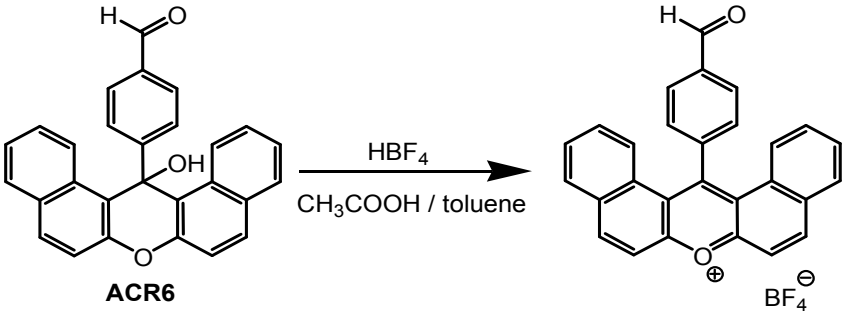

ACR6

A solution of compound **ACR6** (980 mg, 2.44 mmol) dissolved in a mixture of acetic acid (35 mL) and toluene (20 mL) was cooled to 0 ^{O}C, before the slow addition of tetrafluoroboric acid solution (48% wt., 2.0 mL) in a dropwise manner. A red solid appeared immediately upon the addition of the tetrafluoroboric acid. The reaction was protected from light and stirred in an ice-water bath for 1.5 hours. The red solid was filtered off, washed with dry diethyl ether and recrystallised from acetonitrile and diethyl ether. Yield, 865 mg, 1.83 mmol, 75%.

^{1}H NMR (400 MHz, CD_3CN): δ = 10.33 (s, 1H; H of CHO), 8.92 (d, J = 8.8 Hz, 2H; H of Ar), 8.35 (d, J = 8.4 Hz, 4H; H of Ar), 8.30 (d, J = 8.8 Hz, 2H; H of Ar), 7.83 (apparent t, J = 8.4 Hz, 2H; H of Ar), 7.80 (d, J = 8.4 Hz, 2H; H of Ar), 7.49 (apparent t, J = 8.4 Hz, 2H; H of Ar), 7.19 (d, J = 8.4 Hz, 2H; H of Ar) ppm.

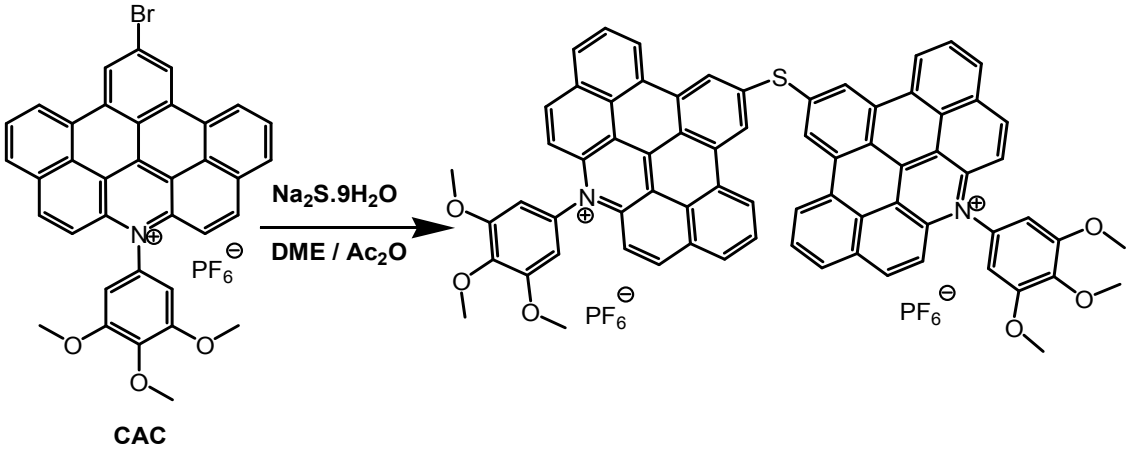

CAC

Sodium sulfide nonahydrate ($Na_2S.9H_2O$) (18 mg, 0.072mmol) was dissolved in 1,2-dimethoxyethane (DME) (5 mL) and was stirred at 80 ^{O}C for 1 hour before compound **CAC** (30 mg, 0.04 mmol) was added. Upon the addition of **CAC**, the colour of the solution changed from green to black. The mixture was stirred for another 30 minutes under nitrogen. The resulting mixture was cooled in an ice bath followed by the addition of acetic anhydride (0.02 mL). After 1 hour the mixture was diluted with dichloromethane and water. The organic layer was separated and washed with water 3 times. The combined organic layers were dried over magnesium sulphate and the solvent was removed under vacuum. There was still some high boiling point solvent left, so saturated aqueous potassium hexafluorophosphate solution was added to help the precipitation of a dark orange solid. The crude product was purified by vapour diffusion of diethyl ether into a solution of the crude solid in acetonitrile. Yield, 6 mg, 0.0044 mmol, 22%.

^{1}H NMR (400 MHz, CD_3CN): δ = 9.54 (s, 4H; H of Ar), 9.32 (d, J = 7.6 Hz, 4H; H of Ar), 8.82 (d, J = 9.2 Hz, 4H; H of Ar), 8.63 (d, J = 7.6 Hz, 4H; H of Ar), 8.20 (apparent t, J = 7.6 Hz, 4H; H of Ar), 8.08 (apparent d, J = 9.2 Hz, 4H; H of Ar), 7.13 (s, 4H; H of Ar), 4.03 (s, 6H; H of OCH_3), 3.88 (s, 12H; H of OCH_3) ppm. FTMS + p NSI: m/z calcd for $[M\text{-}2PF_6]^{2+}$: 533.1533; found: 533.1524. (No mono charged ion was found in the spectrum).

2.4.2 Compounds discussed in chapter 4

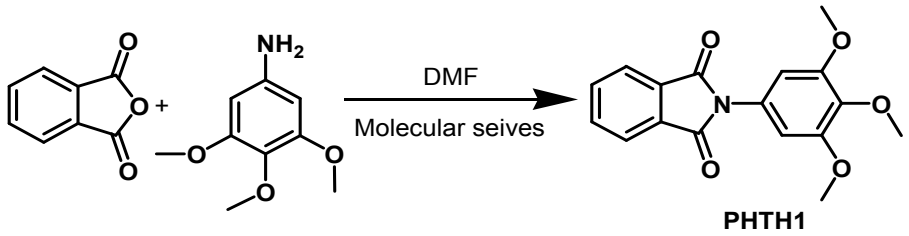

A round-bottomed flask was charged with phthalic anhydride (750 mg, 5.01 mmol), 3,4,5-trimethoxyaniline (916 mg, 5.00 mmol), 10mL of DMF (10 mL) and molecular sieves (1.00 g). The mixture (olive green) was stirred at 120 ^{O}C for 5h. The mixture was cooled to room temperature (a solid precipitated during the cooling process) and dichloromethane was added to dissolve the solid. The molecular sieves were filtered off to afford a green solution. The product precipitated out again after removing of the dichloromethane. The remaining DMF was filtered to afford a white solid, which was washed with small amount of diethyl ether before drying under vacuum. The crude product was purified by recrystalisation from chloroform and diethyl ether using solvent vapour diffusion method to afford white crystals. Yield, 950 mg, 3.03 mmol, 61%.

^{1}H NMR (400 MHz, $CDCl_3$): δ = 7.93 - 7.99 (m, 2H; H of Ar), 7.77 - 7.84 (m, 2H; H of Ar), 6.64 (s, 2H; H of Ar), 1.57 (s, 9H; H of OCH_3). ^{13}C NMR (101 MHz, $CDCl_3$): δ = 167.76, 153.80, 138.21, 134.83, 132.02, 124.11, 104.73, 61.24, 56.56 ppm. EI-MS: m/z calcd. for $[M]^+$: 313.1; found: 313.1. Elemental analysis calcd (%) for $C_{17}H_{15}NO_5$: C 65.17, H 4.83, N 4.47; found: C 65.07, H 4.90, N 4.52. IR $\upsilon_{(max)}$ (film) cm^{-1}: 3060 (υ Ar-H), 2833 - 3006 cm^{-1} (υ C-H of methyl group), 1707 (υ C=O), 1596, 1504, 1458 (υ C=C of Ar). Melting point: 227 - 228 ^{O}C.

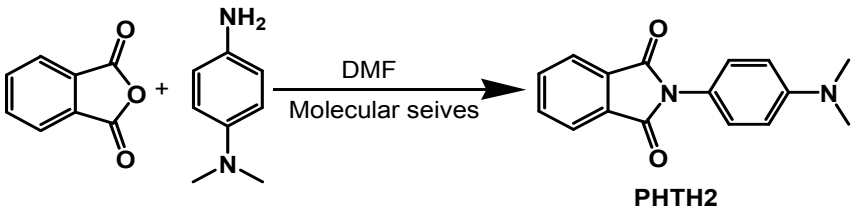

A round-bottomed flask was charged with phthalic anhydride (748 mg, 5.00 mmol), *N,N*-dimethyl-*p*-phenylenediamine (702 mg, 5.00 mmol), DMF (10 mL) and molecular sieves (1.00 g). The mixture (dark green) was stirred at 130 ^{O}C for 5h. Then the mixture was cooled to RT and during the cooling process some green solid precipitated and dichloromethane was added to dissolve the green solid. The molecular sieves were filtered off to leave a green solution. The product precipitated out again after removing all of the dichloromethane. The rest of DMF was filtered to afford a yellowish green solid, which was washed with a small amount of diethyl ether before drying under vacuum. The crude product was purified by recrystalisation from chloroform and diethyl ether using solvent vapour diffusion method to afford yellowish green crystals. Yield, 1.11 g, 4.17 mmol, 83%.

^{1}H NMR (400 MHz, $CDCl_3$): δ = 7.96 - 7.91 (m, 2H; H of Ar), 7.79 - 7.74 (m, 2H; H of Ar), 7.26 - 7.22 (m, 2H; H of Ar), 6.82 - 6.78 (m, 2H; H of Ar), 3.00 (s, 6H; H of NCH_3). ^{13}C NMR (101 MHz, $CDCl_3$): δ = 168.30, 150.62, 134.46, 132.34, 127.87, 123.88, 120.29, 112.85, 40.89 ppm. EI-MS: m/z calcd for $[M]^+$: 266.1; found: 266.0. Elemental analysis calcd (%) for $C_{16}H_{14}N_2O_2$: C 72.37, H 5.50, N 10.51; found: C 72.01, H 5.58, N 10.54. IR $\upsilon_{(max)}$ (film) cm^{-1}: 1697 (υ C=O), 1617, 1527 (υ C=C of aromatic ring). Melting point: 265 - 266 ^{O}C.

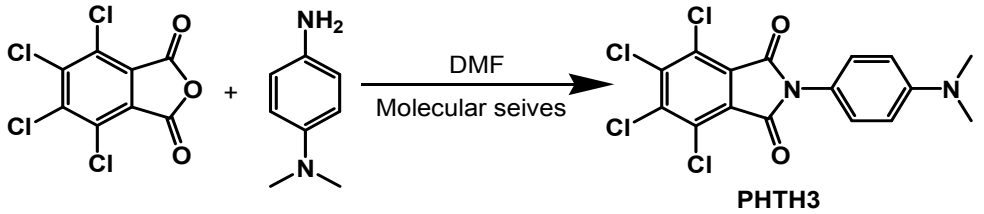

PHTH3

A round-bottomed flask was charged with tetrachlorophthalic anhydride (1.19g, 4.00 mmol), *N,N*-dimethyl-*p*-phenylenediamine (562 mg, 4.00 mmol), DMF (10 mL) and molecular sieves (1.02 g). The mixture (dark brown) was stirred at 130 ^{O}C for 4h. Then the mixture was cooled to RT and during the cooling process some gold yellow solid precipitated and dichloromethane was added to dissolve the solid. The molecular sieves were filtered off to afford a dark brown solution. The product precipitated out again after removing all of the dichloromethane. The rest of the DMF was filtered to afford a orange solid, which was washed with a small amount of diethyl ether before drying under vacuum. The crude product was purified by recrystallisation from chloroform and diethyl ether using solvent vapour diffusion method to afford an orange solid. Yield, 1.10 g, 2.72 mmol, 68%.

^{1}H NMR (400 MHz, $CDCl_3$): δ = 7.23 - 7.19 (m, 2H; H of Ar), 6.80 - 6.76 (m, 2H; H of Ar), 3.01 (s, 6H; H of CH_3). ^{13}C NMR (101 MHz, $CDCl_3$): δ = 163.50, 150.82, 140.52, 130.20, 127.83, 127.70, 119.35, 112.62, 40.78 ppm. FTMS + p NSI: m/z calcd for $[M + H]^+$: 404.9540; found: 404.9539. Elemental analysis calcd (%) for $C_{17}H_{15}NO_2$: C 47.56, H 2.49, N 6.39; found: C 47.50, H 2.58, N 8.02. IR $\upsilon_{(max)}$ (film) cm^{-1}: 1710 (υ C=O), 1616, 1522 cm^{-1} (υ C=C of Ar). Melting point: 257 - 258 ^{O}C.

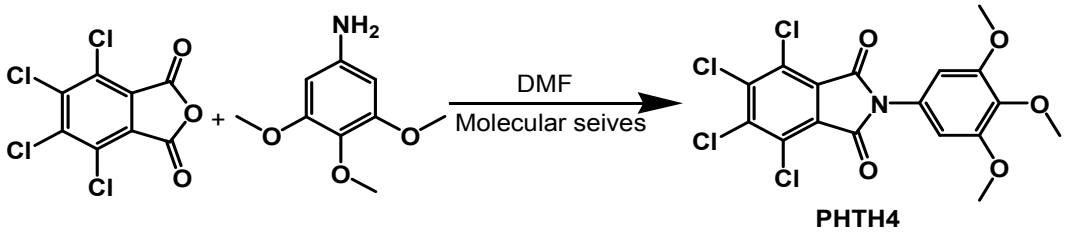

PHTH4

A round-bottomed flask was charged with tetrachlorophthalic anhydride (1.19 g, 4.00 mmol), 3,4,4-trimethoxyaniline (756 mg, 4.00 mmol), DMF (10 mL) and molecular sieves (1.00 g). The mixture (yellow solution) was stirred at 130 ^{O}C for 5.5 hours under nitrogen. Then the mixture was cooled to room temperature and during the cooling process some beige solid precipitated and dichloromethane was added to dissolve the biege solid. The molecular sieves were filtered off to afford a beige solution. The product precipitated out again after removing all of the dichloromethane. The rest of DMF was filtered to afford a biege solid, which was washed with a small amount of diethyl ether before drying under vacuum. Yield, 1.09 g, 2.42 mmol, 60%.

^{1}H NMR (400 MHz, $CDCl_3$): δ = 6.62 (s, 2H; H of Ar), 3.90 (s, 3H; H of CH_3), 3.87 (s, 6H; H of CH_3) ppm. IR $\upsilon_{(max)}$ (film) cm^{-1}: 1704 (υ C=O), 1596.0, 1505 (υ C=C of Ar). Melting point: 333 - 334 ^{O}C.

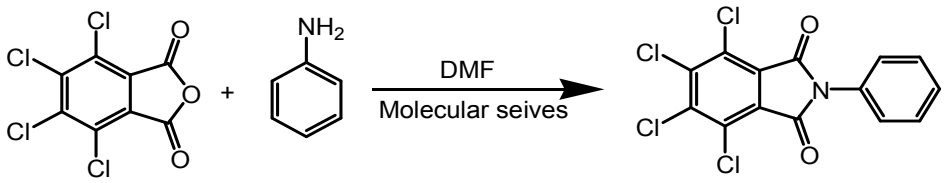

PHTH5

A round-bottomed flask was charged with tetrachlorophthalic anhydride (893 mg, 3.00 mmol), aniline (0.28 mL, 3.04 mmol), DMF (10 mL) and molecular sieves (1.02 g). The mixture (dark brown) was stirred at 135 ^{O}C for 4 hours. Then the mixture was cooled to room temperature and during the cooling process some yellow solid precipitated and dichloromethane was added to dissolve the solid. The molecular sieves were filtered off to afford a brown solution. The product precipitated out again after removing of the dichloromethane. The rest of the DMF was filtered to afford a yellow solid, which was washed with small amount of diethyl ether before drying under vacuum. The crude product was purified by recrystallisation from chloroform and diethyl ether using solvent vapour diffusion method to afford a yellow solid. Yield, 480 mg, 1.33 mmol, 44%.

^{1}H NMR (400 MHz, $CDCl_3$): δ = 7.39 - 7.55 (m, 5H; H of Ar). ^{13}C NMR (101 MHz, $CDCl_3$): δ = 162.90, 140.88, 131.12, 130.51, 129.60, 129.11, 127.59, 126.86 ppm. FTMS + p APCI: m/z calcd for $[M + H]^+$: 361.9118; found: 361.9116. IR $\upsilon_{(max)}$ (film) cm^{-1}: 1709 (υ C=O), 1599, 1500 (υ C=C of Ar).

PHTH6

A round-bottomed flask charged with phthalic anhydride (748 mg, 5.00 mmol), 2,4,6-trimethylaniline (0.72 mL, 5.00 mmol), DMF (10 mL) and molecular sieves (1.00 g). The mixture (dark green) was stirred at 130 ^{O}C for 6h. Then the mixture was cooled to room temperature and during the cooling process some white solid precipitated and DCM was added to dissolve the white solid. The molecular sieves were filtered off to afford a beige solution. The product precipitated out again after removal of the DCM. The rest of the DMF was filtered to afford a white solid, which was washed with small amount of diethyl ether before drying under vacuum. The recrystallisation was carried out by dissolving the crude product in ethanol and the solution was left at room temperature. During the slow evaporation process colourless transparent crystals were obtained. Yield, 1.16 g, 4.37 mmol, 87%.

^{1}H NMR (400 MHz, $CDCl_3$): δ = 7.96 - 7.94 (m, 2H), 7.82 - 7.78 (m, 2H), 7.00 (s, 2H; H of Ar), 2.33 (s, 3H; H of CH_3), 2.12 (s, 6H; H of CH_3). ^{13}C NMR (101 MHz, $CDCl_3$): δ = 167.76, 139.73, 136.80, 134.61, 132.39, 129.64, 127.38, 124.08, 21.49, 18.32 ppm. FTMS + p NSI: m/z calcd for $[M + H]^+$: 266.1176; found: 266.1177. Elemental analysis calcd (%) for $C_{17}H_{15}NO_2$: C 76.96, H 5.70, N 5.28; found: C 76.91, H 5.64, N 5.36. IR $\upsilon_{(max)}$ (film) cm^{-1}: 1697 (υ C=O), 1617, 1527 (υ C=C of Ar). Melting point: 181 - 183 ^{O}C.

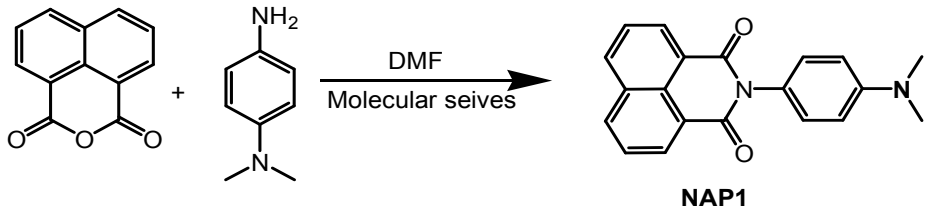

NAP1

A round-bottomed flask was charged with 1,8-naphthalic anhydride (793 mg, 4.00 mmol), *N,N*-dimethyl-*p*-phenylenediamine (562 mg, 4.00 mmol), DMF (10 mL) and molecular sieves (1.00 g). The mixture (dark brown) was stirred at 130 ^{O}C for 4 hours. Then the mixture was cooled to room temperature and during the cooling process some yellowish green solid precipitated and DCM was added to dissolve the solid. The molecular sieves were filtered off to afford a dark brown solution. The product precipitated out again after removing theDCM. The rest of the DMF was filtered to afford a green solid, which was washed with small amount of diethyl ether before drying under vacuum. The crude product was purified by recrystallisation from chloroform and diethyl ether using solvent vapour diffusion method to afford orange crystals. When the solvent pair was changed to DCM and diethyl ether green crystals were obtained. Yield, 1.00 g, 3.16 mmol, 79%.

^{1}H NMR (400 MHz, $CDCl_3$): δ = 8.65 (d, J = 8.0 Hz, 2H; H of Naphth), 8.25 (d, J = 8.0 Hz, 2H; H of Naphth), 7.78 (apparent t, J = 8.0 Hz, 2H; H of Naphth), 7.16 (d, J = 9.2 Hz, 2H; H of Ar), 6.85 (d, J = 9.2 Hz, 2H; H of Ar), 3.02 (s, 6H; H of NCH_3). ^{13}C NMR (101 MHz, $CDCl_3$): δ = 165.11, 150.80, 134.33, 132.05, 131.85, 129.15, 128.85, 127.29, 124.14, 123.43, 113.19, 40.93 ppm. FTMS + p NSI: m/z calcd for $[M + H]^+$: 317.1285; found: 317.1288. Elemental analysis calcd (%) for $C_{20}H_{16}N_2O_2$: C 75.93, H 5.10, N 8.85; found: C 75.10, H 5.12, N 8.83. IR $\upsilon_{(max)}$ (film) cm^{-1}: 1699, 1661 cm^{-1} (υ C=O), 1608, 1584, 1522 cm^{-1} (υ C=C of aromatic ring). Melting points: orange crystals decomposed at 320 ^{O}C; 331 - 332 ^{O}C (green crystals).

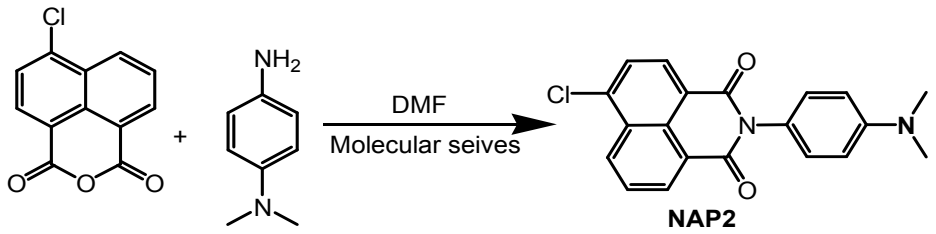

NAP2

A round-bottomed flask was charged with 4-chloro-1,8-naphthalic anhydride (980 mg, 4.00 mmol), *N,N*-dimethyl-*p*-phenylenediamine (562 mg, 4.00 mmol), DMF (10 mL) and molecular sieves (1.00 g). The mixture (dark brown) was stirred at 130 ^{O}C for 4 hours. Then the mixture was cooled to room temperature and during the cooling process some dark brown solid precipitated and DCM was added to dissolve the solid. The molecular sieves were filtered off to afford a dark brown solution. The product precipitated out again after removing of the DCM. The rest of DMF was filtered to afford a white solid, which was washed with a small amount of diethyl ether before drying under vacuum. The crude product was purified by recrystallisation from DCM and diethyl ether using a solvent vapour diffusion method to afford a dark brown solid. Yield, 1.20 g, 3.42 mmol, 86%.

^{1}H NMR (400 MHz, $CDCl_3$): δ = 8.71 (d, *J* = 8.0 Hz, 1H; H of Naphth), 8.65 (d, *J* = 8.0 Hz, 1H; H of Naphth), 8.55 (d, *J* = 8.0 Hz, 1H; H of Naphth), 7.89 (d, *J* = 8.0Hz, 1H; H of Naphth), 7.86 (apparent t, *J* = 8.0 Hz, 1H; H of Naphth), 7.15 (d, *J* = 8.8 Hz, 2H; H of Ar), 6.85 (d, *J* = 8.8 Hz, 2H; H of Ar), 3.02 (s, 6H; H of NCH_3) ppm. FTMS + p NSI: m/z calcd for $[M + H]^+$: 351.0895; found: 351.0899. Elemental analysis calcd (%) for $C_{20}H_{15}N_2O_2Cl$: C 68.48, H 4.31, N 7.98; found: C 66.63, H 4.22, N 7.96. IR $\upsilon_{(max)}$ (film) cm^{-1}: 1705, 1668 (υ C=O), 1609, 1588, 1523 (υ C=C of Ar). Melting point: 296 - 297 ^{O}C.

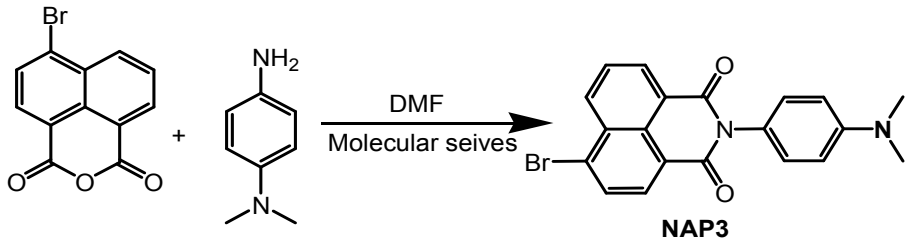

NAP3

A round-bottomed flask was charged with 4-bromo-1,8-naphthalic anhydride (1.17 g, 4.00 mmol), *N,N*-dimethyl-*p*-phenylenediamine (562 mg, 4.00 mmol), DMF (10 mL) and molecular sieves (1.00 g). The mixture (dark brown) was stirred at 130 ^{O}C for 4 hours. Then the mixture was cooled to room temperature and during the cooling process some dark brown solid precipitated and DCM was added to dissolve the solid. The molecular sieves were filtered off to afford a dark brown solution. The product precipitated out again after removing of the DCM. The rest of DMF was filtered to afford a brown solid, which was washed with a small amount of diethyl ether before drying under vacuum. The crude product was purified by recrystallisation from DCM and diethyl ether using a solvent vapour diffusion method to afford a red solid. Yield, 1.20 g, 3.42 mmol, 86%.

^{1}H NMR (400 MHz, $CDCl_3$): δ = 8.70 (dd, *J* = 0.8, 7.2 Hz, 1H; H of Naphth), 8.62 (dd, *J* = 1.2, 8.4 Hz, 1H; H of Naphth), 8.46 (d, *J* = 7.6 Hz, 1H; H of Naphth), 8.07 (d, *J* = 7.6 Hz, 1H; H of Naphth), 7.87 (dd, *J* = 7.2, 8.4 Hz, 1H; H of Naphth), 7.15 (m, 2H; H of Naphth), 6.86 (d, *J* = 8.8 Hz, 2H; H of Naphth), 3.02 (s, 6H; H of NCH_3). ^{13}C NMR (101 MHz, $CDCl_3$): δ = 164.34, 150.59, 134.58, 133.53, 132.51, 131.67, 131.27, 130.88, 130.52, 129.48, 128.88, 128.26, 123.61, 122.75, 112.99, 40.75 ppm.

2.4.3 Compounds discussed in chapter 5

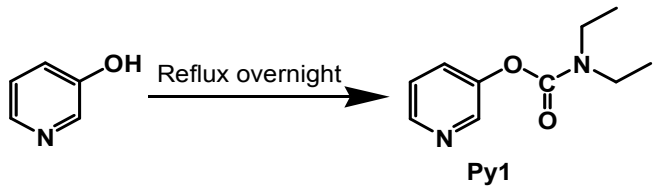

Py1

Pyridin-3-yl ethyl carbamate (Py1)

3-Hydroxypyridine (10 g, 0.105 mol) was dissolved in THF (200 mL) containing triethylamine (60 mL). Then, diethylcarbamyl chloride (20 mL, 0.16 mol) was added in a dropwise manner to the refluxing solution. Some white precipitation appeared during the addition process and the solution turned brown. The solution was refluxed overnight. After cooling to room temperature the white solid was filtered off which left a brown solution. The THF and triethylamine were removed under vacuum to afford a brown oil. The brown oil was diluted in ethyl acetate and washed with water, then dried over magnesium sulphate. The crude product (brown oil) obtained after removal of the solvent was purified by column chromatography (silica gel), eluting with acetone / petroleum ether = 1 / 2, to afford a light yellow oil. Yield, 19.48 g, 0.10 mmol, 95%.

^{1}H NMR (400 MHz, $CDCl_3$): δ = 8.30 (dd, 1H, *J* = 2.8 Hz; H of Py), 8.27 (dd, 1H, *J* = 1.2, 4.8 Hz; H of Py), 7.37 (ddd, 1H, *J* = 1.2, 2.8, 8.4 Hz; H of Py), 7.14 (dd, 1H, *J* = 4.8, 8.4 Hz; H of Py), 3.26 (q, 2H, *J* = 6.8 Hz; H of CH_2), 3.23 (q, 2H, *J* = 6.8 Hz; H of CH_2), 1.09 (t, 3H, *J* = 6.8 H; of CH_3), 1.04 (t, 3H, *J* = 6.8 Hz; H of CH_3). ^{13}C NMR (101 MHz, $CDCl_3$): δ = 153.33, 148.13, 146.00, 143.52, 129.27, 123.60, 42.34, 41.94, 14.13, 13.19 ppm.

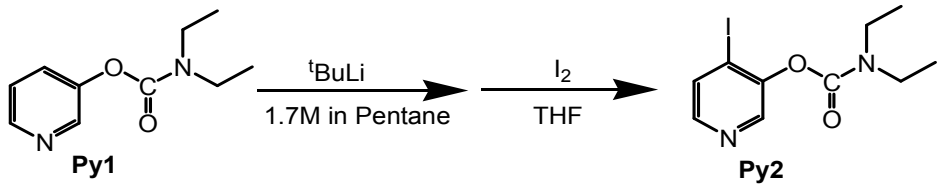

4-Iodopyridin-3-yl diethyl carbamate from pyridin-3-yl ethyl carbamate (Py2)

To a solution of **Py1** (4.5 g, 0.023 mol) in THF (95 mL) was added TMEDA (5 mL). The mixture was cooled to -78 ^{O}C before *tert*-butyllithium solution (1.7 M in pentane, 18 mL, 0.031 mol) was added dropwise over 0.5 hour through a syringe pump. The mixture (orange solution) was stirred at -78 ^{O}C for 1 hour. Then I_2 (8.42 g, 0.033 mol) in THF (30 mL) was added dropwise over 0.5 hour. The mixture (brown solution) was stirred for another 1 hour at -78 ^{O}C. The cool bath was removed to let the reaction flask warm to room temperature and the mixture was stirred overnight. The mixture was diluted with ethyl acetate, washed with sodium metabisulfite, brine and dried over magnesium sulphate. The crude product (brown oil) was purified by column chromatography (silica gel), eluting with acetone / petroleum ether = 1 / 1, to afford a dark brown oil. Yield, 3.88g, 0.012 mmol, 52%.

^{1}H NMR (400 MHz, $CDCl_3$): δ = 8.33 (d, 1H, *J* = 0.8 Hz; H of Py), 8.00 (dd, 1H, *J* = 0.8, 5.2 Hz; H of Py), 7.72 (dd, 1H, *J* = 0.8, 5.2 Hz; H of Py), 3.48 (q, 2H, *J* = 7.2 Hz; H of CH_2), 3.36 (q, 2H, *J* = 7.2 Hz; H of CH_2), 1.29 (t, 3H, *J* = 7.2 Hz; H of CH_3), 1.19 (t, 3H, *J* = 7.2 Hz; H of CH_3). ^{13}C NMR (101 MHz, $CDCl_3$): δ = 152.61, 149.91, 146.74, 144.62, 134.11, 102.43, 42.91, 42.41, 14.74, 13.47 ppm.

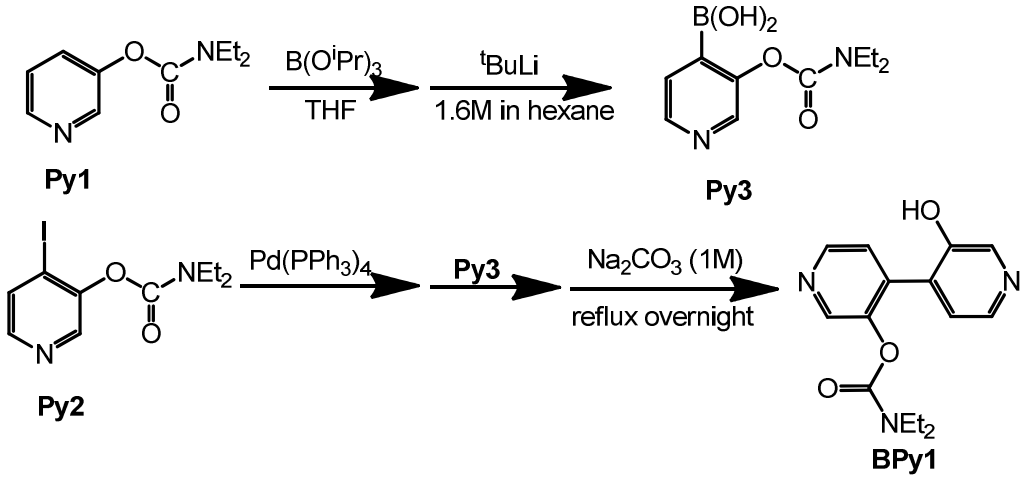

To a two-neck round bottom flask triisopropyl borate (8 mL, 0.035 mol) and a solution of **Py1** (5.0 g, 0.026 mol) in THF (80 mL) were added. The mixture was cooled to -78 ^{O}C and a butyllithium solution (1.6 M in hexane, 22 mL, 0.035 mol) was added dropwise through a syringe over 1h. The mixture was stirred at -78 ^{O}C for 1 hour. The cool bath was removed to allow the flask to warm to room temperature and the mixture was stirred for another 1 hour. Deoxygenated ethanol (30 mL) was added to the solution. The mixture was transferred to a pre-mixed solution of **Py2** (3.0 g, 0.009 mol) and tetrakis-(triphenylphosphine) palladium(0), $Pd(PPh_3)_4$, (700 mg, 0.6 mmol) in DME followed by the addition of deoxygenated ethanol (60 mL) and a sodium carbonate solution (1 M, 35 mL). The mixture was refluxed overnight. Water (150 mL) and ethyl acetate (250 mL) were poured into the solution, which was then filtered to remove insoluble material. The isolated organic layer was washed with sodium carbonate solution (0.2 M). The aqueous layers were extracted with ethyl acetate. The combined organic layers were neutralized with hydrochloric acid (2 M), then dried over magnesium sulphate and filtered. After removal of the organic solvent a yellow oily solid was obtained. Yield, 1.0 g, 3.48 mmol, 39%.

^{1}H NMR (400 MHz, $CDCl_3$): δ = 8.54 (s, 1H; H of Py), 8.50 (d, 1H, *J* = 5.2 Hz; H of Py), 8.37 (s, 1H; H of Py), 8.16 (d, 1H, *J* = 4.8 Hz; H of Py), 7.35 (d, 1H, *J* = 4.8 Hz; H of Py), 7.16 (d, 1H, *J* = 5.2 Hz; H of Py), 3.28 - 3.21 (m, 4H; H of CH_2), 1.05 - 1.00 (m, 6H; H of CH_3). ^{13}C NMR (101 MHz, $CDCl_3$): δ = 153.84, 151.58, 146.68, 145.97, 145.36, 140.47, 139.36, 137.70, 131.25, 125.46, 125.03, 42.85, 42.34, 14.21, 13.35 ppm.

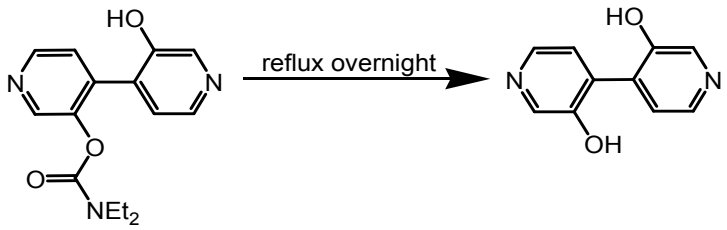

BPy1 **BPy2**

[4,4']bipyridinyl-3,3'-diol (BPy2)

To a round-bottomed flask **BPy1** (1.00 g, 3.48 mmol), sodium hydroxide solution (2 M, 10 mL) and methanol (20 mL) were added. The mixture was refluxed overnight (22 hours) then cooled to room temperature. The insoluble solid was filtered off and the volume of the filtrate was reduced to about 5mL (all methanol was removed). The white insoluble residue was removed to afford an orange solution which was neutralized with hydrochloric acid (6 M) to afford a yellow precipitate. Yield, 0.48 g, 2.55 mmol, 73%.

^{1}H NMR (400 MHz, DMSO): δ = 8.18 (br s, 2H; H of Py), 8.02 (d, 2H, *J* = 4.8 Hz; H of Py), 7.31 (d, 2H, *J* = 4.8 Hz; H of Py). ^{13}C NMR (101 MHz, DMSO): δ = 154.16, 139.20, 138.88, 132.22, 125.74 ppm.

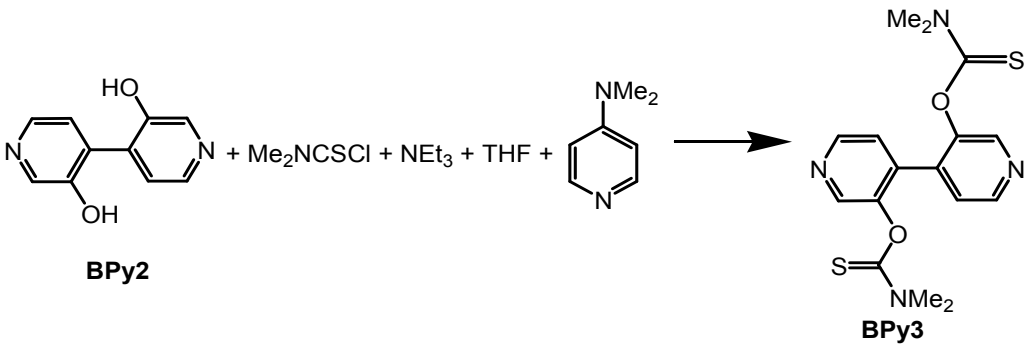

Dimethyl-thiocarbamic acid O-(3'-dimethylthiocarbamoyloxy[4,4']bipyridinyl-3-yl) ester (BPy3)

To a one neck round-bottom flask **BPy2** (400 mg, 2.12 mmol), dimethylthiocarbamoyl chloride (800 mg, 6.47 mmol), triethylamine (20 mL, 143 mmol), 4-dimethylaminopyridine (105 mg, 0.86 mmol) and THF (60 mL) were added. The orange mixture was refluxed at 90 ^{O}C overnight (22 hours, colour of the solution changed from orange to dark brown). After cooling to room temperature the white solid was filtered off. THF was removed to afford a dark brown residue. The residue was dissolved in dichloromethane and then washed with water. The aqueous phase was extracted with dichloromethane. Then combined organic layers were dried over magnesium sulphate. The dichloromethane was removed under vacuum to afford a dark brown residue. The crude product was purified by column chromatography (silica gel) eluting with acetone / petroleum ether = 2 / 1 to afford a beige solid. Yield, 620 mg, 1.71 mmol, 81%.

^{1}H NMR (400 MHz, $CDCl_3$): δ = 8.54 (d, 4H, J = 4.8 Hz; H of Py), 7.41 (d, 2H J = 4.8 Hz; H of Py), 3.32 (s, 6H; H of CH_3), 3.14 (s, 6H; H of CH_3). ^{13}C NMR (101 MHz, $CDCl_3$): δ = 185.59, 147.86, 146.50, 146.40, 136.97, 124.90, 43.78, 39.11ppm. EI-MS: m/z calcd. for $[M]^+$: 362; found: 362.

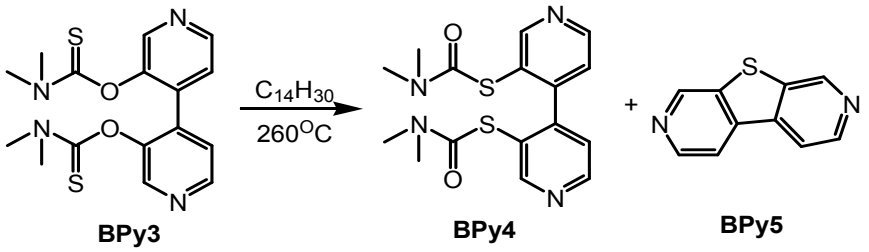

Dimethyl-thiocarbamic acid S-(3'-dimethyl-carbamoylsulfanyl[4,4']bipyridinyl-3-yl) ester (BPy4)

To a one-neck round-bottom flask **BPy3** (1.91 g, 5.26 mmol) and tetradecane (45 mL) were added. The mixture was heated to reflux (temperature of oil bath was 260 ^{O}C) for 9 hours under the protection of nitrogen. The mixture was cooled to room temperature and purified by column chromatography (silica gel) directly, eluting with acetone / petroleum ether = 2 / 1 and acetone / dichloromethane = 1 / 1. The pure product of **BPy4** was obtained as a white solid; **BPy5** was biege colour. Yield, **BPy4**, 1.68 g, 4.63 mmol, 88%; **BPy5**, 15 mg, 0.081mmol, 1.5%.

BPy4 ^{1}H NMR (400 MHz, $CDCl_3$): δ = 8.75 (s, 2H; H of Py), 8.65 (d, 2H, *J* = 4.8 Hz; H of Py), 7.27 (d, 2H, *J* = 4.8 Hz; H of Py), 2.90 (s, 12H; H of CH_3). ^{13}C NMR (101 MHz, $CDCl_3$): δ = 164.93, 156.96, 151.30, 150.14, 125.14, 124.54, 37.14 ppm. EI-MS: m/z calcd. for $[M + H]^+$: 363; found: 363.

BPy5 ^{1}H NMR (400 MHz, $CDCl_3$): δ= 9.29 (s, 2H; H of Py), 8.76 - 8.75 (d, 2H, *J* = 5.2 Hz; H of Py), 8.12 - 8.11 (d, 2H, *J* = 5.2 Hz; H of Py).

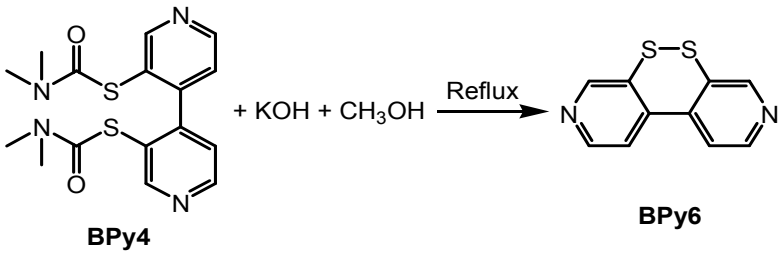

BPy4 **BPy6**

9,10-Dithia-2,7-diaza-phenanthrene (BPy6)

BPy4 (200 mg, 0.55mmol) was dissolved in methanol (20 mL) in a round-bottomed flask and degassed with nitrogen. Then solid potassium hydroxide (0.92 g, 16.40 mmol) was added. The mixture was refluxed for 6.5 hours then cooled to room temperature and water (10 mL) was added. The solution was acidified with hydrochloric acid (2 M) to pH 6-7 and extracted with dichloromethane. The combined organic layers were stirred in air for about 1 hour before drying over magnesium sulphate. The solvent was removed to afford a yellow solid. The crude product was purified by column chromatography (silica gel) and eluted with dichloromethane / acetone = 4 / 1 to afford a bright yellow solid. Yield, 87 mg, 0.40 mmol, 73%.

^{1}H NMR (400 MHz, $CDCl_3$): δ = 8.77 (s, 2H; H of Py), 8.67 (d, 2H, *J* = 5.1 Hz; H of Py), 7.62 (d, 2H, *J* = 5.1 Hz; H of Py). ^{13}C NMR (101 MHz, $CDCl_3$): δ = 150.26, 149.36, 142.77, 133.33, 121.57 ppm. EI-MS: m/z calcd. for $[M]^+$: 218; found: 218. Melting point: 167 - 168 ^{O}C.

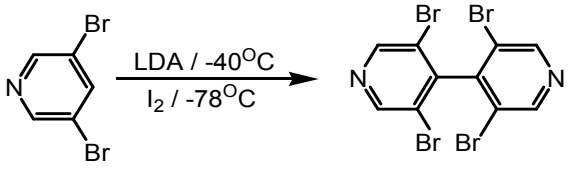

BPyTB

A solution of 3,5-dibromopyridine (5.00 g, 21.11 mmol) dissolved in freshly distilled THF (90 mL) was cooled to -40^{O}C, followed by dropwise addition of lithium diisopropylamide under nitrogen atmosphere. The orange mixture was stirred at this temperature for 1 hour before further cooling to -78^{O}C. Then iodine solution (5.63 g in 30 mL of THF) was added dropwise and the resulting mixture was left at this temperature and stirred for 1 hour. The cool bath was removed and mixture was warmed to room temperature and stirred overnight. Saturated $Na_2S_2O_5$ aqueous solution was added to quench the reaction. The mixture was extracted with ethyl acetate three times and washed with brine three times and dried over magnesium sulphate. The solvent was removed under vacuum. The crude product was purified by column chromatography (silica gel) eluting with petroleum ether / ethyl acetate = 4 / 1 to afford a white solid. Yield, 2.88 g, 6.10 mmol, 29%.

^{1}H NMR (400 MHz, $CDCl_3$): δ = 8.81 (s, 4H; H of Py). ^{13}C NMR (101 MHz, $CDCl_3$): δ = 150.90, 146.81, 120.94 ppm.

All chemical shifts values were consistent with those stated in the literature[5].

[5] M. Abboud, V. Mamane, E. Aubert, C. Lecomte and Y. Fort, *J. Org. Chem.*, 2010, **75**, 3224.

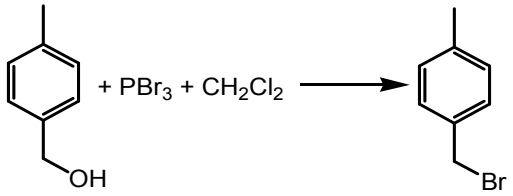

4-Methylbenzyl bromide

At 0 ^{O}C (ice bath), phosphorous tribromide (3.2 mL, 34.05 mmol) was added dropwise to a solution of 4-methylbenzyl alcohol (2.0 g, 16.37 mmol) in dichloromethane (50 mL). The mixture was left in the ice bath and stirred for another 0.5 hour. Then the ice bath was removed and the solution was stirred overnight under the protection of nitrogen. The reaction was quenched with saturated sodium bicarbonate solution (40 mL). The mixture was extracted with chloroform. The combined organic layers were washed with brine three times and dried over magnesium sulphate. The magnesium sulphate was filtered off and the chloroform was removed under vacuum to afford a yellow residue. The crude product was purified by column chromatography (silica gel) eluting with petroleum ether / ethyl acetate = 10 / 1 to afford a white solid. Yield, 2.39 g, 12.91 mmol, 79%.

^{1}H NMR (400 MHz, $CDCl_3$): δ = 7.29 (d, 2H, J = 8.0 Hz; H of Ar), 7.16 (d, 2H, J = 8.0 Hz; H of Ar), 4.50 (s, 2H; H of CH_2), 2.35 (s, 3H; H of CH_3). ^{13}C NMR (101 MHz, $CDCl_3$): δ = 138.67, 135.31, 129.80, 129.29, 33.83, 21.44 ppm. IR $_{(max)}$ (film) cm^{-1}: 3040 (υ Ar-H), 3000, 2918 and 2914 (υ C-H), 1614, 1514 (υ C=C of Ar).

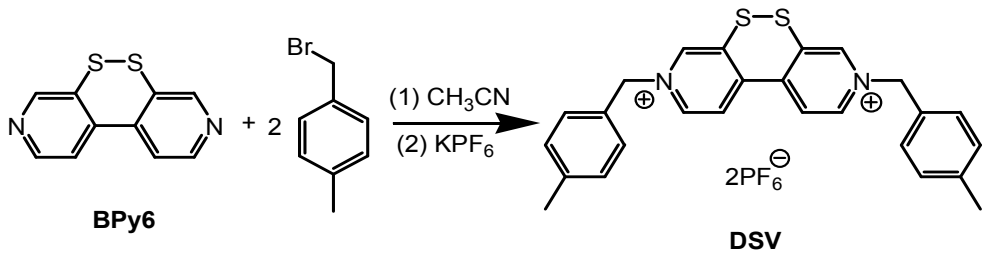

2,7-Bis-(4-methylbenzyl)-9,10-dithia-2,7-diaza-phenanthrene hexafluoro phosphate (DSV)

4-Methylbenzyl bromide (0.50 g, 2.70 mmol) was added to a solution of **BPy6** (50 mg, 0.23 mmol) in acetonitrile (12 mL). The solution was refluxed overnight (colour changed from yellow to orange). Diethyl ether was added to complete the precipitation of the product. The orange solid was filtered off and washed thoroughly with diethyl ether. After drying under vacuum overnight the orange solid was dissolved in distilled water (20 mL) and aqueous potassium hexafluorophosphate (427 mg in 16 mL of water) was added to afford the yellow ion exchanged product. The crude product was purified by recrystallisation from diethyl ether and acetonitrile to afford a yellow solid. Yield, 73 mg, 0.10 mmol, 43%.

^{1}H NMR (400 MHz, $CDCl_3$): δ = 9.65 (s, 2H; H of Py), 9.00 (d, 2H, J = 6.4 Hz; H of Py), 8.92 (dd, 2H, J = 0.8, 6.4 Hz; H of Py), 7.42 (dd, 4H, J = 0.8, 8.0 Hz; H of Ar), 7.31 (d, 4H, J = 8.0 Hz; H of Ar), 5.89 (s, 4H; H of CH_2), 2.35 (s, 6H; H of CH_3) ppm. FT-MS: m/z calcd. for $[M\text{-}PF_6]^+$: 573.1017; found: 573.1010; m/z calcd for $[M\text{-}2PF_6]^+$: 428.1375; found: 428.1372; m/z calcd for $[M\text{-}2PF_6]^{2+}$: 214.0685; found: 214.0686. Elemental analysis calcd (%) for $C_{26}H_{24}N_2S_2 \cdot P_2F_{12}$: C 43.46, H 3.37, N 3.90; found: C 43.59, H 3.34, N 4.02. IR $\upsilon_{(max)}$ (film) cm^{-1}: 3136 (υ Ar-H), 1625, 1550, 1515 and 1460 (υ C=C of Ar), 800 (δ P-F). Melting point: 237 ^{O}C (decomposition).

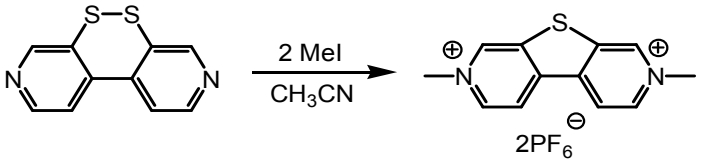

BPy6 **MSV1**

2,7-Dimethyl-9,10-thia-2,7-diaza-phenanthrene hexafluoro phosphate (MSV1)

Iodomethane (0.50 mL, 9.80 mmol) was added to a solution of **BPy6** (40 mg, 0.18 mmol) in acetonitrile (10 mL). The solution was refluxed overnight. Diethyl ether was added to complete the precipitation of the product. The orange solid was filtered off and washed thoroughly with diethyl ether. After drying under vacuum overnight the orange solid was dissolved in distilled water (20 mL) and aqueous potassium hexafluorophosphate (320 mg in 10 mL of water) was added to afford the yellow ion exchanged product. The crude product was purified by recrystallisation from diethyl ether and acetonitrile to afford a yellow solid. Yield, 52 mg, 0.10 mmol, 56%.

^{1}H NMR (400 MHz, $CDCl_3$): δ = 9.57 (s, 2H; H of Py), 8.99 (d, 2H, *J* = 8.8 Hz; H of Py), 8.80 (d, 2H, *J* = 8.8 Hz; H of Py), 4.53 (s, 6H; H of CH_3). ^{13}C NMR (101 MHz, $CDCl_3$): δ (ppm) = 145.15, 144.32, 143.44, 142.03, 124.75, 51.04 ppm. FT-MS: m/z calcd. for $[M\text{-}PF_6]^+$: 361.0358; found: 361.0360.

2.4.4 Compounds discussed in chapter 6

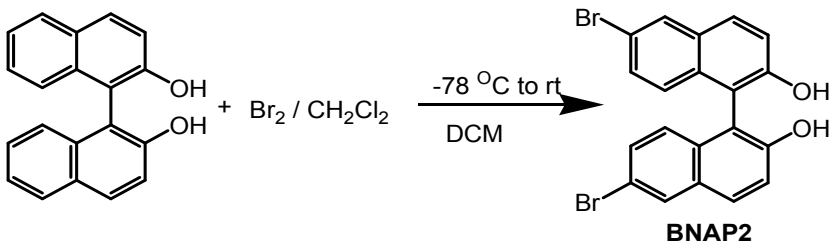

BNAP2

A solution of 1,1-bi-2-naphthol (5.0 g, 17.29 mmol, racemic) was cooled to -78 ^{O}C followed by the slow addition of a bromine solution (2.4 mL in 20mL of dichloromethane) over 30 minutes under the protection of nitrogen. The mixture was stirred for 2 hours under this condition before warming to room temperature and stirring overnight. During the stirring overnight process, a white solid precipitated out of the solution. The reaction was quenched by saturated sodium metabisulfite solution. The organic layer was separated and washed with brine. The combined organic layers were dried over magnesium sulphate and the solvent was removed under vacuum to afford a beige solid. The product was used in the next step without further purification. Yield, 7.68g, 17.29 mmol, 100%.

^{1}H NMR (300 MHz, $CDCl_3$): δ = 8.05 (d, *J* = 1.8 Hz, 2H; H of), 7.89 (d, *J* = 9.0 Hz, 2H; H of binap), 7.39 (d, *J* = 9.0 Hz, 2H; H of binap), 7.37 (dd, *J* = 1.8, 8.7 Hz, 2H; H of binap), 6.96 (d, *J* = 8.7 Hz, 2H; H of binap) 5.06 (s, 2H; H of OH) ppm. ^{13}C NMR (101 MHz $CDCl_3$): δ = 153.11, 132.01, 131.01, 130.85, 130.71, 130.59, 126.01, 119.11, 118.16, 110.75 ppm.

All chemical shifts values were consistent with those stated in the literature[6].

[6] C. Valente, E. Choi, M. E. Belowich, C. J. Doonan, Q. Li, T. B. Gasa, Y. Y. Botros, O. M. Yaghi and J. F. Stoddart, *Chem. Commun.*, 2010, **46**, 4911.

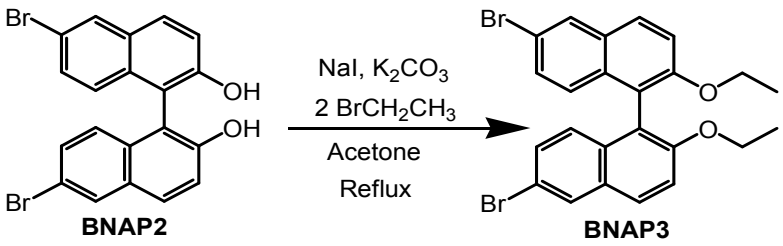

Sodium iodide (18 mg, 0.117 mmol) and potassium carbonate (1.24 g, 9 mmol) were added to a solution of **BNAP2** (1.0 g, 2.25 mmol) in acetone (50 mL). The mixture was heated to reflux following dropwise addition of bromoethane (1.03 mL, 13.5 mmol) under the protection of nitrogen. The mixture was refluxed overnight before cooling to room temperature. During the overnight reflux process, a white solid precipitated out of the solution. The white solid was filtered off to afford a light yellow solution. Acetone was removed under vacuum to afford a beige solid. The solid was dispersed in hexane and sonicated before filtration. The filtered off material was a white solid. The white solid was used in next step without further purification. Yield, 1.01 g, 2.02 mmol, 90%.

^{1}H NMR (400 MHz, $CDCl_3$): δ = 8.00 (d, J = 2.0 Hz, 2H; H of binap), 7.83 (d, J = 8.8 Hz, 2H; H of binap), 7.41 (d, J = 9.2 Hz, 2H; H of binap), 7.25 (dd, J = 2.0, 8.8 Hz, 2H; H of binap), 6.94 (d, J = 9.2 Hz, 2H; H of binap), 4.06 - 4.00 (m, 4H; H of CH_2), 1.07-1.05 (t, J = 6.8 Hz, 6H; H of CH_3). ^{13}C NMR (101 MHz, $CDCl_3$): δ = 154.66, 132.65, 130.35, 129.94, 129.60, 128.59, 127.24, 120.13, 117.41, 116.57, 65.19, 15.06 ppm.
All chemical shifts values were consistent with those stated in the literature[7].

[7] C. Valente, E. Choi, M. E. Belowich, C. J. Doonan, Q. Li, T. B. Gasa, Y. Y. Botros, O. M. Yaghi and J. F. Stoddart, *Chem. Commun.*, 2010, **46**, 4911.

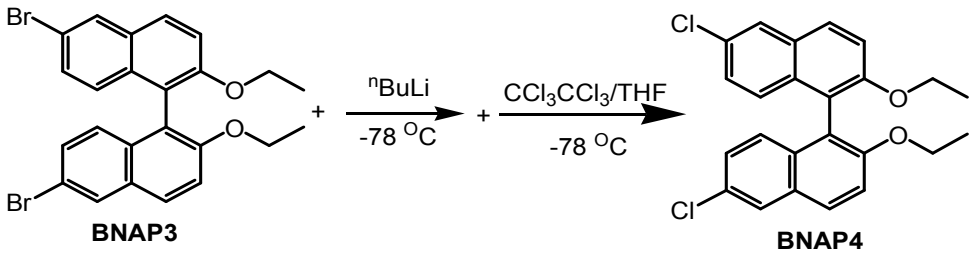

A solution of **BNAP3** (10.00 g, 20 mmol) in THF (125 mL) was cooled to -78 ^{O}C and was followed by the slow addition of a butyllithium solution (2.6 M in hexane, 31 mL) under a nitrogen atmosphere. The resulting mixture was stirred at this temperature for 1 hour before a solution of hexachloroethane (9.57 g, 40 mmol) in THF (25 mL) was added dropwise through a syringe pump. The mixture was stirred for an additional 1 hour before warming gradually to room temperature and was stirred overnight. The reaction was quenched with saturated ammonium chloride solution. The organic layer was separated and washed with brine, and the aqueous layer was extracted with ethyl acetate. The combined organic layers were dried over magnesium sulphate and the solvent was removed under vacuum to afford a brown solid. The solid was suspended in a small amount of hexane and the suspension was filtered to afford a brown solid. The brown solid was used in the next step without further purification (6.37 g, 15.49 mmol, 77%).

^{1}H NMR (400 MHz, $CDCl_3$): δ = 7.85 (d, *J* = 9.2 Hz, 2H; H of binap), 7.83 (d, *J* = 2.0 Hz, 2H; H of binap), 7.43 (d, *J* = 9.2 Hz, 2H; H of binap), 7.15 (dd, *J* = 2.0, 9.2 Hz, 2H; H of binap), 7.02 (d, *J* = 9.2 Hz, 2H; H of binap), 4.07 - 4.00 (m, 4H; H of CH_2), 1.06 (t, *J* = 5.6 Hz, 6H; H of CH_3). ^{13}C NMR (101 MHz, $CDCl_3$): δ = 154.57, 132.45, 129.83, 129.31, 128.59, 127.16, 127.12, 126.63, 120.21, 116.67, 65.23, 15.07 ppm.

All chemical shifts values were consistent with those stated in the literature[8].

[8] C. Valente, E. Choi, M. E. Belowich, C. J. Doonan, Q. Li, T. B. Gasa, Y. Y. Botros, O. M. Yaghi and J. F. Stoddart, *Chem. Commun.*, 2010, **46**, 4911.

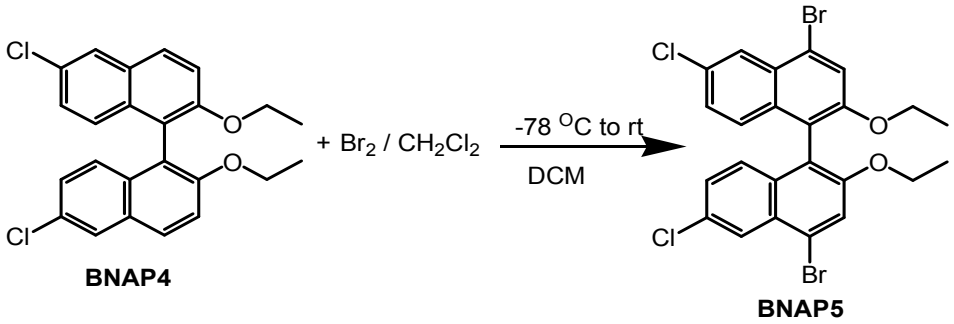

BNAP4 **BNAP5**

A solution of **BNAP4** (5.00 g, 12.16 mmol) in DCM (250 mL) was cooled to -78 ^{O}C followed by the slow addition of a solution of bromine (9.34 mL, 182.34 mmol) in dichloromethane (50 mL) using a syringe pump under a nitrogen atmosphere. The resulting mixture was stirred for an additional 1 hour before warming gradually to room temperature and was then stirred overnight. The reaction was quenched with saturated sodium metabisulfite solution. The organic layer was separated and the aqueous layer was extracted with dichloromethane. The combined organic layers were washed with brine, dried over magnesium sulphate, and the solvent was removed under vacuum to afford a brown solid. The solid was suspended in a small amount of hexane and the suspension was filtered to afford a brown solid. The brown solid was used in the next step without further purification. Yield, 6.62 g, 11.63 mmol, 96%.

^{1}H NMR (400 MHz, $CDCl_3$): δ = 8.23 (d, *J* = 2.0 Hz, 2H; H of binap), 7.73 (s, 2H; H of binap), 7.19 (dd, *J* = 2.0, 8.8 Hz, 2H; H of binap), 7.01 (d, *J* = 8.8 Hz, 2H; H of binap), 4.07 - 4.00 (m, 4H; H of CH_2), 1.11-1.06 (m, 6H; H of CH_3). ^{13}C NMR (101 MHz, $CDCl_3$): δ = 154.17, 132.92, 131.21, 128.57, 128.22, 127.40, 126.28, 122.62, 120.55, 119.33, 65.48, 14.95 ppm.

All chemical shifts values were consistent with those stated in the literature[9].

[9] C. Valente, E. Choi, M. E. Belowich, C. J. Doonan, Q. Li, T. B. Gasa, Y. Y. Botros, O. M. Yaghi and J. F. Stoddart, *Chem. Commun.*, 2010, **46**, 4911.

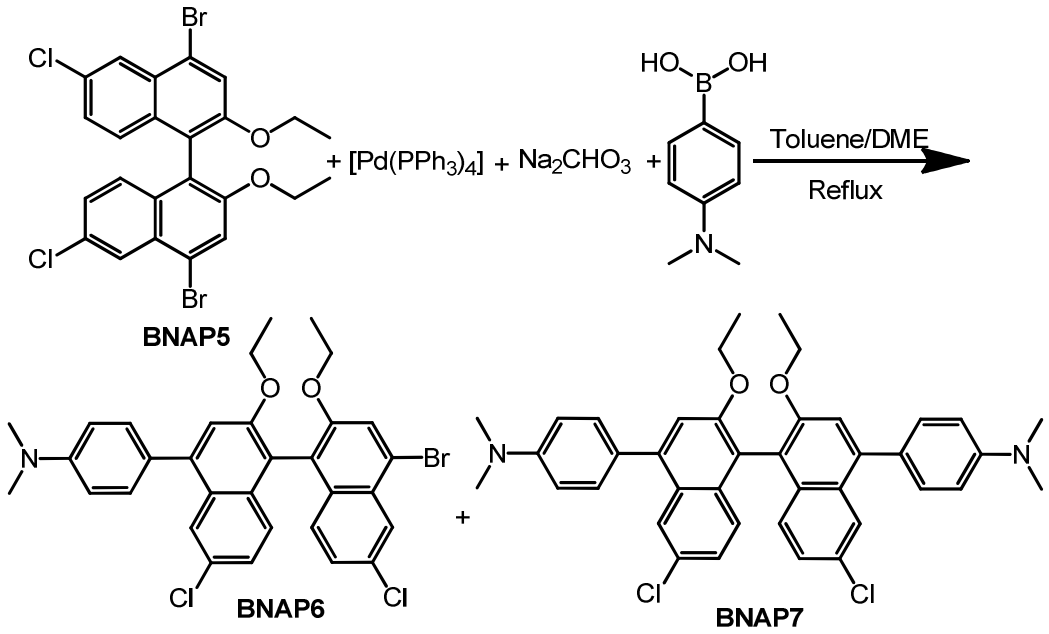

A two-neck round-bottom flask was charged with **BNAP5** (3.00 g, 5.25 mmol), sodium carbonate solution (1M, 26 mL), tetrakis(triphenylphosphine)-palladium (0) (364 mg, 0.31 mmol), 1,2-dimethoxyethane (35 mL) and toluene (70 mL). The solution was bubbled with nitrogen for 10 minutes before 4-(diemthylamino)phenylboronic acid (693 mg, 4.2 mmol) was added. The resulting mixture was bubbled with N_2 for another 10 minutes and heated to reflux for 24 hours under nitrogen atmosphere. The solution was cooled to room temperature and the organic layer was separated. The aqueous layer was extracted with ethyl acetate. The combined organic layers were washed 2 times with brine, dried over magnesium sulphate and the solvent was removed under vacuum to afford a brown oil. The crude product was purified by column chromatography (silica gel) eluting with petroleum ether / ethyl acetate = 4 / 1 to afford **BNAP6** (1.01 g, 1.66 mmol, 40%), **BNAP7** (0.46 mg, 11%) and the starting material (1.29 g).

BNAP6 ^{1}H NMR (400 MHz, $CDCl_3$): δ = 8.28 (s, 1H, H of binap), 8.03 (s, 1H, H of binap), 7.80 (s, 1H, H of binap), 7.51 (d, J = 8.4 Hz, 2H; H of Ar), 7.38 (s, 1H, H of binap), 7.22 (dd, J = 2.0, 8.8 Hz, 1H; H of binap), 7.19 - 7.15 (m, 2H; H of binap), 7.08 (d, J = 8.8 Hz, 1H; H of binap), 6.94 (d, J = 8.4 Hz, 2H; H of Ar), 4.12 - 4.05 (m, 4H; H of CH_2), 3.09 (s, 6H; H of NCH_3), 1.16 -1.13 (t, J = 6.8 Hz, 3H; H of CH_3), 1.12-1.08 (t, J = 6.8 Hz, 3H; H of CH_3). ^{13}C NMR (101 MHz, $CDCl_3$): δ = 154.34, 153.93, 150.15, 141.83, 133.28,

132.72, 131.06, 130.90, 129.41, 128.61, 128.52, 127.93, 127.88, 127.09, 127.03, 126.11, 125.43, 122.09, 120.87, 120.64, 117.54, 116.97, 112.41, 65.55, 64.92, 40.67, 15.07, 14.97 ppm. FTMS + p NSI: m/z calcd for $[M+H]^+$:608.0743; found: 608.0753.

BNAP7 ^{1}H NMR (400 MHz, $CDCl_3$): δ = 8.00 (d, *J* = 2.0 Hz, 2H; H of binap), 7.51 (d, *J* = 8.8 Hz, 4H; H of Ar),7.38 (s, 2H, H of binap), 7.20 - 7.14 (m, 4H; H of binap), 6.93 (d, *J* = 8.8 Hz, 4H; H of Ar), 4.10 (q, *J* = 6.8 Hz , 4H; H of CH_2), 3.09 (s, 12H; H of NCH_3), 1.12 (t, *J* = 6.8 Hz, 6H; H of CH_3). ^{13}C NMR (101 MHz $CDCl_3$): δ = 154.10, 150.14, 141.36, 133.09, 130.97, 129.34, 128.65, 128.20, 127.61, 126.83, 125.33, 118.94, 117.46, 112.46, 65.13, 40.75, 15.17 ppm. FTMS + p NSI: m/z calcd for $[M]^+$: 648.2305; found: 648.2299.

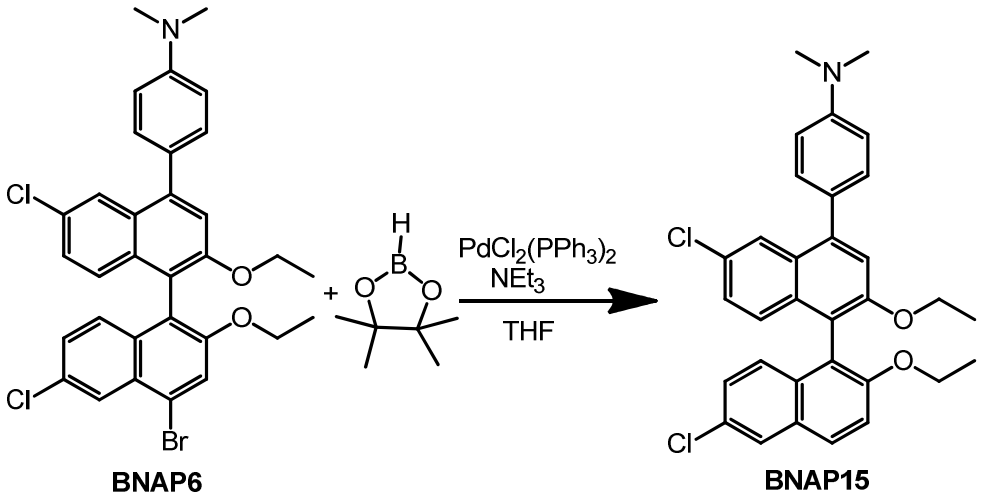

BNAP6 **BNAP15**

BNAP6 (200 mg, 0.33 mmol), bis(triphenylphosphine)palladium(II) dichloride, $PdCl_2(PPh_3)_2$, (24 mg, 0.033 mmol), and triethylamine (0.55 mL) were suspended in THF (8 mL). The mixture was degasssed with nitrogen and was followed by the addition of pinacolborane (85 mg, 0.66 mmol) and the bubbling with nitrogen for another 5 minutes. The resulting mixture was refluxed overnight. The mixture was diluted with ethyl acetate and filtered to remove insoluble solid. The solution was washed with distilled water and dried over magnesium sulphate. The solvent was removed to afford a brown oil. The crude product was purified by column chromatography (silica gel) eluting with petroleum ether / acetone = 5 / 1 to afford a white solid. Yield, 150 mg, 0.28 mmol, 85%.

^{1}H NMR (400 MHz, $CDCl_3$): δ = 7.98 (d, *J* = 1.2 Hz, 1H; H of binap), 7.86 (d, *J* = 9.2 Hz, 1H; H of binap), 7.84(d, *J* = 1.2 Hz, 1H; H of binap), 7.49 (d, *J* = 8.0 Hz, 2H; H of Ar), 7.45 (d, *J* = 9.2 Hz, 1H; H of binap), 7.35 (s, 1H, H of binap), 7.18 - 7.11 (m, 3H; H of binap), 7.07 (d, *J* = 9.2 Hz, 1H; H of binap), 6.92 (d, *J* = 8.0 Hz, 2H; H of Ar), 4.11- 4.01 (m, 4H; H of -CH_2), 3.08 (s, 6H; H of NCH_3), 1.13 - 1.10 (t, *J* = 7.2 Hz, 3H; H of CH_3), 1.07 - 1.04 (t, *J* = 7.2 Hz, 3H; H of CH_3) ppm. FTMS + p NSI: m/z calcd for $[M+H]^+$: 530.1648; found: 530.1644.

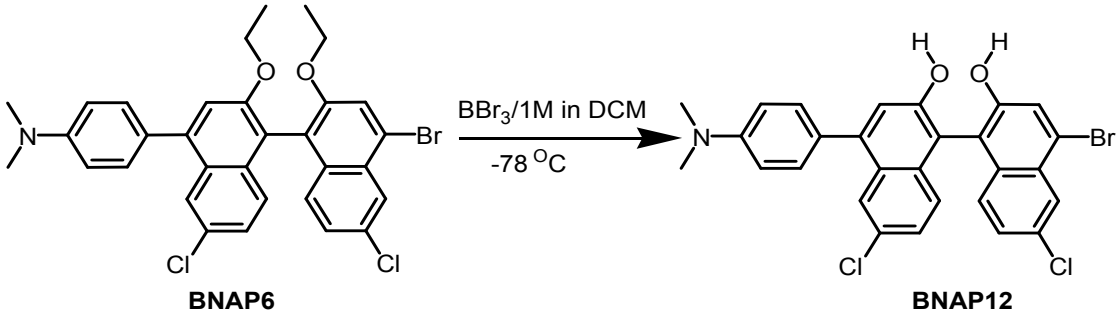

A solution of **BNAP6** (950 mg, 1.56 mmol) in DCM (30 mL) was cooled to -78 ^{O}C and was followed by the slow addition of boron tribromide solution (4.7 mL, 1M in DCM) under a nitrogen atmosphere. The mixture was stirred for another 2 hours under these conditions before warming gradually to room temperature and was then stirred overnight. The reaction was quenched by saturated sodium carbonate solution. The organic layer was separated and the aqueous layer was extracted 3 times with dichloromethane. The combined organic layers were washed with brine and dried over magnesium sulphate. The solvent was removed under vacuum to afford a beige power, which is used in next step without further purification (800 mg, 1.45 mmol, 93%).

^{1}H NMR (400 MHz, $CDCl_3$): δ = 8.29 (d, *J* = 1.6 Hz, 1H; H of binap), 8.02 (s, 1H; H of binap), 7.75 (s, 1H; H of binap), 7.43 (d, *J* = 8.4 Hz, 2H; H of Ar), 7.30 - 7.28 (m, 2H; H of binap), 7.23 (dd, *J* = 1.6, 9.2 Hz, 1H; H of binap), 7.16 (d, *J* = 9.2 Hz, 1H; H of binap), 7.05 (d, *J* = 8.8 Hz, 1H; H of binap), 6.93 (d, *J* = 8.4 Hz, 2H; H of Ar), 3.07 (s, 6H; H of NCH_3). ^{13}C NMR (101 MHz, $CDCl_3$): δ = 152.75, 152.44, 149.90, 132.77, 132.66, 132.28, 131.75, 130.81, 130.33, 129.27, 129.20, 129.11, 128.37, 126.91, 126.68, 126.14, 126.00, 124.49, 123.18, 119.45, 112.95, 112.75, 111.60, 108.76, 40.91 ppm.

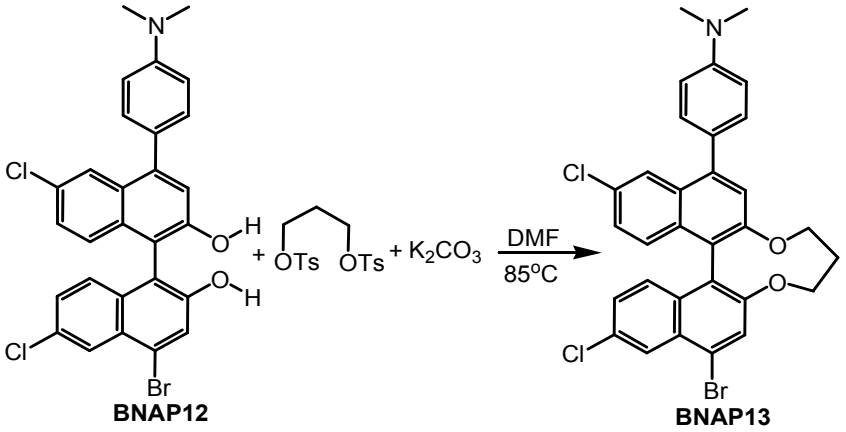

Potassium carbonate (419 mg, 3.03 mmol) was added to a solution of **BNAP12** (600 mg, 1.08 mmol) in DMF (60 mL). The mixture was stirred and heated at 85 ^{o}C for 2 hours under a N_2 atmosphere. Then a solution of $TsO(CH_2)_3OTs$ (458 mg, 1.19 mmol) in DMF (60 mL) was added slowly through a syringe pump over 1.5 hours. After the addition the mixture was further stirred and heated under this condition for another 24 hours. The solvent was removed under vacuum to afford a yellow residue which was dissolved in ethyl acetate and water. The organic layer was separated and then washed with brine for 3 times. Combined organic layers were dried over magnesium sulphate, and solvent was removed under vacuum to afford a brown oily solid. The crude product was purified by column chromatography (silica gel) eluting with petroleum ether / acetone = 1 / 6 to afford starting material (50 mg) and a light yellow solid. Yield, 330 mg, 0.56 mmol, 52%.

^{1}H NMR (400 MHz, $CDCl_3$): δ = 8.31 (d, *J* = 2.0 Hz, 1H; H of binap), 8.05 (d, *J* = 2.0 Hz, 1H; H of binap), 7.83 (s, 1H; H of binap), 7.48 (d, *J* = 8.8 Hz, 2H; H of Ar), 7.42 (s, 1H; H of binap), 7.32 - 7.28 (m, 1H; H of binap), 7.26 (dd, *J* = 2.0, 9.2 Hz, 1H; H of binap), 7.21 (dd, *J* = 2.0, 9.2 Hz, 1H; H of binap), 7.17 (d, *J* = 8.4 Hz, 1H; H of binap), 6.93 (d, *J* = 8.8 Hz, 2H; H of Ar), 4. 45 - 4.29 (m, 4H; H of CH_2), 3.09 (s, 6H; H of NCH_3), 2.06 -1.91 (m, 2H; H of CH_2). ^{13}C NMR (101 MHz $CDCl_3$): δ = 154.94, 154.52, 150.25, 142.44, 132.50, 132.12, 132.01, 130.87, 130.52, 130.02, 129.98, 128.51, 128.27, 127.71, 127.40, 126.52, 125.80, 124.97, 124.24, 122.29, 121.50, 121.25, 120.93, 112.45, 72.68, 71.88, 40.71, 30.65 ppm. FTMS + p NSI: m/z calcd for $[M+H]^+$: 592.0438; found: 592.0440.

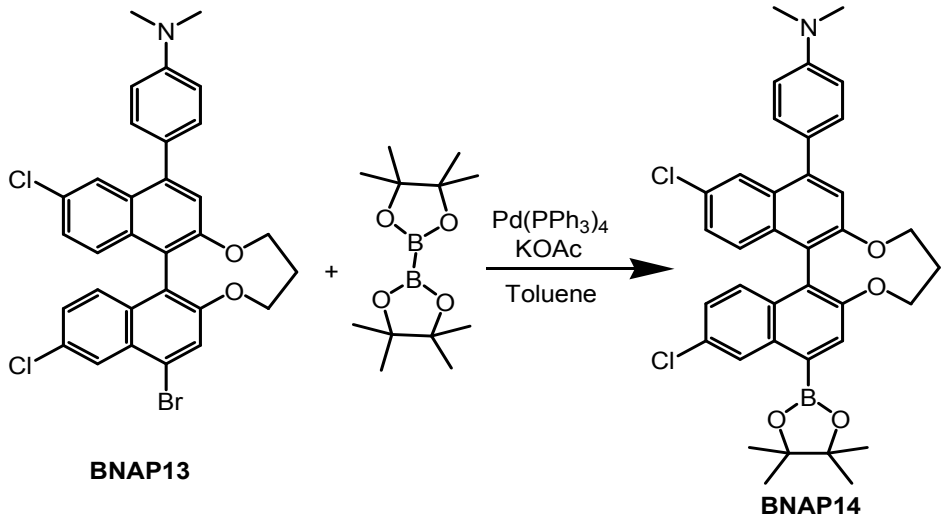

BNAP13 **BNAP14**

Toluene (15 mL) was added to a mixture of **BNAP13** (100 mg, 0.17 mmol), tetrakis-(triphenylphosphine) palladium(0), (6 mg, 0.005 mmol), potassium acetate (166 mg, 1.69 mmol) and bis(pinacolato)diboron (52 mg, 0.21 mmol). The mixture was degassed with nitrogen and refluxed overnight. The mixture was diluted with ethyl acetate and filtered to remove insoluble solid. The solution was washed with distilled water and dried over magnesium sulphate. The solvent was removed to afford a brown oil. The crude product was purified by column chromatography (silica gel) eluting with petroleum ether / acetone = 5 / 1 to afford a white solid. Yield, 70 mg, 0.11 mmol, 65%.

^{1}H NMR (400 MHz, $CDCl_3$): δ = 8.85 - 8.85 (d, *J* = 2.0 Hz, 1H; H of binap), 8.06 (s, 1H; H of binap), 8.01 (s, 1H; H of binap), 7.48 - 7.46 (d, *J* = 8.0 Hz, 2H; H of Ar), 7.41 (s, 1H; H of binap), 7.27 - 7.19 (m, 2H; H of binap), 7.17 - 7.12 (m, 2H; H of binap), 6.93 - 6.91 (d, *J* = 8.0 Hz, 2H; H of Ar), 4. 50 - 4.27 (m, 4H; H of -CH_2), 3.08 (s, 6H; H of N-CH_3), 1.98 (m, 2H; H of -CH_2), 1.47 (s, 12H; H of -CH_3). ^{13}C NMR (101 MHz $CDCl_3$): δ = 154.44, 154.34, 134.73, 133.43, 132.03, 131.97, 130.94, 130.42, 129.88, 129.67, 128.02, 127.96, 127.86, 127.73, 127.51, 127.19, 127.02, 125.56, 125.38, 124.64, 123.60, 123.53, 121.329, 121.00, 84.27, 72.26, 71.93, 60.51, 30.76, 24.98 ppm. FTMS + p NSI: m/z calcd for $[M+H]^+$: 639.2224; found: 639.2217.

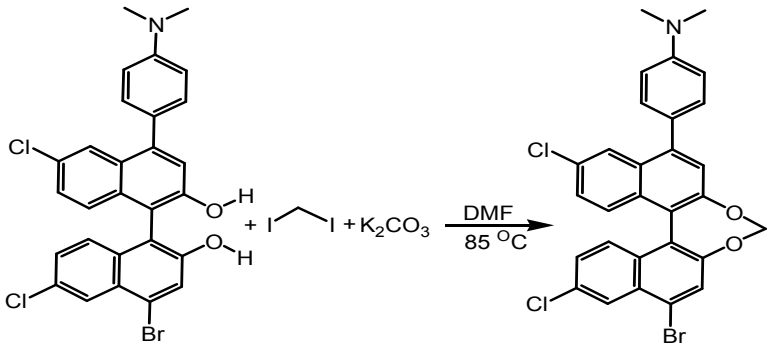

BNAP12 **BNAP16**

Potassium carbonate (240 mg, 1.74 mmol) was added to a solution of **BNAP12** (400 mg, 0.72 mmol) in DMF (40 mL). The suspension was stirred and heated at 85 ^{O}C for 2 hours under a nitrogen atmosphere. Then a solution of diiodomethane (0.065 mL, 0.80 mmol) in DMF (40 mL) was added slowly through a syringe pump over 1 hour. After the addition the mixture was further stirred and heated under this condition for another 24 hours. The solvent was removed under vacuum to afford a yellow residue which was dissolved in a mixture of ethyl acetate and water. The organic layer was separated and washed three times with brine. Combined organic layers were dried over magnesium sulphate, and the solvent was removed under vacuum to afford a brown oily solid. The crude product was purified by column chromatography (silica gel) eluting with petroleum ether / acetone = 6 / 1 to afford starting material (50 mg) and a light yellow solid product. Yield, 140 mg, 0.25 mmol, 35%.

^{1}H NMR (400 MHz, $CDCl_3$): δ = 8.37 (d, *J* = 2.0 Hz, 1H; H of binap), 8.12 (d, *J* = 2.4 Hz, 1H; H of binap), 7.86 (s, 1H; H of binap), 7.52 - 7.50 (d, *J* = 9.2 Hz, 1H; H of binap), 7.46 (d, *J* = 8.0 Hz, 2H; H of Ar), 7.45 (s, 1H; H of binap), 7.38 (d, *J* = 8.8 Hz, 1H; H of binap), 7.31 (dd, *J* = 2.0, 9.2 Hz, 1H; H of binap), 7.25 (dd, *J* = 2.4, 9.2 Hz, 1H; H of binap), 6.93 (d, *J* = 8.8 Hz, 2H; H of Ar), 5.74 - 5.66 (m, 2H; H of CH_2), 3.08 (s, 6H; H of NCH_3). ^{13}C NMR (101 MHz, $CDCl_3$): δ = 151.17, 151.03, 150.31, 143.28, 132.84, 131.39, 131.28, 131.25, 131.11, 130.85, 130.80, 129.06, 128.30, 127.95, 127.13, 126.84, 126.64, 126.60, 126.23, 126.00, 123.48, 122.50, 122.46, 112.40, 103.36, 40.59 ppm. FTMS + p NSI: m/z calcd for $[M+H]^+$: 564.0127; found: 564.0122.

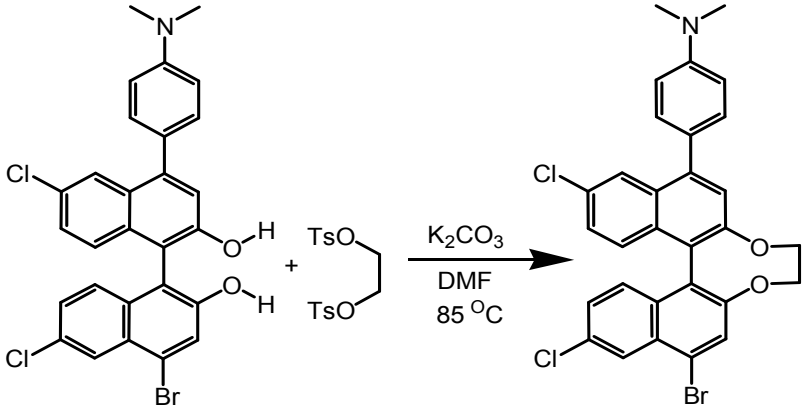

Potassium carbonate (43 mg, 0.31mmol) was added to a solution of **BNAP12** (62 mg, 0.11 mmol) in DMF (10 mL). The mixture was stirred and heated at 85 ^{O}C for 2 hours under a nitrogen atmosphere. Then a solution of $TsO(CH_2)_2OTs$ (46 mg, 0.12 mmol) in DMF (10 mL) was added slowly through a syringe pump with a speed of 20 mL/h. After the addition the mixture was further stirred and heated under this condition for another 24 hours. The solvent was removed under vacuum to afford a yellow residue which was dissolved in ethyl acetate and water. The organic layer was separated and then washed with brine. The combined organic layers were dried over magnesium sulphate, and the solvent was removed under vacuum to afford a brown oily solid. The crude product was purified by column chromatography (silica gel) eluting with petroleum ether / acetone = 5 / 1 to afford a light yellow solid product. Yield, 20 mg, 0.035 mmol, 32%.

^{1}H NMR (400 MHz, $CDCl_3$): δ = 8.30 (s, 1H; H of binap), 8.03 (s, 1H; H of binap), 7.83 (d, *J* = 1.6 Hz, 1H; H of binap), 7.45 (d, *J* = 8.0 Hz, 1H; H of Ar), 7.40 (d, *J* = 2.0 Hz, 1H; H of binap), 7.18 - 7.11 (m, *J* = 8.0 Hz, 3H; H of binap), 7.32 - 7.28 (m, 1H), 7.25 (dd, *J* = 2.0, 9.2 Hz, 1H), 6.91 (bs, 2H; H of Ar), 4. 47 - 4.37 (m, 2H; H of CH_2), 4. 24 - 4.14 (m, 2H; H of CH_2), 3.08 (s, 6H; H of NCH_3) ppm.

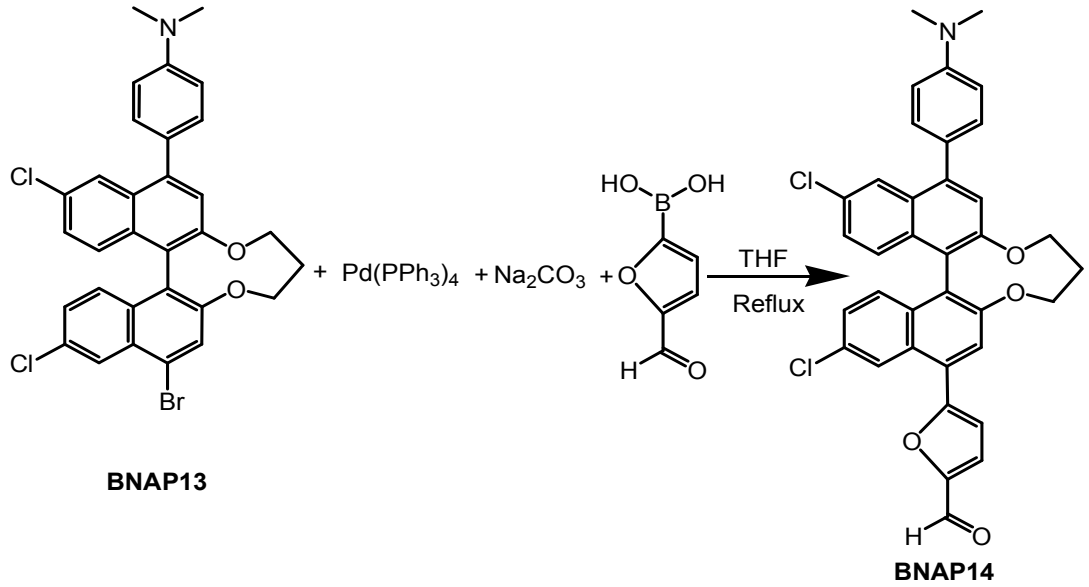

BNAP13 **BNAP14**

A two-neck round-bottom flask was charged with **BNAP13** (100 mg, 0.156 mmol), sodium carbonate solution (1.18 in 5 mL of H_2O), tetrakis(triphenylphosphine)-palladium (0) (13 mg, 7 mol%) and THF (5 mL). The solution was bubbled with N_2 for 10 minutes and heated at 45 ^{O}C for 30 minutes under a nitrogen atmosphere. A solution of 5-formylfuran-2-boronic acid (23 mg, 0.156 mmol) in THF (5 mL) was added slowly. The resulting mixture was bubbled with nitrogen for another 10 minutes and heated to reflux for 1.5 hours under a nitrogen atmosphere. The solution was cooled to room temperature, the organic layer was separated and the aqueous layer was extracted with ethyl acetate. The combined organic layers were washed 3 times with brine, dried over magnesium sulphate and the solvent was removed under vacuum to afford a brown oil. The crude product was purified by column chromatography (silica gel) eluting with petroleum ether / ethyl acetate = 5 / 1 to afford a yellow solid. Yield, 70 mg, 0.115 mmol, 74%.

^{1}H NMR (400 MHz, $CDCl_3$): δ = 9.79 (s, 1H; H of CHO), 8.36 (d, *J* = 2.0 Hz, 1H; H of binap), 8.03 (d, *J* = 2.0 Hz, 1H; H of binap), 7.89 (s, 1H; H of binap), 7.50 (d, *J* = 3.6 Hz, 1H; H of furan), 7.46 (d, *J* = 8.4 Hz, 2H; H of Ar), 7.42 (s, 1H), 7.35 (d, *J* = 9.2 Hz, 1H; H of binap), 7.28 (dd, *J* = 2.0, 9.2 Hz, 1H; H of binap), 7.20 (dd, *J* = 2.0, 8.8 Hz, 1H; H of binap), 7.16 (d, *J* = 8.8 Hz, 1H; H of binap), 7.05 (d, *J* = 3.6 Hz, 1H; H of furan), 6.91 (d,

J = 8.4 Hz, 2H; H of Ar), 4.45 - 4.29 (m, 4H; H of OCH_2), 3.07 (s, 6H; H of NCH_3), 2.08 - 1.93 (m, 2H; H of CH_2). ^{13}C NMR (101 MHz, $CDCl_3$): δ = 177.70, 157.61, 154.80, 154.58, 152.69, 142.56, 133.26, 133.18, 132.57, 132.15, 132.01, 130.89, 130.55, 130.02, 128.82, 128.16, 127.93, 127.70, 127.46, 126.77, 126.64, 125.86, 124.24, 121.83, 121.33, 120.90, 118.05, 112.80, 112.48, 72.70, 71.93, 40.73, 30.70 ppm.

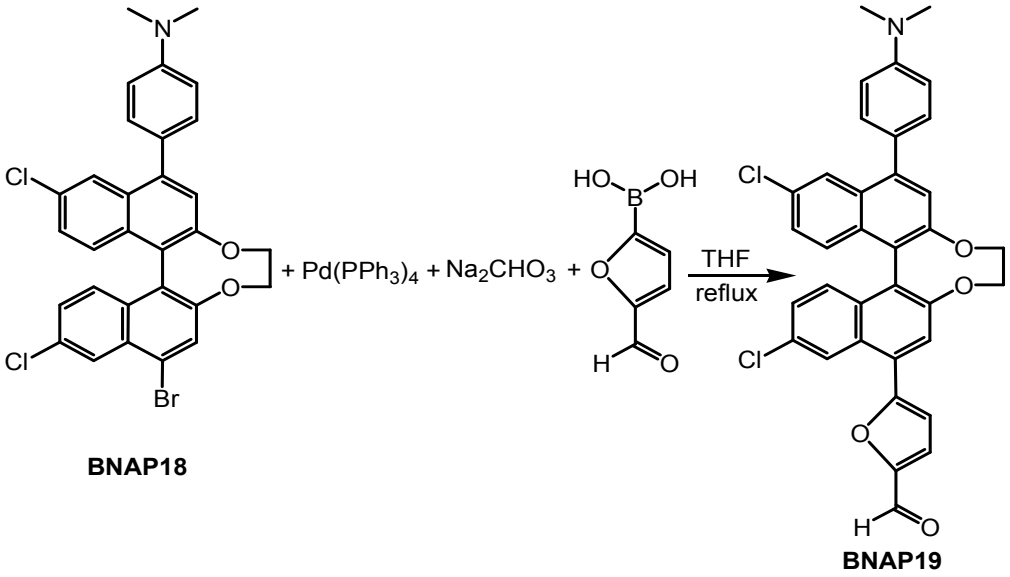

BNAP18 **BNAP19**

A two-neck round-bottom flask was charged with **BNAP18** (20 mg, 0.04 mmol), sodium carbonate solution (301 mg in 2 mL of H_2O), tetrakis(triphenylphosphine)-palladium (0) (3 mg, 7 mol%) and THF (3 mL). The solution was bubbled with nitrogen for 10 minutes and then heated to 45 ^{O}C for 30 minutes under a nitrogen atmosphere. A solution of 5-formylfuran-2-boronic acid (6 mg, 0.04 mmol) in THF (3 mL) was added slowly. The resulting mixture was bubbled with nitrogen for another 10 minutes and heated to reflux for one hour under a nitrogen atmosphere. The solution was cooled to room temperature and the organic layer was separated. The aqueous layer was extracted with ethyl acetate and the combined organic layers were washed three times with brine, dried over magnesium sulphate and the solvent was removed under vacuum to afford a brown oil. The crude product was purified by column chromatography (silica gel) eluting with petroleum ether / ethyl acetate = 5 / 1 to afford a yellow solid. Yield, 7 mg, 0.012 mmol, 30%.

^{1}H NMR (400 MHz, $CDCl_3$): δ = 9.80 (s, 1H; H of CHO), 8.40 (d, *J* = 2.0 Hz, 1H; H of binap), 8.06 (s, 1H; H of binap), 7.92 (s, 1H; H of binap), 7.51 (d, *J* = 3.6 Hz, 1H; H of furan), 7.47 (d, *J* = 8.8 Hz, 2H; H of Ar), 7.43 (s, 1H; H of binap), 7.35 (d, *J* = 8.8 Hz, 1H; H of binap), 7.28 (dd, *J* = 2.0, 8.8 Hz, 1H; H of binap), 7.20 (dd, *J* = 2.0, 8.8 Hz, 1H; H of binap), 7.16 (d, *J* = 2.0, 8.8 Hz, 1H; H of binap), 7.07 (d, *J* = 3.6 Hz, 1H), 6.93 (bs, 2H; H of Ar), 4. 45 - 4.29 (m, 4H; H of OCH_2), 3.07 (s, 6H; H of NCH_3) ppm.

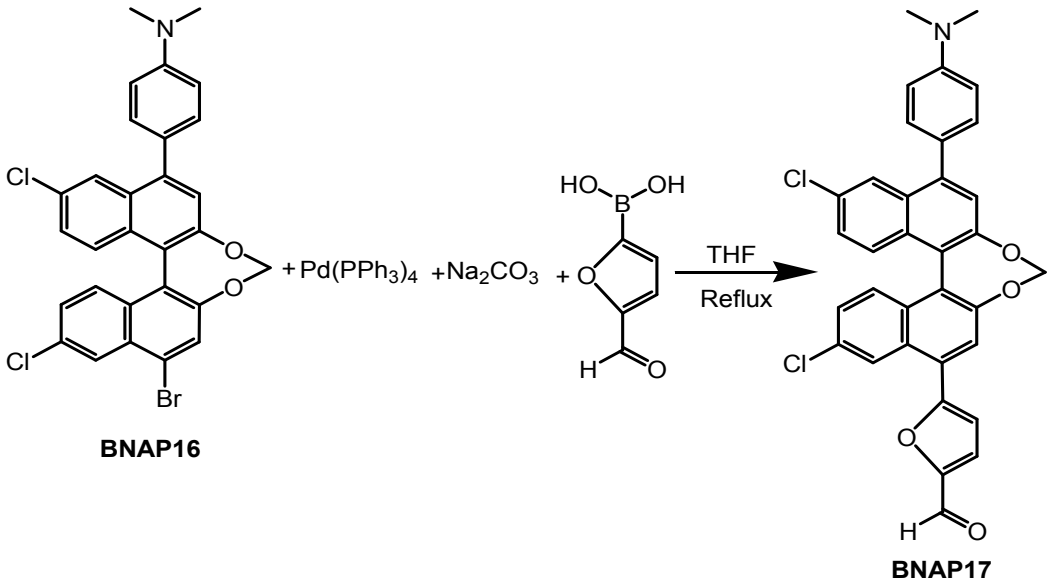

BNAP16 **BNAP17**

A two-neck round-bottom flask was charged with **BNAP16** (134 mg, 0.24 mmol), sodium carbonate solution (1.8 g in 8 mL of H_2O), tetrakis(triphenylphosphine)-palladium (0) (19 mg, 7 mol%) and THF (8 mL). The solution was bubbled with N_2 for 10 minutes and heated at 45 ^{O}C for 30 minutes under a nitrogen atmosphere. A solution of 5-formylfuran-2-boronic acid (34 mg, 0.24 mmol) in THF (8 mL) was added slowly. The resulting mixture was bubbled with nitrogen for another 10 minutes and heated to reflux for 1.5 hours under nitrogen atmosphere. The solution was cooled to room temperature, and the organic layer was separated. The aqueous layer was extracted with ethyl acetate and the combined organics were washed 3 times with brine, dried over magnesium sulphate and the solvent was removed under vacuum to afford a brown oil. The crude product was purified by column chromatography (silica gel) eluting with petroleum ether / ethyl acetate = 5 / 1 to afford a yellow solid. Yield, 56 mg, 0.096 mmol, 40%.

^{1}H NMR (400 MHz, $CDCl_3$): δ = 9.81 (s, 1H; H of CHO), 8.45 (d, *J* = 2.0 Hz, 1H; H of binap), 8.11 (d, *J* = 2.0 Hz, 1H; H of binap), 7.94 (s, 1H), 7.58 (d, *J* = 9.2 Hz, 1H; H of binap), 7.50 (d, J = 3.6 Hz, 1H; H of furan), 7.46 (d, J = 8.8 Hz, 2H; H of Ar), 7.46 (s, 1H), 7.42 (d, J = 9.2 Hz, 1H; H of binap),7.34 (dd, *J* = 2.0, 9.2 Hz, 1H; H of binap), 7.26 (dd, *J* = 2.0, 9.2 Hz, 1H; H of binap), 7.07 (d, *J* = 3.6 Hz, 1H; H of furan), 6.91 (d, *J* = 8.8 Hz, 2H; H of Ar), 5.75 (d, *J* = 3.6 Hz, 1H; H of CH), 5.74 (d, *J* = 3.6 Hz, 1H; H of CH),

3.09 (s, 6H; H of NCH_3). ^{13}C NMR (101 MHz $CDCl_3$): δ = 177.74, 157.30, 152.87, 151.50, 150.91, 150.39, 143.53, 132.88, 131.45, 131.34, 131.28, 130.93, 130.87, 129.45, 129.39, 128.57, 128.35, 127.98, 127.64, 127.24, 126.88, 126.09, 124.53, 123.55, 123.48, 122.59, 112.90, 112.45, 103.29, 40.65 ppm. FTMS + p APCI: m/z calcd for $[M]^+$: 579.0999; found: 579.0998.

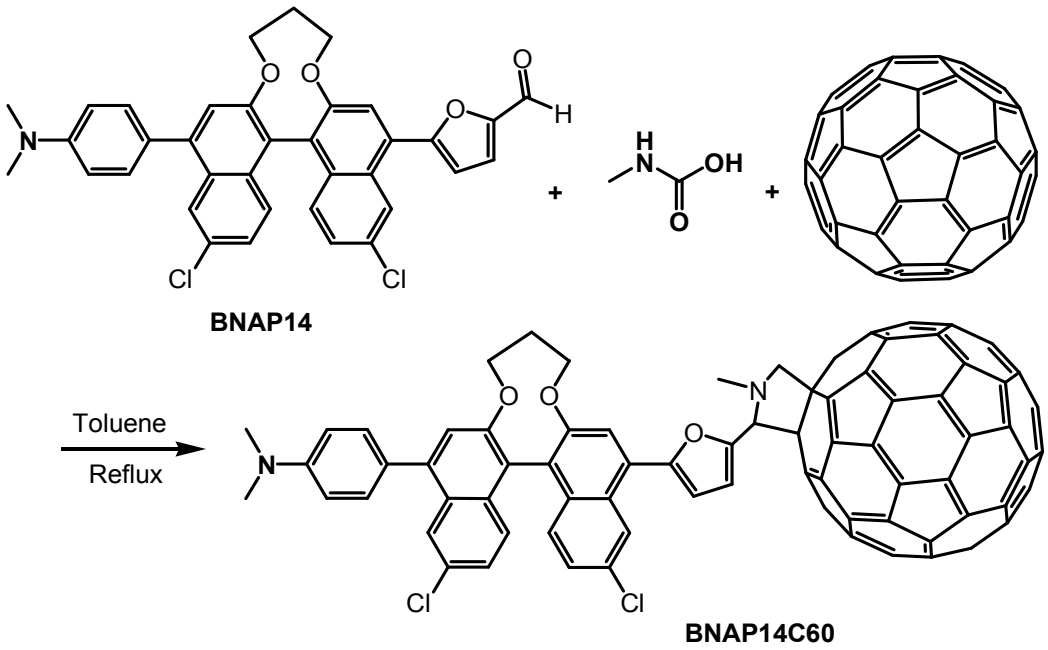

To a solution of **BNAP14** (153 mg, 0.25 mmol) in anhydrous toluene (150 mL) was added C60 (181 mg, 0.25 mmol) and N-methylglycine (sarcosine) (76 mg, 0.85 mmol). The mixture was refluxed overnight under nitrogen. The hot solution was filtered to remove insoluble solid. Then the solvent was removed to afford a dark black residue. The crude product was purified by column chromatography (silica gel) eluting with petroleum ether / toluene = 4 / 1, DCM / toluene = 4 / 1 and DCM / toluene = 1 / 1 to afford a brown solid. Yield, 72 mg, 0.053 mmol, 21%

^{1}H NMR (400 MHz, $CDCl_3$): δ = 8.46 (dd, *J* = 2.0, 6.4 Hz, 1H; H of binap), 8.01 (s, 1H; H of binap), 7.58 - 7.52 (m, 1H; H of furan), 7.46 - 7.44 (d, *J* = 8.8 Hz, 2H; H of Ar), 7.40 - 7.38 (m, 1H; H of binap), 7.30 - 7.14 (m, 5H; H of binap), 7.03 - 7.02 (m, 1H; H of furan), 6.91 (d, *J* = 8.8 Hz, 2H; H of Ar), 5.30 (d, *J* = 7.2 Hz, 1H; H of CH or CH_2), 5.05 (d, *J* = 9.6 Hz, 1H; H of CH or CH_2), 4.40 - 4.24 (m, 4H; H of CH_2), 4.32 (d, *J* = 9.6 Hz, 1H; H of CH or CH_2) 3.07 (s, 6H; H of NCH_3), 3.01 (d, *J* = 4.4 Hz, 3H; H of NCH_3), 1.98 - 1.86 (m, 2H; H of CH_2) ppm.

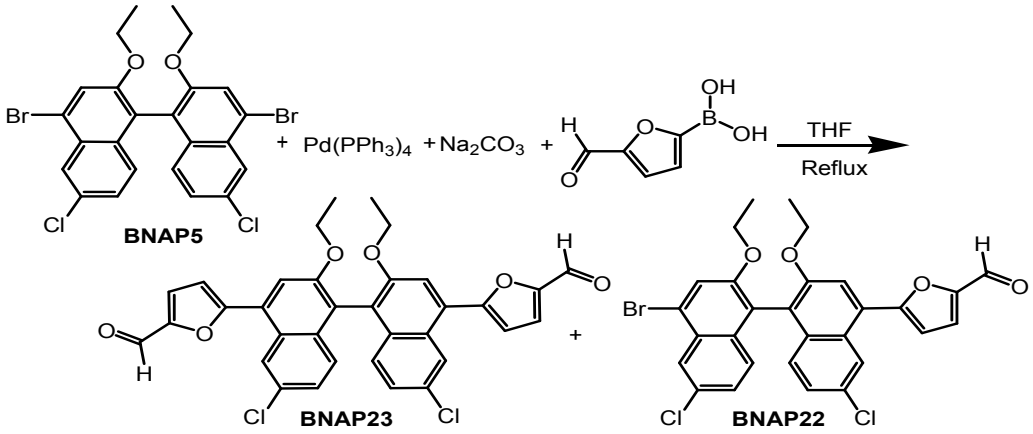

To **BNAP5** (200 mg, 0.35 mmol) dissolved in THF (10 mL) was added a sodium carbonate solution (2.65 g in 12 mL of H_2O) and tetrakis(triphenylphosphine)-palladium (0) (28 mg, 7 mol%). The mixture was bubbled with N_2 for 10 minutes and heated to 45 ^oC for 30 minutes under a nitrogen atmosphere. A solution of 5-formylfuran-2-boronic acid (46 mg, 0.32 mmol) in THF (10 mL) was added slowly. The resulting mixture was bubbled with N_2 for another 10 minutes and heated to reflux overnight. The solution was cooled to room temperature and diluted with ethyl acetate. The organic layer was separated and the aqueous layer was extracted with ethyl acetate. The combined organic layers were washed 3 times with brine, dried over magnesium sulphate and the solvents were removed under vacuum to afford a brown oil. The crude product was purified by column chromatography (silica gel) eluting with petroleum ether / ethyl acetate = 3 / 1 to afford biege solids **BNAP22**(30 mg, 0.051 mmol,16%) and **BNAP23** (20 mg, 0.033 mmol, 9.4%).

BNAP22 ^{1}H NMR (400 MHz, $CDCl_3$): δ = 9.80 (s, 1H; H of CHO), 8.30 (d, *J* = 2.0 Hz, 1H; H of binap), 8.25 (d, *J* = 2.0 Hz, 1H; H of binap), 7.63 (d, *J* = 6.4 Hz, 2H; H of binap), 7.50 (d, *J* = 3.2 Hz, 1H; H of furan), 7.21 (apparent dd, *J* =2.0, 9.2 Hz, 2H; H of binap), 7.10 (d, *J* = 9.2 Hz, 1H; H of binap), 7.05 (d, *J* = 3.2 Hz, 1H; H of furan), 7.03 (d, *J* = 8.0 Hz 1H; H of binap), 4. 15 - 4.02 (m, 4H; H of CH_2), 1.18 -1.08 (m, 6H; H of CH_3).

BNAP23 ^{1}H NMR (300 MHz, $CDCl_3$): δ = 9.79 (s, 2H; H of CHO), 8.32 (d, *J* = 2.1 Hz, 2H; H of binap), 7.79 (s, 2H; H of binap), 7.51 (d, *J* = 3.6 Hz, 2H; H of furan), 7.23 (dd, *J* = 2.1, 12 Hz, 2H; H of binap), 7.12 (dd, *J* = 2.1, 12 Hz, 2H), 7.06 (d, *J* = 3.6 Hz, 2H; H of furan), 4.14 (q, *J* = 7.2 Hz, 4H; H of CH_2), 1.13 - 1.09 (t, *J* = 7.2 Hz, 6H; H of CH_3) ppm.

Chapter 3

New Chromophores for Dye-sensitised Solar Cells

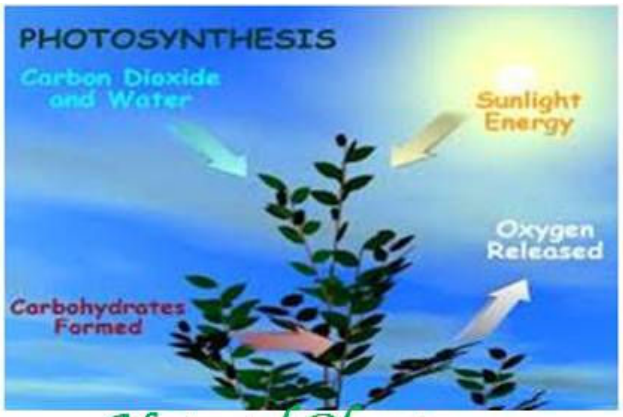

Natural Plants

Artificial Assemblies

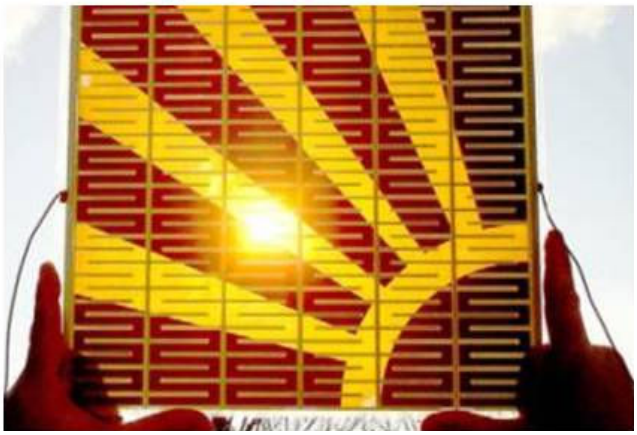

Selected molecular structures discussed in this chapter are shown below.

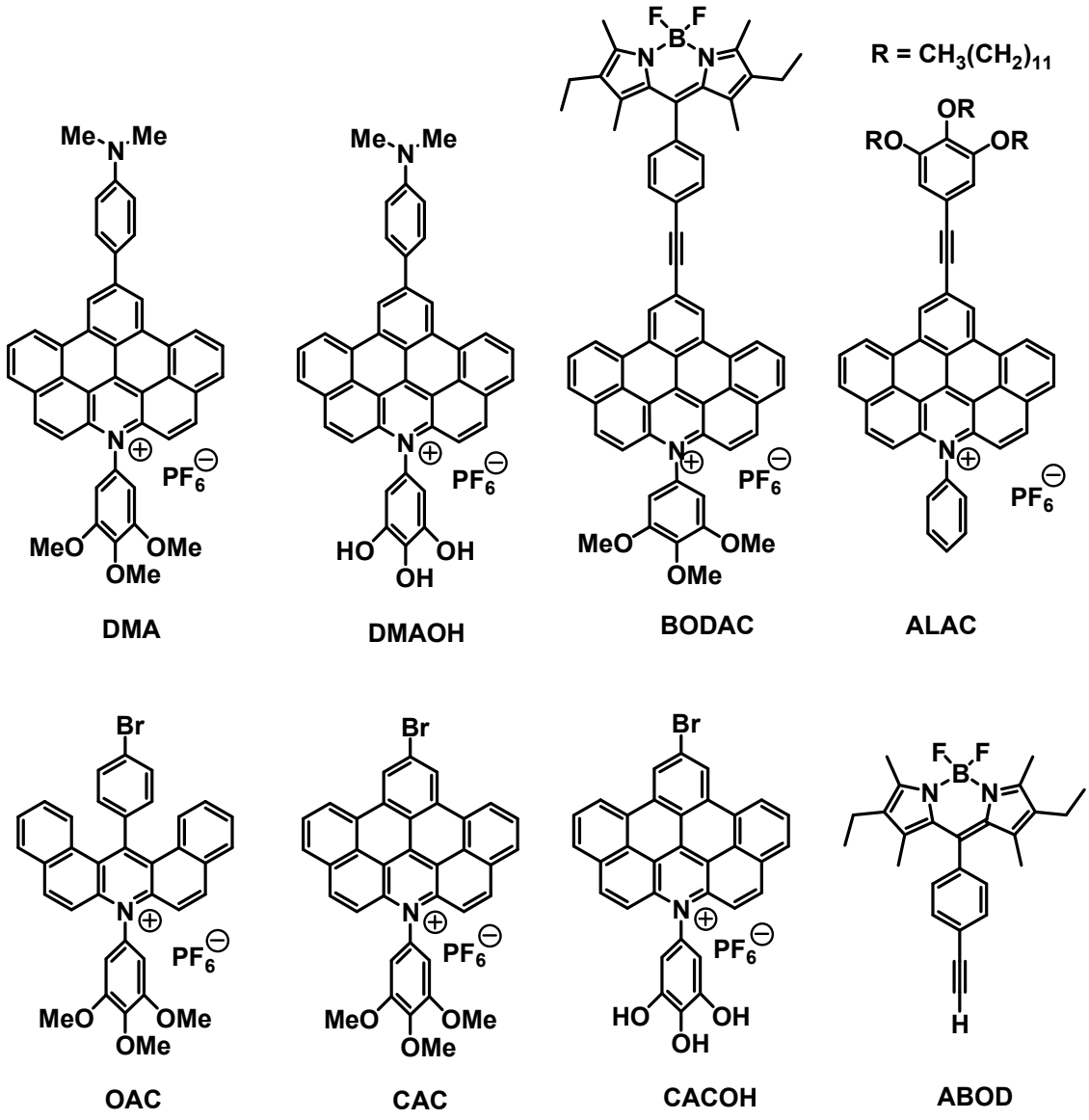

Those involved in this work are acknowledged. Thanks to Dr Ross W. Harrington for the characterisation of crystal structures, to Prof. Nikolai V. Tkachenko's group with the help of calculation for charge transfer process and transient absorption measurements, to Dr Corinne Wills for her help with temperature dependent NMR experiments and finally to Dr Libby Gibson's group for their help on dye sensitised solar cell measurements.

3.1 Introduction

Since the first report of a 7% efficient dye sensitised solar cell (DSSC) by O'Regan and Grätzel,[1] extensive efforts have been devoted to the development of more sophisticated cells with better performance[2]. Over the last 20 years the recorded efficiency has increased steadily, and a recently reported efficiency was quoted as above 12%[3]. In order to improve performance of a DSSC we have to understand certain aspects of efficient natural photosynthesis. One of the central components of natural photosynthesis is the photosynthetic reaction centre complex. The structures of the reaction centres and the light harvesting antennae[4] have been revealed by biophysicists and protein crystallography. Highly organised chlorophyll molecules are capable of moving photons over large distances, and directing them to the reaction centre in the protein environment. There are still no artificial molecular dyads which are capable of transferring photons to a reaction centre with the efficiency seen in natural photosynthesis. One difficulty encountered in artificial photosynthesis is mimicking the efficient and directional charge separation seen in the natural reaction centre[5, 6]. However, despite many set backs we are still making promising progression. For example, "artificial leaf molecular dyads" has been reported by Ziessel *et al.*[7]. In their work they showed that it was possible to manufacture artificial light harvesting arrays which are capable of collecting photons and transferring energy over a relatively large distance to specific sites.

There are usually two approaches in the search for efficient photosynthesis reaction centre mimics; the cascade approach and simple molecular dyads[8]. Based on the cascade approach, numerous efforts have been devoted to the synthesis of different molecular triads[9], tetrads[10], pentads[11] to achieve reasonable charge separation distance, and to tune the absorption of light of different components. More recently, research has also started to pay attention to elaborate three-dimensional molecular arrays, such as

polymers[12], dendrimers[13], and quantum dots dispersed in a polymer film[14]. The aim is to obtain reasonable charge separation (CS) lifetimes to improve the efficiency of solar cells. The disadvantages of this approach is the long synthesis routes and usually low overall yield which makes cells expensive and limits their practical application. Alternatively, the design of simple molecular systems provides a relatively easier and faster way to test the reliability of DSSCs[15]. In principle, slower energy wasting charge recombination can be achieved from orthogonally arranged donor–acceptor dyads. However, they often suffer from localized triplet formation following charge recombination as intersystem crossing is a major decay route. Triplet state species can react with ground-state triplet oxygen to generate destructive singlet oxygen, which will react with the organic dyads and destroy the cells. Even though different sorts of problems are faced, the bridged donor-accepter based dyad approach still shows promise and has attracted the attention of researchers focusing on Bodipy-based (boron dipyrromethene-based) systems[16]. Here we turn our attention to use of a new chromophore developed in our group based on an expanded and highly planar acridinium-like framework (*Figure 1*)[17].

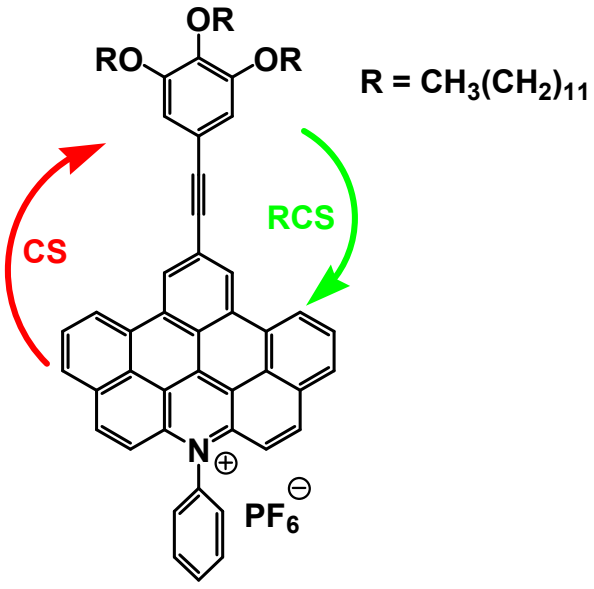

*Figure 1. Molecular structure of **ALAC** with arrows showing excited state electron transfer processes.CS = charge shift; RCS =reverse charge shift.*

Acridinium derivatives have been known for some time and their excellent performance

in different aspects such as biological sensors [18], molecular switches [19], and photocatalyst[20] make them ideal chromophores. There is no example of the application of acridinium derivatives as sensitizers in DSSCs to the best of our knowledge. Photophysical studies reveal that charge shift (CS) occurs in 5 ps following the excitation of **ALAC** by a short laser pulse. The excited state decays back through charge recombination (CR) in 80 ps. The descrimination between these two processes is 16 which is relatively poor. But an advantage of this molecular dyad is that the reverse charge shift does not populate the triplet state on the acridinium[17]. Based on this first successful design of new molecular dyads, our first target molecule is shown in *Figure 2*. *N,N*-dimethylaniline is the donor part of the molecular dye and the acridinium centre is the acceptor part, with the carboxylic acid acting as the anchoring group to attach to TiO_2 semiconductor surface. We expected that upon the irradiation with sunlight, the electron would transport form the donor to acridinium positive center and finally to the carboxylic acid end which is attached to a semiconductor surface.

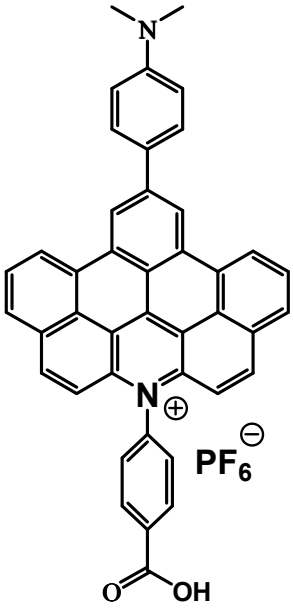

Figure 2. The first target molecular structure containing the carboxylate anchor group.

In this chapter is reported an example of a charge-transfer molecular dyad and an in-depth look into the charge transfer (CT) mechanism. It was also noticed that the acridinium dye did not suffer from population of the triplet state following charge recombination. We also tried to synthesise molecular dyads by coupling the acridinium

moiety with a bodipy moiety, the later unit is well known for its high molar absorption coefficient and high fluorescence quantum yield[21]. Even so, the fluorescence is still effectively quenched. Both of the dyes revealed that charge transfer is effectively taking place to quench the fluorescence[22]. The final obtained molecular dyes are promising sensitizer for DSSCs.

3.2 Synthesis

The synthesis of the target molecules was not straightforward and numerous problems had to be overcome as discussed in this chapter. The first attempted expanded acridinium derivative for the application of dye-sensitized solar cell application was **ACD3** and the synthetic route is shown in *Scheme 1*. Compound **ACR3** was obtained according to the literature reported method[23]. Claisen condensation of one equivalent of 4-bromo-benzaldehyde with two equivalents of 2-naphthol afforded **ACR1** in 78% yield, which required no further purification for the next step. Oxidation of **ACR1** with the mild oxidant lead dioxide in acetic acid afforded **ACR2**. The elimination of water from **ACR2** was performed in the dark to avoid the possible ring closure reaction, which did lead to complications in separation and a reduction in the reaction yield. Both polar (acetonitrile) and non-polar (dichloromethane) solvents were tried in the synthesis of compound **ACR3**. When the reaction was carried out in a solvent mixture of dichloromethane and acetic acid, the reaction was found to be an equilibrium process. Both starting material and product was found in the mixture and completion of the reaction was not achieved even after a long reaction time (2 days). The reaction performed in a mixture of acetonitrile and acetic acid was found to be more efficient. The ring closure reaction was not as clean as an unsubstituted derivative reported by Müller *et al.*[23]. The irradiation of a solution of **ACR3** in acetic acid under sunlight or halogen lamp (filtered through a water tank to remove long wavelength light) afforded mixture of different products which were not easily separated. Therefore, this suggested that the reaction carried out here undergoes different pathway as the reported one. After the consideration of the separation of the

mixture of salts or looking for alternative method, we decided to choose the later one.

One alterative way to reach the target molecule might be to insert the aniline derivative to xanthenylium before the ring closure reaction. No expected product was achieved when ethyl 4-aminobenzoate was refluxed with **ACR3** in freshly distilled THF or in NMP (1-methy-2-pyrrolidinone) in the presence of molecular sieves. We hypothesised that activation of the amine group perhaps might promote the reaction, at least according to the mechanism proposed by Müller *et al.* [23]. Therefore, we modified our target molecule to **DMA** (*Scheme 2*). The reaction between **ACR3** and 3,4,5-trimethoxyaniline in THF did not afford the expected product **OAC**. ^{1}H NMR analysis showed a mixture of products and after separation only the hydrolysis product, i.e., **ACR2** was obtained. It is very possible even a trace amount of water can drive the reaction to go backwards to compound **ACR3**.

Alternative conditions, i.e., reflux in NMP in the presence of molecular sieves, were tried and the product obtained was **ACR4** instead of **OAC** in a yield of 38%. Reactions under lower temperatures (80 ^{O}C and 150 ^{O}C) were also carried out, which afforded only the hydrolysis of the xanthenylium product, i.e., compound **ACR2**. The harsh condition was essential for the reaction. The ring-open form acridinium **OAC** was obtained in 66% optimised yield from **ACR4** following similar procedures used in the preparation of our first expanded acridinium derivatives[17] without any major problems. The structure was confirmed by NMR, MS and a crystal structure. There are only a few examples reported in the literature for the conversion of a xanthenylium salt to an acridinium[23]. The method developed here shows another possible way to obtain acridinium derivatives.

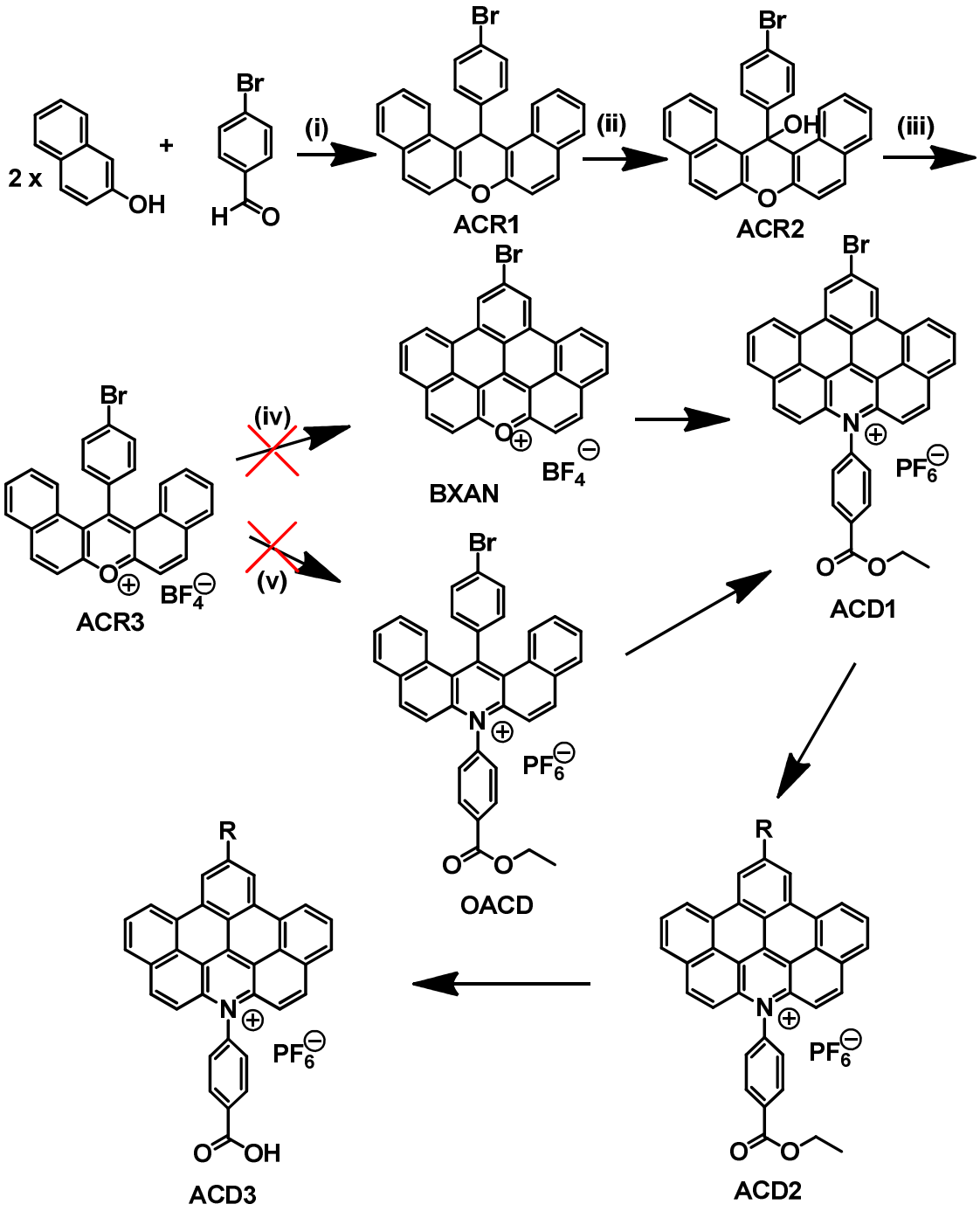

*Scheme 1. Reagents and Conditions: (i) Acetic acid, HCl (37%), reflux; (ii) PbO_2, acetic acid, reflux; (iii) acetic acid, acetonitrile, HBF_4, in dark; (iv) sunlight, acetic acid (v) ethyl 4-aminobenzoate, reflux. Problems were encountered in step (iv) and (v), so the target **ACD3** cannot be achieved.*

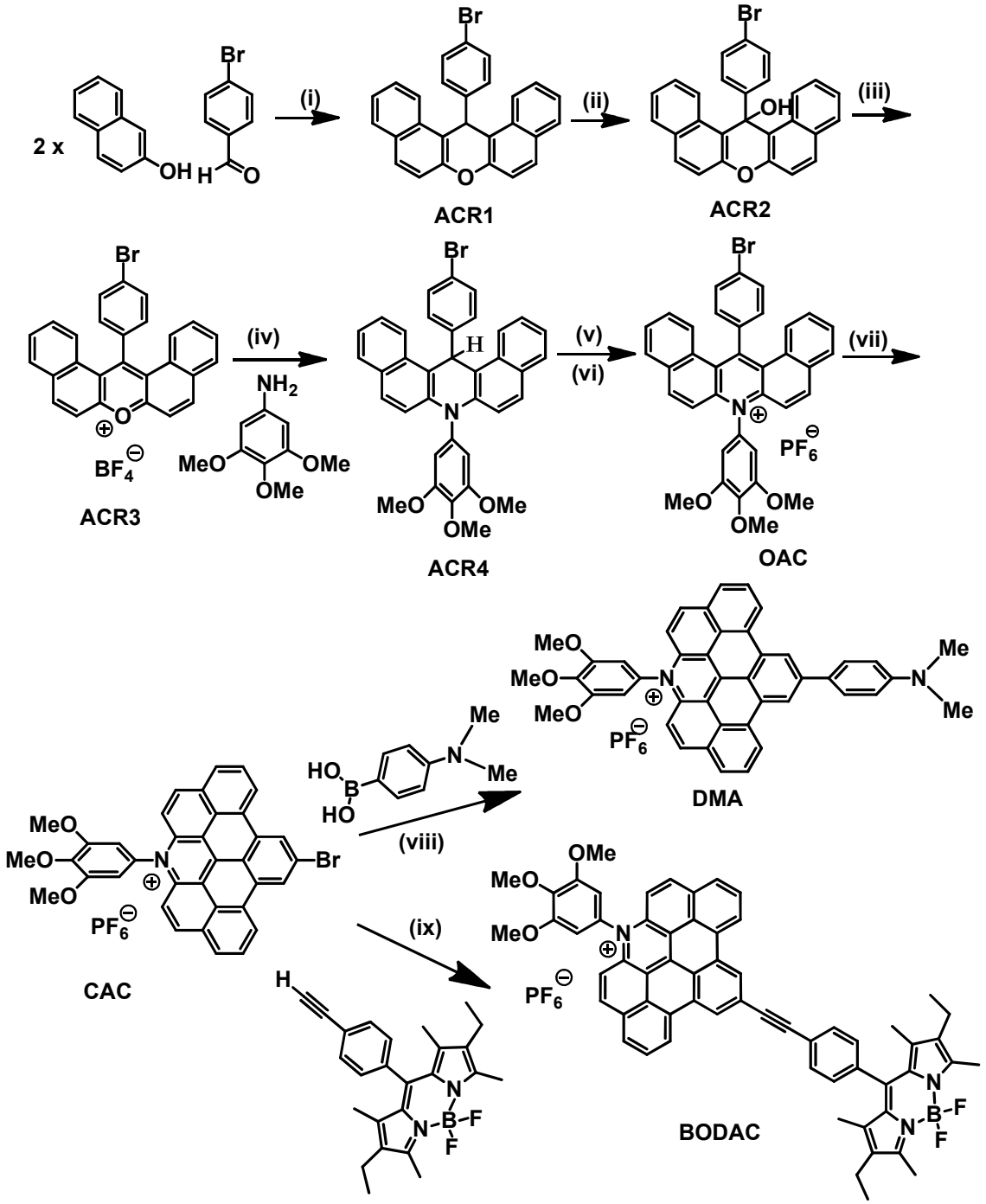

Scheme 2. Reagents and Conditions: (i) Acetic acid, HCl (37%), reflux; (ii) PbO_2, acetic acid, reflux; (iii) acetic acid / acetonitrile, HBF_4, in dark; (iv) molecular sieves, NMP, reflux; (v) MnO_2, acetic anhydride, HCl (g); (vi) HCl (37%), acetic acid; (vii) sunlight, acetonitile, water; (viii) $Pd(PPh_3)_4$, Na_2CO_3, DME, DMF, 95 ^{O}C.(ix) $Pd(PPh_3)_4$, CuI, Et_3N, DMF, 80 ^{O}C.

A photo-illuminated ring closure reaction afforded **CAC** in very good 92% yield. The ring closure reaction was extremely slow in pure acetonitrile as monitored by ^{1}H NMR spectroscopy. No product was obtained even after several weeks under sunlight illumination. The addition of one equivalent of water in the solvent sped up the reaction

dramatically. The colour of the solution changed from yellow to orange after one day's illumination under sunlight, and as the reaction proceeded an orange solid precipitated out of the solution. The reaction was monitored by ^{1}H NMR spectroscopy until no starting material was observed. Different reaction paths / mechanisms have been proposed for the similar ring-closure reaction, including the half-closed product proposed by Dilthey *et al.*[24] and fully closed product suggested by Benniston and co-workers[25]. In this experiment, no half-closed product was seen in the ^{1}H NMR spectrum. It is interesting to note that every ^{1}H NMR spectrum obtained showed only the starting material and the fully-closed product and changes in their ratios (see details in ^{1}H NMR spectral data). It is not possible to monitor the intermediate of the reaction by ^{1}H NMR spectroscopy. Short-lived radical intermediates could be a possibility involved in the reaction. Four hydrogens must be lost during reaction, and the possible acceptor under the reaction conditions applied here is the acetonitrile molecules. The acetonitrile could possibly be reduced to ethanimine or ethanamine, or alternatively it is possible that there is hydrogen gas released during the reaction. Further experiments are needed to confirmed these proposals. Standard Suzuki coupling reaction between **CAC** and N,N-dimethyl-4-phenyl-boronic acid afforded dark purple **DMA**. Sonogashira coupling of **ABOD** and **CAC** resulted in reddish **BODAC**. Demethylation of **CAC** and **DMA** afforded **CACOH** and **DMAOH**, respectively (*Scheme 3*).

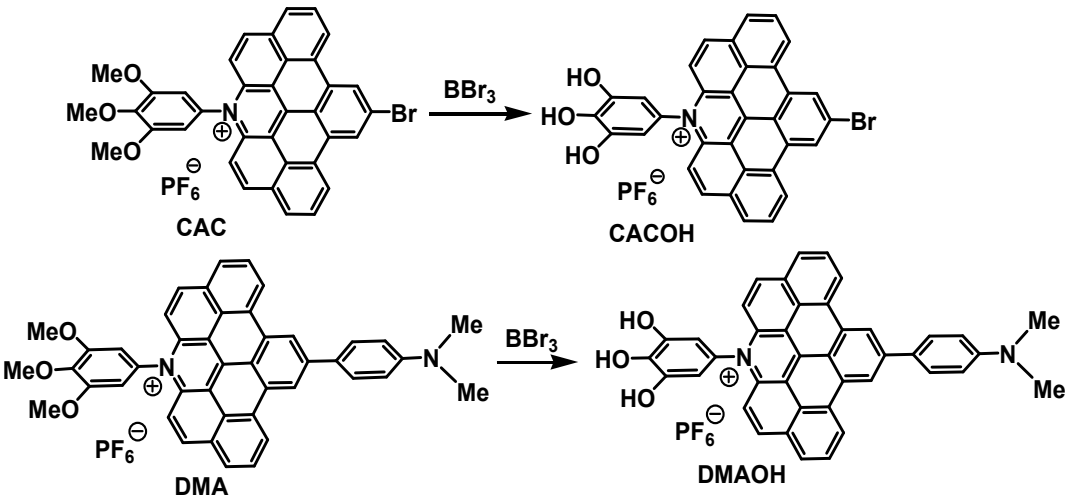

Scheme 3. Reagents and Conditions: BBr_3, -78 ^{O}C for 2 hours then room temperature overnight.

A different route to the other dyads (**CBOD1**) by coupling the expanded acridinium and BODIPY moieties was tried (*Scheme 4*). The difference between **BODAC** and **CBOD1** is the distance between the donor-acceptor units, which should result in a change in the photophysical properties such as the charge transfer lifetime, charge recombination lifetime and fluorescence quantum yield. However, the problem was encountered in step (vi), where oxidation of **HBOD** with either PbO_2, or MnO_2 did not give a satisfactory yield. Mass spectrometry analysis showed that another product, with the same mass as **OHBOD**, was obtained as well. Even extensive column chromatography did not afford pure enough **OHBOD**. The reaction of **ACR6** under standard BODIPY synthesis reaction did not afford the expected product **OHBOD** as well. Finally conversion of **ACR6** to the xanthenylium derivative then insertion of aniline, applying similar reaction conditions as for the synthesis of **ACR4** from **ACR2**, was also tried. The xanthenylium derivative was obtained but the insertion of the aniline to the oxygen centre failed.

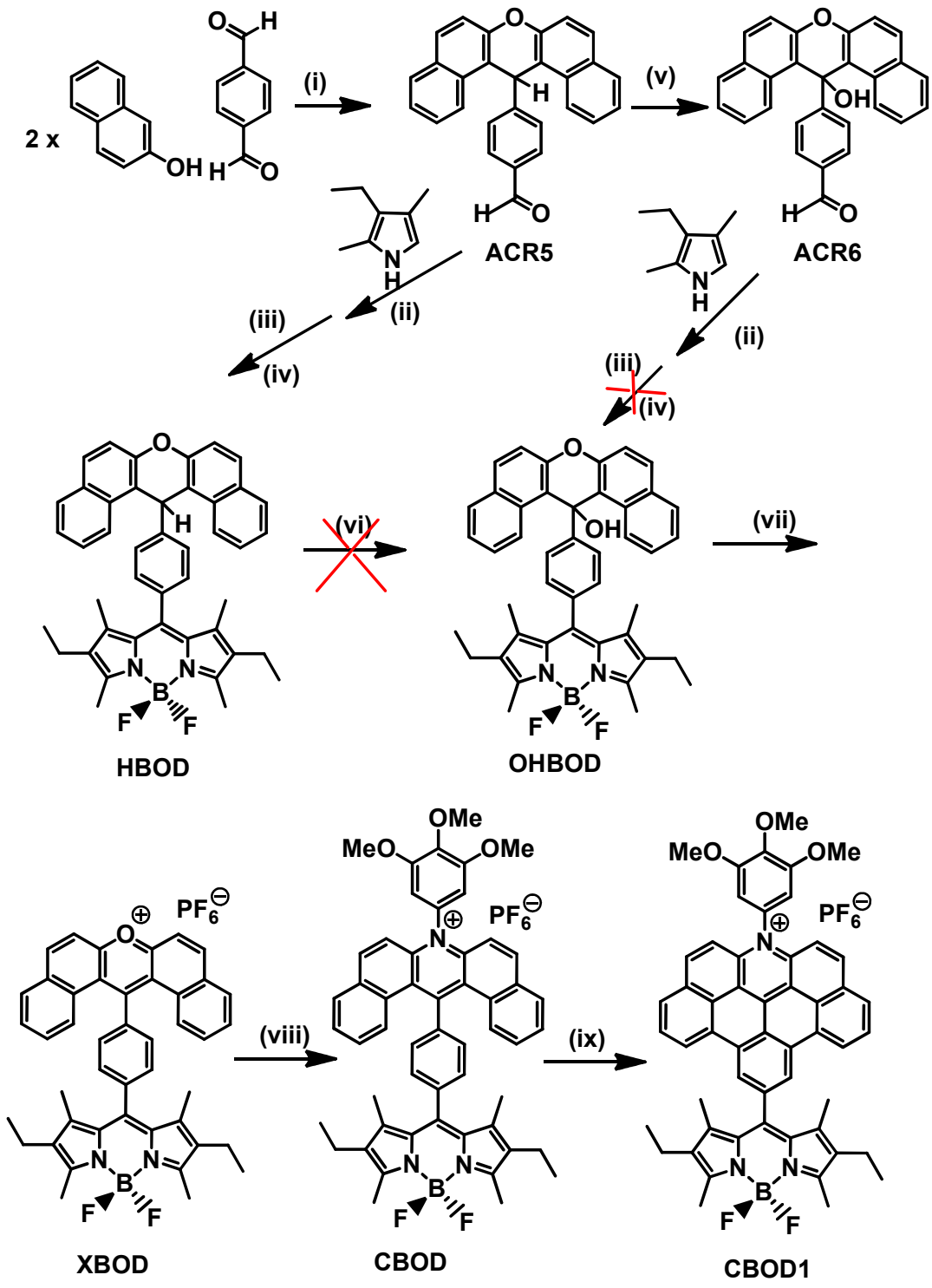

*Scheme 4. Reagents and Conditions. (i) Acetic acid, HCl (37%), reflux; (ii) N,N-dimethyl-p-phenylenediamine, trifluoroacetic aicd, DCM; (iii) dichlorodicyanobenzo quinone ; (iv) $BF_3.Et_2O$, (v) PbO_2, acetic acid, reflux; (vi) PbO_2, acetic acid, reflux; or MnO_2, acetic anhydride, HCl (g); (vii) HCl (37%), acetic acid, KPF_6; (viii) 3,4,5-trimethoxyaniline / THF; (ix) sunlight, acetonitrile, water. The target molecule **CBOB1** was not achieved as problems were encountered in synthesis of **OHBOD** indicating by red crosses.*

3.3 ^{1}H NMR spectral data

The ring closure reaction from **OAC** to **CAC** was monitored by ^{1}H NMR spectroscopy, as presented in *Figure 3*. As we can see from the aromatic region of the spectra (*Figure 3, (1) to (4)*), as the ring closure reaction proceeded the spectrum started to become more complicated showing a mixture of **OAC** and **CAC** (*Figure 3, (2) to (3)*). Finally, only the peaks corresponding to **CAC** were observed. The aliphatic region of the spectra (*Figure 4*) for the tri-methoxy group also clearly indicated the evolution of the reaction. Only two peaks at 3.81 ppm and 3.96 ppm were observed for **OAC** and as the reaction proceeded two additional peaks appeared, and the reaction was complete when only two downfield peaks at 3.86 ppm and 4.01 ppm were observed.

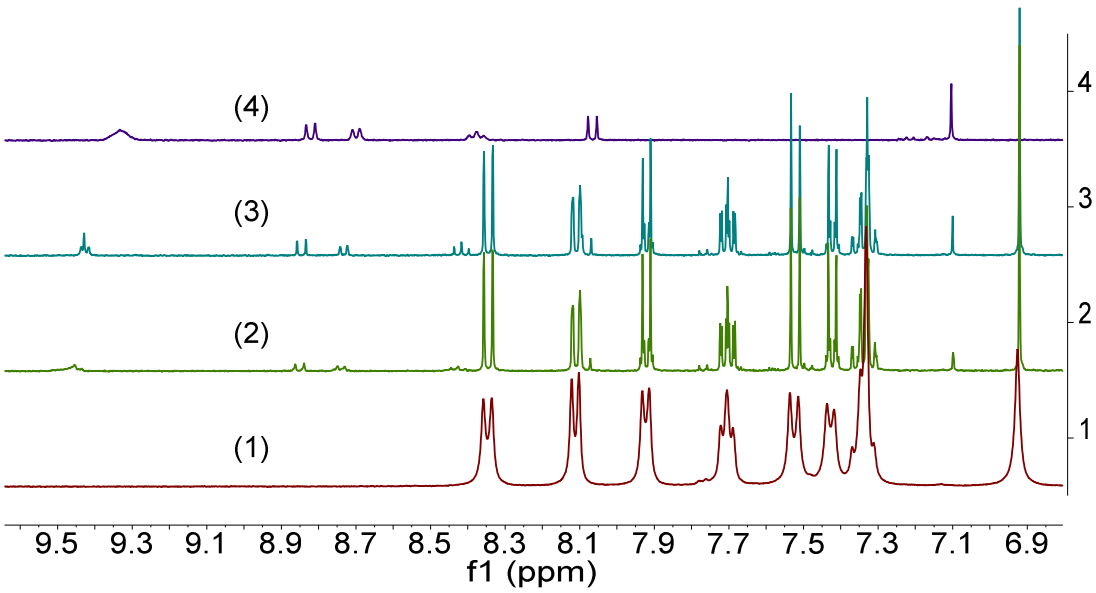

*Figure 3. ^{1}H NMR spectra for the aromatic region of the photo irradiation reaction from **OAC** to **CAC**, as the time move on the spectra changed from (1) to (4).*

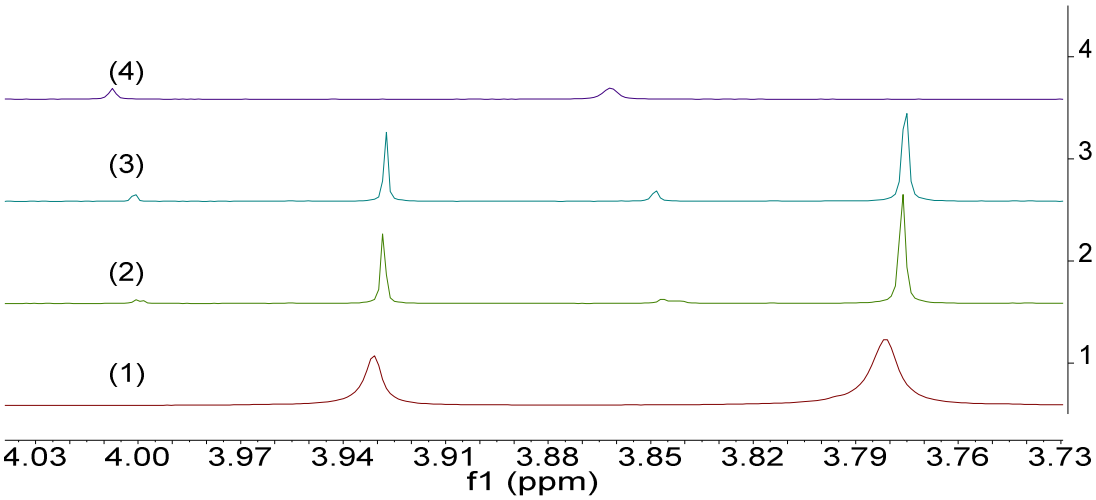

*Figure 4. The ^{1}H NMR spectra for the aliphatic region, trimethoxy group, of the photo irradiation reaction from **OAC** to **CAC**, as the time move on the spectra changed from (1) to (4).*

The spectra of both **OAC** and **CAC** are shown in *Figure 5* and *Figure 6*. One singlet with chemical shift at 6.95 ppm was observed for **OAC** corresponding to *proton a* (*Figure 5*) and this proton was shifted downfield to 7.10 ppm in **CAC** (*Figure 6*). The other singlet assigned to *proton b* for **CAC** overlapped with a doublet and appears as a broad singlet at 9.33 ppm.

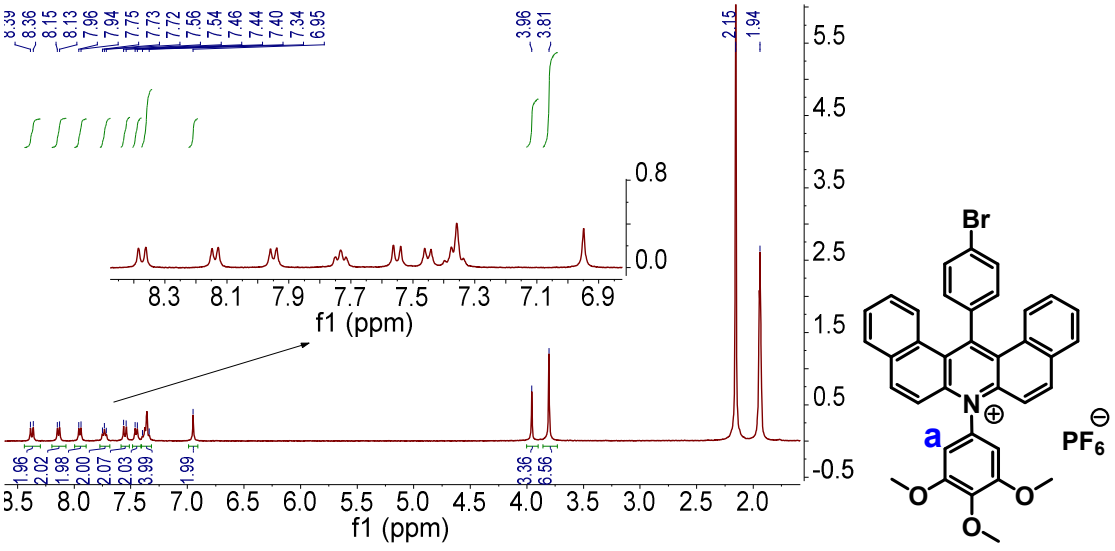

*Figure 5. The ^{1}H NMR spectrum, and the expanded aromatic region for **OAC**, recorded in CD_3CN at RT.*

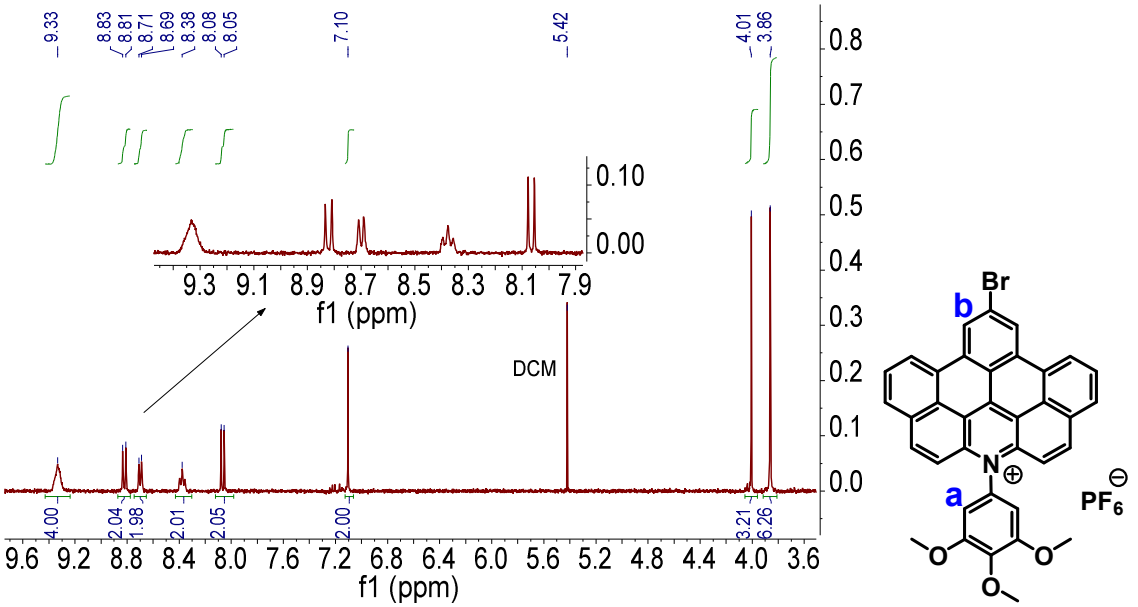

*Figure 6. The ^{1}H NMR spectrum for **CAC** recorded in CD_3CN at RT. The insert shows the expanded region for the aromatic protons.*

A COSY spectrum (*Figure 7*) of **DMA** was taken to help with identification of the aromatic protons. The assignment of protons in different positions (*Figure 8* and *Table 1*) are analysed as follow:

(1) *Proton i* and *c* should appear as singlet and the peak corresponding to *i* is upfield relative to *c* as indicated from spectra of **OAC** and **CAC**.

(2) There is only one apparent triplet (it is actually a doublet of doublet which have very similar coupling constant and overlap with each other) which can be readily assigned to *e* and a COSY correlations between *e* and *d* and *e* and *f* were observed. But with the data obtained is not possible to give concluding identification of the peaks.

(3) *Proton a* and *b* belongs to a single aromatic ring (in the ring of *N,N*-dimethylaniline) and their chemical shifts are expected to be upfield in comparison to those in the expanded acridinium part. *Proton a* is expected to be more shielded, as the strong electron donor *N,N*-dimethyl group is closer to *proton a*, therefore it is able to accept electron density from the N,N-dimethyl group.

(4) The final two doublet peaks should belong to *g* and/or *h*. Considering the strong deshielding effect from the positive quaternary nitrogen the downfield peak was assigned to *h*.

(5) The ratio of the integral between *k* and *j* is 3 / 6, therefore the peak with a chemical shift of 4.07 ppm was assigned to *k*. Finally the only peak left is *l*.

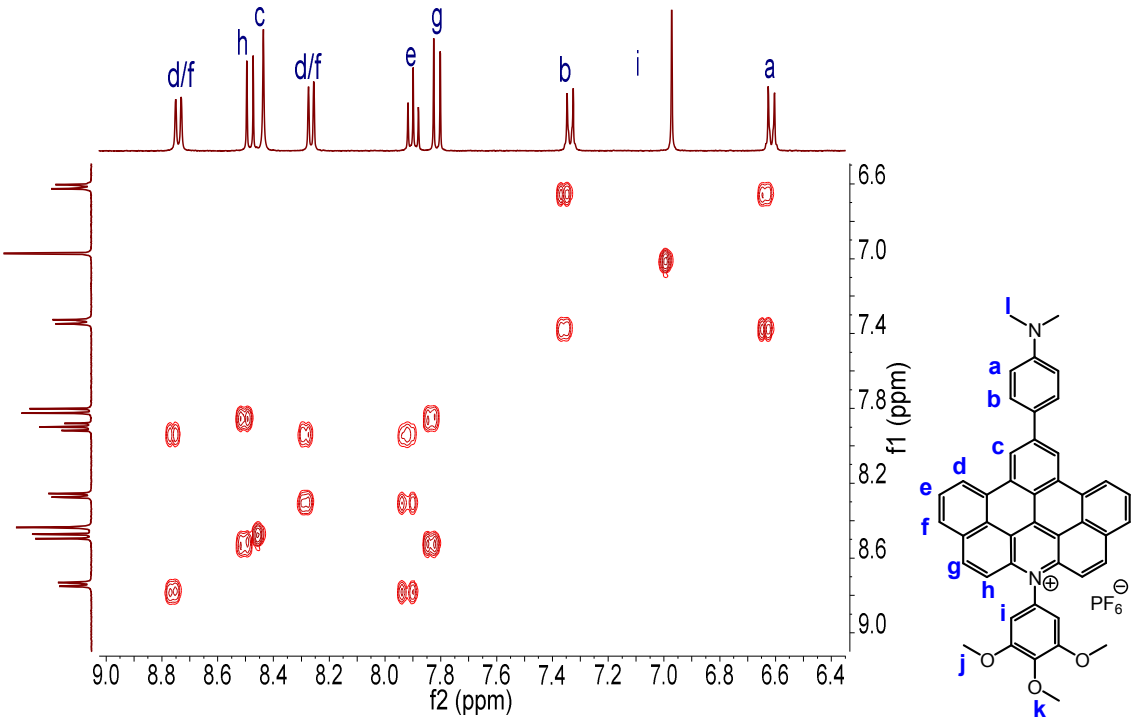

*Figure 7. The aromatic region for the COSY spectrum of **DMA** recorded in CD_3CN in RT.*

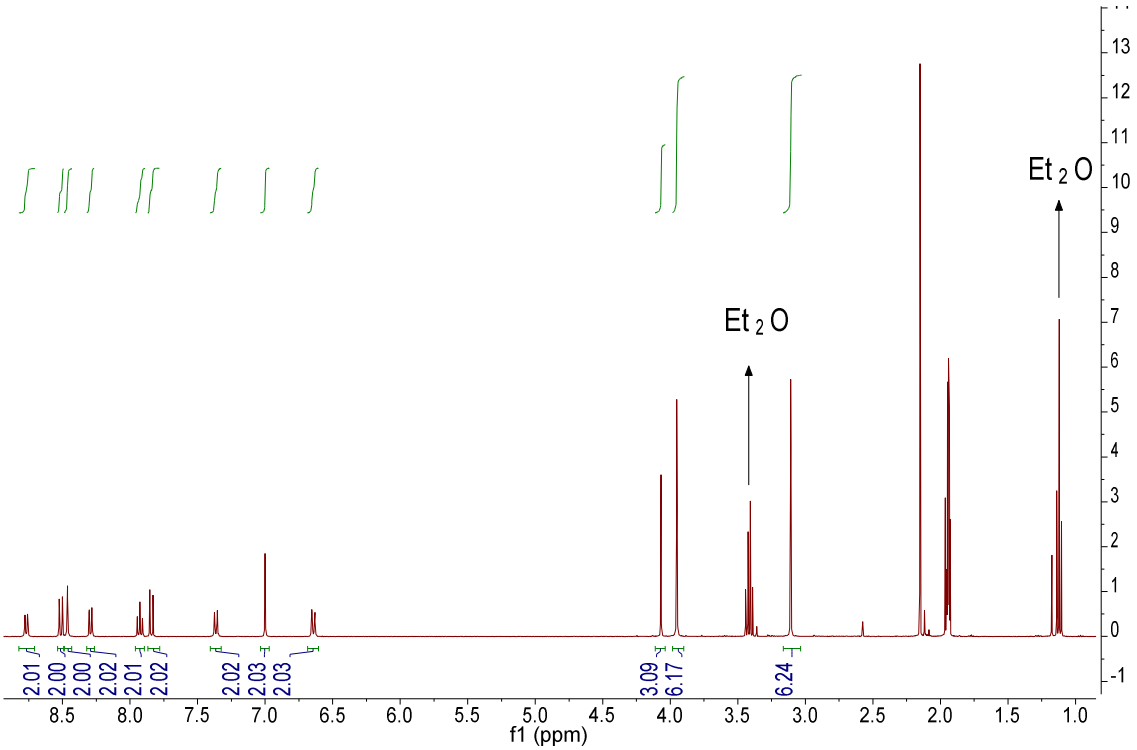

*Figure 8. The ^1H NMR spectrum of **DMA** recorded in CD_3CN in RT.*

*Table 1. The ^1H NMR peak assignment for **DMA** in CD_3CN in RT.*

Chemical shift (to 2 d.p) (ppm)	Intensity (no. of H atoms)	Multiplicity	Assignment
8.78	2	d	d/f
8.52	2	d	h
8.46	2	s	c
8.30	2	d	d/f
7.93	2	apparent t	e
7.85	2	d	g
7.38	2	d	b
7.00	2	s	i
6.65	2	d	a
4.07	3	s	k
3.95	6	s	j
3.10	6	s	l

Temperature dependent ^{1}H NMR spectra were collected for **DMA** (*Figure 9*), a downfield shift trend (the spectra were corrected to reference CH_3CN) was observed for protons in aromatic rings as the temperature increased from 294K to 348K. Aliphatic protons did not exhibit any changes within this temperature range. The chemical shifts corresponding to protons of Et_2O, another internal reference, did not shift as well. Besides these non-exchangeable protons, the protons for the **HDO** molecule displayed an opposite shift trend, i.e., upfield shift with the increasing temperature relative to those in the aromatic rings. Plots of the peaks positions (δ) against temperature (T) indicated a linear relationship between these two parameters (*Figure 10*). Usually, aggregation[26], π-π stacking[27] and hydrogen bonding[28] are the possible reasons for the observation of concentration dependent spectra. Temperature, concentration and solvent dependent ^{1}H NMR for exchangeable protons is well known[29]. There are a few reported concentration dependent examples which lead to cross-over of the signal for non-exchangeable protons. Mitra and co-workers reported a study of concentration dependent hydrogen chemical shifts of non-exchangeable proton of aromatic protons in a single solvent[30]. It was confirmed that in electron-rich acridine (*Figure 11*)[30], H_9 exhibited the most significant shift in $CDCl_3$. A summary of the gradients from plots

corresponding to the proton shifts (*Table 2*) revealed that the largest peak shift was seen for *hydrogen c* of **DMA**; an increase of 0.55 ppm for a temperature change from 294 K to 348K. A crossover of the *proton c* and *proton g* was indicated at 294K.

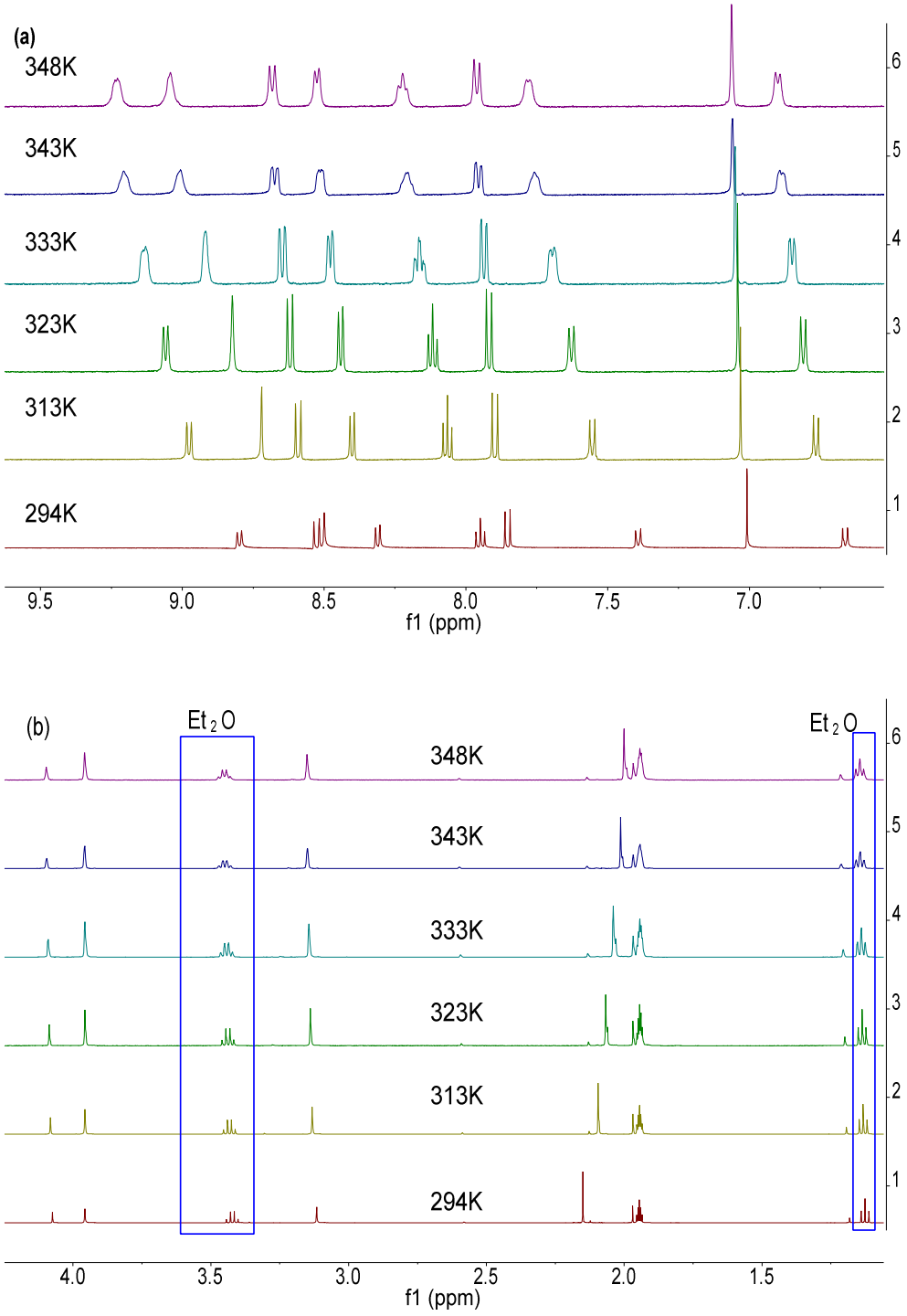

*Figure 9. Temperature dependent ^{1}H NMR spectra for **DMA** measured in CD_3CN. The blue box shows the peaks corresponding to diethyl ether, both acetonitrile and diethyl ether can be used as internal references. (a) Aromatic region; (b) aliphatic region.*

There is no quantitative explanation for the temperature dependence shift, but there are following possible reasons which could lead to this phenomenon. One main reason could be electrostatic interaction; there are cations and anions which may be in some form of association/dissociation equilibrium. In solution it is likely that with increasing temperature the solvent cage will break down and the distance between positive and negative ions decreases. A decrease in electron density at the aromatic group would result in a downfield shift for protons in the NMR spectrum. The other possible reasons could be hydrogen bonding (between fluorine atoms and protons), aggregation, π-π stacking along the planar expanded acridinium ring and the effect of intermolecular charge transfer. Exchange of $[PF_6]^-$ with the other anions (e.g. $[B(C_6H_5)_4]^-$ and $[B_{12}H_{12}]^{2-}$) can help us to identify the influence of electrostatic interaction in the temperature dependence NMR spectra. Concentration dependence experiments can provide further information for the identification of aggregation effects.

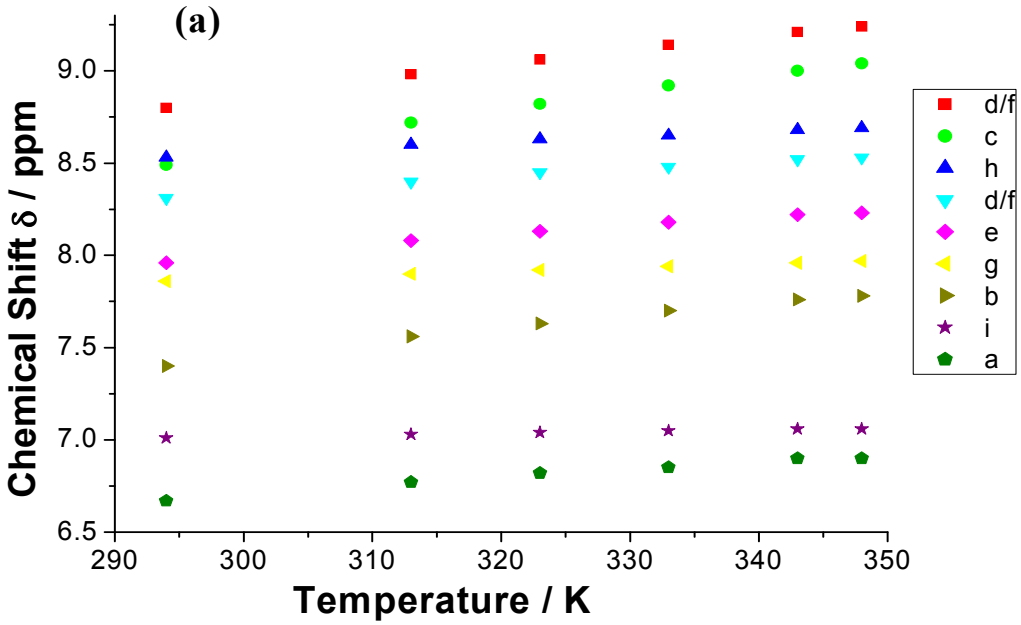

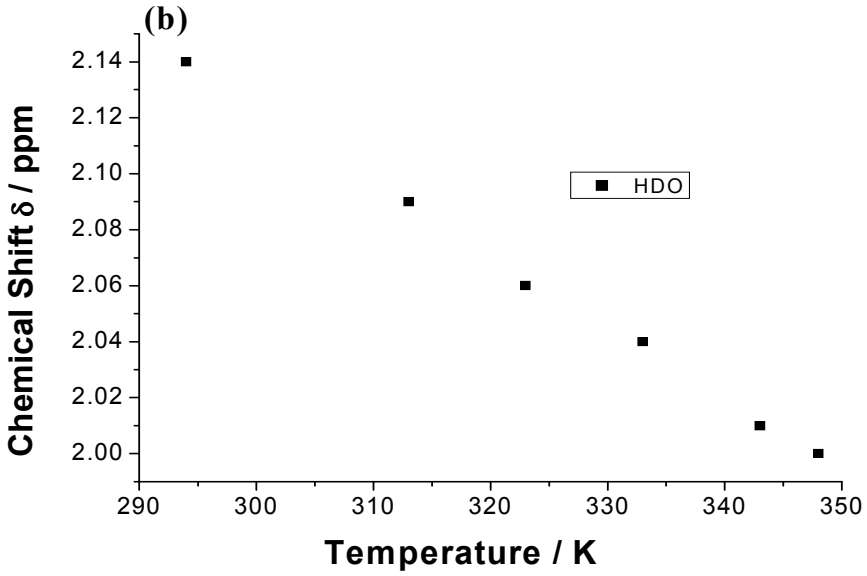

*Figure 10. Plots of hydrogen chemical shifts (δ) against temperature ranging from 294 to 348 K. (a) Aromatic region; (b) Hydrogen in **HDO**.*

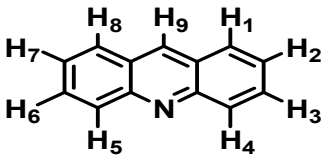

Figure 11. Example of an acridine studied by Mitra et al.

Table 2. Slopes obtained from the linear relationship between chemical shifts and temperatures.

Proton	d/f	c	h	d/f	e	g	b	i	a	HDO
Slope (ppm /K * 10^{-3})	8.1	10.1	2.9	4.1	5.0	2.0	7.1	1.0	4.3	-2.6

The presence of counter ion $[PF_6]^-$ was confirmed by ^{19}F NMR and ^{31}P NMR spectroscopies. The six fluorides are octahedrally arranged and they are chemically equivalent (have the same chemical shift). The nuclei spin for both ^{19}F (100%) and ^{31}P (100%) is 1/2. Therefore, ^{19}F NMR (*Figure 12*) appeared as a doublet due to the splitting from the directly-bonded ^{31}P nucleus, and the correspondingly spectrum for the ^{31}P nucleus (*Figure 13*) shows as a septet split by the six equivalent fluorine nuclei.

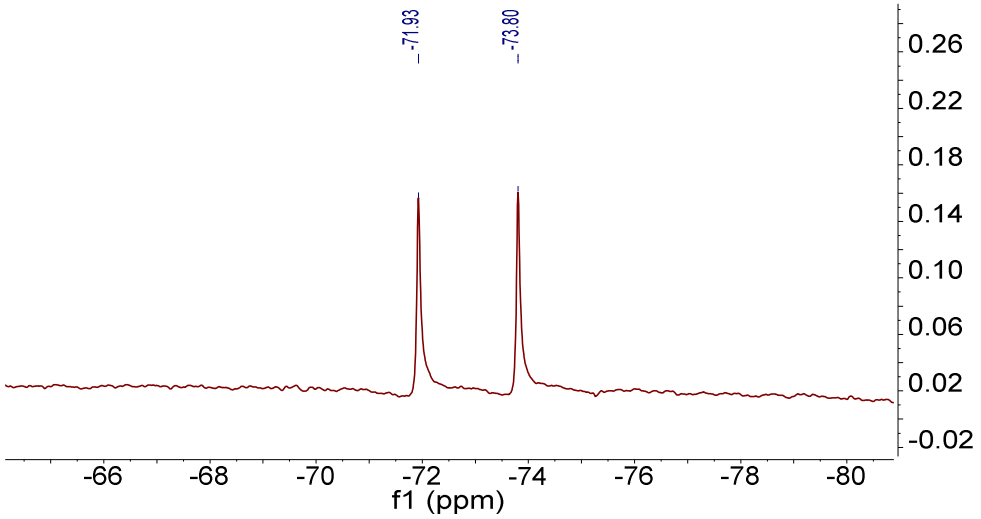

*Figure 12. ^{19}F NMR spectrum for **DMA** measured at CD_3CN.*

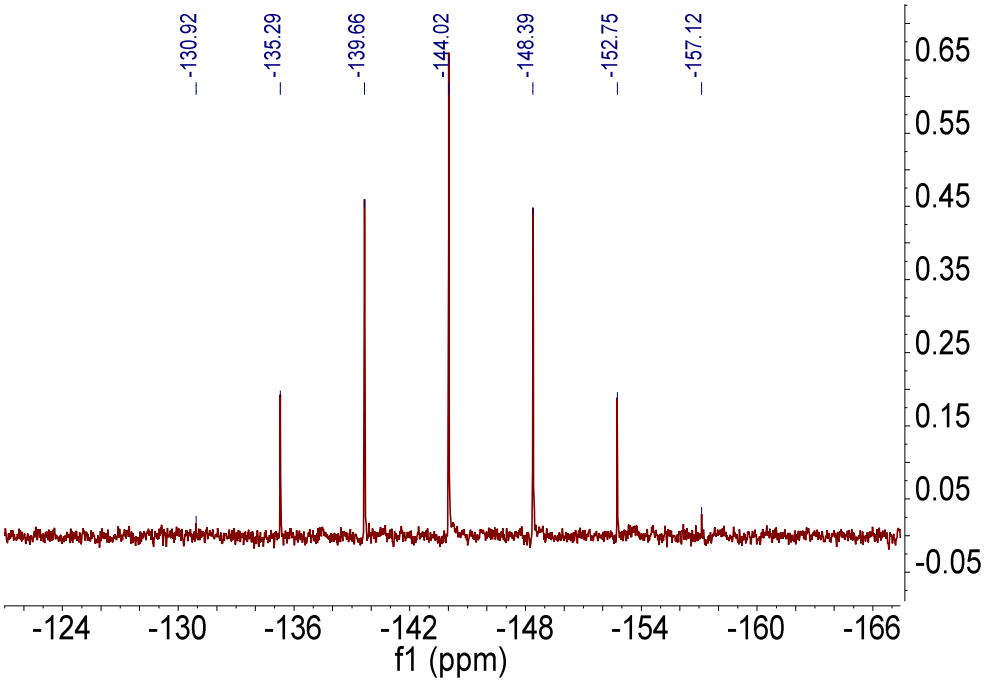

*Figure13. ^{31}P NMR spectrum for **DMA** measured in CD_3CN.*

3.4 Crystal structures

X-ray diffraction quality crystals of several intermediates were obtained during the synthesis. It was interesting to observe the elegant evolution of the structures from basic xanthene derivatives to the ring closed expanded acridinium derivatives. The geometry of product **ACR1** (*Figure 14*) shows as a T-shape structure with the phenyl ring almost perpendicular to the xanthene core. The dihedral angle is 87^{O} between the planes

creating along the xanthene core and the phenyl ring. Two naphthalene rings are symmetrical to the central pyran ring.

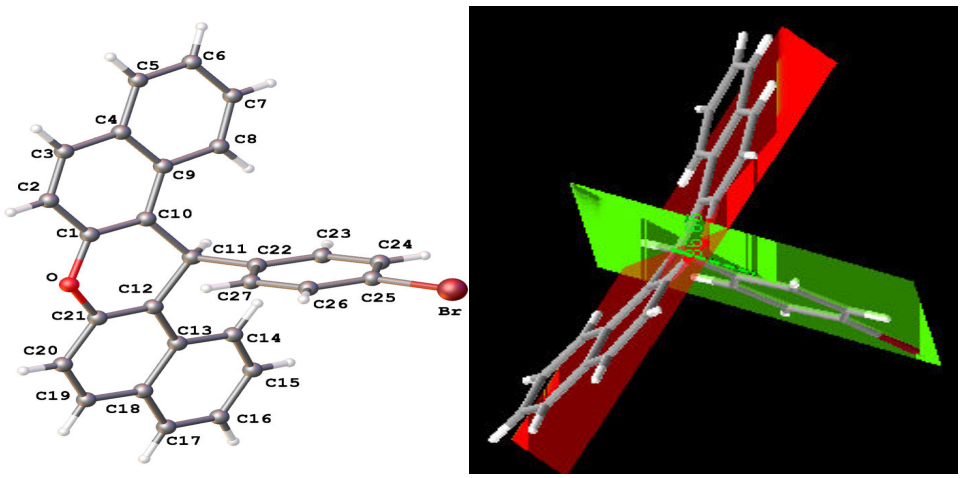

*Figure 14. Left: Molecular structure of **ACR1**; Right: the dihedral angle between xanthene core and the phenyl ring. Carbon (grey), oxygen (red), hydrogen (white), bromine (russetish).*

The oxidation and elimination reaction afforded xanthenylium derivative **ACR3**. The formation of the pyrilium ring increases aromaticity in the structure and forces the phenyl ring to be lifted up; the dihedral angle is 62^{O} (*Figure 15*). At the same time the two naphthalene rings are twisted to two sides of the pyran ring plane.

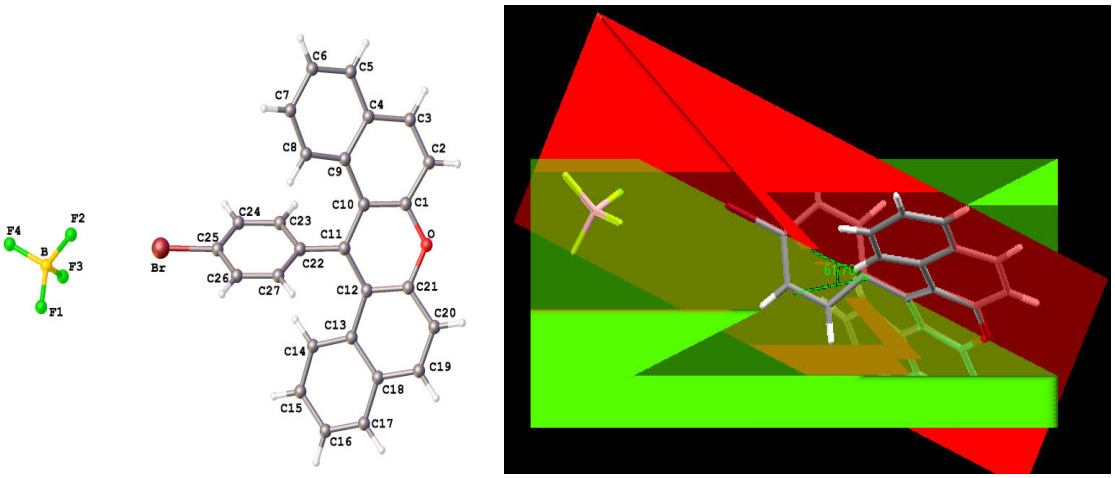

*Figure 15. Left: Molecular structure of **ACR3**; Right: Shows the dihedral angle between the phenyl ring and pyran ring. Carbon (grey), oxygen (red), hydrogen (white), bromine (russetish), boron (yellow), fluorine(green).*

Formation of the ring-open acridinium derivative **OAC** further increases the number of rings in the molecule. The two naphthalene rings on **OAC** are twisted to decrease the interaction with the two phenyl rings (*Figure 16*).

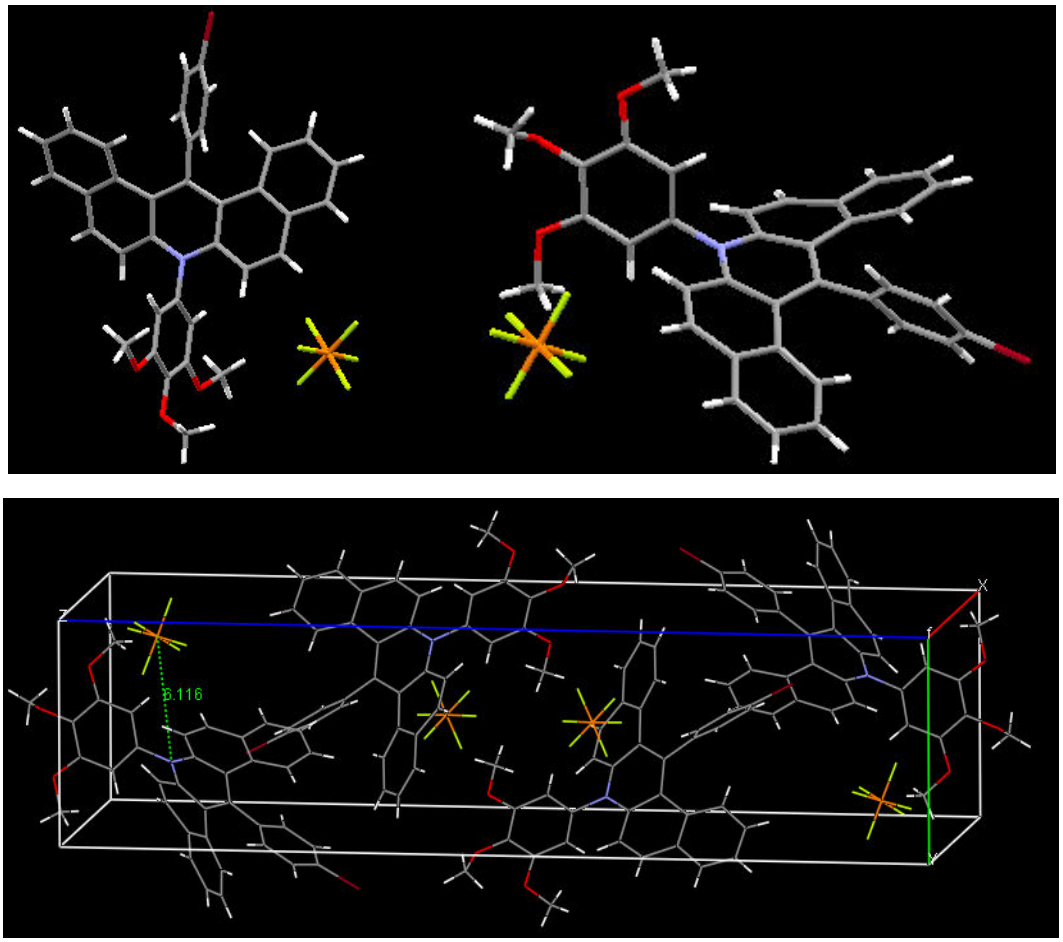

*Figure 16. Top: Molecular structure of **OAC**. Bottom: Packing diagram of **OAC**; carbon (grey), oxygen (red), hydrogen (white), nitrogen (blue), bromine (russetish), phosphorus (orange), fluorine(green).*

Upon closure of the ring a planar structure is constructed (*Figure 17*), containing eight six-membered rings. The packing of the structure displays a head-to-tail π-stacking motif. The PF_6^- counter ions appear to reside in between two nearest neighbour molecules (with the same orientation) at almost the same distance to the quaternary nitrogen centre, 5.7 Å. The crystal packing diagram for **CAC** shows interesting features.

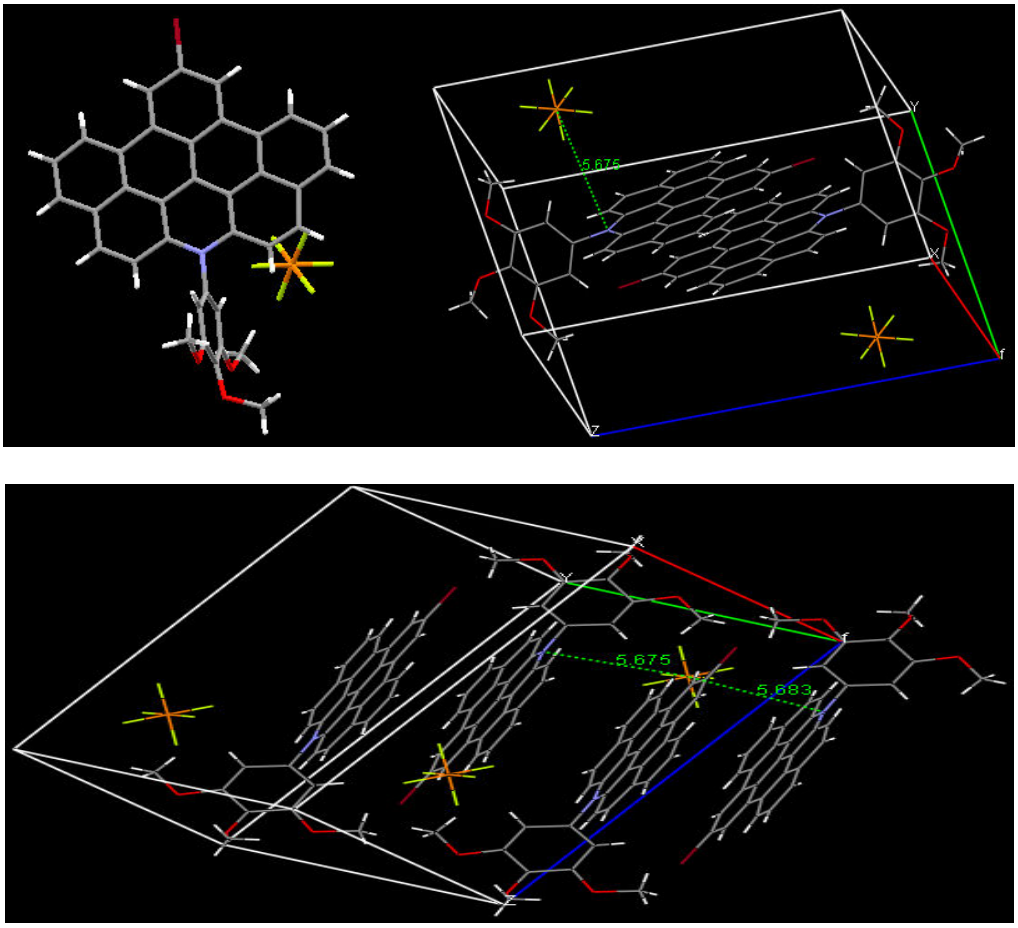

*Figure 17. Top: Molecular structure of **CAC**. Bottom: Packing diagram of **CAC**: carbon (grey), oxygen (red), hydrogen (white), nitrogen (blue), bromine (russetish), phosphorus (orange), fluorine(green).*

The molecular structure of **DMA** (*Figure 18*) appeared as two disparate asymmetric units. The other feature was the on-set of planarity between the *N,N*-dimethylaniline group and the expanded acridinium ring. The dihedral angles between planes created using the two ring systems, *N,N*-dimethylaniline group and the expanded acridinium ring, are 24.98 ^{O} and 29.02 ^{O}. When planes were created using 3,4,5-trimethoxy-benzene group and expanded acridinium ring the dihedral angles were 69.87 ^{O} and 70.72 ^{O}. The molecules adopt head-to-tail packing as shown in the packing diagram. The 3,4,5-trimethoxybenzene and *N,N*-dimethylaniline groups appear in turn on the two sides of the aromatic rings. The distance between PF_6^- counter ions and the neighbouring quaternary nitrogen centres varied (4.6 Å, 5.4 Å and 5.6 Å), indicating that association strength between the cations and anions are not the same.

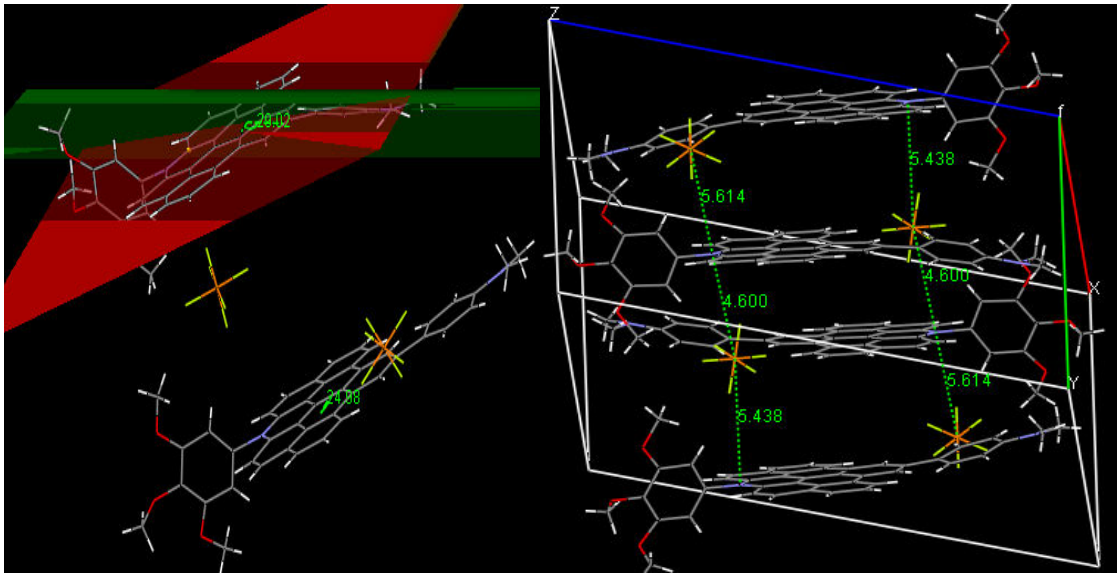

*Figure 18. Left: molecular structure of **DMA**. Right: Packing diagram of **DMA**: carbon (grey), oxygen (red), hydrogen (white), nitrogen (blue), bromine (russetish), phosphorus (orange), fluorine(green).*

3.5 Electrochemistry

The redox behaviour of acridinium derivatives was investigated in dry solvent (acetonitrile or dichloromethane) containing 0.2 M TBATFB background electrolyte by cyclic voltammetry (CV). All solutions were thoroughly purged with nitrogen before measurements. Both **OAC** (*Figure 19*) and **CAC** (*Figure 20*) showed two quasi-reversible one-electron reduction waves and no oxidation waves were observed within the applied potential window. Values (*Table 3*) for the half-wave potentials ($E_{1/2}$) of **CAC** were -0.67 V (78 mV) and -1.39 V (78 mV), vs. Fc^{+}/Fc, which are 0.17 V and 0.33 V more negative than those of **OAC**, respectively. The differences can be reasoned by the fact that the fully planar acridinium core of **CAC** enhances the conjugation effect from the tri-methoxy group. A conjugation effect of the lone pair of electron on bromine can increase the electron density on the positive centre of the acridinium core. Such effect would make **CAC** more difficult to reduce in comparison to **OAC**. It was reported previously that the reduction process of **ALAC** involved addition of two electrons to the acridinium ion core[17]; the addition of the first electron neutralised the ring and pushed the second reduction to a more cathodic potential. Similar reduction

processes occurred on the acridinium core for both **OAC** and **CAC**.

*Table 3. The redox potentials values of acridinium derivatives. E values vs. Fc^+/Fc ($E_{1/2}$ = 0.44 V). *oxidation of the trialkyloxybenzene group connecting with the acridinium core through a alkyne group.*

Compounds	E_1	E_2	E_3	E_4
OAC	-	-1.06 V (52 mV)	-0.50 V (80 mV)	-
CAC	-	-1.39 V (78 mV)	-0.67 V (80 mV)	-
ALAC	-	-1.81 V (110 mV)	-1.09 V (150 mV)	+0.89 V (180 mV)*
DMA	-	-	-0.71V (150 mV)	+0.87V (80 mV)
BODAC	-1.25 V (90 mV)	-1.16 V (78 mV)	-0.57 (85 mV)	+1.13 V (80 mV)

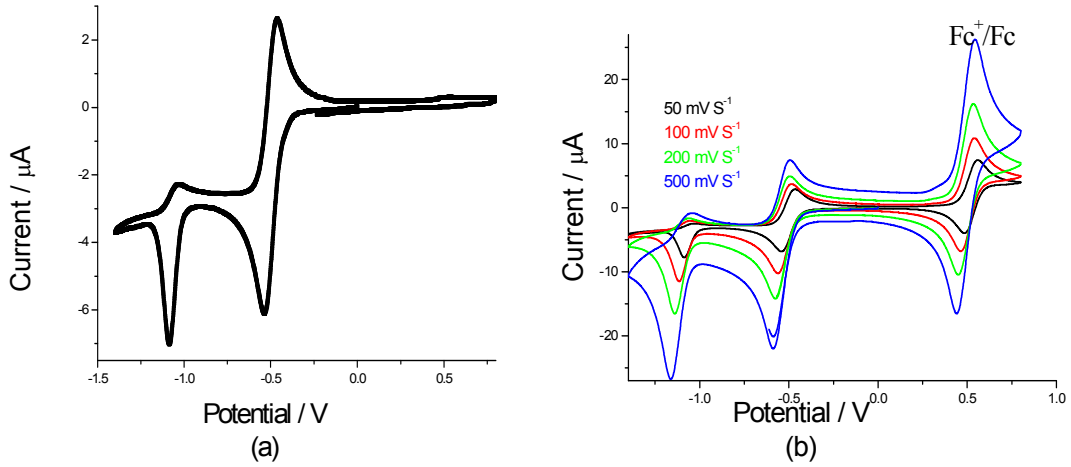

*Figure 19. Recorded cyclic voltammograms for **OAC** in dry CH_2Cl_2 (a) the scan rate was 50 mV s^{-1};(b) under different scan rates with ferrocene as internal reference, the current increased as the scan rate increased and the redox process can be repeated without any major changes.*

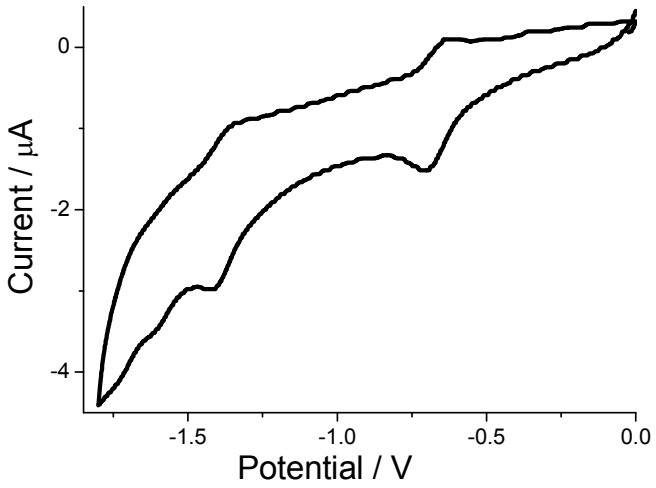

*Figure 20. Recorded cyclic voltammogram of **CAC** in dry CH_2Cl_2 (top).*

The CV of **DMA** was recorded in dry MeCN and only a single one-electron quasi-reversible wave at -0.71 V (150 mV) vs. Fc^+/Fc (*Table 3*) was observed within the negative scan portion. In comparison to **OAC** and **CAC**, it is obvious that the second reduction peak is not observed. If we ignore the difference of solvents used in the experiments, the value of the first reduction potential is more negative in comparison to **CAC**. Therefore, reduction is more difficult. It is very possible that the *N,N*-dimethylaniline is a relatively good electron donor which could result in an increase of electron density on the expanded acridinium rings. Therefore, after the addition of the first electron, the molecule became more difficult to be reduced relative to the same process in **CAC**. The reduction potential was shifted to more negative than -2.0 V, which is outside the experimental potential window. A quasi-reversible wave was seen at $E_{1/2}$ = 0.87 eV (80 mV) vs Fc^+/Fc in positive potential range, and it was readily assigned to oxidation of the *N,N*-dimethylaniline group in comparison to literature examples[31].

The oxidative scan for **BODAC** (*Figure 21*) was dominant by an one-electron quasi-reversible wave located at +1.13 V (80 mV). This wave corresponds to the oxidation of the bodipy part (in **ABOD** molecule). Three one-electron waves were seen on the

reductive scan, which was more complicated than the others. The first wave, -0.57 V (85 mV), was assigned to the reduction of the positive centre of the molecular framework, and the assignment of the second and third waves was not straightforward as they are located close to each other. One of the waves is associated with reduction of the acridinium core and the other one arose from reduction of the bodipy part. The Bodipy moiety played an opposite role to *N,N*-dimethylaniline, i.e., it was an electron acceptor relative to the acridinium core. This was deduced from the value of the reduction potentials in comparison to **CAC**. The addition of the Bodipy moiety makes the acridinium easier to be reduced, i.e., the reduction wave was seen at a less cathodic potential.

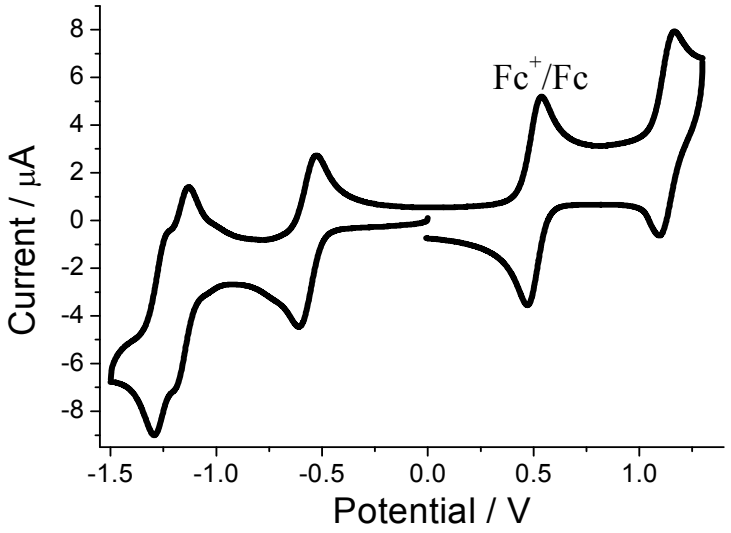

*Figure 21. Recorded cyclic voltammogram of **BODAC** in dry CH_3CN at the scan rate 50 mV s^{-1}.*

3.6 Molecular orbital calculations

The energy-minimised structure for **DMA** (*Figure 22*)[22] was calculated using Density Functional Theory (B3LYP, 6-311G) and the Gaussian O3 [32] package. The 3,4,5-trimethoxybenzene is almost perpendicular to the planar expanded acridinium ring which is in agreement with the crystal structure of **DMA**.

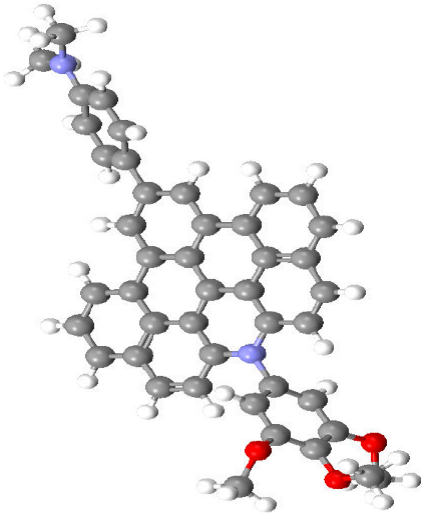

*Figure 22. Calculated structures for **DMA** using DFT.*

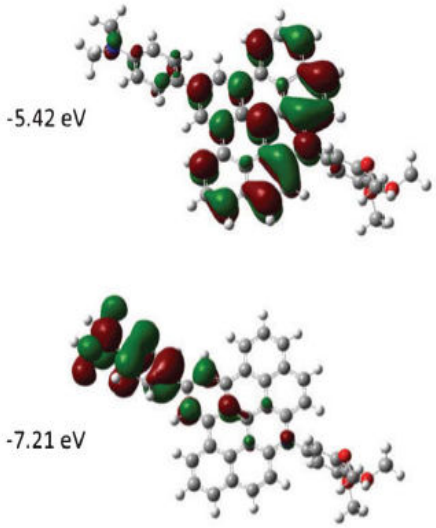

*Figure 23. Representation of the HOMO (bottom) and LUMO (top) for **DMA** as computed using Gaussian03 at the DFT level using B3LYP and a 6-311G basis set.*

The other feature was tending toward planar between the *N,N*-dimethylaniline group and the expanded acridinium ring. The dihedral angle between planes created using the two ring systems is only 31.7 ^{O} which is larger than that observed in the crystal structure (24.98 ^{O} and 29.02 ^{O}). This is consistent with the observation in electrochemistry that the electron is partially donated from the *N,N*-dimethylaniline to the quaternary nitrogen. Even so, the localisation of the HOMO and LUMO is still very distinct as shown in *Figure 23*. The majority of the HOMO is located on the *N,N*-dimethylaniline group and LUMO is on the expanded acridinium plane. The HOMO-LUMO gap is 1.79 eV somewhat similar to the experimental value 1.5 eV observed from electrochemistry. The

HOMO-LUMO gap is associated with the energy needed for the excitation of one electron from N,N-dimethylaniline donor part to the expanded acridinium ring acceptor part.

3.7 Photophysical measurements

3.7.1 Absorption and fluorescence

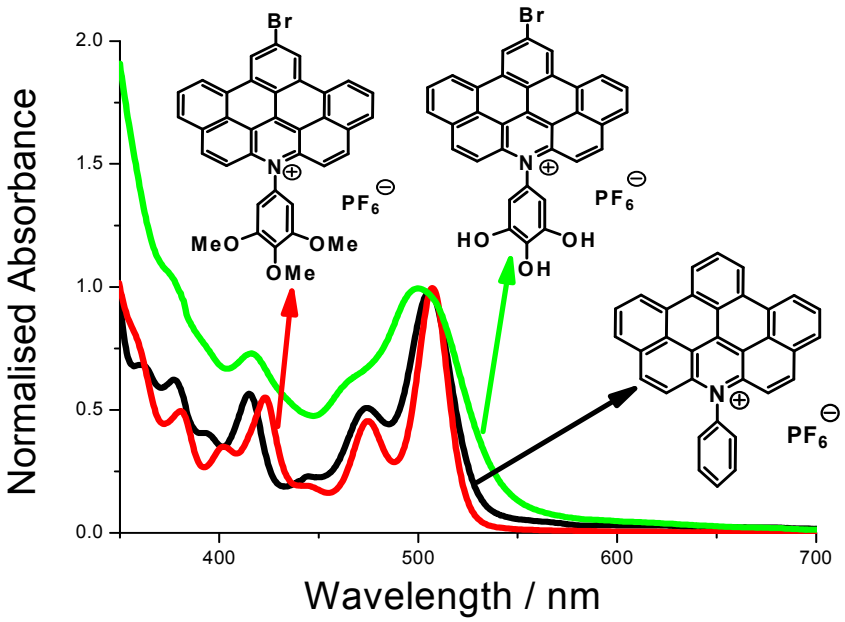

*Figure 24. Normalised room temperature absorption spectra of **ACBN** (black line), **CAC** (red line) and **CACOH** (green line) recorded in acetonitrile.*

Normalized electronic absorption spectrum for **CAC** in dilute acetonitrile is shown in *Figure 24*. It can be seen that orange coloured **CAC** exhibited multiple electronic transition bands with an intense peak maximum at 507 nm. The maximum absorption peak only red shift 1 nm in comparison to reference compound **ACBN** (*Figure 24*). The largest shift of the peak in visible range was observed at 422 nm (red shift 8 nm relative to **ACBN**). The peaks of **ACBN** were slightly broader than that of **CAC**. The absorption maximum for **CACOH** (*Figure 24*) is shifted to 500 nm and overlaps with a neighbouring less intense absorbance at about 472 nm, resulting in further broadening

of the peak. There are no significant "gaps" in the spectral window, at least up to around 540 nm, as seen for example in **ALAC** reported previously[17] and some porphyrin-based derivatives[33]. The broad absorbance will enhance the light absorbing efficiency in DSSC, but the defect of **ACBN** is the lack of strong absorption in red region. This is not true for **DMA** discussed in the following part, which is a dark purple solid. The most pronounced difference for the electronic transition spectrum (*Figure 25*) of **DMA** was the broad shoulder which tails off from the sharp band located at 506 nm when compared to the reference compound **ACBN**[22]. The absorption maximums are summarised in *Table 4*.

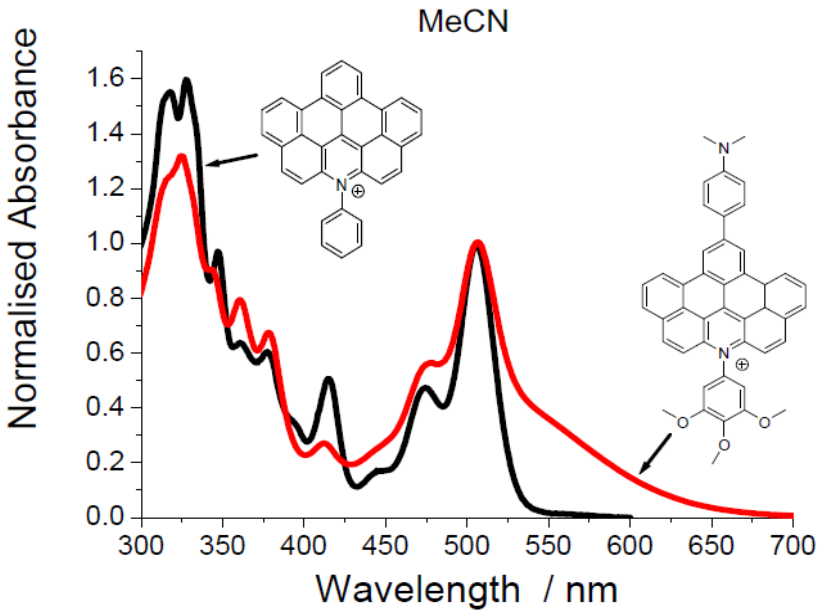

*Figure 25. Normalised room temperature absorption spectra of **ACBN** (black line), **DMA** (red line) recorded in acetonitrile*[22].

Table 4. Selective absorption maximum for acridinium derivatives recorded in acetonitrile.

Compounds	λ_1 (nm)	λ_2 (nm)	λ_3 (nm)
CAC	415	474	507
ACBN	422	474	506
CACOH	416	464	500
DMA	422	465	501

Fluorescence is extremely weak from a dilute acetonitrile solution of highly purified **DMA** upon excitation at 480 nm (*Figure 26*). The quantum yield (Φ_{FLU}) < 0.001. In comparison, **ACBN** showed strong fluorescence and the quantum yield of fluorescence

(Φ_{FLU}) and lifetime (τ_s) are 0.71 and 7 ns, respectively. The quenching of fluorescence of **DMA** can be explained as illustrated in *Figure 27*. Excitation of ground state **ACBN** molecules generates singlet state **ACBN***. The excited **ACBN*** decays back to the ground state and releases energy through fluorescence. This decay process is prohibited or unfavoured for **DMA**, as there is a smaller energy gap between singlet exited state (S_1*) and charge separation state (CSS). Therefore, the fluorescence for **DMA** was quenched by a charge transfer process.

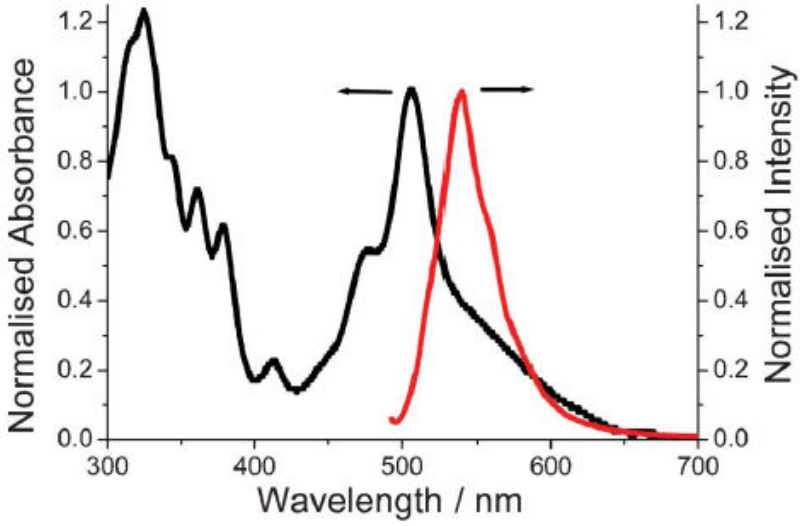

*Figure 26. Normalised Room temperature absorption (black) and fluorescence spectra (red) for **DMA** collected in acetonitrile*[22].

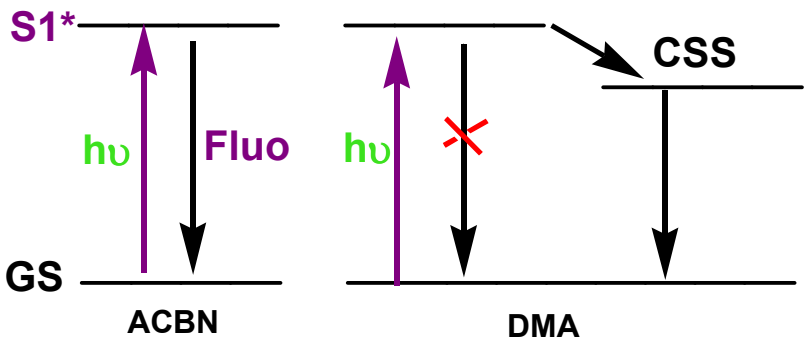

*Figure 27. Explanation of different decay processes for **ACBN** and **DMA**. Ground state (GS), singlet state (S1*), fluorescence (Fluo), charge separation state (CSS).*

The fully corrected **DMA** fluorescence excitation spectrum (*Figure 28*) does not match

over a wide spectral region with the absorption spectrum, or even with **ACBN**[22]. Excitation of **DMA** via the charge transfer (CT) band at 550 nm did not generate any fluorescence. This suggested that not all electronic transitions which constitute the overall absorption profile resulted in fluorescence. Another CT transition is also possible, for example, as a result of the close proximity of the trimethoxybenzene (even though it is not a good electron donor) and the planar expanded acridinium positive centre[22].

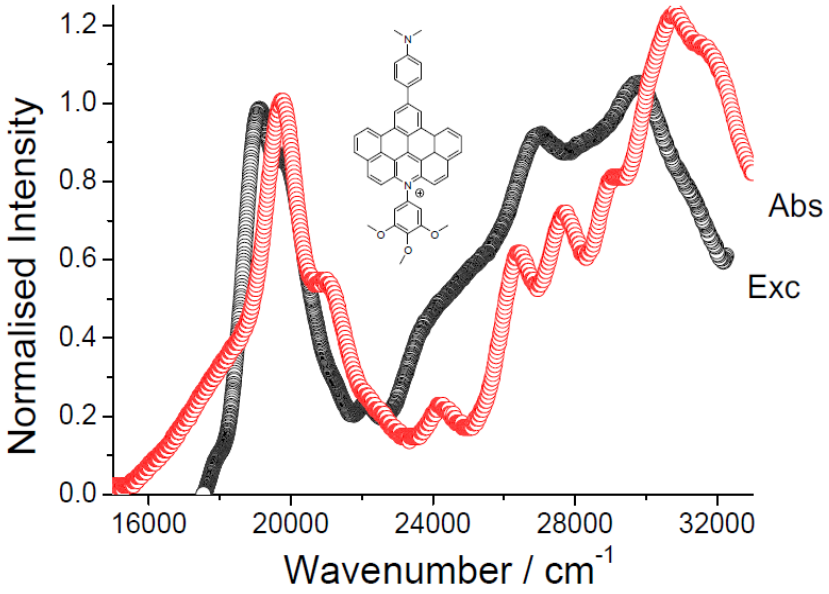

*Figure 28. Normalised Room temperature absorption spectrum (red) and corrected excitation spectrum (black) for **DMA** collected in acetonitrile*[22].

The coupling of expanded acridinium **CAC** and **ABOD** moieties afforded **BODAC** which exhibited interesting electronic transition and fluorescence spectra (*Figure 29*). The absorbance in the 450 - 550 nm region displayed the strongest band. This is the overlap between the absorption of the bodipy part (transition between ground state to first singlet state usually shows around 500 nm[34]) and the acridinium part. Absorption and fluorescence spectra of phenyl bodipy (*Figure 30*) were taken to compare with **BODAC**. As shown in the spectra, the broad band with a shoulder between 450 and 550 nm was the sum of the different transitions. One of the advantages of this dyad is the intensive absorbance in the range between 250 and 550 nm but a defect is the lack of absorbance in the red region. The fluorescence quantum yield of **BODAC** was extremely small (0.001) as well. **BODIPY** derivatives are well known for their strong

fluorescence properties, however this is not seen for **BODAC**. One answer to this is that the fluorescence is quenched by the presence of the quaternary nitrogen center. Thus, it is feasible that charge shift competes with radiative decay (fluorescence). The fluorescence maximum for **BODAC** is red shifted by some 14 nm in comparison to phenyl bodipy. The fluorescence band for **BODAC** is broader than **DMA**.

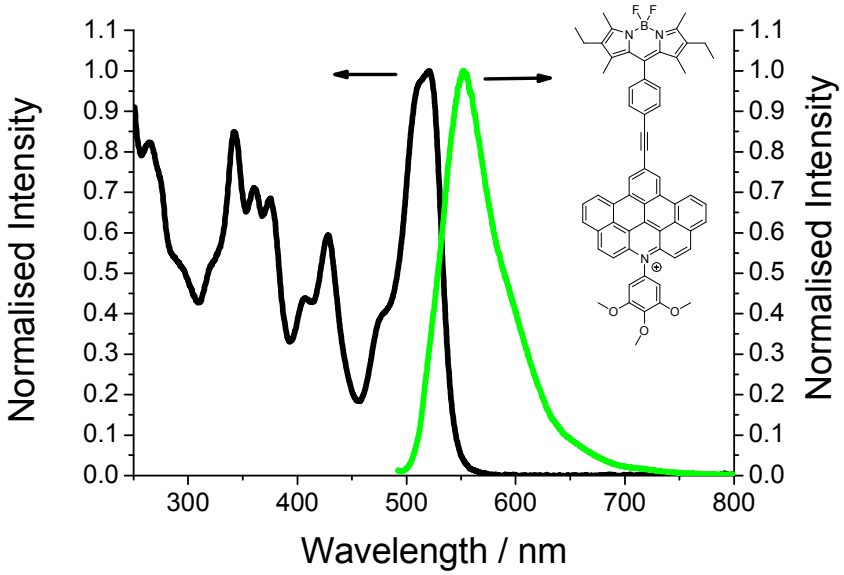

*Figure 29. Normalised room temperature absorption spectrum (black) and fluorescence spectrum for **BODAC** collected in acetonitrile.*

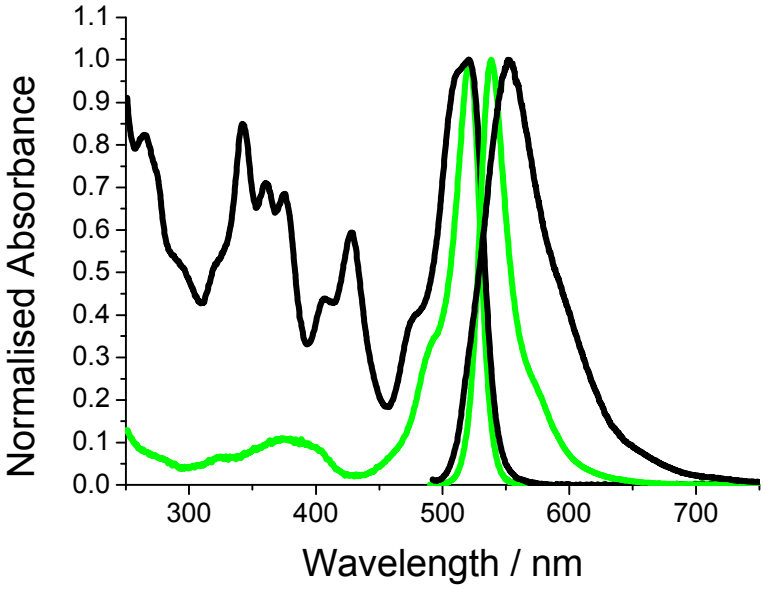

*Figure 30. Normalised room temperature absorption and fluorescence spectra for **BODAC** (black) and reference compound phenyl bodipy (green) collected in acetonitrile.*

3.7.2 Charge transfer studies and analysis of DMA[22]

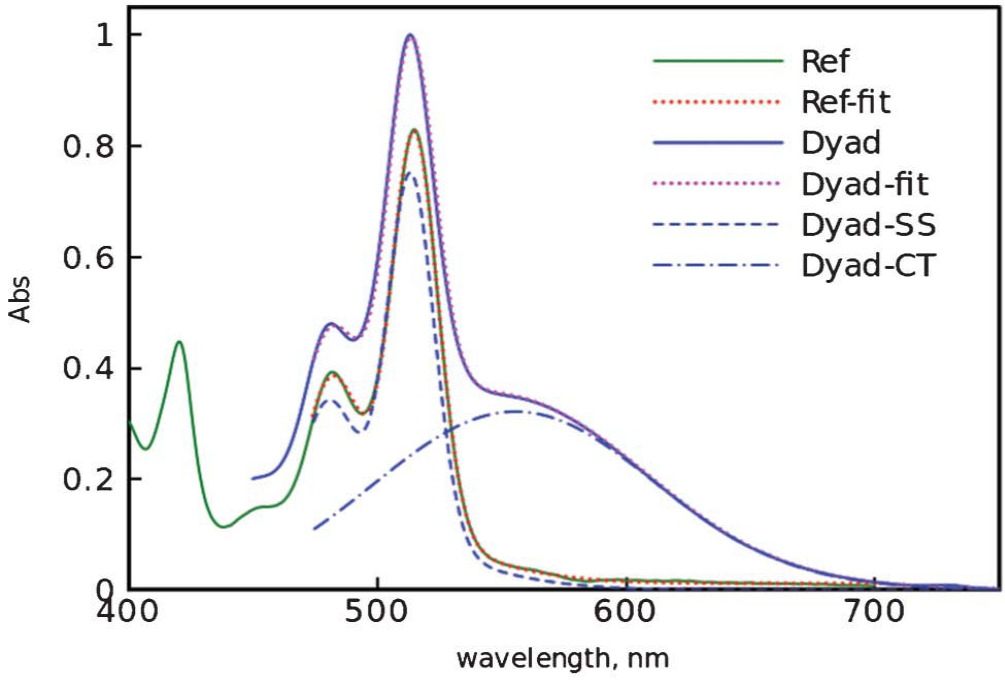

*Figure 31. Normalised absorption spectra (solid lines) for **ACBN** (Ref) and **DMA** (Dyad) in DCE. The dotted lines show the fit curves, and the dashed and dashed- and dotted lines present deconvolution of the dyad spectrum into singlet–singlet and CT absorption bands[22].*

The electronic absorption spectra for **DMA** were obtained in a range of solvents and the

spectra were analysed in detail by deconvolution into a series of Guassians. Absorption spectra for **ACBN** were recorded in the same range of solvents, and they were used as a reference to help distinguish the sharp singlet-singlet and broad CT absorption bands. Compounds **DMA** and **ACBN** were analysed together in each solvent. The recorded absorption spectrum and deconvoluted spectra of the dyad in DCE are presented in *Figure 31*.

Firstly, a basic model was generated to an approximate absorption profile for the reference compound in the wavelength range 474-700 nm (*Figure 31* Ref-fit). Three Gaussian bands were used at this step (Equation 1), where a_i is the band intensity, λ_i and $\Delta\lambda_i$ are the positions and widths of the bands.

$$A_{SS}(\lambda) = \sum_{i=1}^{3} a_i \exp\left[-\frac{1}{2}\left(\frac{\lambda_i}{\Delta\lambda_i}\right)^2\left(\frac{\lambda_i}{\lambda}-1\right)^2\right] \qquad (1)$$

The best-fit band positions (half widths) were 515 nm (9.2 nm), 482 nm (11.9 nm), and 503 nm (32.7 nm). The ratios of the band intensities were a_2/a_1 = 0.422 and a_3/a_1 = 0.115.

The position of singlet-singlet transition bands for **DMA** are blue shifted about 1.5 nm in comparison to **ACBN**. Hence, in the second step of the fitting, the ratios of a_2/a_1 and a_3/a_1 were kept constant for both **ACBN** (the reference) and **DMA** (the dyad) spectra. An additional CT absorption was added to the model for the dyad and identical S_1-S_1 band values were set for the dyad corresponding to that of the reference compound. Almost the same fitting spectrum was obtained for reference compound as that from the first step.

Semi-quantum electron transfer theory considers possible photoinduced transitions between the lowest vibrational level of the electronic ground state and the vibration levels of the CT state[35]. The CT band was analysed according to this theory and an

approximation can be presented as equation (2)

$$A_{CT}(\lambda) = A_0 \sum_{n=0}^{\infty} \frac{S^n}{n!} \exp\left[\frac{-\left(\Delta G^0 + E_s + nE_v - \frac{hc}{\lambda}\right)}{4E_s k_B T}\right] \qquad (2)$$

The terms in the equation are explained as follow:

ΔG^0 --- free energy

E_S --- solvent reorganisation energy

E_v --- fundamental vibration mode energy

S --- vibrational electronic coupling element, is the ratio of internal reorganisation energy (E_i) to the vibrational energy

T--- Temperature

k_B --- Boltzmann constant

A_0 --- constant

The goal of the spectral fits for the dyad in different solvents was to separate the absorption into two parts; namely, the singlet-singlet and CT bands, $A(\lambda) = A_{SS} + A_{CT}(\lambda)$, and to evaluate the parameters ΔG^0, E_S, E_v, and S associated with the CT absorption band shape (*Table 5*).

Table 5. Parameters obtained from the analysis of charge transfer band in different solvent. Refractive index n and solvent dielectric constant were obtained from literature. Solvent polarity funcetion is calculated according to equation $f = n^{-2} - \varepsilon^{-1}$. [a] Methoxybenzene, [b] Methyltetrahydrofuran, [c] Tetrahydrofuran, [d] Dichloromethane, [e] 1,2-Dichloroethane, [f] N,N-dimethylformamide, [g] Propan-2-one.[22]

solvent	n	ε	f^h	ΔG^0, eV	E_s, eV	E_v, eV	S
Anisole[a]	1.517	4.33	0.204	1.58	0.60	0.19	0.82
MeTHF[b]	1.406	6.97	0.362	1.64	0.57	0.21	0.69
THF[c]	1.4052	7.52	0.373	1.63	0.57	0.21	0.60
DCM[d]	1.4241	8.93	0.381	1.70	0.41	0.18	0.99
DCE[e]	1.4448	10.4	0.383	1.69	0.42	0.19	0.92
DMF[f]	1.4305	36.7	0.461	1.62	0.61	0.18	0.84
Acetone[g]	1.3591	21.0	0.494	1.62	0.63	0.17	0.86
$MeNO_2$	1.3935	39.4	0.489	1.54	0.73	0.17	0.77
MeCN	1.346	36.6	0.525	1.59	0.66	0.14	1.02

3.7.3 Transient absorption spectroscopy and a decay model

Transient spectroscopy is a powerful tool to study the electronic and structural properties of short-lived excited states for photoactive molecules. Absorption of photons generates excited state molecules and because of changes to the absorption profiles, the excited state can be probed. Transient absorption spectra for **DMA** were recorded in both 1,2-dichloroethane (DCE) and acetonitrile.

The DCE solution of **DMA** was excited with a 70 fs laser pulse at 395 nm to obtain a series of spectra (*Figure 32*)[22]. It is clear that there is a bleach effect at around 515 nm and 570 nm within the 1 ps time delay. The bleaching at 570 nm is associated with the intramolecular charge transfer band. The negative band moved towards shorter wavelength as the time evolved, indicating a structure change occurred which reduced π-conjugation during the relaxation process. A positive band at 470 nm of the transient profiles is a characteristic peak of the mono-reduced radical of the dyad[17]. A new negative feature is seen to grow very quickly between 600 - 725 nm, where there is little ground-state absorption. This is very characteristic of stimulated emission. After around

6 ps, a new positive broad feature is clearly evident at around 690 nm. This feature decays over some 300 ps and there is no sign of a long-lived species from the temporal profiles.

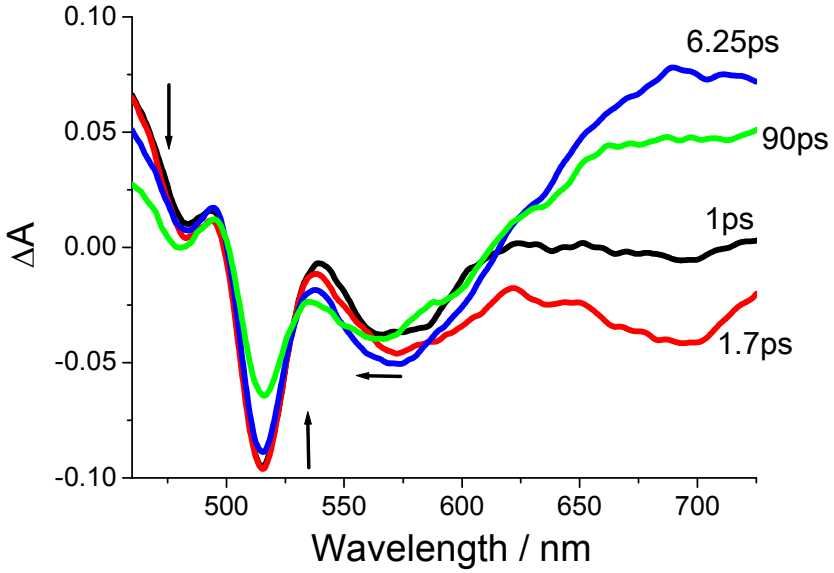

*Figure 32. Transient absorption spectra of **DMA** recorded in DCE solution*[22].

Decay kinetics were monitored at a single wavelength (*Figure 33*) from the transient profiles, revealing that at least three decay processes are involved. The lifetime monitored at 455 nm and 569 nm are in good agreement. Three-exponential model is required to fit the transient records (*Figure 34*). The three lifetimes are τ_1 = 0.7 ps, τ_2 = 4.7 ps and τ_3 = 196 ps.

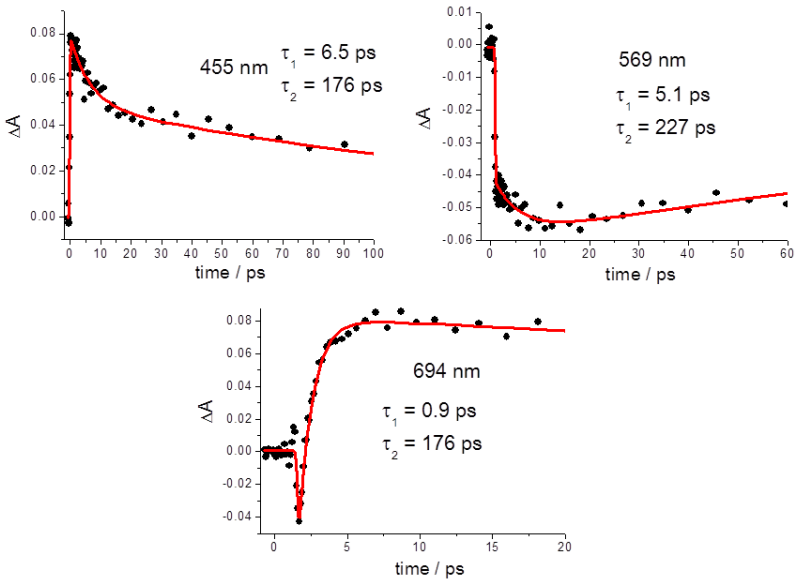

*Figure 33. Decay profile monitored in single wavelength of **DMA** recorded in DCE solution.*

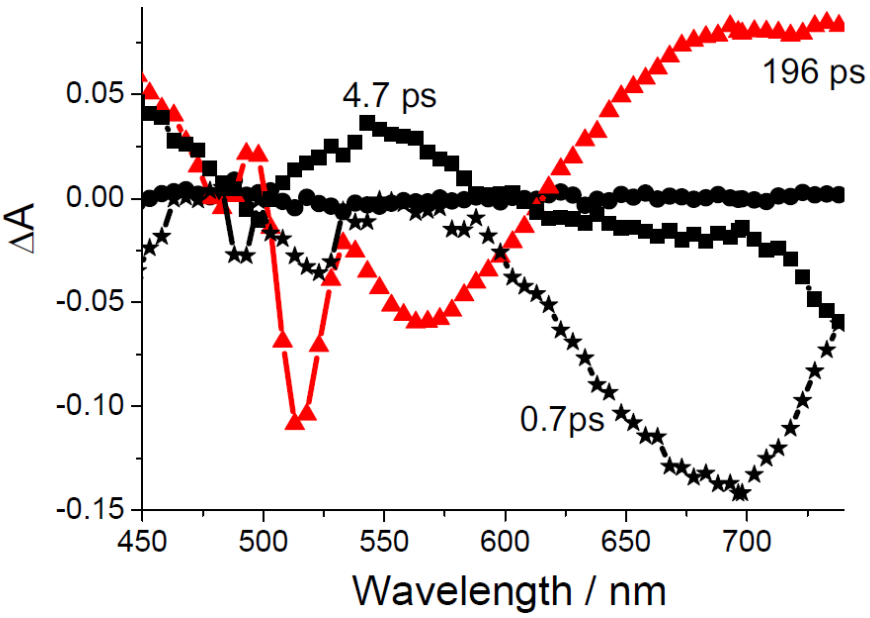

*Figure 34. Three-exponential model of a global decay fit of the transient for **DMA** records in DCE.*

The same transient absorption decay profiles were also recorded in acetonitrile *(Figure 35*), but they are simpler than those obtained from **DCE**. Two-exponential model is adequate to analyse the decay process. There is an extremely fast decay within 0.5 ps which is at the limit of the machine and the other transient decays over 12 ps with similar character seen in DCE.

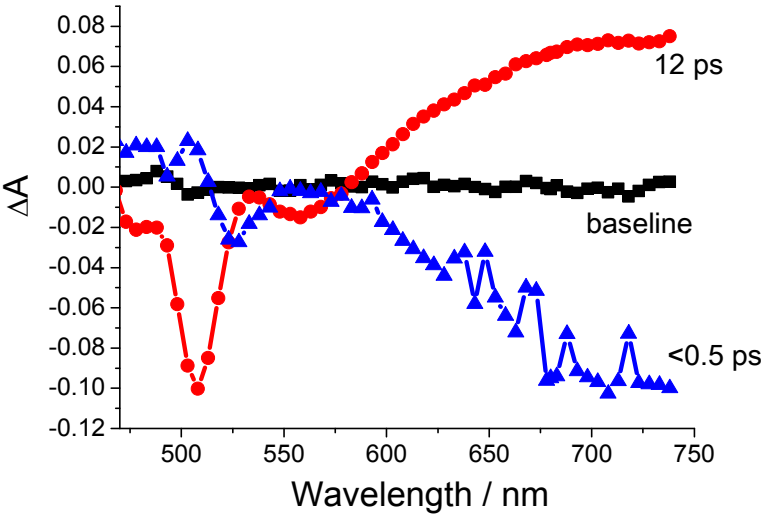

*Figure 35. Two-exponential model of a global decay fit of the transient for **DMA** records in CH_3CN.*

Based on these observations from transient records, a decay model (*Figure 36*) can be proposed[22]. Three lifetimes in DCE corresponds to three processes after the excitation of the ground state molecules. Upon the excitation of the molecule, the ground state molecule goes through the Frank-Condon state which rapidly transfers an electron to form the highly planar charge shift (CS) state in less than 1 ps. Such a process would increase the overall π-conjugation. To alleviate steric interaction between the hydrogen atoms on the acridinium core rings and phenyl ring, a structural reorganisation (SR) takes place (k_{SR} = 2 x 10^{11} s^{-1}). There is a reduction in π-conjugation as revealed from the transient profiles (bleaching of the band shifted to higher energy side). Finally, the ground state is reformed through charge recombination (CR) at slower rate k_{CR} = 5 x 10^9 s^{-1} . The discrimination of the forward and backward charge transfer process is about 200 which is comparable to other molecular dyads.

In more polar solvents, such as acetonitrile, the extent of ground state charge transfer is greater as a consequence of the solvent stabilisation effect. Therefore, the geometry is close to Frank-Condon state and both charge transfer and structure reorganisation occurred in less than 0.5 ps.

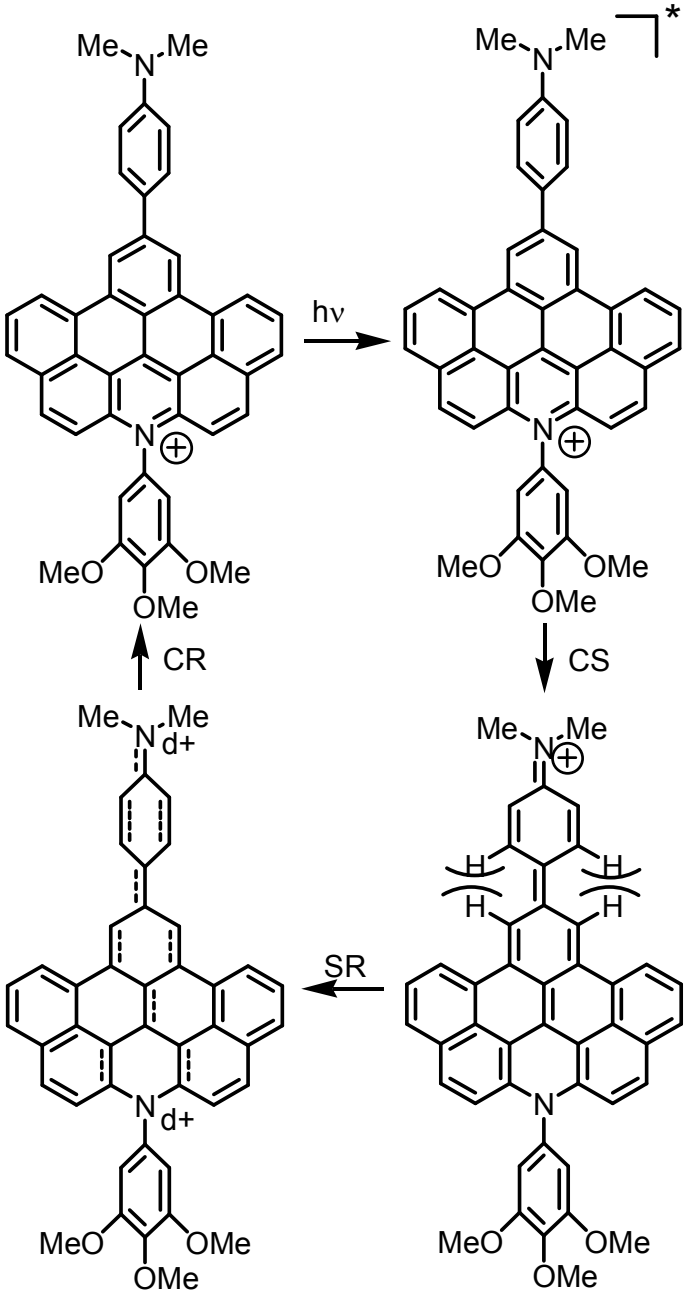

*Figure 36. Proposed decay model of **DMA** upon the radiation of laser at 395 nm.*

3.8 Surface binding study and measurements

The ability of dyads to adsorb onto semiconductor surfaces was tested through UV absorption studies (*Figure 37*). The absorbance of FTO (fluorine doped tin oxide) glass was taken as the background. A NiO coated glass was left in dye bath (0.03 mM **CACOH** acetonitrile solution) overnight and washed with ethanol and dried before recording the electronic transition spectrum. The film was then treated with heat and

soaked with electrolyte solution, and after each treatment a spectrum was recorded. No significant change was found between the three spectra. Therefore, the attachment of **CACOH** to semiconductor surface is relatively robust. The three main peaks at greater than 400 nm are red shifted in comparison to the absorption spectrum in solution (*Table 6*). One possible reason is that there is an enhancement of electron density to the whole molecular the dyad upon attaching to the semiconductor surface. The intensity of the three peaks are more similar in the film, i.e., the molar absorption coefficients are almost the same for these three peaks. A new broad tail between 600 to 800 nm was observed in the spectra recorded from solid films. This broad band is possibly due to charge transfer between **CACOH** and the semiconductor surface. Similar results (*Figure 38*) were obtained for **CACOH** attached on a TiO_2 coated semiconductor surface. A schematic presentation of the attachment of hydroxyl group to semiconductor surface is shown in *Figure 39*.

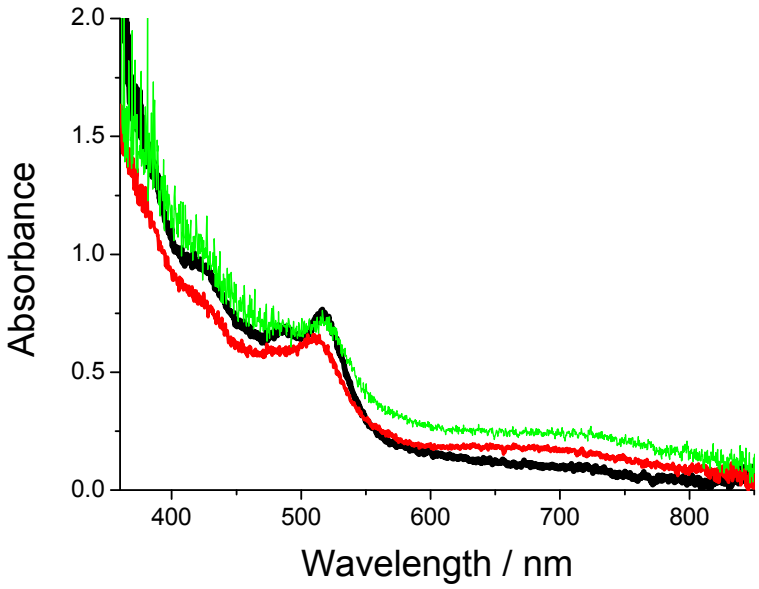

*Figure 37. (1) Electronic absorption spectra of **CACOH** on NiO coated ITO glass surface (black line); (2) spectrum after the treatment of (1) with heat (120 ^{O}C for 10 minutes), (red line); (3) spectrum after the treatment of (2) with soaking in electrolyte solution for 3 hours (green line).*

*Table 6. Selective comparison of **CACOH** absorption peaks maximum in solution and solid film.*

UV absorption of **CACOH**	Selected Peak Maximum Wavelength / nm		
Solution	415	465	500
Film on NiO surface	420	485	515

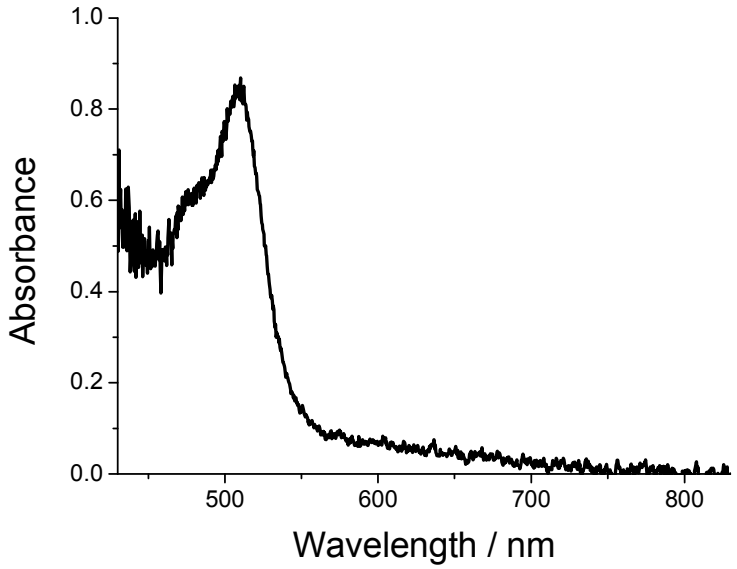

*Figure 38. Electronic sbsorption spectrum of **CACOH** on TiO_2 coated ITO glass surface.*

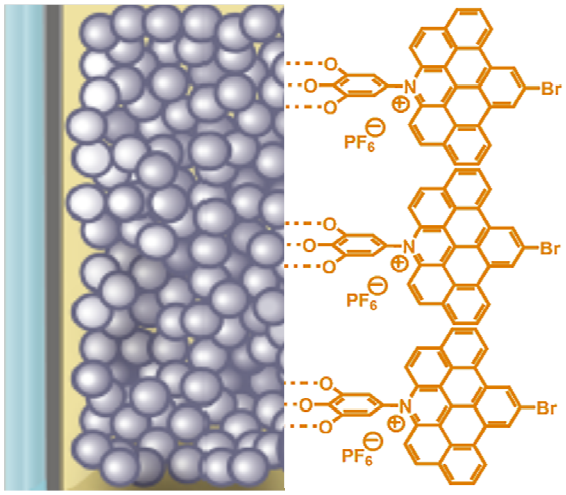

*Figure 39. Schematic presentation of attachment of **CACOH** to semiconductor surface (TiO_2 or NiO).*

The assembled sandwich cells consist of dye-sensitised working electrodes and platinum-coated conducting glass counter electrodes. The two electrodes were placed on top of each other and sealed from the edge through a thin transparent Surlyn polymer

film, which also creates a space for the electrolyte. A drop of 1.0 M LiI and 0.1 M I_2 in acetonitrile electrolyte was added through a predrilled hole in the counter electrode by vacuum backfilling, and was sealed by a piece of Surlyn polymer film. The area of the cell was 0.196 cm^2. The current generated from the cell was characterised by photocurrent density-photovoltage curve (*Figure 40* and *Figure 41*). The open-circuit photovoltage (Voc) and photocurrent density (J_{SC}) were obtained directly from the curve. When the photovoltage is 0, the corresponding photocurrent density is J_{SC}, and Voc is the photovoltage when photocurrent density is 0. The power is P = J*V. When the power is at a maximum both photocurrent and photovoltage are optimised, so the maximum integral photocurrent density (J_{max}) and maximum photovoltage V_{max} can be obtained. The fill factor is FF = P_{max}/P_{theor}. The efficiency = J_{SC}*Voc*FF/1. The parameters obtained from the plot are shown in *Table 7*. It is also interesting to realise that the acridinium based dye works in both p- and n-type cells. Finally the anchoring group used in here is different from conventional carboxylic acid and phosphate acid, the closest structure to this is the catechol group. Usually, the catechol group is applied as the anchoring group in a n-type cell. There is only one other example to the best of our knowledge which it is used in a p-type cell and this is with a ruthenium(II) polypyridine complex as a sensitizer[36].

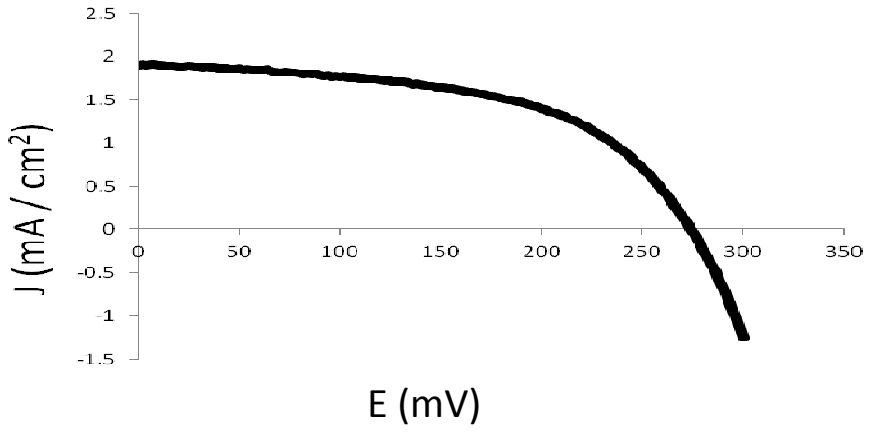

*Figure 40.Photocurrent-photovoltage measurement of **CACOH** on n-type (TiO_2) cell.*

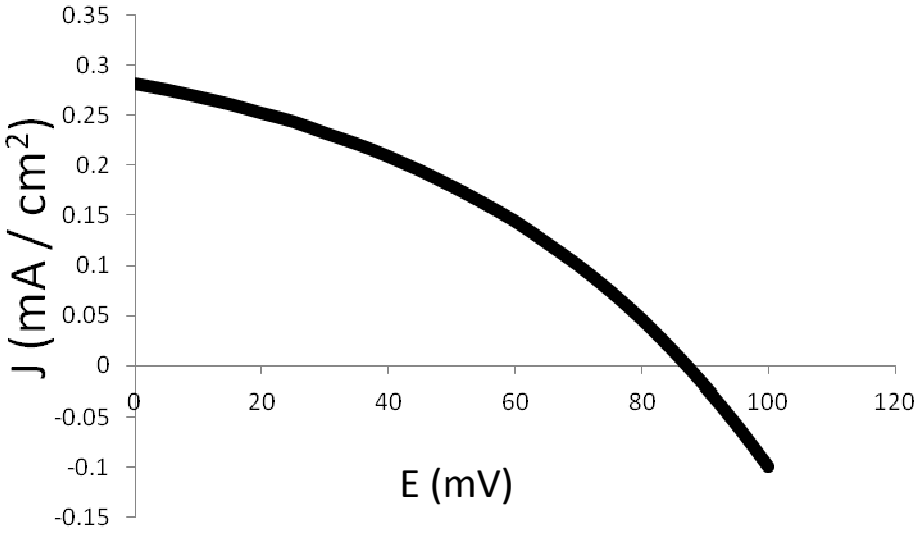

*Figure 41. Photocurrent-photovoltage measurement of **CACOH** on p-type (NiO) cell*

*Table 7. Parameters obtained from current-voltage measuremen for **CACOH**.*

Cell	J_{sc} (mA/cm^{-2})	V_{oc} (V)	J_{max} (mA/cm^{-2})	V_{max} (V)	P_{max}	P_{theor}	FF %	Efficiency η (%)
n-type	1.90	0.27	1.40	0.2	0.28	0.52	54	0.28
p-type	0.28	0.085	0.18	0.05	0.009	0.024	38	0.009

The same p-type cell (NiO) was made using **DMAOH** as sensitizer. We expected that the **DMAOH** absorbs a broader range of light and could improve the efficiency. However, the efficiency (*Figure 41* and *Table 8*) is still low in comparison to the reported highest efficiency p-type cell (1.3%)[37] and we reasoned that this is due to fast charge recombination. The transient absorption data indicated that the charge recombination in acetonitrile is fast, i.e., 12 ps, but in non-polar solvent like DCE, the process was slowed down almost 20 times. The problem with non-polar solvent is that the solubility is low.

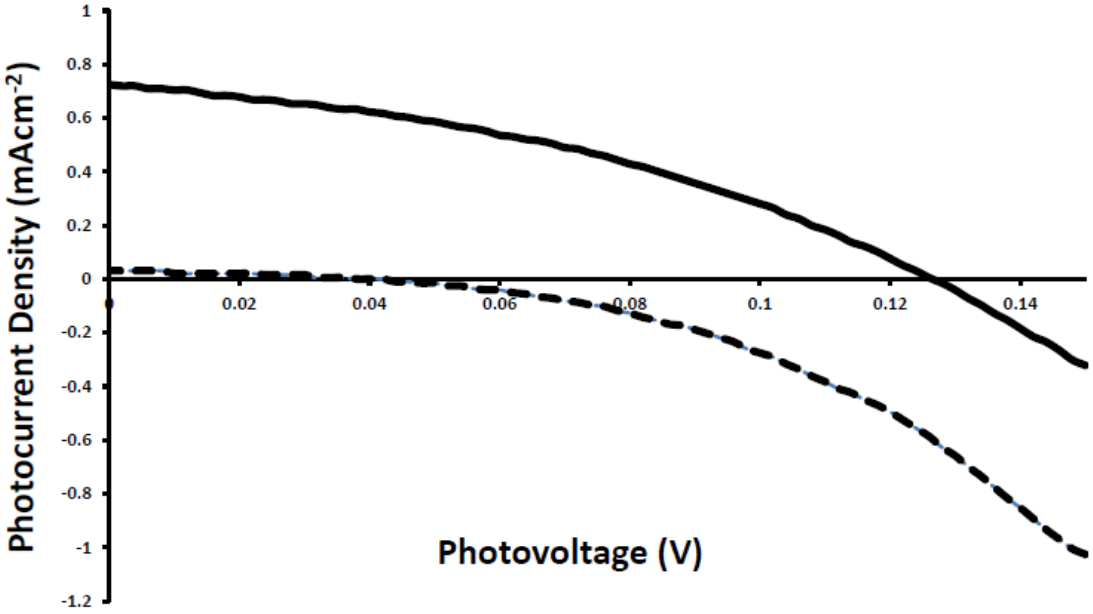

*Figure 41. Photocurrent-photovoltage measurement of **DMAOH** on p-type (NiO) cell,the solid line (-)is the current generated under photo-radiation, the dashed line (--)is the dark current. The dark current line indicated that the current passing through the cell is almost zero in dark. Therefore the current measured upon photo-excitation (solid line) is purely due to the dye sensing effect.*

*Table 8. Parameters obtained from current-voltage measurement for **DMAOH**.*

Cell	J_{sc} (mA/cm^{-2})	V_{oc} (V)	V_{max} (V)	J_{max} (mA/cm^{-2})	P_{max}	P_{theor}	FF (%)	η (%)
P-type	0.73	0.13	0.076	0.46	0.035	0.091	38.23	0.035

3.9 Concluding remarks

This chapter has described the discovery of synthetic routes to new acridinium dyes and the measurement of their photophysical properties. A new rout was explored for the synthesis of acridinium derivatives **DMA** and **BODAC**. The photo-radiation of ring **OAC** leaded to ring closure product **CAC** in a very good yield, 92%. The details of the reaction mechanism are not known, but the possible oxidant in the reaction could be acetonitrile or oxygen, hydrogen gas could be a possible product from the reaction. It was also found that in the absence of water the reaction is extremely slow, almost no conversion even after several weeks' sunlight irradiation. Therefore the water must play

an important role in the detailed mechanism. Laine and co-workers[38] reported a photo-radiation conversion of a hexa-branched pyridiniums derivative in methanol solution (saturated with oxygen) to the corresponding hemifused pyridinium product is very similar to the reaction we observed in here. A four hydrides transferred process was also involved in the reaction. But the details of the reaction path are not known yet. The other known fused aromatic rings formation reactions (e.g. stilbene formation and oligophenylene formation) are usually performed in the presence of oxidants (e.g. I_2 and DDQ) or weak Lewis acid (e.g. $FeCl_3$ and $CuCl_2$)[39]. Further experiments need to be carried out to discover the detailed mechanism in involved in our four hydride transferred process. Solvent polarity dependence UV-Vis absorption spectroscopy study reveals the intramolecular charge transfer properties of **DMA**. In comparison to the reference compound **ACBN**, the fluorescence of **DMA** was not observed due to the presence of a low-lying charge transfer state. Similarly, the fluorescence was not observed in **BODAC**, even though bodipy derivatives are well known for their high fluorescence quantum yields[40]. It is very possibly that the fluorescence of the BODAC is quenched by the competing charge transfer process.

It was shown that the **DMAOH** acted as a sensitizer for p-type DSSCs with efficiency less than 0.04%, which is more than 30 times less efficient in comparison to the recorded efficiency reported by Bach and co-workers[37]. Despite these, we still for the first demonstrate that the acridinium derivatives are viable candidates for DSSCs cells. The possible reason for the low efficiency is that the fast charge recombination process is very fast, 12 ps, as it is revealed from the transient absorption measurement of the **DMA** in acetonitrile. Long charge recombination lifetimes have been found in naphthalenediimide based molecular dyads in μs range[41], which is by a factor of 10^6 longer than **DMA**. We can tune the properties through the modification of the structure, for instance, to alter the distance between the acridinium positive core and the anchoring group to slow down the charge recombination rate. It should be possible to functionalise the acridinium rings to change their redox potentials, and to modify the donor part of

the molecules to expand the absorbing range to longer wavelength. We have also shown that hydroxyl groups are relatively robust for attaching to semiconductor surface for both types of cells.

The synthetic routes developed enable us to open up more diverse acridinium-based dye chemistry. There is the possibility to tune the acridinium-based dye structure for different practical applications. The positive centre in the molecule makes it a promising candidate for plasmon resonance energy transfer sensing especially if we attach the dye to a nanoparticle surface. The counter ion could be exchanged to alter the solubility in organic or inorganic solvents. We expect that more work will be done on these types of acridinium-based derivatives to fully discover their properties and potential applications.

3.10 References

[1] B. O'Regan and M. Grätzel, *Nature*, 1991, **353**, 737.

[2] (i) M. K. Nazeeruddin, E. Baranoff and M. Grätzel, *Sol. Energy*, 2011, **85**,1172; (ii) E. Baranoff, J. H. Yum, M. Grätzel and M. K. Nazeeruddin, *J. Organomet. Chem.*, 2009, **694**, 2661; (iii) Danuta Wrobela and Andrzej Graja, *Coord. Chem. Rev.*, 2011, **255**, 2555; (iv) S. Fantacci and F. D. Angelis, *Coord. Chem. Rev.*, 2011, **255**, 2704; (v) R. Menzel, D. Ogermann, S. Kupfer, D. Wei, H. Görls, K. Kleinermanns, L. González and R. Beckert, *Dyes and Pigments*, 2012, **94**, 512; (vi) M. R. Mohammadi, R. R. M. Louca, D. J. Fray and M. E. Welland, *Sol. Energy*, 2012, **86**, 2654; (vii) T. Yoshida, J. Zhang, D. Komatsu, S. Sawatani, H. Minoura, T. Pauporté, D. Lincot, T. Oekermann, D. Schlettwein, H. Tada, D. Wohrle, K. Funabiki, M. Matsui, H. Miura and H. Yanagi, *Adv. Funct. Mater.*, 2009, **19**, 17; (viii) M. Grätzel, *Acc. Chem. Res.*, 2009, **42**, 1788.

[3] A. Yella, H. W. Lee, H. N. Tsao, C. Y. Yi, A. K. Chandiran, M. K. Nazeeruddin, E. W. G. Diau, C. Y. Yeh, S. M. Zakeeruddin and M. Grätzel, *Sci.*, 2011, **334**, 629.

[4] (i) G. McDermott, S. M. Prince, A. A. Freer, A. M. Hawthornthwaite-Lawless, M. Z. Papiz, R. J. Cogdell and N. W. Isaacs, *Nature*, 1995, **374**, 517; (ii) J. Deisenhofer, O. Epp, K. Miki, R. Huber and H. Michel, *J. Mol. Biol.*, 1984, **180**, 385; (iii) J. Deisenhofer, O. Epp, K. Miki, R. Huber and H. Michel, *Nature*, 1985, **318**, 618.

[5] G. S. Engel, T. R. Calhoun, E. L. Read, T. K. Ahn, T. Mancal, Y. C. Cheng, R. E. Blankenship and G. R. Fleming, *Nature*, 2007, **446**, 782.

[6] Z. E. X. Dance, S. M. Mickley, T. M. Wilson, A. Butler Ricks, A. M. Scott, M. A. Ratner and M. R. Wasielewski, *J. Phys. Chem. A*, 2008, **112**, 4194.

[7] J. Iehl, J. F. Nierengarten, A. Harriman, T. Bura and R. Ziessel, *J. Am. Chem. Soc.*, 2012, **134**, 988.

[8] A. Benniston and A. Harriman, *Mater. Today*, 2008, **11**, 26.

[9] J. W. Verhoeven, *J. Photochem. Photobiol. C*, 2006, **7**, 40.

[10] D. Gust, T. A. Moore, A. L. Moore, G. Seely, P. Liddell, D. Barrett, L. O. Harding, X. C. Ma,

S. J. Lee and F. Gao, *Tetrahedron*, 1989, **45**, 4867.

[11] D. Gust, T. A. Moore, A. L. Moore, S. J. Lee, E. Bittersmann, D. K. Luttrull, A. A. Rehms, J. M. D. Graziano, X. C. Ma, F. Gao, R. E. Belford and T. T. Trier, *Science*, 1990, **248**, 199.

[12] (i) D. A. Holden and J. E. Guillet, *Macromolecules*, 1980, **13**, 289; (ii) S. E. Webber, *Chem. Rev.*, 1990, **90**, 1469; (iii) E. Collini and G. D. Scholes, *Science*, 2009, **323**, 369.

[13] (i) A. Adronov, S. L. Gilat, J. M. J. Frechet, K. Ohta, F. V. R. Neuwahl and G. R. Fleming, *J. Am. Chem. Soc.*, 2000, **122**, 1175; (ii) E. K. L. Yeow, K. P. Ghiggino, J. N. H. Reek, M. J. Crossley, A. W.Bosman, A. P. H. J. Schenning and E. W. Meijer, *J. Phys. Chem. B*, 2000, **104**, 2596; (iii) M. S. Choi, T. Yamazaki, I. Yamazaki and T. Aida, *Angew. Chem. Int. Ed.*, 2004, **43**, 150.

[14] K. W. J. Barnham, J. L. Marques, J. Hassard and P. O'Brien, *Appl. Phys. Lett.*, 2000, **76**, 1197.

[15] A. C. Benniston, G. Copley, H. Lemmetyinen and N. V. Tkachenko, *Eur. J. Org. Chem.*, 2010, **15**, 2867.

[16] A. C. Benniston, G. Copley, H. Lemmetyinen and N. V. Tkachenko, *ChemPhysChem*, 2010, **11**, 1685.

[17] A. C. Benniston, J. Hagon, X. He, H. Lemmetyinen, N. V. Tkachenko, W. Clegg and R. W. Harrington, *Phys. Chem. Chem. Phys.*, 2012, **14**, 3194.

[18] (i) K. Gleu and W. Petsch, *Angew. Chem.*, 1935, **48**, 57; (ii) A. Natrajan, D. Sharpe and D. Wen, *Org. Biomol. Chem.*, 2012, **10**, 1883.

[19] (i) W. Abraham, K. Buck, M. O. Zgadzaj, S. S. Schaffer and U. W. Grummt, *Chem. Commun.*, 2007, **29**, 3094; (ii) W. Abraham, A. Wlosnewski, K. Buck and S. Jacob, *Org. Biomol. Chem.*, 2009, **7**, 142; (iii) Y. Duo, S. Jacob and W. Abraham, *Org. Biomol. Chem.*, 2011, **9**, 3549.

[20] K. Ohkubo, K. Mizushima, R. Iwata and S. Fukuzumi, *Chem. Sci.*, 2011, **2**, 715.

[21] G. Ulrich, R. Ziessel and A. Harriman, *Angew. Chem. Int. Ed.*, 2008, **47**, 11.

[22] A. C. Benniston, X. He, H. Lemmetyinenb and Nikolai V. Tkachenko, *RSC Adv.*, 2013, **3**, 4995.

[23] (i) D. Q.Wu, X. L. Feng, M. Takase, M. C. Haberecht and K. Müllen, *Tetrahedron*, 2008, **64**, 11379; (ii) D. Q. Wu, W. Pisula, M. C. Haberecht, X. Feng and K. Müllen, *Org. Lett.*, 2009, **11**, 5686.

[24] W. Dilthey, F. Quint and J. Heinen, *J. Prakt. Chem.*, 1939, **152**, 49.

[25] A. C. Benniston and D. B. Rewinska, *Org. Biomol. Chem.*, 2006, **4**, 3886.

[26] (i) M. Iqbal and P. Balaram, *Biopolymers*, 1982, **21**, 1427;(ii) X. Qin, M. Liu, D. Yang and X. Zhang, *J. Phys. Chem. B*, 2010, **114**, 3863.

[27] (i) J. Fortage, F. Tuyeras, P. Ochsenbein, F. Puntoriero, F. Nastasi, S. Campagna, S. Griveau, F. Bedioui, I. Ciofini and P. P. Laine, *Chem. Eur. J.*, 2010, **16**, 11047; (ii) I. Tabushi and H. Yamada, *Tetrahedron*, 1977, **33**,1101.

[28] (i) R. J. Abraham and M. Mobli, *Magn. Reson. Chem.*, 2007, **45**, 865; (ii) M. A. Wendt, J. Meiler, F. Weinhold and T. C. Farrar, *Mol. Phys.*, 1998, **93**, 145; (iii) N. J. Baxter and M. P. Williamson, *J. Biomolecular NMR*, 1997, **9**, 359.

[29] (i) P. L. Corio, R. L. Rutledge and J. R. Zimmerman, *J. Mol. Spec.*, 1959, **3**, 592; (ii) W. Drinkard and D. J. Kivelson, *J. Phys. Chem.*, 1958, **62**, 1494.

[30] A. Mitra, P. J. Seaton, R. A. Assarpour and T. Williamson, *Tetrahedron*, 1998, **54**, 15489.

[31] T. L. Macdonald, W. G. Gutheim, R. B. Martin and F. P. Guengerich, *Biochemistry*, 1989, **28**, 2071.

[32] M. J. Frisch, G. W. Trucks, H. B. Schlegel, G. E. Scuseria, M. A. Robb, J. R. Cheeseman, J. A. Montgomery Jr., T. Vreven, K. N. Kudin, J. C. Burant, J. M. Millam, S. S. Iyengar, J. Tomasi, V. Barone, B. Mennucci, M. Cossi, G. Scalmani, N. Rega, G. A. Petersson, H. Nakatsuji, M. Hada, M. Ehara, K. Toyota, R. Fukuda, J. Hasegawa, M. Ishida, T. Nakajima, Y. Honda, O. Kitao, H. Nakai, M. Klene, X. Li, J. E. Knox, H. P. Hratchian, J. B. Cross, V. Bakken, C. Adamo, J. Jaramillo, R. Gomperts, R. E. Stratmann, O. Yazyev, A. J. Austin, R. Cammi, C. Pomelli, J. W. Ochterski, P. Y. Ayala, K. Morokuma, G. A. Voth, P. Salvador, J. J. Dannenberg, V. G. Zakrzewski, S. Dapprich, A. D. Daniels, M. C. Strain, O. Farkas, D. K. Malick, A. D. Rabuck, K. Raghavachari, J. B. Foresman, J. V. Ortiz, Q. Cui, A. G. Baboul, S. Clifford, J. Cioslowski, B. B. Stefanov, G. Liu, A. Liashenko, P. Piskorz, I. Komaromi, R. L.

Martin, D. J. Fox, T. Keith, M. A. Al-Laham, C. Y. Peng, A. Nanayakkara, M. Challacombe, P. M. W. Gill, B. Johnson, W. Chen, M. W. Wong, C. Gonzalez and J. A. Pople, Gaussian 03, Gaussian, Inc., Wallingford CT, 2004.

[33] The absorption profile between the porphyrin Soret and Q-bands (B430-500 nm) is rather flat and deviod of electronic transitions

[34] A. C. Benniston, G. Copley, K. J. Elliott, R. W. Harrington and William Clegg, *Eur. J. Org. Chem.*, 2008, **16**, 2659.

[35] (i) R. A. Marcus, *J. Phys. Chem.*, 1989, **93**, 3078; (ii) V. Chukharev, N. V. Tkachenko, E. Efimov and H. Lemmetyinen, *Chem. Phys. Lett.*, 2005, **411**, 501.

[36] Y. Pellegrin, L. L. Pleuxa, E. Blart, A. Renaud, B. Chavillon, N. Szuwarski, M. Boujtita, L. Cario, S. Jobic, D. Jacquemina and F. Odobela, *J. Photochem. Photobiol. A*, 2011, **219**, 235.

[37] S. Powar, T. Daeneke, M. T. Ma, D. Fu, N. W. Duffy, G. Gotz, M. Weidelener, A. Mishra, P. Bauerle, L. Spiccia and U. Bach, *Angew. Chem. Int. Ed.*, 2013, **52**, 602.

[38] J. Fortage, F. Tuyeras, P. Ochsenbein, F. Puntoriero, F. Nastasi, S. Campagna, S. Griveau, F. Bedioui, I. Ciofini and P. P. Laine, *Chem. Eur. J.*, 2010, **16**, 11047.

[39] (i) M. Müller, C. Kübel and K. Müllen, *Chem. Eur. J.*, 1998, **4**, 2099; (ii) F. B. Mallory, C. S. Wood, J. T. Gordon, L. C. Lindquist and M. L. Savitz, *J. Am. Chem. Soc.*, 1962*,* **84***,* 4361; (iii) F. B. Mallory, C. S. Wood and J. T. Gordon*, J. Am. Chem. Soc.*, 1964, **86**, 3094; (iv) L. Liu, B. Yang, T. J. Katz and M. K. Poindexter, *J. Org. Chem.*, 1991, **56**, 3769.

[40] A. C. Benniston and G. Copley, *Phys. Chem. Chem. Phys.*, 2009, **11**, 4124.

[41] (i) E. A. Gibson, A. L. Smeigh, L. L. Pleux, J. Fortage, G. Boschloo, E. Blart, Y. Pellegrin, F. Odobel, A. Hagfeldt, L. Hammarstrom, *Angew. Chem. Int. Ed.*, 2009, **48**, 4402; (ii) A. Nattestad, A. J. Mozer, M. K. R. Fischer, Y. B. Cheng, A. Mashra, P. Bauerle and U. Bach, *Nat. Mater.*, 2010, **9**, 31.

Chapter 4

Charge Transfer Fluorescence in the Crystalline State

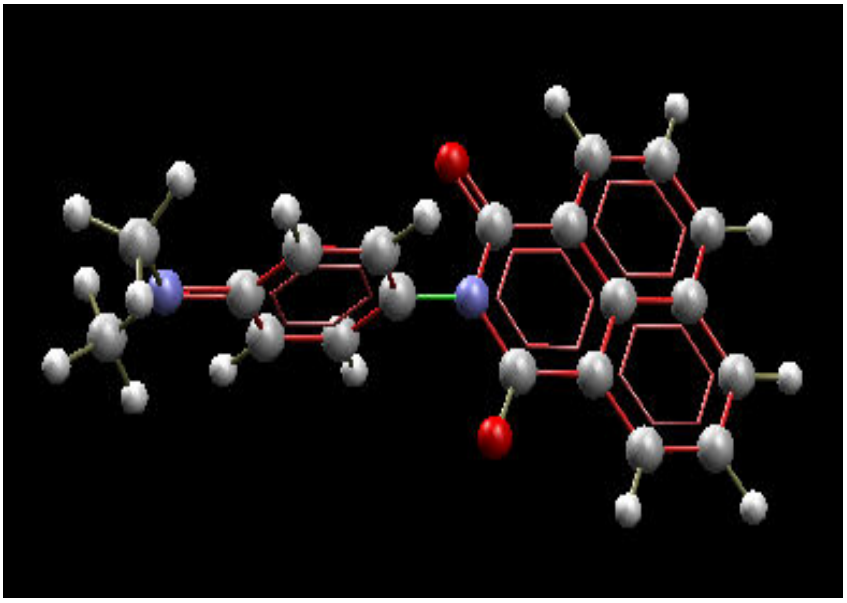

Selected molecular structures discussed in this chapter are shown below.

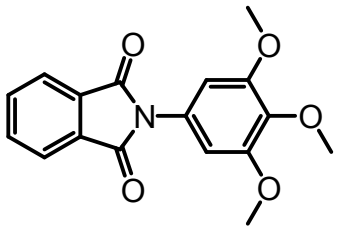

PHTH1

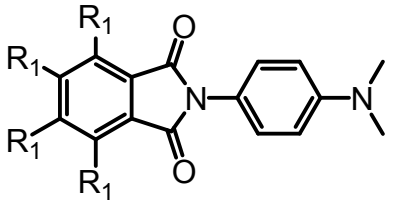

R_1 = H, **PHTH2**; R_1 = Cl, **PHTH3**

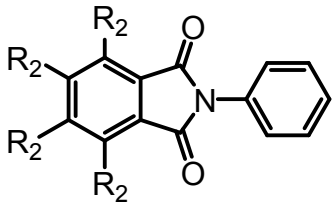

R_2 = H, **PHTH4**; R_2 = Cl, **PHTH5**

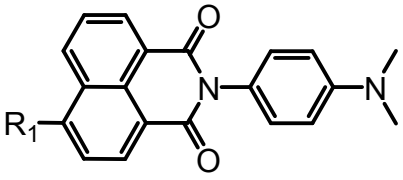

R_1 = H, **NAP1**
R_1 = Cl, **NAP2**
R_1 = Br, **NAP3**

We acknowledge those involved in the work described in this Chapter. Thanks to Dr Ross W. Harrington for the characterisation of crystal structures. To Prof. Nikolai V. Tkachenko's group for fluorescence lifetime measurements, to Noor Aniza Harun for her help with the confocal microscopy measurements and finally to Jonathan Pate for current-voltage measurement on crystals.

4.1 Introduction

Organic chromophores usually exhibit fluorescence properties in dilute solution and they have shown potentials in various areas such as chemical ion sensors[1], viscosity probes[2], gas sensors[3] and dye-sensitised solar cells[4]. Fluorescence from most organic chromophores is not observed in concentrated solution, or in the crystalline state, due to quenching by aggregation. However, practical molecular devices such as organic light emitting diode (OLED) materials used in display technology applications (e.g., smartphones, laptops and television screens) require crystalline materials with high stability. Due to increasing demands on solid state emitters, researchers found that instead of conventional aggregation quenched fluorescence, some molecules display the interesting property of "aggregation induced fluorescence". Tang *et al.*[5], reported that silole (1-methyl-1,2,3,4,5-pentaphenylsilole) displayed this interesting property. They reasoned this phenomenon is a result of restricted intramolecular rotation and emission is enhanced upon aggregation. Since then, increasing amount of research has been devoted to the synthesis of organic or polymeric materials which emit in the crystalline form[6].

Naphthalimide derivatives are efficient fluorescence materials. Their applications have been found in many aspects such as laser dyes[7], p-channel semiconductors[8], molecular logic gates[9] and chemosensors[10]. In this work we describe one step synthesis of naphthalimide and phthalimide derivatives. We expected to study their photophysical properties in the solid state and to exam their potential as solid state emitters. We also observed polymorphism in one of the naphthalimide derivatives. A polymorph is described as identical asymmetric units with disparate arrangements[11]. There are several factors which contribute to the formation of a polymorph such as solvents, concentration, temperature and pH[12]. Under different conditions there is a kinetically favoured product and is formed as the dominant product. The dissimilar orientations of

the identical units results in diversity in colours, melting points, chemical reactivity, solubility and mechanical properties[13]. The advantage of the existence of a polymorph is that we can easily tune the properties with minimum modification of the chemical composition. Polymorphism is also of vital importance in drug synthesis for the pharmaceutical industry. In this chapter we discovered polymorphs in a naphthalimide derivative and they displayed different properties such as colours, melting points and emission lifetimes.

4.2 Synthesis

The synthesis of naphthalimide and phthalimide derivatives followed the literature method[14]. When reactions were carried out in the absence of molecular sieves, longer reaction times were required and the yields were low. Therefore, molecular sieves were used to absorb water to reduce the reaction time and improve the yield. The advantage of using molecular sieves instead of another drying reagent is the simplicity of the purification process. Molecular sieves can be easily removed by filtration. When the temperature was high the product dissolved readily in DMF, but once the temperature decreased the product began to precipitate out of solution. Since the precipitated product coated the molecular sieves the material after filtration was dissolved in DCM, filtered and removed to recover the product. Reactions were carried out in DMF (dried over 4 Å molecular sieves before usage) at 120-130^{o}C for 4-5 hours affording yields between 70 - 80%. The synthesis of phthalimide and naphthalimide derivatives is shown in *Scheme 1*.

The products were purified by recrystallisation and two methods were used:

1: Vapour diffusion. The crude was dissolved in a “good solvent” (i.e. one in which the compound was fully soluble) and put into a small sample vial. The sample vial was placed in a large vial which contained an anti-solvent. The good solvents used here were generally chloroform or dichloromethane, and the anti-solvents were generally diethyl ether or petroleum ether.

2: Evaporation. The crude product was dissolved in ethanol and left at room temperature.

With evaporation of the ethanol, crystals formed in the sample vials. Specific details for each compound were described in chapter 2.

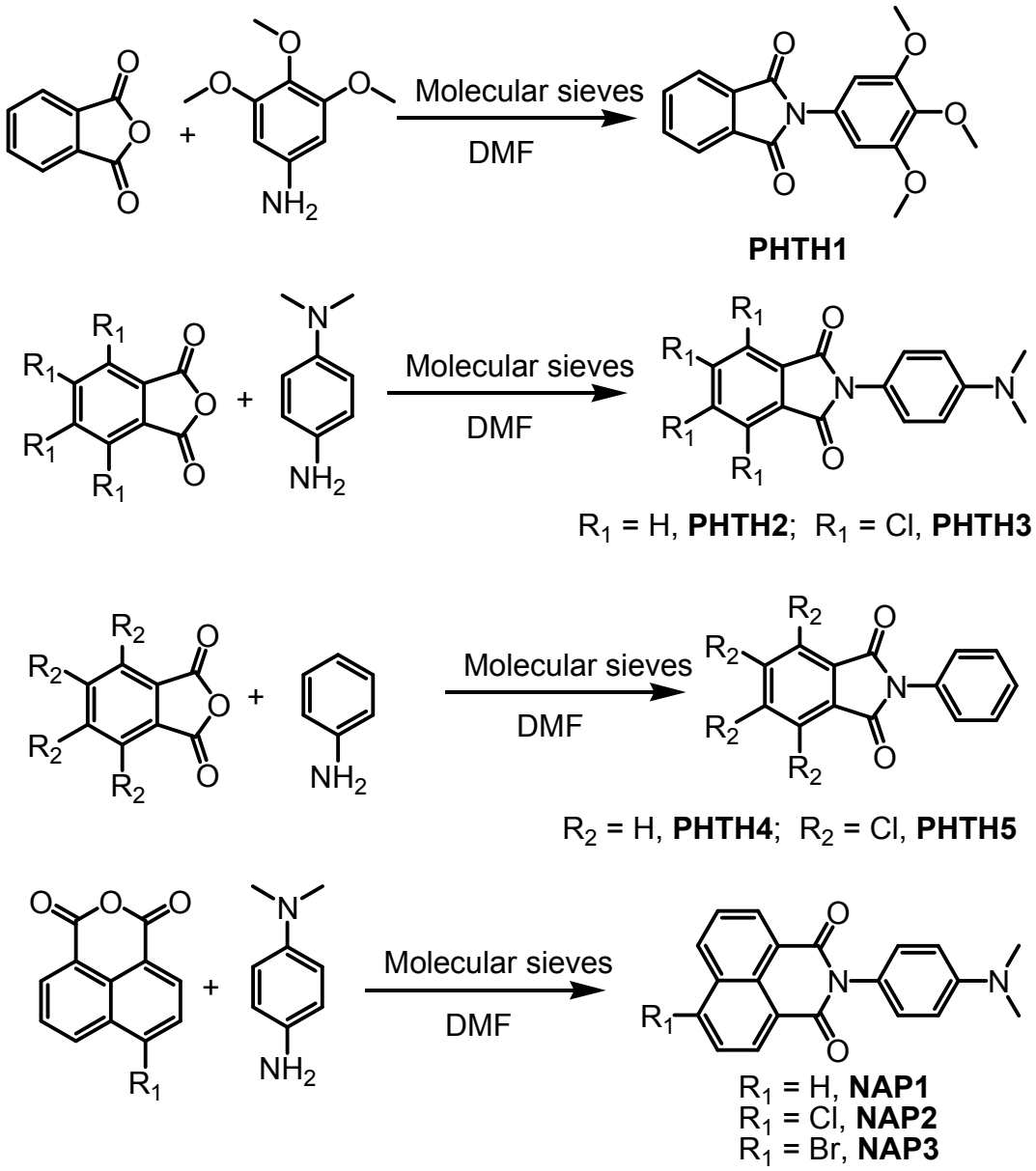

Scheme 1. Synthesis of the naphthalimide and phthalimide derivatives.

A general reaction mechanism[15] (phthalimide is shown as an example) is illustrated in *Scheme 2*. One of the side products from the reaction can be the carboxylic acid which is derived from hydrolysis of the anhydride. The second step is slower than the first step, i.e. the second step is rate determining control step. Therefore, in the absence of molecular sieves the completion of the reaction is slow and inefficient. Presence of water also promotes hydrolysis of the final amide. To achieve the target products in a reasonable

yield, the presence of the absorbent for water is essential. The identity of all products was confirmed by routine analysis including, NMR spectroscopy, MS, combustion analysis and X-ray crystallography.

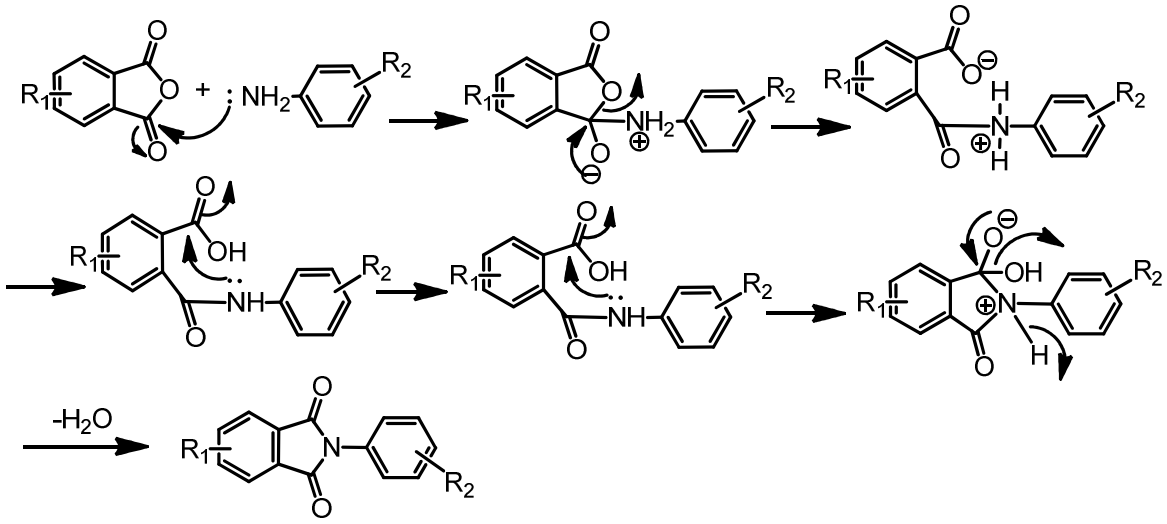

Scheme 2. Reaction mechanism for acylation of an amine with an anhydride.

It is worth noting that the crystals of **NAP 1** were obtained as green colour (**NAP1-G**) when the crude product was recrystallised from dichloromethane and diethyl ether. If the solution was left for longer times orange coloured crystals (**NAP1-O**) started to appear on the top of green crystals. This seems to us that the two crystal forms are polymorphs of **NAP1** and the green coloured crystals are the kinetically favoured product. We therefore set out to explore whether it was possible to obtain orange crystals under different conditions. Indeed, we found that orange crystals could be obtained when chloroform was used as a "good solvent" instead of DCM. The orange crystals achieved from chloroform and diethyl ether turned out to be very large long needles. Without crystal structures we firstly suspected that the disparate colours were due to the presence of solvents in the crystal lattice. The crystal structures (section 4.3 crystal structures) confirm that it is not impurities but different conformers. No solvent molecules were found in either crystal structures, and packing of the structures varied from each other. The melting point of **NAP1-G** was 332 ^{O}C while **NAP1-O** started to decompose at 320 ^{O}C.

4.3 Crystal structures

Single crystals for a few compounds were obtained and their structures are shown in *Figure 1* to *Figure 6*.

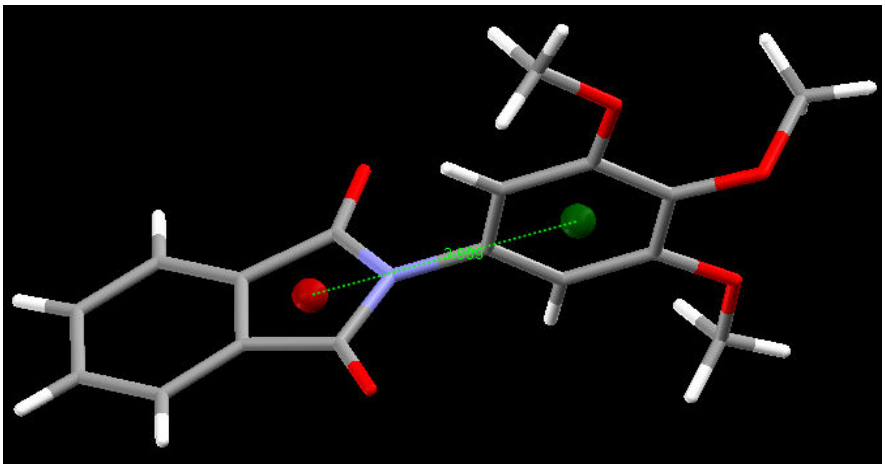

*Figure 1. Molecular structure of **PHTH1**: carbon (grey), oxygen (red), hydrogen (white), nitrogen (blue). Dihedral angle between plane of donor part and plane of acceptor part is 70.26. Intramolecular distance between donor centre (red dot) and acceptor (green dot) is 4.0 Å.*

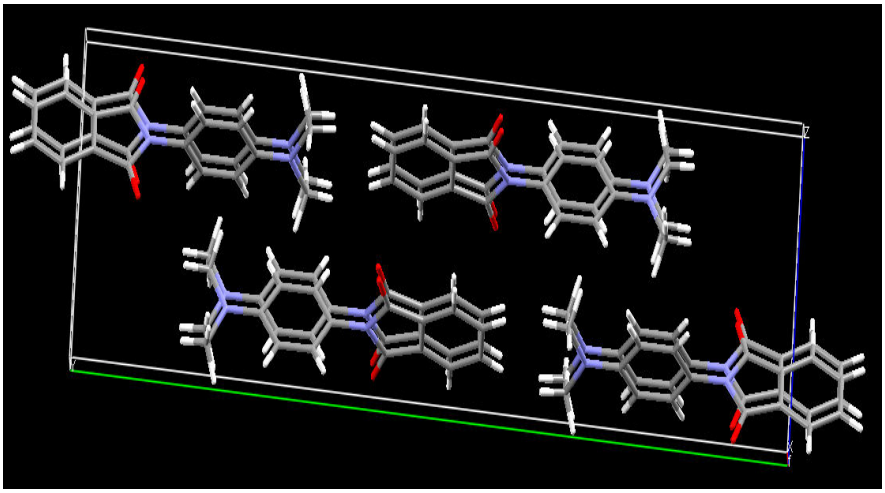

*Figure 2. Molecular structure of **PHTH2**: carbon (grey), oxygen (red), hydrogen (white), nitrogen (blue).*

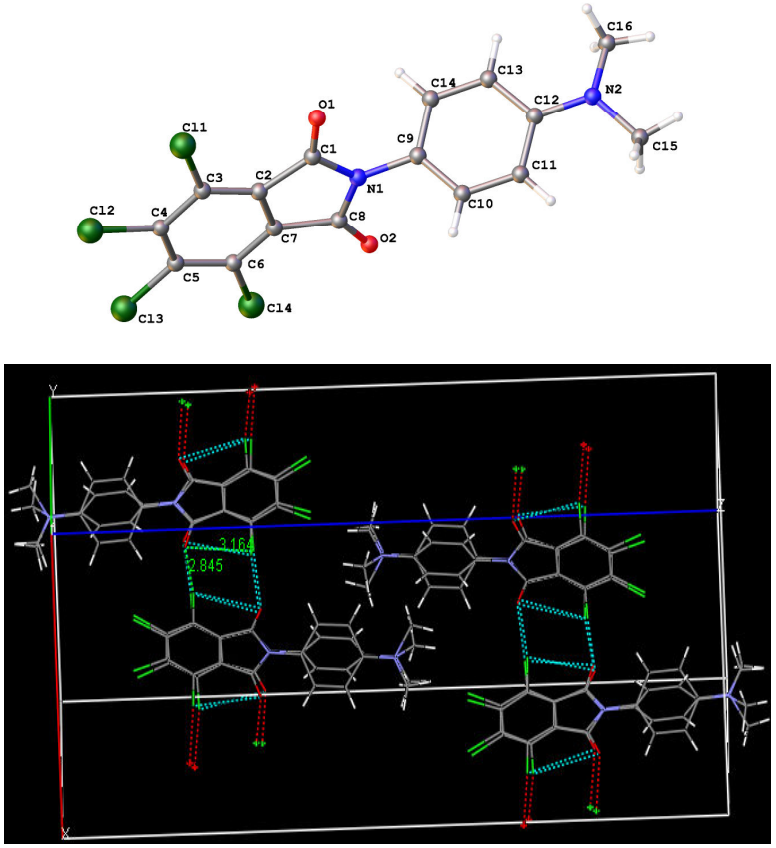

*Figure 3. Molecular structure of **PHTH3**: carbon (grey), oxygen (red), hydrogen (white), nitrogen (blue), chloride (green). Intermolecular oxygen and chlorine atoms distances are 2.8 Å which are shorter than the sum of Van der Waals radius of chloride and oxygen (175 pm +152 pm = 3.24 Å).*

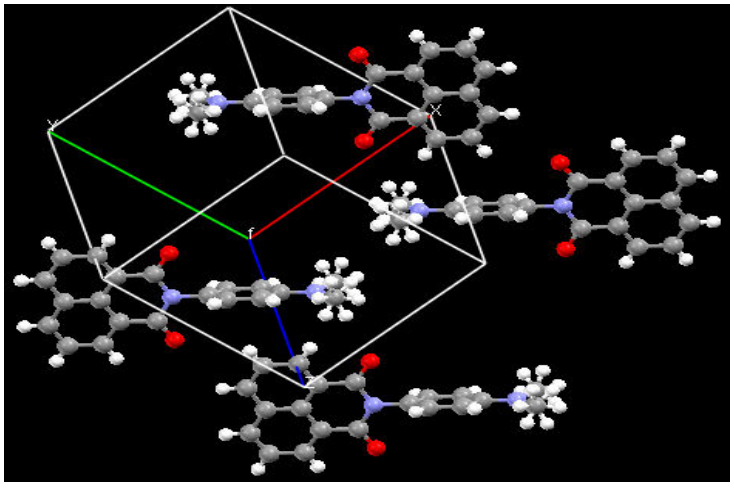

*Figure 4. Molecular structure of **NAP1-G**: carbon (grey), oxygen (red), hydrogen (white), nitrogen (blue). The head-to-tail stacking means that the N,N-dimethyl phenyl ring is sandwiched between the two naphthalimide rings. There are defects in the crystal structures, the final R indices is 0.0452.*

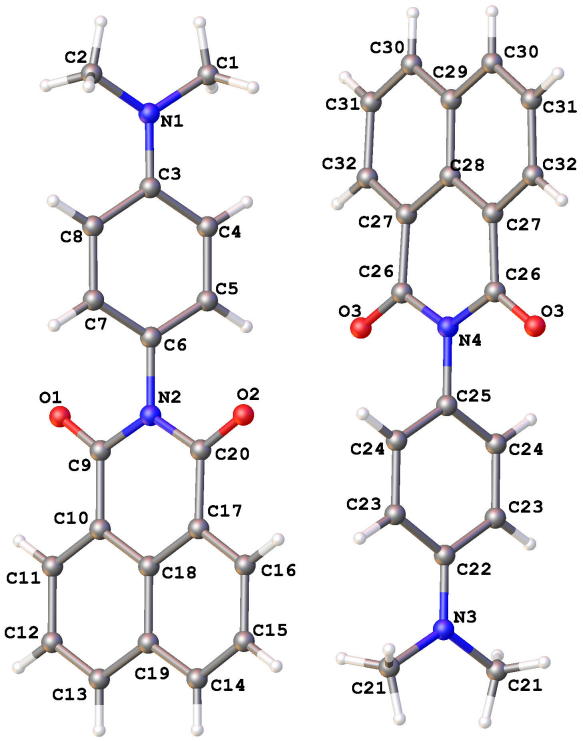

*Figure 5. Molecular structure of **NAP1-O**: carbon (grey), oxygen (red), hydrogen (white), nitrogen (blue). The final R indices obtained from the structure analysis is 0.0452.*

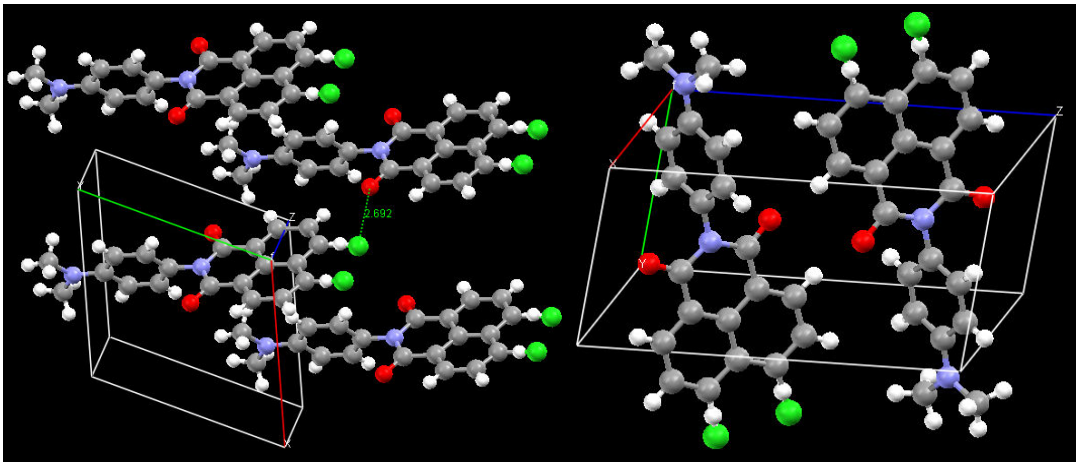

*Figure 6. Molecular structure of **NAP2**: carbon (grey), oxygen (red), hydrogen (white), nitrogen (blue), chloride (green). Chloride shown in both 3 and 7 position of the naphthalimide ring is due to the defects of the crystals. The final R indices obtained from the structure analysis is 0.0421. Intermolecular oxygen and chlorine atoms distances are 2.7 Å.*

Intramolecular distances of donors and acceptor ($d_{D\text{-}A}$, *Table 1*) show no significant differences. The dihedral angles (*Table 1*) between the planes of the donor and acceptor units for **NAP1-O** are 89^{O} and 69^{O}. The distance between donor planes ($d'_{D\text{-}D}$) or between acceptor planes ($d'_{A\text{-}A}$) were similar for phthalimide derivatives. Donor/ acceptor

planes of **NAP2** and acceptor planes of **NAP1** are not parallel (intersect with each other among neighbouring molecules), therefore the distances were not determined. **PHTH2**, **NAP1-O** have similar values of d'_{D-D}, around 3 Å, and smaller than **PHTH1** and **PHTH3**. It was suggested by Langhals *et al.*[16] that an intermolecular donor/acceptor plane distance less than 5-6 Å leads to quenching of solid-state fluorescence, due to the enhancement of exciton coupling. However this rule is not applicable to some of these phthalimide and naphthalimide derivatives. For **PHTH3** and **NAP2** the intermolecular oxygen and chlorine atoms distances are about 2.8 Å which are shorter than the sum of Van der Waals radius of chloride and oxygen (175 pm +152 pm = 3.24 Å). So there might be halogen bonding to support the solid state charge transfer fluorescence. Other examples exempt to this rule were also reported by Dreuw and co-workers[17] in their study of solid-state fluorescence behavior of organic Pigment Yellow 101 derivatives. They suggested that intramolecular hydrogen bonding play an important role for the solid state fluorescence properties.

Table 1. Comparison of crystal packing diagrams of phthalimides and naphthalimides derivatives.

Compounds	d_{D-A} [(a)] / (Å)	Dihedral angle [(b)] / (^{O})	d'_{D-D} [(c)] / (Å)	d'_{A-A} [(d)] / (Å)
PHTH1	4.0 [(e)]	71	3.8	3.4
PHTH2	6.8	65	3.0	3.0
PHTH3	7.4	69	5.0 [(f)]	5.0 [(g)]
NAP1-O	7.0	89 / 69	3.0	-
NAP1-G	7.0	71	-	-
NAP2	7.0	70	-	-

(a) Intramolecular distance of donor centres and acceptors centres; (b) Dihedral angles between donor planes and acceptor planes, an example of measurement was shown in Figure 1; (c) Distance of intermolecular planes of donors; (d) Distance of intermolecular planes of acceptors; (e) The centre of the aromatic ring was set as the centre of tri-methoxy groups; (f) Distance between N and N. (g) Distance between centroids of phthalimide rings.

When we compare the crystal packing diagrams of all derivatives, it is clear that the phthalimide molecules pack in a "heads to heads and tails to tails" manner, i.e. donors to donors and acceptors to acceptors between neighbouring molecules. In contrast to naphthalimide derivatives adopt a "head to tail" (i.e. donors to acceptors) arrangement. This packing feature leads to disparate intermolecular donor to acceptor distances, which is one possible reason for the variations in photophysical properties among these systems.

The observation of **NAP1** polymorphs led us to exam the variation of their properties in the solid state in more depth, and to further understand how packing in the crystalline materials might affect their optical properties. The intermolecular distance from amino nitrogen to the centroid of the naphthalimide (red dot) (*Figure 7 and Figure 8*) shows subtle differences for the polymorphs as summarised in *Table 2*.

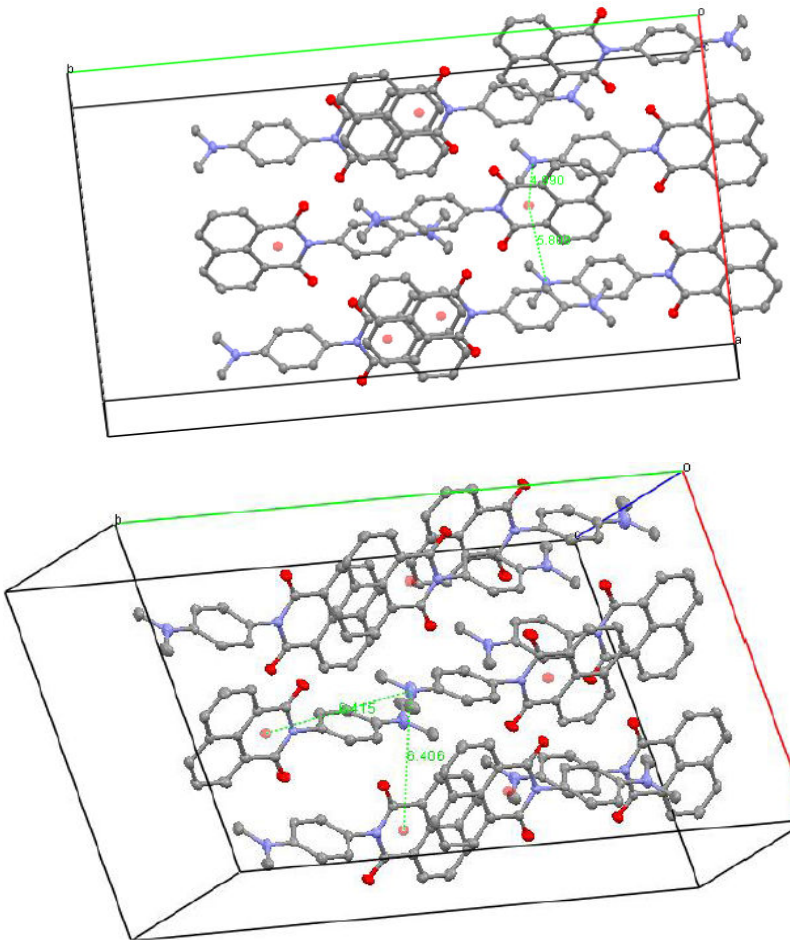

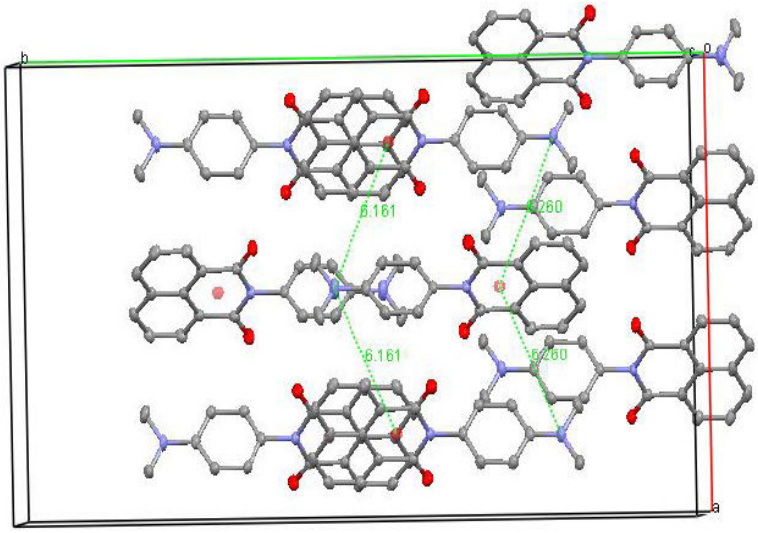

*Figure 7. Several views for the crystal packing diagram for **NAP1-O** showing a selection of the intermolecular amino-naphthalimide separation distances. Carbon (grey), oxygen (red), nitrogen (blue).*

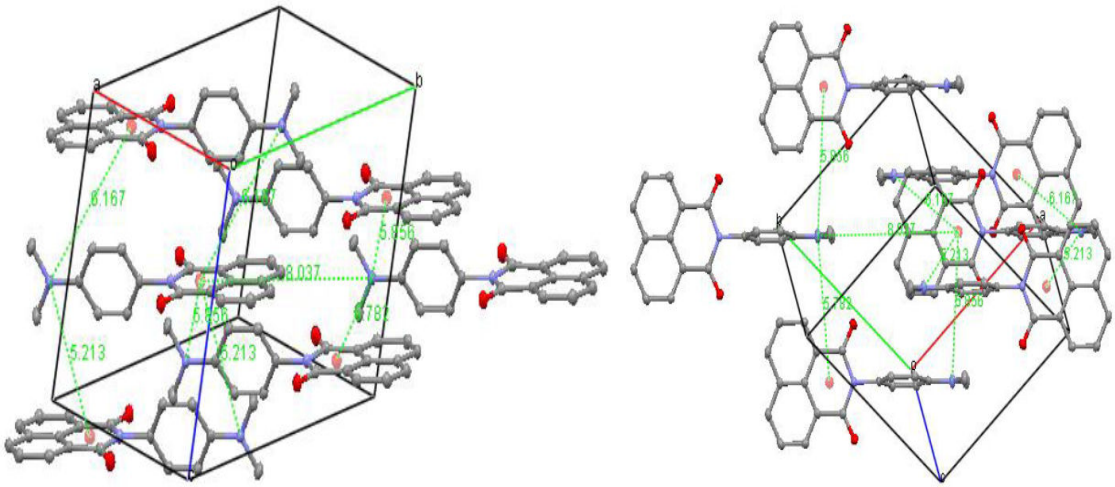

*Figure 8. Several views for the crystal packing diagram for **NAP1-G** showing a selection of the intermolecular amino-naphthalimide separation distances*

Table 2. Selected intermolecular N-amino to naphthalimide centroid distances for the two polymorphs.

Compound	Selected intermolecular distances / Å					
NAP1-O	4.99	5.81	6.16	6.26	6.41	6.42
NAP1-G	5.21	5.78	5.86	6.17	6.68	7.92

One side product from formation of **NAP2** reaction was **NAPA** (*Figure 9*). The formation

of **NAPA** is possibly because of coupling of the halide with the amine. The most well known aryl halide amination reaction is the Buchwald-Hartwig coupling reaction[18]. The reaction usually proceeds in the presence of palladium catalyst and specific ligands, and generally chloride is not as reactive as bromide and iodide. Under our reaction conditions neither metal catalyst nor ligand was used. Therefore, the observation of **NAPA** from crystallography analysis was unexpected. It is very likely that **NAPA** is formed as side product and we were lucky enough to pick up the **NAPA** crystal during the analysis. It is possible that the reaction proceeds without catalyst because of the high temperature used in the reaction.

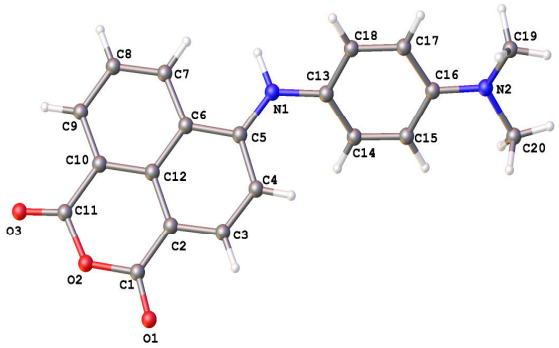

*Figure 9. Crystal structure of **NAPA**: carbon (grey), oxygen (red), hydrogen (white), nitrogen (blue).*

4.4 Electrochemical investigation

The redox properties of phthalimide and naphthalimide derivatives were studied by cyclic voltammetry. The experiment was carried out in a conventional three electrode cell consisting of a glassy carbon working electrode, a platinum wire counter electrode and Ag/AgCl reference electrode. The phthalimide/naphthalimide derivative (1 mM) was dissolved in anhydrous DCM containing tetrabutylammonium tetrafluoroborate (TBATFB, 0.2 M) background electrolyte. The solution was deoxygenated before the measurement and kept under nitrogen during the whole experiment. The same concentration (1 mM) of ferrocene was added as internal reference.

Cyclic voltammograms recorded for the phthalimide and naphthalimide derivatives are

shown in *Figure 10* and *Figure 11*, respectively. Each compound exhibited a one-electron, quasi-reversible oxidation peak and a one-electron, quasi-reversible reduction peak. The oxidation peaks are assigned to removal of an electron from the *N*-amino/methoxy group, while the reduction peaks are due to addition of an electron to the naphthalimide/phthalimide units. The difference between the oxidation and reduction potentials (ΔE) is reported in *Table 3*. The reduction potentials of **PHTH1** and **PHTH2** were similar, while for **PHTH3** the value was shifted more than 300 mV to a less negative potential. This shift is likely the effect of six chlorine atoms in the phthalimide ring which remove electron density from the ring and make **PHTH3** easier to reduce. The highest oxidation potential was seen for **PHTH1** with $E_{1/2}$ = 1.51 V, which is about 500 mV more positive than the other two phthalimide derivative. The oxidation and reduction potentials for naphthalimide derivatives are similar.

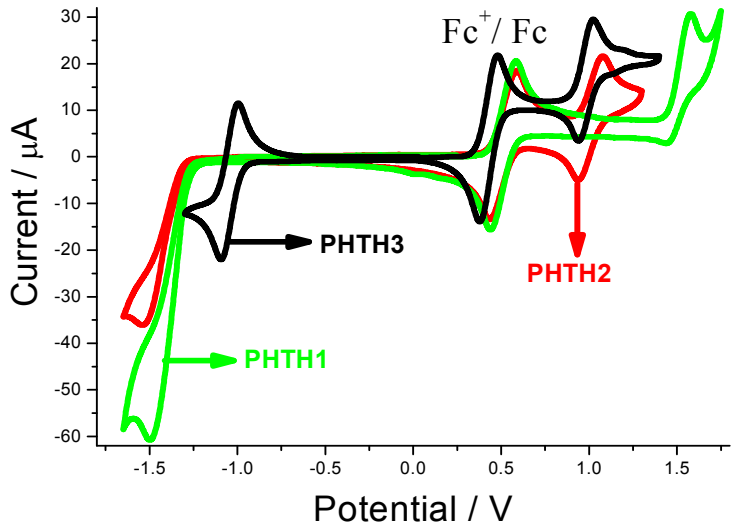

*Figure 10. The cyclic voltammogram recorded for **PHTH1** (green), **PHTH2** (red) and **PHTH3** (black) in CH_2Cl_2 (0.2 M TBATFB). Scan rate = 50 mV s^{-1}.*

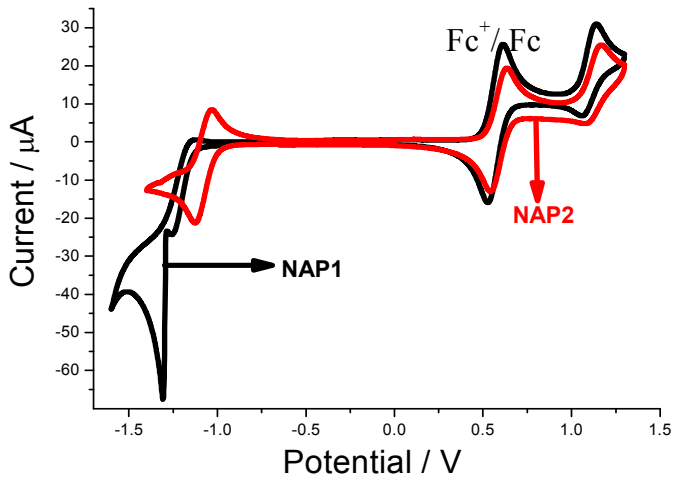

*Figure 11. The cyclic voltammogram recorded for **NAP1** (black) and **NAP2** (red) in CH_2Cl_2 (0.2 M TBATFB). Scan rate = 50 mV s^{-1}.*

Table 3. Summary of potential difference between oxidation and reduction potentials.

Compound	**PHTH1**	**PHTH2**	**PHTH3**	**NAP1**	**NAP2**
E_1 (V)	1.51	1.0	0.98	1.10	1.12
(Δ_E / mV)[a]	(130 mV)	(140 mV)	(100 mV)	(80 mV)	(90 mV)
E_2 (V)	-1.37	-1.40	-1.05	-1.20	-1.08
(Δ_E / mV)[a]	(260 mV)	(255 mV)	(105 mV)	(110 mV)	(100 mV)
ΔE (V)	2.88	2.40	2.03	2.30	2.20

[a]Separation between E_{pa} and E_{pc}.

4.5 Molecular orbital calculations

The HOMO-LUMO energy gap obtained from the gas phase DFT calculated (B3LYP, 6-311G$^+$)[19] energy-minimised structure for **NAP1** is 2.53 eV (*Figure 12*). The HOMO resides on the *N,N*-dimethylaniline group while the LUMO is localised on the naphthalimide subunit.

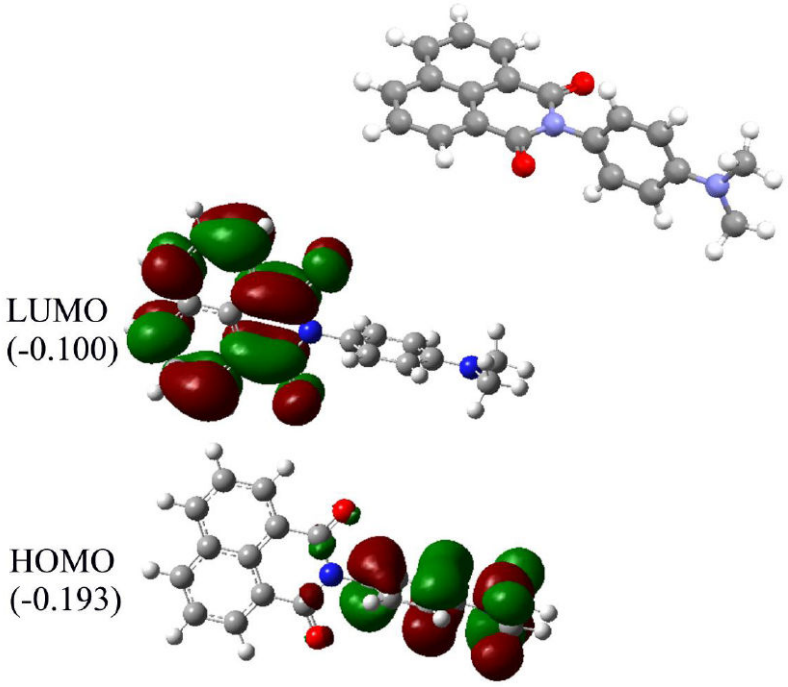

Figure 12. DFT (B3LYP 6-311G) energy-minimized structure for ***NAP1*** *calculated using Gaussian O3. Representation of the HOMO and LUMO for the molecule. Energy in Hartrees.*

4.6 Photophysical studies

4.6.1 Absorption spectra

Absorption spectra of phthalimide and naphthalimide derivatives are shown in *Figure 13* to *Figure 15*. There is one common feature of these compounds which is a broad tail as seen from the spectrum (see inset expansion in *Figure 13* to *Figure 15*). The broad tails are characteristic for charge transfer transition bands. To further confirm that the broad band is due to charge transfer between donor and acceptor, the absorption spectrum of reference compound **PHTH5** (*Figure 16*, without *N,N*-dimethylamino donor group), was measured and compared with **PHTH3**.

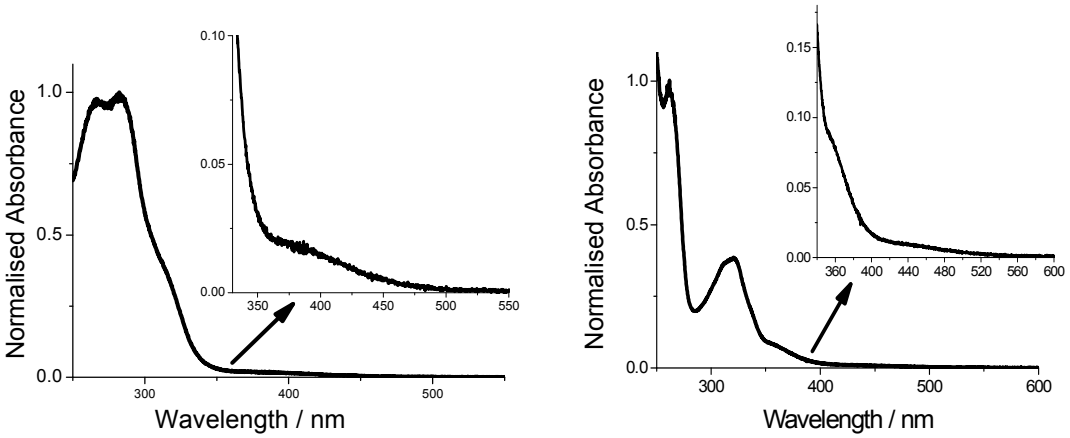

*Figure 13. Left: normalized absorption spectrum of **PHTH2** and the inset shows expansion between 350 and 550 nm. Right: normalized absorption spectrum of **PHTH3** and the inset displays expansion of the spectrum between 370 and 600 nm. The spectra were recorded in DCM at room temperature.*

Two main peaks for **PHTH2** (*Figure 13, left*) were observed at 270 nm and 280 nm, and around 310 nm another peak was seen as a shoulder. The peak at longer wavelength is most likely due to the n-π∗ transition of the carbonyl group, since similar peak values, 280 nm and 300 nm, were reported for phthalimide derivatives[20]. **PHTH3** (*Figure 13, right*) exhibited different electronic transition characteristics, the first peak was seen at 260 nm and second one at 320 nm. This means that **PHTH3** displayed a blue shift for the higher energy transition band, and a red shift for lower energy transition band. The blue shift might be a result of the chlorine atoms on the phthalimide ring which decreases the electron density on the rings and increases the energy gap for π-π* transition. And the lone pair of electrons on chlorine can add additional n-π∗ transition bands to the absorption spectrum.

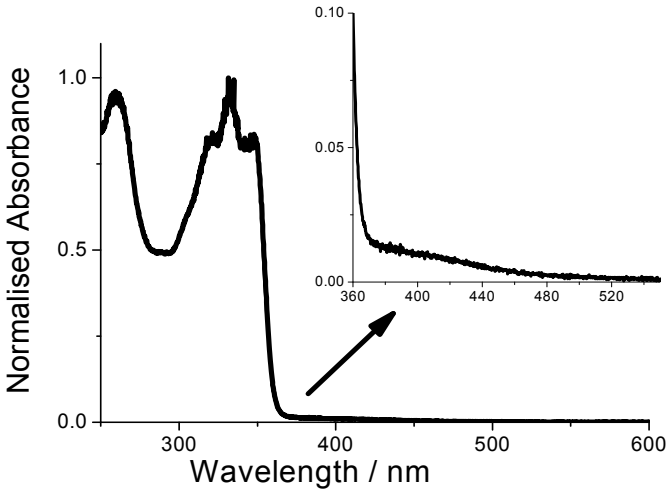

*Figure 14. Normalized absorption spectrum of **NAP1** recorded in DCM at room temperature.*

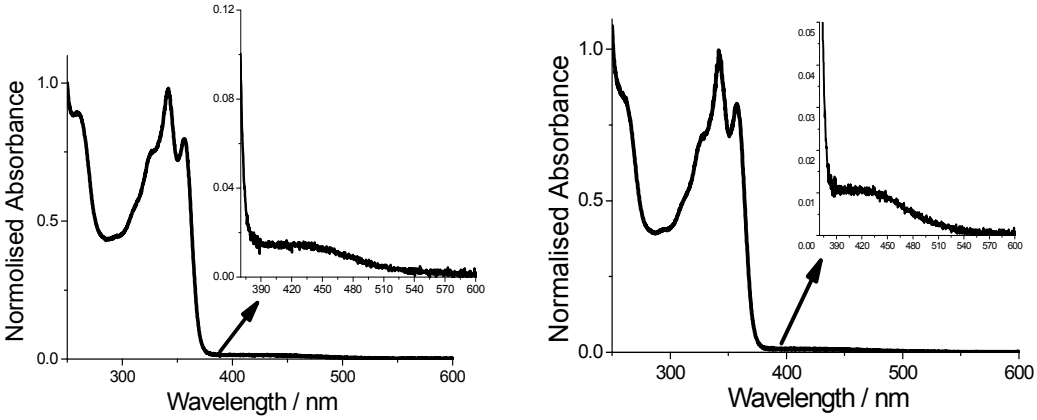

*Figure 15. Left: normalized absorption spectrum of **NAP2** and the inset shows expansion between 360 and 550 nm. Right: normalized absorption spectrum of **NAP3** and the inset displays expansion of the spectrum between 360 and 550 nm. The spectra were recorded in DCM at room temperature.*

Four main peaks at 260 nm, 320 nm, 332 nm and 348 nm, are observed in the electronic absorption spectrum for **NAP1** (*Figure 14*). Wintgens and co-workers reported that the maximum absorption bands for 1,8-naphthalimides are around 230 nm with a shoulder on both sides, and longer wavelength peaks at around 330 nm and 345 nm[21]. The values at longer wavelength are close to our experimental ones. The small 2-3 nm variation is within experimental error and one additional peak at 320 nm was observed for **NAP1** in our experiment. Any absorbance bands at a wavelength shorter than 250 nm were not measured in our experiment so only the one peak at about 260 nm was seen. Absorption

spectra for **NAP2** and **NAP3** (*Figure 15*) are similar, characterised by four peaks at 260 nm, 327 nm, 340 nm and 356 nm. The peak in lower energy side is the same as **NAP1** and those in longer wavelength, over 300 nm, were red shifted about 8 nm. The red shift can be reasoned to the lone pair on the chlorine/bromine atoms, similar mechanism as for the red shift observation of **PHTH2**. A summary of the absorption bands and molar absorption coefficient was shown in *Table 4*.

Table 4. Absorption maximum and molar absorption coefficient for phthalimide and naphthalimde derivatives recorded in DCM at room temperature.

Compound	λ_1 (nm)	$\varepsilon_1/10^4$ (M^{-1} cm^{-1})	λ_2 (nm)	$\varepsilon_2/10^4$ (M^{-1} cm^{-1})	λ_3 (nm)	$\varepsilon_3/10^4$ (M^{-1} cm^{-1})	λ_4 (nm)	$\varepsilon_4/10^4$ (M^{-1} cm^{-1})
PHTH2	267	1.15	282	1.17	312	0.46	-	-
PHTH3	260	1.55	-	-	320	0.79	-	-
NAP1	260	1.44	320	1.25	332	1.5	348	1.25
NAP2	260	1.8	327	1.53	340	1.99	356	1.63
NAP3	260	1.47	327	1.26	340	1.26	356	1.44

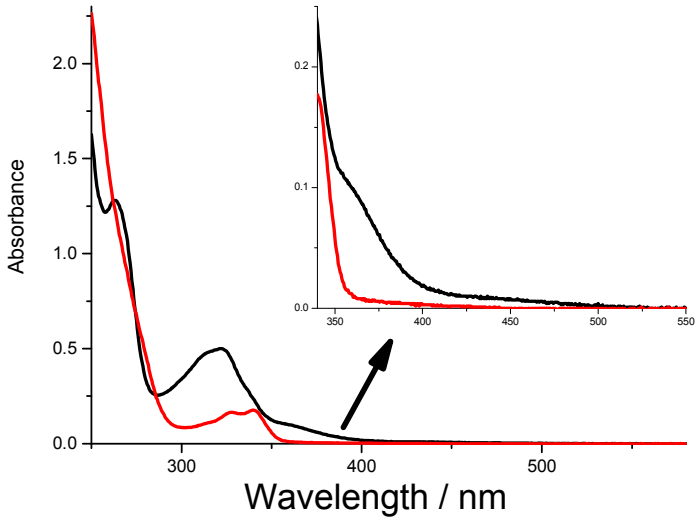

*Figure 16. Comparison of absorption spectra of **PHTH3** (black) and **PHTH5** (red). The inset shows the expansion of spectra between 330 nm and 550 nm.*

4.6.2 Solid state fluorescence

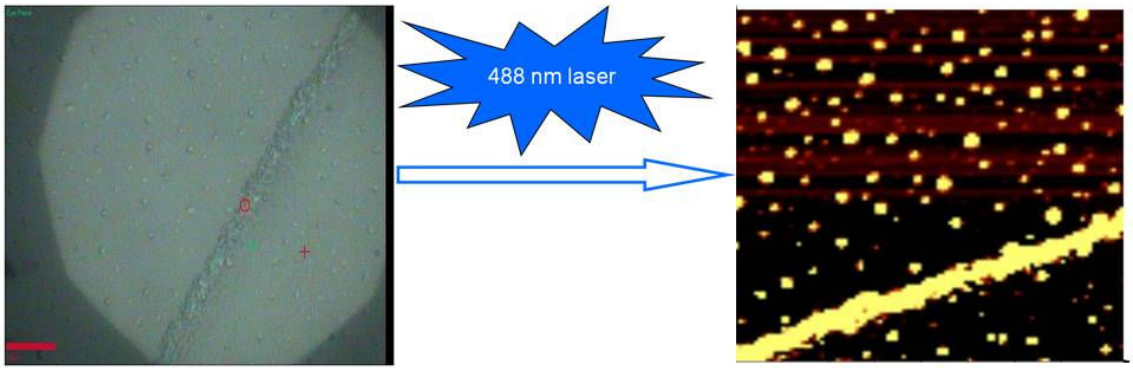

Figure 17. Images under confocal microscope for ***NAP1*** *before (left) and after (right) laser excitation.*

Solid-state fluorescence spectra were measured by confocal microscopy with a 488 nm laser as light source. Images under microscope before and after laser excitation are shown in *Figure 20*. A micro-crystalline solid is observed in the image (*Figure 17*, left). Crystals form a thick long band where more material was deposited on the glass slide. The micro-crystals were observed as bright spots under laser excitation and the thick crystals band was seen as a bright yellow band in the image (*Figure 17*, *right*). An emission spectrum was collected for each point of the image, and by taking an average of all the spots we obtained a complete emission spectrum.

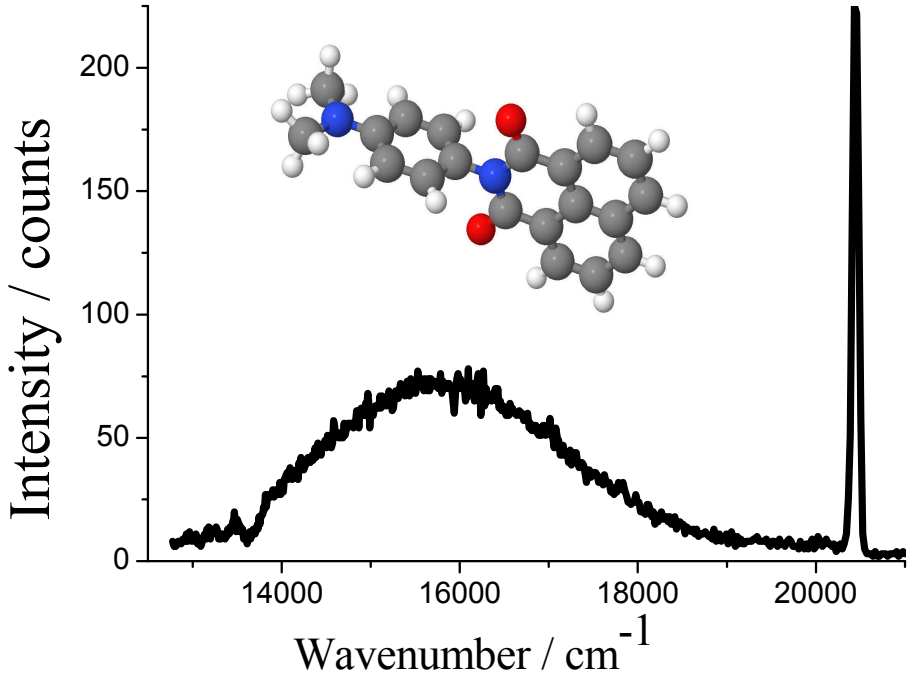

*Figure 18. Solid-state fluorescence spectrum recorded for **NAP1**.*

A representative fluorescence spectrum for **NAP1** is shown in *Figure 18*. The sharp peak is due to the excitation laser (λ_{ex} = 488 nm), which is used as a reference during the experiments. The broad featureless band is assigned to charge transfer fluorescence. Spectra were collected for all the samples. In most cases the emission bands were distorted, and so peaks were fitted as a Gaussian (*Figure 19*) to obtain the peak maximum (λ_{EM}) and the FWHM (full width at half maximum). The broad fluorescence spectrum for **PHTH3** required fitting as two Gaussian bands. The FWHM of **PHTH1** (*Table 5*) was larger than the others, this is possibly due to the three methoxy groups which are more flexible than the N,N-dimethyl group leading to a larger reorganisation energy. The reorganisation energy (λ_T) is proportional to the square of FWHM[22].

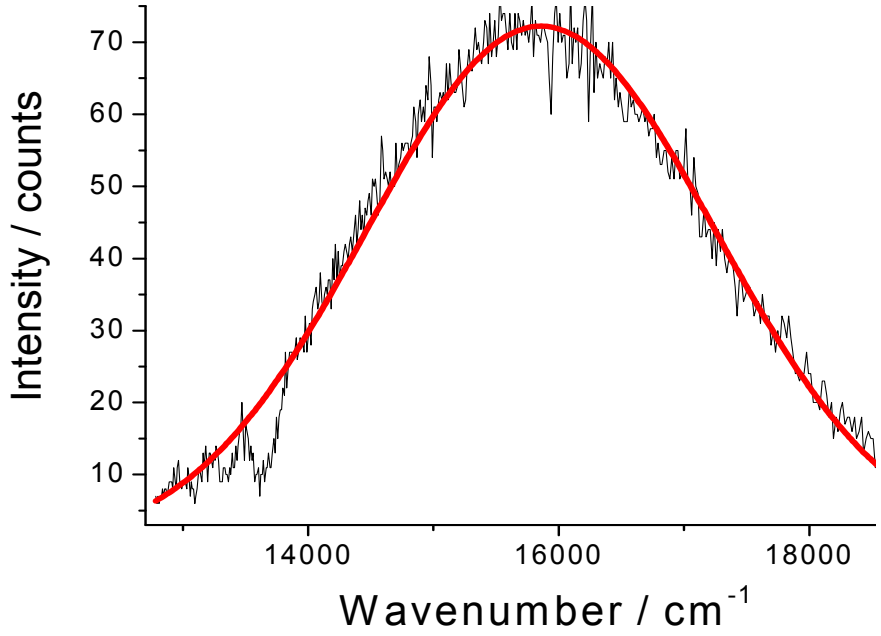

*Figure 19. Observed solid state fluorescence spectrum for **NAP1** (black) and fitted spectrum (red).*

Table 5. Parameters obtained from emission spectra in the solid state.

Compound	**PHTH1**	**PHTH2**	**PHTH3**	**NAP1**	**NAP2**
λ_{EM} / cm^{-1}	17085	17400	15860/18840	15855	17300
FWHM / cm^{-1}	4250	3290	3700	3285	3720

NAP1-O was obtained as long needle shape crystals and we realised that fluorescence could be observed by placing the crystals under 355 nm UV light (*Figure 20*). This observation indicated to us that it might be possible to obtain a fluorescence spectrum using a normal fluorescence spectrometer.

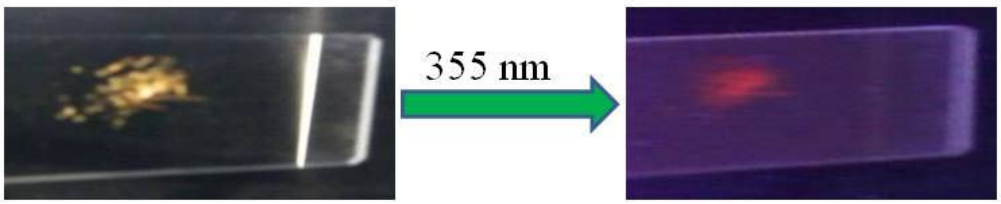

*Figure 20. Images of crystalline **NAP1-O** upon radiation of 355 nm UV light.*

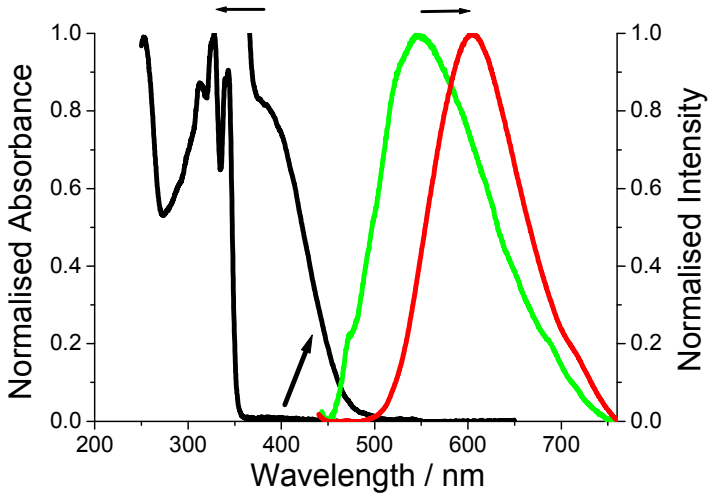

*Figure 21. Room temperature absorption spectrum for **NAP1** in dilute cyclohexane and the expansion of the region around 400 nm. The fluorescence spectrum recorded for crystalline **NAP1-O** (red) and **NAP1-G** (green).*

The crystals were carefully aligned with the centre of the excitation light source. The solid state fluorescence from crystals was obtained for **NAP1-O** and **NAP1-G** respectively (*Figure 21*). The peak maximum for **NAP1-G** is λ_{EM} = 605 nm while that for **NAP1-O** was blue shifted to λ_{EM} = 549 nm. No reproducible fluorescence was observed from a dilute cyclohexane solution of **NAP1** at room temperature. The fluorescence is unique to the crystalline sample, the emission profiles in the solid state cannot be assigned to the structured emission seen in solution at around λ_{EM} = 378 nm as previously reported for 1,8-naphthalimide[15]. It was reported that the fluorescence intensity and quantum yield of *N*-alkylnaphthalimide decreased when the alkyl side chain contained an amino group[23]. The quenching of **NAP1** fluorescence in solution is likely the result of the presence of a low-lying charge transfer state.

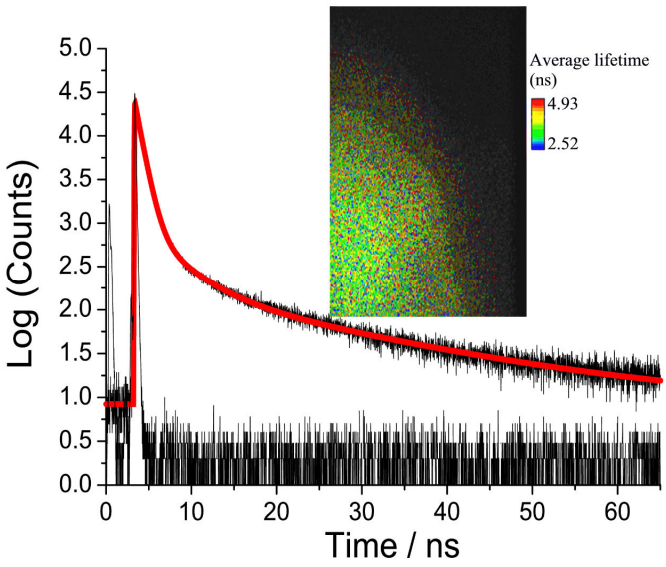

*Figure 22. Room temperature emission decay curve and instrument response function recorded for **NAP1-O** and the least-squares fit to a tri-exponential (red line). Insert shows a typical lifetime imaging picture taken for the crystal sample.*

Picosecond fluorescence lifetime imaging experiments were performed on both crystal polymorphs. A decay profile and image for **NAP1-O** are shown in *Figure 22*. The fluorescence decay profile was best fit to a tri-exponential model ($\tau_{obs} = A_1\exp(-t/\tau_1) + A_2\exp(-t/\tau_2) + A_3\exp(-t/\tau_3)$). Data collected on different crystals, orientations and from multiple areas of a crystal could be analysed in an identical manner. Values for lifetimes and pre-exponential factors were within error identical. The major lifetime (τ_1) is 1.20 ns and represents 92% of the fluorescence decay profile. The two longer lifetime components contribute to the remaining fraction of the decay. Assigning significance to the τ_3 component is risky; the error is ca. 16% and the A_3 contribution is small.

An identical lifetime imaging experiment performed on **NAP1-G** (*Figure 23*) resulted in decay profile that was similarly analysed as a tri-exponential. However, τ_1 is reduced significantly to only 350 ps, but the A_1 value is still comparable to the case for **NAP1-O** (*Table 6*). Again, the longer lifetime components contribute only a small fraction to the decay curve. For comparison purposes we concentrate on τ_1 values for both the polymorphic crystals. The effect on the τ_1 lifetime by alteration in the crystal packing for **NAP1** is striking.

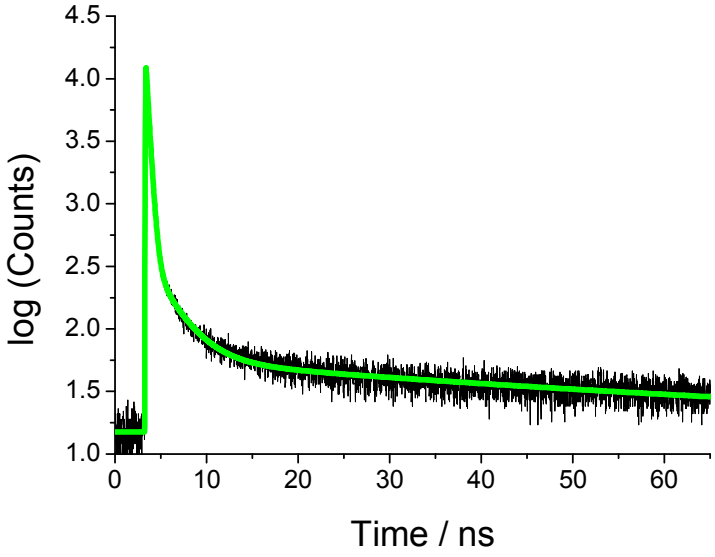

*Figure 23. Room temperature emission decay curve and instrument response function recorded for **NAP1-G** and the least-squares fit to a tri-exponential (green line).*

*Table 6. Emission lifetimes and pre-exponential parameters measured for **NAP1** polymorphic crystals.*

Compound	τ_1 (ns)	A_1	τ_2 (ns)	A_2	τ_3 (ns)	A_3
NAP1-O	1.20 (0.06)	0.92	6.4 (1.5)	0.06	31 (5)	0.02
NAP1-G	0.33 (0.01)	0.97	2.7 (0.4)	0.02	55 (14)	0.01

4.7 Explanation of solid state fluorescence

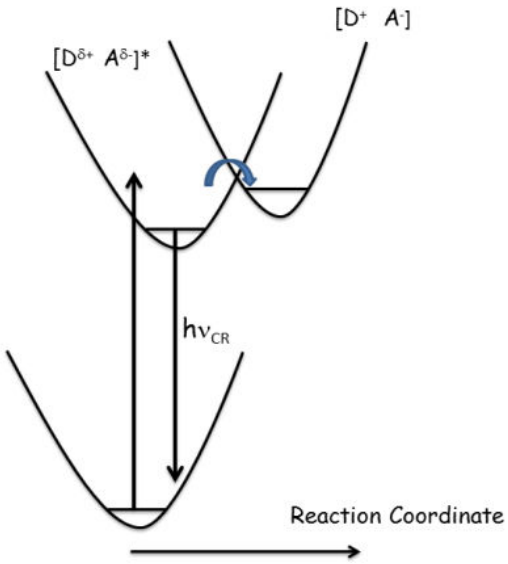

Figure 24. Simple potential energy surface diagrams for naphthalimide/phthalimide derivatives in the crystalline state.

An excited charge transfer state (CTS) within naphthalimide/phthalimide derivatives measured in here, is produced following photo-induced partial electron donation from the *N,N*-dimethylamino/trimethoxy group to the naphthalimide/phthalimide unit. Both electrochemical and theoretical calculations are supportive of this notion, and in agreement with previous literature examples. Excited state decay following return electron transfer (i.e., charge recombination), in general, is via a non-radiative route. In solution, solvent molecules encapsulating a molecular donor acceptor system act as the energy sink. Cases arise where energy is dissipated in the form of emission (i.e. namely charge recombination fluorescence). Considering the situation for **NAP1** the observed emission is assigned to the photonic energy dissipated during charge recombination. Formation of the completely formed charge transfer state is considered unfavoured owing to the inability of the environment to stabilise the two fully charged radicals (*Figure 24*). A key point to note is the observation of photoinduced electron transfer within the dyad in the crystalline state. Like in the natural photosynthetic reaction centre complex, where

the protein blanket supports charge separation, the local dipoles (e.g., CO group) of neighbouring molecules presumably play a similar role.

4.8 Voltage-current measurement on NAP1-O crystals

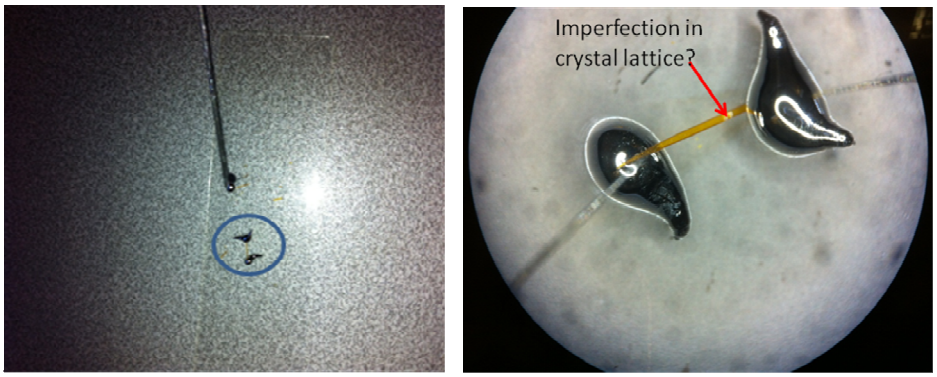

Figure 25. Left: Ga/In eutetic paste. Right: ***NAP1-O*** *crystal connected by Ga/In eutetic paste.*

Organic charge transfer crystals can be potential candidates for photoconductive materials[24]. Several thousands of organic charge transfer crystals have been synthesized and a large number of them are based on tetrathiafulvalene tetracyanoquinodimethane, acene-tetrathiafulvalene and their derivatives[25]. We were hoping to find out the photoconductivity of **NAP1-O** crystals, and to examine the possibility of using them as photoconductive materials. Voltage-current measurements were carried out on the long needle shape **NAP1-O** crystal. If the crystal is regarded as a cylinder, the diameter is 0.2 mm and the length is 1.7 mm. The experiment was carried out at 20 ^{O}C under an atmosphere of nitrogen. Voltage scans range from -3 to +3 V (30 mV intervals). Direct contact with the probe needle to the crystal surface results in the crystal 'shattering' upon impact. Therefore, each end of the crystal was connected to a drop of Ga/In eutectic paste, which serves as the two electrodes. The probe needle then contacts the eutetic paste (*Figure 25*). From the image (*Figure 25, right*) we obtained, it is possible that there is imperfection in crystal lattice. The measurement was carried out under dark and light conditions (*Figure 26*). A small current was obtained from the experiment, but no variation of current was seen between dark and under light experiments. Fragility of crystals made measurements through direct contact of a crystal with the electrodes

difficult. In addition, the crystal fractures which may inhibit electrical conductance along the length of the crystal.

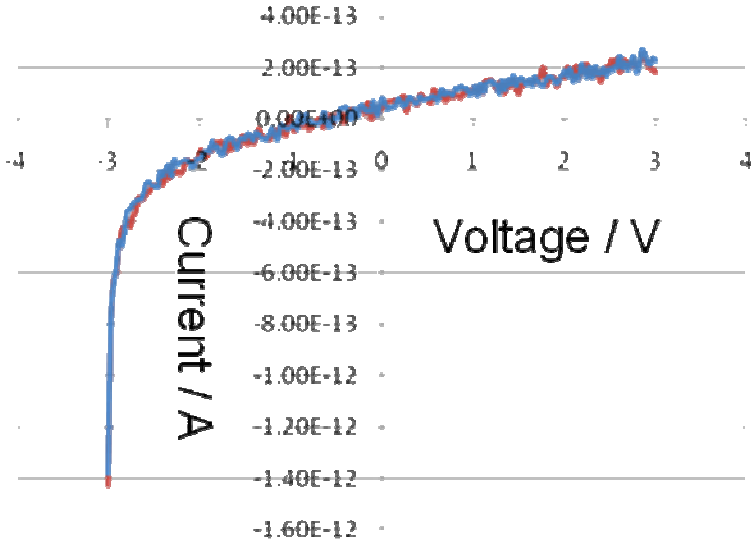

Figure 26. Voltage-current measurement in dark (blue line) and under light (red line)

4.9 Conclusions

In this chapter we have demonstrated that phthalimide/naphthalimide derivatives exhibited solid state charge transfer fluorescence properties. Charge transfer process was confirmed by electronic transition spectra and electrochemistry measurements. Fluorescence was found to be exclusive to the solid state, and both measurements by confocal microscopy and conventional fluorescence spectroscopy support this conclusion. The emission wavelength can be tuned by appropriate substitution of either donor or acceptor, providing important opportunities to optimise the system via crystal engineering. The work is rendered more challenging by the onset of polymorphs of **NAP1-O** and **NAP1-G**. Dreuw and co-workers[17] suggested that intramolecular hydrogen bonding play an important role for the induction of organic Pigment Yellow 101 derivatives' solid state fluorescence properties. This rule does not seem to be applicable to all of the naphthalimide and phthalimide derivatives especially for **PHTH3** and **NAP2**. There is no obvious intramolecular/intermolecular hydrogen bonding observed from crystal structure analysis. However, we notice that the intermolecular oxygen and chlorine atoms distances are about 2.8 Å which are shorter

than the sum of Van der Waals radius of chloride and oxygen (3.24 Å). So there might be halogen bonding to support the solid state charge transfer fluorescence for these two compounds. The possible intramolecular interaction for naphthalimide and phthalimide derivatives discussed in this chapter is the interaction between the oxygen atoms on carbonyl group and the hydrogen atoms on phenyl rings. However, the distance between hydrogen and oxygen atoms measured from crystal structure packing diagram is about 2.8 Å, which is longer than the usual hydrogen bonding length (about 2 Å). Steric effects of bulky cyclics have been proposed by Tang *et al*. for the arisen of solid state emission properties in silole derivatives[5, 6]. Inorganic metal complexes have also been shown to exhibit solid state emission properties. For instance, De Cole and co-workers[26] reported that two polymorphs of a dinuclear rhenium complex $[Re_2(\mu\text{-}Cl)_2(CO)_6(\mu\text{-}4,5\text{-}(Me_3Si)_2\text{-pyridazine})]$ exhibited one order of magnitude higher solid state fluorescence quantum yield in comparison to that in solution. The restricted rotation of Me_3Si was proposed to be responsible for the enhanced emission in solid.

The complete origin of the effect is not clear but we speculate that alterations in the non-radiative decay process may be a contributor to the lifetime variations. The shift in the emission profile is probably an environment effect associated with perturbation of the emitting state. In addition, the emission properties for crystals can be highly sensitive to packing within the crystal lattice. We expect to build-up a clearer picture by temperature dependent studies, and a complete description in terms of electron transfer theory. It is worth to note that the findings from our work suggest that especially naphthalimide derivatives can be potential candidates for solid state emitters. This allows us to measure certain properties that characterise the charge-transfer event in the solid. The work advances our understanding of electron transfer in the solid state.

4.10 References

[1] (i) X. Peng, J. Du, J. Fan, J. Wang, Y. Wu, J. Zhao, S. Sun, T. Xu, *J. Am.Chem. Soc.,* 2007, **129**, 1500; (ii) A. Coskun, M. D. Yilmaz and E. U. Akkay, *Org. Lett.,* 2007, **9**, 607; (iii) W. Chen, X. Tu and X. Guo, *Chem. Commum.*, 2009, **13**, 1736; (iv) S. S. Tan, S. J. Kim and E. T. Kool, *J. Am. Chem. Soc.*, 2011, **133**, 2664.

[2] (i) M. A. H. Alamiry, A. C. Benniston, G. Copley, K. J. Elliott, A. Harriman, B. Stewart and Y. G. Zhi, *Chem. Mater.*, 2008, **20**, 4024; (ii) M. K. Kuimova, G. Yahioglu, J. A. Levitt and K. Suhling, *J. Am. Chem. Soc.*, 2008, **130**, 6672.

[3] (i) R. Ziessel, G. Ulrich, A. Harriman, A. A. H. Alamimiry, B. Stewart and P. Retailleau, *Chem. Eur. J.*, 2009, **15**, 1359; (ii) Y. Liu, Y. Tang, N. N. Barashkov, I. S. Irgibaeva, J. W. Y. Lam, R. Hu, D. Birimzhanova, Y. Yu and B. Z. Tang, *J. Am. Chem. Soc.*, 2010, **132**, 13951; (iii) J. He, T.-Y. Zhang and G. Chen, *J. Colloid Interface Sci.*, 2012, **373**, 94.

[4] (i) M. G. Walter, A. B. Rudine and C. C. Wamser, *J. Porphyrins Phthalocyanines*, 2010, **14**, 760; (ii) Y. Pellegrin, L. L. Pleuxa, E. Blart, A. Renaud, B. Chavillon, N. Szuwarski, M. Boujtita, L. Cario, S. Jobic, D. Jacquemina and F. Odobela, *J. Photochem. Photobiol. A: Chemistry*, 2011, **219**, 235; (iii) F. Odobel, L. Pleux, Y. Pellegrin and E. Blart, *Acc. Chem. Res.*, 2010, **43**, 1063; (iv) M. Grätzel, *Acc. Chem. Res.*, 2009, **42**, 1788; (v) S. K. Balasingam, M. Lee, M. G. Kang and Y. Jun, *Chem. Commun.*, 2013, **49**, 1471; (vi) M. Liang and J. Chen, *Chem. Commun.*, 2013, **42**, 3453.

[5] (i) J. Luo, Z. Xie, J. W. Y. Lam, L. Cheng, H. Chen, C. Qiu, H. S. Kwok, X. Zhan, Y. Liu, D. Zhu and B. Z. Tang, *Chem. Commun.*, 2001, **18**, 1740.

[6] (i) Y. Hong, J. W.Y. Lam and B. Z. Tang, *Chem. Commun.*, 2009, **29**, 4332; (ii) J. Liu, J. W.Y. Lam and B. Z. Tang, *J. Inorg. Organomet. Polym.*, 2009, **19**, 249; (iii) J. Wu, W. Liu, J. Ge, H. Zhang and P. Wang, *Chem. Soc. Rev.*, 2011, **40**, 3483; (iv) A. Qin, J. W. Y. Lam and B. Z. Tang, *Prog. Polym. Sci.*, 2012, **37**, 182.

[7] A. Pardo, A. Martin, J. M. L. Poyato and J. J. Camacho, *J. Photochem. Photobiol. A: Chemistry*, 1989, **48**, 259.

[8] S. L. Suraru, U. Zschieschang, H. Klauk and F. Wurthner, *Chem. Commun.*, 2011, **47**, 11504.

[9] H. Wang, H. Wu, L. Xue, Y. Shi and X. Li, *Org. Biomol. Chem.*, 2011, **9**, 5436.

[10] R. M. Duke, E. B. Veale, F. M. Pfeffer, P. E. Krugerc and T. Gunnlaugsson, *Chem. Soc. Rev.*, 2010, **39**, 3936.

[11] Polymorphism in Molecular Crystals, Joel Bernstein, 2007, Oxford University Press; (ii) R. J. Davey, N. Blagden, G. D. Potts and R. Docherty, *J. Am. Chem. Soc.*,1997, **119**, 1767; (iii) A. Mahieu, J. f. Willart, E. Dudognon, M. D. Eddleston, W. Jones, F. Danède and M. Descamps, *J. Pharm. Sci.*, 2013, **102**, 462.

[12] (i) Y. V. Seryotkin, T. N. Drebushchak and E. V. Boldyreva, *Acta Cryst*. 2013, **B69**, 77; (ii) V.V. Krisyuk , I. A. Baidina, I. V. Korolkov, P. P. Semyannikov, P. A. Stabnikov, S. V. Trubin and A. E. Turgambaeva, *Polyhedron*, 2013, **49**, 1; (iii) G. J. Han, S. Thirunahari, P. S. Chow and R. B. H. Tan, *Cryst. Eng. Comm.*, 2013, **15**, 1218; (iv) C. S. Towler, R. J. Davey, R. W. Lancaster and C. J. Price, *J. Am. Chem. Soc*., 2004, **126**, 13347.

[13] (i) S. Varughese, M. S. R. N. Kiran, U. Ramamurty and G. R. Desiraju, *Angew. Chem. Int. Ed.*, 2013, **52**, 2701; (ii) N. Masó, H. Beltrán, E. Cordoncillo, D. C. Sinclair and A. R. West, *J. Am. Ceram. Soc.*, 2008, **91**, 144; (iii) M. C. Menard, B. L. Drake, G. T. McCandless, K. R. Thomas, R. D. Hembree, N. Haldolaarachchige, J. F. DiTusa, D. P. Young and J. Y. Chan, *Eur. J. Inorg. Chem.*, 2011, **26**, 3909; (iv) J. O. Williams and J. M. Thomas, *Trans. Faraday Soc.*, 1967, **63**, 1720; (v) J. M. Thomas and J. O. Williams, *Trans. Faraday Soc.*, 1967, **63**, 1922.

[14] M. Palucki, D. L Hughes, N. Yasuda, C. Yang and P. J Reider, *Tetrahedron Lett.*, 2001, **42**, 6811.

[15] Polyimides Fundamentals and Applications, T. Takekoshi, 1996, Marcel Dekker, New York.

[16] H. Langhals, T. Potrawa, H. Noth and G. Linti, *Angew. Chem.*, 1989, **101**, 497.

[17] A. Dreuw, J. Plötner, L. Lorenz, J. Wachtveitl, J. E. Djanhan, J. Brüning, T. Metz, M. Bolte, and M. U. Schmidt, *Angew. Chem. Int. Ed.*, 2005, **44**, 7783.

[18] (i) A. S. Guram and S. L. Buchwald, *J. Am. Chem. Soc.*, 1994, **116**, 7901; (ii) J. P. Wolfe, S. Wagaw and S. L. Buchwald, *J. Am. Chem. Soc.*, 1996, **118**, 7215; (iii) M. S. Driver and J. F. Hartwig, *J. Am. Chem. Soc.*, 1996, **118**, 7217.

[19] M. J. Frisch, G. W. Trucks, H. B. Schlegel, G. E. Scuseria, M. A. Robb, J. R. Cheeseman, J. A. Montgomery Jr., T. Vreven, K. N. Kudin, J. C. Burant, J. M. Millam, S. S. Iyengar, J. Tomasi, V. Barone, B. Mennucci, M. Cossi, G. Scalmani, N. Rega, G. A. Petersson, H. Nakatsuji, M. Hada, M. Ehara, K. Toyota, R. Fukuda, J. Hasegawa, M. Ishida, T. Nakajima, Y. Honda, O. Kitao, H. Nakai, M. Klene, X. Li, J. E. Knox, H. P. Hratchian, J. B. Cross, V. Bakken, C. Adamo, J. Jaramillo, R. Gomperts, R. E. Stratmann, O. Yazyev, A. J. Austin, R. Cammi, C. Pomelli, J. W. Ochterski, P. Y. Ayala, K. Morokuma, G. A. Voth, P. Salvador, J. J. Dannenberg, V. G. Zakrzewski, S. Dapprich, A. D. Daniels, M. C. Strain, O. Farkas, D. K. Malick, A. D. Rabuck, K. Raghavachari, J. B. Foresman, J. V. Ortiz, Q. Cui, A. G. Baboul, S. Clifford, J. Cioslowski, B. B. Stefanov, G. Liu, A. Liashenko, P. Piskorz, I. Komaromi, R. L. Martin, D. J. Fox, T. Keith, M. A. Al-Laham, C. Y. Peng, A. Nanayakkara, M. Challacombe, P. M. W. Gill, B. Johnson, W. Chen, M. W. Wong, C. Gonzalez and J. A. Pople, Gaussian 03, Gaussian, Inc., Wallingford CT, 2004.

[20] A. G. Griesbeck, J. Neudörfl and A. de Kiff, *Beilstein J. Org. Chem.*, 2011, **7***,* 518.

[21] V. Wintgens, P. Valat and J. Kossanyi, *J. Chem. Soc. Faraday Trans.*, 1994, **90**, 411.

[22] W. Hayes, H. Ambaye and J. R. Manson**,** *J. Phys.: Condens. Matter,* 2007, **19**, 305007.

[23] A. Pardo, E. Martin, J. M. L. Poyato, J. J. Camacho, J. M. Guerra, R. Weigang, M. F. Brana and J. M. Castellano, *J . Photochem. Photobiol. A Chemistry,* 1989, **48**, 259.

[24] (i)W. Yu, X. Y. Wang, J. Li, Z. T. Li, Y. K. Yan, W. Wang and J. Pei, *Chem. Commun.*, 2013, **49**, 54. (ii) G. Horowitz, F. Kouki and P. Valat, *Phys. Rev. B*, 1999, **59**, 10651. (iii) J. H. Sharp, *J. Phys. Chem.*, 1967, **71**, 2587.

[25] (i) T. Hasegawa and J. Takeya, *Sci. Technol. Adv. Mater.*, 2009, **10**, 024314. (ii) T. Mori, *J. Phys.: Condens. Matter*, 2008, **20**, 184010. (iii) G. Saito and Y. Yoshida, *Bull. Chem. Soc. Jpn*., 2007, **80**, 1.

[26] E. Q. Procopio, M. Mauro, M. Panigati, D. Donghi, P. Mercandelli, A. Sironi, G. D'Alfonso, and L. De Cola, *J. Am. Chem. Soc.*, 2010, **132**, 14397.

Chapter 5

Multi-electron Storage Molecular Systems

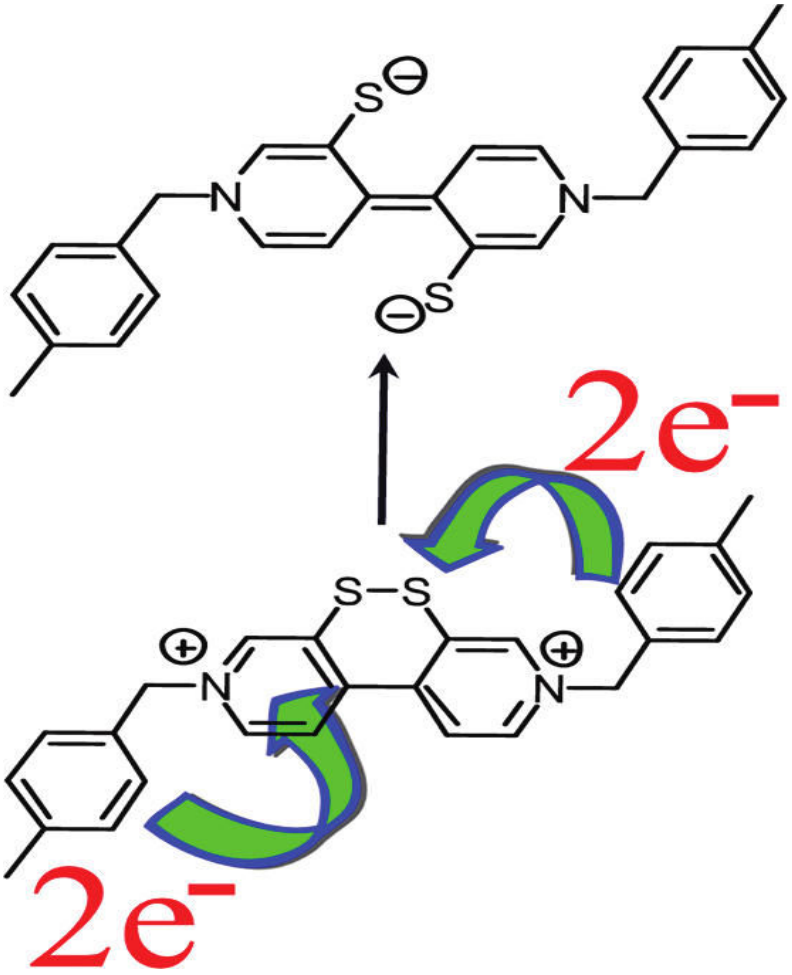

Selected molecular structures discussed in this chapter are shown below.

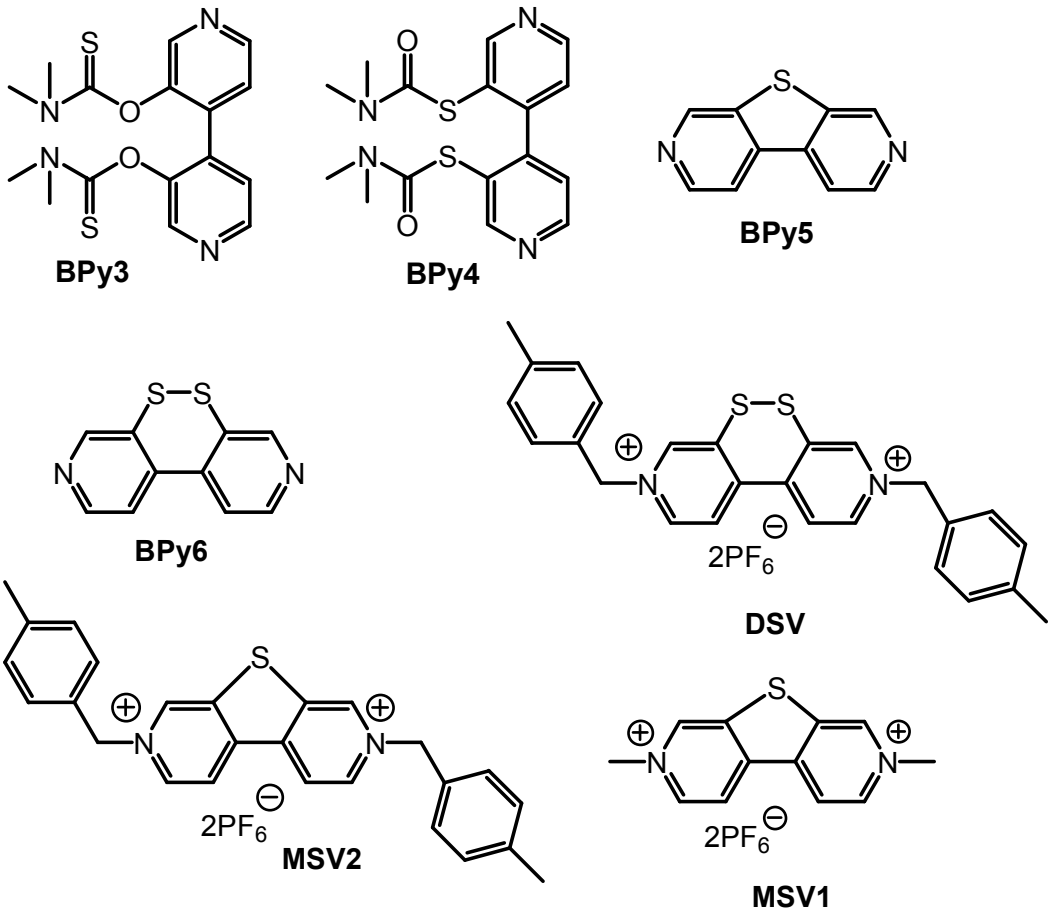

We acknowledge those involved in this work. Thanks to Dr Ross W. Harrington for the measurement of crystal structures and to Dr Jerry Hagon for the molecular orbital calculations.

5.1 Introduction

It is easy to see how battery technology has revolutionized mobile phones. Instead of the cumbersome large battery operated phones seen in the late 1980s, pocket-size long-lasting devices are now commonplace. This shift in technology can be traced to the development of high-density lithium carbon-based storage cells[1]. The efficient and high-density storage of charge in molecular systems, in the form of positive holes or electrons, is of fundamental importance[2]. Upon conformation changes (e.g. bond angles, ring opening and ring closure) of a carefully designed molecular system the reversible process, i.e., charge/discharge (ON/OFF) states, can be achieved under the stimulation of photons or electrons[3]. In the design of a functional charge storage "bank" two key aspects need to be considered: (i) The "lifetime" (the times of the reversible process) of the molecule and (ii) the capacity per unit (the amount of data that can be stored per unit).

Generally speaking inorganic materials, especially metal oxides (e.g., IrO_2), are abundantly capable of multiple charge storage, their electronic band shape, lattice defect structure, and mixed-valence oxidation state formation often providing the means to support mass charge accumulation[4]. One problem often encountered is the slowness by which charging the material takes place[5]. By comparison, multiple charge storage, at a reasonable thermodynamic potential, within a single organic molecule is less easy to achieve[6]. The advantage, however, is the fast charging/discharging generally observed in organic molecules[7].

A redox responsive unit, 3, 8-diiodo-dibenzo[1,2] dithiine (*Figure 1*), has been shown to be a potential molecular memory storage bank by our group[8]. A theoretical and experimental study has shown that the reduction and oxidation (applied mildly anodic potential) process, i.e. the writing and reading process, of this system can be repeated many times without destruction of the molecules. The advantages of this molecular

system are its relatively simple structure and the easy way it can be integrated into a complex architecture as a molecular switch. Therefore, to further this study we decided to synthesis and study systems with similar size, while possessing higher capacitance of each redox responsive unit. *N,N*-alkylated bipyridinium cation (viologen) is well-known for its reversible electrochemistry[9]. The viologens accumulate two electrons and their reduction potentials are readily manipulated by controlling the dihedral angle[10]. S-S in is known for its two electron reducible properties[11]. *Figure 2* shows the target viologen derivatives, and it was expected that the viologen system could store four to six electrons depending on the substituent. It is expected that reversible addition and reduction of electron properties of the viologen based system can also find interesting applications in the multi-electron processes, such as working as an electron mediator in water oxidation because of the low reduction potentials of viologen derivatives.

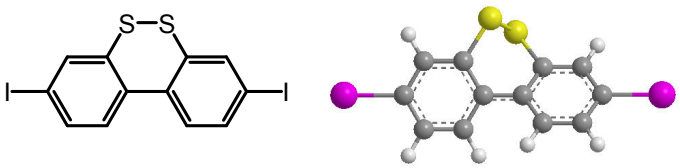

Figure 1. The structure of 3, 8-diiodo-dibenzo[1,2] dithiine.

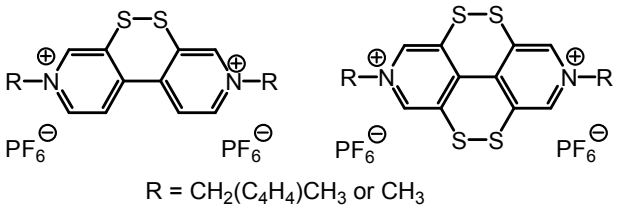

Figure 2. Structures of the target viologen-based data storage molecules.

5.2 Synthesis

The synthetic protocol is shown in *Scheme 1*. The strategy of the synthesis was derived from the literature[8, 12]. Compound **BPy2** was prepared following the literature method. One of the key steps in the synthesis of **BPy2** involved a Suzuki coupling reaction[13] (the mechanism of the reaction will be discussed later), which was a rather easy and efficient method for the formation of the C-C bond linking the two pyridine rings. Step (i) involved

the protection of the hydroxyl group of 3-hydroxypyridine by forming a carbamyl group. One-pot Suzuki coupling reaction (**Py3** was used directly in step four without any work up or purification) and work up afforded the mono-protected product **BPy1** which was in agreement with the literature report[8]. After hydrolysis under basic condition **BPy2** was obtained as yellow solid in 74% yield. **BPy3** was prepared with similar reaction conditions as preparation of **Py1** from 3-hydroxypyridine. Step (vii) was a Newman-Kwart rearrangement[14] (mechanism will be discussed later), which was an efficient method to obtain a protected *S*-thiocarbamate. The side product from the Newman-Kwart rearrangement in this step was the thiophene derivative (**BPy5**). Temperature and reaction time have been shown to be the most important factors which influence the ratio of bis-*S*-thiolcarbamate esters product and thiophene derivatives[15]. Deprotection of thiol groups under basic conditions followed by work up in dichloromethane afforded the bright yellow solid **BPy6** in 72% yield. The deprotection of the thiol groups afforded the dithiol which was readily oxidised to the thiine product (**BPy6**) on exposure in air (by stirring) in the presence of dichloromethane. During the neutralisation process, the colour of the solution changed from light yellow to orange. The changes of the colour may be assigned to the oxidation of dithiol groups to the corresponding thiine. Substitution of hydroxy group on *p*-tolylmethanol afforded 1-(bromomethyl)-4-methylbenzene[16]. Under milder conditions and controlled reaction times, it was possible to alkylate **BPy6** with 1-bromo-methyl-4-methylbenzene to afford **DSV**[17]. The crude product was purified by recrystallisation (solvent vapour diffusion method) from diethyl ether and acetonitrile to afford yellow crystals. However, this sample when left in acetonitrile solution for prolonged times, especially in the presence of water, decomposed to give the monosulfur adduct **MSV2**. The presence of monsulfur adduct was unexpected from the beginning until we got results from crystallography, as the product had been confirmed by NMR spectroscopy, mass spectrometry and elemental analysis. The stronger alkylating agent of iodomethane produced after reflux with **BPy6** and metathesis with hexafluorophosphate, **MSV1**[17]. The six-membered disulfide ring appears to eject one sulfur to form the central five-membered ring.

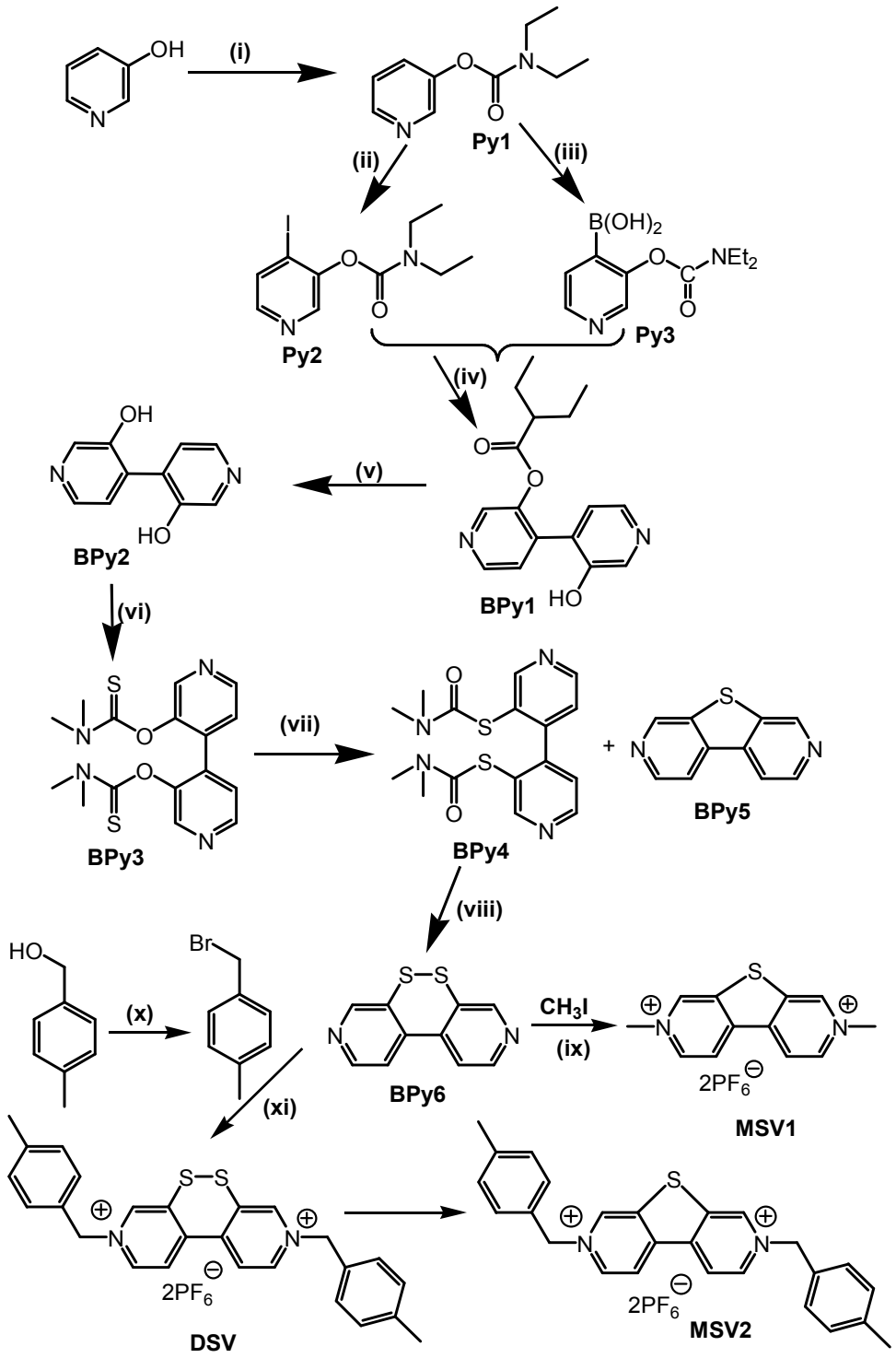

Scheme 1. Reaction conditions: (i) Et_2NCOCl, Et_3N, THF, 54%; (ii)TMEDA, ^tBuLi, I_2, THF, 96%; (iii) $B(O^iPr)_3$, ^nBuLi; (iv) $Pd(PPh_3)_4$, DME, deoxygenated EtOH, Na_2CO_3, 37%; (v) NaOH, EtOH, 74%; (vi) Me_2NCSCl, NEt_3, THF, 79%; (vii) $C_{14}H_{30}$, 260 ^OC, 88%; (viii) KOH, air, MeOH, DCM, 72%; (ix) CH_3CN, KPF_6, 56%; (x) PBr_3, DCM, 79%; (xi) CH_3CN, KPF_6, 44%.

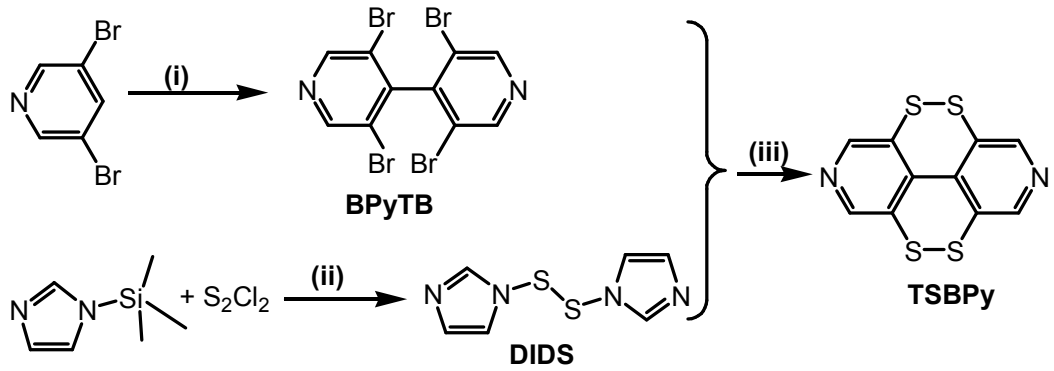

Scheme 2. Reaction condition: (i) -40 ^{O}C, THF, Lithium diisoprpylamide, -78 ^{O}C, I_2 then room temperature; (ii) Toluene, under the protection of N_2, room temperature; (iii) -78 ^{O}C, ^{n}BuLi then room temperature.

Before we realised the possible decomposition of **DSV**, synthesis of **TSBPy** (*Scheme 2*) was tried. Step (i)[18] proceeded well without any major problem except that purification needed to be carried out two to three times by column chromatography (silica gel) due to the similar polarity and low solubility of the side product in the chosen solvent system (petroleum ether / ethyl acetate = 4 / 1). The side product (less polar in comparison to the expected product **BPyTB**) came out of the column before **BPyTB**, but the lower solubility led to partial precipitation of the side product on the column. As a result, some of the side product was actually eluted out at the same time as **BPyTB**. Step (ii) was carried out at room temperature and the yellow solid **DIDS** precipitated out immediately as soon as the sulfur monochloride was added to the stirred solution of 1-trimethylsilylimidazole. **DIDS** was found to be extremely insoluble in organic solvents, even in dimethyl sulfoxide, and was moisture sensitive. If it was exposed to air, the yellow solid started to became an oily solid. Therefore, after removing the toluene under vacuum the material was used directly in step (iii) without any characterisation. Reaction of compound **BPyTB** and **DIDS** afforded a very oily yellow solid, which was only soluble in dimethyl sulfoxide. The ^{1}H NMR spectrum showed a singlet peak at 7.69 ppm in the range for a pyridine ring, but the ^{13}C NMR spectrum did not show the corresponding resonance peaks for carbons in the pyridine ring. The singlet peak in the ^{1}H NMR could be an artifact. Therefore, this method was not really feasible under the conditions applied.

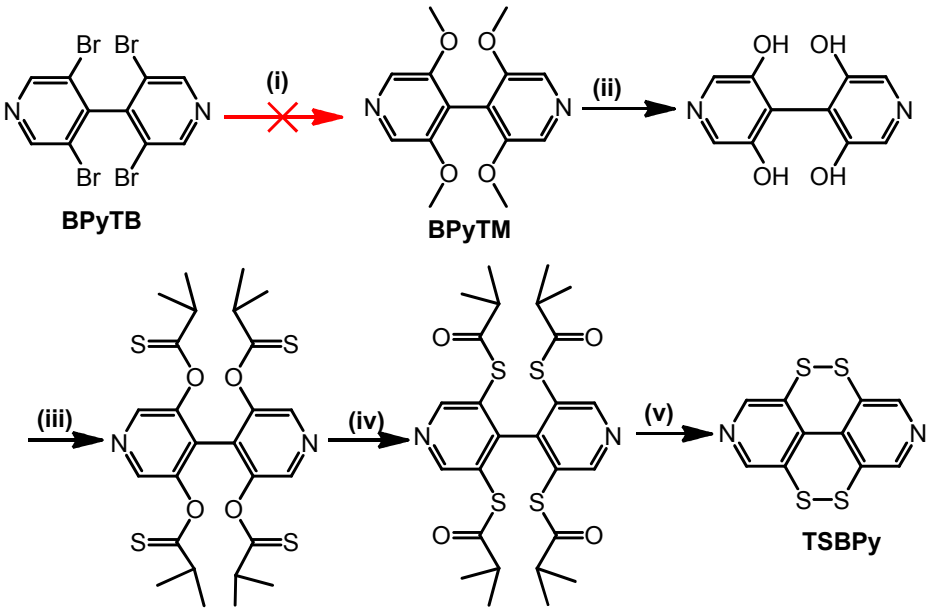

Scheme 3. Reaction conditions: (i) NaOMe, MeOH, reflux; (ii) BBr_3, DCM; (iii) N, N-dimethylthiocarbanoyl, triethylamine, 4-dimethylaminopyridine, THF; (iv) $C_{14}H_{30}$, 260 ^{O}C, reflux 10h; (v) KOH, MeOH, 80 ^{O}C. The reaction was failed in step (i).

The second synthetic route to **TSBPy** is shown in Scheme 3. Compound **BPyTB** was obtained by the same first route, however the main problem was encountered in the second step. The substitution reaction of 3,5,3',5'-tetrabromo-[4,4'] bipyridinyl was found to be difficult even though in the literature the conversion of 1,3,5-tribromobenzene to 1,3,5-trimethoxybenzene was found to be successful [19]. Different reaction conditions (*Table 1*) were tried, and from the mass spectrum of the crude product from experiment **2** (*Figure 3*) the desired mass of the expected product was seen. Unfortunately, after column chromatograph only several milligrams (starting with 500mg of **BPyTB**) of a mixture of the different substituted or reduced products were obtained. The extremely low yield and the separation difficulty indicated that it was not an efficient method for the target compound. However, at the same time the tiny amount of product observed in the mass spectrum showed that further modification of the reaction condition (for example, higher temperature, higher ratio of sodium methoxide, more efficient catalyst and longer reaction time) may afford a better result. Unfortunately, all of the attempted reaction conditions did not give a better result, even though the unidentified products from each reaction showed the methoxy group in the ^{1}H NMR spectrum.

Therefore, it suggested that the substitution of four bromine atoms in one reaction was a really harsh process. On a positive side, the presence of the methoxy group inferred from the ^{1}H NMR spectrum indicated that substitution was possible (i.e., bromide can be substituted by the methoxy group). Therefore, substitution of two bromide atoms at once may be possible.

*Table 1. Different attempted reaction conditions for the substitution reaction of **BPyTB**.*

Experiment No.	Pyridyltetrabromide : Sodium methoxide	Catalyst (mol %)	Solvent	Product
1	1: 17	None	DMF	-
2	1: 47	$CuBr_2$ 38	MeOH	-
3	1:70	$CuBr_2$ 26	DMF & MeOH	-
4	1:60	CuI 40	Isopropanol	-
5	1:53	CuI 49	MeOH	-
6	1:47	CuBr 40	MeOH	-
7	1:40	CuBr 30	MeOH	-

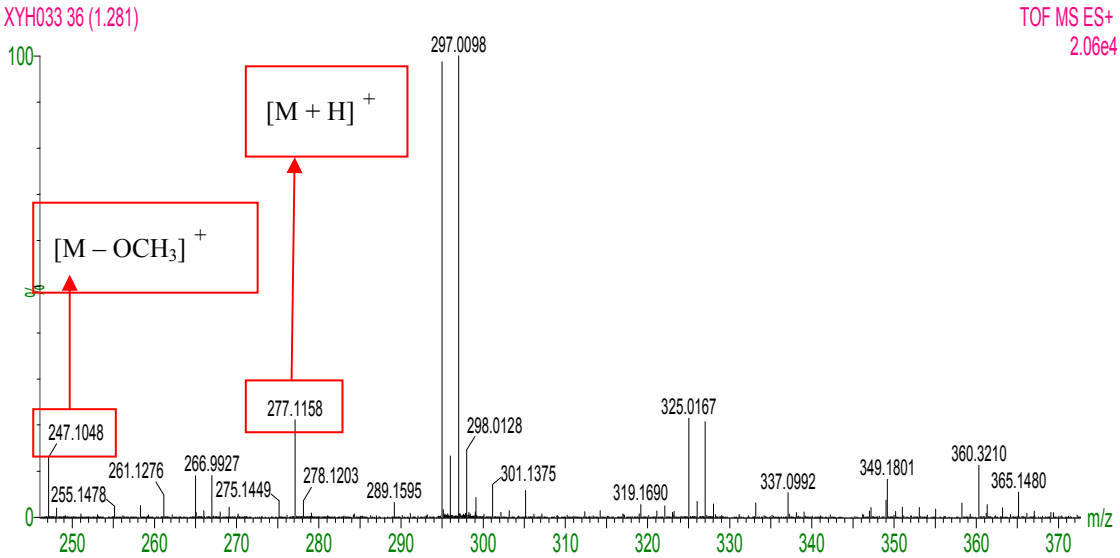

*Figure 3. Mass spectrum of crude product from conversion of **BPyTB** to **BPyTM**.*

When we were going forward to an alternative synthetic rout, crystallography for **DSV** came to us and it showed that instead of **DSV** the crystal structure we obtained was **MSV2**. Therefore, instead of moving forward the synthesise the **TSBPy**, we started to analyse the possible decomposition pathways for **DSV**. The decomposition possibly invoked an intramolecular ring contraction owing to presence of the quaternerized nitrogens (see section 5.8 and 5.9). The reaction may even proceed once one nitrogen is alkylated. This analysis indicated that even though we might achieve preparation of the tetrasulfur derivative it is likely that it will undergo similar decomposition route. The only possible way to utilise **DSV** as a four electron bridge is to find a way to stabilise the disulfide bridges. This is difficult and we have to seek another target for the practical application.

5.3 Reaction mechanisms

5.3.1 Suzuki coupling

Suzuki coupling reaction[13] (*Equation 1*) has been shown to be a convenient and easy way to carry out method to generate a carbon carbon bond.

$$R^1B(OH)_2 \; + \; R^2X \xrightarrow[\text{Base}]{\text{Pd(0)}L_4} R^1\text{-}R^2$$

Equation 1. X = Br, I. R^2 = alkenyl, alkynyl, benzyl, allyl, aryl.

Generally the coupling reaction is catalysed by palladium (0) complex (PdL_4) (catalytic cycle, *Figure 4*) and forms a C-C bond from an organoboron and an organohalide under basic or neutral conditions. The oxidative addition (step i) has been considered as the rate determining step. The reductive elimination (step iv) has been proposed to undergo through *cis* configuration (*Figure 5*); the *trans* intermediate firstly isomerises to the *cis* one and then undergoes further reaction[13]. Various bases, ranging from very weak one like potassium acetate to very strong one like sodium hydroxide, can be used in the reaction depending on the properties of the reactants.

For the Suzuki coupling reaction involved in the synthesis of **BPy1**, the sodium carbonate was used as base and the reaction was carried out under homogeneous conditions by adding the aqueous base in 1,2-dimethoxyethane. The yield of the reaction (37%) was not high which might be due to the competitive hydrolytic deboronation of **Py3** under aqueous conditions.

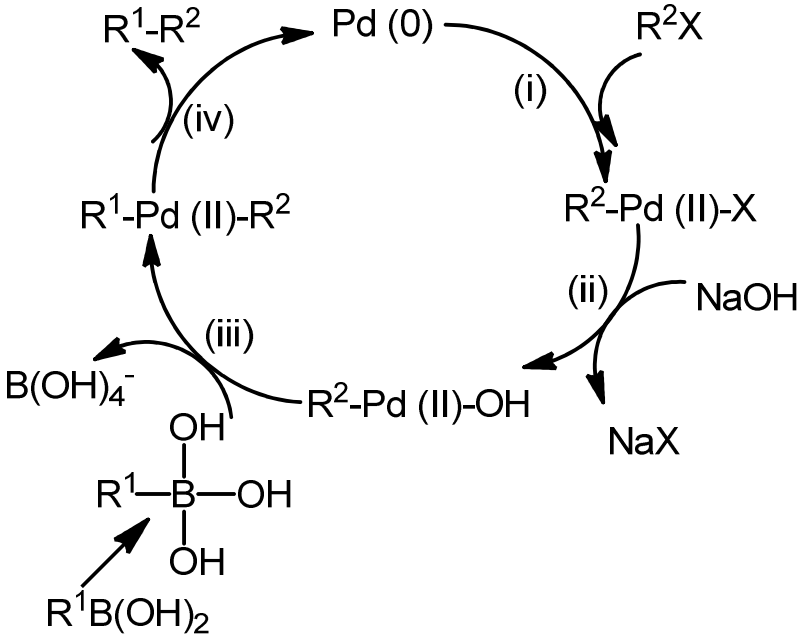

Figure 4. A catalytic cycle (use sodium hydroxide as base) of Suzuki coupling reaction, X = Br, I. R^2 = alkenyl, alkynyl, benzyl, allyl, aryl [13].

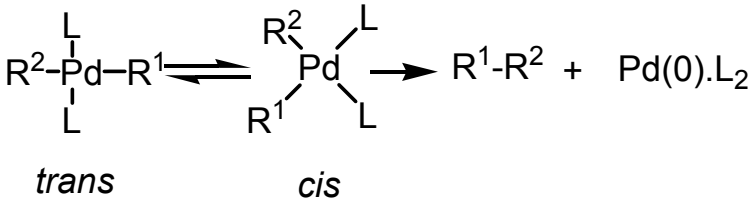

Figure 5. Reductive elimination of the intermediate in the Suzuki coupling reaction[13].

5.3.2 Newman-Kwart rearrangement

The rearrangement of a thiocarbonyl group was first reported by Schonberg and co-workers[20], and later the method was developed and shown to be an important method in the conversion of aromatic hydroxides to aromatic thiols. The conversion of thione to thiol now is generally known as Newman-Kwart rearrangement (*Figure 6*)[14]. The mechanism of the rearrangement (*Figure 7*) involves the four membered ring

intermediate. It was suggested that the driving force for the reaction is the stronger nucleophilicity of sulphur in comparison to oxygen. The substituent (R^1 and R^2, *Figure 7*) of the starting material played a key role in the determination of the reaction rate. The influence of different substituents (R^1 and R^2) on the reaction rate was studied by Miyazaki *et al.*[21]. It was shown that the stronger electron-withdrawing ability of R^1 and the stronger electron-donating ability of the R^2 led to the stabilisation of the intermediate and in term resulted in a higher reaction rate[21, 22]. The dimethylamino groups helped the stabilisation of the four membered ring intermediate in rearrangement of **BPy3** to **BPy4** (*Figure 8*).

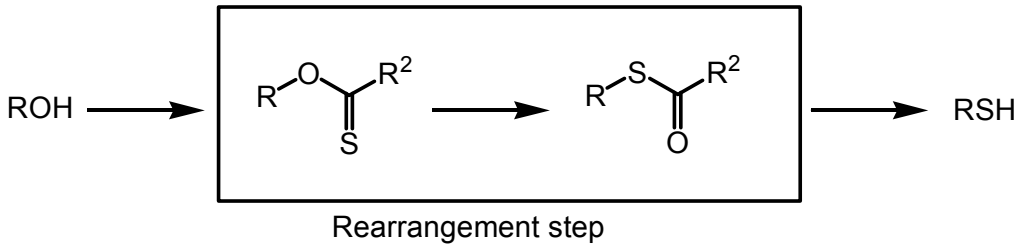

Figure 6. The general steps in the preparation of an aromatic thiol from an aromatic hydroxide. R = Aryl, X has been suggested to be N, N-dialkyls which usually results in a better reaction yield.

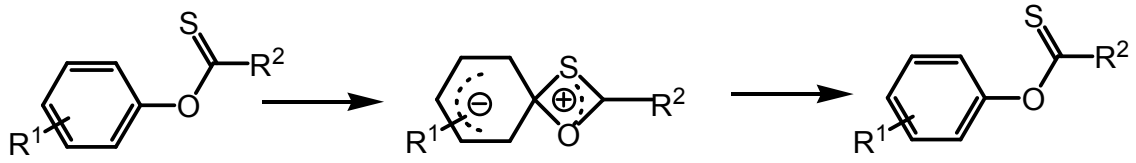

Figure 7. The general steps of the rearrangement of thiolcarbamoyl involving a four-membered ring intermediate.

The side product from the rearrangement was the thiophene derivative (**BPy5**). Controlling reaction temperature and reaction time minimised the yield of the thiophene product. In contrast, thiophene derivative can also be obtained as a major product by carefully choosing the reaction time and reaction temperature. The rearrangement reaction involved here was carried out under refluxing conditions and tetradecane (boiling point 252-254 ^{O}C) as solvent to help maintain the temperature. Even though the temperature was brought to reflux quickly, inevitably some of the starting material still underwent the side reaction. The yield of the major product (**BPy4**) is 88% indicating that the reaction works well under the applied conditions.

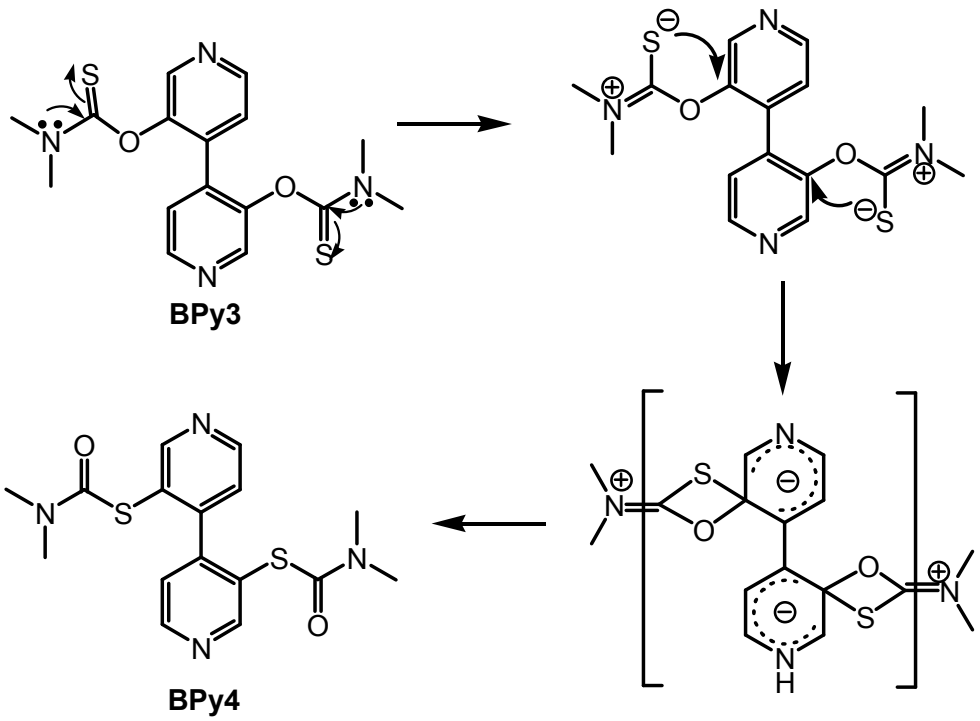

*Figure 8. The proposed reaction mechanism of the conversion compound **BPy3** to **BPy4**.*

5.4 NMR spectra

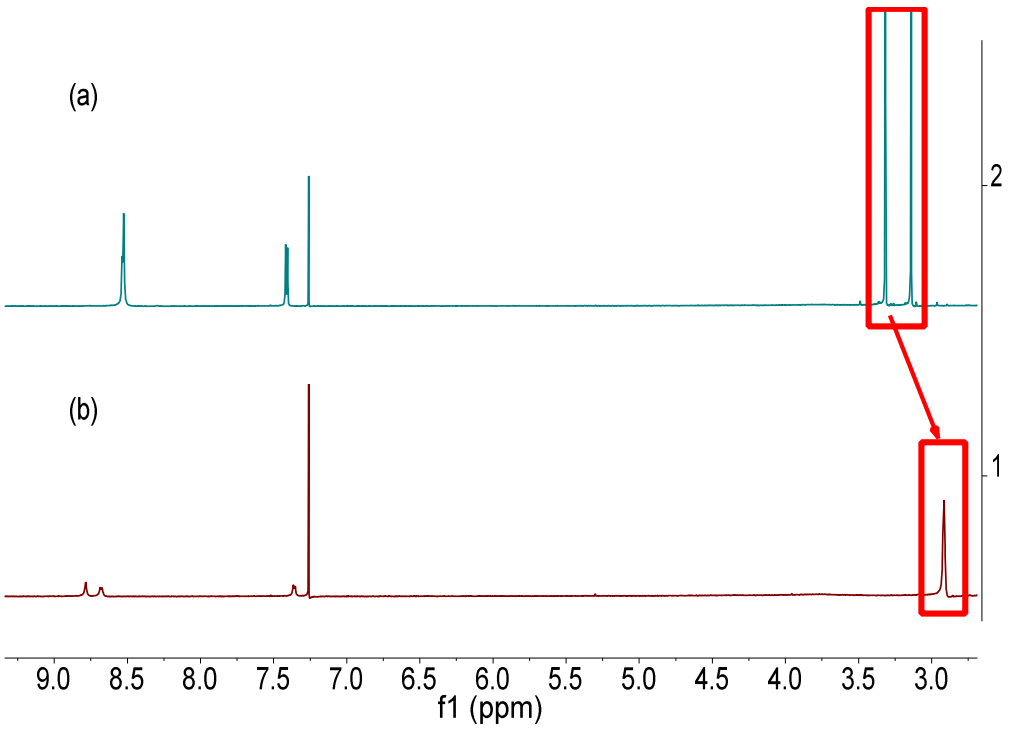

*Figure 9. Comparison of the ^{1}H NMR spectra of the Newman-Kwart rearrangement reaction. (a) Spectrum of **BPy3**, (b) Spectrum of **BPy4**.*

The ^{1}H NMR spectrum of the dimethyl derivative of **BPy3** and **BPy4** (before and after rearrangement) showed interesting changes in terms of patterns of the peaks. The protons of the four methyl groups were non-equivalent before rearrangement, showing two singlet peaks, while after the rearrangement all of the protons became equivalent and only a singlet peak was observed (*Figure 9*). This observation was in agreement with the literature report[23].

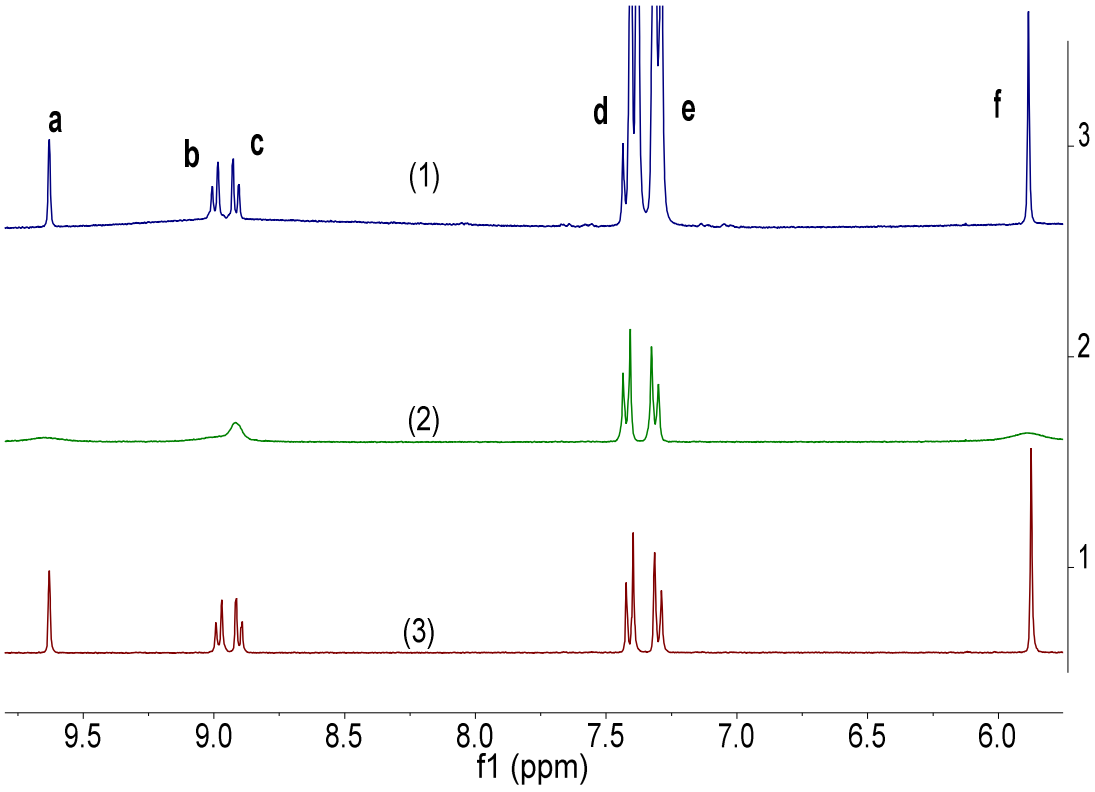

*Figure 10. Expanded ^{1}H NMR spectra of **BMVS**: (1) Spectrum from saturated solution; (2) Spectrum from dilution of solution (1) 4 times; (3) Spectrum of the same sample as (2) left overnight in dark at room temperature.*

Peaks distortion (*Figure 10 (1)*) was observed when a freshly made saturated solution of **DSV** was used to carry out a ^{1}H NMR experiment. A broad rolling baseline was observed as a big bump under the main peaks, especially for peaks b and c. The integral according to **DSV** can only be obtained by integrating over a very wide range including the broad peak. When the solution was diluted 4 times and the ^{1}H NMR spectrum was measured again, the distorted peaks (peak a, b, c and f) observed in *Figure 10 (1)* changed to three broad peaks shown as *Figure 10 (2)*. If we look closely there is a tiny peak on the left side of the main doublet peak d and the chemical shift is same as the

corresponding peak d in the spectrum (2). The sample (2) was sealed and left in the dark overnight and the measurement repeated again. The three broad peaks became sharp (*Figure 10 (3)*) and the peak patterns fitted well with the proposed structure of **DSV**. This observation is possibly due to a dynamic process taking place in the solution.

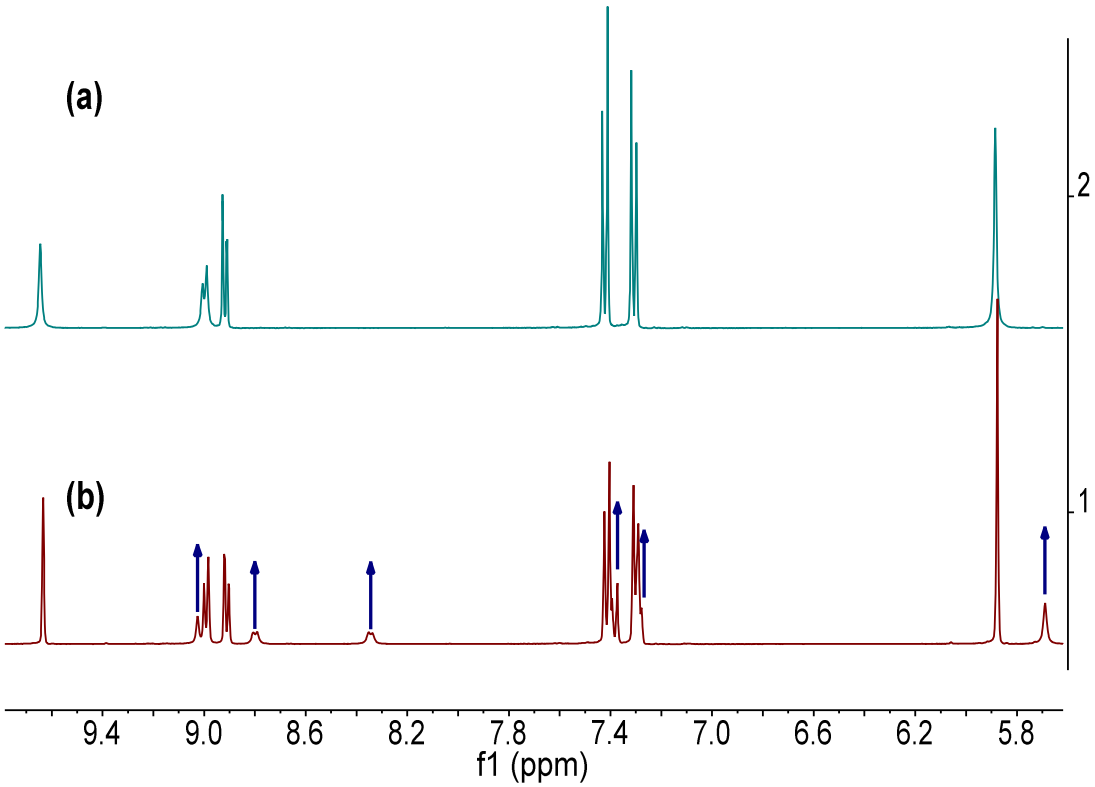

*Figure 11. ^{1}H NMR spectra indicating decomposition of **DSV**.*

To further examine the stability of **DSV** (we realised degradation of the sample occurred from crystallography experiment which will be discussed later), we took a ^{1}H NMR spectrum (*Figure 11 (a)*) of a solution before it was heated in air and boiled the solution (volume of the acetonitrile reduced from 0.9 mL to 0.45 mL). Then the ^{1}H NMR spectrum was measured again. No changes were observed from the spectrum. The sample was left overnight and some solid precipitated out of the tube the next morning. The measurement was repeated again and new peaks were found (*Figure 11 (b)*, blue arrows) with a very similar peak-pattern to the original peaks but with different chemical shifts. Therefore, the experiment seems to suggest that there is decomposition undergoing in the solution, the potential factors could be oxygen and moisture.

5.5 Mass spectrometry

High resolution mass spectra for **DSV** and **MSV1** were obtained to confirm the structures. The **DSV** molecule losing one PF_6^- counter, $[\mathbf{DSV}\text{-}PF_6]^+$, was observed with m/z = 573.1010 (*Figure 12*) which is very close to the theoretical value 573.1017. The mass spectrum for **MSV1** is shown in *Figure 13*. The peaks with m/z = 361.0354 and m/z = 867.0348 are corresponds to $[\mathbf{MSV1}\text{-}PF_6]^+$ and $[2\mathbf{MSV1}\text{-}PF_6]^+$ respectively.

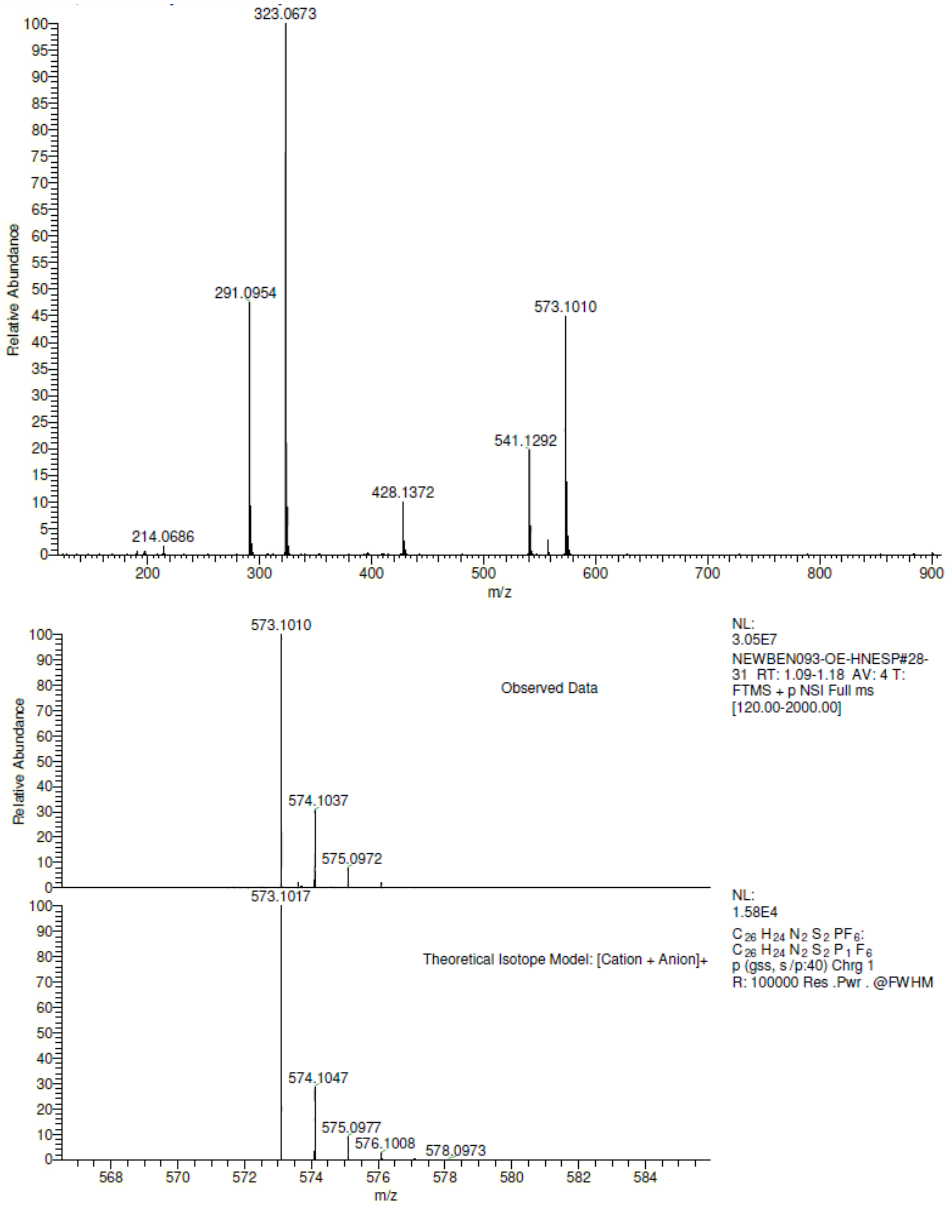

*Figure 12. Mass spectrum of **DSV**.*

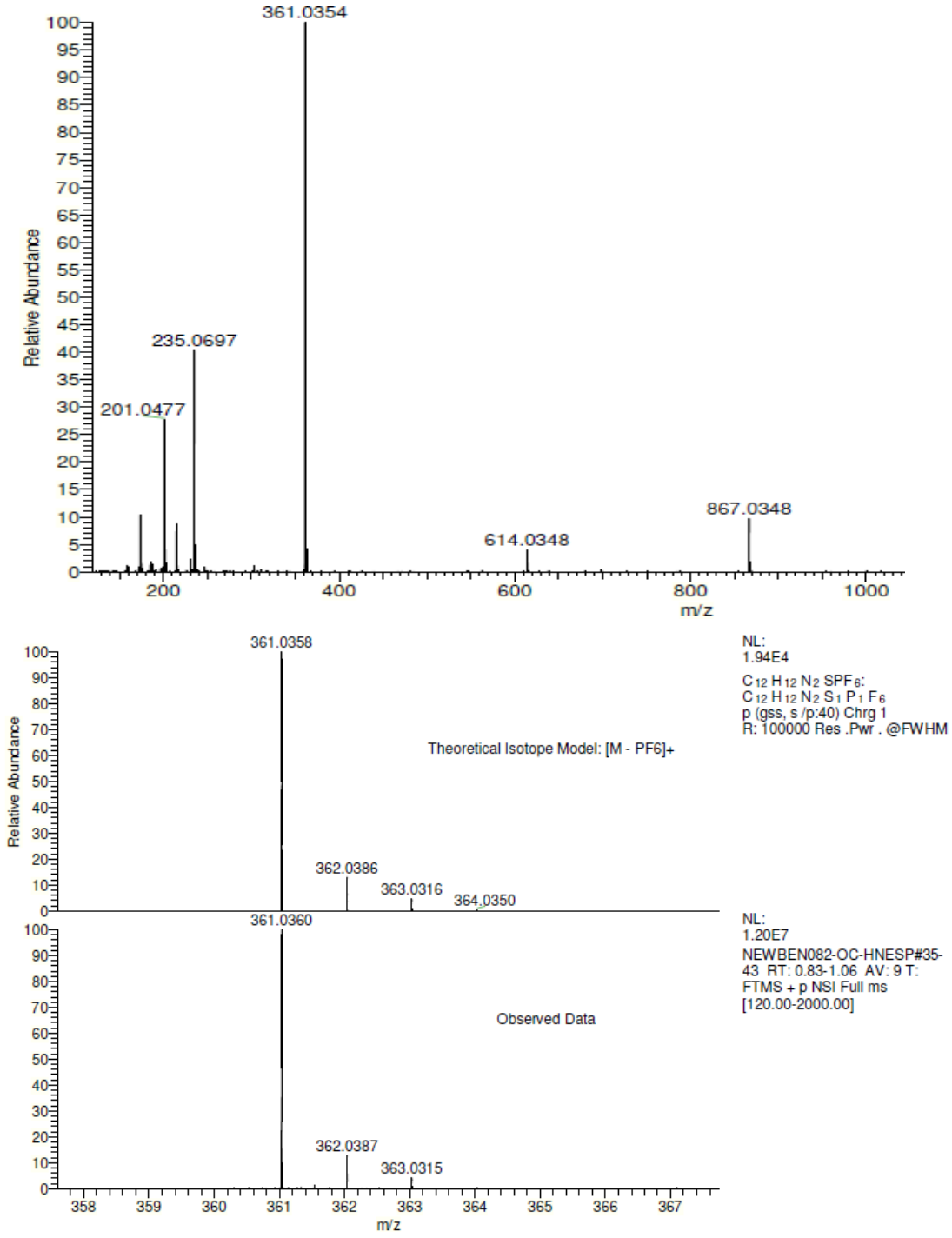

*Figure 13. Mass spectrum of **MSV1**.*

5.6 Crystal structures

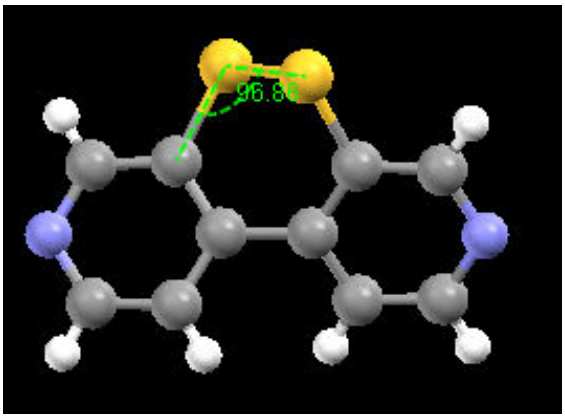

*Figure 14. X-ray crystallographic structure for **BPy6**. Carbon (grey), sulfur (yellow), hydrogen (white), nitrogen (blue).*

A few crystals were obtained during the synthesis. The crystal structure of **BPy6** (*Figure 14*)[17] clearly shows that there is a disulfide bond connecting the two pyridine rings on the 3,3' positions. The confirmation of the structure of **BPy6** was important since one explanation for **MSV2** or **MSV1** was the wrong starting material was used in the synthesis. The disulfide ring is puckered and the C-S-S bond angle is 96.86 ^{O}. The twist in the molecule as measured by the dihedral angel between planes created using the two pyridine rings is 32 ^{O}.

Suitable **DSV** crystals could not be obtained due to the problem with the decomposition of the compound during the slow crystallisation process[17]. However, the crystals of **MSV1** (*Figure 15*) and **MSV2** (*Figure 16*) were obtained and the structures are confirmed by X-ray analysis. The crystal packing diagram for **MSV2** was especially notable as illustrated in *Figure 17*. The asymmetric units align, as viewed along the a-axis, to create a tunnel-like motif. The tolyl groups of one molecular unit appear to point inward toward another subunit creating a hollow for CH_3CN solvent molecules. Each asymmetric unit is in fact slightly displaced from each other. The PF_6^- counter ions appear to reside in channels as observed along the b-axis direction.

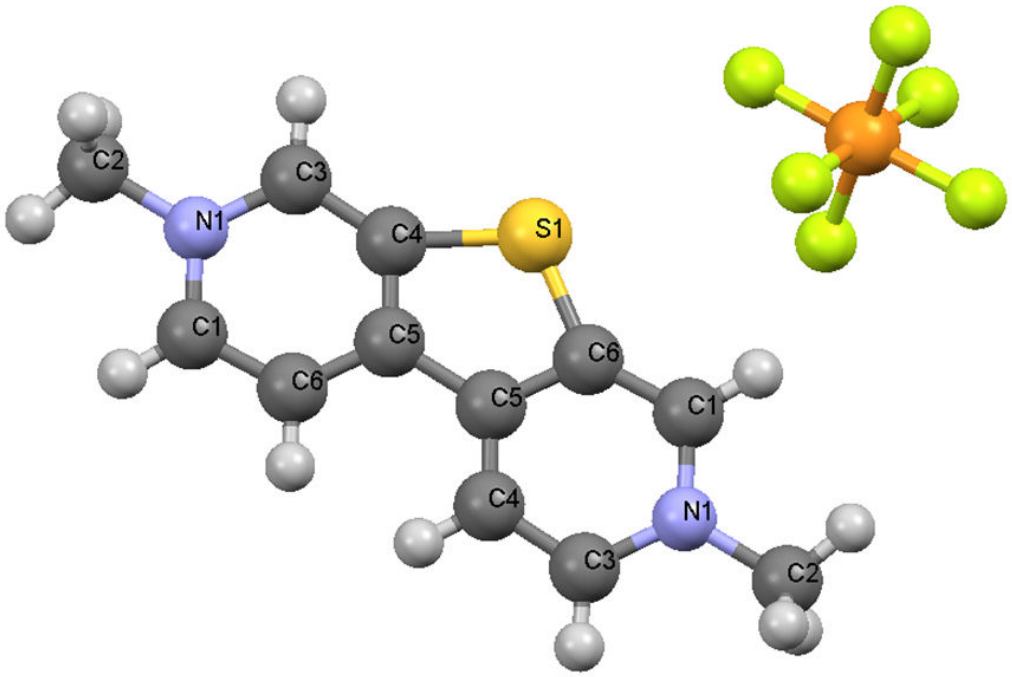

*Figure 15. X-ray crystallographic structure for **MSV1** (second PF_6^- is not shown): carbon (grey), hydrogen (white), nitrogen (blue), phosphorus (orange), fluorine(green), sulphur (yellow). There are defects in the crystals. The final R indices obtained from the structure analysis is 0.0599.*

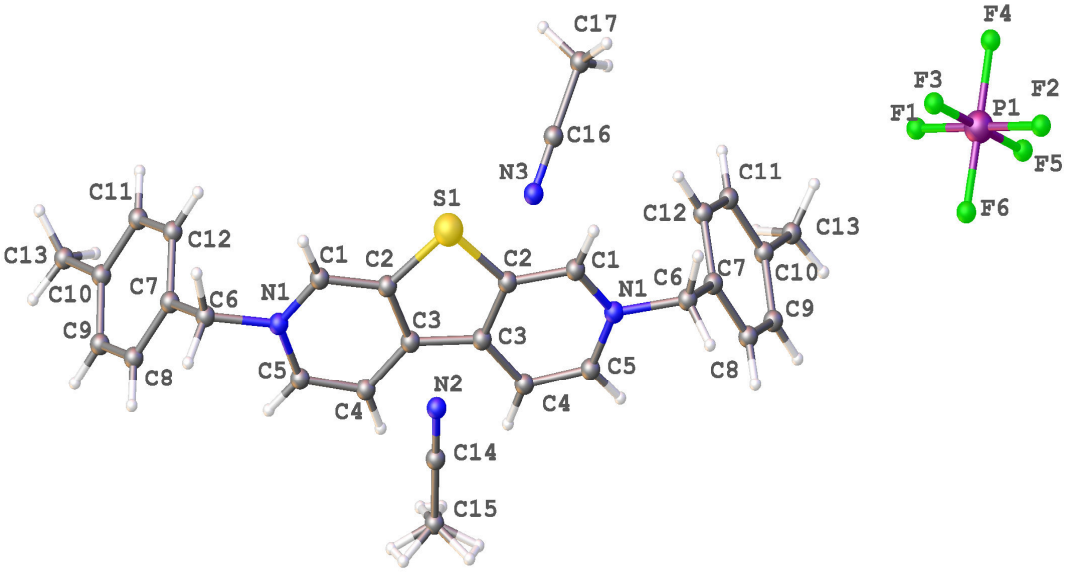

*Figure 16. X-ray crystallographic structure for **MSV2** (second PF_6^- is not shown): carbon (grey), hydrogen (white), nitrogen (blue), phosphorus (orange), fluorine(green), sulphur (yellow). There are defects in the crystals and the final R indices obtained from the structure analysis is 0.0720.*

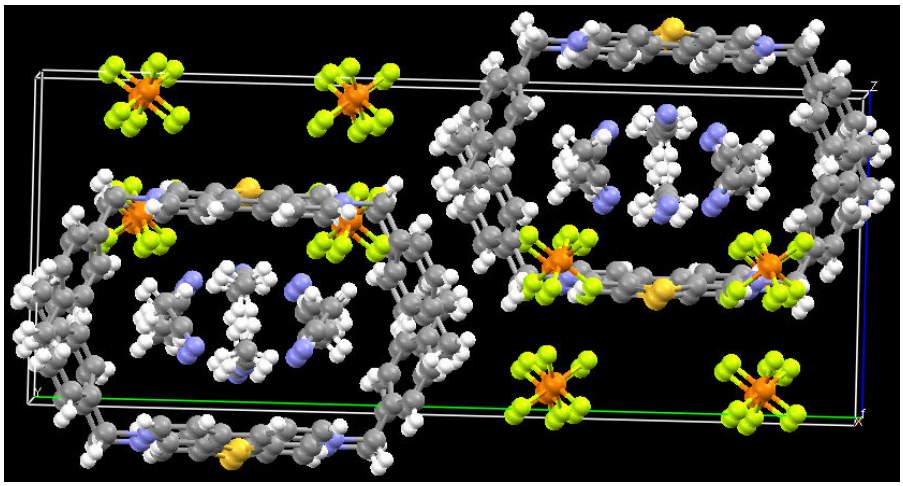

*Figure 17. Crystal packing diagram for **MSV2** showing the tunnel-like structure and the CH_3CN solvate molecules. Carbon (grey), sulfur (yellow), hydrogen (white), nitrogen (blue), phosphorus (orange), fluorine (green).*

5.7 Electrochemical investigations

The electrochemical properties of **DSV** and **MSV1** were studied by cyclic voltammetry. Experiments were carried out in a conventional three electrode cell consisting of a glassy carbon working electrode, a platinum wire counter electrode and Ag/AgCl reference electrode. **DSV** or **MSV1** was dissolved in anhydrous acetonitrile (1 mM) and TBATFB (0.2 M) was used as background electrolyte. The solution was deoxygenated before the measurement and kept under nitrogen during the whole experiment. Ferrocene was added in the same concentration as **DSV**/**MSV1** as a internal reference.

Two reversible one-electron waves are observed for **MSV1** (*Figure 18*)[17] from the cyclic voltammogram measurement. The first wave was seen at $E_{1/2}$ = -0.34 V (70 mV) vs Ag/AgCl, which is associated with the production of the monocation, and the potential is slightly more anodic when compared to simple methyl viologen ($E_{1/2}$ = -0.40 V vs Ag/AgCl) measured under identical conditions. The five-membered sulphur ring essentially forces the two pyridinium units to be nearly coplanar. This geometry is highly favourable to facilitate one-electron reduction, since this process introduces more double-bond character into the connector C-C bond. The second wave is at - 0.83 V (80 mV) corresponding to the addition of second electron to the mono-reduced viologen to

produce the neutral species. It is well separated from the first wave and more cathodic because of increased π-conjugation.

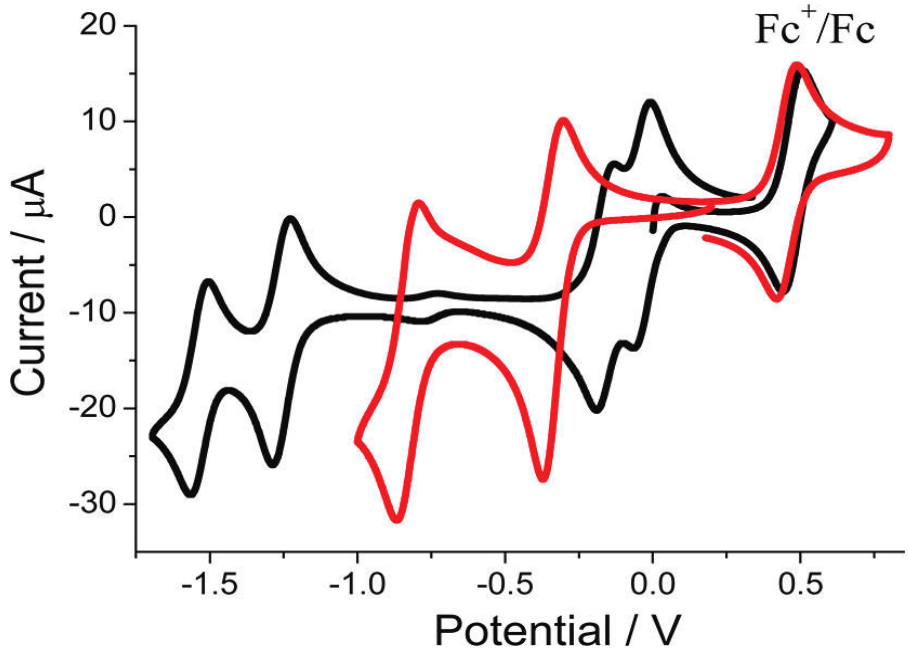

*Figure 18. Cyclic voltammograms recorded for **DSV** (black) and **MSV1** (red) in dry CH3CN containing 0.2 M TBATFB. Scan rate = 50 mV s^{-1}.*[17]

In comparison, the reductive electrochemistry for **DSV** (*Figure 18*) is far more richer displaying four distinctive reversible one-electron waves. The first two one-electron reduction waves are closely spaced occurring at $E_{1/2}$ = -0.04 V (65 mV) and $E_{1/2}$= -0.16V (70 mV) vs Ag/AgCl. After the addition of two electrons the species produced is neutral irrespective of the sites for reduction. Preliminary EPR data is consistent with production, in the first instance, of a non sulfur-based radical. The final two one-electron reduction waves are well separated from the first two and occur at $E_{1/2}$ = -1.26 V (60 mV) and $E_{1/2}$ = -1.54 V(64 mV) vs Ag/AgCl. It is noted that the difference (ΔE) between these two waves is only 280 mV, supporting the notion that the two negative charges are separated spatially. By comparison to the electrochemical behaviour for dibenzo[1,2]dithiine[8] the final two waves are attributed to sulfur-based reduction. However, there is one major difference: for dibenzo[1,2]dithiine the process consists of a single two-electron reduction which is irreversible. The electrochemical irreversibility is removed by the incorporation of the disulfide bridge into the viologen unit.

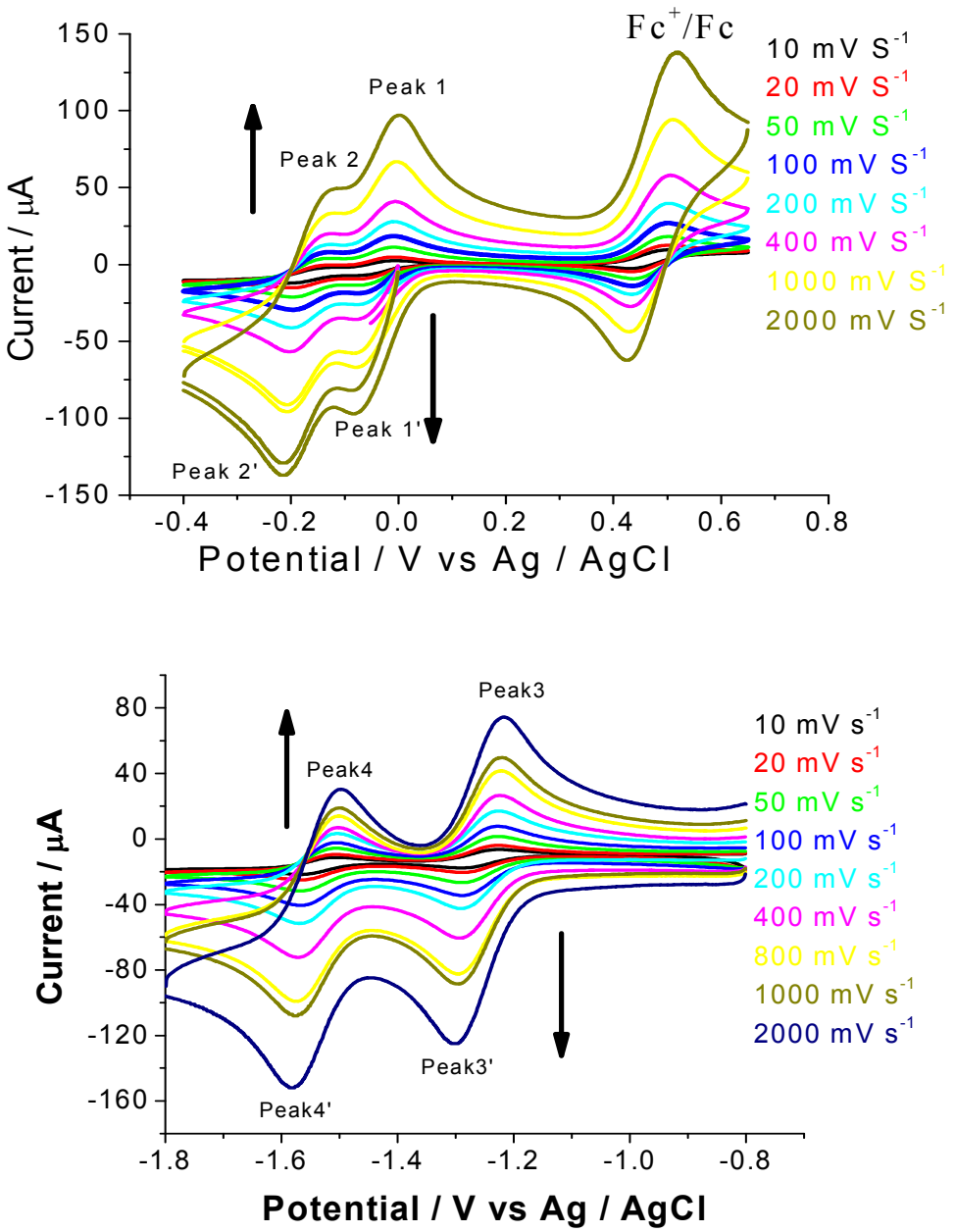

*Figure 19. Cyclic voltammograms of **DSV** at different scan rates.*

Different scan rates were applied to further study the reduction and oxidation processes. The reduction peaks currents increased as the scan rate increased from 10 mV s^{-1} to 2000 mV s^{-1} along with the oxidation peaks currents (*Figure 19*). The peak currents (i_{pa}, use anodic current as represent) increased linearly with the square root of the scan rate ($\upsilon^{1/2}$) (*Figure 20*), and this result fitted well with the relationship between peak currents and scan rates according to *Equation 2*. The oxidation and reduction were electrochemically quasi-reversible (*Table 2*, ΔE_p = 60 - 90 mV, $I_{p,a}$ / $I_{p,c}$ = 0.6 - 1.4) over the applied scan

rates.

$$I_p = 2.69 \times 10^{-5} A n^{2/3} D^{1/2} \upsilon^{1/2} C \quad (\textit{Equation 2})$$

I_p – peak current, A – surface area of the electrode (cm^2), n – number of electron transferred, D – diffusion coefficient ($cm^2\ s^{-1}$), C – concentration ($mol\ cm^{-3}$).

*Table 2. Summary of peak potentials and peak currents of **DSV** at different scan rates.*

	Peak 1			**Peak 2**		
Scan rate ($mV\ s^{-1}$)	$E_{1/2}$ / mV	$I_{p,a}$ / μA	$I_{p,a}$ / $I_{p,c}$	$E_{1/2}$ / mV	$I_{p,a}$ / μA	$I_{p,a}$ / $I_{p,c}$
10	-40.00 (65)	4.53	0.62	-165.62 (75)	5.87	1.21
20	-44.91 (70)	5.31	0.57	-165.62 (73)	7.60	1.31
50	-42.89 (65)	9.51	0.75	-165.04 (70)	11.53	1.46
100	-42.89 (65)	14.87	0.89	-162.73 (67)	15.87	1.32
200	-43.47 (70)	21.03	0.90	-164.17 (70)	21.26	1.23
400	-43.18 (75)	30.08	0.94	-163.88 (76)	28.90	1.20
1000	-40.29 (75)	48.63	0.80	-165.90 (85)	44.04	1.10
2000	-41.74 (85)	67.67	0.78	-167.35 (95)	61.93	1.12

	Peak 3			**Peak 4**		
Scan rate ($mV\ s^{-1}$)	$E_{1/2}$ / mV	$I_{p,a}$ / μA	$I_{p,a}$ / $I_{p,c}$	$E_{1/2}$ / mV	$I_{p,a}$ / μA	$I_{p,a}$ / $I_{p,c}$
10	-1257 (64)	7.15	0.97	-1538 (64)	5.86	1.03
20	-1258 (60)	9.14	0.94	-1540 (65)	8.78	1.05
50	-1258 (60)	13.13	0.92	-1538 (64)	12.68	1.07
100	-1258 (60)	18.41	0.92	-1536 (61)	17.90	1.12
200	-1260 (65)	25.80	0.87	-1536 (67)	25.11	1.09
400	-1259 (65)	36.11	0.87	-1538 (70)	33.76	1.09
1000	-1259 (75)	50.71	0.84	-1540 (75)	47.92	1.09
2000	-1260 (75)	56.86	0.84	-1538 (77)	56.77	1.16

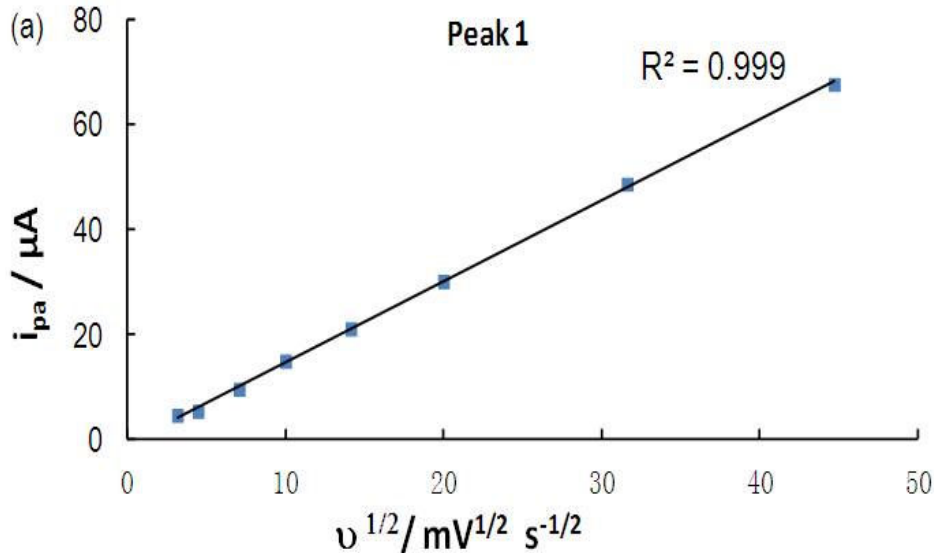
(a)
Peak 1
R² = 0.999
i_{pa} / μA
υ 1/2/ mV1/2 s-1/2

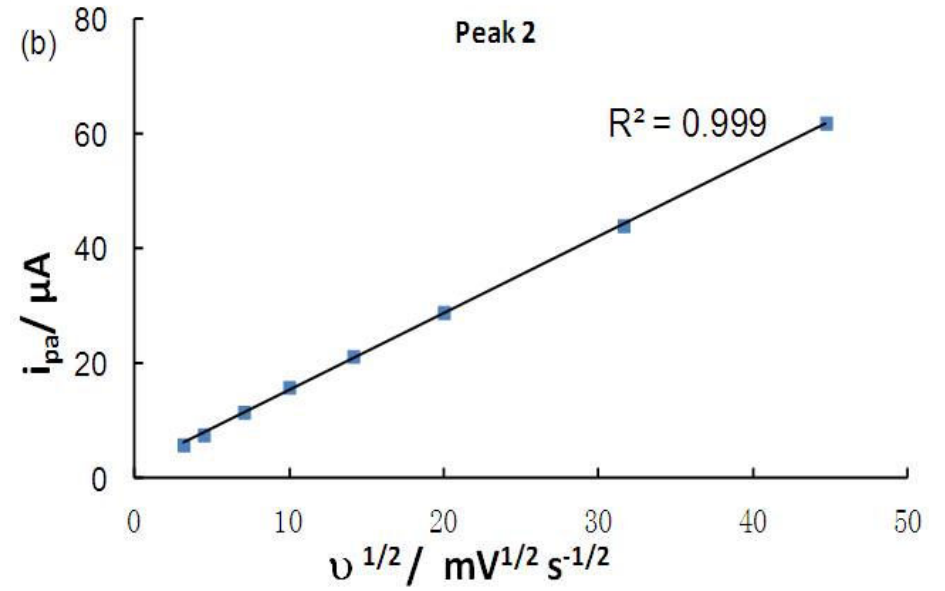
(b)
Peak 2
R² = 0.999
i_{pa}/ μA
υ 1/2 / mV1/2 s-1/2

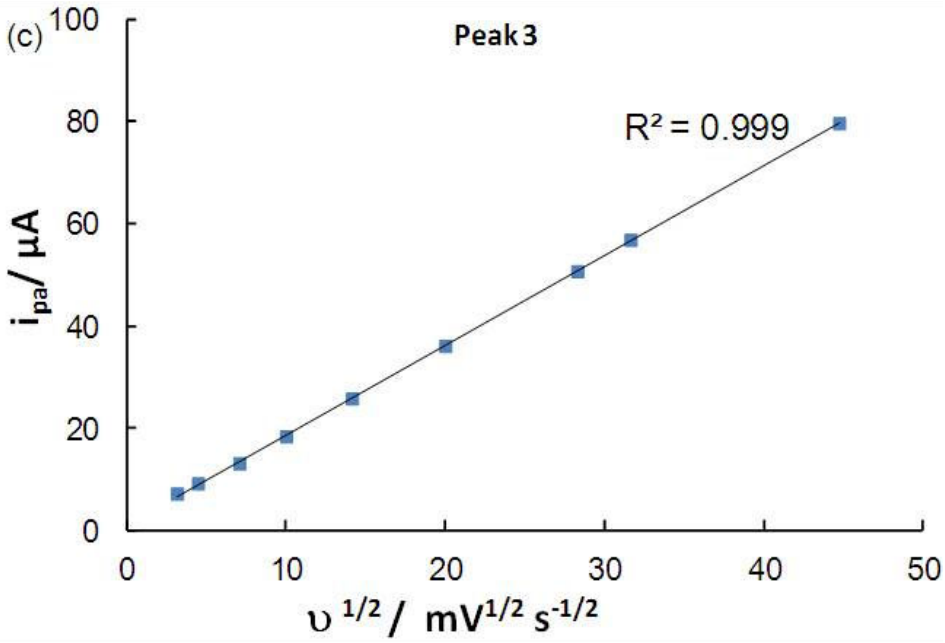
(c)
Peak 3
R² = 0.999
i_{pa}/ μA
υ 1/2 / mV1/2 s-1/2

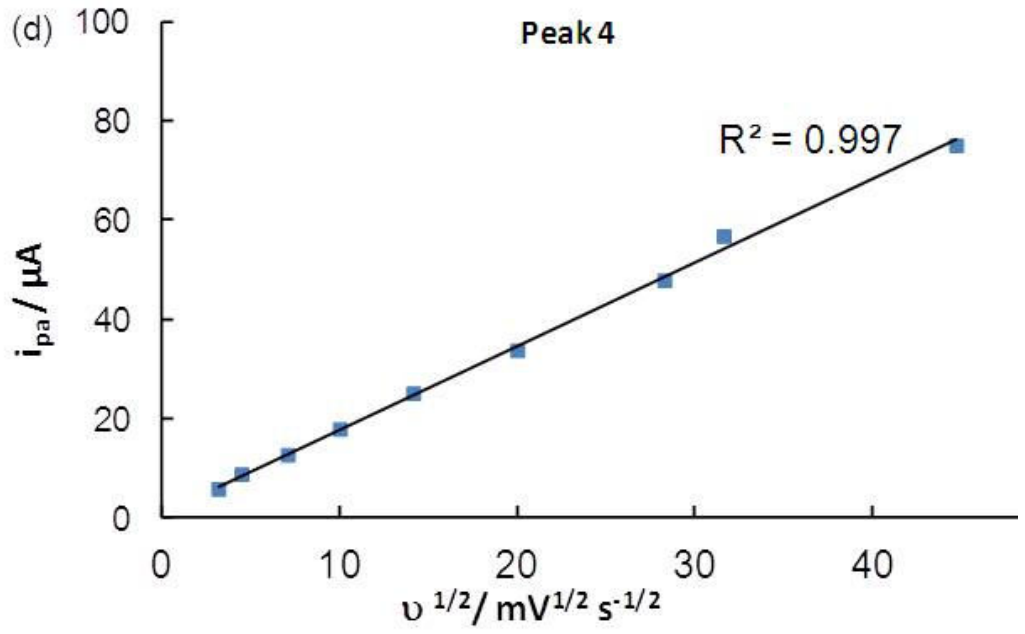

*Figure 20. Plot of peak currents vs scan rates for **DSV**.*

5.8 Molecular orbital calculations

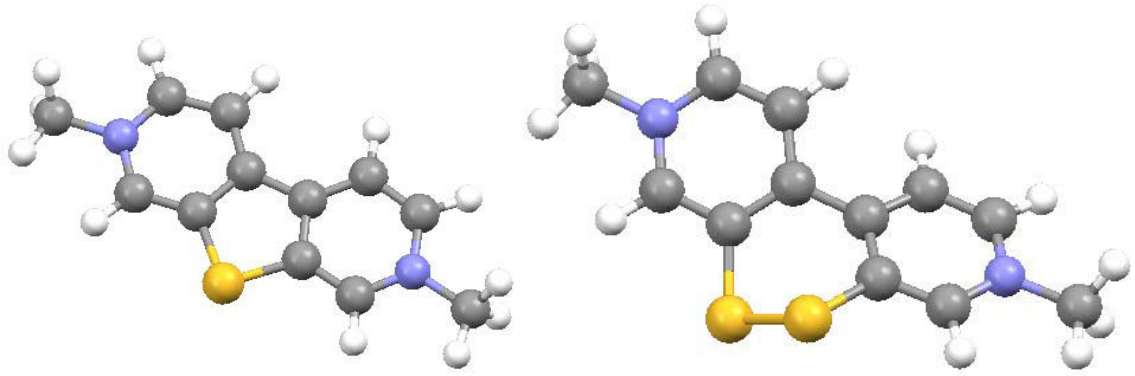

*Figure 21. Computer calculated energy-minimized structure for the cation **MSV1** (left) and **DSV** (right).*

High-level computational study was undertaken to elucidate more information on the two disparate sulfur-based viologen derivatives. To simplify the calculations, the N-methyl group was chosen instead of the more flexible tolyl group. In the first case, the basic energy minimized ground-state molecular geometries for **MSV1** and **DSV** were calculated in the gas phase at the Hartree-Fock level (6-31G) using Gaussian 03[24]. Further refinement was then carried out using DFT (B3LYP) and the 6-311G^{++}(3df)

basis set to account for the two sulfur atoms. The computer-generated energy-minimized structures for the two derivatives are shown in *Figure 21*.

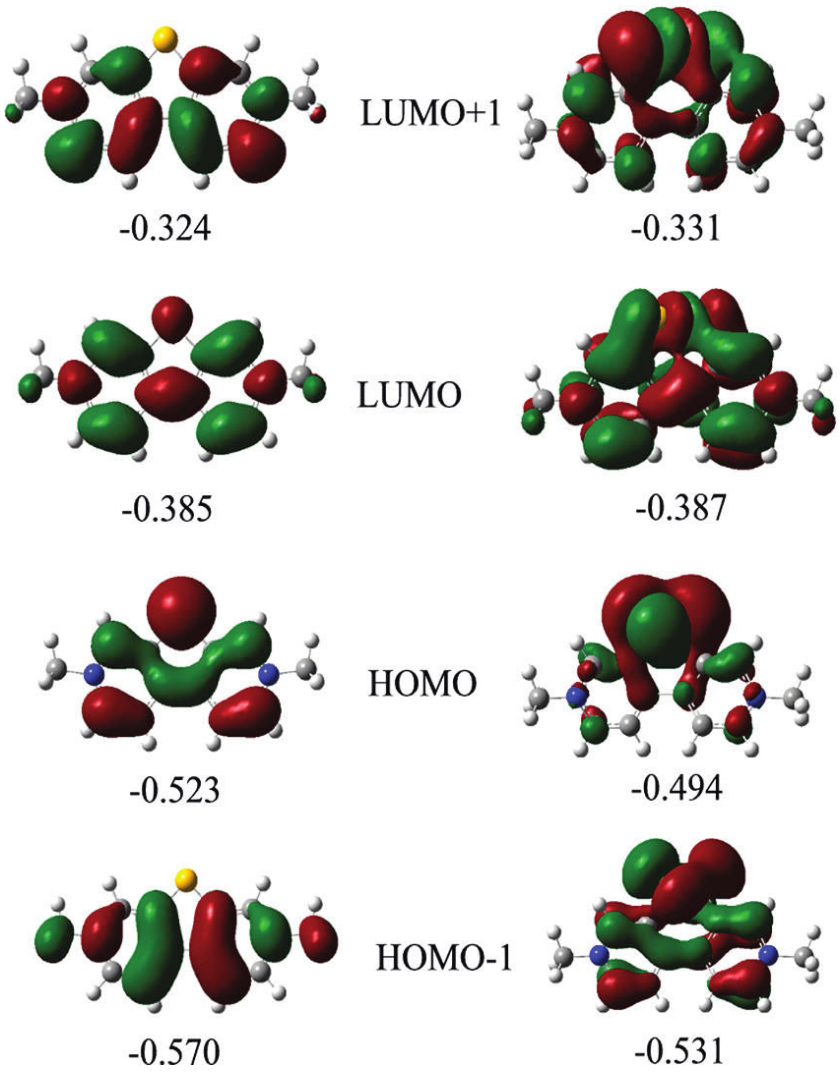

*Figure 22. Illustrations of selected molecular orbitals associated with **MSV1** (left) and **DSV** (right) calculated using DFT(B3LYP) and the 6-311G^{++}(3df) basis set. Energies are given in hartrees.*

For comparison purposes, a selection of the generated HOMOs and LUMOs associated with the two cations are shown in *Figure 22*. The HOMO for **DSV** is located almost exclusively on the two sulfur atoms; a somewhat similar picture is seen for the HOMO-1. In comparison, the HOMO, and to a greater extent the HOMO-1, for **MSV1** is situated on the viologen moiety. The energies for the LUMOs of both cations are remarkably similar, but their localization is very different. The LUMO for **DSV** is delocalized over the entire cation, whereas the LUMO+1 is localized on the disulfide bridge. The LUMO and LUMO+1 for **MSV1** are situated on the viologen moiety. We

infer from these calculations that addition of the first electron to **MSV1** is very much viologen-based, but the case for **DSV** is somewhat less clear-cut. However, assuming that addition of two electrons to **DSV** is exclusively viologen-based, the neutral product formed contains double bond character in the C-C connector bond. Addition of a single electron to this species produces a radical anion. A DFT energy minimization calculation (B3LYP, 6-311G^{++}(3df)) starting from this compound is interesting. After the addition of the third electrons, the S-S bond increases significantly to ca. 3.5 Å (*Figure 23*). In addition, the connector C-C bond length (1.43 Å) is elongated and hence has reduced double bond character.

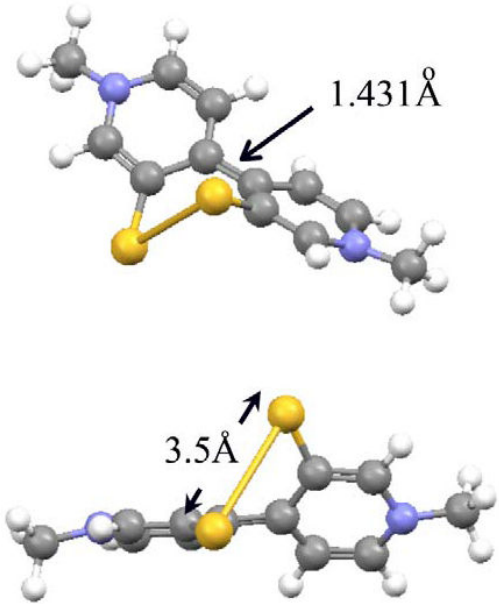

*Figure 23. Computer calculated energy-minimized structure for the three electron reduced **DSV** molecule. Note: the central connector bond is too long to be considered a pure double bond and the molecule is twisted to alleviate strain.*

5.9 Proposed disulfide bond "spring open" model[17]

As discussed previously for the molecular structure calculations, the addition of one electron to the doubly reduced neutral species facilitates sulfur-sulfur bond cleavage. On electrostatic repulsion grounds, energy minimized structures and in fitting with the ΔE value, the final one electron addition must occur in the conformation where the two sulfurs are anti to each other[17]. Anti and syn forms show significant change in bond length for the central connector bond, and the driving force for formation of the anti

arrangement is large (*Figure 24*)[17]. In essence, the molecule "springs open" assists this process. Again, such behavior is dissimilar to dibenzo[1,2]dithiine where only after concurrent two-electron reduction does the molecule twist to alleviate electrostatic repulsion[8,17].

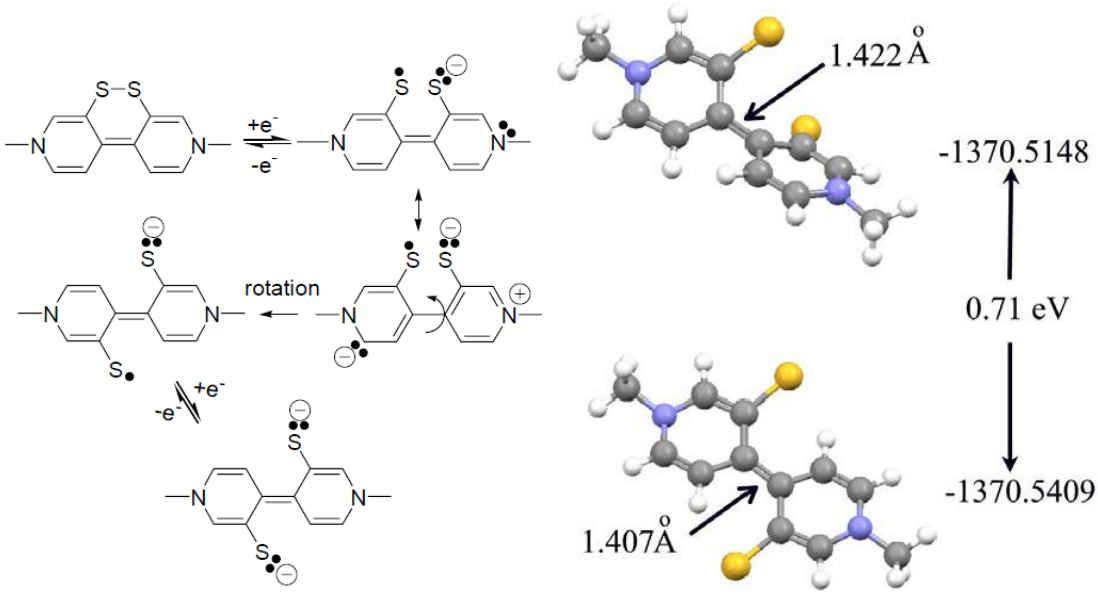

Figure 24. Simplified representation of the proposed 'spring opening' from the doubly reduced ***DSV*** *(left), and the difference in energies for the fully reduced molecules in the syn and anti conformations (right)*[17].

5.10 Conclusions

We have shown that a viologen based four-electron storage molecule **DSV** can be achieved by incorporation of the disulfide bridge into the viologen dication with a potential less than ca. -1.6 V vs Ag/AgCl. Two-electron reduction is known for viologen derivatives. The first reduction step is highly feasible with a reduction potential around -0.3 V vs Ag/AgCl. The second reduction potential is usually found in the range of -0.5 V to -1.0 V vs Ag/AgCl as reported previously[25]. Maran and co-workers reported that electrochemical reduction of aryl disulfides also involved a two electron process[26]. These are consistence with our finding that upon the incorporation of a disulfide bridge into a viologen a four electron reduction is feasible. Both of the viologen and the disulfide bridge maintain their reduction properties in **DSV**. Furthermore, the addition of the first two electrons is extremely facile, making **DSV** one

of the easiest to reduce viologen derivatives to date[25].

It is very likely that the cleavage process of disulfide bond in **DSV** is similar to the reduction of sulfur-containing amino acid derivative (e.g. cysteine, cyastine and methionine residues)[27] found in biological systems. *Figure 25* illustrated a possible pathway of the disulfide bond cleavage upon the interaction with hydrated electrons (e_{aq}^-) and H· radical proposed by Chatgilialoglu and co-workers[28].

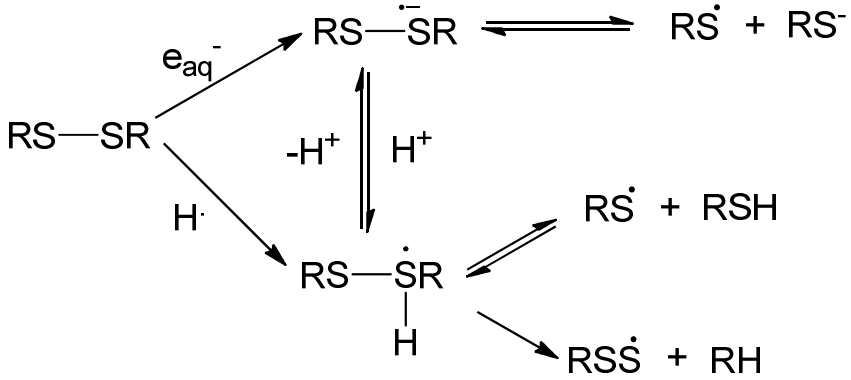

Figure 25.The possible reaction of e_{aq}^- and H· with a disulfide-containing amino acid derivatives in aqueous solution proposed by Chatgilialoglu and co-workers[28].

We were expected to exploit the rather unique redox properties of **DSV** in multiple charge accumulation for applications in artificial photosynthesis and molecular memory devices. This does not seem to be feasible unless we can find a way to enhance the stability of the disulfide bridge. One prospects of **DSV** is to incorporate the disulfide bridge into a gold nanoparticle surface and to study its properties on a nanoparticle surface.

5.11 References

[1] L. Ji, Z. Lin, M. Alcoutlabi and X. Zhang, *Energy Environ. Sci.,* 2011, **4**, 2682.

[2] (i) B. Peng and J. Chen, *Coord. Chem. Rev.*, 2009, **253**, 2805; (ii) D. Gust, T. A. Moore and A. L. Moore, *Acc. Chem. Res.*, 2009, **42**, 1890; (iii) X. P. Gao and H. X. Yang, *Energy Environ. Sci.*, 2010, **3**, 174.

[3] (i) P. Belser, L. D. Cola, F. Hartl, V. Adamo, B. Bozic, Y. Chriqui, V. M. Iyer, R. T. F. Jukes, J. Kühni, M. Querol, S. Roma and N. Salluce, *Adv. Funct. Mater.* 2006, **16**, 195; (ii) M. Irie, *Photochem. Photobiol. Sci.*, 2010, **9**, 1535; (iii) C. C. Corredor, Z. Huang and K. D. Belfield*, Adv. Mater.* 2006, **18**, 2910; (iv) S. Pu, D. Jiang, W. Liu, G. Liu and S. Cui, *J. Mater. Chem.*, 2012, **22**, 3517; (v) M. Natali and S. Giordani, *Chem. Soc. Rev.,* 2012, **41**, 4010; (vi) H. Bouas-Laurent and H. Durr, *Pure Appl. Chem.*, 2001, **73**, 639; (vii) D. Dulic, S. J. van der Molen, T. Kudernac, H. T. Jonkman, J. J. D. de Jong, T. N. Bowden, J. van Esch, B. L. Feringa and B. J. van Wees, *Phys. Rev. Lett.*, 2003, **91**, 207402; (viii) S. H. Kawai, S. L. Gilat, R. Ponsinet and J.-M. Lehn, *Chem. Eur. J.*, 1995, **1**, 285.

[4] W. Wei, X. Cui, W. Chen and D. G. Ivey, *Chem. Soc. Rev.*, 2011, **40**, 1697.

[5] W. J. Youngblood, S. H. A. Lee, Y. Kobayashi, E. A. Hernandez-Pagan, P. G. Hoertz, T. A. Moore, A. L. Moore, D. Gust and T. E. Mallouk, *J. Am. Chem. Soc.,* 2009, **131**, 926.

[6] H. Nishide and K. Oyaizu, *Science*, 2008, **319**, 737.

[7] M. Fukai, A. Kitani, C. Degrand and L. L. Miller, *J. Am. Chem. Soc.*, 1982, **104**, 28.

[8] A. C. Benniston, B. D. Allen, A. Harriman, I. Llarena, J. P. Rostron and B. Stewart, *New. J. Chem.*, 2009, **33**, 417.

[9] C. L. Bird and A. T. Kuhn, *Chem. Soc. Rev.*, 1981, **10**, 49.

[10] A. C. Benniston, A. Harriman, P. Li and J. P. Rostron, *Tetrahedron Lett.*, 2005, **46**, 7291.

[11] C. S. Sevier and C. A. Kaiser, *Nat. Rev. Mol. Cell Bio.*, 2002, **3**, 836.

[12] (i) A. C. Benniston, A. Harriman, P. Li, J. P. Rostron, R. W. Harrington and W. Clegg, *Chem. Eur. J.*, 2007, **13**, 7838; (ii) M. A. J. Miah and V. Snieckus, *J. Org. Chem.*, 1985, **50**, 5436; (iii) H. M. Wuest and E. H. Sakal, *J. Am. Chem. Soc*., 1951, **73**, 1210.

[13] N. Miyaura and A. Suzuki, *Chem. Rev.*, 1995, **95**, 2457.

[14] (i) M. S. Newman and H. A. Karnes, *J. Org. Chem.*, 1966, **31**, 3980; (ii) H. Kwart and E. R. Evans, *J. Org. Chem.*, 1966, **31**, 410.

[15] (i) O. D. Lucchi, *Pure & Appl Chem*, 1996, **68**, 945; (ii) Y. H. Cho, A. K. Kina and T. Shimada, T. Hayashi, *J. Org. Chem.*, 2004, **69**, 3811; (iii) S. Cossu, O. D. Lucchi, D. Fabbri, G. Valle, G. F. Painter, R. A. J. Smith, *Tetrahedron,* 1997, **53**, 6073.

[16] X. Yang, Q. Shi, Y. Liu, G. Zhao, K. F. Bastow, J. Lin, S. Yang, P. Yang and K. Lee, *J. Med. Chem.*, 2009, **52**, 5262.

[17] A.C. Benniston, J. Hagon, X. He, S. Yang and R. W. Harrington, *Org. Lett.*, 2012, **14**, 506.

[18] M. Abboud, V. Mamane, E. Aubert, C. Lecomte and Y. Fort, *J. Org. Chem.*, 2010, **75**, 3224.

[19] A. McKillop, B. D. Howarth and R. J. Kobylecki, *Synthetic Commun.*, 1974, **4**, 35.

[20] A. Schonberg and L. Varga, *Ber. Dtsch. Chem. Ges.*, 1930, **63**, 178.

[21] K. Miyazaki, *Tetrahedron Lett.*, 1968, **9**, 2793.

[22] A. Kaji, Y. Araki and K. Miyazaki, *Bull Chem. Soc. Japan*, 1971, **44**, 1393.

[23] M. Hori, M. Ban, E. Imai, N. Iwata, Y. Baba, H. Fujimura, M. Nozaki and M. Niwa, *Heterocycles*, 1983, **20**, 2359.

[24] M. J. Frisch, G. W. Trucks, H. B. Schlegel, G. E. Scuseria, M. A. Robb, J. R. Cheeseman, J. A. Montgomery Jr., T. Vreven, K. N. Kudin, J. C. Burant, J. M. Millam, S. S. Iyengar, J. Tomasi, V. Barone, B. Mennucci, M. Cossi, G. Scalmani, N. Rega, G. A. Petersson, H. Nakatsuji, M. Hada, M. Ehara, K. Toyota, R. Fukuda, J. Hasegawa, M. Ishida, T. Nakajima, Y. Honda, O. Kitao, H. Nakai, M. Klene, X. Li, J. E. Knox, H. P. Hratchian, J. B. Cross, V. Bakken, C. Adamo, J. Jaramillo, R. Gomperts, R. E. Stratmann, O. Yazyev, A. J. Austin, R. Cammi, C. Pomelli, J. W. Ochterski, P. Y. Ayala, K. Morokuma, G. A. Voth, P. Salvador, J. J. Dannenberg, V. G. Zakrzewski, S. Dapprich, A. D. Daniels, M. C. Strain, O. Farkas, D. K. Malick, A. D. Rabuck, K. Raghavachari, J. B. Foresman, J. V. Ortiz, Q. Cui, A. G. Baboul, S. Clifford, J. Cioslowski, B. B. Stefanov, G. Liu, A. Liashenko, P. Piskorz, I. Komaromi, R. L. Martin, D. J. Fox, T. Keith, M. A. Al-Laham, C. Y. Peng, A. Nanayakkara, M. Challacombe, P.

M. W. Gill, B. Johnson, W. Chen, M. W. Wong, C. Gonzalez and J. A. Pople, Gaussian 03, Gaussian, Inc., Wallingford CT, 2004.

[25] (i) A. L. Black and L. A. Summers, *J. Heterocycl. Chem.*, 1971, **8**, 29; (ii) C. L. Bird and A. T. Kuhn, *Chem. Soc. Rev.*, 1981, **10**, 49; (iii) L. Michaelis and E. S. Hill, *J. Gen. Physiol.*, 1933, **16**, 859; (iv) T. Kawata and M. Yamamoto, *Jpn. J. Appl. Phys.*, 1975, **14**, 725.

[26] S. Antonello, K. Daasbjerg, H. Jensen, F. Taddei and F. Maran, *J. Am. Chem. Soc.*, 2003, **125**, 14905.

[27] (i) S. P. Mezyk, *J. Phys. Chem.*, 1996, **100**, 8861; (ii) S. P. Mezyk, *J. Phys. Chem.*, 1996, **100**, 8295; (iii) M. Z. Hoffman and E. Hayon, *J. Am. Chem. Soc.*, 1972, **94**, 7950.

[28] C. Chatgilialoglu, C. Ferreri, A. Torreggiani, A. M. Salzano, G. Renzone and A. Scaloni, J. Proteomics, 2011, **74**, 2264.

Chapter 6

Molecular Dyads with Conformation Variations on Conjugated Bridges

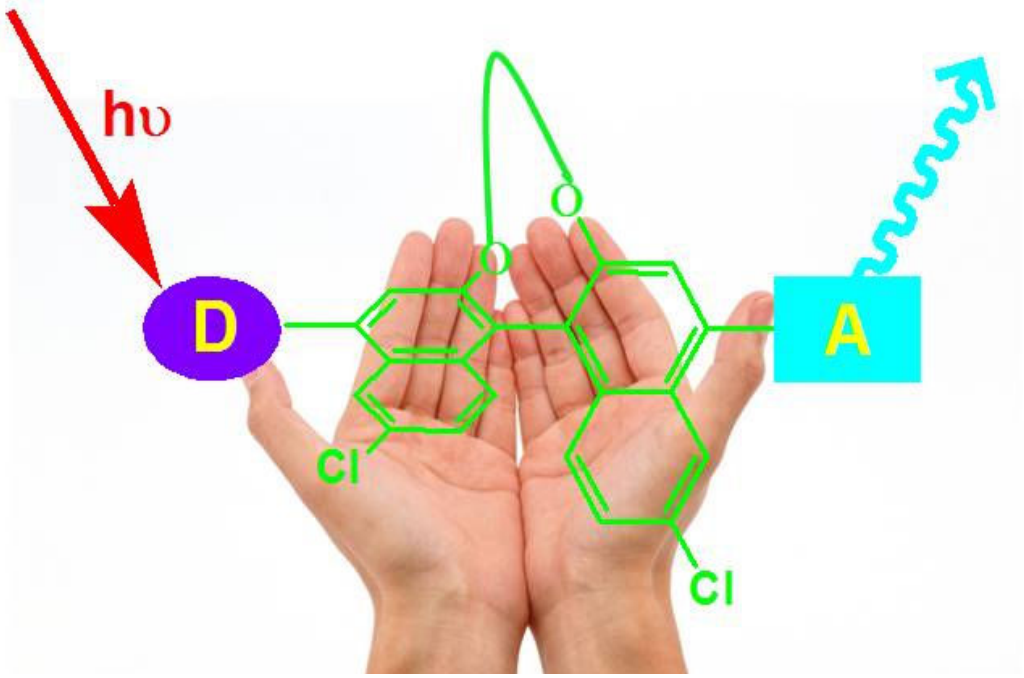

Selected molecular structures discussed in this chapter are shown below.

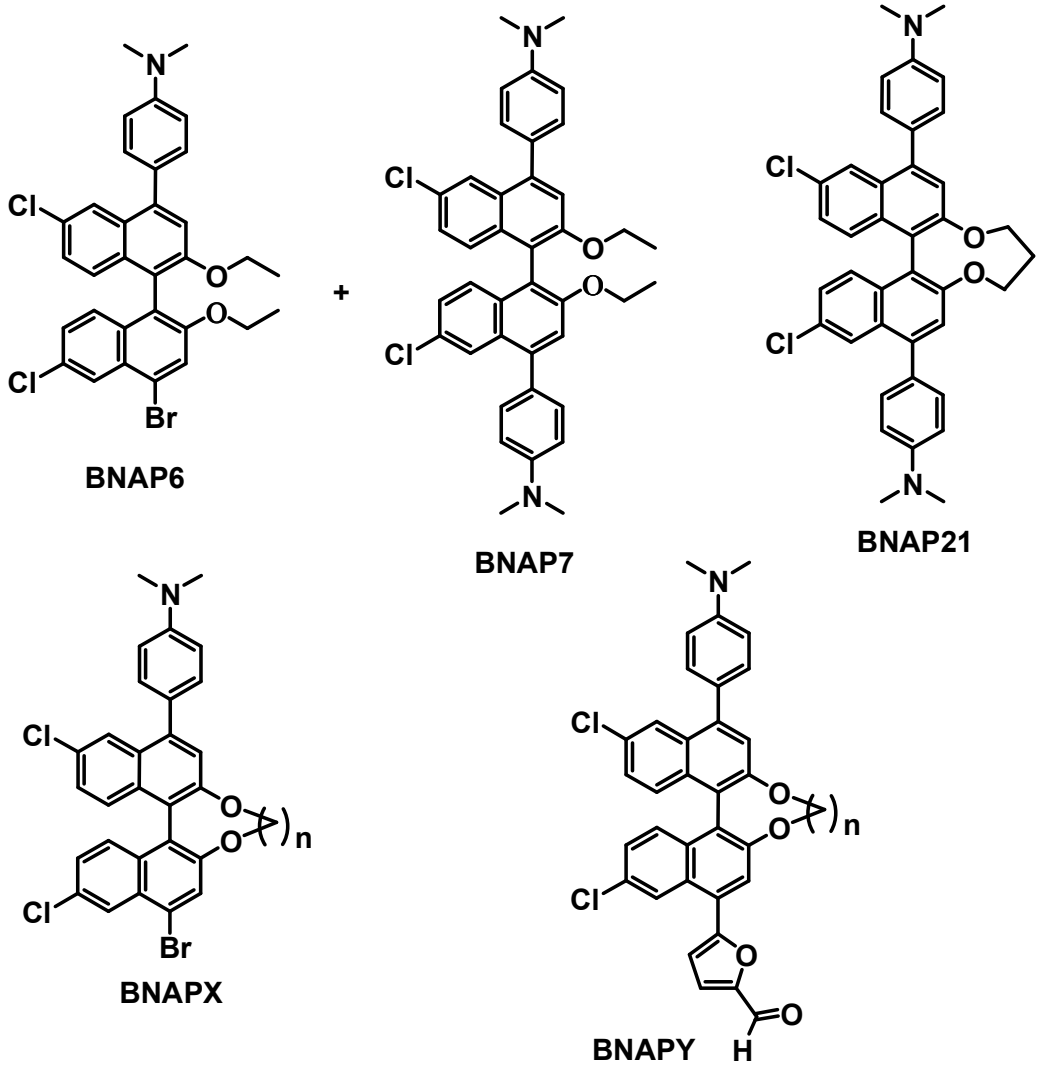

n = 1, BNAPX = BNAP16, BNAPY = BNAP17;
n = 2, BNAPX = BNAP18, BNAPY = BNAP19;
n = 3, BNAPX = BNAP13, BNAPY = BNAP14.

6.1 Introduction

Long range energy transfer rate constants depend on the energetics of the system and strength of electronic coupling (H_{DA}). These two factors are correlated with each other by the nuclear mode of the molecular system during the electron/energy transfer process and the surrounding environment[1]. The surrounding environment such as the bridges between two units is important, and it is found that conformations of the conjugated bridges between donors and acceptors play a significant role in determination of the energy transfer rate[2]. For instance, it is believed that the molecular conductivity reaches maximum when the neighbouring aromatic rings are arranged in a coplanar conformation[3]. There was found nearly a five-fold differences in the non-radiative decay rate between orthogonal and coplanar geometrically restricted *p*-quaterphenyls[4]. The square of strength of a donor and an acceptor electronic coupling ($\{H_{DA}\}^2$) is an exponential function of the distance (R_{DA}) between two units[1].

$$\{H_{DA}\}^2 \propto \exp(-\beta R_{DA}).$$

where β is a coefficient.

Over the past decades, numerous theoretical [5] and experimental [6] studies have investigated how the geometry of the spacer unit can determine the magnitude of H_{DA}. In this chapter we focus on the unsymmetrical functionalisation of 1,1'-bi-2-naphthol (**BINOL**) rings at the 4,4'-position and attempting to control the geometry through length of a dialkoxy strap. Another interesting point about binaphthol arise of the bridge is chiral, which can give us further opportunities to study the affect of chirality on the energy or electron transfer processes. The application of **BINOL** as chiral units have been found in many aspects such as enantioselective sensing[7], optically molecular electronic wires[8], helical receptor-anion complexes[9] and selective enantioselective catalysts [10] . Therefore, we envisaged to discover an approach to achieve binaphthol-bridged molecular dyads and to control the conformation through the

dialkoxy straps. Study of the photophysical properties can give us an insight into the energy/electron transfer dynamics with chiral spacer upon the separation of the enantiomers or by starting from optically pure binaphthol. Therefore, the first goal here was to discover the synthetic approaches which allowed us to achieve unsymmetrical molecular dyads.

6.2 Synthesis

The first five steps to binaphthalene-spaced molecules are shown in *Scheme 1*. Following the literature reported method **BNAP5** was obtained without major problems[11]. Direct bromination of the 4,4' positions of binaphthol was not possible. Binaphthol (racemic) was brominated with a solution of bromine in dichloromethane to yield 6,6'-dibromo-1,1'-binaphthyl-2,2'-diol (**BNAP2**). Iodomethane was firstly tried in the protection of the diol group and the reaction proceeded without any problem with almost 100% yield. However, problems arose in next step, since we found that a mixture of starting material and product existed at the end of the reaction. The starting material cannot be fully converted to the product. Separation of the mixture was difficult because of the high similarity of the starting material and product. When bromoethane was used instead of iodomethane the problem was solved. Therefore, the diol group was protected with ethyl groups to afford **BNAP3**. One may also argue that if we link the two hydroxyl groups in this step (i.e. do the protection and linkage of the diol group at the same time), it will shorten the synthesis route and improve the overall yield. We did attempt this synthetic route but once again separation of products was challenging. In the following step, bromine atoms were exchanged with chlorines to give **BNAP4**. This exchange is to deactivate and avoid coupling reaction with boronic acid on these positions in further steps. The chlorination of 6,6' positions activated the 4,4' positions which made bromination of **BNAP4** and its conversion to **BNAP5** possible. The yields of these steps were very good and over 90%.

Standard Suzuki coupling of **BNAP5** with 4-(dimethylamino)phenyl boronic acid

afforded a mixture of **BNAP6** and **BNAP7**. The ratio of the **BNAP5** and boronic acid was controlled (1:0.8) in order to achieve higher yield of the mono-coupled product, **BNAP6**. The crude mixture, including starting material **BNAP5**, was separated by column chromatography without any major problem. When the ratio was increased to 1:2, the dominant product was the di-coupled **BNAP7**.

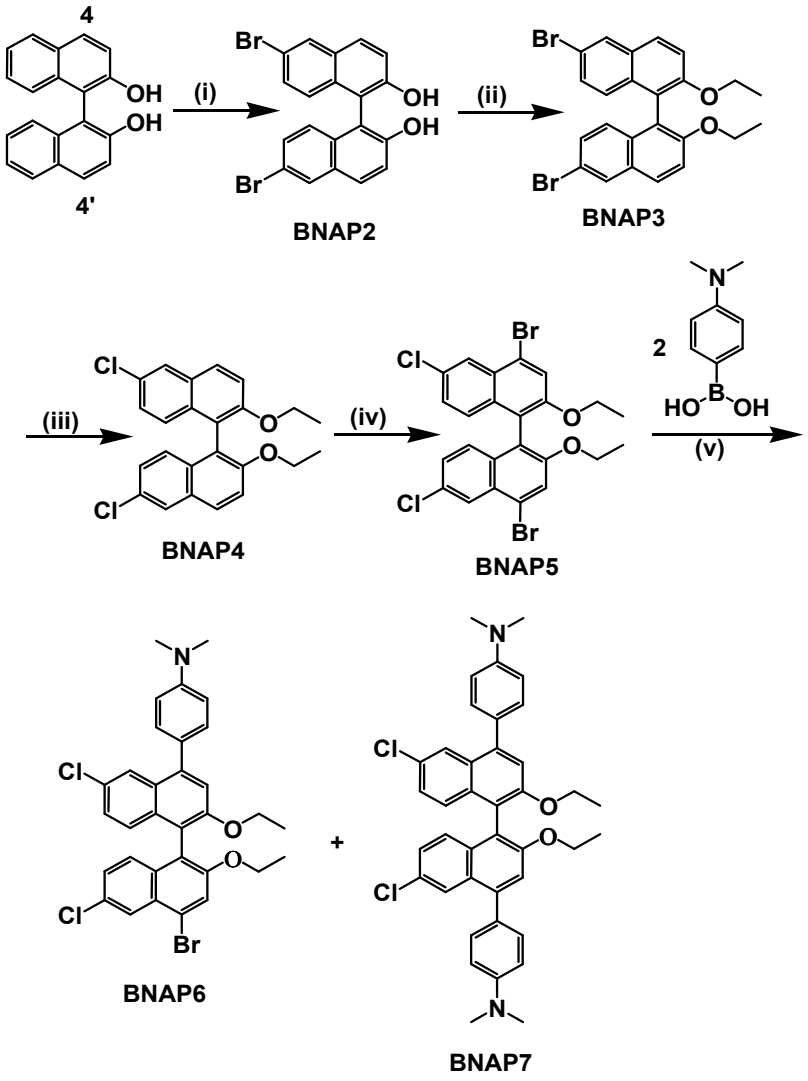

*Scheme 1 Synthesis of **BNAP6** as basic precursor for straped-binaphthol-spaced derivatives. Reaction conditions: (i) Br_2 (1M in DCM), -78 ^{O}C 2 hours, room temperature overnight, CH_2Cl_2;(ii) NaI, K_2CO_3, CH_3CH_2Br, acetone, reflux;(iii) $^{n}BuLi$, -78 ^{O}C, CCl_3CCl_3, THF, -78 ^{O}C; (iv) Br_2 (1M in DCM), -78 ^{O}C 2 hours, room temperature overnight; (v) $Pd(PPh_3)_4$, Na_2CO_3, toluene, 1,2-dimethoxyethane.*

The method to **BNAP10** with different length of straps was firstly tried by carrying out a coupling reaction between **BNAP6** and phthalimide (*Scheme 2*). The reaction is

similar to Buchwald-Hartwig coupling reaction. Usually electron poor aryl bromides, and electron rich primary / secondary amines will activate the coupling reaction[12]. However, both aryl bromide (**BNAP6**) and amide are not reactive in Buchwald-Hartwig coupling reaction. **BNAP6** bears a relatively strong electron donating dimethyl amino group. The secondary amine in phthalimide is directly connected to two electron withdrawing carbonyl groups. Therefore, the reaction is extremely difficult. Attempts with Buchwald-coupling reaction did not yield the expected product.

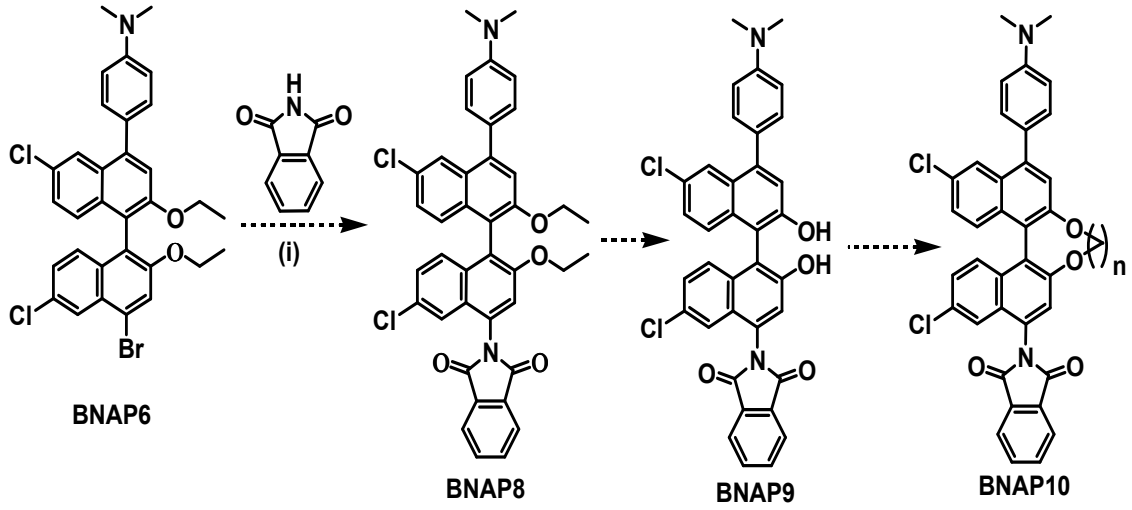

Scheme 2. First proposed synthetic route to the strapped targets. Reaction conditions: (i) $[P(O\text{-}MeC_6H_4)_3]_2PdCl_2$, KO^tBu, toluene, 100 ^OC.

The reaction between aryl halides and amide groups on phthalimides to form C-N bond is not so common in the literature. We found that Bacon and co-workers[13] published work on the extended application of the Gabriel reaction[14] from alkyl halides to aryl halides. The reaction between potassium phthalimide and *p*-bromobenzonitrile proved successful in the presence of copper (I) iodide as catalyst and dimethylacetamide as solvent with a yield of 94%. Similarly, reaction between potassium phthalimide and **BNAP5** (*Scheme 3*) was carried out under the same conditions as reported. A white solid was obtained after extensive column chromatography and the characteristic peaks corresponding to protons on the phthalimide were clearly observed in the ^{1}H-NMR spectrum, but there was still small amount of impurities which were easily separated. Therefore, **BNAP11** with small amount of impurities was used directly in the next step

for the Suzuki coupling reaction. After separation of the reaction mixture, we realised that there were more peaks in the ^{1}H NMR spectrum than expected for **BNAP8** (*Figure 1*). We suspected that the triplet peak for the aromatic region at 6.91 ppm (*Figure 1*) did not actually belong to **BNAP8**. For the aliphatic region and additional peak is also seen at 3.03 ppm. If we rule out these two peaks, all of the other peaks fit with the proposed product. Therefore, it is possible that the spectrum we actually recorded is a mixture of two products. Even after column chromatography and preparative thin layer chromatography no separation was achieved. Before carrying on any further experiments we decided to try and confirm the preparation of **BNAP8** by mass spectrometry. The results turned to be disappointing, the molecular fragments did not prove the successful achievement of the reaction. As we observed for the synthetic route from binaphthol to **BNAP6**, we thought that maybe it was worth putting on the strap between diol groups first, and then apply a similar reaction conditions. Unfortunately, the expected **BNAP10** was still not produced.

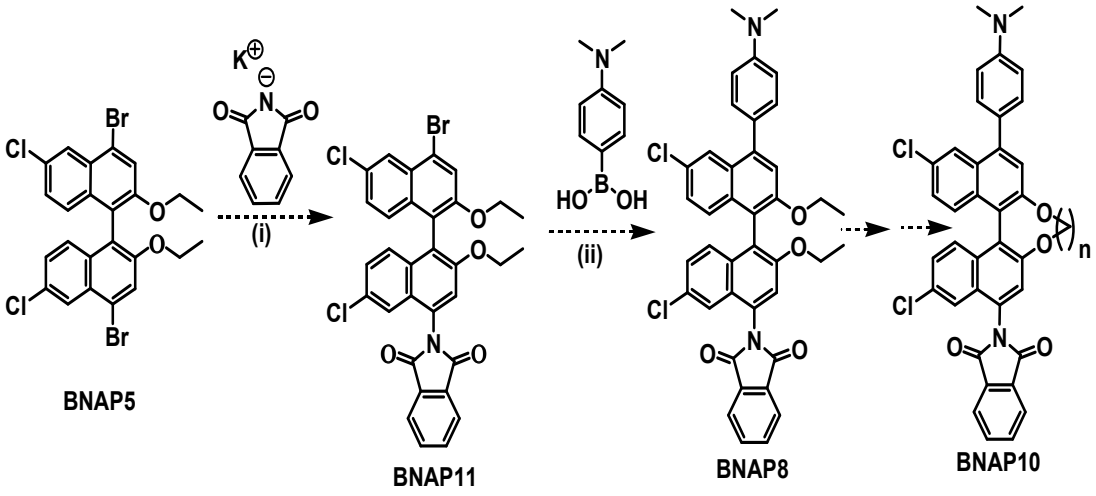

Scheme 3. Second proposed synthetic route to the strapped targets. Reaction conditions: (i) CuI, N,N-dimethylacetamide, molecular sieves (4 Å); (ii) $Pd(PPh_3)_4$, Na_2CO_3, toluene, 1,2-dimethoxyethane.

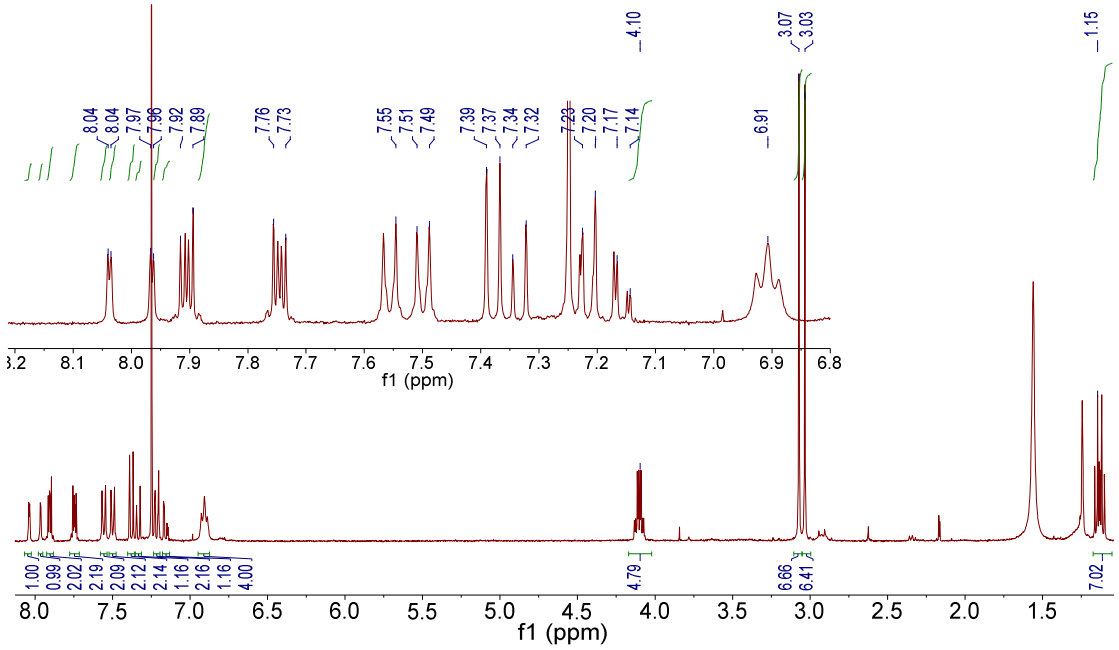

*Figure 1. ^{1}H NMR spectrum from the attempted synthesis of **BNAP8**.*

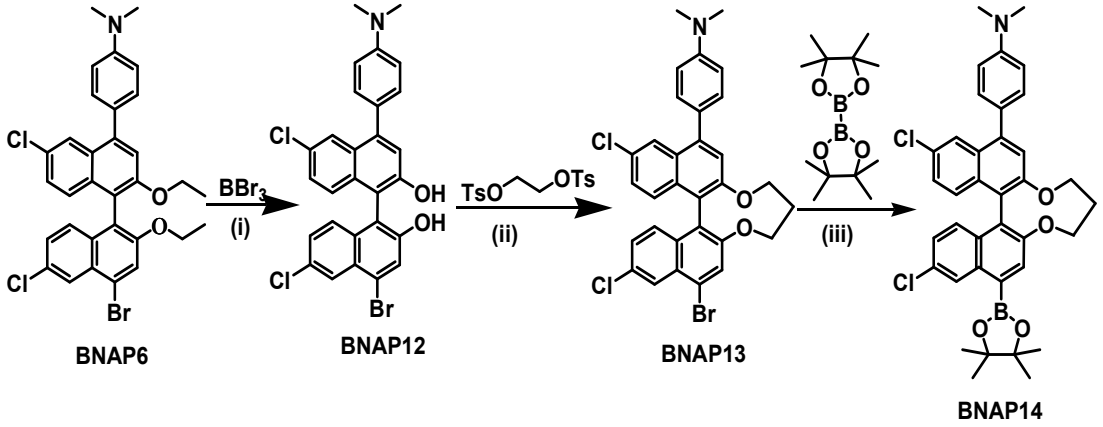

*Scheme 4. Synthesis of boronic ester derivative **BNAP14**, TsO- = $CH_3C_6H_4SO_2O$-. Reaction conditions: (i) BBr_3, 1M in CH_2Cl_2, -78 ^{O}C 2 hours, room temperature overnight, CH_2Cl_2; (ii) K_2CO_3, DMF, 85 ^{O}C; (iii) $Pd(PPh_3)_4$, KOAc, toluene, reflux.*

After all of these failures we put our final expectation to the conversion of **BNAP6** or **BNAP13** (*Scheme 4*) to boranes derivatives. The final reaction would then be a Suzuki coupling reaction to attach the phthalimide acceptor part to the molecular dyads. The conversion of the bromide to a boronic ester using Suzuki coupling only succeeded between **BNAP13** and bis(pinacolato)diboron (*Scheme 4*)[15]. The reaction between **BNAP6** and pinacolborane afforded mainly debromination product, **BNAP15** (*Scheme 5*). Dehalogenation of aryl halide is one usual side reaction in C-C bond formation

coupling reaction, as the coupling reaction catalyst can also be effective for dehalogenation reaction[16]. **BNAP14** was tried in the next Suzuki coupling reaction with N-bromophthalimide, but once again no product was produced.

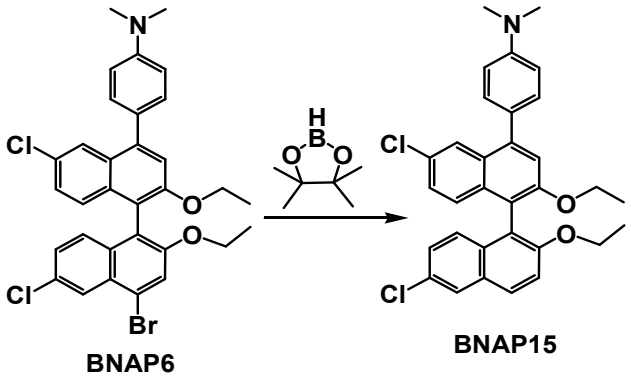

*Scheme 5. Reaction between **BNAP6** and pinacolborane, reaction conditions: $PdCl_2(PPh_3)_2$, NEt_3, THF.*

After all of these fails, we decided to modify the design of our target dyads. The final obtained derivative is shown in *Scheme 6*. One advantage of choosing aldehyde as the ending group for **BNAPY** is that further reactions are possible, such as the reaction with C60.

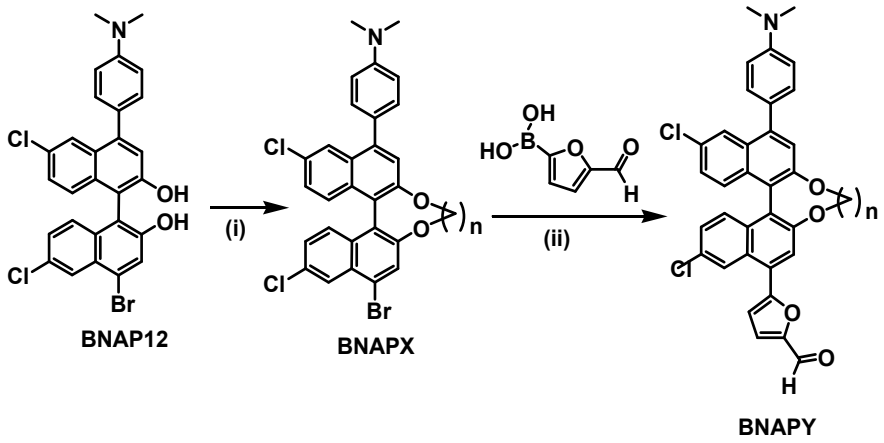

*Scheme 6. Synthesis of strapped-binaphthol bridged molecular dyads, $TsO(CH_2)OTs$ = $CH_3C_6H_4SO_2O(CH_2)OSO_2C_6H_4CH_3$. (1) (i) ICH_2I, K_2CO_3, DMF, 85 ^{O}C, n = 1, **BNAPX** = **BNAP16**, **BNAPY** = **BNAP17**; (2) (i) $TsO(CH_2)_2OTs$, K_2CO_3, DMF, 85 ^{O}C, n = 2, **BNAPX** = **BNAP18**, **BNAPY** = **BNAP19**; (3) (i) $TsO(CH_2)_3OTs$, K_2CO_3, DMF, 85 ^{O}C, n = 3, **BNAPX** = **BNAP13**, **BNAPY** = **BNAP14**. (ii) $Pd(PPh_3)_4$, Na_2CO_3, THF, reflux.*

Conversion of **BNAP7** to the strapped product was also achieved (*Scheme 7*). **BNAP21**

can also be regarded as a donor-bridge-acceptor type molecular dyad. Mild oxidation of only one N,N-dimethylamino groups forms a positive hole and the other neutral moiety can act as a donor. It is possible to study charge transfer (CT) if the appropriate CT band is observed in the spectro-electrochemical experiments.

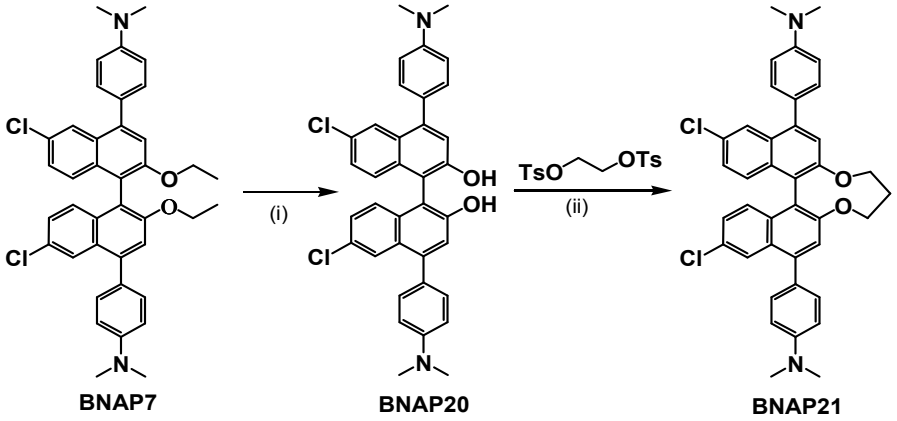

*Scheme 7. Synthesis of **BNAP21**, $TsO(CH_2)_2OTs$ = $CH_3C_6H_4SO_2O(CH_2)_2OSO_2C_6H_4CH_3$. Reaction conditions: (i) BBr_3 (1M in DCM), -78 ^{O}C 2 hours, room temperature overnight, CH_2Cl_2; (ii) K_2CO_3, dimethylformamide, 85 ^{O}C.*

BNAP 22 was synthesised as reference compound for photophysical studies. An excess (9%) of **BNAP5** was used in the Suzuki coupling reaction (*Scheme 8*), but both mono- and di-coupled products were obtained.

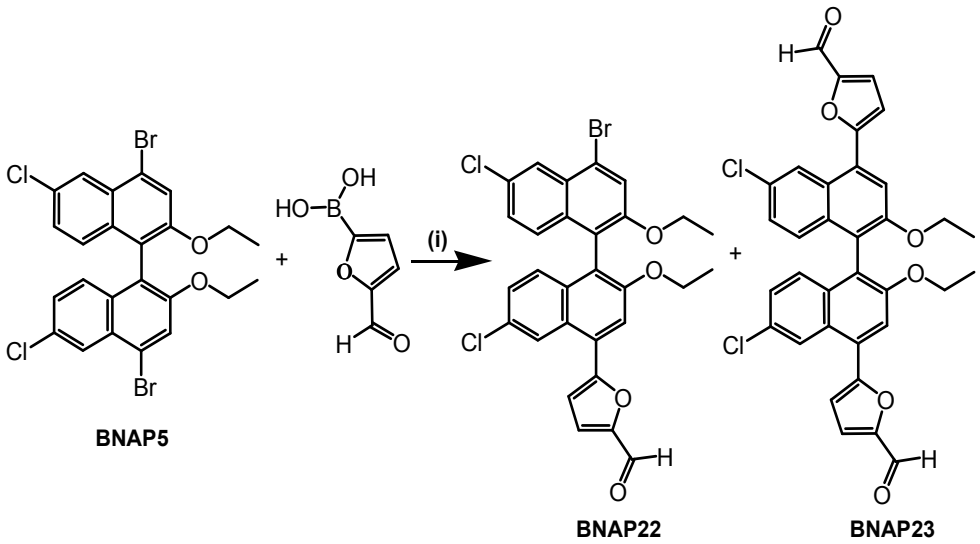

*Scheme 8. Synthesis of **BNAP22**. Reaction conditions: (i) $Pd(PPh_3)_4$, Na_2CO_3, THF, reflux.*

6.3 NMR spectra

6.3.1 Interpretation of ^{1}H NMR spectra

The COSY spectrum for **BNAP14** (*Figure 2*) was taken to assist identification of protons on the aromatic rings. The assignment of the peaks for the spectrum is shown in *Figure 2*. Summary of the peaks assignment is shown in *Table 1*.The reasons for the assignment of the peaks are:

(1) Firstly, we expected that all naphthalene ring protons which are close to the dimethylaniline group side possess higher electron density in comparison to those near the furan rings. Therefore, they are expected to appear upfield in the spectrum.

(2) It is expected that four singlet peaks should be observed for protons c, i, j and f. But there are only two singlets if we try to look at the structure again, it is possible that there is a possible "W-Coupling" between hydrogen d and c, and between g and i (the spectra for **BNAP2** / **BNAP3**/ **BNAP4** in the following section also prove this). Exclusion of c and i, leaves j and f. According to (1) we can assign j and f as shown in *Figure 2*. Usually, the coupling constant for "W-Coupling" in aromatic ring is 2 to 3 Hz[17]. Proton i is expected to appear more downfield in comparison to proton c, as described in (1). So we can assign these two protons as shown in *Figure 2*.

(3) Hydrogens d and g are expected to be a doublet of doublets, based on the analysis discussed in part (2). Proton d couples with c and e and g couples with i and h, so we can identify d and g.

(4) Hydrogens e and h should couple to d and g, respectively. Therefore, we can assign their peaks in the spectrum.

(5) Finally, there are protons a, b, k, and l left. The chemical shifts for a and b are expected to be more upfield in comparison to k and l, based on the analysis of (1). Besides, the coupling constants for furan protons are expected to be around 3.5 Hz[18]. The same principles as (1) is used to identify peaks a and b. Therefore the most upfield doublet peak on the expanded COSY spectrum was assigned to proton a.

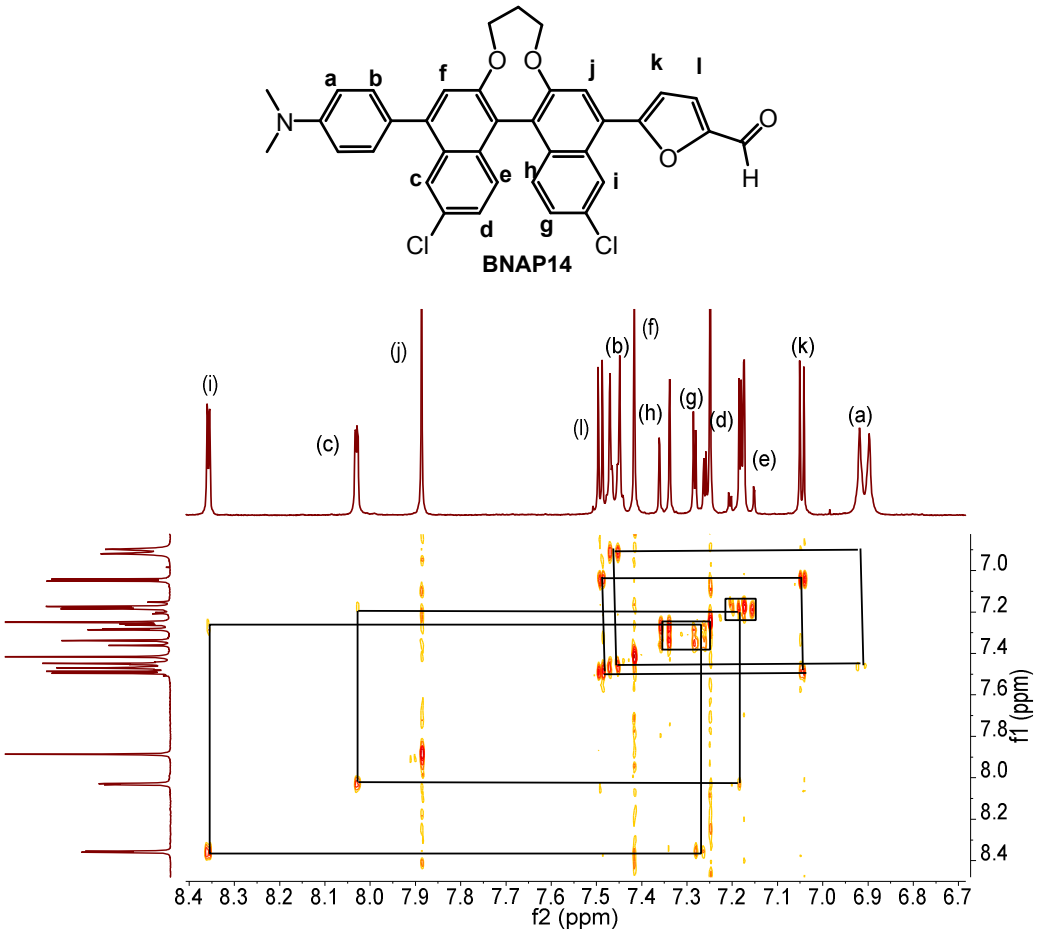

Figure 2. Molecular structure (top) and the aromatic region of the COSY spectrum (bottom) of ***BNAP14****. The black square map the coupling between protons.*

Table1. The aromatic region ^{1}*H NMR spectral peak assignments for* ***BNAP14****.*

Chemical shift (to 2 d.p) (ppm)	**Intensity (no. of H atoms)**	**Multiplicity**	**Assignment**
8.36	1	d	i
8.03	1	d	c
7.89	1	s	j
7.50	1	d	l
7.46	2	d	b
7.42	1	s	f
7.35	1	d	h
7.27	1	dd	g
7.20	1	dd	d
7.16	1	d	e
7.05	1	d	k
6.91	2	d	a

6.3.2 Interpretation of properties from ^{1}H NMR spectra

Hydroxy group is an electron donating group and the reactive positions for electrophilic aromatic substitution reactions are expected to occur at ortho/para postitions. 4,4' position of the 1,1'-bi-2-naphthol (*Figure 3, left*) are in meta position relative to the hydroxy groups, therefore the electrophilic aromatic substitution reaction cannot take place in these positions. Chemical shifts of peaks in the ^{1}H-NMR spectrum corresponding to aromatic protons of binaphthol derivatives can give us an insight into the electron density distribution on the naphthalene rings. This can help us explain the reason for the difficult direct bromination of the 4,4' positions of 1,1'-bi-2-naphthol. *Figure 3* shows the chemical shift for each proton on 1,1'-bi-2-naphthol and indicates that lowest electron density for the 4,4' positions. The positions 8 and 8' are the most reactive site towards electrophiles in terms of electron density distribution, however there is strong steric hindrance on these places. A steric effect can decrease the reactivity of an electrophilic addition reaction. The interaction between two naphthalene rings and the presence of hydroxy groups decrease the reactivity on 8/8', 7/7' and 3/3' positions. Therefore, the most reactive sites in our experiment were 6 and 6' for 1,1-bi-2-naphthol. Electrophilic bromination of 6 and 6' position yielded **BNAP2**, and using a COSY spectrum we can assign the peaks in the spectrum (*Figure 4* and *Table 2*). The protection of the diol group in **BNAP2** yielded **BNAP3**. Exchange of bromine atoms with chlorines afforded **BNAP4**. According to the chemical shifts for the ^{1}H NMR spectrum (*Figure 4 (3)*) for **BNAP4**, the electron density on aromatic protons from high to low are in the order 8,8'>7,7'>3,3'>4,4'>5,5'. However, a steric hindered effect (caused by bromine atoms, hydroxy groups and the interaction between two naphthalene rings) decreases the reactivity on 8,8', 7,7' 5,5' and 3,3' positions. Therefore, the bromination reaction of **BNAP4** was found to take place at the 4,4' positions.

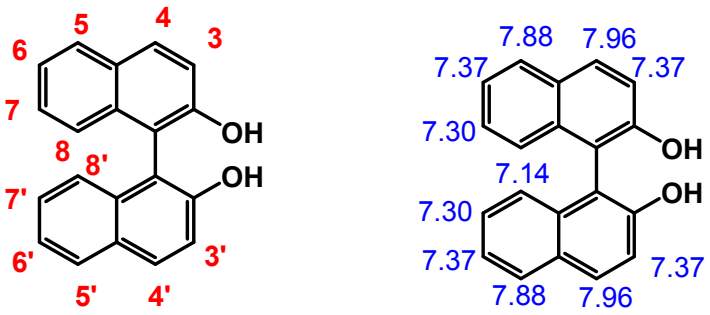

Figure 3. Molecular structure and the numbering of the rings (left) of 1,1'-bi-2-naphthol; molecular structure and ChemDraw predicted chemical shifts for each proton (right).

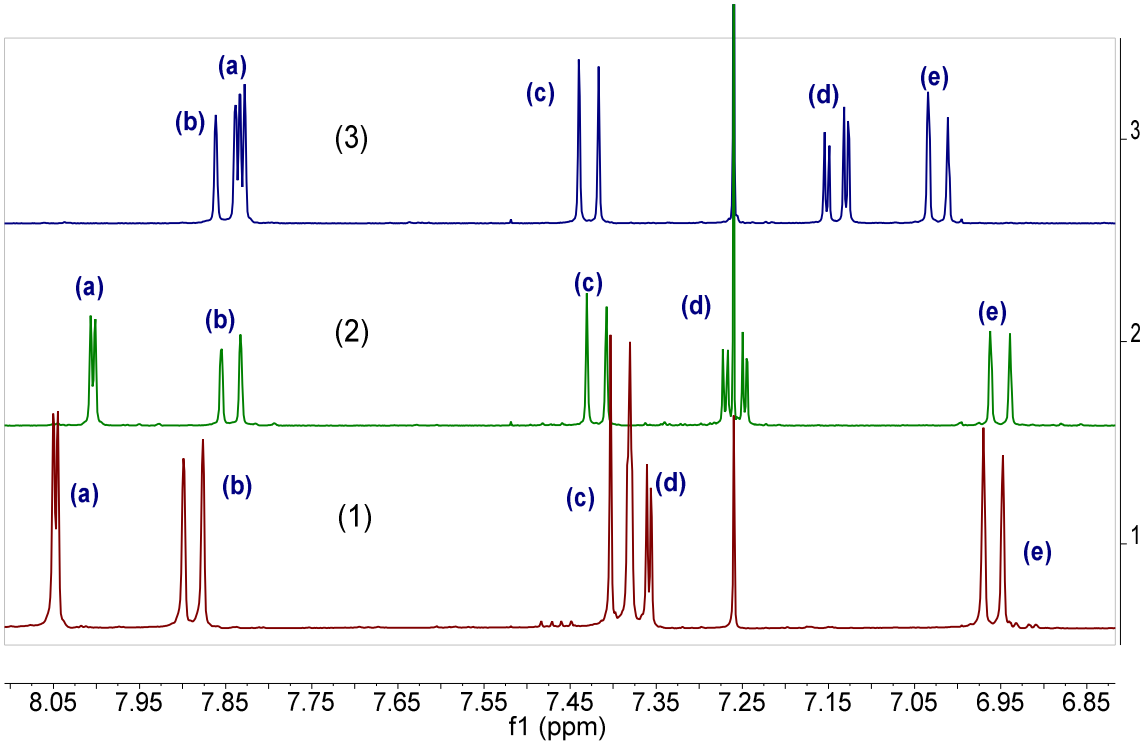

*Figure 4. ^{1}H NMR spectra of binaphthol derivatives. (1) **BNAP2**; (2) **BNAP3**; (3) **BNAP4**.*

Table 2. Assignment of ^{1}H NMR spectra (Figure 3) for binaphthol derivatives.

Position on binaphthol derivatives	Peak positions on ^{1}H NMR spectra
3 and 3'	c
4 and 4'	b
5 and 5'	a
7 and 7'	d
8 and 8'	e

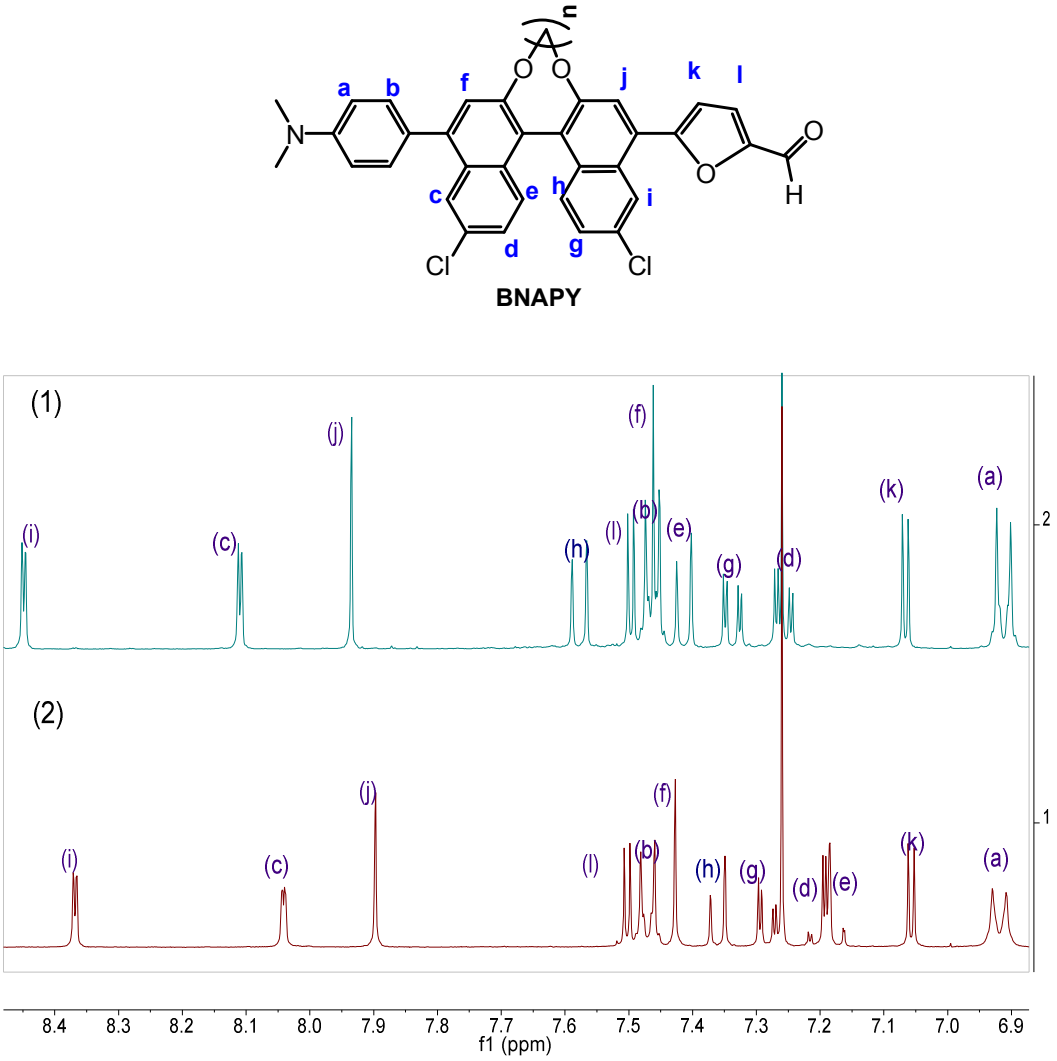

Figure 5. Top: Molecular structure of binaphthalene derivatives, n = 1, ***BNAPY*** *=* ***BNAP17****; n = 3,* ***BNAPY*** *=* ***BNAP14****. Bottom: [1]H NMR spectrum of (1)* ***BNAP17****; (2)* ***BNAP14****.*

Strap length effect on the electron density distribution within the molecular dyads can be qualitatively analysed from chemical shifts of proton resonances in the ^{1}H NMR spectrum. The comparison of the spectral data for **BNAP14** and **BNAP17** (*Figure 5*) clearly indicated the change of the electron density on the molecular dyads. A summary of the assignment of the peaks corresponding to each proton is displayed in *Table 3*. The most significant shift is seen for e and h, as shown in the cluster bar chart (*Figure 6*). The peak corresponding to proton e moves more downfield than peaks g and d as the strap length is reduced. Protons i, c, j, f, g and d exhibit slightly downfield shifts as the length of the strap decreased from n = 3 to n = 1. Almost no changes are observed for a, b, k, and l. Overall, there is almost no effect of strap length on the electron density for

the donor and acceptor parts of the molecular dyads. The main variation is found on the bridge parts of the dyads, i.e., the binaphthalene rings. The length of the strap changes can lead to variation of dihedral angle between two naphthalene planes. The chemical shift of the protons on the naphthalene rings for **BNAP17** displayed a downfield shift trend in comparison to that on **BNAP14**. We can deduce that as the length of the strap decreased there is a decrease of electron density on the binaphthol bridge.

*Table 3. Summary of the assignment of aromatic protons on ^1H NMR spectra for **BNAP17** and **BNAP14**.*

Proton	**BNAP17** **Chemical shift (δ / ppm)**	**BNAP14** **Chemical shift (δ / ppm)**
i	8.45	8.36
c	8.11	8.03
j	7.94	7.89
l	7.49	7.50
b	7.46	7.46
f	7.46	7.42
h	7.58	7.35
g	7.33	7.27
d	7.25	7.20
e	7.41	7.16
k	7.06	7.05
a	6.91	6.91

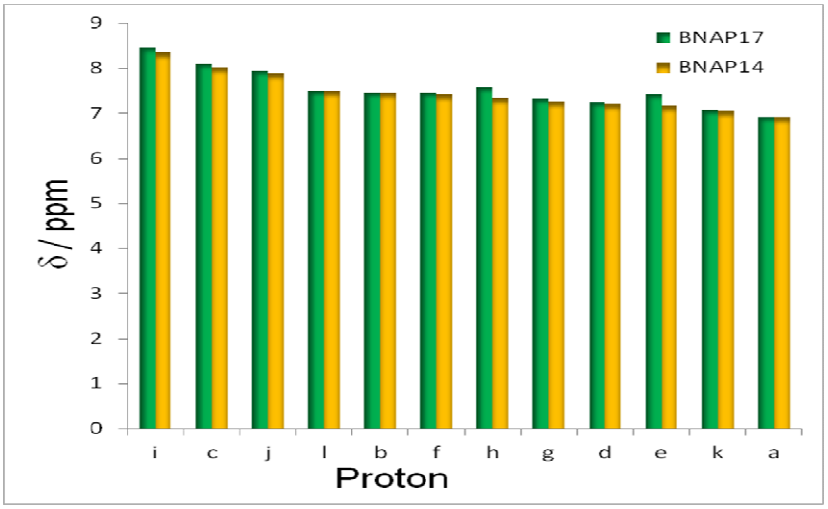

*Figure 6.Comparison of aromatic protons chemical shifts (δ) of **BNAP17** and **BNAP14**.*

6.3.3 Spectra simulation

The none-equivalent chemical environment for protons on the straps was evident by inspection of ^{1}H NMR spectra. For the simplest dyad, **BNAP17**, where there is only two protons on the strap, the resonances appear as two doublets in the spectrum. The more interesting observation is for molecular dyad, **BNAP21** which contains a donor group either side of the bridge. If the chemical environment of H_1, H_2, H_3 and H_4 (*Figure 7*) are equivalent (and H_5, H_6), a simple triplet should be observed in the ^{1}H NMR spectrum. However, the peaks shown in the spectrum (*Figure 7*) are much more complicated. This phenomenon is due to the presence of the chiral binaphthalene centre and the creation of diasteriotopic protons. In order to look into the coupling pattern in more detail the spectrum was simulated.

Firstly, it is supposed that the individual chemical environments for the proton pairs H_1/H_3, H_2/H_4 and H_5/H_6 are the same. Chemical shifts for proton pairs were taken from the middle positions for each set of peaks. The chemical shifts for H_1/H_3, H_2/H_4 and H_5/H_6 are 4.351 ppm, 4.428 ppm and 1.991 ppm, respectively. Coupling constants calculated from the peaks between 4.41 - 4.45 ppm were 9.6 Hz, 3.2 Hz and1.6 Hz, if the peaks were considered as a doublet of a triplet (two sets of triplet exhibit

non-identical coupling constants). The value from this calculation gives us an indication to estimate the actual value. The coupling constant J_{12}, J_{34} and J_{56} are estimated based on the literature value[19]. The two sets of peaks (4.12 - 4.37 and 4.41 - 4.45 ppm) appeared as different splitting pattern, therefore we expected that H_5 and H_6 coupled with the other protons with a slightly different J value. After the adjustment of the coupling constant, we put the following value of the coupling constants into the simulation program, $J_{12} = J_{34} = J_{56} = 12$ Hz; $J_{15} = J_{35} = 1.5$ Hz; $J_{16} = J_{36} = 6.5$ Hz; $J_{25} = J_{45} = 1.5$ Hz; $J_{26} = 3.00$ Hz; $J_{46} = 3.5$ Hz (*Table 4*). The simulated spectrum corresponding to proton H_1 to H_6 is shown in *Figure 8* and *Figure 9*. The simulated spectrum shows fairly good agreement with the experimental one.

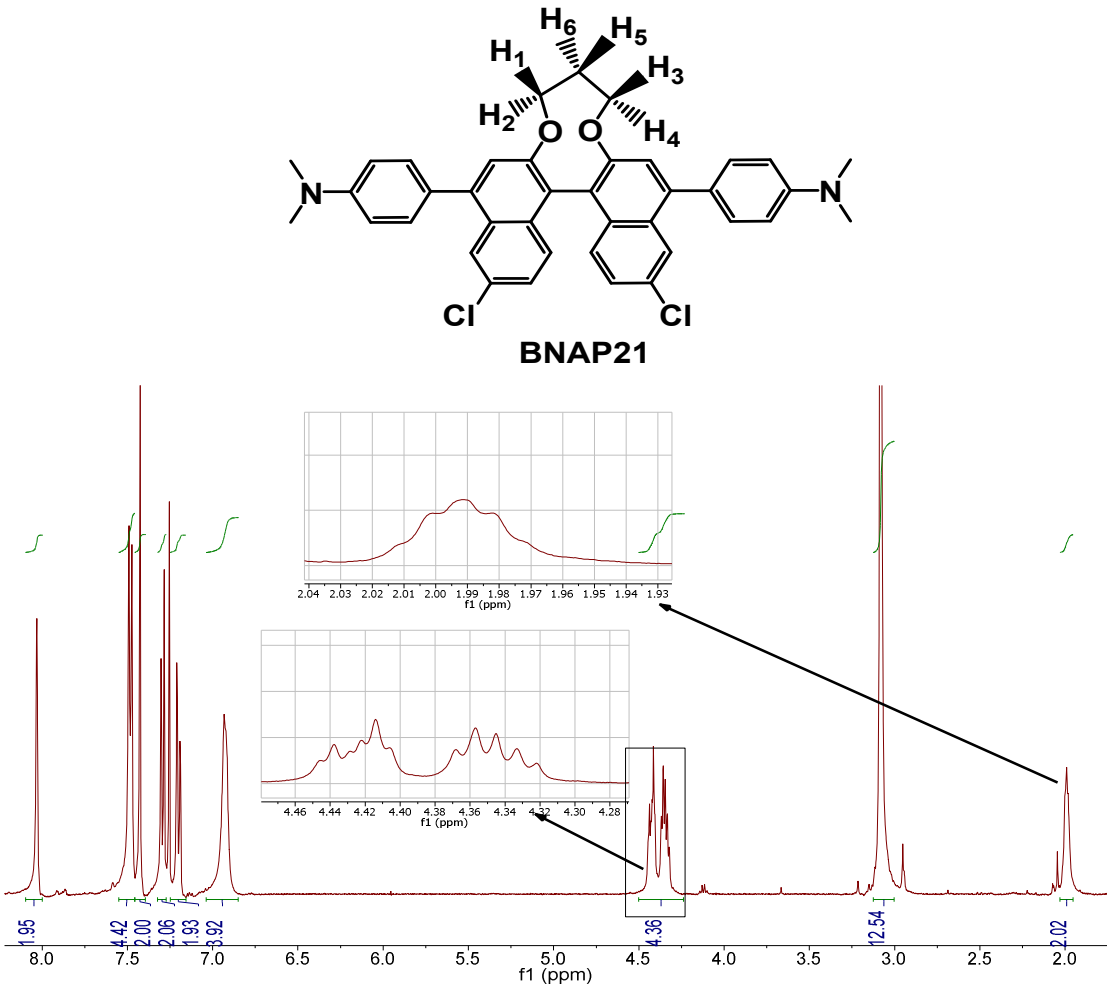

*Figure 7. Molecular structure of **BNAP21** (top); ^{1}H NMR spectrum and the expanded regions for H_1 to H_6 for **BNAP21** (bottom).*

Table 4. Coupling constants between H_1, H_2, H_3, H_4, H_5 and H_6.

	Coupling constant (Hz)					
Proton (Chemical shift, ppm)	H_1	H_2	H_3	H_4	H_5	H_6
H_1 (4.428)	-	12.00	-	-	1.50	6.50
H_2 (4.352)	12.00	-	-	-	9.00	3.00
H_3 (4.428)	-	-	-	12.00	1.50	6.50
H_4 (4.352)	-	-	12.00	-	9.00	3.50
H_5 (1.991)	1.50	9.00	1.50	9.00	-	12.00
H_6 (1.991)	6.50	3.00	6.50	3.50	12.00	-

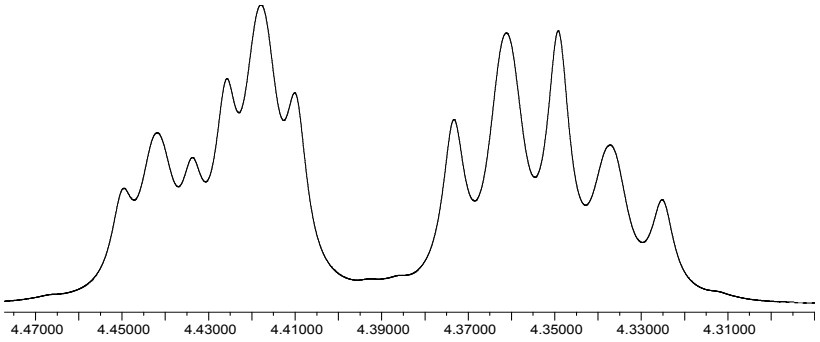

Figure 8. Simulated spectrum corresponding to the peaks for H_1, H_2, H_3 and H_4.

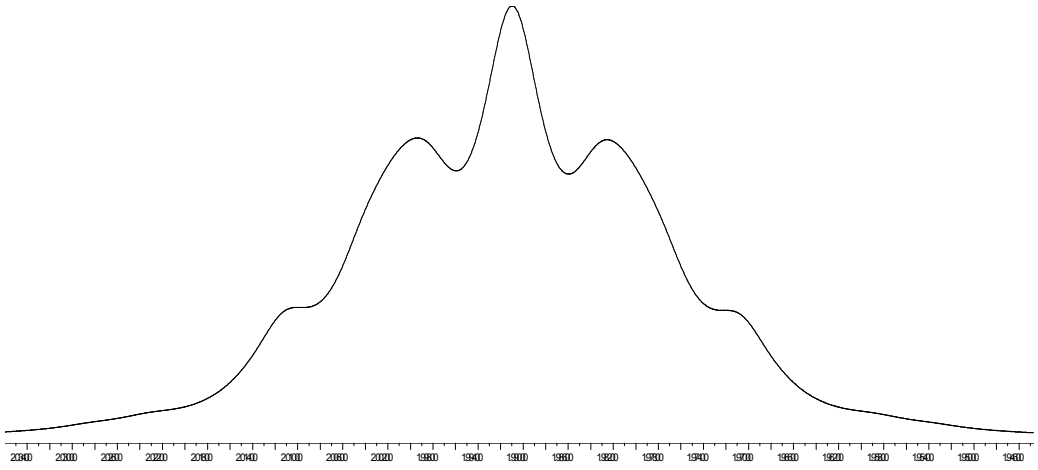

Figure 9. Simulated spectrum corresponding to the peaks for H_5 and H_6.

6.4 Electrochemistry

The electrochemical behaviour of the binaphthol derivatives was measured by cyclic voltammetry (CV) in dry CH_2Cl_2 containing 0.2 M tetrabutylammonium tetrafluoroborate (TBATFB) electrolyte. Gold electrode, platinum electrode and Ag/AgCl were used as working electrode, counter electrode and reference electrode respectively.

Ferrocene (same concentration as the measured binaphthol derivatives) was used as an internal reference.

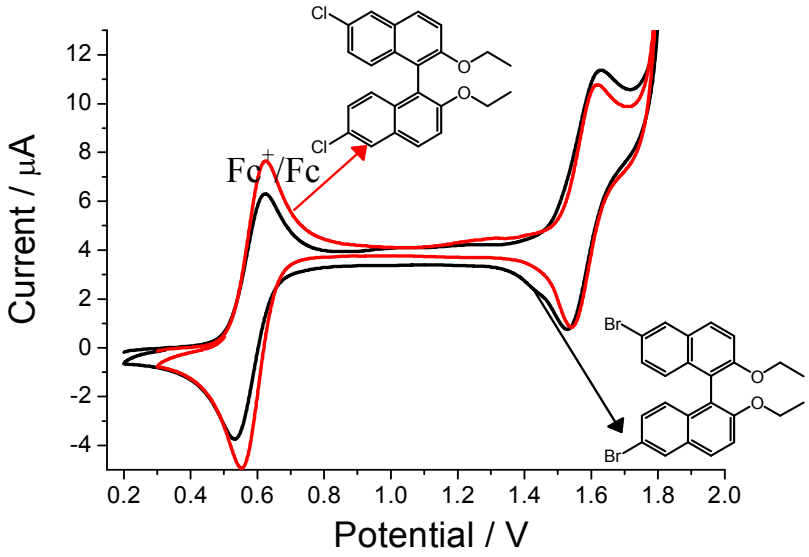

*Figure 10. The cyclic voltammogram recorded for **BNAP3** (black) and **BNAP4** (red) in CH_2Cl_2 (0.2 M TBATFB). Scan rate = 50 mV s^{-1}.*

Only a single one-electron oxidation peak with a half-wave potential of 1.58 V (ΔE = 100 mV) was observed for **BNAP3** (*Figure 10*), which indicates that it is possible for redox at the binaphthol. Almost no variation was seen between **BNAP3** and **BNAP4**. No reductive peak was found for either of them. In comparison to **BNAP4**, there is an additional quasi-reversible oxidative wave with a half-wave potential of 1.00 V observed for **BNAP15** (*Figure 11*). The addition wave corresponds to one-electron oxidation of the *N,N*-dimethylaniline [20]. A larger peak separation (ΔE = 130 mV) was seen for the oxidative wave of the binaphthol unit in **BNAP15** at 1.50 V compared to **BNAP3**. Therefore, we can deduce that the first electron is removed from *N,N*-dimethylaniline group and second one from binaphthol bridge when **BNAP15** is oxidised.

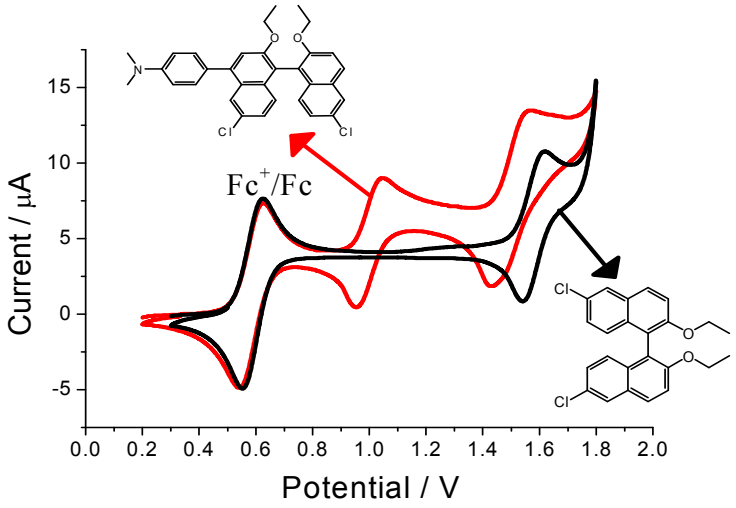

Figure 11. The cyclic voltammograms recorded for ***BNAP4*** *(black) and* ***BNAP15*** *(red) in CH_2Cl_2 (0.2 M TBATFB). Scan rate = 50 mV s^{-1}.*

Adding another *N,N*-dimethylaniline group to the binaphthol ring did not lead to a significant alteration to the electrochemical properties. The CV spectrum for **BNAP7** is fairly similar to **BNAP15** (*Figure 12*). It infers that after removal of two electrons from **BNAP7**, the further oxidation of the **BNAP7**$^{+2\cdot}$ becomes extremely difficult, even though *N,N*-dimethylaniline unit can be oxidized.

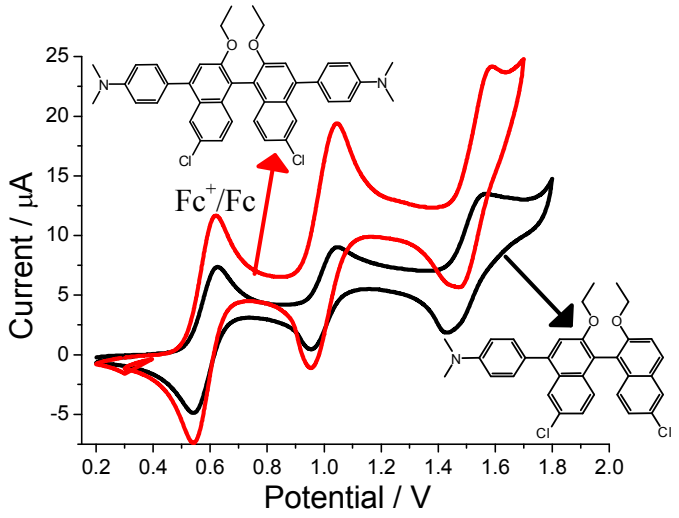

Figure 12. The cyclic voltammogram recorded for ***BNAP15*** *(black) and* ***BNAP7*** *(red) in CH_2Cl_2 (0.2 M TBATFB). Scan rate = 50 mV s^{-1}.*

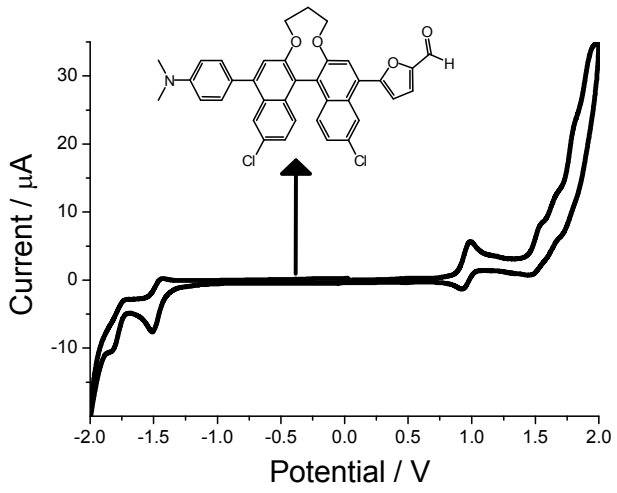

*Figure 13. The cyclic voltammogram recorded for **BNAP14** in CH_2Cl_2 (0.2 M TBATFB). Scan rate = 50 mV s-1.*

When the CV spectrum was recorded to full potential window range (-2.0 V to 2.0 V) for **BNAP14**, there were two one-electron quasi-reversible reduction waves observed with half-wave potentials of $E_{1/2}$ = -1.78 V (ΔE = 130 mV) and $E_{1/2}$ = -1.47 V (ΔE = 85 mV) (*Figure 13*). The oxidative segment of the spectrum was slightly complicated. One reversible oxidation peak ($E_{1/2}$ = 0.96 V, ΔE = 60 mV) was clearly found and there were additional peaks between 1.5 V and 2.0 V which were not easy to identify. Slowing down or increasing the scan rate did not give us better resolution. The experiment was repeated again and the potential window was controlled in the range -1.8 to 1.3 V. This time one quasi-reversible reduction wave and one reversible oxidation wave was observed in the whole range (*Figure 14*). Reduction waves were assigned to one electron addition to the furan ring (acceptor part of the molecular dyad). There is no big difference in CV spectra between **BNAP7** and **BNAP21**. The strap between the diol group did not affect the electrochemical properties at least within the experimental measured range.

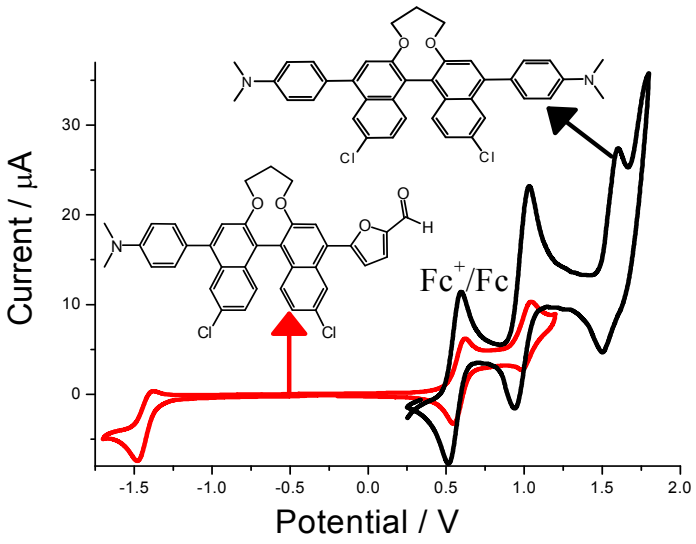

*Figure 14. The cyclic voltammogram recorded for **BNAP21** (black) and **BNAP14** (red) in CH_2Cl_2 (0.2 M TBATFB). Scan rate = 50 mV s^{-1}.*

6.5 Photophysical properties

Normalised absorption spectrum for **BNAP4**, **BNAP13** and **BNAP14** are shown in *Figure 15*. A peak maximum was found at 346 nm for **BNAP4** which overlapped with the second most intensive peak (peak maximum at 334 nm). These peaks are due to π-π transition in the binaphthol rings. Coupling of the *N,N*-dimethylaniline (as a donor) made the **BNAP13** absorption spectrum more broader in comparison to **BNAP4**, even though we can still see the shoulder at 334 nm and the new broad band with peak maximum at 351 nm. The small red shift in the peak maximum of 5 nm is possibly due to the addition of the donor to the binaphthol ring which increases π-conjugation in the whole system and decrease the energy gap between ground state and first excited singlet state. The broadening of the peak may arise from additional π-π transitions from the dimethylaniline ring. The electronic transition bands for **BNAP14** are the broadest among these three binaphthol derivatives. In addition, the maximum absorbance was shifted to longer wavelength of 365 nm. There is no "gap" in the spectrum window between 300 nm and 425 nm for **BNAP14**.

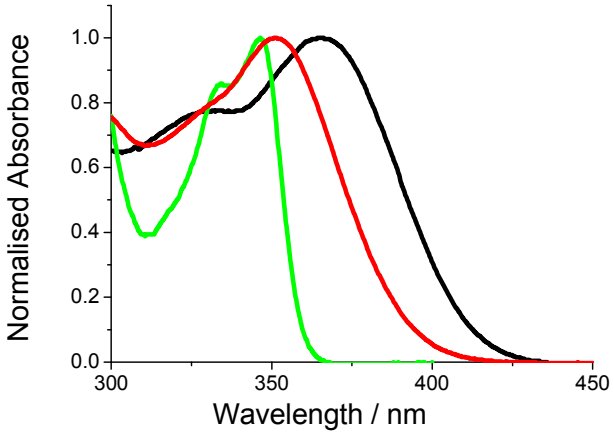

*Figure 15. Normalised absorption spectra of **BNAP4** (green), **BNAP13** (red) and **BNAP14** (black) recorded in acetonitrile at room temperature.*

Emission spectra for these derivatives were also recorded. The emission peak maximum was found at 376 nm for **BNAP4** in acetonitrile following excitation at 336 nm (*Figure 16*). Although chlorine atoms are present the heavy atom effect did not quench the fluorescence to any great extent. The fluorescence quantum yield for **BNAP4** was moderate (ϕ_{FLU} = 0.6). The Stokes' shift is large, c.a. 30 nm.

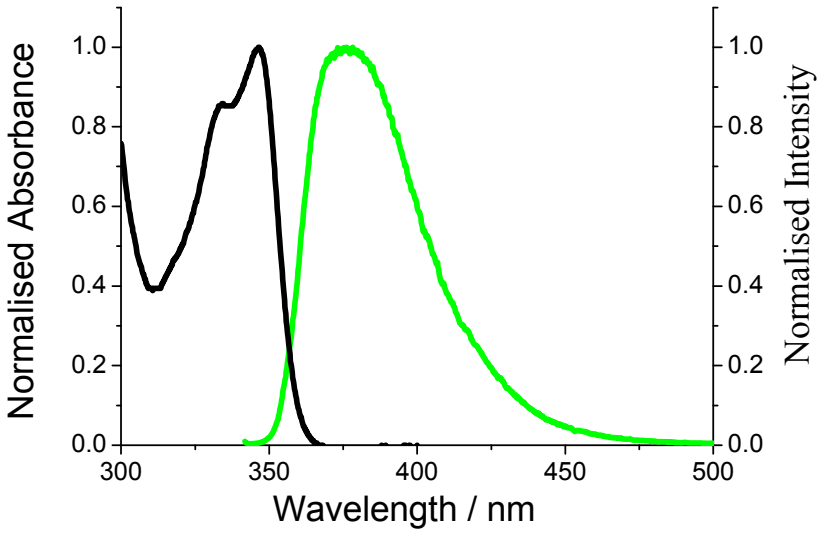

*Figure 16. Normalised absorption spectrum (black) and emission spectrum (green) for **BNAP4** recorded in acetonitrile at room temperature.*

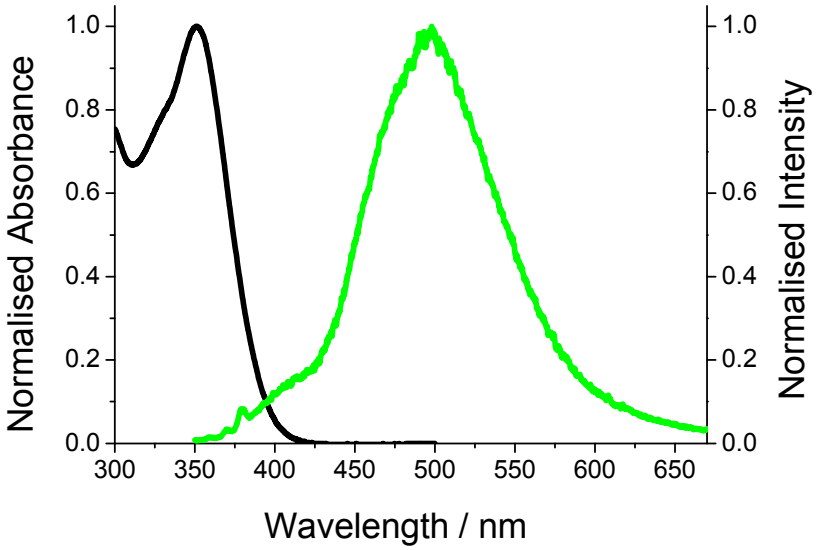

*Figure 17. Normalised absorption spectrum (black) and emission spectrum (green) for **BNAP13** recorded in acetonitrile at room temperature.*

The fluorescence was observed at 497 nm in acetonitrile upon the excitation of **BNAP13** at 340 nm (*Figure 17*). When the non-polar solvent, cyclohexane, was used and a dilute solution was excited at 340 nm, the emission maximum was found at the shorter wavelength of 413 nm (*Figure 18*). The peak maximum in the absorption spectrum exhibited only 1 nm blue shift. This variation is likely due to the nature of the excited state for **BNAP13** which is probably localised on the binaphthalene unit in the non-polar solvent of cyclohexane. In the polar solvent there is the possibility of forming an intramolecular charge transfer state. The fluorescence quantum yields are 0.03 and 0.54 in acetonitrile and cyclohexane, respectively.

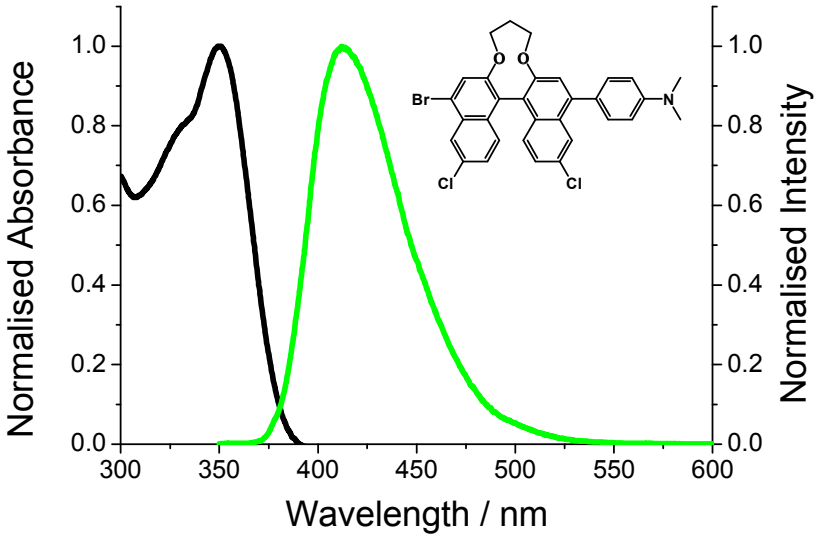

Figure 18. Normalised absorption spectrum (black) and emission spectrum (green) for ***BNAP13*** *recorded in cyclohexane at room temperature.*

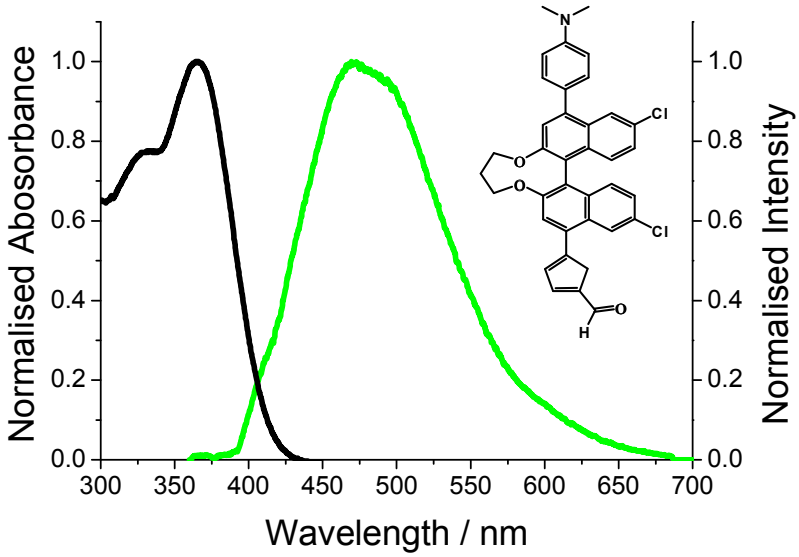

Figure 19. Normalised absorption spectrum (black) and emission spectrum (green) for ***BNAP14*** *recorded in acetonitrile at room temperature.*

The **BNAP14** fluorescence spectrum was recorded in acetonitrile at room temperature (*Figure 19*) upon excitation at 340 nm. The maximum emission was observed at 472 nm and the fluorescence quantum yield was 0.017. When the emission spectrum was recorded in non-polar cyclohexane (*Figure 20*), a similar peak maximum shift was seen as for **BNAP13** (i.e., the peak blue shifted 22 nm to 450 nm). The absorption spectra

exhibited a larger variation between those recorded in polar and non-polar solvents in terms of their peaks shapes. The intensity of peak at lower energy, 324 nm, was higher than the peak at 361 nm. The absorption and fluorescence bands are summarised in *Table 5*.

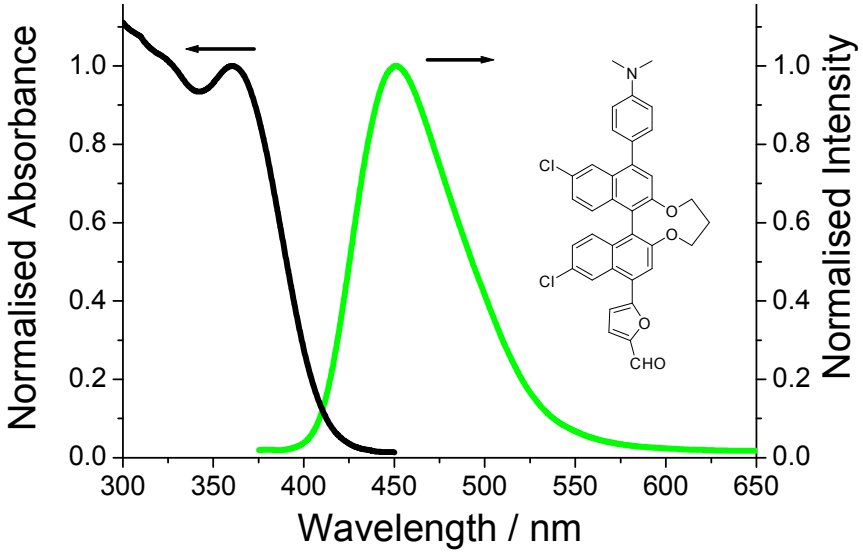

Figure 20. Normalised absorption spectrum (black) and emission spectrum (green) for ***BNAP14*** *recorded in cyclohexane at room temperature.*

Table 5. Absorption and fluorescence maximum for binaphthol derivatives record at room temperature.

Compound	Solvent	Absorption	Fluorescence
		λ_1 (nm)	λ (nm)
BNAP4	CH_3CN	346	376
BNAP13	CH_3CN	351	497
	Cyclohexane	350	413
BNAP14	CH_3CN	365	472
	Cyclohexane	360	450

From the experiments we found that after the electron donating group *N,N*-dimethylaniline was attached to the **BNAP4** to obtain **BNAP 13**, the fluorescence quantum yield in actetonitrile was significantly reduced from 0.6 to 0.03. The recovery of **BNAP13** fluorescence was found in non-polar cyclohexane with a quantum yield of 0.54. The fluorescence quantum yield is further decreased to 0.017 in **BNAP14** in

acetonitrile. Therefore, if we excite the centre binaphthol bridge of **BNAP14**, the possible quenching routes include electron transfer between donor (*N,N*-dimethylaniline) and bridge (binaphthol rings). Alternatively, electron transfer is possible between the bridge and the acceptor (furan ring). The possible charge transfer between donor and acceptor needs more work to confirm the hypothesis.

6.6 Incorporation of fullerene to binaphthol derivatives

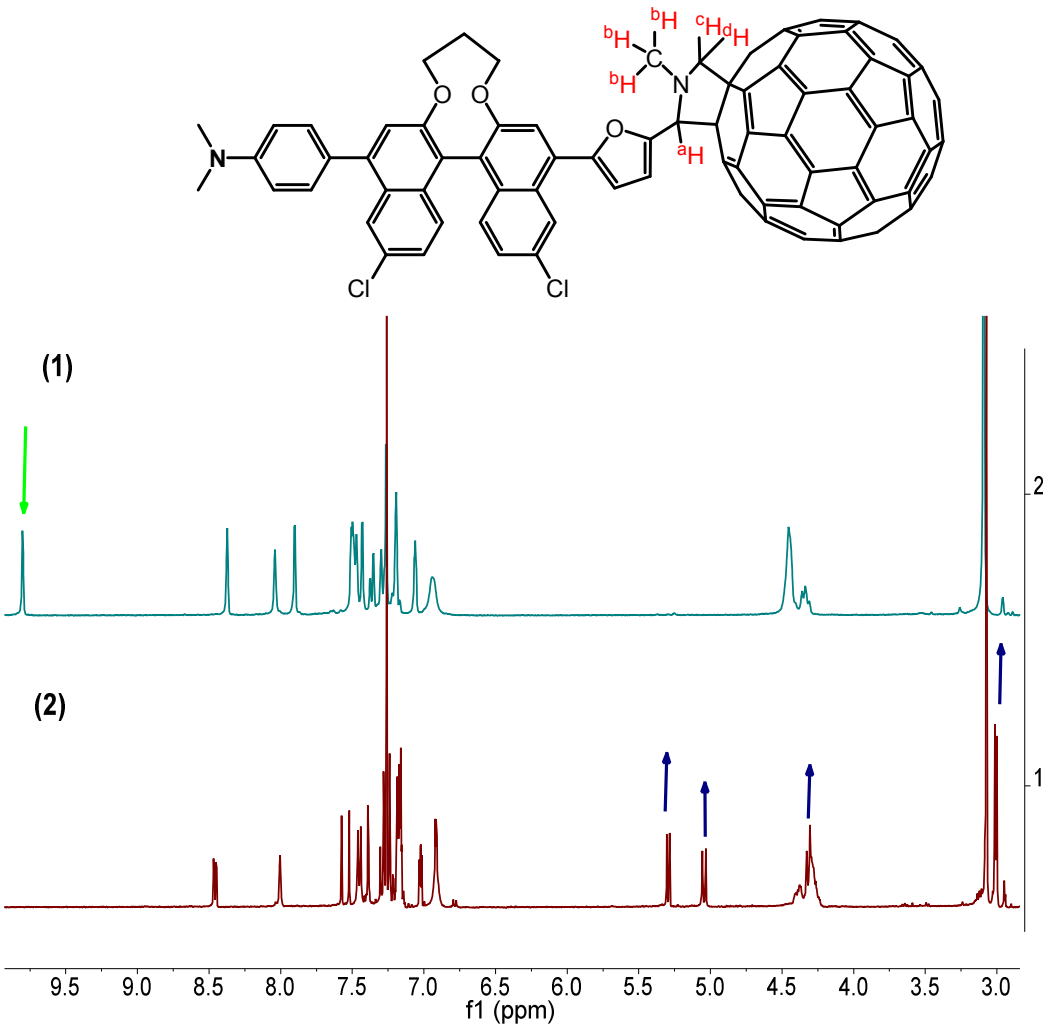

*Figure 21. Top: Molecular structure of **BNAPC60**. Bottom: comparison of ^{1}H NMR spectra for **BNAP14** (1) and **BNAPC60**(2).*

In order to introduce a much better electron acceptor the C60 group was introduced. Thus, coupling of C60 to **BNAP14** through the aldehyde group was carried out. The ^{1}H-NMR spectrum clearly indicated that the coupling product **BNAPC60** was achieved.

Figure 21 shows as the reaction proceeded, the proton on the aldehyde group (indicated by the green arrow) disappeared. Four new peaks (indicated by the blue arrow) appeared in the spectrum for **BNAPC60**. These four peaks correspond to the protons shown in red in the **BNAPC60** molecular structure (*Figure 21*). The peaks at 5.29, 5.04, 4.32 and 3.00 ppm belongs to protons c, d, a and b. It is noticed that all of the four new peaks appear as doublets which is not exactly as we firstly expected. Protons c and d are diasteriotopic, they couple with each other and lead to the appearance of two doublets in the spectrum. There are two possible reasons for proton a and b to show up as a doublet in the spectrum. The presence of two chiral centres in the molecule leads to the existence of diastereomers which were not separated by column chromotography. If this is the case then the doublet is more likely to be two singlets. It is also possible that there is a long range coupling between proton c, d and the protons on the furan ring. The compound seems to be unstable in air, even though we could get the ^{1}H NMR spectrum of **BNAPC60**. Purification of the product needed to be carried out immediately after the work up of the reaction. Long time expose on the column chromatography caused the degradation.

6.7 Conclusions and future work

Overall, we have demonstrated a method to synthesize unsymmetrical molecular dyads with different central dihedral angles based on the 1,1'-bi-2-naphthol group. The incorporation of fullerene was shown to be possible. Primary photophysical study confirms that a charge transfer process takes between the donor (*N,N*-dimethylaniline) and the bridge (binaphthol). Further experiments need to be carried out to confirm the charge transfer process between donor and acceptor. It is hoped that further photophysical measurements will be carried out on these binaphthol-based molecular dyads to understand how the conformation variations on the bridge affect their properties. We expect to obtain optically pure derivatives in the future and to investigate the role of chirality on energy/electron transfer processes. It is also possible to further

functionalise the molecular dyads with carboxylic acid groups for attachment to semiconductor surface for applications as dye-sensitised solar cells.

6.8 References

[1] M. D. Newton, *Theor. Chem. Acc.*, 2003, **110**, 307.

[2] (i) D. V. Matyushov and G. A. Voth, *J. Chem. Phys.*, 2000, **113**, 5413; (ii) L.W. Ungar, M. D. Newton and G. A. Voth, *J. Phys. Chem. B*, 1999, **103**,7367; (iii) D.W. Small, D.V. Matyushov and G. A. Voth, *J. Am. Chem. Soc.*, 2003, **125**, 7470; (iv) D. V. Matyushov and M. D. Newton, *J. Phys. Chem. A*, 2001, **105**, 8516; (v) D. V. Matyushov and G. A.Voth, *J. Phys. Chem. A*, 1999, **103**, 10981.

[3] E. A. Weiss, M. J. Tauber, R. F. Kelley, M. J. Ahrens, M. A. Ratner, and M. R. Wasielweski, *J. Am. Chem. Soc*., 2005, **127**, 11842.

[4] B. D. Allen, A. C. Benniston, A. Harriman, I. Llarena and C. A. Sams, *J. Phys. Chem. A,* 2007, **111**, 14, 2641.

[5] (i) M. D. Newton, *Int. J. Quantum Chem.*, 2000, **77**, 255. (ii) C. A. Naleway, L. A. Curtiss and J. R. Miller, *Chem. Phys.*, 1991, **95**, 8434.

[6] (i) A. Harriman and J. P. Sauvage, *Chem. Soc. Rev.*, 1996, **25**, 41; (ii) M. R. Wasielewski, *Chem. Rev.*,1992, **92**, 435; (iii) D. Gust, T. A. Moore and A. L. Moore, *Acc. Chem. Res.*,2001, **34**, 40; (iv) M. N. Paddon-Row, *Adv. Phys. Org. Chem.*, 2003, **38**, 1; (v) D. Kim and A. Osuka, *Acc. Chem. Res.*, 2004, **37**, 735; (vi) J. L. Sessler, M. Sathiosatham, C. T. Brown, T. A. Rhodes and G. Wiederrecht, *J. Am. Chem. Soc.* 2001, **123**, 3655.

[7] S. J. Lee and W. Lin, *J. Am. Chem. Soc.*, 2002, **124**, 4554.

[8] Y. Zhu, N. Gergel, N. Majumdar, L. R. Harriott, J. C. Bean and L. Pu, *Org. Lett.*, 2006, **8**, 355.

[9] Y. Haketa, Y. Bando, K. Takaishi, M. Uchiyama, A. Muranaka, M. Naito, H. Shibaguchi, T. Kawai and H. Maeda, *Angew. Chem. Int. Ed.*, 2012, **51**, 7967.

[10] (i) M. Kant, S. Bischoff, R. Siefken, E. Gründemann and A. Köckritz, *Eur. J. Org. Chem.* 2001, **3**, 477; (ii) A. Hu, H. L. Ngo and W. Lin, *Angew. Chem. Int. Ed.*, 2004, **43**, 2501.

[11] C. Valente, E. Choi, M. E. Belowich, C. J. Doonan, Q. Li, T. B. Gasa, Y. Y. Botros, O. M. Yaghi and J. F. Stoddart, *Chem. Commun.*, 2010, **46**, 4911.

[12] (i) A. S. Guram and S. L. Buchwald, *J. Am. Chem. Soc.*, 1994, **116**, 7901; (ii) J. P. Wolfe, S. Wagaw and S. L. Buchwald, *J. Am. Chem. Soc.*, 1996, **118**, 7215; (iii) M. S. Driver and J. F. Hartwig, *J. Am. Chem. Soc.*, 1996, **118**, 7217.

[13] (i) R. G. Bacon and A. Karim, *J. C. S. Perkin I*, 1972, **3**, 272; (ii) R. G. Bacon and A. Karim, *Chem. Comm.*, 1969, **9**, 486.

[14] (i) S. Gabriel, *Chemische Berichte*, 1887, **20**, 2224; (ii) M. S. Gibson, R. W. Bradshaw, *Angew. Chem. Int. Ed. Engl.*, 1968, **7**, 919.

[15] (i) C. Sooambar, V. Troiani, C. Bruno, M. Marcaccio, F. Paolucci, A. Listorti, A. Belbakra, N. Armaroli, A. Magistrato, R. D. Zorzi, S. Geremia and D. Bonifazi, *Org. Biomol. Chem.*, 2009, **7**, 2402; (ii) D. Bonifazi, G. Accorsi, N. Armaroli, F. Song, A. Palkar, L. Echegoyen, M. Scholl, P. Seiler, B. Jaun and F. Diederich, *Helv. Chim. Acta*, 2005, **88**, 1839.

[16] O. Navarro, H. Kaur, P. Mahjoor and S. P. Nolan, *J. Org. Chem.*, 2004, **69**, 3173.

[17] H. Gunther and G. Jlikeli, *Chem. Rev.*, 1977, **77**, 599.

[18] K. Spirkov and R. Kada, *Chem. Papers*, 1987, **41**, 787.

[19] T. R. Hoye, P. R. Hanson and J. R. Vyvyan, *J. Org. Chem.*, 1994, **59**, 4096.

[20] A. C. Benniston, X. He, H. Lemmetyinen and N. V. Tkachenko, *RSC Adv.*, 2013, **3**, 4995.

Chapter 7

Appendix: Crystal Structures

The crystal structures data are in the order that they appear in the thesis. The full data is attached electronically in the attached CD.

7.1 Crystal data and structure refinement for ACR1

Table 1. Crystal data and structure refinement for **ACR1**.

Identification code	**ACR1**
Chemical formula (moiety)	$C_{27}H_{17}BrO$
Chemical formula (total)	$C_{27}H_{17}BrO$
Formula weight	437.32
Temperature	150(2) K
Radiation, wavelength	MoKα, 0.71073 Å
Crystal system, space group	orthorhombic, $Pna2_1$
Unit cell parameters	a = 14.036(2) Å α = 90°
	b = 17.400(4) Å β = 90°
	c = 7.8622(12) Å γ = 90°
Cell volume	1920.2(6) $Å^3$
Z	4
Calculated density	1.513 g/cm^3
Absorption coefficient μ	2.157 mm^{-1}
F(000)	888
Crystal colour and size	colourless, 0.40 × 0.03 × 0.03 mm^3
Reflections for cell refinement	1799 (θ range 3.1 to 28.5°)
Data collection method	Oxford Diffraction Gemini A Ultra diffractometer
	thick-slice ω scans
θ range for data collection	3.1 to 28.6°
Index ranges	h –18 to 17, k –21 to 21, l –8 to 10
Completeness to θ = 25.0°	99.7 %
Reflections collected	9299
Independent reflections	3707 (R_{int} = 0.0490)
Reflections with $F^2>2\sigma$	2954
Absorption correction	semi-empirical from equivalents
Min. and max. transmission	0.4791 and 0.9381
Structure solution	direct methods
Refinement method	Full-matrix least-squares on F^2
Weighting parameters a, b	0.0370, 0.4729
Data / restraints / parameters	3707 / 1 / 262
Final R indices [$F^2>2\sigma$]	R1 = 0.0434, wR2 = 0.0879
R indices (all data)	R1 = 0.0629, wR2 = 0.0978
Goodness-of-fit on F^2	1.044
Absolute structure parameter	0.002(11)
Largest and mean shift/su	0.001 and 0.000
Largest diff. peak and hole	0.64 and –0.68 e $Å^{-3}$

7.2 Crystal data and structure refinement for ACR3

Table 2. Crystal data and structure refinement for **ACR3**.

Identification code	**ACR3**	
Chemical formula (moiety)	$C_{27}H_{16}BBrF_4O$	
Chemical formula (total)	$C_{27}H_{16}BBrF_4O$	
Formula weight	523.12	
Temperature	150(2) K	
Radiation, wavelength	MoKα, 0.71073 Å	
Crystal system, space group	rhombohedral, $R\bar{3}$	
Unit cell parameters	a = 35.533(2) Å	α = 90°
	b = 35.533(2) Å	β = 90°
	c = 9.0525(8) Å	γ = 120°
Cell volume	9898.3(12) $Å^3$	
Z	18	
Calculated density	1.580 g/cm^3	
Absorption coefficient μ	1.921 mm^{-1}	
F(000)	4716	
Reflections for cell refinement	1484 (θ range 3.0 to 28.2°)	
Data collection method	Oxford Diffraction Gemini A Ultra diffractometer	
	thick-slice ω scans	
θ range for data collection	3.0 to 25.0°	
Index ranges	h –40 to 42, k –36 to 36, l –10 to 8	
Completeness to θ = 25.0°	99.7 %	
Reflections collected	7376	
Independent reflections	3873 (R_{int} = 0.0381)	
Reflections with $F^2>2\sigma$	2761	
Absorption correction	semi-empirical from equivalents	
Min. and max. transmission	0.88939 and 1.00000	
Structure solution	direct methods	
Refinement method	Full-matrix least-squares on F^2	
Weighting parameters a, b	0.0361, 5.0468	
Data / restraints / parameters	3873 / 0 / 308	
Final R indices [$F^2>2\sigma$]	R1 = 0.0479, wR2 = 0.0925	
R indices (all data)	R1 = 0.0786, wR2 = 0.1028	
Goodness-of-fit on F^2	1.039	
Extinction coefficient	0.00000(3)	
Largest and mean shift/su	0.232 and 0.001	
Largest diff. peak and hole	0.50 and –0.41 e $Å^{-3}$	

7.3 Crystal data and structure refinement for OAC

Table 3. Crystal data and structure refinement for **OAC**.

Identification code	**OAC**	
Chemical formula (moiety)	$C_{36}H_{27}BrF_6NO_3P$	
Chemical formula (total)	$C_{36}H_{27}BrF_6NO_3P$	
Formula weight	746.47	
Temperature	150(2) K	
Radiation, wavelength	MoKα, 0.71073 Å	
Crystal system, space group	monoclinic, $P12_1/c1$	
Unit cell parameters	a = 10.5148(4) Å	α = 90°
	b = 8.7448(3) Å	β = 93.098(3)°
	c = 34.5974(11) Å	γ = 90°
Cell volume	3176.58(19) $Å^3$	
Z	4	
Calculated density	1.561 g/cm^3	
Absorption coefficient μ	1.419 mm^{-1}	
F(000)	1512	
Crystal colour and size	yellow, 0.50 × 0.05 × 0.05 mm^3	
Reflections for cell refinement	9108 (θ range 2.9 to 28.5°)	
Data collection method	Xcalibur, Atlas, Gemini ultra thick-slice ω scans	
θ range for data collection	3.0 to 28.6°	
Index ranges	h –12 to 14, k –11 to 11, l –34 to 43	
Completeness to θ = 25.0°	99.8 %	
Reflections collected	28287	
Independent reflections	7008 (R_{int} = 0.0333)	
Reflections with $F^2>2\sigma$	5783	
Absorption correction	semi-empirical from equivalents	
Min. and max. transmission	0.5373 and 0.9324	
Structure solution	direct methods	
Refinement method	Full-matrix least-squares on F^2	
Weighting parameters a, b	0.0400, 5.1123	
Data / restraints / parameters	7008 / 0 / 436	
Final R indices [$F^2>2\sigma$]	R1 = 0.0419, wR2 = 0.0963	
R indices (all data)	R1 = 0.0556, wR2 = 0.1027	
Goodness-of-fit on F^2	1.028	
Largest and mean shift/su	0.001 and 0.000	
Largest diff. peak and hole	0.84 and –0.56 e $Å^{-3}$	

7.4 Crystal data and structure refinement for CAC

Table 4. Crystal data and structure refinement for **CAC**.

Identification code	**CAC**	
Chemical formula (moiety)	$C_{36}H_{23}BrNO_3^+ \cdot PF_6^- \cdot 2H_2O$	
Chemical formula (total)	$C_{36}H_{27}BrF_6NO_5P$	
Formula weight	778.47	
Temperature	150(2) K	
Radiation, wavelength	synchrotron, 0.68890 Å	
Crystal system, space group	triclinic, $p\bar{1}$	
Unit cell parameters	a = 9.074(9) Å	α = 81.276(10)°
	b = 11.340(12) Å	β = 84.685(11)°
	c = 17.023(18) Å	γ = 67.049(11)°
Cell volume	1593(3) $Å^3$	
Z	2	
Calculated density	1.623 g/cm^3	
Absorption coefficient μ	1.322 mm^{-1}	
F(000)	788	
Crystal colour and size	red, 0.40 × 0.10 × 0.10 mm^3	
Reflections for cell refinement	4552 (θ range 2.3 to 24.5°)	
Data collection method	Crystal Logic diffractometer and Rigaku Saturn 724+ CCD thick-slice ω scans	
θ range for data collection	1.2 to 24.2°	
Index ranges	h –9 to 10, k –12 to 13, l –20 to 20	
Completeness to θ = 24.2°	95.3 %	
Reflections collected	10201	
Independent reflections	5373 (R_{int} = 0.0815)	
Reflections with $F^2>2\sigma$	3908	
Absorption correction	semi-empirical from equivalents	
Min. and max. transmission	0.6198 and 0.8791	
Structure solution	direct methods	
Refinement method	Full-matrix least-squares on F^2	
Weighting parameters a, b	0.2000, 0.0000	
Data / restraints / parameters	5373 / 0 / 437	
Final R indices [$F^2>2\sigma$]	R1 = 0.2252, wR2 = 0.5015	
R indices (all data)	R1 = 0.2541, wR2 = 0.5214	
Goodness-of-fit on F^2	2.090	
Extinction coefficient	7.4(8)	
Largest and mean shift/su	0.294 and 0.023	
Largest diff. peak and hole	3.78 and –1.41 e $Å^{-3}$	

7.5 Crystal data and structure refinement for DMA

Table 5. Crystal data and structure refinement for **DMA**.

Identification code	**DMA**	
Chemical formula (moiety)	$C_{44}H_{33}F_6N_2O_3P$	
Chemical formula (total)	$C_{44}H_{33}F_6N_2O_3P$	
Formula weight	782.69	
Temperature	100(2) K	
Radiation, wavelength	synchrotron, 0.6889 Å	
Crystal system, space group	triclinic, $P\bar{1}$	
Unit cell parameters	a = 10.226(9) Å	α = 106.360(9)°
	b = 18.309(15) Å	β = 97.926(10)°
	c = 22.041(19) Å	γ = 91.902(9)°
Cell volume	3910(6) $Å^3$	
Z	4	
Calculated density	1.329 g/cm^3	
Absorption coefficient μ	0.098 mm^{-1}	
F(000)	1616	
Crystal colour and size	red, 0.04 × 0.04 × 0.005 mm^3	
Reflections for cell refinement	1076 (θ range 2.3 to 19.9°)	
Data collection method	Rigaku Saturn 724+ on kappa diffractometer wide-frame ω scans	
θ range for data collection	0.9 to 21.3°	
Index ranges	h –10 to 10, k –19 to 19, l –23 to 23	
Completeness to θ = 24.4°	66.8 %	
Reflections collected	23234	
Independent reflections	9464 (R_{int} = 0.2185)	
Reflections with $F^2>2\sigma$	3450	
Absorption correction	none	
Structure solution	direct methods	
Refinement method	Full-matrix least-squares on F^2	
Weighting parameters a, b	0.1189,	
Data / restraints / parameters	9464 / 0 / 1020	
Final R indices [$F^2>2\sigma$]	R1 = 0.0996, wR2 = 0.2169	
R indices (all data)	R1 = 0.2457, wR2 = 0.2853	
Goodness-of-fit on F^2	0.947	
Extinction coefficient	0.039(2)	
Largest and mean shift/su	0.000 and 0.000	
Largest diff. peak and hole	0.42 and –0.37 e $Å^{-3}$	

7.6 Crystal data and structure refinement for PHTH1

Table 6. Crystal data and structure refinement for **PHTH1**.

Identification code	**PHTH1**	
Chemical formula (moiety)	$C_{17}H_{15}NO_5$	
Chemical formula (total)	$C_{17}H_{15}NO_5$	
Formula weight	313.30	
Temperature	150(2) K	
Radiation, wavelength	MoKα, 0.71073 Å	
Crystal system, space group	triclinic, $P\bar{1}$	
Unit cell parameters	a = 5.2034(5) Å	α = 68.696(6)°
	b = 12.1688(8) Å	β = 78.984(7)°
	c = 12.5890(9) Å	γ = 83.613(7)°
Cell volume	728.21(10) $Å^3$	
Z	2	
Calculated density	1.429 g/cm^3	
Absorption coefficient μ	0.106 mm^{-1}	
F(000)	328	
Reflections for cell refinement	2547 (θ range 3.3 to 28.5°)	
Data collection method	Oxford Diffraction Gemini A Ultra diffractometer	
	thick-slice ω scans	
θ range for data collection	3.3 to 28.6°	
Index ranges	h –6 to 6, k –12 to 15, l –16 to 16	
Completeness to θ = 26.0°	97.7 %	
Reflections collected	5749	
Independent reflections	3022 (R_{int} = 0.0365)	
Reflections with $F^2>2\sigma$	2200	
Absorption correction	semi-empirical from equivalents	
Min. and max. transmission	0.80972 and 1.00000	
Structure solution	direct methods	
Refinement method	Full-matrix least-squares on F^2	
Weighting parameters a, b	0.0649, 0.0000	
Data / restraints / parameters	3022 / 0 / 212	
Final R indices [$F^2>2\sigma$]	R1 = 0.0486, wR2 = 0.1140	
R indices (all data)	R1 = 0.0722, wR2 = 0.1312	
Goodness-of-fit on F^2	1.028	
Extinction coefficient	0.012(4)	
Largest and mean shift/su	0.000 and 0.000	
Largest diff. peak and hole	0.26 and –0.22 e $Å^{-3}$	

7.7 Crystal data and structure refinement for PHTH2

Table 7. Crystal data and structure refinement for **PHTH2**.

Identification code	**PHTH2**	
Chemical formula (moiety)	$C_{16}H_{14}N_2O_2$	
Chemical formula (total)	$C_{16}H_{14}N_2O_2$	
Formula weight	266.29	
Temperature	150(2) K	
Radiation, wavelength	CuKα, 1.54178 Å	
Crystal system, space group	orthorhombic, Pcnb	
Unit cell parameters	a = 5.5271(7) Å	α = 90°
	b = 28.565(5) Å	β = 90°
	c = 7.9350(17) Å	γ = 90°
Cell volume	1252.8(4) $Å^3$	
Z	4	
Calculated density	1.412 g/cm^3	
Absorption coefficient μ	0.767 mm^{-1}	
F(000)	560	
Reflections for cell refinement	1435 (θ range 3.1 to 62.3°)	
Data collection method	Xcalibur, Atlas, Gemini ultra thick-slice ω scans	
θ range for data collection	3.1 to 62.3°	
Index ranges	h –4 to 6, k –29 to 32, l –8 to 9	
Completeness to θ = 62.3°	98.0 %	
Reflections collected	3341	
Independent reflections	981 (R_{int} = 0.0385)	
Reflections with $F^2>2\sigma$	808	
Absorption correction	semi-empirical from equivalents	
Min. and max. transmission	0.52486 and 1.00000	
Structure solution	direct methods	
Refinement method	Full-matrix least-squares on F^2	
Weighting parameters a, b	0.0662, 0.1872	
Data / restraints / parameters	981 / 0 / 95	
Final R indices [$F^2>2\sigma$]	R1 = 0.0417, wR2 = 0.1077	
R indices (all data)	R1 = 0.0517, wR2 = 0.1180	
Goodness-of-fit on F^2	1.077	
Extinction coefficient	0.0009(4)	
Largest and mean shift/su	0.000 and 0.000	
Largest diff. peak and hole	0.17 and –0.16 e $Å^{-3}$	

7.8 Crystal data and structure refinement for PHTH3

Table 8. Crystal data and structure refinement for **PHTH3**.

Identification code	**PHTH3**	
Chemical formula (moiety)	$C_{16}H_{10}Cl_4N_2O_2$	
Chemical formula (total)	$C_{16}H_{10}Cl_4N_2O_2$	
Formula weight	404.06	
Temperature	150(2) K	
Radiation, wavelength	synchrotron, 0.68890 Å	
Crystal system, space group	orthorhombic, Pbca	
Unit cell parameters	a = 16.608(3) Å	α = 90°
	b = 6.6724(14) Å	β = 90°
	c = 29.798(6) Å	γ = 90°
Cell volume	3302.1(11) $Å^3$	
Z	8	
Calculated density	1.626 g/cm^3	
Absorption coefficient μ	0.663 mm^{-1}	
F(000)	1632	
Crystal colour and size	yellow, 0.10 × 0.10 × 0.00 mm^3	
Reflections for cell refinement	9912 (θ range 2.7 to 27.4°)	
Data collection method	Rigaku Spider CCD diffractometer thick-slice ω scans	
θ range for data collection	1.8 to 27.4°	
Index ranges	h –15 to 21, k –8 to 8, l –39 to 39	
Completeness to θ = 27.4°	97.5 %	
Reflections collected	31172	
Independent reflections	4029 (R_{int} = 0.0517)	
Reflections with $F^2>2\sigma$	3432	
Absorption correction	semi-empirical from equivalents	
Min. and max. transmission	0.9366 and 0.9987	
Structure solution	direct methods	
Refinement method	Full-matrix least-squares on F^2	
Weighting parameters a, b	0.0412, 2.0510	
Data / restraints / parameters	4029 / 0 / 220	
Final R indices [$F^2>2\sigma$]	R1 = 0.0342, wR2 = 0.0878	
R indices (all data)	R1 = 0.0412, wR2 = 0.0914	
Goodness-of-fit on F^2	1.039	
Extinction coefficient	0.0036(7)	
Largest and mean shift/su	0.001 and 0.000	
Largest diff. peak and hole	0.32 and –0.31 e $Å^{-3}$	

7.9 Crystal data and structure refinement for NAP1-G

Table 9. Crystal data and structure refinement for **NAP1-G**.

Identification code	**NAP1-G**	
Chemical formula (moiety)	$C_{20}H_{16}N_2O_2$	
Chemical formula (total)	$C_{20}H_{16}N_2O_2$	
Formula weight	316.35	
Temperature	150(2) K	
Radiation, wavelength	MoKα, 0.71073 Å	
Crystal system, space group	triclinic, $P\bar{1}$	
Unit cell parameters	a = 9.4336(8) Å	α = 115.803(9)°
	b = 9.5749(8) Å	β = 97.324(7)°
	c = 9.9183(9) Å	γ = 104.839(7)°
Cell volume	749.69(11) $Å^3$	
Z	2	
Calculated density	1.401 g/cm^3	
Absorption coefficient μ	0.092 mm^{-1}	
F(000)	332	
Crystal colour and size	yellow, 0.30 × 0.20 × 0.20 mm^3	
Reflections for cell refinement	2145 (θ range 3.2 to 28.6°)	
Data collection method	Xcalibur, Atlas, Gemini ultra thick-slice ω scans	
θ range for data collection	3.2 to 28.6°	
Index ranges	h –12 to 11, k –9 to 11, l –11 to 12	
Completeness to θ = 25.0°	99.7 %	
Reflections collected	5582	
Independent reflections	3090 (R_{int} = 0.0207)	
Reflections with $F^2>2\sigma$	2403	
Absorption correction	semi-empirical from equivalents	
Min. and max. transmission	0.9730 and 0.9819	
Structure solution	direct methods	
Refinement method	Full-matrix least-squares on F^2	
Weighting parameters a, b	0.0551, 0.2663	
Data / restraints / parameters	3090 / 0 / 220	
Final R indices [$F^2>2\sigma$]	R1 = 0.0452, wR2 = 0.1115	
R indices (all data)	R1 = 0.0599, wR2 = 0.1260	
Goodness-of-fit on F^2	1.027	
Extinction coefficient	0.014(3)	
Largest and mean shift/su	0.004 and 0.000	
Largest diff. peak and hole	0.31 and –0.26 e $Å^{-3}$	

7.10 Crystal data and structure refinement for NAP1-O

Table 10. Crystal data and structure refinement for **NAP1-O**.

Identification code	**NAP1-O**	
Chemical formula (moiety)	$C_{60}H_{48}N_6O_6$	
Chemical formula (total)	$C_{60}H_{48}N_6O_6$	
Formula weight	949.04	
Temperature	150(2) K	
Radiation, wavelength	MoKα, 0.71073 Å	
Crystal system, space group	monoclinic, C12/c1	
Unit cell parameters	a = 17.3700(9) Å	α = 90°
	b = 29.0684(13) Å	β = 94.498(4)°
	c = 8.8805(4) Å	γ = 90°
Cell volume	4470.1(4) $Å^3$	
Z	4	
Calculated density	1.410 g/cm^3	
Absorption coefficient μ	0.092 mm^{-1}	
F(000)	1992	
Crystal colour and size	orange, 0.20 × 0.08 × 0.08 mm^3	
Reflections for cell refinement	5796 (θ range 3.3 to 28.5°)	
Data collection method	Xcalibur, Atlas, Gemini ultra thick-slice ω scans	
θ range for data collection	3.3 to 28.6°	
Index ranges	h –23 to 22, k –39 to 38, l –10 to 11	
Completeness to θ = 26.0°	99.4 %	
Reflections collected	23905	
Independent reflections	5091 (R_{int} = 0.0278)	
Reflections with $F^2>2\sigma$	3685	
Absorption correction	semi-empirical from equivalents	
Min. and max. transmission	0.9818 and 0.9926	
Structure solution	direct methods	
Refinement method	Full-matrix least-squares on F^2	
Weighting parameters a, b	0.0588, 1.9423	
Data / restraints / parameters	5091 / 0 / 331	
Final R indices [$F^2>2\sigma$]	R1 = 0.0429, wR2 = 0.1098	
R indices (all data)	R1 = 0.0653, wR2 = 0.1247	
Goodness-of-fit on F^2	1.029	
Largest and mean shift/su	0.001 and 0.000	
Largest diff. peak and hole	0.19 and –0.24 e $Å^{-3}$	

7.11 Crystal data and structure refinement for NAP2

Table 11. Crystal data and structure refinement for **NAP2**.

Identification code	**NAP2**	
Chemical formula (moiety)	$C_{20}H_{15}ClN_2O_2$	
Chemical formula (total)	$C_{20}H_{15}ClN_2O_2$	
Formula weight	350.79	
Temperature	150(2) K	
Radiation, wavelength	MoKα, 0.71073 Å	
Crystal system, space group	triclinic, $P\bar{1}$	
Unit cell parameters	a = 8.0297(10) Å	α = 98.082(8)°
	b = 8.7857(8) Å	β = 98.708(9)°
	c = 12.6909(12) Å	γ = 114.068(11)°
Cell volume	787.47(14) $Å^3$	
Z	2	
Calculated density	1.479 g/cm^3	
Absorption coefficient μ	0.259 mm^{-1}	
F(000)	364	
Reflections for cell refinement	2225 (θ range 3.3 to 28.4°)	
Data collection method	Xcalibur, Atlas, Gemini ultra	
	thick-slice ω scans	
θ range for data collection	3.3 to 28.5°	
Index ranges	h –10 to 9, k –10 to 11, l –16 to 13	
Completeness to θ = 28.5°	83.1 %	
Reflections collected	6845	
Independent reflections	3307 (R_{int} = 0.0255)	
Reflections with $F^2>2\sigma$	2636	
Absorption correction	semi-empirical from equivalents	
Min. and max. transmission	0.89753 and 1.00000	
Structure solution	direct methods	
Refinement method	Full-matrix least-squares on F^2	
Weighting parameters a, b	0.0427, 0.2462	
Data / restraints / parameters	3307 / 0 / 241	
Final R indices [$F^2>2\sigma$]	R1 = 0.0421, wR2 = 0.0970	
R indices (all data)	R1 = 0.0575, wR2 = 0.1088	
Goodness-of-fit on F^2	1.067	
Extinction coefficient	0.004(2)	
Largest and mean shift/su	0.001 and 0.000	
Largest diff. peak and hole	0.25 and –0.25 e $Å^{-3}$	

7.12 Crystal data and structure refinement for NAP

Table 12. Crystal data and structure refinement for **NAP**.

Identification code	**NAP**	
Chemical formula (moiety)	$C_{20}H_{16}N_2O_3$	
Chemical formula (total)	$C_{20}H_{16}N_2O_3$	
Formula weight	332.35	
Temperature	120(2) K	
Radiation, wavelength	synchrotron, 0.68890 Å	
Crystal system, space group	orthorhombic, Pbca	
Unit cell parameters	a = 12.938(4) Å	α = 90°
	b = 8.719(3) Å	β = 90°
	c = 28.518(10) Å	γ = 90°
Cell volume	3217.0(19) $Å^3$	
Z	8	
Calculated density	1.372 g/cm^3	
Absorption coefficient μ	0.094 mm^{-1}	
F(000)	1392	
Crystal colour and size	red, 0.07 × 0.05 × 0.01 mm^3	
Reflections for cell refinement	4012 (θ range 3.0 to 24.0°)	
Data collection method	Rigaku	
	thick-slice ω scans	
θ range for data collection	2.8 to 24.4°	
Index ranges	h –10 to 15, k –10 to 10, l –34 to 34	
Completeness to θ = 24.4°	99.1 %	
Reflections collected	23938	
Independent reflections	2873 (R_{int} = 0.0964)	
Reflections with $F^2>2\sigma$	1875	
Absorption correction	semi-empirical from equivalents	
Min. and max. transmission	0.9935 and 0.9995	
Structure solution	direct methods	
Refinement method	Full-matrix least-squares on F^2	
Weighting parameters a, b	0.0657, 1.5391	
Data / restraints / parameters	2873 / 0 / 233	
Final R indices [$F^2>2\sigma$]	R1 = 0.0505, wR2 = 0.1222	
R indices (all data)	R1 = 0.0909, wR2 = 0.1447	
Goodness-of-fit on F^2	1.021	
Extinction coefficient	0.021(4)	
Largest and mean shift/su	0.000 and 0.000	
Largest diff. peak and hole	0.23 and –0.24 e $Å^{-3}$	

7.13 Crystal data and structure refinement for BPy6

Table 13. Crystal data and structure refinement for **BPy6**.

Identification code	**BPy6**	
Chemical formula (moiety)	$C_{10}H_6N_2S_2$	
Chemical formula (total)	$C_{10}H_6N_2S_2$	
Formula weight	218.29	
Temperature	150(2) K	
Radiation, wavelength	MoKα, 0.71073 Å	
Crystal system, space group	monoclinic, C12/c1	
Unit cell parameters	a = 12.3446(6) Å	α = 90°
	b = 7.2892(3) Å	β = 105.901(5)°
	c = 10.3201(5) Å	γ = 90°
Cell volume	893.09(7) $Å^3$	
Z	4	
Calculated density	1.623 g/cm^3	
Absorption coefficient μ	0.547 mm^{-1}	
F(000)	448	
Crystal colour and size	yellow, 0.32 × 0.10 × 0.10 mm^3	
Reflections for cell refinement	1676 (θ range 3.0 to 28.3°)	
Data collection method	Xcalibur, Atlas, Gemini ultra thick-slice ω scans	
θ range for data collection	3.3 to 28.3°	
Index ranges	h –16 to 16, k –9 to 7, l –10 to 13	
Completeness to θ = 26.0°	97.7 %	
Reflections collected	2095	
Independent reflections	928 (R_{int} = 0.0130)	
Reflections with $F^2>2\sigma$	842	
Absorption correction	semi-empirical from equivalents	
Min. and max. transmission	0.8443 and 0.9473	
Structure solution	direct methods	
Refinement method	Full-matrix least-squares on F^2	
Weighting parameters a, b	0.0334, 0.7770	
Data / restraints / parameters	928 / 0 / 64	
Final R indices [$F^2>2\sigma$]	R1 = 0.0247, wR2 = 0.0655	
R indices (all data)	R1 = 0.0277, wR2 = 0.0662	
Goodness-of-fit on F^2	1.083	
Largest and mean shift/su	0.001 and 0.000	
Largest diff. peak and hole	0.34 and –0.23 e $Å^{-3}$	

7.14 Crystal data and structure refinement for MSV1

Table 14. Crystal data and structure refinement for **MSV1**.

Identification code	**MSV1**	
Chemical formula (moiety)	$C_{12}H_{12}F_{12}N_2P_2S$	
Chemical formula (total)	$C_{12}H_{12}F_{12}N_2P_2S$	
Formula weight	506.24	
Temperature	293(2) K	
Radiation, wavelength	CuKα, 1.54178 Å	
Crystal system, space group	monoclinic, $P2_1/c$	
Unit cell parameters	a = 6.1108(5) Å	α = 90°
	b = 11.5152(8) Å	β = 99.776(8)°
	c = 12.9622(9) Å	γ = 90°
Cell volume	898.87(11) $Å^3$	
Z	2	
Calculated density	1.870 g/cm^3	
Absorption coefficient μ	4.481 mm^{-1}	
F(000)	504	
Crystal colour and size	colourless, 0.40 × 0.04 × 0.04 mm^3	
Reflections for cell refinement	1067 (θ range 3.5 to 61.8°)	
Data collection method	Xcalibur, Atlas, Gemini ultra thick-slice ω scans	
θ range for data collection	7.7 to 50.4°	
Index ranges	h –5 to 6, k –7 to 11, l –12 to 12	
Completeness to θ = 50.4°	99.4 %	
Reflections collected	1717	
Independent reflections	932 (R_{int} = 0.0233)	
Reflections with $F^2>2\sigma$	822	
Absorption correction	semi-empirical from equivalents	
Min. and max. transmission	0.2673 and 0.8411	
Structure solution	direct methods	
Refinement method	Full-matrix least-squares on F^2	
Weighting parameters a, b	0.0891, 3.0674	
Data / restraints / parameters	932 / 98 / 166	
Final R indices [$F^2>2\sigma$]	R1 = 0.0599, wR2 = 0.1571	
R indices (all data)	R1 = 0.0666, wR2 = 0.1633	
Goodness-of-fit on F^2	1.070	
Extinction coefficient	0.0015(8)	
Largest and mean shift/su	0.022 and 0.001	
Largest diff. peak and hole	0.67 and –0.32 e $Å^{-3}$	

7.15 Crystal data and structure refinement for MSV2

Table 15. Crystal data and structure refinement for **MSV2**.

Identification code	**MSV2**	
Chemical formula (moiety)	$C_{32}H_{33}F_{12}N_5P_2S$	
Chemical formula (total)	$C_{32}H_{33}F_{12}N_5P_2S$	
Formula weight	809.63	
Temperature	150(2) K	
Radiation, wavelength	MoKα, 0.71073 Å	
Crystal system, space group	orthorhombic, Pnma	
Unit cell parameters	a = 9.9868(5) Å	α = 90°
	b = 30.2095(15) Å	β = 90°
	c = 11.8887(5) Å	γ = 90°
Cell volume	3586.8(3) $Å^3$	
Z	4	
Calculated density	1.499 g/cm^3	
Absorption coefficient μ	0.274 mm^{-1}	
F(000)	1656	
Crystal colour and size	yellow, 0.24 × 0.20 × 0.20 mm^3	
Reflections for cell refinement	1377 (θ range 2.6 to 26.8°)	
Data collection method	Xcalibur, Atlas, Gemini ultra thick-slice ω scans	
θ range for data collection	2.7 to 25.0°	
Index ranges	h −7 to 11, k −35 to 32, l −14 to 12	
Completeness to θ = 25.0°	99.9 %	
Reflections collected	8454	
Independent reflections	3220 (R_{int} = 0.0842)	
Reflections with $F^2>2\sigma$	1790	
Absorption correction	semi-empirical from equivalents	
Min. and max. transmission	0.9372 and 0.9472	
Structure solution	direct methods	
Refinement method	Full-matrix least-squares on F^2	
Weighting parameters a, b	0.0902, 0.8138	
Data / restraints / parameters	3220 / 0 / 244	
Final R indices [$F^2>2\sigma$]	R1 = 0.0720, wR2 = 0.1611	
R indices (all data)	R1 = 0.1392, wR2 = 0.2031	
Goodness-of-fit on F^2	1.021	
Largest and mean shift/su	0.000 and 0.000	
Largest diff. peak and hole	0.42 and −0.41 e $Å^{-3}$	

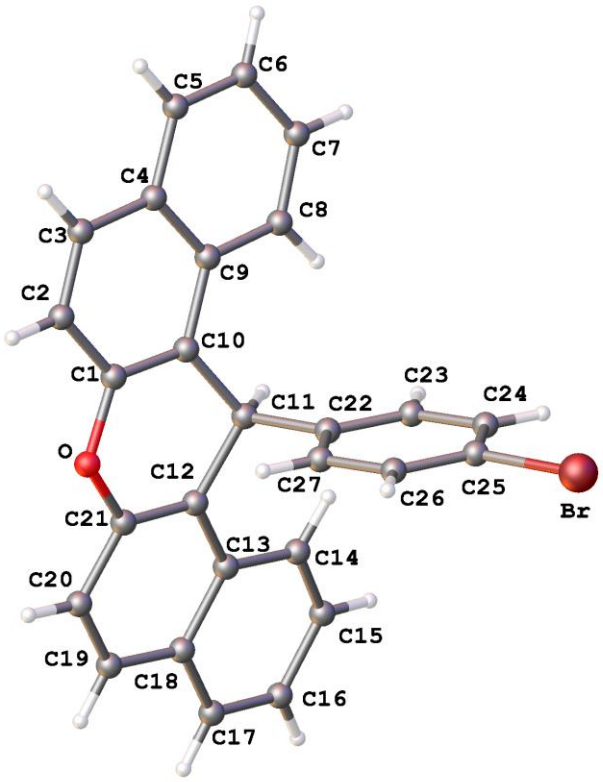
C6
C5
C7
C4
C8
C3
C9
C2
C10
C1
C23
C24
C11
C22
O
C12
C27
C26
C25
Br
C21
C13
C14
C20
C15
C19
C18
C16
C17

Table 1. Crystal data and structure refinement for **ACR1**.

Identification code	**ACR1**	
Chemical formula (moiety)	$C_{27}H_{17}BrO$	
Chemical formula (total)	$C_{27}H_{17}BrO$	
Formula weight	437.32	
Temperature	150(2) K	
Radiation, wavelength	MoKα, 0.71073 Å	
Crystal system, space group	orthorhombic, $Pna2_1$	
Unit cell parameters	a = 14.036(2) Å	α = 90°
	b = 17.400(4) Å	β = 90°
	c = 7.8622(12) Å	γ = 90°
Cell volume	1920.2(6) $Å^3$	
Z	4	
Calculated density	1.513 g/cm^3	
Absorption coefficient μ	2.157 mm^{-1}	
F(000)	888	
Crystal colour and size	colourless, 0.40 × 0.03 × 0.03 mm^3	
Reflections for cell refinement	1799 (θ range 3.1 to 28.5°)	
Data collection method	Oxford Diffraction Gemini A Ultra diffractometer thick-slice ω scans	
θ range for data collection	3.1 to 28.6°	
Index ranges	h −18 to 17, k −21 to 21, l −8 to 10	
Completeness to θ = 25.0°	99.7 %	
Reflections collected	9299	
Independent reflections	3707 (R_{int} = 0.0490)	
Reflections with $F^2>2\sigma$	2954	
Absorption correction	semi-empirical from equivalents	
Min. and max. transmission	0.4791 and 0.9381	
Structure solution	direct methods	
Refinement method	Full-matrix least-squares on F^2	
Weighting parameters a, b	0.0370, 0.4729	
Data / restraints / parameters	3707 / 1 / 262	
Final R indices [$F^2>2\sigma$]	R1 = 0.0434, wR2 = 0.0879	
R indices (all data)	R1 = 0.0629, wR2 = 0.0978	
Goodness-of-fit on F^2	1.044	
Absolute structure parameter	0.002(11)	
Largest and mean shift/su	0.001 and 0.000	
Largest diff. peak and hole	0.64 and −0.68 e $Å^{-3}$	

Table 2. Atomic coordinates and equivalent isotropic displacement parameters ($Å^2$) for acb175. U_{eq} is defined as one third of the trace of the orthogonalized U^{ij} tensor.

	x	y	z	U_{eq}
Br	0.92899(3)	0.56273(3)	0.23481(8)	0.05483(17)
O	0.47821(18)	0.50401(17)	0.7794(3)	0.0384(7)
C(1)	0.5377(3)	0.4443(3)	0.8261(5)	0.0345(10)
C(2)	0.4976(4)	0.3697(3)	0.8138(5)	0.0424(11)
C(3)	0.5488(4)	0.3084(3)	0.8564(5)	0.0485(13)
C(4)	0.6443(4)	0.3156(2)	0.9143(5)	0.0416(11)
C(5)	0.7004(4)	0.2515(2)	0.9630(6)	0.0499(13)
C(6)	0.7906(4)	0.2587(3)	1.0193(6)	0.0550(14)
C(7)	0.8308(4)	0.3320(3)	1.0290(5)	0.0459(12)
C(8)	0.7807(3)	0.3958(2)	0.9821(5)	0.0369(10)
C(9)	0.6862(3)	0.3900(2)	0.9250(4)	0.0316(9)
C(10)	0.6301(3)	0.4555(2)	0.8778(5)	0.0294(9)
C(11)	0.6730(3)	0.5352(2)	0.8755(5)	0.0284(9)
C(12)	0.5949(3)	0.5963(2)	0.8745(4)	0.0282(9)
C(13)	0.6154(3)	0.6744(2)	0.9212(4)	0.0265(8)
C(14)	0.7046(3)	0.6992(2)	0.9856(4)	0.0296(9)
C(15)	0.7196(3)	0.7735(2)	1.0324(5)	0.0372(10)
C(16)	0.6479(4)	0.8292(3)	1.0152(5)	0.0421(11)
C(17)	0.5615(3)	0.8076(3)	0.9503(5)	0.0417(11)
C(18)	0.5419(3)	0.7307(2)	0.9040(5)	0.0343(10)
C(19)	0.4518(3)	0.7070(3)	0.8455(5)	0.0392(11)
C(20)	0.4327(3)	0.6333(3)	0.8088(5)	0.0388(11)
C(21)	0.5056(3)	0.5783(2)	0.8231(5)	0.0317(9)
C(22)	0.7369(2)	0.54294(17)	0.7182(5)	0.0230(7)
C(23)	0.8332(2)	0.55926(19)	0.7318(7)	0.0308(7)
C(24)	0.8902(3)	0.5640(2)	0.5883(5)	0.0337(9)
C(25)	0.8506(3)	0.5521(2)	0.4306(5)	0.0316(9)
C(26)	0.7556(3)	0.5358(2)	0.4127(5)	0.0328(9)
C(27)	0.6992(3)	0.5313(2)	0.5571(5)	0.0274(9)

Table 3. Bond lengths [Å] and angles [°] for acb175.

Br–C(25)	1.901(4)	O–C(1)	1.382(5)
O–C(21)	1.392(5)	C(1)–C(2)	1.417(6)
C(1)–C(10)	1.374(6)	C(2)–H(2A)	0.950
C(2)–C(3)	1.329(7)	C(3)–H(3A)	0.950
C(3)–C(4)	1.421(7)	C(4)–C(5)	1.418(7)
C(4)–C(9)	1.425(6)	C(5)–H(5A)	0.950
C(5)–C(6)	1.347(7)	C(6)–H(6A)	0.950
C(6)–C(7)	1.396(7)	C(7)–H(7A)	0.950
C(7)–C(8)	1.366(6)	C(8)–H(8A)	0.950
C(8)–C(9)	1.404(6)	C(9)–C(10)	1.434(6)
C(10)–C(11)	1.511(6)	C(11)–H(11A)	1.000
C(11)–C(12)	1.526(6)	C(11)–C(22)	1.534(5)
C(12)–C(13)	1.437(6)	C(12)–C(21)	1.353(5)
C(13)–C(14)	1.418(5)	C(13)–C(18)	1.429(5)
C(14)–H(14A)	0.950	C(14)–C(15)	1.360(6)
C(15)–H(15A)	0.950	C(15)–C(16)	1.404(6)
C(16)–H(16A)	0.950	C(16)–C(17)	1.368(7)
C(17)–H(17A)	0.950	C(17)–C(18)	1.414(6)
C(18)–C(19)	1.408(6)	C(19)–H(19A)	0.950
C(19)–C(20)	1.342(6)	C(20)–H(20A)	0.950
C(20)–C(21)	1.406(6)	C(22)–C(23)	1.385(5)
C(22)–C(27)	1.388(5)	C(23)–H(23A)	0.950
C(23)–C(24)	1.385(6)	C(24)–H(24A)	0.950
C(24)–C(25)	1.374(6)	C(25)–C(26)	1.370(6)
C(26)–H(26A)	0.950	C(26)–C(27)	1.387(5)
C(27)–H(27A)	0.950		

C(1)–O–C(21)	117.8(3)	O–C(1)–C(2)	115.5(4)
O–C(1)–C(10)	122.8(4)	C(2)–C(1)–C(10)	121.7(4)
C(1)–C(2)–H(2A)	119.9	C(1)–C(2)–C(3)	120.2(5)
H(2A)–C(2)–C(3)	119.9	C(2)–C(3)–H(3A)	119.3
C(2)–C(3)–C(4)	121.4(4)	H(3A)–C(3)–C(4)	119.3
C(3)–C(4)–C(5)	122.8(4)	C(3)–C(4)–C(9)	119.2(4)
C(5)–C(4)–C(9)	118.1(4)	C(4)–C(5)–H(5A)	118.8
C(4)–C(5)–C(6)	122.5(5)	H(5A)–C(5)–C(6)	118.8
C(5)–C(6)–H(6A)	120.6	C(5)–C(6)–C(7)	118.9(5)
H(6A)–C(6)–C(7)	120.6	C(6)–C(7)–H(7A)	119.3
C(6)–C(7)–C(8)	121.3(5)	H(7A)–C(7)–C(8)	119.3
C(7)–C(8)–H(8A)	119.5	C(7)–C(8)–C(9)	121.0(4)
H(8A)–C(8)–C(9)	119.5	C(4)–C(9)–C(8)	118.3(4)
C(4)–C(9)–C(10)	118.8(4)	C(8)–C(9)–C(10)	123.0(4)
C(1)–C(10)–C(9)	118.8(4)	C(1)–C(10)–C(11)	120.2(4)
C(9)–C(10)–C(11)	120.9(4)	C(10)–C(11)–H(11A)	108.8
C(10)–C(11)–C(12)	110.7(3)	C(10)–C(11)–C(22)	108.8(3)
H(11A)–C(11)–C(12)	108.8	H(11A)–C(11)–C(22)	108.8
C(12)–C(11)–C(22)	110.8(3)	C(11)–C(12)–C(13)	120.9(3)
C(11)–C(12)–C(21)	120.4(4)	C(13)–C(12)–C(21)	118.7(4)
C(12)–C(13)–C(14)	123.8(4)	C(12)–C(13)–C(18)	118.6(4)
C(14)–C(13)–C(18)	117.5(4)	C(13)–C(14)–H(14A)	119.3
C(13)–C(14)–C(15)	121.5(4)	H(14A)–C(14)–C(15)	119.3
C(14)–C(15)–H(15A)	119.3	C(14)–C(15)–C(16)	121.3(4)
H(15A)–C(15)–C(16)	119.3	C(15)–C(16)–H(16A)	120.6
C(15)–C(16)–C(17)	118.7(4)	H(16A)–C(16)–C(17)	120.6

C(16)–C(17)–H(17A)	119.0	C(16)–C(17)–C(18)	121.9(4)
H(17A)–C(17)–C(18)	119.0	C(13)–C(18)–C(17)	118.9(4)
C(13)–C(18)–C(19)	118.6(4)	C(17)–C(18)–C(19)	122.4(4)
C(18)–C(19)–H(19A)	119.0	C(18)–C(19)–C(20)	122.0(4)
H(19A)–C(19)–C(20)	119.0	C(19)–C(20)–H(20A)	120.4
C(19)–C(20)–C(21)	119.2(4)	H(20A)–C(20)–C(21)	120.4
O–C(21)–C(12)	123.0(4)	O–C(21)–C(20)	114.3(4)
C(12)–C(21)–C(20)	122.7(4)	C(11)–C(22)–C(23)	121.8(4)
C(11)–C(22)–C(27)	120.0(3)	C(23)–C(22)–C(27)	118.2(4)
C(22)–C(23)–H(23A)	119.6	C(22)–C(23)–C(24)	120.9(4)
H(23A)–C(23)–C(24)	119.6	C(23)–C(24)–H(24A)	120.3
C(23)–C(24)–C(25)	119.5(4)	H(24A)–C(24)–C(25)	120.3
Br–C(25)–C(24)	118.8(3)	Br–C(25)–C(26)	120.0(3)
C(24)–C(25)–C(26)	121.2(4)	C(25)–C(26)–H(26A)	120.5
C(25)–C(26)–C(27)	118.9(4)	H(26A)–C(26)–C(27)	120.5
C(22)–C(27)–C(26)	121.4(4)	C(22)–C(27)–H(27A)	119.3
C(26)–C(27)–H(27A)	119.3		

Table 4. Anisotropic displacement parameters ($Å^2$) for acb175. The anisotropic displacement factor exponent takes the form: $-2\pi^2[h^2a^{*2}U^{11} + ...+ 2hka^*b^*U^{12}]$

	U^{11}	U^{22}	U^{33}	U^{23}	U^{13}	U^{12}
Br	0.0459(3)	0.0634(3)	0.0552(3)	–0.0063(3)	0.0280(3)	–0.0042(2)
O	0.0277(14)	0.0501(18)	0.0374(16)	–0.0034(13)	–0.0009(13)	–0.0122(14)
C(1)	0.035(2)	0.043(3)	0.0254(19)	–0.0042(17)	0.0040(18)	–0.013(2)
C(2)	0.051(3)	0.048(3)	0.0284(18)	–0.0123(19)	0.0117(19)	–0.026(2)
C(3)	0.074(4)	0.035(3)	0.037(2)	–0.010(2)	0.016(2)	–0.025(3)
C(4)	0.063(3)	0.034(3)	0.027(2)	0.0021(18)	0.011(2)	–0.014(2)
C(5)	0.086(4)	0.019(2)	0.044(2)	0.0014(19)	0.022(3)	–0.011(2)
C(6)	0.085(4)	0.032(3)	0.049(3)	0.008(2)	0.013(3)	0.010(3)
C(7)	0.066(3)	0.035(3)	0.036(2)	0.010(2)	0.000(2)	0.005(2)
C(8)	0.053(3)	0.026(2)	0.032(2)	0.0073(17)	0.001(2)	–0.001(2)
C(9)	0.045(3)	0.028(2)	0.0218(18)	–0.0040(16)	0.0044(18)	–0.0069(19)
C(10)	0.032(2)	0.032(2)	0.0245(19)	0.0009(15)	0.0022(17)	–0.0105(17)
C(11)	0.027(2)	0.031(2)	0.028(2)	0.0009(16)	–0.0066(17)	–0.0033(18)
C(12)	0.027(2)	0.038(2)	0.0193(18)	0.0009(16)	0.0041(15)	–0.0037(18)
C(13)	0.028(2)	0.032(2)	0.0195(17)	0.0028(16)	0.0040(16)	0.0024(17)
C(14)	0.027(2)	0.036(2)	0.0255(19)	0.0021(16)	0.0038(16)	–0.0017(18)
C(15)	0.042(3)	0.036(3)	0.034(2)	–0.0061(19)	0.007(2)	–0.003(2)
C(16)	0.059(3)	0.031(3)	0.037(2)	0.0005(19)	0.007(2)	–0.001(2)
C(17)	0.053(3)	0.036(3)	0.036(2)	–0.0011(19)	0.011(2)	0.013(2)
C(18)	0.034(2)	0.044(3)	0.025(2)	0.0022(18)	0.0068(18)	0.0057(19)
C(19)	0.035(2)	0.055(3)	0.027(2)	0.0085(19)	0.0028(17)	0.012(2)
C(20)	0.025(2)	0.061(3)	0.030(2)	0.005(2)	0.0008(17)	0.001(2)
C(21)	0.029(2)	0.047(3)	0.0191(17)	0.0002(16)	0.0027(16)	–0.0062(19)
C(22)	0.0203(17)	0.0181(17)	0.0306(18)	0.0034(18)	0.0021(17)	0.0010(12)
C(23)	0.0279(17)	0.0261(19)	0.0383(18)	0.0071(19)	–0.002(2)	0.0000(15)
C(24)	0.025(2)	0.029(2)	0.047(2)	0.0062(18)	–0.0016(19)	–0.0003(18)
C(25)	0.030(2)	0.022(2)	0.043(2)	0.0010(17)	0.0140(19)	0.0027(17)
C(26)	0.029(2)	0.035(2)	0.035(2)	–0.0038(17)	0.0009(18)	–0.0017(18)
C(27)	0.0209(19)	0.029(2)	0.032(2)	–0.0023(17)	0.0004(17)	–0.0031(17)

Table 5. Hydrogen coordinates and isotropic displacement parameters ($Å^2$) for acb175.

	x	y	z	U
H(2A)	0.4340	0.3636	0.7749	0.051
H(3A)	0.5210	0.2588	0.8479	0.058
H(5A)	0.6734	0.2015	0.9557	0.060
H(6A)	0.8263	0.2147	1.0517	0.066
H(7A)	0.8943	0.3375	1.0691	0.055
H(8A)	0.8102	0.4449	0.9882	0.044
H(11A)	0.7129	0.5421	0.9798	0.034
H(14A)	0.7550	0.6631	0.9964	0.036
H(15A)	0.7797	0.7879	1.0776	0.045
H(16A)	0.6592	0.8810	1.0480	0.051
H(17A)	0.5133	0.8454	0.9360	0.050
H(19A)	0.4030	0.7444	0.8316	0.047
H(20A)	0.3706	0.6185	0.7735	0.047
H(23A)	0.8605	0.5673	0.8409	0.037
H(24A)	0.9562	0.5754	0.5988	0.040
H(26A)	0.7289	0.5278	0.3031	0.039
H(27A)	0.6333	0.5200	0.5455	0.033

Table 6. Torsion angles [°] for acb175.

C(21)–O–C(1)–C(2)	166.4(3)	C(21)–O–C(1)–C(10)	−14.9(5)
O–C(1)–C(2)–C(3)	−179.7(4)	C(10)–C(1)–C(2)–C(3)	1.6(6)
C(1)–C(2)–C(3)–C(4)	−0.3(6)	C(2)–C(3)–C(4)–C(5)	179.1(4)
C(2)–C(3)–C(4)–C(9)	−0.7(6)	C(3)–C(4)–C(5)–C(6)	−179.4(4)
C(9)–C(4)–C(5)–C(6)	0.4(6)	C(4)–C(5)–C(6)–C(7)	−0.4(7)
C(5)–C(6)–C(7)–C(8)	−0.3(7)	C(6)–C(7)–C(8)–C(9)	1.1(6)
C(7)–C(8)–C(9)–C(4)	−1.1(5)	C(7)–C(8)–C(9)–C(10)	178.6(4)
C(3)–C(4)–C(9)–C(8)	−179.8(4)	C(3)–C(4)–C(9)–C(10)	0.4(5)
C(5)–C(4)–C(9)–C(8)	0.3(5)	C(5)–C(4)–C(9)–C(10)	−179.4(4)
O–C(1)–C(10)–C(9)	179.5(3)	O–C(1)–C(10)–C(11)	−3.7(5)
C(2)–C(1)–C(10)–C(9)	−1.8(5)	C(2)–C(1)–C(10)–C(11)	174.9(3)
C(4)–C(9)–C(10)–C(1)	0.8(5)	C(4)–C(9)–C(10)–C(11)	−175.9(3)
C(8)–C(9)–C(10)–C(1)	−178.9(4)	C(8)–C(9)–C(10)–C(11)	4.4(5)
C(1)–C(10)–C(11)–C(12)	20.4(5)	C(1)–C(10)–C(11)–C(22)	−101.6(4)
C(9)–C(10)–C(11)–C(12)	−162.9(3)	C(9)–C(10)–C(11)–C(22)	75.1(4)
C(10)–C(11)–C(12)–C(13)	161.9(3)	C(10)–C(11)–C(12)–C(21)	−20.7(5)
C(22)–C(11)–C(12)–C(13)	−77.3(4)	C(22)–C(11)–C(12)–C(21)	100.1(4)
C(11)–C(12)–C(13)–C(14)	−6.1(5)	C(11)–C(12)–C(13)–C(18)	174.6(3)
C(21)–C(12)–C(13)–C(14)	176.4(3)	C(21)–C(12)–C(13)–C(18)	−2.9(5)
C(12)–C(13)–C(14)–C(15)	−178.2(3)	C(18)–C(13)–C(14)–C(15)	1.1(5)
C(13)–C(14)–C(15)–C(16)	−1.5(6)	C(14)–C(15)–C(16)–C(17)	0.1(6)
C(15)–C(16)–C(17)–C(18)	1.5(6)	C(16)–C(17)–C(18)–C(13)	−1.7(6)
C(16)–C(17)–C(18)–C(19)	176.6(4)	C(12)–C(13)–C(18)–C(17)	179.7(3)
C(12)–C(13)–C(18)–C(19)	1.4(5)	C(14)–C(13)–C(18)–C(17)	0.4(5)
C(14)–C(13)–C(18)–C(19)	−178.0(3)	C(13)–C(18)–C(19)–C(20)	1.2(6)
C(17)–C(18)–C(19)–C(20)	−177.1(4)	C(18)–C(19)–C(20)–C(21)	−2.3(6)
C(11)–C(12)–C(21)–O	4.1(5)	C(11)–C(12)–C(21)–C(20)	−175.6(3)
C(13)–C(12)–C(21)–O	−178.3(3)	C(13)–C(12)–C(21)–C(20)	1.9(5)
C(1)–O–C(21)–C(12)	14.7(5)	C(1)–O–C(21)–C(20)	−165.5(3)
C(19)–C(20)–C(21)–O	−179.1(3)	C(19)–C(20)–C(21)–C(12)	0.7(6)
C(10)–C(11)–C(22)–C(23)	−120.2(3)	C(10)–C(11)–C(22)–C(27)	57.8(4)
C(12)–C(11)–C(22)–C(23)	117.9(4)	C(12)–C(11)–C(22)–C(27)	−64.1(4)
C(11)–C(22)–C(23)–C(24)	178.3(3)	C(27)–C(22)–C(23)–C(24)	0.1(5)
C(22)–C(23)–C(24)–C(25)	−0.2(6)	C(23)–C(24)–C(25)–Br	177.6(3)
C(23)–C(24)–C(25)–C(26)	0.2(6)	Br–C(25)–C(26)–C(27)	−177.5(3)
C(24)–C(25)–C(26)–C(27)	−0.2(6)	C(25)–C(26)–C(27)–C(22)	0.1(6)
C(11)–C(22)–C(27)–C(26)	−178.2(4)	C(23)–C(22)–C(27)–C(26)	−0.1(6)

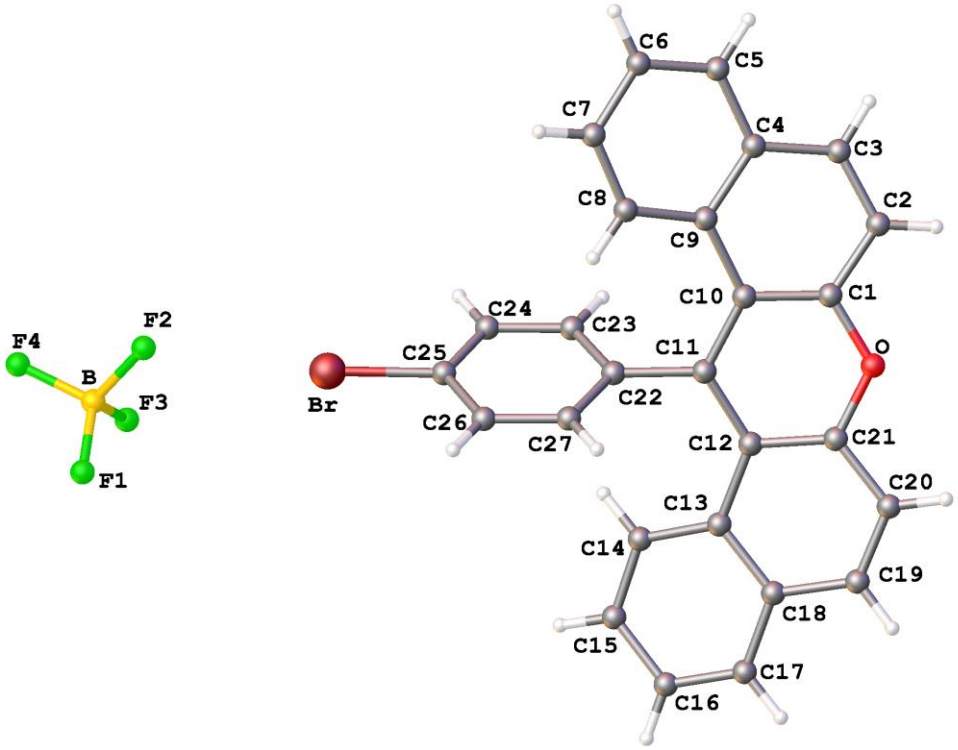
F4
F2
B
F3
F1
C6
C5
C7
C4
C3
C8
C2
C9
C10
C1
C24
C23
C25
C11
O
Br
C22
C26
C27
C12
C21
C20
C13
C14
C19
C18
C15
C17
C16

Table 1. Crystal data and structure refinement for **ACR3**.

Identification code	**ACR3**	
Chemical formula (moiety)	$C_{27}H_{16}BBrF_4O$	
Chemical formula (total)	$C_{27}H_{16}BBrF_4O$	
Formula weight	523.12	
Temperature	150(2) K	
Radiation, wavelength	MoKα, 0.71073 Å	
Crystal system, space group	rhombohedral, $R\bar{3}$	
Unit cell parameters	a = 35.533(2) Å	α = 90°
	b = 35.533(2) Å	β = 90°
	c = 9.0525(8) Å	γ = 120°
Cell volume	9898.3(12) $Å^3$	
Z	18	
Calculated density	1.580 g/cm^3	
Absorption coefficient μ	1.921 mm^{-1}	
F(000)	4716	
Reflections for cell refinement	1484 (θ range 3.0 to 28.2°)	
Data collection method	Oxford Diffraction Gemini A Ultra diffractometer thick-slice ω scans	
θ range for data collection	3.0 to 25.0°	
Index ranges	h −40 to 42, k −36 to 36, l −10 to 8	
Completeness to θ = 25.0°	99.7 %	
Reflections collected	7376	
Independent reflections	3873 (R_{int} = 0.0381)	
Reflections with $F^2>2\sigma$	2761	
Absorption correction	semi-empirical from equivalents	
Min. and max. transmission	0.88939 and 1.00000	
Structure solution	direct methods	
Refinement method	Full-matrix least-squares on F^2	
Weighting parameters a, b	0.0361, 5.0468	
Data / restraints / parameters	3873 / 0 / 308	
Final R indices [$F^2>2\sigma$]	R1 = 0.0479, wR2 = 0.0925	
R indices (all data)	R1 = 0.0786, wR2 = 0.1028	
Goodness-of-fit on F^2	1.039	
Extinction coefficient	0.00000(3)	
Largest and mean shift/su	0.232 and 0.001	
Largest diff. peak and hole	0.50 and –0.41 e $Å^{-3}$	

Table 2. Atomic coordinates and equivalent isotropic displacement parameters ($Å^2$) for acb177. U_{eq} is defined as one third of the trace of the orthogonalized U^{ij} tensor.

	x	y	z	U_{eq}
Br	0.722878(13)	0.053050(13)	0.23921(4)	0.04020(18)
O	0.52793(8)	0.10846(8)	–0.1610(3)	0.0307(6)
F(1)	0.84401(9)	0.02651(9)	0.1070(2)	0.0653(8)
F(2)	0.84471(10)	0.08706(8)	0.1840(3)	0.0737(9)
F(3)	0.79939(8)	0.02286(8)	0.2852(3)	0.0736(8)
F(4)	0.87025(8)	0.05412(8)	0.3307(2)	0.0553(7)
B	0.83968(15)	0.04787(14)	0.2250(5)	0.0325(11)
C(1)	0.55911(12)	0.13770(12)	–0.0724(4)	0.0305(9)
C(2)	0.55410(14)	0.17301(13)	–0.0350(5)	0.0431(11)
C(3)	0.58500(15)	0.20406(15)	0.0521(5)	0.0563(13)
C(4)	0.62355(15)	0.20383(14)	0.0912(5)	0.0469(11)
C(5)	0.65803(17)	0.24012(15)	0.1637(5)	0.0604(13)
C(6)	0.69722(16)	0.24281(15)	0.1865(5)	0.0598(14)
C(7)	0.70355(14)	0.20959(14)	0.1361(4)	0.0462(11)
C(8)	0.67066(12)	0.17357(12)	0.0698(4)	0.0361(10)
C(9)	0.62919(12)	0.16841(12)	0.0489(4)	0.0320(9)
C(10)	0.59249(11)	0.13108(11)	–0.0213(4)	0.0271(9)
C(11)	0.58691(11)	0.08912(11)	–0.0391(4)	0.0242(8)
C(12)	0.55087(11)	0.05666(11)	–0.1189(4)	0.0235(8)
C(13)	0.53888(11)	0.01130(11)	–0.1392(4)	0.0244(8)
C(14)	0.55489(11)	–0.01079(11)	–0.0535(4)	0.0262(8)
C(15)	0.54298(12)	–0.05336(12)	–0.0823(4)	0.0299(9)
C(16)	0.51417(12)	–0.07627(12)	–0.1958(4)	0.0347(10)
C(17)	0.49593(12)	–0.05676(12)	–0.2744(4)	0.0326(9)
C(18)	0.50698(11)	–0.01370(12)	–0.2474(4)	0.0270(9)
C(19)	0.48513(11)	0.00473(13)	–0.3248(4)	0.0300(9)
C(20)	0.49254(11)	0.04488(13)	–0.2952(4)	0.0318(9)
C(21)	0.52442(11)	0.06978(11)	–0.1908(4)	0.0262(8)
C(22)	0.61911(10)	0.07943(11)	0.0279(4)	0.0223(8)
C(23)	0.62377(11)	0.08015(11)	0.1798(4)	0.0263(8)
C(24)	0.65440(11)	0.07221(11)	0.2430(4)	0.0270(9)
C(25)	0.68014(11)	0.06300(11)	0.1534(4)	0.0275(8)
C(26)	0.67596(11)	0.06172(11)	0.0017(4)	0.0269(8)
C(27)	0.64544(11)	0.07013(11)	–0.0614(4)	0.0280(9)

Table 3. Bond lengths [Å] and angles [°] for acb177.

Br–C(25)	1.890(3)	O–C(1)	1.341(4)
O–C(21)	1.344(4)	F(1)–B	1.363(5)
F(2)–B	1.364(5)	F(3)–B	1.366(5)
F(4)–B	1.380(5)	C(1)–C(2)	1.394(5)
C(1)–C(10)	1.398(5)	C(2)–H(2A)	0.950
C(2)–C(3)	1.354(6)	C(3)–H(3A)	0.950
C(3)–C(4)	1.419(6)	C(4)–C(5)	1.419(6)
C(4)–C(9)	1.422(5)	C(5)–H(5A)	0.950
C(5)–C(6)	1.363(7)	C(6)–H(6A)	0.950
C(6)–C(7)	1.385(6)	C(7)–H(7A)	0.950
C(7)–C(8)	1.367(5)	C(8)–H(8A)	0.950
C(8)–C(9)	1.404(5)	C(9)–C(10)	1.461(5)
C(10)–C(11)	1.412(5)	C(11)–C(12)	1.420(5)
C(11)–C(22)	1.480(5)	C(12)–C(13)	1.458(5)
C(12)–C(21)	1.401(5)	C(13)–C(14)	1.410(5)
C(13)–C(18)	1.423(5)	C(14)–H(14A)	0.950
C(14)–C(15)	1.377(5)	C(15)–H(15A)	0.950
C(15)–C(16)	1.391(5)	C(16)–H(16A)	0.950
C(16)–C(17)	1.362(5)	C(17)–H(17A)	0.950
C(17)–C(18)	1.398(5)	C(18)–C(19)	1.425(5)
C(19)–H(19A)	0.950	C(19)–C(20)	1.342(5)
C(20)–H(20A)	0.950	C(20)–C(21)	1.399(5)
C(22)–C(23)	1.384(5)	C(22)–C(27)	1.396(5)
C(23)–H(23A)	0.950	C(23)–C(24)	1.378(5)
C(24)–H(24A)	0.950	C(24)–C(25)	1.379(5)
C(25)–C(26)	1.379(5)	C(26)–H(26A)	0.950
C(26)–C(27)	1.384(5)	C(27)–H(27A)	0.950

C(1)–O–C(21)	122.0(3)	F(1)–B–F(2)	111.2(3)
F(1)–B–F(3)	108.9(3)	F(1)–B–F(4)	109.5(4)
F(2)–B–F(3)	109.4(4)	F(2)–B–F(4)	109.5(3)
F(3)–B–F(4)	108.2(3)	O–C(1)–C(2)	114.5(3)
O–C(1)–C(10)	120.6(3)	C(2)–C(1)–C(10)	124.9(4)
C(1)–C(2)–H(2A)	121.3	C(1)–C(2)–C(3)	117.3(4)
H(2A)–C(2)–C(3)	121.3	C(2)–C(3)–H(3A)	118.9
C(2)–C(3)–C(4)	122.2(4)	H(3A)–C(3)–C(4)	118.9
C(3)–C(4)–C(5)	120.5(4)	C(3)–C(4)–C(9)	120.1(4)
C(5)–C(4)–C(9)	119.3(4)	C(4)–C(5)–H(5A)	119.3
C(4)–C(5)–C(6)	121.4(4)	H(5A)–C(5)–C(6)	119.3
C(5)–C(6)–H(6A)	120.5	C(5)–C(6)–C(7)	119.1(4)
H(6A)–C(6)–C(7)	120.5	C(6)–C(7)–H(7A)	119.5
C(6)–C(7)–C(8)	121.0(4)	H(7A)–C(7)–C(8)	119.5
C(7)–C(8)–H(8A)	118.9	C(7)–C(8)–C(9)	122.1(4)
H(8A)–C(8)–C(9)	118.9	C(4)–C(9)–C(8)	116.8(4)
C(4)–C(9)–C(10)	117.6(4)	C(8)–C(9)–C(10)	125.4(3)
C(1)–C(10)–C(9)	116.0(3)	C(1)–C(10)–C(11)	117.2(3)
C(9)–C(10)–C(11)	126.8(3)	C(10)–C(11)–C(12)	120.6(3)
C(10)–C(11)–C(22)	118.8(3)	C(12)–C(11)–C(22)	120.5(3)
C(11)–C(12)–C(13)	127.5(3)	C(11)–C(12)–C(21)	116.7(3)
C(13)–C(12)–C(21)	115.8(3)	C(12)–C(13)–C(14)	124.7(3)
C(12)–C(13)–C(18)	118.5(3)	C(14)–C(13)–C(18)	116.6(3)
C(13)–C(14)–H(14A)	119.3	C(13)–C(14)–C(15)	121.3(3)
H(14A)–C(14)–C(15)	119.3	C(14)–C(15)–H(15A)	119.5

C(14)–C(15)–C(16)	121.0(3)	H(15A)–C(15)–C(16)	119.5
C(15)–C(16)–H(16A)	120.4	C(15)–C(16)–C(17)	119.1(4)
H(16A)–C(16)–C(17)	120.4	C(16)–C(17)–H(17A)	119.3
C(16)–C(17)–C(18)	121.4(4)	H(17A)–C(17)–C(18)	119.3
C(13)–C(18)–C(17)	120.2(3)	C(13)–C(18)–C(19)	119.9(3)
C(17)–C(18)–C(19)	119.8(3)	C(18)–C(19)–H(19A)	119.1
C(18)–C(19)–C(20)	121.8(3)	H(19A)–C(19)–C(20)	119.1
C(19)–C(20)–H(20A)	120.9	C(19)–C(20)–C(21)	118.3(3)
H(20A)–C(20)–C(21)	120.9	O–C(21)–C(12)	120.8(3)
O–C(21)–C(20)	114.5(3)	C(12)–C(21)–C(20)	124.7(3)
C(11)–C(22)–C(23)	120.2(3)	C(11)–C(22)–C(27)	120.3(3)
C(23)–C(22)–C(27)	119.5(3)	C(22)–C(23)–H(23A)	119.7
C(22)–C(23)–C(24)	120.5(3)	H(23A)–C(23)–C(24)	119.7
C(23)–C(24)–H(24A)	120.3	C(23)–C(24)–C(25)	119.3(3)
H(24A)–C(24)–C(25)	120.3	Br–C(25)–C(24)	119.5(3)
Br–C(25)–C(26)	119.1(3)	C(24)–C(25)–C(26)	121.4(3)
C(25)–C(26)–H(26A)	120.4	C(25)–C(26)–C(27)	119.1(3)
H(26A)–C(26)–C(27)	120.4	C(22)–C(27)–C(26)	120.1(3)
C(22)–C(27)–H(27A)	119.9	C(26)–C(27)–H(27A)	119.9

Table 4. Anisotropic displacement parameters ($Å^2$) for acb177. The anisotropic displacement factor exponent takes the form: $-2\pi^2[h^2a^{*2}U^{11} + ...+ 2hka^*b^*U^{12}]$

	U^{11}	U^{22}	U^{33}	U^{23}	U^{13}	U^{12}
Br	0.0434(3)	0.0471(3)	0.0385(3)	–0.0074(2)	–0.0134(2)	0.0290(2)
O	0.0283(14)	0.0343(15)	0.0337(15)	0.0054(13)	0.0043(12)	0.0189(13)
F(1)	0.089(2)	0.091(2)	0.0333(14)	–0.0224(14)	–0.0130(14)	0.0583(18)
F(2)	0.113(2)	0.0363(15)	0.0663(18)	0.0088(13)	–0.0119(16)	0.0333(16)
F(3)	0.0437(16)	0.0582(17)	0.094(2)	0.0039(16)	0.0228(15)	0.0065(14)
F(4)	0.0591(16)	0.0503(15)	0.0426(14)	–0.0097(12)	–0.0191(13)	0.0170(13)
B	0.038(3)	0.030(3)	0.023(2)	–0.003(2)	–0.004(2)	0.012(2)
C(1)	0.034(2)	0.032(2)	0.027(2)	0.0027(19)	0.0073(19)	0.0175(19)
C(2)	0.046(3)	0.042(3)	0.051(3)	0.000(2)	0.012(2)	0.029(2)
C(3)	0.064(3)	0.046(3)	0.064(3)	–0.010(3)	0.017(3)	0.031(3)
C(4)	0.051(3)	0.044(3)	0.041(3)	–0.008(2)	0.010(2)	0.021(2)
C(5)	0.075(4)	0.038(3)	0.057(3)	–0.019(2)	0.006(3)	0.019(3)
C(6)	0.050(3)	0.050(3)	0.049(3)	–0.012(2)	0.001(3)	0.002(3)
C(7)	0.043(3)	0.043(3)	0.038(2)	0.002(2)	0.005(2)	0.010(2)
C(8)	0.033(2)	0.032(2)	0.030(2)	0.0025(18)	0.0043(19)	0.0062(19)
C(9)	0.038(2)	0.031(2)	0.021(2)	0.0039(17)	0.0097(18)	0.0129(19)
C(10)	0.027(2)	0.031(2)	0.0204(19)	0.0044(17)	0.0103(17)	0.0121(18)
C(11)	0.0233(19)	0.032(2)	0.0142(18)	0.0029(16)	0.0072(16)	0.0120(17)
C(12)	0.0197(19)	0.033(2)	0.0183(18)	0.0027(16)	0.0057(15)	0.0132(17)
C(13)	0.0215(19)	0.032(2)	0.0204(19)	0.0027(16)	0.0080(16)	0.0139(17)
C(14)	0.0196(19)	0.032(2)	0.025(2)	0.0015(17)	0.0040(16)	0.0111(17)
C(15)	0.029(2)	0.031(2)	0.032(2)	0.0049(19)	0.0072(18)	0.0167(18)
C(16)	0.035(2)	0.029(2)	0.036(2)	0.0008(19)	0.010(2)	0.0133(19)
C(17)	0.028(2)	0.035(2)	0.030(2)	–0.0050(19)	0.0030(18)	0.0114(19)
C(18)	0.0220(19)	0.035(2)	0.022(2)	–0.0006(17)	0.0042(16)	0.0124(17)
C(19)	0.021(2)	0.042(2)	0.020(2)	0.0032(18)	0.0015(16)	0.0111(18)
C(20)	0.023(2)	0.043(2)	0.032(2)	0.007(2)	0.0042(18)	0.0188(19)
C(21)	0.025(2)	0.027(2)	0.027(2)	0.0043(17)	0.0077(17)	0.0137(17)
C(22)	0.0192(18)	0.0234(19)	0.0222(19)	–0.0011(16)	–0.0004(16)	0.0091(16)
C(23)	0.025(2)	0.027(2)	0.023(2)	–0.0021(17)	0.0024(16)	0.0104(17)
C(24)	0.029(2)	0.025(2)	0.0186(19)	0.0008(16)	–0.0012(17)	0.0078(17)
C(25)	0.026(2)	0.026(2)	0.027(2)	–0.0032(17)	–0.0076(17)	0.0102(17)
C(26)	0.0209(19)	0.029(2)	0.027(2)	–0.0041(17)	0.0023(16)	0.0099(17)
C(27)	0.026(2)	0.033(2)	0.0209(19)	–0.0020(17)	–0.0005(17)	0.0121(18)

Table 5. Hydrogen coordinates and isotropic displacement parameters ($Å^2$) for acb177.

	x	y	z	U
H(2A)	0.5300	0.1752	–0.0692	0.052
H(3A)	0.5807	0.2268	0.0882	0.068
H(5A)	0.6537	0.2630	0.1970	0.073
H(6A)	0.7199	0.2671	0.2363	0.072
H(7A)	0.7312	0.2119	0.1478	0.055
H(8A)	0.6760	0.1513	0.0369	0.043
H(14A)	0.5743	0.0040	0.0257	0.031
H(15A)	0.5546	–0.0673	–0.0237	0.036
H(16A)	0.5073	–0.1051	–0.2183	0.042
H(17A)	0.4753	–0.0728	–0.3491	0.039
H(19A)	0.4648	–0.0119	–0.3996	0.036
H(20A)	0.4765	0.0561	–0.3438	0.038
H(23A)	0.6057	0.0862	0.2410	0.032
H(24A)	0.6577	0.0731	0.3473	0.032
H(26A)	0.6938	0.0552	–0.0586	0.032
H(27A)	0.6424	0.0696	–0.1658	0.034

Table 6. Torsion angles [°] for acb177.

C(21)–O–C(1)–C(2)	−170.5(3)	C(21)–O–C(1)–C(10)	7.7(5)
O–C(1)–C(2)–C(3)	−178.8(3)	C(10)–C(1)–C(2)–C(3)	3.1(6)
C(1)–C(2)–C(3)–C(4)	6.9(6)	C(2)–C(3)–C(4)–C(5)	170.5(4)
C(2)–C(3)–C(4)–C(9)	−5.2(7)	C(3)–C(4)–C(5)–C(6)	−172.1(4)
C(9)–C(4)–C(5)–C(6)	3.6(7)	C(4)–C(5)–C(6)–C(7)	0.8(7)
C(5)–C(6)–C(7)–C(8)	−2.8(7)	C(6)–C(7)–C(8)–C(9)	0.2(6)
C(7)–C(8)–C(9)–C(4)	4.0(5)	C(7)–C(8)–C(9)–C(10)	179.7(3)
C(3)–C(4)–C(9)–C(8)	169.9(4)	C(3)–C(4)–C(9)–C(10)	−6.2(6)
C(5)–C(4)–C(9)–C(8)	−5.8(6)	C(5)–C(4)–C(9)–C(10)	178.1(4)
O–C(1)–C(10)–C(9)	168.1(3)	O–C(1)–C(10)–C(11)	−13.5(5)
C(2)–C(1)–C(10)–C(9)	−14.0(5)	C(2)–C(1)–C(10)–C(11)	164.5(3)
C(4)–C(9)–C(10)–C(1)	14.8(5)	C(4)–C(9)–C(10)–C(11)	−163.4(3)
C(8)–C(9)–C(10)–C(1)	−160.8(3)	C(8)–C(9)–C(10)–C(11)	20.9(6)
C(1)–C(10)–C(11)–C(12)	6.1(5)	C(1)–C(10)–C(11)–C(22)	−173.4(3)
C(9)–C(10)–C(11)–C(12)	−175.6(3)	C(9)–C(10)–C(11)–C(22)	4.9(5)
C(10)–C(11)–C(12)–C(13)	−175.7(3)	C(10)–C(11)–C(12)–C(21)	6.6(5)
C(22)–C(11)–C(12)–C(13)	3.8(5)	C(22)–C(11)–C(12)–C(21)	−173.9(3)
C(11)–C(12)–C(13)–C(14)	16.4(5)	C(11)–C(12)–C(13)–C(18)	−167.2(3)
C(21)–C(12)–C(13)–C(14)	−165.8(3)	C(21)–C(12)–C(13)–C(18)	10.5(4)
C(12)–C(13)–C(14)–C(15)	−178.1(3)	C(18)–C(13)–C(14)–C(15)	5.5(5)
C(13)–C(14)–C(15)–C(16)	−1.0(5)	C(14)–C(15)–C(16)–C(17)	−3.3(5)
C(15)–C(16)–C(17)–C(18)	2.8(5)	C(16)–C(17)–C(18)–C(13)	2.0(5)
C(16)–C(17)–C(18)–C(19)	−175.8(3)	C(12)–C(13)–C(18)–C(17)	177.3(3)
C(12)–C(13)–C(18)–C(19)	−4.8(5)	C(14)–C(13)–C(18)–C(17)	−6.0(5)
C(14)–C(13)–C(18)–C(19)	171.8(3)	C(13)–C(18)–C(19)–C(20)	−2.5(5)
C(17)–C(18)–C(19)–C(20)	175.3(3)	C(18)–C(19)–C(20)–C(21)	3.6(5)
C(1)–O–C(21)–C(12)	6.1(5)	C(1)–O–C(21)–C(20)	−174.7(3)
C(19)–C(20)–C(21)–O	−176.1(3)	C(19)–C(20)–C(21)–C(12)	3.1(5)
C(11)–C(12)–C(21)–O	−12.9(5)	C(11)–C(12)–C(21)–C(20)	167.9(3)
C(13)–C(12)–C(21)–O	169.1(3)	C(13)–C(12)–C(21)–C(20)	−10.1(5)
C(10)–C(11)–C(22)–C(23)	64.4(4)	C(10)–C(11)–C(22)–C(27)	−114.7(4)
C(12)–C(11)–C(22)–C(23)	−115.2(4)	C(12)–C(11)–C(22)–C(27)	65.8(4)
C(11)–C(22)–C(23)–C(24)	−178.4(3)	C(27)–C(22)–C(23)–C(24)	0.6(5)
C(22)–C(23)–C(24)–C(25)	−0.7(5)	C(23)–C(24)–C(25)–Br	178.9(2)
C(23)–C(24)–C(25)–C(26)	0.2(5)	Br–C(25)–C(26)–C(27)	−178.3(3)
C(24)–C(25)–C(26)–C(27)	0.4(5)	C(25)–C(26)–C(27)–C(22)	−0.5(5)
C(11)–C(22)–C(27)–C(26)	179.0(3)	C(23)–C(22)–C(27)–C(26)	0.0(5)

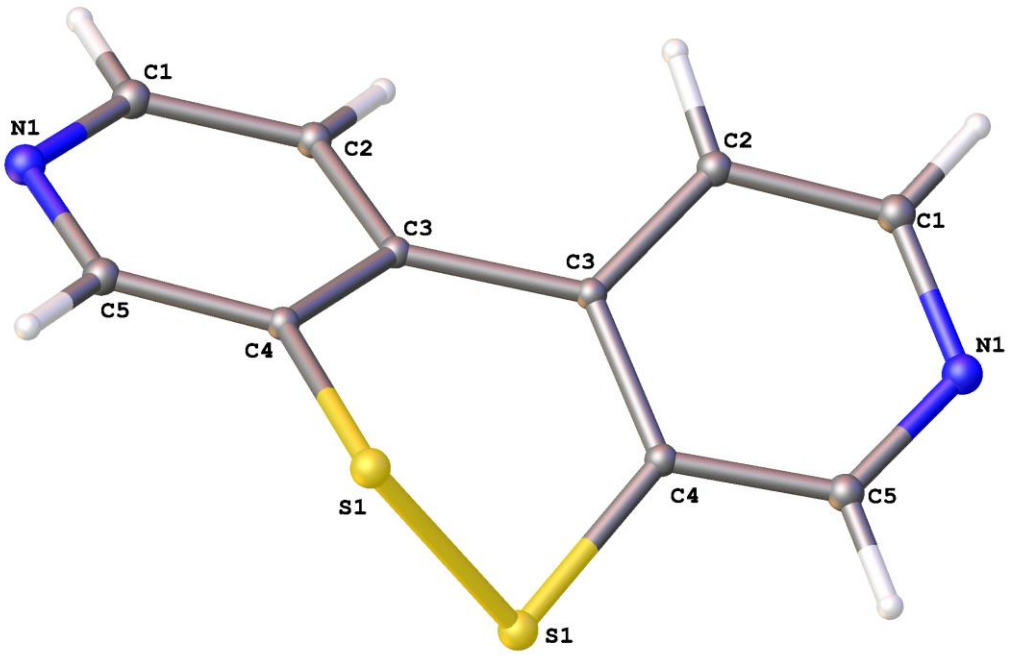
C1
N1
C2
C3
C5
C4
S1
S1
C4
C3
C2
C1
N1
C5

Table 1. Crystal data and structure refinement for **BPy6**.

Identification code	**BPy6**	
Chemical formula (moiety)	$C_{10}H_6N_2S_2$	
Chemical formula (total)	$C_{10}H_6N_2S_2$	
Formula weight	218.29	
Temperature	150(2) K	
Radiation, wavelength	MoKα, 0.71073 Å	
Crystal system, space group	monoclinic, C12/c1	
Unit cell parameters	a = 12.3446(6) Å	α = 90°
	b = 7.2892(3) Å	β = 105.901(5)°
	c = 10.3201(5) Å	γ = 90°
Cell volume	893.09(7) $Å^3$	
Z	4	
Calculated density	1.623 g/cm^3	
Absorption coefficient μ	0.547 mm^{-1}	
F(000)	448	
Crystal colour and size	yellow, 0.32 × 0.10 × 0.10 mm^3	
Reflections for cell refinement	1676 (θ range 3.0 to 28.3°)	
Data collection method	Xcalibur, Atlas, Gemini ultra thick-slice ω scans	
θ range for data collection	3.3 to 28.3°	
Index ranges	h –16 to 16, k –9 to 7, l –10 to 13	
Completeness to θ = 26.0°	97.7 %	
Reflections collected	2095	
Independent reflections	928 (R_{int} = 0.0130)	
Reflections with $F^2>2\sigma$	842	
Absorption correction	semi-empirical from equivalents	
Min. and max. transmission	0.8443 and 0.9473	
Structure solution	direct methods	
Refinement method	Full-matrix least-squares on F^2	
Weighting parameters a, b	0.0334, 0.7770	
Data / restraints / parameters	928 / 0 / 64	
Final R indices [$F^2>2\sigma$]	R1 = 0.0247, wR2 = 0.0655	
R indices (all data)	R1 = 0.0277, wR2 = 0.0662	
Goodness-of-fit on F^2	1.083	
Largest and mean shift/su	0.001 and 0.000	
Largest diff. peak and hole	0.34 and –0.23 e $Å^{-3}$	

Table 2. Atomic coordinates and equivalent isotropic displacement parameters ($Å^2$) for acb99. U_{eq} is defined as one third of the trace of the orthogonalized U^{ij} tensor.

	x	y	z	U_{eq}
S(1)	0.50663(3)	0.11705(5)	0.85148(4)	0.02276(15)
N(1)	0.29633(11)	0.48480(19)	0.93684(12)	0.0233(3)
C(1)	0.31706(12)	0.6332(2)	0.87120(15)	0.0218(3)
C(2)	0.39451(12)	0.6361(2)	0.79584(15)	0.0182(3)
C(3)	0.45672(11)	0.4801(2)	0.78781(13)	0.0146(3)
C(4)	0.43332(11)	0.3241(2)	0.85441(14)	0.0157(3)
C(5)	0.35334(12)	0.3334(2)	0.92640(14)	0.0201(3)

Table 3. Bond lengths [Å] and angles [°] for acb99.

S(1)–S(1A)	2.0557(7)	S(1)–C(4)	1.7643(15)
N(1)–C(1)	1.338(2)	N(1)–C(5)	1.329(2)
C(1)–H(1A)	0.950	C(1)–C(2)	1.388(2)
C(2)–H(2A)	0.950	C(2)–C(3)	1.388(2)
C(3)–C(3A)	1.486(3)	C(3)–C(4)	1.399(2)
C(4)–C(5)	1.3904(19)	C(5)–H(5A)	0.950

S(1A)–S(1)–C(4)	96.86(5)	C(1)–N(1)–C(5)	116.83(12)
N(1)–C(1)–H(1A)	118.2	N(1)–C(1)–C(2)	123.56(14)
H(1A)–C(1)–C(2)	118.2	C(1)–C(2)–H(2A)	120.1
C(1)–C(2)–C(3)	119.88(14)	H(2A)–C(2)–C(3)	120.1
C(2)–C(3)–C(3A)	121.38(9)	C(2)–C(3)–C(4)	116.41(12)
C(3A)–C(3)–C(4)	122.21(9)	S(1)–C(4)–C(3)	120.72(10)
S(1)–C(4)–C(5)	119.57(11)	C(3)–C(4)–C(5)	119.69(13)
N(1)–C(5)–C(4)	123.58(14)	N(1)–C(5)–H(5A)	118.2
C(4)–C(5)–H(5A)	118.2		

Symmetry operations for equivalent atoms
A –x+1,y,–z+3/2

Table 4. Anisotropic displacement parameters ($Å^2$) for acb99. The anisotropic displacement factor exponent takes the form: $-2\pi^2[h^2a^{*2}U^{11} + ...+ 2hka^*b^*U^{12}]$

	U^{11}	U^{22}	U^{33}	U^{23}	U^{13}	U^{12}
S(1)	0.0342(2)	0.0163(2)	0.0229(2)	0.00458(15)	0.01658(16)	0.00532(16)
N(1)	0.0176(6)	0.0343(8)	0.0200(6)	0.0010(6)	0.0084(5)	0.0042(6)
C(1)	0.0169(7)	0.0269(8)	0.0216(7)	–0.0015(6)	0.0055(6)	0.0064(6)
C(2)	0.0180(7)	0.0182(7)	0.0185(7)	0.0000(6)	0.0050(6)	0.0012(6)
C(3)	0.0126(6)	0.0179(7)	0.0127(6)	–0.0026(5)	0.0022(5)	–0.0020(5)
C(4)	0.0156(6)	0.0173(7)	0.0142(6)	–0.0011(5)	0.0040(5)	0.0003(6)
C(5)	0.0183(7)	0.0265(8)	0.0172(7)	0.0027(6)	0.0074(6)	–0.0009(6)

Table 5. Hydrogen coordinates and isotropic displacement parameters ($Å^2$) for acb99.

	x	y	z	U
H(1A)	0.2766	0.7425	0.8764	0.026
H(2A)	0.4049	0.7448	0.7498	0.022
H(5A)	0.3386	0.2257	0.9705	0.024

Table 6. Torsion angles [°] for acb99.

C(5)–N(1)–C(1)–C(2)	−0.7(2)	N(1)–C(1)–C(2)–C(3)	−1.2(2)
C(1)–C(2)–C(3)–C(3A)	−177.78(15)	C(1)–C(2)–C(3)–C(4)	2.3(2)
C(2)–C(3)–C(4)–S(1)	179.92(10)	C(2)–C(3)–C(4)–C(5)	−1.6(2)
C(3A)–C(3)–C(4)–S(1)	0.0(2)	C(3A)–C(3)–C(4)–C(5)	178.42(15)
S(1A)–S(1)–C(4)–C(3)	−46.08(12)	S(1A)–S(1)–C(4)–C(5)	135.46(11)
C(1)–N(1)–C(5)–C(4)	1.4(2)	S(1)–C(4)–C(5)–N(1)	178.24(11)
C(3)–C(4)–C(5)–N(1)	−0.2(2)		

Symmetry operations for equivalent atoms
A −x+1,y,−z+3/2

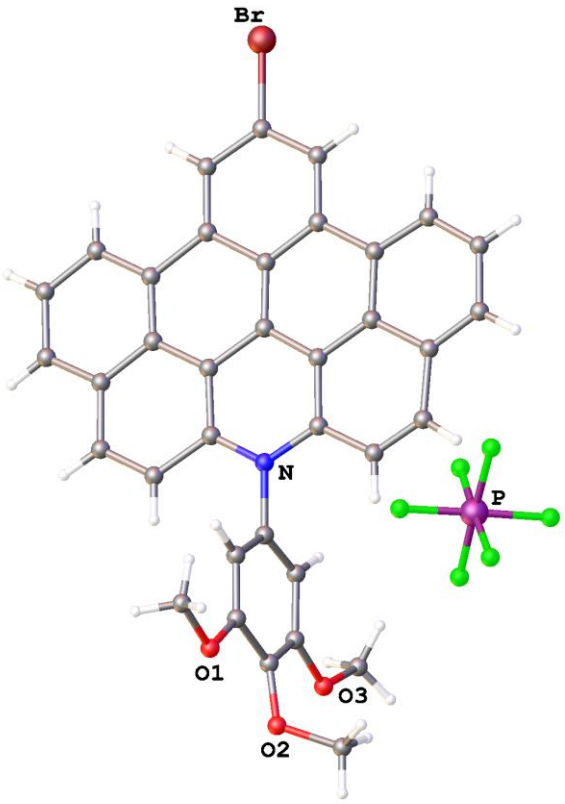
Br
N
P
O1
O3
O2

Table 1. Crystal data and structure refinement for **CAC**.

Identification code	**CAC**	
Chemical formula (moiety)	$C_{36}H_{23}BrNO_3^+ \cdot PF_6^- \cdot 2H_2O$	
Chemical formula (total)	$C_{36}H_{27}BrF_6NO_5P$	
Formula weight	778.47	
Temperature	150(2) K	
Radiation, wavelength	synchrotron, 0.68890 Å	
Crystal system, space group	triclinic, $p\bar{1}$	
Unit cell parameters	a = 9.074(9) Å	α = 81.276(10)°
	b = 11.340(12) Å	β = 84.685(11)°
	c = 17.023(18) Å	γ = 67.049(11)°
Cell volume	1593(3) $Å^3$	
Z	2	
Calculated density	1.623 g/cm^3	
Absorption coefficient μ	1.322 mm^{-1}	
F(000)	788	
Crystal colour and size	red, 0.40 × 0.10 × 0.10 mm^3	
Reflections for cell refinement	4552 (θ range 2.3 to 24.5°)	
Data collection method	Crystal Logic diffractometer and Rigaku Saturn 724+ CCD thick-slice ω scans	
θ range for data collection	1.2 to 24.2°	
Index ranges	h −9 to 10, k −12 to 13, l −20 to 20	
Completeness to θ = 24.2°	95.3 %	
Reflections collected	10201	
Independent reflections	5373 (R_{int} = 0.0815)	
Reflections with $F^2>2\sigma$	3908	
Absorption correction	semi-empirical from equivalents	
Min. and max. transmission	0.6198 and 0.8791	
Structure solution	direct methods	
Refinement method	Full-matrix least-squares on F^2	
Weighting parameters a, b	0.2000, 0.0000	
Data / restraints / parameters	5373 / 0 / 437	
Final R indices [$F^2>2\sigma$]	R1 = 0.2252, wR2 = 0.5015	
R indices (all data)	R1 = 0.2541, wR2 = 0.5214	
Goodness-of-fit on F^2	2.090	
Extinction coefficient	7.4(8)	
Largest and mean shift/su	0.294 and 0.023	
Largest diff. peak and hole	3.78 and −1.41 e $Å^{-3}$	

Table 2. Atomic coordinates and equivalent isotropic displacement parameters ($Å^2$) for acb12. U_{eq} is defined as one third of the trace of the orthogonalized U^{ij} tensor.

	x	y	z	U_{eq}
Br	–0.2215(2)	1.55444(19)	–0.79933(11)	0.0920(14)
P	–0.2742(5)	0.9490(4)	–0.2435(3)	0.0832(16)
F(1)	–0.1569(13)	0.9348(13)	–0.1713(8)	0.118(4)
F(2)	–0.1937(16)	0.7906(8)	–0.2413(7)	0.112(4)
F(3)	–0.3881(15)	0.9589(14)	–0.3150(7)	0.120(4)
F(4)	–0.3552(16)	1.1027(9)	–0.2443(7)	0.116(4)
F(5)	–0.1353(13)	0.9597(10)	–0.3095(8)	0.107(3)
F(6)	–0.4050(16)	0.9352(13)	–0.1765(9)	0.126(4)
N	–0.2734(12)	1.4533(11)	–0.2621(7)	0.067(3)
O(1)	–0.2024(15)	1.5658(12)	–0.0001(9)	0.096(4)
O(2)	–0.2856(17)	1.3700(13)	0.0729(9)	0.100(4)
O(3)	–0.3965(15)	1.2369(11)	–0.0047(8)	0.092(3)
C(1)	–0.2323(13)	1.5347(12)	–0.6862(9)	0.062(3)
C(2)	–0.3684(13)	1.6194(10)	–0.6455(9)	0.058(3)
C(3)	–0.3771(11)	1.6036(9)	–0.5626(9)	0.056(3)
C(4)	–0.5197(12)	1.6890(10)	–0.5147(8)	0.052(3)
C(5)	–0.6503(13)	1.7859(13)	–0.5558(9)	0.066(3)
C(6)	–0.7835(13)	1.8629(10)	–0.5117(11)	0.068(4)
C(7)	–0.7889(13)	1.8455(11)	–0.4280(10)	0.064(3)
C(8)	–0.6551(12)	1.7493(9)	–0.3875(8)	0.054(3)
C(9)	–0.6591(13)	1.7359(10)	–0.3017(9)	0.063(3)
C(10)	–0.5343(14)	1.6395(10)	–0.2603(8)	0.059(3)
C(11)	–0.3938(14)	1.5512(10)	–0.3035(9)	0.060(3)
C(12)	–0.1411(14)	1.3694(14)	–0.3011(9)	0.067(3)
C(13)	–0.0112(16)	1.2690(13)	–0.2588(10)	0.068(3)
C(14)	0.1192(14)	1.1957(13)	–0.2932(12)	0.079(4)
C(15)	0.1415(14)	1.2014(10)	–0.3825(10)	0.065(4)
C(16)	0.2723(15)	1.1256(10)	–0.4220(10)	0.068(4)
C(17)	0.2819(17)	1.1417(12)	–0.5055(12)	0.078(4)
C(18)	0.1657(16)	1.2344(11)	–0.5486(10)	0.066(3)
C(19)	0.0234(13)	1.3160(10)	–0.5140(7)	0.052(3)
C(20)	–0.1091(12)	1.4181(10)	–0.5591(8)	0.055(3)
C(21)	–0.1014(14)	1.4341(12)	–0.6441(10)	0.063(4)
C(22)	–0.5222(12)	1.6705(9)	–0.4319(9)	0.058(3)
C(23)	–0.3887(13)	1.5712(10)	–0.3892(8)	0.053(3)
C(24)	–0.1296(13)	1.3872(10)	–0.3875(7)	0.052(3)
C(25)	0.0072(11)	1.3053(10)	–0.4278(8)	0.055(3)
C(26)	–0.2411(11)	1.4974(9)	–0.5160(8)	0.053(3)
C(27)	–0.2549(12)	1.4842(10)	–0.4331(9)	0.055(3)
C(28)	–0.2861(14)	1.4360(12)	–0.1704(9)	0.066(3)
C(29)	–0.2382(14)	1.5127(13)	–0.1310(10)	0.075(4)
C(30)	–0.2437(13)	1.4977(12)	–0.0502(8)	0.058(3)
C(31)	–0.2976(19)	1.3974(15)	–0.0077(10)	0.079(4)
C(32)	–0.3443(16)	1.3280(16)	–0.0507(10)	0.078(4)
C(33)	–0.3322(16)	1.3413(12)	–0.1342(10)	0.072(4)
C(34)	–0.144(2)	1.6572(19)	–0.0431(14)	0.100(6)
C(35)	–0.178(4)	1.242(2)	0.1028(18)	0.132(9)

C(36)	–0.437(3)	1.148(2)	–0.0434(14)	0.114(7)

Table 3. Bond lengths [Å] and angles [°] for acb12.

Br–C(1)	1.902(15)	P–F(1)	1.649(12)
P–F(2)	1.650(9)	P–F(3)	1.632(14)
P–F(4)	1.604(10)	P–F(5)	1.638(12)
P–F(6)	1.604(14)	N–C(11)	1.372(16)
N–C(12)	1.393(18)	N–C(28)	1.54(2)
O(1)–C(30)	1.396(19)	O(1)–C(34)	1.42(2)
O(2)–C(31)	1.37(2)	O(2)–C(35)	1.44(3)
O(3)–C(32)	1.405(18)	O(3)–C(36)	1.46(2)
C(1)–C(2)	1.430(18)	C(1)–C(21)	1.44(2)
C(2)–H(2A)	0.950	C(2)–C(3)	1.39(2)
C(3)–C(4)	1.531(15)	C(3)–C(26)	1.528(15)
C(4)–C(5)	1.417(17)	C(4)–C(22)	1.392(19)
C(5)–H(5A)	0.950	C(5)–C(6)	1.412(19)
C(6)–H(6A)	0.950	C(6)–C(7)	1.41(2)
C(7)–H(7A)	0.950	C(7)–C(8)	1.426(17)
C(8)–C(9)	1.44(2)	C(8)–C(22)	1.422(15)
C(9)–H(9A)	0.950	C(9)–C(10)	1.387(17)
C(10)–H(10A)	0.950	C(10)–C(11)	1.491(16)
C(11)–C(23)	1.441(19)	C(12)–C(13)	1.438(19)
C(12)–C(24)	1.45(2)	C(13)–H(13A)	0.950
C(13)–C(14)	1.30(2)	C(14)–H(14A)	0.950
C(14)–C(15)	1.51(2)	C(15)–C(16)	1.353(19)
C(15)–C(25)	1.499(16)	C(16)–H(16A)	0.950
C(16)–C(17)	1.40(2)	C(17)–H(17A)	0.950
C(17)–C(18)	1.34(2)	C(18)–H(18A)	0.950
C(18)–C(19)	1.401(18)	C(19)–C(20)	1.481(15)
C(19)–C(25)	1.452(19)	C(20)–C(21)	1.43(2)
C(20)–C(26)	1.407(17)	C(21)–H(21A)	0.950
C(22)–C(23)	1.455(17)	C(23)–C(27)	1.460(16)
C(24)–C(25)	1.418(16)	C(24)–C(27)	1.426(16)
C(26)–C(27)	1.396(19)	C(28)–C(29)	1.39(2)
C(28)–C(33)	1.35(2)	C(29)–H(29A)	0.950
C(29)–C(30)	1.36(2)	C(30)–C(31)	1.48(2)
C(31)–C(32)	1.35(2)	C(32)–C(33)	1.41(2)
C(33)–H(33A)	0.950	C(34)–H(34A)	0.980
C(34)–H(34B)	0.980	C(34)–H(34C)	0.980
C(35)–H(35A)	0.980	C(35)–H(35B)	0.980
C(35)–H(35C)	0.980	C(36)–H(36A)	0.980
C(36)–H(36B)	0.980	C(36)–H(36C)	0.980

F(1)–P–F(2)	88.5(7)	F(1)–P–F(3)	178.5(7)
F(1)–P–F(4)	91.5(7)	F(1)–P–F(5)	90.1(7)
F(1)–P–F(6)	88.0(8)	F(2)–P–F(3)	90.0(7)
F(2)–P–F(4)	178.8(8)	F(2)–P–F(5)	89.0(6)
F(2)–P–F(6)	89.9(7)	F(3)–P–F(4)	90.0(7)
F(3)–P–F(5)	89.8(7)	F(3)–P–F(6)	92.1(8)
F(4)–P–F(5)	92.2(7)	F(4)–P–F(6)	88.9(7)
F(5)–P–F(6)	177.8(7)	C(11)–N–C(12)	121.4(12)
C(11)–N–C(28)	119.0(11)	C(12)–N–C(28)	119.6(10)
C(30)–O(1)–C(34)	112.2(14)	C(31)–O(2)–C(35)	116.5(16)
C(32)–O(3)–C(36)	120.0(15)	Br–C(1)–C(2)	119.5(9)
Br–C(1)–C(21)	118.5(9)	C(2)–C(1)–C(21)	122.0(13)
C(1)–C(2)–H(2A)	120.3	C(1)–C(2)–C(3)	119.4(11)

H(2A)–C(2)–C(3)	120.3	C(2)–C(3)–C(4)	122.6(10)
C(2)–C(3)–C(26)	120.0(10)	C(4)–C(3)–C(26)	117.4(11)
C(3)–C(4)–C(5)	119.0(12)	C(3)–C(4)–C(22)	120.5(10)
C(5)–C(4)–C(22)	120.4(10)	C(4)–C(5)–H(5A)	120.5
C(4)–C(5)–C(6)	119.1(13)	H(5A)–C(5)–C(6)	120.4
C(5)–C(6)–H(6A)	119.3	C(5)–C(6)–C(7)	121.5(11)
H(6A)–C(6)–C(7)	119.3	C(6)–C(7)–H(7A)	120.6
C(6)–C(7)–C(8)	118.8(10)	H(7A)–C(7)–C(8)	120.6
C(7)–C(8)–C(9)	118.3(10)	C(7)–C(8)–C(22)	119.7(13)
C(9)–C(8)–C(22)	122.0(10)	C(8)–C(9)–H(9A)	120.1
C(8)–C(9)–C(10)	119.8(9)	H(9A)–C(9)–C(10)	120.1
C(9)–C(10)–H(10A)	119.6	C(9)–C(10)–C(11)	120.7(12)
H(10A)–C(10)–C(11)	119.6	N–C(11)–C(10)	120.3(12)
N–C(11)–C(23)	121.3(10)	C(10)–C(11)–C(23)	118.3(10)
N–C(12)–C(13)	122.2(13)	N–C(12)–C(24)	119.2(11)
C(13)–C(12)–C(24)	118.5(12)	C(12)–C(13)–H(13A)	118.1
C(12)–C(13)–C(14)	123.8(15)	H(13A)–C(13)–C(14)	118.1
C(13)–C(14)–H(14A)	118.8	C(13)–C(14)–C(15)	122.3(13)
H(14A)–C(14)–C(15)	118.8	C(14)–C(15)–C(16)	125.3(12)
C(14)–C(15)–C(25)	114.6(11)	C(16)–C(15)–C(25)	120.0(14)
C(15)–C(16)–H(16A)	119.8	C(15)–C(16)–C(17)	120.4(12)
H(16A)–C(16)–C(17)	119.8	C(16)–C(17)–H(17A)	119.2
C(16)–C(17)–C(18)	121.7(13)	H(17A)–C(17)–C(18)	119.2
C(17)–C(18)–H(18A)	118.7	C(17)–C(18)–C(19)	122.6(15)
H(18A)–C(18)–C(19)	118.7	C(18)–C(19)–C(20)	124.5(12)
C(18)–C(19)–C(25)	118.2(11)	C(20)–C(19)–C(25)	117.1(10)
C(19)–C(20)–C(21)	120.2(11)	C(19)–C(20)–C(26)	118.2(11)
C(21)–C(20)–C(26)	121.6(10)	C(1)–C(21)–C(20)	118.8(10)
C(1)–C(21)–H(21A)	120.6	C(20)–C(21)–H(21A)	120.6
C(4)–C(22)–C(8)	120.5(10)	C(4)–C(22)–C(23)	120.9(9)
C(8)–C(22)–C(23)	118.6(12)	C(11)–C(23)–C(22)	120.4(10)
C(11)–C(23)–C(27)	119.6(10)	C(22)–C(23)–C(27)	119.8(11)
C(12)–C(24)–C(25)	119.7(10)	C(12)–C(24)–C(27)	121.4(11)
C(25)–C(24)–C(27)	118.9(12)	C(15)–C(25)–C(19)	116.8(10)
C(15)–C(25)–C(24)	120.9(12)	C(19)–C(25)–C(24)	122.3(10)
C(3)–C(26)–C(20)	118.1(11)	C(3)–C(26)–C(27)	118.2(10)
C(20)–C(26)–C(27)	123.6(9)	C(23)–C(27)–C(24)	116.9(12)
C(23)–C(27)–C(26)	123.0(10)	C(24)–C(27)–C(26)	119.9(10)
N–C(28)–C(29)	117.8(12)	N–C(28)–C(33)	117.6(13)
C(29)–C(28)–C(33)	124.4(15)	C(28)–C(29)–H(29A)	120.3
C(28)–C(29)–C(30)	119.4(12)	H(29A)–C(29)–C(30)	120.3
O(1)–C(30)–C(29)	128.0(12)	O(1)–C(30)–C(31)	113.9(12)
C(29)–C(30)–C(31)	118.1(12)	O(2)–C(31)–C(30)	119.0(13)
O(2)–C(31)–C(32)	122.0(15)	C(30)–C(31)–C(32)	118.7(14)
O(3)–C(32)–C(31)	114.2(15)	O(3)–C(32)–C(33)	123.3(16)
C(31)–C(32)–C(33)	122.4(14)	C(28)–C(33)–C(32)	116.7(14)
C(28)–C(33)–H(33A)	121.7	C(32)–C(33)–H(33A)	121.7
O(1)–C(34)–H(34A)	109.5	O(1)–C(34)–H(34B)	109.5
O(1)–C(34)–H(34C)	109.5	H(34A)–C(34)–H(34B)	109.5
H(34A)–C(34)–H(34C)	109.5	H(34B)–C(34)–H(34C)	109.5
O(2)–C(35)–H(35A)	109.5	O(2)–C(35)–H(35B)	109.5
O(2)–C(35)–H(35C)	109.5	H(35A)–C(35)–H(35B)	109.5
H(35A)–C(35)–H(35C)	109.5	H(35B)–C(35)–H(35C)	109.5
O(3)–C(36)–H(36A)	109.5	O(3)–C(36)–H(36B)	109.5
O(3)–C(36)–H(36C)	109.5	H(36A)–C(36)–H(36B)	109.5

H(36A)–C(36)–H(36C)	109.5	H(36B)–C(36)–H(36C)	109.5

Table 4. Anisotropic displacement parameters ($Å^2$) for acb12. The anisotropic displacement factor exponent takes the form: $-2\pi^2[h^2a^{*2}U^{11} + ...+ 2hka^*b^*U^{12}]$

	U^{11}	U^{22}	U^{33}	U^{23}	U^{13}	U^{12}
Br	0.0976(17)	0.1161(18)	0.0739(17)	0.0062(9)	–0.0118(9)	–0.0579(11)
P	0.082(3)	0.070(2)	0.079(3)	0.0054(17)	–0.019(2)	–0.0098(17)
F(1)	0.101(7)	0.138(9)	0.097(8)	–0.006(7)	–0.043(6)	–0.021(6)
F(2)	0.165(10)	0.059(4)	0.093(8)	0.000(4)	–0.017(7)	–0.022(5)
F(3)	0.116(8)	0.158(11)	0.077(7)	–0.001(7)	–0.018(6)	–0.043(7)
F(4)	0.151(9)	0.075(5)	0.092(8)	–0.007(5)	–0.033(7)	–0.006(5)
F(5)	0.112(7)	0.097(6)	0.110(9)	–0.024(6)	0.014(6)	–0.037(5)
F(6)	0.115(8)	0.116(8)	0.129(11)	0.013(7)	–0.002(8)	–0.037(6)
N	0.059(6)	0.084(7)	0.063(7)	0.010(5)	–0.022(5)	–0.037(5)
O(1)	0.092(7)	0.100(7)	0.091(9)	–0.006(6)	–0.007(6)	–0.033(6)
O(2)	0.128(10)	0.110(8)	0.085(9)	–0.001(7)	0.000(7)	–0.074(8)
O(3)	0.116(8)	0.081(6)	0.086(8)	0.023(5)	–0.021(7)	–0.055(6)
C(1)	0.044(5)	0.064(6)	0.076(9)	0.007(5)	–0.008(5)	–0.024(5)
C(2)	0.054(6)	0.046(5)	0.074(9)	0.007(5)	–0.010(6)	–0.022(4)
C(3)	0.035(5)	0.044(5)	0.089(10)	–0.001(5)	–0.010(5)	–0.016(4)
C(4)	0.042(5)	0.054(5)	0.061(8)	–0.002(5)	–0.007(5)	–0.020(4)
C(5)	0.039(5)	0.081(7)	0.069(9)	0.005(6)	–0.006(5)	–0.017(5)
C(6)	0.040(5)	0.040(5)	0.120(14)	–0.009(6)	–0.018(6)	–0.008(4)
C(7)	0.042(5)	0.055(6)	0.090(11)	–0.008(6)	–0.004(6)	–0.014(4)
C(8)	0.035(5)	0.041(5)	0.084(9)	–0.001(5)	–0.011(5)	–0.014(4)
C(9)	0.042(5)	0.044(5)	0.084(10)	–0.001(5)	–0.001(5)	0.001(4)
C(10)	0.059(6)	0.053(6)	0.059(8)	–0.007(5)	–0.009(5)	–0.014(5)
C(11)	0.059(6)	0.048(5)	0.069(9)	0.003(5)	–0.001(6)	–0.021(5)
C(12)	0.049(6)	0.090(8)	0.068(9)	–0.004(7)	–0.014(6)	–0.032(6)
C(13)	0.072(8)	0.070(7)	0.071(9)	–0.002(6)	–0.018(6)	–0.035(6)
C(14)	0.042(6)	0.071(7)	0.116(14)	0.005(7)	–0.022(7)	–0.014(5)
C(15)	0.056(6)	0.039(5)	0.099(11)	0.013(5)	–0.013(6)	–0.023(4)
C(16)	0.064(7)	0.038(5)	0.097(12)	–0.007(5)	–0.018(7)	–0.010(4)
C(17)	0.068(8)	0.053(6)	0.115(14)	–0.016(7)	0.006(8)	–0.025(6)
C(18)	0.072(7)	0.057(6)	0.074(9)	–0.004(6)	–0.014(6)	–0.026(5)
C(19)	0.052(6)	0.050(5)	0.054(7)	–0.002(4)	–0.008(5)	–0.022(4)
C(20)	0.050(6)	0.050(5)	0.070(8)	0.013(5)	–0.021(5)	–0.029(5)
C(21)	0.057(6)	0.065(6)	0.091(11)	–0.027(6)	0.012(6)	–0.045(5)
C(22)	0.040(5)	0.041(5)	0.092(10)	–0.018(5)	0.001(6)	–0.010(4)
C(23)	0.054(6)	0.052(5)	0.055(7)	–0.007(5)	–0.013(5)	–0.020(4)
C(24)	0.057(6)	0.047(5)	0.054(7)	0.000(4)	–0.016(5)	–0.021(4)
C(25)	0.031(5)	0.054(5)	0.080(9)	–0.010(5)	–0.006(5)	–0.015(4)
C(26)	0.038(5)	0.048(5)	0.072(9)	–0.001(5)	–0.018(5)	–0.015(4)
C(27)	0.045(5)	0.049(5)	0.077(9)	–0.005(5)	–0.018(5)	–0.020(4)
C(28)	0.057(6)	0.069(7)	0.070(9)	0.004(6)	–0.006(6)	–0.025(5)
C(29)	0.050(6)	0.080(8)	0.101(12)	0.018(7)	–0.022(7)	–0.038(6)
C(30)	0.053(6)	0.070(6)	0.055(8)	0.001(5)	–0.014(5)	–0.026(5)
C(31)	0.089(9)	0.086(9)	0.065(10)	–0.033(7)	–0.002(7)	–0.027(7)
C(32)	0.063(7)	0.099(9)	0.063(9)	0.015(7)	–0.003(6)	–0.030(7)
C(33)	0.071(7)	0.064(7)	0.075(10)	–0.002(6)	–0.017(7)	–0.019(6)
C(34)	0.091(10)	0.100(11)	0.124(17)	0.007(10)	–0.043(10)	–0.052(9)
C(35)	0.17(2)	0.090(12)	0.12(2)	0.010(12)	–0.008(17)	–0.043(13)

C(36)	0.162(19)	0.118(14)	0.101(15)	–0.049(12)	0.018(14)	–0.087(14)

Table 5. Hydrogen coordinates and isotropic displacement parameters ($Å^2$) for acb12.

	x	y	z	U
H(2A)	–0.4522	1.6859	–0.6747	0.070
H(5A)	–0.6484	1.7989	–0.6123	0.079
H(6A)	–0.8713	1.9279	–0.5391	0.082
H(7A)	–0.8801	1.8969	–0.3990	0.077
H(9A)	–0.7470	1.7930	–0.2737	0.075
H(10A)	–0.5383	1.6297	–0.2038	0.071
H(13A)	–0.0213	1.2554	–0.2024	0.082
H(14A)	0.2035	1.1364	–0.2610	0.095
H(16A)	0.3582	1.0611	–0.3931	0.082
H(17A)	0.3730	1.0855	–0.5322	0.094
H(18A)	0.1805	1.2452	–0.6048	0.080
H(21A)	–0.0116	1.3795	–0.6723	0.076
H(29A)	–0.2019	1.5752	–0.1602	0.090
H(33A)	–0.3553	1.2862	–0.1636	0.086
H(34A)	–0.2168	1.7444	–0.0336	0.150
H(34B)	–0.1380	1.6498	–0.1000	0.150
H(34C)	–0.0372	1.6403	–0.0253	0.150
H(35A)	–0.1876	1.2300	0.1610	0.198
H(35B)	–0.0674	1.2318	0.0863	0.198
H(35C)	–0.2046	1.1779	0.0814	0.198
H(36A)	–0.4242	1.0695	–0.0062	0.172
H(36B)	–0.3666	1.1244	–0.0904	0.172
H(36C)	–0.5489	1.1890	–0.0594	0.172

Table 6. Torsion angles [°] for acb12.

Br–C(1)–C(2)–C(3)	179.1(8)	C(21)–C(1)–C(2)–C(3)	–1.1(17)
C(1)–C(2)–C(3)–C(4)	–179.1(10)	C(1)–C(2)–C(3)–C(26)	0.6(16)
C(2)–C(3)–C(4)–C(5)	1.6(17)	C(2)–C(3)–C(4)–C(22)	–179.2(10)
C(26)–C(3)–C(4)–C(5)	–178.1(10)	C(26)–C(3)–C(4)–C(22)	1.0(15)
C(3)–C(4)–C(5)–C(6)	178.7(10)	C(22)–C(4)–C(5)–C(6)	–0.4(18)
C(4)–C(5)–C(6)–C(7)	0.1(19)	C(5)–C(6)–C(7)–C(8)	1.2(18)
C(6)–C(7)–C(8)–C(9)	177.4(10)	C(6)–C(7)–C(8)–C(22)	–2.1(16)
C(7)–C(8)–C(9)–C(10)	177.1(11)	C(22)–C(8)–C(9)–C(10)	–3.3(17)
C(8)–C(9)–C(10)–C(11)	1.4(18)	C(12)–N–C(11)–C(10)	179.9(11)
C(12)–N–C(11)–C(23)	0.1(18)	C(28)–N–C(11)–C(10)	0.2(17)
C(28)–N–C(11)–C(23)	–179.6(10)	C(9)–C(10)–C(11)–N	–177.8(12)
C(9)–C(10)–C(11)–C(23)	2.0(18)	C(11)–N–C(12)–C(13)	177.9(12)
C(11)–N–C(12)–C(24)	0.8(18)	C(28)–N–C(12)–C(13)	–2.4(19)
C(28)–N–C(12)–C(24)	–179.5(10)	N–C(12)–C(13)–C(14)	–174.5(13)
C(24)–C(12)–C(13)–C(14)	3(2)	C(12)–C(13)–C(14)–C(15)	–5(2)
C(13)–C(14)–C(15)–C(16)	–178.2(13)	C(13)–C(14)–C(15)–C(25)	4.7(19)
C(14)–C(15)–C(16)–C(17)	–178.3(12)	C(25)–C(15)–C(16)–C(17)	–1.4(18)
C(15)–C(16)–C(17)–C(18)	2(2)	C(16)–C(17)–C(18)–C(19)	–4(2)
C(17)–C(18)–C(19)–C(20)	–179.0(12)	C(17)–C(18)–C(19)–C(25)	4.6(19)
C(18)–C(19)–C(20)–C(21)	3.6(17)	C(18)–C(19)–C(20)–C(26)	–176.5(11)
C(25)–C(19)–C(20)–C(21)	–179.9(9)	C(25)–C(19)–C(20)–C(26)	–0.1(15)
C(19)–C(20)–C(21)–C(1)	–179.8(10)	C(26)–C(20)–C(21)–C(1)	0.3(16)
Br–C(1)–C(21)–C(20)	–179.5(7)	C(2)–C(1)–C(21)–C(20)	0.6(17)
C(3)–C(4)–C(22)–C(8)	–179.6(10)	C(3)–C(4)–C(22)–C(23)	0.9(16)
C(5)–C(4)–C(22)–C(8)	–0.5(17)	C(5)–C(4)–C(22)–C(23)	180.0(11)
C(7)–C(8)–C(22)–C(4)	1.8(16)	C(7)–C(8)–C(22)–C(23)	–178.7(10)
C(9)–C(8)–C(22)–C(4)	–177.7(10)	C(9)–C(8)–C(22)–C(23)	1.8(16)
N–C(11)–C(23)–C(22)	176.2(11)	N–C(11)–C(23)–C(27)	1.4(17)
C(10)–C(11)–C(23)–C(22)	–3.6(17)	C(10)–C(11)–C(23)–C(27)	–178.4(10)
C(4)–C(22)–C(23)–C(11)	–178.7(10)	C(4)–C(22)–C(23)–C(27)	–4.0(16)
C(8)–C(22)–C(23)–C(11)	1.7(16)	C(8)–C(22)–C(23)–C(27)	176.5(9)
N–C(12)–C(24)–C(25)	177.7(11)	N–C(12)–C(24)–C(27)	–3.4(18)
C(13)–C(12)–C(24)–C(25)	0.5(17)	C(13)–C(12)–C(24)–C(27)	179.4(11)
C(12)–C(24)–C(25)–C(15)	–0.7(17)	C(12)–C(24)–C(25)–C(19)	178.2(10)
C(27)–C(24)–C(25)–C(15)	–179.6(10)	C(27)–C(24)–C(25)–C(19)	–0.7(17)
C(18)–C(19)–C(25)–C(15)	–3.6(15)	C(18)–C(19)–C(25)–C(24)	177.4(11)
C(20)–C(19)–C(25)–C(15)	179.8(9)	C(20)–C(19)–C(25)–C(24)	0.8(16)
C(14)–C(15)–C(25)–C(19)	179.3(10)	C(14)–C(15)–C(25)–C(24)	–1.7(16)
C(16)–C(15)–C(25)–C(19)	2.1(16)	C(16)–C(15)–C(25)–C(24)	–178.9(11)
C(19)–C(20)–C(26)–C(3)	179.4(9)	C(19)–C(20)–C(26)–C(27)	–0.8(16)
C(21)–C(20)–C(26)–C(3)	–0.7(15)	C(21)–C(20)–C(26)–C(27)	179.1(10)
C(2)–C(3)–C(26)–C(20)	0.3(15)	C(2)–C(3)–C(26)–C(27)	–179.6(10)
C(4)–C(3)–C(26)–C(20)	180.0(9)	C(4)–C(3)–C(26)–C(27)	0.2(15)
C(3)–C(26)–C(27)–C(23)	–3.4(16)	C(3)–C(26)–C(27)–C(24)	–179.3(9)
C(20)–C(26)–C(27)–C(23)	176.8(10)	C(20)–C(26)–C(27)–C(24)	0.9(17)
C(12)–C(24)–C(27)–C(23)	4.8(16)	C(12)–C(24)–C(27)–C(26)	–179.1(10)
C(25)–C(24)–C(27)–C(23)	–176.3(9)	C(25)–C(24)–C(27)–C(26)	–0.2(16)
C(11)–C(23)–C(27)–C(24)	–3.8(16)	C(11)–C(23)–C(27)–C(26)	–179.8(10)
C(22)–C(23)–C(27)–C(24)	–178.6(10)	C(22)–C(23)–C(27)–C(26)	5.4(17)
C(11)–N–C(28)–C(29)	–82.7(15)	C(11)–N–C(28)–C(33)	101.9(14)

C(12)–N–C(28)–C(29)	97.6(14)	C(12)–N–C(28)–C(33)	−77.7(15)
N–C(28)–C(29)–C(30)	−178.2(11)	C(33)–C(28)–C(29)–C(30)	−3(2)
C(28)–C(29)–C(30)–O(1)	−179.3(12)	C(28)–C(29)–C(30)–C(31)	1.3(18)
C(34)–O(1)–C(30)–C(29)	−2.2(19)	C(34)–O(1)–C(30)–C(31)	177.2(13)
C(35)–O(2)–C(31)–C(30)	−115.4(18)	C(35)–O(2)–C(31)–C(32)	59(2)
O(1)–C(30)–C(31)–O(2)	−7.3(18)	O(1)–C(30)–C(31)–C(32)	178.3(12)
C(29)–C(30)–C(31)–O(2)	172.1(13)	C(29)–C(30)–C(31)–C(32)	−2.2(19)
O(2)–C(31)–C(32)–O(3)	7(2)	O(2)–C(31)–C(32)–C(33)	−169.4(14)
C(30)–C(31)–C(32)–O(3)	−178.8(12)	C(30)–C(31)–C(32)–C(33)	5(2)
C(36)–O(3)–C(32)–C(31)	−174.8(16)	C(36)–O(3)–C(32)–C(33)	2(2)
N–C(28)–C(33)–C(32)	−179.5(11)	C(29)–C(28)–C(33)–C(32)	5.5(19)
O(3)–C(32)–C(33)–C(28)	177.6(13)	C(31)–C(32)–C(33)–C(28)	−6(2)

Table 1. Crystal data and structure refinement for **DMA**.

Identification code	**DMA**	
Chemical formula (moiety)	$C_{44}H_{33}F_6N_2O_3P$	
Chemical formula (total)	$C_{44}H_{33}F_6N_2O_3P$	
Formula weight	782.69	
Temperature	100(2) K	
Radiation, wavelength	synchrotron, 0.6889 Å	
Crystal system, space group	triclinic, $P\bar{1}$	
Unit cell parameters	a = 10.226(9) Å	α = 106.360(9)°
	b = 18.309(15) Å	β = 97.926(10)°
	c = 22.041(19) Å	γ = 91.902(9)°
Cell volume	3910(6) $Å^3$	
Z	4	
Calculated density	1.329 g/cm^3	
Absorption coefficient μ	0.098 mm^{-1}	
F(000)	1616	
Crystal colour and size	red, 0.04 × 0.04 × 0.005 mm^3	
Reflections for cell refinement	1076 (θ range 2.3 to 19.9°)	
Data collection method	Rigaku Saturn 724+ on kappa diffractometer wide-frame ω scans	
θ range for data collection	0.9 to 21.3°	
Index ranges	h −10 to 10, k −19 to 19, l −23 to 23	
Completeness to θ = 24.4°	66.8 %	
Reflections collected	23234	
Independent reflections	9464 (R_{int} = 0.2185)	
Reflections with $F^2>2\sigma$	3450	
Absorption correction	none	
Structure solution	direct methods	
Refinement method	Full-matrix least-squares on F^2	
Weighting parameters a, b	0.1189,	
Data / restraints / parameters	9464 / 0 / 1020	
Final R indices [$F^2>2\sigma$]	R1 = 0.0996, wR2 = 0.2169	
R indices (all data)	R1 = 0.2457, wR2 = 0.2853	
Goodness-of-fit on F^2	0.947	
Extinction coefficient	0.039(2)	
Largest and mean shift/su	0.000 and 0.000	
Largest diff. peak and hole	0.42 and –0.37 e $Å^{-3}$	

The asymmetric unit contains two cations and two anions, together with some highly disordered solvent that is probably DMF and has been treated with the SQUEEZE procedure of PLATON.

Table 2. Atomic coordinates and equivalent isotropic displacement parameters ($Å^2$) for acb130007. U_{eq} is defined as one third of the trace of the orthogonalized U^{ij} tensor.

	x	y	z	U_{eq}
N(1)	0.1091(9)	–0.0182(5)	0.3031(4)	0.056(2)
N(2)	0.5058(12)	0.1232(7)	0.9075(5)	0.108(4)
C(1)	0.2078(11)	–0.0571(6)	0.3253(6)	0.060(3)
C(2)	0.2746(10)	–0.1115(6)	0.2806(5)	0.059(3)
C(3)	0.3695(10)	–0.1527(6)	0.3032(6)	0.058(3)
C(4)	0.4095(11)	–0.1441(6)	0.3695(5)	0.057(3)
C(5)	0.5093(10)	–0.1869(6)	0.3929(6)	0.057(3)
C(6)	0.5439(11)	–0.1745(6)	0.4587(6)	0.059(3)
C(7)	0.4841(10)	–0.1200(6)	0.5026(6)	0.060(3)
C(8)	0.3848(10)	–0.0739(6)	0.4820(6)	0.053(3)
C(9)	0.3211(10)	–0.0170(5)	0.5284(5)	0.047(3)
C(10)	0.3544(10)	–0.0012(6)	0.5942(6)	0.056(3)
C(11)	0.2930(10)	0.0519(6)	0.6387(5)	0.054(3)
C(12)	0.1891(10)	0.0896(6)	0.6144(5)	0.056(3)
C(13)	0.1495(11)	0.0757(6)	0.5478(5)	0.051(3)
C(14)	0.0402(11)	0.1159(6)	0.5225(5)	0.054(3)
C(15)	–0.0309(11)	0.1690(6)	0.5630(5)	0.056(3)
C(16)	–0.1330(11)	0.2078(6)	0.5381(6)	0.055(3)
C(17)	–0.1654(10)	0.1932(6)	0.4720(6)	0.056(3)
C(18)	–0.0961(10)	0.1410(6)	0.4295(5)	0.049(3)
C(19)	–0.1317(10)	0.1221(6)	0.3607(5)	0.056(3)
C(20)	–0.0676(11)	0.0714(6)	0.3189(6)	0.062(3)
C(21)	0.0424(11)	0.0347(6)	0.3445(5)	0.057(3)
C(22)	0.0049(11)	0.1020(6)	0.4550(5)	0.056(3)
C(23)	0.0791(11)	0.0480(6)	0.4125(5)	0.051(3)
C(24)	0.1802(10)	0.0081(5)	0.4360(5)	0.041(3)
C(25)	0.2460(10)	–0.0444(6)	0.3926(5)	0.050(3)
C(26)	0.3484(10)	–0.0887(6)	0.4150(5)	0.051(3)
C(27)	0.2162(10)	0.0223(5)	0.5035(5)	0.045(3)
C(28)	0.0705(10)	–0.0300(6)	0.2322(5)	0.049(3)
C(29)	0.1009(11)	0.0292(7)	0.2083(5)	0.058(3)
C(30)	0.0558(12)	0.0192(7)	0.1423(6)	0.061(3)
C(31)	–0.0166(12)	–0.0500(8)	0.1064(6)	0.065(3)
C(32)	–0.0399(11)	–0.1097(7)	0.1316(6)	0.056(3)
C(33)	–0.0016(11)	–0.0999(7)	0.1964(5)	0.059(3)
C(34)	0.1426(15)	0.1482(8)	0.1491(6)	0.105(5)
C(35)	–0.1815(12)	–0.0259(7)	0.0263(6)	0.083(4)
C(36)	–0.0989(11)	–0.2428(7)	0.1111(5)	0.070(4)
C(37)	0.3435(11)	0.0668(6)	0.7080(6)	0.060(3)
C(38)	0.4127(11)	0.0157(7)	0.7336(6)	0.065(3)
C(39)	0.4658(11)	0.0327(6)	0.7989(6)	0.069(4)
C(40)	0.4520(13)	0.1074(7)	0.8423(5)	0.073(4)
C(41)	0.3803(13)	0.1586(8)	0.8180(6)	0.090(5)
C(42)	0.3263(11)	0.1394(6)	0.7517(6)	0.073(4)
C(43)	0.6041(12)	0.0772(7)	0.9280(6)	0.080(4)
C(44)	0.4672(14)	0.1902(9)	0.9540(6)	0.112(6)
O(1)	0.0737(8)	0.0734(5)	0.1112(4)	0.074(2)
O(2)	–0.0582(8)	–0.0601(4)	0.0399(3)	0.072(2)

O(3)	–0.1060(8)	–0.1756(5)	0.0890(3)	0.067(2)
N(3)	0.7796(9)	0.3887(5)	0.2960(4)	0.055(2)
N(4)	0.7243(12)	0.6055(7)	0.8987(5)	0.102(4)
C(45)	0.8694(11)	0.3611(6)	0.3354(5)	0.052(3)
C(46)	0.9636(10)	0.3074(6)	0.3101(5)	0.052(3)
C(47)	1.0518(11)	0.2819(6)	0.3493(5)	0.059(3)
C(48)	1.0577(10)	0.3063(6)	0.4171(5)	0.052(3)
C(49)	1.1519(11)	0.2799(6)	0.4587(5)	0.059(3)
C(50)	1.1594(10)	0.3063(6)	0.5253(6)	0.059(3)
C(51)	1.0749(10)	0.3629(6)	0.5522(5)	0.050(3)
C(52)	0.9790(10)	0.3902(5)	0.5137(5)	0.046(3)
C(53)	0.8851(10)	0.4464(6)	0.5406(5)	0.048(3)
C(54)	0.8831(10)	0.4735(6)	0.6071(5)	0.053(3)
C(55)	0.7954(10)	0.5276(6)	0.6336(5)	0.051(3)
C(56)	0.7083(11)	0.5545(6)	0.5910(5)	0.054(3)
C(57)	0.7052(10)	0.5321(6)	0.5244(5)	0.052(3)
C(58)	0.6129(10)	0.5590(6)	0.4805(5)	0.050(3)
C(59)	0.5238(10)	0.6170(6)	0.5013(6)	0.059(3)
C(60)	0.4408(10)	0.6442(6)	0.4600(6)	0.052(3)
C(61)	0.4393(11)	0.6160(6)	0.3936(5)	0.058(3)
C(62)	0.5248(10)	0.5580(6)	0.3693(5)	0.055(3)
C(63)	0.5235(11)	0.5276(6)	0.3018(5)	0.062(3)
C(64)	0.6035(10)	0.4694(6)	0.2769(5)	0.054(3)
C(65)	0.6933(10)	0.4454(6)	0.3200(5)	0.054(3)
C(66)	0.6104(10)	0.5312(6)	0.4120(5)	0.049(3)
C(67)	0.6985(10)	0.4730(6)	0.3878(6)	0.054(3)
C(68)	0.7889(10)	0.4472(6)	0.4306(5)	0.048(3)
C(69)	0.8749(10)	0.3873(6)	0.4039(5)	0.048(3)
C(70)	0.9714(10)	0.3632(6)	0.4455(5)	0.049(3)
C(71)	0.7935(10)	0.4737(6)	0.4994(5)	0.049(3)
C(72)	0.7736(10)	0.3559(7)	0.2259(5)	0.053(3)
C(73)	0.8225(11)	0.4006(7)	0.1909(6)	0.062(3)
C(74)	0.8242(11)	0.3677(7)	0.1254(6)	0.058(3)
C(75)	0.7738(12)	0.2894(8)	0.0960(6)	0.059(3)
C(76)	0.7266(12)	0.2489(7)	0.1323(6)	0.066(3)
C(77)	0.7204(11)	0.2802(6)	0.2007(6)	0.060(3)
C(78)	0.8665(14)	0.4868(7)	0.1056(6)	0.087(4)
C(79)	0.8944(13)	0.2207(8)	0.0148(6)	0.101(5)
C(80)	0.6279(14)	0.1258(7)	0.1356(6)	0.092(4)
C(81)	0.7894(11)	0.5507(7)	0.7050(5)	0.060(3)
C(82)	0.8185(11)	0.5028(7)	0.7431(6)	0.064(3)
C(83)	0.8034(11)	0.5211(7)	0.8072(6)	0.072(4)
C(84)	0.7492(13)	0.5895(7)	0.8357(6)	0.075(4)
C(85)	0.7214(11)	0.6390(7)	0.7987(5)	0.070(4)
C(86)	0.7393(11)	0.6214(6)	0.7346(5)	0.063(3)
C(87)	0.7920(18)	0.5665(9)	0.9432(7)	0.134(7)
C(88)	0.6646(15)	0.6750(8)	0.9262(6)	0.110(5)
O(4)	0.8596(9)	0.4038(5)	0.0846(4)	0.077(3)
O(5)	0.7729(8)	0.2573(4)	0.0308(4)	0.070(2)
O(6)	0.6787(8)	0.1720(5)	0.0991(4)	0.074(2)
P(1)	0.4756(3)	0.2110(2)	0.31861(16)	0.0701(11)
F(1)	0.5549(8)	0.2933(4)	0.3349(4)	0.101(3)
F(2)	0.5963(6)	0.1694(4)	0.2850(3)	0.082(2)
F(3)	0.4112(7)	0.2208(5)	0.2512(3)	0.108(3)
F(4)	0.3576(6)	0.2507(4)	0.3527(3)	0.086(2)

F(5)	0.5449(7)	0.1998(5)	0.3839(3)	0.107(3)
F(6)	0.3952(7)	0.1294(4)	0.3010(5)	0.124(3)
P(2)	0.0831(4)	0.32517(18)	0.73326(16)	0.0669(10)
F(7)	0.1211(7)	0.4126(3)	0.7349(3)	0.076(2)
F(8)	0.1743(6)	0.2950(3)	0.6788(3)	0.0691(19)
F(9)	–0.0428(6)	0.3212(3)	0.6785(3)	0.0716(19)
F(10)	–0.0093(7)	0.3556(3)	0.7886(3)	0.077(2)
F(11)	0.2098(6)	0.3289(3)	0.7878(3)	0.077(2)
F(12)	0.0443(6)	0.2375(3)	0.7313(3)	0.0723(19)

Table 3. Bond lengths [Å] and angles [°] for acb130007.

N(1)–C(1)	1.369(13)	N(1)–C(21)	1.397(13)
N(1)–C(28)	1.510(13)	N(2)–C(40)	1.410(14)
N(2)–C(43)	1.440(14)	N(2)–C(44)	1.465(15)
C(1)–C(2)	1.452(14)	C(1)–C(25)	1.431(14)
C(2)–H(2)	0.950	C(2)–C(3)	1.374(14)
C(3)–H(3)	0.950	C(3)–C(4)	1.424(14)
C(4)–C(5)	1.435(14)	C(4)–C(26)	1.438(14)
C(5)–H(5)	0.950	C(5)–C(6)	1.395(14)
C(6)–H(6)	0.950	C(6)–C(7)	1.402(14)
C(7)–H(7)	0.950	C(7)–C(8)	1.448(14)
C(8)–C(9)	1.478(14)	C(8)–C(26)	1.417(14)
C(9)–C(10)	1.387(14)	C(9)–C(27)	1.443(13)
C(10)–H(10)	0.950	C(10)–C(11)	1.405(14)
C(11)–C(12)	1.413(13)	C(11)–C(37)	1.487(14)
C(12)–H(12)	0.950	C(12)–C(13)	1.415(13)
C(13)–C(14)	1.489(14)	C(13)–C(27)	1.437(14)
C(14)–C(15)	1.418(14)	C(14)–C(22)	1.427(14)
C(15)–H(15)	0.950	C(15)–C(16)	1.417(14)
C(16)–H(16)	0.950	C(16)–C(17)	1.395(14)
C(17)–H(17)	0.950	C(17)–C(18)	1.420(14)
C(18)–C(19)	1.448(14)	C(18)–C(22)	1.417(13)
C(19)–H(19)	0.950	C(19)–C(20)	1.367(14)
C(20)–H(20)	0.950	C(20)–C(21)	1.457(14)
C(21)–C(23)	1.442(14)	C(22)–C(23)	1.468(14)
C(23)–C(24)	1.409(13)	C(24)–C(25)	1.412(13)
C(24)–C(27)	1.428(13)	C(25)–C(26)	1.462(14)
C(28)–C(29)	1.375(13)	C(28)–C(33)	1.419(14)
C(29)–H(29)	0.950	C(29)–C(30)	1.423(15)
C(30)–C(31)	1.412(15)	C(30)–O(1)	1.377(13)
C(31)–C(32)	1.387(15)	C(31)–O(2)	1.426(12)
C(32)–C(33)	1.387(14)	C(32)–O(3)	1.388(12)
C(33)–H(33)	0.950	C(34)–H(34A)	0.980
C(34)–H(34B)	0.980	C(34)–H(34C)	0.980
C(34)–O(1)	1.482(13)	C(35)–H(35A)	0.980
C(35)–H(35B)	0.980	C(35)–H(35C)	0.980
C(35)–O(2)	1.458(12)	C(36)–H(36A)	0.980
C(36)–H(36B)	0.980	C(36)–H(36C)	0.980
C(36)–O(3)	1.445(12)	C(37)–C(38)	1.389(14)
C(37)–C(42)	1.437(14)	C(38)–H(38)	0.950
C(38)–C(39)	1.409(14)	C(39)–H(39)	0.950
C(39)–C(40)	1.454(15)	C(40)–C(41)	1.386(15)
C(41)–H(41)	0.950	C(41)–C(42)	1.426(15)
C(42)–H(42)	0.950	C(43)–H(43A)	0.980
C(43)–H(43B)	0.980	C(43)–H(43C)	0.980
C(44)–H(44A)	0.980	C(44)–H(44B)	0.980
C(44)–H(44C)	0.980	N(3)–C(45)	1.381(12)
N(3)–C(65)	1.421(12)	N(3)–C(72)	1.484(13)
N(4)–C(84)	1.397(14)	N(4)–C(87)	1.481(16)
N(4)–C(88)	1.441(15)	C(45)–C(46)	1.451(14)
C(45)–C(69)	1.442(14)	C(46)–H(46)	0.950
C(46)–C(47)	1.349(13)	C(47)–H(47)	0.950
C(47)–C(48)	1.425(14)	C(48)–C(49)	1.428(14)
C(48)–C(70)	1.451(14)	C(49)–H(49)	0.950

C(49)–C(50)	1.399(14)	C(50)–H(50)	0.950
C(50)–C(51)	1.425(13)	C(51)–H(51)	0.950
C(51)–C(52)	1.404(13)	C(52)–C(53)	1.487(13)
C(52)–C(70)	1.434(13)	C(53)–C(54)	1.413(13)
C(53)–C(71)	1.416(13)	C(54)–H(54)	0.950
C(54)–C(55)	1.416(14)	C(55)–C(56)	1.405(13)
C(55)–C(81)	1.521(14)	C(56)–H(56)	0.950
C(56)–C(57)	1.404(13)	C(57)–C(58)	1.456(14)
C(57)–C(71)	1.460(14)	C(58)–C(59)	1.440(14)
C(58)–C(66)	1.447(14)	C(59)–H(59)	0.950
C(59)–C(60)	1.367(13)	C(60)–H(60)	0.950
C(60)–C(61)	1.406(14)	C(61)–H(61)	0.950
C(61)–C(62)	1.432(14)	C(62)–C(63)	1.431(14)
C(62)–C(66)	1.398(14)	C(63)–H(63)	0.950
C(63)–C(64)	1.399(14)	C(64)–H(64)	0.950
C(64)–C(65)	1.401(14)	C(65)–C(67)	1.429(14)
C(66)–C(67)	1.453(14)	C(67)–C(68)	1.417(14)
C(68)–C(69)	1.472(13)	C(68)–C(71)	1.449(13)
C(69)–C(70)	1.421(13)	C(72)–C(73)	1.395(15)
C(72)–C(77)	1.400(14)	C(73)–H(73)	0.950
C(73)–C(74)	1.403(15)	C(74)–C(75)	1.441(15)
C(74)–O(4)	1.337(13)	C(75)–C(76)	1.356(15)
C(75)–O(5)	1.390(12)	C(76)–C(77)	1.465(15)
C(76)–O(6)	1.427(13)	C(77)–H(77)	0.950
C(78)–H(78A)	0.980	C(78)–H(78B)	0.980
C(78)–H(78C)	0.980	C(78)–O(4)	1.455(13)
C(79)–H(79A)	0.980	C(79)–H(79B)	0.980
C(79)–H(79C)	0.980	C(79)–O(5)	1.470(13)
C(80)–H(80A)	0.980	C(80)–H(80B)	0.980
C(80)–H(80C)	0.980	C(80)–O(6)	1.451(13)
C(81)–C(82)	1.387(14)	C(81)–C(86)	1.423(14)
C(82)–H(82)	0.950	C(82)–C(83)	1.390(14)
C(83)–H(83)	0.950	C(83)–C(84)	1.402(15)
C(84)–C(85)	1.392(15)	C(85)–H(85)	0.950
C(85)–C(86)	1.398(14)	C(86)–H(86)	0.950
C(87)–H(87A)	0.980	C(87)–H(87B)	0.980
C(87)–H(87C)	0.980	C(88)–H(88A)	0.980
C(88)–H(88B)	0.980	C(88)–H(88C)	0.980
P(1)–F(1)	1.609(8)	P(1)–F(2)	1.627(7)
P(1)–F(3)	1.600(7)	P(1)–F(4)	1.597(7)
P(1)–F(5)	1.584(7)	P(1)–F(6)	1.601(8)
P(2)–F(7)	1.625(7)	P(2)–F(8)	1.608(7)
P(2)–F(9)	1.624(7)	P(2)–F(10)	1.631(7)
P(2)–F(11)	1.626(7)	P(2)–F(12)	1.628(7)

C(1)–N(1)–C(21)	122.0(9)	C(1)–N(1)–C(28)	120.5(9)
C(21)–N(1)–C(28)	117.4(9)	C(40)–N(2)–C(43)	120.7(11)
C(40)–N(2)–C(44)	119.4(11)	C(43)–N(2)–C(44)	119.7(10)
N(1)–C(1)–C(2)	120.1(11)	N(1)–C(1)–C(25)	120.3(10)
C(2)–C(1)–C(25)	119.6(10)	C(1)–C(2)–H(2)	120.2
C(1)–C(2)–C(3)	119.7(11)	H(2)–C(2)–C(3)	120.2
C(2)–C(3)–H(3)	118.3	C(2)–C(3)–C(4)	123.4(11)
H(3)–C(3)–C(4)	118.3	C(3)–C(4)–C(5)	123.2(10)
C(3)–C(4)–C(26)	118.2(10)	C(5)–C(4)–C(26)	118.6(10)
C(4)–C(5)–H(5)	120.1	C(4)–C(5)–C(6)	119.7(10)

H(5)–C(5)–C(6)	120.1	C(5)–C(6)–H(6)	119.4
C(5)–C(6)–C(7)	121.1(10)	H(6)–C(6)–C(7)	119.4
C(6)–C(7)–H(7)	119.1	C(6)–C(7)–C(8)	121.8(11)
H(7)–C(7)–C(8)	119.1	C(7)–C(8)–C(9)	121.6(11)
C(7)–C(8)–C(26)	116.2(10)	C(9)–C(8)–C(26)	122.1(10)
C(8)–C(9)–C(10)	123.6(10)	C(8)–C(9)–C(27)	117.7(10)
C(10)–C(9)–C(27)	118.7(9)	C(9)–C(10)–H(10)	118.0
C(9)–C(10)–C(11)	123.9(10)	H(10)–C(10)–C(11)	118.0
C(10)–C(11)–C(12)	117.5(10)	C(10)–C(11)–C(37)	118.5(10)
C(12)–C(11)–C(37)	124.0(10)	C(11)–C(12)–H(12)	119.3
C(11)–C(12)–C(13)	121.4(10)	H(12)–C(12)–C(13)	119.3
C(12)–C(13)–C(14)	121.2(9)	C(12)–C(13)–C(27)	119.8(10)
C(14)–C(13)–C(27)	119.1(9)	C(13)–C(14)–C(15)	122.5(10)
C(13)–C(14)–C(22)	119.8(9)	C(15)–C(14)–C(22)	117.7(10)
C(14)–C(15)–H(15)	119.2	C(14)–C(15)–C(16)	121.7(10)
H(15)–C(15)–C(16)	119.2	C(15)–C(16)–H(16)	120.3
C(15)–C(16)–C(17)	119.4(10)	H(16)–C(16)–C(17)	120.3
C(16)–C(17)–H(17)	119.5	C(16)–C(17)–C(18)	120.9(10)
H(17)–C(17)–C(18)	119.5	C(17)–C(18)–C(19)	122.0(10)
C(17)–C(18)–C(22)	119.1(10)	C(19)–C(18)–C(22)	118.7(10)
C(18)–C(19)–H(19)	118.4	C(18)–C(19)–C(20)	123.1(10)
H(19)–C(19)–C(20)	118.4	C(19)–C(20)–H(20)	120.6
C(19)–C(20)–C(21)	118.7(11)	H(20)–C(20)–C(21)	120.6
N(1)–C(21)–C(20)	120.3(10)	N(1)–C(21)–C(23)	118.5(9)
C(20)–C(21)–C(23)	121.1(10)	C(14)–C(22)–C(18)	121.1(10)
C(14)–C(22)–C(23)	118.4(9)	C(18)–C(22)–C(23)	120.5(10)
C(21)–C(23)–C(22)	117.7(10)	C(21)–C(23)–C(24)	120.1(9)
C(22)–C(23)–C(24)	122.2(10)	C(23)–C(24)–C(25)	119.6(10)
C(23)–C(24)–C(27)	119.5(9)	C(25)–C(24)–C(27)	120.8(9)
C(1)–C(25)–C(24)	119.4(10)	C(1)–C(25)–C(26)	119.2(10)
C(24)–C(25)–C(26)	121.3(10)	C(4)–C(26)–C(8)	122.5(10)
C(4)–C(26)–C(25)	119.9(10)	C(8)–C(26)–C(25)	117.6(9)
C(9)–C(27)–C(13)	118.7(10)	C(9)–C(27)–C(24)	120.3(9)
C(13)–C(27)–C(24)	121.0(10)	N(1)–C(28)–C(29)	117.7(9)
N(1)–C(28)–C(33)	116.8(10)	C(29)–C(28)–C(33)	125.4(11)
C(28)–C(29)–H(29)	121.5	C(28)–C(29)–C(30)	117.0(11)
H(29)–C(29)–C(30)	121.5	C(29)–C(30)–C(31)	118.0(12)
C(29)–C(30)–O(1)	124.7(11)	C(31)–C(30)–O(1)	117.3(11)
C(30)–C(31)–C(32)	123.1(11)	C(30)–C(31)–O(2)	117.4(12)
C(32)–C(31)–O(2)	119.3(11)	C(31)–C(32)–C(33)	119.6(11)
C(31)–C(32)–O(3)	116.0(11)	C(33)–C(32)–O(3)	124.3(12)
C(28)–C(33)–C(32)	116.6(11)	C(28)–C(33)–H(33)	121.7
C(32)–C(33)–H(33)	121.7	H(34A)–C(34)–H(34B)	109.5
H(34A)–C(34)–H(34C)	109.5	H(34A)–C(34)–O(1)	109.5
H(34B)–C(34)–H(34C)	109.5	H(34B)–C(34)–O(1)	109.5
H(34C)–C(34)–O(1)	109.5	H(35A)–C(35)–H(35B)	109.5
H(35A)–C(35)–H(35C)	109.5	H(35A)–C(35)–O(2)	109.5
H(35B)–C(35)–H(35C)	109.5	H(35B)–C(35)–O(2)	109.5
H(35C)–C(35)–O(2)	109.5	H(36A)–C(36)–H(36B)	109.5
H(36A)–C(36)–H(36C)	109.5	H(36A)–C(36)–O(3)	109.5
H(36B)–C(36)–H(36C)	109.5	H(36B)–C(36)–O(3)	109.5
H(36C)–C(36)–O(3)	109.5	C(11)–C(37)–C(38)	123.9(10)
C(11)–C(37)–C(42)	119.3(10)	C(38)–C(37)–C(42)	116.7(11)
C(37)–C(38)–H(38)	118.6	C(37)–C(38)–C(39)	122.9(11)
H(38)–C(38)–C(39)	118.6	C(38)–C(39)–H(39)	120.1

C(38)–C(39)–C(40)	119.8(11)	H(39)–C(39)–C(40)	120.1
N(2)–C(40)–C(39)	118.9(12)	N(2)–C(40)–C(41)	122.9(11)
C(39)–C(40)–C(41)	118.1(11)	C(40)–C(41)–H(41)	119.6
C(40)–C(41)–C(42)	120.7(11)	H(41)–C(41)–C(42)	119.6
C(37)–C(42)–C(41)	121.6(11)	C(37)–C(42)–H(42)	119.2
C(41)–C(42)–H(42)	119.2	N(2)–C(43)–H(43A)	109.5
N(2)–C(43)–H(43B)	109.5	N(2)–C(43)–H(43C)	109.5
H(43A)–C(43)–H(43B)	109.5	H(43A)–C(43)–H(43C)	109.5
H(43B)–C(43)–H(43C)	109.5	N(2)–C(44)–H(44A)	109.5
N(2)–C(44)–H(44B)	109.5	N(2)–C(44)–H(44C)	109.5
H(44A)–C(44)–H(44B)	109.5	H(44A)–C(44)–H(44C)	109.5
H(44B)–C(44)–H(44C)	109.5	C(30)–O(1)–C(34)	118.0(9)
C(31)–O(2)–C(35)	113.5(8)	C(32)–O(3)–C(36)	115.0(9)
C(45)–N(3)–C(65)	122.8(9)	C(45)–N(3)–C(72)	117.5(8)
C(65)–N(3)–C(72)	119.6(9)	C(84)–N(4)–C(87)	120.9(10)
C(84)–N(4)–C(88)	119.0(11)	C(87)–N(4)–C(88)	117.5(11)
N(3)–C(45)–C(46)	121.9(10)	N(3)–C(45)–C(69)	120.3(9)
C(46)–C(45)–C(69)	117.7(9)	C(45)–C(46)–H(46)	119.5
C(45)–C(46)–C(47)	121.1(10)	H(46)–C(46)–C(47)	119.5
C(46)–C(47)–H(47)	119.0	C(46)–C(47)–C(48)	122.0(10)
H(47)–C(47)–C(48)	119.0	C(47)–C(48)–C(49)	122.1(10)
C(47)–C(48)–C(70)	119.5(10)	C(49)–C(48)–C(70)	118.3(10)
C(48)–C(49)–H(49)	119.3	C(48)–C(49)–C(50)	121.5(10)
H(49)–C(49)–C(50)	119.3	C(49)–C(50)–H(50)	120.3
C(49)–C(50)–C(51)	119.3(10)	H(50)–C(50)–C(51)	120.3
C(50)–C(51)–H(51)	119.1	C(50)–C(51)–C(52)	121.8(10)
H(51)–C(51)–C(52)	119.1	C(51)–C(52)–C(53)	122.8(10)
C(51)–C(52)–C(70)	118.8(9)	C(53)–C(52)–C(70)	118.3(9)
C(52)–C(53)–C(54)	121.7(9)	C(52)–C(53)–C(71)	120.2(10)
C(54)–C(53)–C(71)	118.1(9)	C(53)–C(54)–H(54)	118.8
C(53)–C(54)–C(55)	122.4(9)	H(54)–C(54)–C(55)	118.8
C(54)–C(55)–C(56)	117.6(10)	C(54)–C(55)–C(81)	120.6(10)
C(56)–C(55)–C(81)	121.7(10)	C(55)–C(56)–H(56)	118.0
C(55)–C(56)–C(57)	123.9(10)	H(56)–C(56)–C(57)	118.0
C(56)–C(57)–C(58)	123.6(9)	C(56)–C(57)–C(71)	116.2(9)
C(58)–C(57)–C(71)	119.9(9)	C(57)–C(58)–C(59)	123.3(10)
C(57)–C(58)–C(66)	121.2(9)	C(59)–C(58)–C(66)	115.4(10)
C(58)–C(59)–H(59)	118.4	C(58)–C(59)–C(60)	123.2(11)
H(59)–C(59)–C(60)	118.4	C(59)–C(60)–H(60)	119.8
C(59)–C(60)–C(61)	120.4(10)	H(60)–C(60)–C(61)	119.8
C(60)–C(61)–H(61)	120.2	C(60)–C(61)–C(62)	119.6(10)
H(61)–C(61)–C(62)	120.2	C(61)–C(62)–C(63)	120.5(10)
C(61)–C(62)–C(66)	119.5(10)	C(63)–C(62)–C(66)	120.0(9)
C(62)–C(63)–H(63)	119.2	C(62)–C(63)–C(64)	121.6(10)
H(63)–C(63)–C(64)	119.2	C(63)–C(64)–H(64)	121.0
C(63)–C(64)–C(65)	118.0(10)	H(64)–C(64)–C(65)	121.0
N(3)–C(65)–C(64)	119.3(10)	N(3)–C(65)–C(67)	117.7(9)
C(64)–C(65)–C(67)	122.9(9)	C(58)–C(66)–C(62)	121.9(9)
C(58)–C(66)–C(67)	118.3(10)	C(62)–C(66)–C(67)	119.8(10)
C(65)–C(67)–C(66)	117.5(10)	C(65)–C(67)–C(68)	122.1(9)
C(66)–C(67)–C(68)	120.4(10)	C(67)–C(68)–C(69)	118.5(9)
C(67)–C(68)–C(71)	122.6(9)	C(69)–C(68)–C(71)	118.8(9)
C(45)–C(69)–C(68)	118.4(9)	C(45)–C(69)–C(70)	121.4(9)
C(68)–C(69)–C(70)	119.7(10)	C(48)–C(70)–C(52)	120.3(9)
C(48)–C(70)–C(69)	118.0(10)	C(52)–C(70)–C(69)	121.7(9)

C(53)–C(71)–C(57)	121.5(10)	C(53)–C(71)–C(68)	120.9(9)
C(57)–C(71)–C(68)	117.5(9)	N(3)–C(72)–C(73)	119.2(10)
N(3)–C(72)–C(77)	115.4(11)	C(73)–C(72)–C(77)	125.4(11)
C(72)–C(73)–H(73)	120.6	C(72)–C(73)–C(74)	118.8(11)
H(73)–C(73)–C(74)	120.6	C(73)–C(74)–C(75)	119.3(12)
C(73)–C(74)–O(4)	126.1(11)	C(75)–C(74)–O(4)	114.4(11)
C(74)–C(75)–C(76)	119.3(11)	C(74)–C(75)–O(5)	119.2(12)
C(76)–C(75)–O(5)	121.5(11)	C(75)–C(76)–C(77)	124.1(11)
C(75)–C(76)–O(6)	115.3(11)	C(77)–C(76)–O(6)	120.5(12)
C(72)–C(77)–C(76)	113.0(11)	C(72)–C(77)–H(77)	123.5
C(76)–C(77)–H(77)	123.5	H(78A)–C(78)–H(78B)	109.5
H(78A)–C(78)–H(78C)	109.5	H(78A)–C(78)–O(4)	109.5
H(78B)–C(78)–H(78C)	109.5	H(78B)–C(78)–O(4)	109.5
H(78C)–C(78)–O(4)	109.5	H(79A)–C(79)–H(79B)	109.5
H(79A)–C(79)–H(79C)	109.5	H(79A)–C(79)–O(5)	109.5
H(79B)–C(79)–H(79C)	109.5	H(79B)–C(79)–O(5)	109.5
H(79C)–C(79)–O(5)	109.5	H(80A)–C(80)–H(80B)	109.5
H(80A)–C(80)–H(80C)	109.5	H(80A)–C(80)–O(6)	109.5
H(80B)–C(80)–H(80C)	109.5	H(80B)–C(80)–O(6)	109.5
H(80C)–C(80)–O(6)	109.5	C(55)–C(81)–C(82)	123.3(10)
C(55)–C(81)–C(86)	119.9(11)	C(82)–C(81)–C(86)	116.5(11)
C(81)–C(82)–H(82)	118.2	C(81)–C(82)–C(83)	123.7(10)
H(82)–C(82)–C(83)	118.2	C(82)–C(83)–H(83)	120.1
C(82)–C(83)–C(84)	119.8(11)	H(83)–C(83)–C(84)	120.1
N(4)–C(84)–C(83)	120.1(12)	N(4)–C(84)–C(85)	122.5(11)
C(83)–C(84)–C(85)	117.4(11)	C(84)–C(85)–H(85)	118.7
C(84)–C(85)–C(86)	122.7(11)	H(85)–C(85)–C(86)	118.7
C(81)–C(86)–C(85)	119.8(11)	C(81)–C(86)–H(86)	120.1
C(85)–C(86)–H(86)	120.1	N(4)–C(87)–H(87A)	109.5
N(4)–C(87)–H(87B)	109.5	N(4)–C(87)–H(87C)	109.5
H(87A)–C(87)–H(87B)	109.5	H(87A)–C(87)–H(87C)	109.5
H(87B)–C(87)–H(87C)	109.5	N(4)–C(88)–H(88A)	109.5
N(4)–C(88)–H(88B)	109.5	N(4)–C(88)–H(88C)	109.5
H(88A)–C(88)–H(88B)	109.5	H(88A)–C(88)–H(88C)	109.5
H(88B)–C(88)–H(88C)	109.5	C(74)–O(4)–C(78)	116.8(9)
C(75)–O(5)–C(79)	114.0(9)	C(76)–O(6)–C(80)	117.8(9)
F(1)–P(1)–F(2)	90.9(4)	F(1)–P(1)–F(3)	89.1(5)
F(1)–P(1)–F(4)	89.7(4)	F(1)–P(1)–F(5)	90.7(5)
F(1)–P(1)–F(6)	178.8(5)	F(2)–P(1)–F(3)	89.3(4)
F(2)–P(1)–F(4)	178.7(4)	F(2)–P(1)–F(5)	88.1(4)
F(2)–P(1)–F(6)	89.2(4)	F(3)–P(1)–F(4)	91.8(4)
F(3)–P(1)–F(5)	177.4(4)	F(3)–P(1)–F(6)	89.7(5)
F(4)–P(1)–F(5)	90.8(4)	F(4)–P(1)–F(6)	90.2(4)
F(5)–P(1)–F(6)	90.5(5)	F(7)–P(2)–F(8)	90.0(4)
F(7)–P(2)–F(9)	89.5(3)	F(7)–P(2)–F(10)	90.1(3)
F(7)–P(2)–F(11)	90.6(4)	F(7)–P(2)–F(12)	179.7(4)
F(8)–P(2)–F(9)	90.1(4)	F(8)–P(2)–F(10)	179.9(4)
F(8)–P(2)–F(11)	89.5(4)	F(8)–P(2)–F(12)	90.0(3)
F(9)–P(2)–F(10)	90.1(4)	F(9)–P(2)–F(11)	179.6(4)
F(9)–P(2)–F(12)	90.2(3)	F(10)–P(2)–F(11)	90.3(4)
F(10)–P(2)–F(12)	90.0(4)	F(11)–P(2)–F(12)	89.7(4)

Table 4. Torsion angles [°] for acb130007.

C(21)–N(1)–C(1)–C(2)	−179.9(10)	C(21)–N(1)–C(1)–C(25)	−0.1(16)
C(28)–N(1)–C(1)–C(2)	−1.3(15)	C(28)–N(1)–C(1)–C(25)	178.6(10)
N(1)–C(1)–C(2)–C(3)	−177.2(10)	C(25)–C(1)–C(2)–C(3)	3.0(16)
C(1)–C(2)–C(3)–C(4)	−1.4(17)	C(2)–C(3)–C(4)–C(5)	−179.6(10)
C(2)–C(3)–C(4)–C(26)	−0.8(16)	C(3)–C(4)–C(5)–C(6)	179.3(10)
C(26)–C(4)–C(5)–C(6)	0.6(16)	C(4)–C(5)–C(6)–C(7)	−1.0(16)
C(5)–C(6)–C(7)–C(8)	−0.4(16)	C(6)–C(7)–C(8)–C(9)	179.4(10)
C(6)–C(7)–C(8)–C(26)	2.1(15)	C(7)–C(8)–C(9)–C(10)	2.8(15)
C(7)–C(8)–C(9)–C(27)	−175.4(9)	C(26)–C(8)–C(9)–C(10)	180.0(10)
C(26)–C(8)–C(9)–C(27)	1.7(15)	C(8)–C(9)–C(10)–C(11)	−179.0(10)
C(27)–C(9)–C(10)–C(11)	−0.8(16)	C(9)–C(10)–C(11)–C(12)	1.7(16)
C(9)–C(10)–C(11)–C(37)	−176.5(10)	C(10)–C(11)–C(12)–C(13)	−1.1(16)
C(37)–C(11)–C(12)–C(13)	176.9(10)	C(11)–C(12)–C(13)–C(14)	−179.7(10)
C(11)–C(12)–C(13)–C(27)	−0.3(15)	C(12)–C(13)–C(14)–C(15)	−0.9(16)
C(12)–C(13)–C(14)–C(22)	178.4(10)	C(27)–C(13)–C(14)–C(15)	179.6(10)
C(27)–C(13)–C(14)–C(22)	−1.1(15)	C(13)–C(14)–C(15)–C(16)	178.8(10)
C(22)–C(14)–C(15)–C(16)	−0.5(16)	C(14)–C(15)–C(16)–C(17)	0.5(16)
C(15)–C(16)–C(17)–C(18)	−1.0(15)	C(16)–C(17)–C(18)–C(19)	177.1(10)
C(16)–C(17)–C(18)–C(22)	1.6(15)	C(17)–C(18)–C(19)–C(20)	−179.3(10)
C(22)–C(18)–C(19)–C(20)	−3.7(16)	C(18)–C(19)–C(20)–C(21)	−0.3(16)
C(1)–N(1)–C(21)–C(20)	−176.2(10)	C(1)–N(1)–C(21)–C(23)	−0.2(15)
C(28)–N(1)–C(21)–C(20)	5.1(15)	C(28)–N(1)–C(21)–C(23)	−178.8(9)
C(19)–C(20)–C(21)–N(1)	179.2(10)	C(19)–C(20)–C(21)–C(23)	3.3(16)
C(17)–C(18)–C(22)–C(14)	−1.6(16)	C(17)–C(18)–C(22)–C(23)	−179.5(10)
C(19)–C(18)–C(22)–C(14)	−177.3(10)	C(19)–C(18)–C(22)–C(23)	4.8(15)
C(13)–C(14)–C(22)–C(18)	−178.2(10)	C(13)–C(14)–C(22)–C(23)	−0.3(15)
C(15)–C(14)–C(22)–C(18)	1.1(16)	C(15)–C(14)–C(22)–C(23)	179.0(10)
N(1)–C(21)–C(23)–C(22)	−178.1(10)	N(1)–C(21)–C(23)–C(24)	−0.1(15)
C(20)–C(21)–C(23)–C(22)	−2.1(15)	C(20)–C(21)–C(23)–C(24)	175.9(10)
C(14)–C(22)–C(23)–C(21)	−179.9(10)	C(14)–C(22)–C(23)–C(24)	2.1(16)
C(18)–C(22)–C(23)–C(21)	−2.0(15)	C(18)–C(22)–C(23)–C(24)	−180.0(10)
C(21)–C(23)–C(24)–C(25)	0.6(15)	C(21)–C(23)–C(24)–C(27)	179.6(9)
C(22)–C(23)–C(24)–C(25)	178.5(10)	C(22)–C(23)–C(24)–C(27)	−2.5(15)
C(23)–C(24)–C(25)–C(1)	−0.8(15)	C(23)–C(24)–C(25)–C(26)	−178.0(9)
C(27)–C(24)–C(25)–C(1)	−179.8(9)	C(27)–C(24)–C(25)–C(26)	3.0(15)
N(1)–C(1)–C(25)–C(24)	0.6(16)	N(1)–C(1)–C(25)–C(26)	177.8(10)
C(2)–C(1)–C(25)–C(24)	−179.6(10)	C(2)–C(1)–C(25)–C(26)	−2.4(16)
C(7)–C(8)–C(26)–C(4)	−2.5(15)	C(7)–C(8)–C(26)–C(25)	178.5(9)
C(9)–C(8)–C(26)–C(4)	−179.8(10)	C(9)–C(8)–C(26)–C(25)	1.2(15)
C(3)–C(4)–C(26)–C(8)	−177.6(10)	C(3)–C(4)–C(26)–C(25)	1.4(15)
C(5)–C(4)–C(26)–C(8)	1.2(16)	C(5)–C(4)–C(26)–C(25)	−179.8(10)
C(1)–C(25)–C(26)–C(4)	0.2(15)	C(1)–C(25)–C(26)–C(8)	179.2(10)
C(24)–C(25)–C(26)–C(4)	177.3(10)	C(24)–C(25)–C(26)–C(8)	−3.6(15)
C(23)–C(24)–C(27)–C(9)	−178.9(9)	C(23)–C(24)–C(27)–C(13)	1.0(14)
C(25)–C(24)–C(27)–C(9)	0.1(14)	C(25)–C(24)–C(27)–C(13)	−180.0(9)
C(12)–C(13)–C(27)–C(9)	1.2(15)	C(12)–C(13)–C(27)–C(24)	−178.7(9)
C(14)–C(13)–C(27)–C(9)	−179.4(9)	C(14)–C(13)–C(27)–C(24)	0.7(15)
C(8)–C(9)–C(27)–C(13)	177.7(9)	C(8)–C(9)–C(27)–C(24)	−2.4(14)
C(10)–C(9)–C(27)–C(13)	−0.6(14)	C(10)–C(9)–C(27)–C(24)	179.3(9)
C(1)–N(1)–C(28)–C(29)	−110.5(12)	C(1)–N(1)–C(28)–C(33)	73.3(12)

C(21)–N(1)–C(28)–C(29)	68.2(13)	C(21)–N(1)–C(28)–C(33)	−108.0(11)
N(1)–C(28)–C(29)–C(30)	−175.7(9)	C(33)–C(28)–C(29)–C(30)	0.2(16)
C(28)–C(29)–C(30)–C(31)	0.2(16)	C(28)–C(29)–C(30)–O(1)	177.9(10)
C(29)–C(30)–C(31)–C(32)	−3.3(17)	C(29)–C(30)–C(31)–O(2)	−178.3(9)
O(1)–C(30)–C(31)–C(32)	178.9(10)	O(1)–C(30)–C(31)–O(2)	3.8(15)
C(30)–C(31)–C(32)–C(33)	6.0(17)	C(30)–C(31)–C(32)–O(3)	−176.4(10)
O(2)–C(31)–C(32)–C(33)	−179.0(9)	O(2)–C(31)–C(32)–O(3)	−1.4(14)
C(31)–C(32)–C(33)–C(28)	−5.3(15)	O(3)–C(32)–C(33)–C(28)	177.3(9)
N(1)–C(28)–C(33)–C(32)	178.3(9)	C(29)–C(28)–C(33)–C(32)	2.4(16)
C(10)–C(11)–C(37)–C(38)	−23.5(16)	C(10)–C(11)–C(37)–C(42)	153.5(11)
C(12)–C(11)–C(37)–C(38)	158.5(11)	C(12)–C(11)–C(37)–C(42)	−24.5(17)
C(11)–C(37)–C(38)–C(39)	176.4(11)	C(42)–C(37)–C(38)–C(39)	−0.6(17)
C(37)–C(38)–C(39)–C(40)	−1.7(18)	C(43)–N(2)–C(40)–C(39)	18(2)
C(43)–N(2)–C(40)–C(41)	−165.4(13)	C(44)–N(2)–C(40)–C(39)	−166.0(13)
C(44)–N(2)–C(40)–C(41)	11(2)	C(38)–C(39)–C(40)–N(2)	179.9(11)
C(38)–C(39)–C(40)–C(41)	3.2(19)	N(2)–C(40)–C(41)–C(42)	−179.1(12)
C(39)–C(40)–C(41)–C(42)	−2(2)	C(40)–C(41)–C(42)–C(37)	0(2)
C(11)–C(37)–C(42)–C(41)	−175.8(11)	C(38)–C(37)–C(42)–C(41)	1.4(18)
C(29)–C(30)–O(1)–C(34)	−1.3(16)	C(31)–C(30)–O(1)–C(34)	176.4(11)
C(30)–C(31)–O(2)–C(35)	−84.0(12)	C(32)–C(31)–O(2)–C(35)	100.7(12)
C(31)–C(32)–O(3)–C(36)	164.5(9)	C(33)–C(32)–O(3)–C(36)	−18.0(14)
C(65)–N(3)–C(45)–C(46)	−175.1(10)	C(65)–N(3)–C(45)–C(69)	2.7(15)
C(72)–N(3)–C(45)–C(46)	5.7(15)	C(72)–N(3)–C(45)–C(69)	−176.5(10)
N(3)–C(45)–C(46)–C(47)	179.1(10)	C(69)–C(45)–C(46)–C(47)	1.2(15)
C(45)–C(46)–C(47)–C(48)	−0.4(16)	C(46)–C(47)–C(48)–C(49)	−179.4(10)
C(46)–C(47)–C(48)–C(70)	−3.2(16)	C(47)–C(48)–C(49)–C(50)	177.8(10)
C(70)–C(48)–C(49)–C(50)	1.6(16)	C(48)–C(49)–C(50)–C(51)	−2.5(16)
C(49)–C(50)–C(51)–C(52)	3.4(16)	C(50)–C(51)–C(52)–C(53)	176.9(9)
C(50)–C(51)–C(52)–C(70)	−3.5(15)	C(51)–C(52)–C(53)–C(54)	−2.8(15)
C(51)–C(52)–C(53)–C(71)	177.9(10)	C(70)–C(52)–C(53)–C(54)	177.5(10)
C(70)–C(52)–C(53)–C(71)	−1.8(14)	C(52)–C(53)–C(54)–C(55)	179.3(9)
C(71)–C(53)–C(54)–C(55)	−1.4(16)	C(53)–C(54)–C(55)–C(56)	−0.1(16)
C(53)–C(54)–C(55)–C(81)	175.4(10)	C(54)–C(55)–C(56)–C(57)	−1.4(16)
C(81)–C(55)–C(56)–C(57)	−176.7(10)	C(55)–C(56)–C(57)–C(58)	178.7(10)
C(55)–C(56)–C(57)–C(71)	4.0(16)	C(56)–C(57)–C(58)–C(59)	6.3(17)
C(56)–C(57)–C(58)–C(66)	−177.2(10)	C(71)–C(57)–C(58)–C(59)	−179.2(10)
C(71)–C(57)–C(58)–C(66)	−2.7(15)	C(57)–C(58)–C(59)–C(60)	177.4(10)
C(66)–C(58)–C(59)–C(60)	0.7(15)	C(58)–C(59)–C(60)–C(61)	−0.2(16)
C(59)–C(60)–C(61)–C(62)	0.5(16)	C(60)–C(61)–C(62)–C(63)	179.1(10)
C(60)–C(61)–C(62)–C(66)	−1.2(16)	C(61)–C(62)–C(63)–C(64)	−178.3(11)
C(66)–C(62)–C(63)–C(64)	2.0(17)	C(62)–C(63)–C(64)–C(65)	−4.9(16)
C(63)–C(64)–C(65)–N(3)	−177.5(10)	C(63)–C(64)–C(65)–C(67)	5.5(16)
C(45)–N(3)–C(65)–C(64)	−178.9(10)	C(45)–N(3)–C(65)–C(67)	−1.8(15)
C(72)–N(3)–C(65)–C(64)	0.2(15)	C(72)–N(3)–C(65)–C(67)	177.4(10)
C(61)–C(62)–C(66)–C(58)	1.8(16)	C(61)–C(62)–C(66)–C(67)	−179.3(10)
C(63)–C(62)–C(66)–C(58)	−178.5(10)	C(63)–C(62)–C(66)–C(67)	0.4(16)
C(57)–C(58)–C(66)–C(62)	−178.3(10)	C(57)–C(58)–C(66)–C(67)	2.8(15)
C(59)–C(58)–C(66)–C(62)	−1.5(15)	C(59)–C(58)–C(66)–C(67)	179.6(9)
N(3)–C(65)–C(67)–C(66)	179.8(9)	N(3)–C(65)–C(67)–C(68)	2.1(15)
C(64)–C(65)–C(67)–C(66)	−3.2(16)	C(64)–C(65)–C(67)–C(68)	179.1(10)
C(58)–C(66)–C(67)–C(65)	179.1(10)	C(58)–C(66)–C(67)–C(68)	−3.2(15)
C(62)–C(66)–C(67)–C(65)	0.2(15)	C(62)–C(66)–C(67)–C(68)	177.9(10)

C(65)–C(67)–C(68)–C(69)	−3.2(15)	C(65)–C(67)–C(68)–C(71)	−178.9(10)
C(66)–C(67)–C(68)–C(69)	179.2(9)	C(66)–C(67)–C(68)–C(71)	3.5(16)
N(3)–C(45)–C(69)–C(68)	−3.8(15)	N(3)–C(45)–C(69)–C(70)	−176.3(9)
C(46)–C(45)–C(69)–C(68)	174.2(9)	C(46)–C(45)–C(69)–C(70)	1.6(15)
C(67)–C(68)–C(69)–C(45)	4.0(14)	C(67)–C(68)–C(69)–C(70)	176.7(10)
C(71)–C(68)–C(69)–C(45)	179.8(9)	C(71)–C(68)–C(69)–C(70)	−7.5(14)
C(45)–C(69)–C(70)–C(48)	−5.0(15)	C(45)–C(69)–C(70)–C(52)	178.8(9)
C(68)–C(69)–C(70)–C(48)	−177.5(9)	C(68)–C(69)–C(70)–C(52)	6.3(15)
C(51)–C(52)–C(70)–C(48)	2.5(14)	C(51)–C(52)–C(70)–C(69)	178.7(9)
C(53)–C(52)–C(70)–C(48)	−177.8(9)	C(53)–C(52)–C(70)–C(69)	−1.6(14)
C(47)–C(48)–C(70)–C(52)	−178.0(9)	C(47)–C(48)–C(70)–C(69)	5.8(15)
C(49)–C(48)–C(70)–C(52)	−1.6(15)	C(49)–C(48)–C(70)–C(69)	−177.9(9)
C(52)–C(53)–C(71)–C(57)	−176.4(9)	C(52)–C(53)–C(71)–C(68)	0.4(15)
C(54)–C(53)–C(71)–C(57)	4.3(15)	C(54)–C(53)–C(71)–C(68)	−179.0(9)
C(67)–C(68)–C(71)–C(53)	179.9(10)	C(67)–C(68)–C(71)–C(57)	−3.2(15)
C(69)–C(68)–C(71)–C(53)	4.2(15)	C(69)–C(68)–C(71)–C(57)	−178.9(9)
C(56)–C(57)–C(71)–C(53)	−5.5(15)	C(56)–C(57)–C(71)–C(68)	177.7(10)
C(58)–C(57)–C(71)–C(53)	179.7(10)	C(58)–C(57)–C(71)–C(68)	2.8(14)
C(45)–N(3)–C(72)–C(73)	−108.6(11)	C(45)–N(3)–C(72)–C(77)	70.0(12)
C(65)–N(3)–C(72)–C(73)	72.2(13)	C(65)–N(3)–C(72)–C(77)	−109.2(11)
N(3)–C(72)–C(73)–C(74)	176.0(9)	C(77)–C(72)–C(73)–C(74)	−2.5(17)
C(72)–C(73)–C(74)–C(75)	0.9(16)	C(72)–C(73)–C(74)–O(4)	175.4(10)
C(73)–C(74)–C(75)–C(76)	−0.4(16)	C(73)–C(74)–C(75)–O(5)	178.6(9)
O(4)–C(74)–C(75)–C(76)	−175.5(10)	O(4)–C(74)–C(75)–O(5)	3.5(15)
C(74)–C(75)–C(76)–C(77)	1.3(18)	C(74)–C(75)–C(76)–O(6)	179.9(9)
O(5)–C(75)–C(76)–C(77)	−177.7(10)	O(5)–C(75)–C(76)–O(6)	0.9(16)
N(3)–C(72)–C(77)–C(76)	−175.4(9)	C(73)–C(72)–C(77)–C(76)	3.1(15)
C(75)–C(76)–C(77)–C(72)	−2.5(16)	O(6)–C(76)–C(77)–C(72)	178.9(9)
C(54)–C(55)–C(81)–C(82)	−28.5(16)	C(54)–C(55)–C(81)–C(86)	158.1(10)
C(56)–C(55)–C(81)–C(82)	146.7(11)	C(56)–C(55)–C(81)–C(86)	−26.7(16)
C(55)–C(81)–C(82)–C(83)	−174.8(11)	C(86)–C(81)–C(82)–C(83)	−1.2(18)
C(81)–C(82)–C(83)–C(84)	3.7(19)	C(87)–N(4)–C(84)–C(83)	20(2)
C(87)–N(4)–C(84)–C(85)	−160.0(14)	C(88)–N(4)–C(84)–C(83)	−178.0(13)
C(88)–N(4)–C(84)–C(85)	2(2)	C(82)–C(83)–C(84)–N(4)	175.1(12)
C(82)–C(83)–C(84)–C(85)	−4.5(19)	N(4)–C(84)–C(85)–C(86)	−176.4(12)
C(83)–C(84)–C(85)–C(86)	3.2(19)	C(84)–C(85)–C(86)–C(81)	−0.9(18)
C(55)–C(81)–C(86)–C(85)	173.6(10)	C(82)–C(81)–C(86)–C(85)	−0.2(16)
C(73)–C(74)–O(4)–C(78)	−15.6(16)	C(75)–C(74)–O(4)–C(78)	159.1(10)
C(74)–C(75)–O(5)–C(79)	90.0(12)	C(76)–C(75)–O(5)–C(79)	−91.0(13)
C(75)–C(76)–O(6)–C(80)	179.6(11)	C(77)–C(76)–O(6)–C(80)	−1.8(15)

Table 5. Anisotropic displacement parameters ($Å^2$) for acb130007. The anisotropic displacement factor exponent takes the form: $-2\pi^2[h^2a^{*2}U^{11} + ...+ 2hka^*b^*U^{12}]$

	U^{11}	U^{22}	U^{33}	U^{23}	U^{13}	U^{12}
N(1)	0.053(6)	0.057(6)	0.054(6)	0.012(5)	0.003(5)	–0.001(5)
N(2)	0.109(10)	0.145(11)	0.050(7)	–0.002(7)	–0.003(7)	0.062(9)
C(1)	0.046(7)	0.060(8)	0.071(9)	0.014(7)	0.014(7)	0.010(7)
C(2)	0.050(7)	0.067(8)	0.050(7)	0.008(6)	–0.003(6)	0.005(7)
C(3)	0.043(7)	0.054(7)	0.071(9)	0.006(6)	0.009(6)	0.006(6)
C(4)	0.059(8)	0.050(7)	0.060(8)	0.010(6)	0.015(7)	–0.004(6)
C(5)	0.053(8)	0.049(7)	0.068(9)	0.012(6)	0.011(7)	0.016(6)
C(6)	0.055(8)	0.037(7)	0.077(9)	0.007(6)	0.000(7)	0.009(6)
C(7)	0.048(7)	0.048(7)	0.080(9)	0.017(7)	0.005(7)	–0.007(6)
C(8)	0.034(7)	0.046(7)	0.079(9)	0.019(7)	0.010(6)	–0.002(6)
C(9)	0.035(7)	0.034(6)	0.065(8)	0.003(6)	0.008(6)	0.005(5)
C(10)	0.044(7)	0.046(7)	0.069(9)	0.006(6)	0.007(7)	–0.004(6)
C(11)	0.049(7)	0.040(7)	0.063(8)	0.001(6)	0.001(6)	0.010(6)
C(12)	0.041(7)	0.049(7)	0.072(9)	0.008(6)	0.009(6)	–0.002(6)
C(13)	0.059(8)	0.042(7)	0.048(7)	0.009(6)	0.010(6)	0.002(6)
C(14)	0.056(7)	0.051(7)	0.046(7)	–0.002(6)	0.007(6)	0.014(6)
C(15)	0.060(8)	0.049(7)	0.063(8)	0.019(6)	0.014(7)	0.005(6)
C(16)	0.056(8)	0.039(7)	0.074(9)	0.017(6)	0.020(7)	0.008(6)
C(17)	0.046(7)	0.049(7)	0.068(9)	0.014(6)	–0.002(7)	0.000(6)
C(18)	0.039(7)	0.038(6)	0.066(8)	0.011(6)	0.003(6)	0.006(6)
C(19)	0.038(7)	0.055(8)	0.073(9)	0.019(7)	–0.004(7)	0.000(6)
C(20)	0.054(8)	0.061(8)	0.074(8)	0.022(7)	0.010(7)	0.020(7)
C(21)	0.062(8)	0.050(7)	0.064(8)	0.022(6)	0.012(7)	0.010(6)
C(22)	0.049(7)	0.048(7)	0.069(9)	0.015(6)	0.004(6)	0.011(6)
C(23)	0.060(8)	0.039(7)	0.046(7)	0.002(5)	0.008(6)	0.016(6)
C(24)	0.049(7)	0.023(6)	0.050(7)	0.010(5)	0.004(6)	–0.003(5)
C(25)	0.049(7)	0.035(7)	0.054(8)	–0.002(6)	0.002(6)	–0.006(6)
C(26)	0.044(7)	0.051(7)	0.055(8)	0.011(6)	0.004(6)	0.009(6)
C(27)	0.045(7)	0.034(6)	0.055(7)	0.007(6)	0.019(6)	–0.005(6)
C(28)	0.040(7)	0.039(7)	0.067(8)	0.015(7)	0.008(6)	–0.015(6)
C(29)	0.055(8)	0.053(8)	0.064(9)	0.015(7)	0.002(7)	–0.009(7)
C(30)	0.059(8)	0.050(8)	0.076(10)	0.019(8)	0.011(7)	0.005(7)
C(31)	0.062(9)	0.081(10)	0.056(9)	0.023(8)	0.013(7)	0.016(8)
C(32)	0.052(8)	0.055(8)	0.055(9)	0.009(7)	0.005(7)	0.009(7)
C(33)	0.056(8)	0.063(8)	0.058(8)	0.013(7)	0.012(7)	–0.001(7)
C(34)	0.122(13)	0.088(11)	0.106(12)	0.042(10)	0.001(10)	–0.049(10)
C(35)	0.081(10)	0.092(10)	0.084(10)	0.037(8)	0.012(8)	0.025(8)
C(36)	0.061(8)	0.074(9)	0.063(8)	0.005(7)	–0.004(7)	0.001(7)
C(37)	0.056(8)	0.049(7)	0.072(9)	0.015(7)	0.005(7)	0.015(6)
C(38)	0.064(8)	0.058(8)	0.070(9)	0.020(7)	–0.003(7)	0.011(7)
C(39)	0.069(9)	0.060(8)	0.068(9)	0.004(7)	0.001(7)	0.017(7)
C(40)	0.081(9)	0.077(9)	0.046(8)	–0.005(7)	0.007(7)	0.022(8)
C(41)	0.086(10)	0.098(11)	0.059(9)	–0.015(8)	–0.018(8)	0.042(9)
C(42)	0.060(8)	0.063(8)	0.086(10)	0.002(7)	0.012(7)	0.029(7)
C(43)	0.075(9)	0.087(10)	0.080(9)	0.030(8)	0.000(8)	0.004(8)
C(44)	0.090(11)	0.151(14)	0.063(9)	–0.013(9)	–0.014(8)	0.034(10)
O(1)	0.091(7)	0.059(6)	0.075(6)	0.031(5)	0.002(5)	–0.006(5)
O(2)	0.070(6)	0.087(6)	0.054(5)	0.011(4)	0.007(4)	0.028(5)

O(3)	0.065(5)	0.078(6)	0.059(5)	0.015(5)	0.014(4)	0.015(5)
N(3)	0.053(6)	0.054(6)	0.048(6)	0.003(5)	−0.001(5)	0.001(5)
N(4)	0.142(11)	0.106(9)	0.062(8)	0.015(7)	0.036(8)	0.068(8)
C(45)	0.053(7)	0.045(7)	0.054(8)	0.012(6)	−0.001(6)	0.009(6)
C(46)	0.046(7)	0.053(7)	0.058(7)	0.016(6)	0.010(6)	0.014(6)
C(47)	0.067(8)	0.051(7)	0.060(8)	0.008(6)	0.022(7)	0.012(7)
C(48)	0.048(7)	0.047(7)	0.061(8)	0.013(6)	0.007(7)	0.007(6)
C(49)	0.045(7)	0.069(8)	0.064(8)	0.017(7)	0.019(7)	0.004(6)
C(50)	0.044(7)	0.061(8)	0.072(9)	0.014(7)	0.019(6)	0.013(6)
C(51)	0.049(7)	0.052(7)	0.051(7)	0.014(6)	0.011(6)	0.012(6)
C(52)	0.039(7)	0.031(6)	0.066(8)	0.010(6)	0.012(6)	−0.005(5)
C(53)	0.049(7)	0.039(6)	0.058(8)	0.013(6)	0.009(6)	0.011(6)
C(54)	0.043(7)	0.055(7)	0.064(8)	0.023(6)	0.000(6)	0.022(6)
C(55)	0.036(7)	0.052(7)	0.065(8)	0.016(6)	0.008(6)	−0.001(6)
C(56)	0.061(8)	0.048(7)	0.056(8)	0.018(6)	0.013(6)	0.025(6)
C(57)	0.045(7)	0.056(7)	0.048(7)	0.006(6)	0.004(6)	0.007(6)
C(58)	0.042(7)	0.041(7)	0.061(8)	0.007(6)	0.002(6)	−0.005(6)
C(59)	0.040(7)	0.053(7)	0.081(9)	0.017(7)	0.010(7)	0.003(6)
C(60)	0.042(7)	0.040(7)	0.078(9)	0.028(6)	−0.003(6)	0.011(6)
C(61)	0.049(7)	0.065(8)	0.055(8)	0.016(6)	−0.007(6)	0.004(6)
C(62)	0.043(7)	0.057(8)	0.059(8)	0.006(6)	0.004(6)	0.015(6)
C(63)	0.058(8)	0.066(8)	0.051(8)	0.004(6)	−0.003(6)	0.011(7)
C(64)	0.051(7)	0.057(8)	0.059(7)	0.022(6)	0.011(6)	0.007(6)
C(65)	0.052(7)	0.041(7)	0.060(8)	0.000(6)	−0.003(7)	0.014(6)
C(66)	0.049(7)	0.044(7)	0.052(7)	0.009(6)	0.013(6)	0.005(6)
C(67)	0.035(7)	0.049(7)	0.074(9)	0.013(7)	0.004(6)	0.002(6)
C(68)	0.045(7)	0.053(7)	0.046(7)	0.004(6)	0.019(6)	0.018(6)
C(69)	0.033(6)	0.044(7)	0.066(8)	0.019(6)	0.002(6)	−0.002(6)
C(70)	0.042(7)	0.041(7)	0.055(8)	0.007(6)	−0.002(6)	−0.002(6)
C(71)	0.041(7)	0.045(7)	0.062(8)	0.015(6)	0.017(6)	0.005(6)
C(72)	0.035(7)	0.054(8)	0.058(8)	0.002(7)	−0.006(6)	0.001(6)
C(73)	0.059(8)	0.053(8)	0.070(9)	0.015(7)	0.004(7)	0.002(7)
C(74)	0.056(8)	0.052(9)	0.068(9)	0.023(8)	0.005(7)	0.005(7)
C(75)	0.057(8)	0.068(10)	0.050(8)	0.014(8)	0.006(7)	−0.002(7)
C(76)	0.065(9)	0.049(8)	0.069(9)	0.000(8)	0.001(7)	−0.004(7)
C(77)	0.066(8)	0.046(8)	0.071(9)	0.023(7)	0.009(7)	0.010(7)
C(78)	0.111(12)	0.066(10)	0.091(10)	0.029(8)	0.022(9)	0.013(8)
C(79)	0.081(10)	0.120(12)	0.095(11)	0.008(9)	0.039(9)	0.026(9)
C(80)	0.118(12)	0.064(9)	0.082(10)	−0.003(8)	0.029(9)	−0.026(9)
C(81)	0.055(8)	0.066(8)	0.049(8)	−0.001(7)	0.007(6)	0.004(7)
C(82)	0.067(8)	0.076(9)	0.057(8)	0.026(7)	0.016(7)	0.034(7)
C(83)	0.069(9)	0.085(10)	0.060(9)	0.018(7)	0.001(7)	0.035(7)
C(84)	0.102(11)	0.074(9)	0.055(8)	0.018(7)	0.025(8)	0.038(8)
C(85)	0.072(9)	0.083(9)	0.049(8)	0.004(7)	0.019(7)	0.030(7)
C(86)	0.058(8)	0.065(8)	0.058(8)	0.008(6)	−0.001(6)	0.019(7)
C(87)	0.200(19)	0.146(15)	0.067(10)	0.022(10)	0.060(11)	0.068(14)
C(88)	0.125(13)	0.130(14)	0.086(11)	0.033(10)	0.039(10)	0.044(11)
O(4)	0.102(7)	0.059(6)	0.067(6)	0.014(5)	0.009(5)	0.014(5)
O(5)	0.079(6)	0.069(5)	0.053(5)	0.003(4)	0.010(4)	0.007(5)
O(6)	0.091(6)	0.055(6)	0.067(5)	0.002(5)	0.016(5)	−0.012(5)
P(1)	0.066(2)	0.070(3)	0.070(2)	0.0107(18)	0.0073(19)	0.032(2)
F(1)	0.110(6)	0.065(5)	0.121(6)	0.005(4)	0.045(5)	−0.001(4)
F(2)	0.076(5)	0.079(5)	0.098(5)	0.027(4)	0.023(4)	0.045(4)

F(3)	0.114(6)	0.139(7)	0.059(5)	0.008(4)	0.000(4)	0.071(5)
F(4)	0.076(5)	0.085(5)	0.094(5)	0.010(4)	0.034(4)	0.030(4)
F(5)	0.091(6)	0.167(8)	0.091(5)	0.075(5)	0.018(4)	0.056(5)
F(6)	0.077(5)	0.072(5)	0.202(9)	0.004(6)	0.026(6)	0.000(4)
P(2)	0.087(3)	0.051(2)	0.060(2)	0.0125(16)	0.010(2)	0.0174(19)
F(7)	0.096(5)	0.045(4)	0.084(5)	0.010(3)	0.012(4)	0.021(4)
F(8)	0.072(4)	0.060(4)	0.076(4)	0.013(3)	0.026(4)	0.016(3)
F(9)	0.079(5)	0.056(4)	0.076(4)	0.016(3)	0.002(4)	0.018(3)
F(10)	0.099(5)	0.063(4)	0.070(4)	0.014(3)	0.029(4)	0.025(4)
F(11)	0.087(5)	0.063(4)	0.071(4)	0.011(3)	−0.006(4)	0.007(4)
F(12)	0.084(5)	0.053(4)	0.083(5)	0.025(3)	0.009(4)	0.011(4)

Table 6. Hydrogen coordinates and isotropic displacement parameters ($Å^2$) for acb130007.

	x	y	z	U
H(2)	0.2528	–0.1185	0.2359	0.070
H(3)	0.4107	–0.1888	0.2730	0.070
H(5)	0.5517	–0.2235	0.3638	0.068
H(6)	0.6091	–0.2035	0.4740	0.071
H(7)	0.5094	–0.1132	0.5471	0.072
H(10)	0.4228	–0.0278	0.6102	0.067
H(12)	0.1448	0.1252	0.6434	0.067
H(15)	–0.0095	0.1788	0.6081	0.067
H(16)	–0.1789	0.2435	0.5662	0.066
H(17)	–0.2347	0.2186	0.4552	0.067
H(19)	–0.2031	0.1461	0.3439	0.068
H(20)	–0.0942	0.0603	0.2741	0.074
H(29)	0.1498	0.0747	0.2348	0.070
H(33)	–0.0225	–0.1381	0.2159	0.071
H(34A)	0.0968	0.1706	0.1854	0.158
H(34B)	0.1422	0.1824	0.1220	0.158
H(34C)	0.2342	0.1409	0.1648	0.158
H(35A)	–0.2550	–0.0545	0.0358	0.124
H(35B)	–0.1971	–0.0275	–0.0189	0.124
H(35C)	–0.1752	0.0272	0.0530	0.124
H(36A)	–0.0069	–0.2561	0.1163	0.106
H(36B)	–0.1537	–0.2853	0.0797	0.106
H(36C)	–0.1314	–0.2324	0.1523	0.106
H(38)	0.4248	–0.0329	0.7059	0.078
H(39)	0.5105	–0.0045	0.8146	0.083
H(41)	0.3670	0.2069	0.8457	0.109
H(42)	0.2778	0.1754	0.7362	0.088
H(43A)	0.5652	0.0249	0.9195	0.121
H(43B)	0.6349	0.0987	0.9740	0.121
H(43C)	0.6790	0.0765	0.9046	0.121
H(44A)	0.5120	0.2364	0.9502	0.169
H(44B)	0.4928	0.1859	0.9974	0.169
H(44C)	0.3711	0.1929	0.9457	0.169
H(46)	0.9632	0.2900	0.2652	0.062
H(47)	1.1118	0.2466	0.3312	0.071
H(49)	1.2106	0.2436	0.4409	0.071
H(50)	1.2203	0.2867	0.5522	0.071
H(51)	1.0836	0.3828	0.5974	0.060
H(54)	0.9428	0.4547	0.6352	0.064
H(56)	0.6478	0.5900	0.6083	0.064
H(59)	0.5228	0.6374	0.5459	0.070
H(60)	0.3837	0.6824	0.4762	0.063
H(61)	0.3820	0.6353	0.3650	0.070
H(63)	0.4670	0.5474	0.2733	0.074
H(64)	0.5971	0.4469	0.2320	0.065
H(73)	0.8541	0.4523	0.2111	0.074
H(77)	0.6840	0.2520	0.2254	0.072
H(78A)	0.7831	0.5037	0.1200	0.131

H(78B)	0.8813	0.5066	0.0700	0.131
H(78C)	0.9397	0.5060	0.1410	0.131
H(79A)	0.9696	0.2592	0.0279	0.151
H(79B)	0.8845	0.1965	–0.0315	0.151
H(79C)	0.9101	0.1819	0.0372	0.151
H(80A)	0.6971	0.1233	0.1703	0.138
H(80B)	0.6008	0.0741	0.1075	0.138
H(80C)	0.5513	0.1487	0.1537	0.138
H(82)	0.8505	0.4548	0.7243	0.076
H(83)	0.8297	0.4874	0.8317	0.086
H(85)	0.6890	0.6868	0.8178	0.084
H(86)	0.7179	0.6565	0.7108	0.076
H(87A)	0.7894	0.5117	0.9216	0.201
H(87B)	0.7472	0.5746	0.9808	0.201
H(87C)	0.8844	0.5873	0.9567	0.201
H(88A)	0.7308	0.7184	0.9367	0.165
H(88B)	0.6317	0.6720	0.9652	0.165
H(88C)	0.5908	0.6818	0.8954	0.165

Table 1. Crystal data and structure refinement for **MSV1**.

Identification code	**MSV1**	
Chemical formula (moiety)	$C_{12}H_{12}F_{12}N_2P_2S$	
Chemical formula (total)	$C_{12}H_{12}F_{12}N_2P_2S$	
Formula weight	506.24	
Temperature	293(2) K	
Radiation, wavelength	CuKα, 1.54178 Å	
Crystal system, space group	monoclinic, $P2_1/c$	
Unit cell parameters	a = 6.1108(5) Å	α = 90°
	b = 11.5152(8) Å	β = 99.776(8)°
	c = 12.9622(9) Å	γ = 90°
Cell volume	898.87(11) $Å^3$	
Z	2	
Calculated density	1.870 g/cm^3	
Absorption coefficient μ	4.481 mm^{-1}	
F(000)	504	
Crystal colour and size	colourless, 0.40 × 0.04 × 0.04 mm^3	
Reflections for cell refinement	1067 (θ range 3.5 to 61.8°)	
Data collection method	Xcalibur, Atlas, Gemini ultra thick-slice ω scans	
θ range for data collection	7.7 to 50.4°	
Index ranges	h −5 to 6, k −7 to 11, l −12 to 12	
Completeness to θ = 50.4°	99.4 %	
Reflections collected	1717	
Independent reflections	932 (R_{int} = 0.0233)	
Reflections with $F^2>2\sigma$	822	
Absorption correction	semi-empirical from equivalents	
Min. and max. transmission	0.2673 and 0.8411	
Structure solution	direct methods	
Refinement method	Full-matrix least-squares on F^2	
Weighting parameters a, b	0.0891, 3.0674	
Data / restraints / parameters	932 / 98 / 166	
Final R indices [$F^2>2\sigma$]	R1 = 0.0599, wR2 = 0.1571	
R indices (all data)	R1 = 0.0666, wR2 = 0.1633	
Goodness-of-fit on F^2	1.070	
Extinction coefficient	0.0015(8)	
Largest and mean shift/su	0.022 and 0.001	
Largest diff. peak and hole	0.67 and −0.32 e $Å^{-3}$	

Table 2. Atomic coordinates and equivalent isotropic displacement parameters ($Å^2$) for acb93. U_{eq} is defined as one third of the trace of the orthogonalized U^{ij} tensor.

	x	y	z	U_{eq}
S(1)	0.2702(4)	0.4430(2)	0.0812(2)	0.0379(9)
P(1)	0.0020(2)	0.13993(14)	0.17183(11)	0.0392(7)
F(1)	–0.0328(7)	0.0184(4)	0.1103(3)	0.0872(16)
F(2)	0.0367(7)	0.2561(4)	0.2358(4)	0.0993(17)
F(3)	–0.0343(7)	0.2041(5)	0.0644(3)	0.0980(18)
F(4)	0.0389(7)	0.0703(4)	0.2775(3)	0.0788(14)
F(5)	0.2688(5)	0.1347(4)	0.1856(3)	0.0665(13)
F(6)	–0.2659(5)	0.1442(3)	0.1572(3)	0.0552(11)
N(1)	0.4828(7)	0.7746(4)	0.0953(3)	0.0376(13)
C(1)	0.6149(10)	0.7528(6)	0.0323(5)	0.0509(17)
C(2)	0.4755(13)	0.8908(6)	0.1348(7)	0.078(2)
C(3)	0.3567(11)	0.6916(6)	0.1205(5)	0.0519(17)
C(4)	0.548(5)	0.5684(17)	0.0091(18)	0.040(5)
C(5)	0.663(4)	0.666(2)	–0.0117(16)	0.045(4)
C(6)	0.401(5)	0.5722(19)	0.069(2)	0.038(5)
C(4A)	0.442(5)	0.552(2)	0.0334(19)	0.042(5)
C(5A)	0.583(4)	0.623(2)	–0.0020(14)	0.035(4)
C(6A)	0.322(4)	0.5893(17)	0.0983(16)	0.044(4)

Table 3. Bond lengths [Å] and angles [°] for acb93.

S(1)–C(4A)	1.75(3)	S(1)–C(5A)	1.64(2)
S(1)–C(6)	1.71(2)	S(1)–C(4A)	1.81(3)
S(1)–C(5AA)	1.66(2)	S(1)–C(6A)	1.721(19)
P(1)–F(1)	1.607(4)	P(1)–F(2)	1.569(4)
P(1)–F(3)	1.559(4)	P(1)–F(4)	1.569(4)
P(1)–F(5)	1.611(4)	P(1)–F(6)	1.616(3)
N(1)–C(1)	1.266(8)	N(1)–C(2)	1.437(8)
N(1)–C(3)	1.304(8)	C(1)–H(1A)	0.930
C(1)–C(5)	1.209(19)	C(1)–C(5A)	1.56(3)
C(2)–H(2A)	0.960	C(2)–H(2B)	0.960
C(2)–H(2C)	0.960	C(3)–H(3A)	0.930
C(3)–C(6)	1.57(3)	C(3)–C(6A)	1.223(19)
C(4)–S(1A)	1.75(3)	C(4)–C(4A)	1.68(4)
C(4)–C(5)	1.38(2)	C(4)–C(6)	1.28(3)
C(4)–C(6A)	1.96(4)	C(5)–S(1A)	1.64(2)
C(6)–C(4A)	1.96(4)	C(4A)–C(4AA)	1.71(4)
C(4A)–C(5A)	1.32(3)	C(4A)–C(6A)	1.28(2)
C(5A)–S(1A)	1.66(2)		

C(4A)–S(1)–C(5A)	47.9(9)	C(4A)–S(1)–C(6)	69.0(9)
C(4A)–S(1)–C(4A)	49.8(6)	C(4A)–S(1)–C(5AA)	23.1(8)
C(4A)–S(1)–C(6A)	92.1(9)	C(5A)–S(1)–C(6)	116.8(9)
C(5A)–S(1)–C(4A)	97.6(9)	C(5A)–S(1)–C(5AA)	25.4(6)
C(5A)–S(1)–C(6A)	139.9(8)	C(6)–S(1)–C(4A)	19.4(9)
C(6)–S(1)–C(5AA)	91.7(9)	C(6)–S(1)–C(6A)	23.4(6)
C(4A)–S(1)–C(5AA)	72.6(9)	C(4A)–S(1)–C(6A)	42.4(8)
C(5AA)–S(1)–C(6A)	115.0(9)	F(1)–P(1)–F(2)	177.9(3)
F(1)–P(1)–F(3)	89.0(3)	F(1)–P(1)–F(4)	88.6(3)
F(1)–P(1)–F(5)	93.9(2)	F(1)–P(1)–F(6)	85.5(2)
F(2)–P(1)–F(3)	93.1(3)	F(2)–P(1)–F(4)	89.3(3)
F(2)–P(1)–F(5)	86.0(2)	F(2)–P(1)–F(6)	94.6(2)
F(3)–P(1)–F(4)	177.6(3)	F(3)–P(1)–F(5)	96.0(2)
F(3)–P(1)–F(6)	83.8(2)	F(4)–P(1)–F(5)	83.8(2)
F(4)–P(1)–F(6)	96.3(2)	F(5)–P(1)–F(6)	179.4(2)
C(1)–N(1)–C(2)	118.4(6)	C(1)–N(1)–C(3)	119.0(6)
C(2)–N(1)–C(3)	122.5(6)	N(1)–C(1)–H(1A)	112.8
N(1)–C(1)–C(5)	134.4(14)	N(1)–C(1)–C(5A)	108.1(11)
H(1A)–C(1)–C(5)	112.8	H(1A)–C(1)–C(5A)	138.9
C(5)–C(1)–C(5A)	26.6(9)	N(1)–C(2)–H(2A)	109.5
N(1)–C(2)–H(2B)	109.5	N(1)–C(2)–H(2C)	109.5
H(2A)–C(2)–H(2B)	109.5	H(2A)–C(2)–H(2C)	109.5
H(2B)–C(2)–H(2C)	109.5	N(1)–C(3)–H(3A)	123.8
N(1)–C(3)–C(6)	112.4(10)	N(1)–C(3)–C(6A)	137.2(13)
H(3A)–C(3)–C(6)	123.8	H(3A)–C(3)–C(6A)	98.9
C(6)–C(3)–C(6A)	25.0(10)	S(1A)–C(4)–C(4A)	95(2)
S(1A)–C(4)–C(5)	61.8(13)	S(1A)–C(4)–C(6)	175(2)
S(1A)–C(4)–C(6A)	54.5(12)	C(4A)–C(4)–C(5)	156(3)
C(4A)–C(4)–C(6)	82(3)	C(4A)–C(4)–C(6A)	40.2(13)
C(5)–C(4)–C(6)	121.5(19)	C(5)–C(4)–C(6A)	116(2)
C(6)–C(4)–C(6A)	122(2)	S(1A)–C(5)–C(1)	174(2)
S(1A)–C(5)–C(4)	70.3(17)	C(1)–C(5)–C(4)	114.1(16)
S(1)–C(6)–C(3)	127.0(19)	S(1)–C(6)–C(4)	114(2)
S(1)–C(6)–C(4A)	56.5(9)	C(3)–C(6)–C(4)	118.5(17)

C(3)–C(6)–C(4A)	174.3(19)	C(4)–C(6)–C(4A)	58(2)
S(1)–C(4A)–C(4AA)	90(2)	S(1)–C(4A)–C(5A)	174(2)
S(1)–C(4A)–C(6A)	65.0(15)	C(4AA)–C(4A)–C(5A)	85(3)
C(4AA)–C(4A)–C(6A)	155(3)	C(5A)–C(4A)–C(6A)	120.2(19)
S(1A)–C(5A)–C(1)	124.1(19)	S(1A)–C(5A)–C(4A)	113(2)
C(1)–C(5A)–C(4A)	123.1(16)	S(1)–C(6A)–C(3)	173.7(17)
S(1)–C(6A)–C(4A)	72.7(18)	C(3)–C(6A)–C(4A)	112.3(15)

Symmetry operations for equivalent atoms
A –x+1,–y+1,–z

Table 4. Anisotropic displacement parameters ($Å^2$) for acb93. The anisotropic displacement factor exponent takes the form: $-2\pi^2[h^2a^{*2}U^{11} + ...+ 2hka^*b^*U^{12}]$

	U^{11}	U^{22}	U^{33}	U^{23}	U^{13}	U^{12}
S(1)	0.0371(17)	0.0417(18)	0.0391(17)	0.0051(13)	0.0184(13)	–0.0078(13)
P(1)	0.0323(10)	0.0526(12)	0.0337(10)	0.0019(7)	0.0079(7)	–0.0042(7)
F(1)	0.077(3)	0.093(3)	0.097(3)	–0.045(3)	0.031(2)	–0.010(2)
F(2)	0.076(3)	0.068(3)	0.153(5)	–0.043(3)	0.018(3)	–0.006(2)
F(3)	0.060(3)	0.162(5)	0.073(3)	0.055(3)	0.013(2)	–0.011(3)
F(4)	0.076(3)	0.109(4)	0.052(3)	0.028(2)	0.014(2)	0.001(2)
F(5)	0.036(2)	0.109(3)	0.056(2)	0.002(2)	0.0123(16)	–0.0026(19)
F(6)	0.035(2)	0.078(3)	0.055(2)	0.0002(19)	0.0150(16)	–0.0025(16)
N(1)	0.037(3)	0.040(3)	0.037(3)	0.002(2)	0.008(2)	–0.001(2)
C(1)	0.039(4)	0.063(4)	0.053(4)	0.024(3)	0.011(3)	0.006(3)
C(2)	0.077(6)	0.060(5)	0.089(6)	–0.023(5)	–0.004(4)	0.016(4)
C(3)	0.048(4)	0.073(4)	0.035(4)	0.013(4)	0.008(3)	–0.008(4)
C(4)	0.030(12)	0.059(6)	0.031(9)	0.026(9)	0.002(8)	0.004(8)
C(5)	0.028(10)	0.061(10)	0.048(9)	0.022(7)	0.012(7)	–0.004(7)
C(6)	0.032(12)	0.051(7)	0.030(15)	0.030(6)	0.002(8)	–0.014(8)
C(4A)	0.027(12)	0.069(7)	0.029(13)	0.012(6)	0.000(8)	–0.008(7)
C(5A)	0.030(11)	0.066(9)	0.010(7)	0.019(10)	0.011(6)	0.011(9)
C(6A)	0.037(10)	0.070(6)	0.027(9)	0.018(7)	0.011(6)	–0.002(8)

Table 5. Hydrogen coordinates and isotropic displacement parameters ($Å^2$) for acb93.

	x	y	z	U
H(1A)	0.6924	0.8181	0.0164	0.061
H(2A)	0.4677	0.9451	0.0781	0.117
H(2B)	0.6069	0.9055	0.1852	0.117
H(2C)	0.3469	0.8996	0.1676	0.117
H(3A)	0.2523	0.7017	0.1643	0.062

Table 6. Torsion angles [°] for acb93.

C(2)–N(1)–C(1)–C(5)	178.0(15)	C(2)–N(1)–C(1)–C(5A)	−177.6(9)
C(3)–N(1)–C(1)–C(5)	−2.9(17)	C(3)–N(1)–C(1)–C(5A)	1.4(10)
C(1)–N(1)–C(3)–C(6)	2.3(13)	C(1)–N(1)–C(3)–C(6A)	−1.6(18)
C(2)–N(1)–C(3)–C(6)	−178.7(11)	C(2)–N(1)–C(3)–C(6A)	177.4(16)
N(1)–C(1)–C(5)–S(1A)	143(20)	N(1)–C(1)–C(5)–C(4)	1(3)
C(5A)–C(1)–C(5)–S(1A)	134(22)	C(5A)–C(1)–C(5)–C(4)	−8(2)
S(1A)–C(4)–C(5)–C(1)	176(2)	C(4A)–C(4)–C(5)–S(1A)	−11(7)
C(4A)–C(4)–C(5)–C(1)	165(6)	C(6)–C(4)–C(5)–S(1A)	−175(3)
C(6A)–C(4)–C(5)–S(1A)	−1.4(17)	C(6)–C(4)–C(5)–C(1)	1(4)
C(6A)–C(4)–C(5)–C(1)	175.0(14)	S(1A)–C(4)–C(6)–S(1)	51(21)
S(1A)–C(4)–C(6)–C(3)	−128(20)	S(1A)–C(4)–C(6)–C(4A)	46(20)
C(4A)–C(4)–C(6)–S(1)	4(2)	C(4A)–C(4)–C(6)–C(3)	−175(2)
C(5)–C(4)–C(6)–S(1)	178(2)	C(5)–C(4)–C(6)–C(3)	−1(4)
C(5)–C(4)–C(6)–C(4A)	173(4)	C(6A)–C(4)–C(6)–S(1)	4(2)
C(6A)–C(4)–C(6)–C(3)	−175(2)	C(6A)–C(4)–C(6)–C(4A)	0.000(2)
N(1)–C(3)–C(6)–S(1)	−179.4(15)	N(1)–C(3)–C(6)–C(4)	−1(3)
N(1)–C(3)–C(6)–C(4A)	−53(24)	C(6A)–C(3)–C(6)–S(1)	−6(2)
C(6A)–C(3)–C(6)–C(4)	173(5)	C(6A)–C(3)–C(6)–C(4A)	120(25)
C(4A)–S(1)–C(6)–C(3)	174(2)	C(4A)–S(1)–C(6)–C(4)	−4(2)
C(5A)–S(1)–C(6)–C(3)	175.8(16)	C(5A)–S(1)–C(6)–C(4)	−3(2)
C(5A)–S(1)–C(6)–C(4A)	1.3(15)	C(4A)–S(1)–C(6)–C(3)	168(6)
C(4A)–S(1)–C(6)–C(4)	−11(3)	C(4A)–S(1)–C(6)–C(4A)	−7(4)
C(5AA)–S(1)–C(6)–C(3)	178.8(19)	C(5AA)–S(1)–C(6)–C(4)	0(2)
C(5AA)–S(1)–C(6)–C(4A)	4.3(13)	C(6A)–S(1)–C(6)–C(3)	4.4(18)
C(6A)–S(1)–C(6)–C(4)	−175(5)	C(6A)–S(1)–C(6)–C(4A)	−170(3)
C(4A)–S(1)–C(4A)–C(4AA)	−5.8(15)	C(4A)–S(1)–C(4A)–C(5A)	−34(18)
C(4A)–S(1)–C(4A)–C(6A)	178(2)	C(5A)–S(1)–C(4A)–C(4AA)	−7(2)
C(5A)–S(1)–C(4A)–C(5A)	−35(19)	C(5A)–S(1)–C(4A)–C(6A)	177.4(16)
C(6)–S(1)–C(4A)–C(4AA)	166(6)	C(6)–S(1)–C(4A)–C(5A)	138(22)
C(6)–S(1)–C(4A)–C(6A)	−10(4)	C(5AA)–S(1)–C(4A)–C(4AA)	−2.4(16)
C(5AA)–S(1)–C(4A)–C(5A)	−30(19)	C(5AA)–S(1)–C(4A)–C(6A)	−178.2(19)
C(6A)–S(1)–C(4A)–C(4AA)	176(3)	C(6A)–S(1)–C(4A)–C(5A)	148(20)
S(1)–C(4A)–C(5A)–S(1A)	32(19)	S(1)–C(4A)–C(5A)–C(1)	−145(18)
C(4AA)–C(4A)–C(5A)–S(1A)	3(2)	C(4AA)–C(4A)–C(5A)–C(1)	−173.5(18)
C(6A)–C(4A)–C(5A)–S(1A)	178(2)	C(6A)–C(4A)–C(5A)–C(1)	1(4)
N(1)–C(1)–C(5A)–S(1A)	−177.8(11)	N(1)–C(1)–C(5A)–C(4A)	−1(2)
C(5)–C(1)–C(5A)–S(1A)	−5(2)	C(5)–C(1)–C(5A)–C(4A)	172(4)
N(1)–C(3)–C(6A)–S(1)	142(17)	N(1)–C(3)–C(6A)–C(4A)	1(3)
C(6)–C(3)–C(6A)–S(1)	133(20)	C(6)–C(3)–C(6A)–C(4A)	−8(3)
S(1)–C(4A)–C(6A)–C(3)	175.8(19)	C(4AA)–C(4A)–C(6A)–S(1)	−10(7)
C(4AA)–C(4A)–C(6A)–C(3)	166(6)	C(5A)–C(4A)–C(6A)–S(1)	−176(3)
C(5A)–C(4A)–C(6A)–C(3)	0(4)	C(4A)–S(1)–C(6A)–C(3)	−144(18)
C(4A)–S(1)–C(6A)–C(4A)	−1.2(17)	C(5A)–S(1)–C(6A)–C(3)	−146(17)
C(5A)–S(1)–C(6A)–C(4A)	−4(2)	C(6)–S(1)–C(6A)–C(3)	−134(20)
C(6)–S(1)–C(6A)–C(4A)	8(3)	C(4A)–S(1)–C(6A)–C(3)	−142(18)
C(5AA)–S(1)–C(6A)–C(3)	−141(18)	C(5AA)–S(1)–C(6A)–C(4A)	2(2)

Symmetry operations for equivalent atoms
A −x+1,−y+1,−z

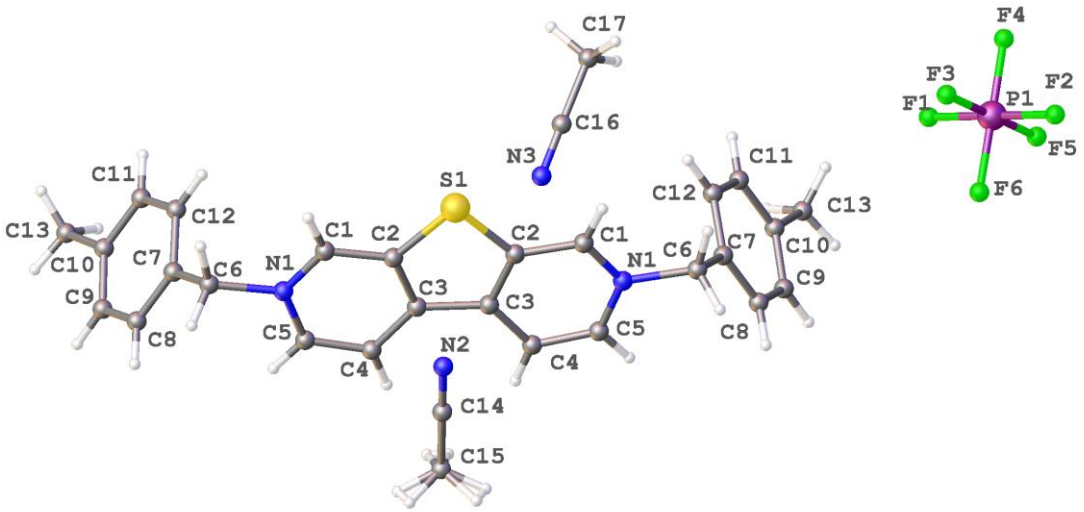

Second PF6 anion not shown

Table 1. Crystal data and structure refinement for **MSV2**.

Identification code	**MSV2**	
Chemical formula (moiety)	$C_{32}H_{33}F_{12}N_5P_2S$	
Chemical formula (total)	$C_{32}H_{33}F_{12}N_5P_2S$	
Formula weight	809.63	
Temperature	150(2) K	
Radiation, wavelength	MoKα, 0.71073 Å	
Crystal system, space group	orthorhombic, Pnma	
Unit cell parameters	a = 9.9868(5) Å	α = 90°
	b = 30.2095(15) Å	β = 90°
	c = 11.8887(5) Å	γ = 90°
Cell volume	3586.8(3) $Å^3$	
Z	4	
Calculated density	1.499 g/cm^3	
Absorption coefficient μ	0.274 mm^{-1}	
F(000)	1656	
Crystal colour and size	yellow, 0.24 × 0.20 × 0.20 mm^3	
Reflections for cell refinement	1377 (θ range 2.6 to 26.8°)	
Data collection method	Xcalibur, Atlas, Gemini ultra thick-slice ω scans	
θ range for data collection	2.7 to 25.0°	
Index ranges	h –7 to 11, k –35 to 32, l –14 to 12	
Completeness to θ = 25.0°	99.9 %	
Reflections collected	8454	
Independent reflections	3220 (R_{int} = 0.0842)	
Reflections with $F^2>2\sigma$	1790	
Absorption correction	semi-empirical from equivalents	
Min. and max. transmission	0.9372 and 0.9472	
Structure solution	direct methods	
Refinement method	Full-matrix least-squares on F^2	
Weighting parameters a, b	0.0902, 0.8138	
Data / restraints / parameters	3220 / 0 / 244	
Final R indices [$F^2>2\sigma$]	R1 = 0.0720, wR2 = 0.1611	
R indices (all data)	R1 = 0.1392, wR2 = 0.2031	
Goodness-of-fit on F^2	1.021	
Largest and mean shift/su	0.000 and 0.000	
Largest diff. peak and hole	0.42 and –0.41 e $Å^{-3}$	

Table 2. Atomic coordinates and equivalent isotropic displacement parameters ($Å^2$) for acb119a. U_{eq} is defined as one third of the trace of the orthogonalized U^{ij} tensor.

	x	y	z	U_{eq}
S(1)	0.7125(2)	0.7500	0.64275(16)	0.0346(5)
P(1)	0.51642(15)	0.37647(5)	0.06675(11)	0.0370(4)
F(1)	0.4700(4)	0.41626(13)	–0.0073(3)	0.0796(13)
F(2)	0.5640(4)	0.33687(13)	0.1440(3)	0.0756(12)
F(3)	0.6114(4)	0.40871(13)	0.1359(3)	0.0726(12)
F(4)	0.6369(3)	0.36630(13)	–0.0167(2)	0.0589(10)
F(5)	0.4223(4)	0.34466(14)	–0.0009(3)	0.0722(12)
F(6)	0.3987(3)	0.38712(11)	0.1536(2)	0.0506(9)
N(1)	0.5101(4)	0.63717(13)	0.6043(3)	0.0273(10)
N(2)	0.1939(12)	0.7500	0.3958(8)	0.080(3)
N(3)	0.5955(7)	0.6843(2)	0.3565(5)	0.0732(19)
C(1)	0.6120(6)	0.66400(16)	0.6252(4)	0.0278(12)
C(2)	0.5910(5)	0.70951(16)	0.6238(4)	0.0277(12)
C(3)	0.4637(5)	0.72597(15)	0.6022(4)	0.0269(11)
C(4)	0.3572(5)	0.69664(15)	0.5836(4)	0.0305(12)
C(5)	0.3848(5)	0.65236(16)	0.5850(4)	0.0306(12)
C(6)	0.5313(6)	0.58783(15)	0.6052(4)	0.0326(13)
C(7)	0.4905(5)	0.56726(14)	0.4939(4)	0.0284(12)
C(8)	0.3754(6)	0.54334(16)	0.4852(5)	0.0385(14)
C(9)	0.3412(6)	0.52359(17)	0.3849(5)	0.0446(15)
C(10)	0.4194(7)	0.52715(18)	0.2910(5)	0.0475(17)
C(11)	0.5369(7)	0.55139(18)	0.3005(5)	0.0478(16)
C(12)	0.5727(6)	0.57167(17)	0.4011(4)	0.0367(13)
C(13)	0.3856(8)	0.5053(2)	0.1803(5)	0.075(2)
C(14)	0.0804(15)	0.7500	0.3794(8)	0.065(3)
C(15)	–0.0637(11)	0.7500	0.3582(9)	0.078(3)
C(16)	0.6737(8)	0.6693(2)	0.2965(6)	0.060(2)
C(17)	0.7749(7)	0.6497(2)	0.2225(5)	0.0642(19)

Table 3. Bond lengths [Å] and angles [°] for acb119a.

S(1)–C(2)	1.737(5)	S(1)–C(2A)	1.737(5)
P(1)–F(1)	1.561(4)	P(1)–F(2)	1.581(4)
P(1)–F(3)	1.589(4)	P(1)–F(4)	1.590(3)
P(1)–F(5)	1.567(4)	P(1)–F(6)	1.597(3)
N(1)–C(1)	1.324(6)	N(1)–C(5)	1.353(6)
N(1)–C(6)	1.505(6)	N(2)–C(14)	1.151(14)
N(3)–C(16)	1.152(8)	C(1)–H(1A)	0.950
C(1)–C(2)	1.391(7)	C(2)–C(3)	1.389(7)
C(3)–C(3A)	1.452(9)	C(3)–C(4)	1.403(6)
C(4)–H(4A)	0.950	C(4)–C(5)	1.366(7)
C(5)–H(5A)	0.950	C(6)–H(6A)	0.990
C(6)–H(6B)	0.990	C(6)–C(7)	1.518(7)
C(7)–C(8)	1.362(7)	C(7)–C(12)	1.382(7)
C(8)–H(8A)	0.950	C(8)–C(9)	1.377(7)
C(9)–H(9A)	0.950	C(9)–C(10)	1.366(8)
C(10)–C(11)	1.388(9)	C(10)–C(13)	1.511(7)
C(11)–H(11A)	0.950	C(11)–C(12)	1.390(7)
C(12)–H(12A)	0.950	C(13)–H(13A)	0.980
C(13)–H(13B)	0.980	C(13)–H(13C)	0.980
C(14)–C(15)	1.461(17)	C(15)–H(15A)	0.980
C(15)–H(15B)	0.980	C(15)–H(15C)	0.980
C(16)–C(17)	1.465(10)	C(17)–H(17A)	0.980
C(17)–H(17B)	0.980	C(17)–H(17C)	0.980

C(2)–S(1)–C(2A)	89.5(3)	F(1)–P(1)–F(2)	178.8(2)
F(1)–P(1)–F(3)	89.8(2)	F(1)–P(1)–F(4)	91.2(2)
F(1)–P(1)–F(5)	90.2(2)	F(1)–P(1)–F(6)	89.5(2)
F(2)–P(1)–F(3)	89.1(2)	F(2)–P(1)–F(4)	89.4(2)
F(2)–P(1)–F(5)	90.8(2)	F(2)–P(1)–F(6)	89.87(19)
F(3)–P(1)–F(4)	89.39(19)	F(3)–P(1)–F(5)	179.7(2)
F(3)–P(1)–F(6)	88.95(18)	F(4)–P(1)–F(5)	90.86(19)
F(4)–P(1)–F(6)	178.2(2)	F(5)–P(1)–F(6)	90.80(19)
C(1)–N(1)–C(5)	122.3(4)	C(1)–N(1)–C(6)	119.8(4)
C(5)–N(1)–C(6)	117.8(4)	N(1)–C(1)–H(1A)	120.4
N(1)–C(1)–C(2)	119.2(5)	H(1A)–C(1)–C(2)	120.4
S(1)–C(2)–C(1)	126.1(4)	S(1)–C(2)–C(3)	114.3(4)
C(1)–C(2)–C(3)	119.6(5)	C(2)–C(3)–C(3A)	111.0(3)
C(2)–C(3)–C(4)	119.9(4)	C(3A)–C(3)–C(4)	129.2(3)
C(3)–C(4)–H(4A)	121.2	C(3)–C(4)–C(5)	117.6(5)
H(4A)–C(4)–C(5)	121.2	N(1)–C(5)–C(4)	121.4(5)
N(1)–C(5)–H(5A)	119.3	C(4)–C(5)–H(5A)	119.3
N(1)–C(6)–H(6A)	109.4	N(1)–C(6)–H(6B)	109.4
N(1)–C(6)–C(7)	111.2(4)	H(6A)–C(6)–H(6B)	108.0
H(6A)–C(6)–C(7)	109.4	H(6B)–C(6)–C(7)	109.4
C(6)–C(7)–C(8)	120.6(5)	C(6)–C(7)–C(12)	119.9(5)
C(8)–C(7)–C(12)	119.5(5)	C(7)–C(8)–H(8A)	119.8
C(7)–C(8)–C(9)	120.3(5)	H(8A)–C(8)–C(9)	119.8
C(8)–C(9)–H(9A)	118.9	C(8)–C(9)–C(10)	122.1(6)
H(9A)–C(9)–C(10)	118.9	C(9)–C(10)–C(11)	117.3(5)
C(9)–C(10)–C(13)	123.3(6)	C(11)–C(10)–C(13)	119.4(6)
C(10)–C(11)–H(11A)	119.4	C(10)–C(11)–C(12)	121.3(6)
H(11A)–C(11)–C(12)	119.4	C(7)–C(12)–C(11)	119.5(5)
C(7)–C(12)–H(12A)	120.3	C(11)–C(12)–H(12A)	120.3

C(10)–C(13)–H(13A)	109.5	C(10)–C(13)–H(13B)	109.5
C(10)–C(13)–H(13C)	109.5	H(13A)–C(13)–H(13B)	109.5
H(13A)–C(13)–H(13C)	109.5	H(13B)–C(13)–H(13C)	109.5
N(2)–C(14)–C(15)	179.8(12)	C(14)–C(15)–H(15A)	109.5
C(14)–C(15)–H(15B)	109.5	C(14)–C(15)–H(15C)	109.5
H(15A)–C(15)–H(15B)	109.5	H(15A)–C(15)–H(15C)	109.5
H(15B)–C(15)–H(15C)	109.5	N(3)–C(16)–C(17)	178.6(8)
C(16)–C(17)–H(17A)	109.5	C(16)–C(17)–H(17B)	109.5
C(16)–C(17)–H(17C)	109.5	H(17A)–C(17)–H(17B)	109.5
H(17A)–C(17)–H(17C)	109.5	H(17B)–C(17)–H(17C)	109.5

Symmetry operations for equivalent atoms
A x,–y+3/2,z

Table 4. Anisotropic displacement parameters ($Å^2$) for acb119a. The anisotropic displacement factor exponent takes the form: $-2\pi^2[h^2a^{*2}U^{11} + ...+ 2hka^*b^*U^{12}]$

	U^{11}	U^{22}	U^{33}	U^{23}	U^{13}	U^{12}
S(1)	0.0286(11)	0.0318(10)	0.0435(11)	0.000	–0.0011(9)	0.000
P(1)	0.0309(9)	0.0514(9)	0.0286(7)	–0.0052(7)	0.0032(7)	–0.0025(8)
F(1)	0.082(3)	0.089(3)	0.068(3)	0.030(2)	0.006(2)	0.021(3)
F(2)	0.074(3)	0.082(3)	0.071(3)	0.028(2)	0.020(2)	0.028(2)
F(3)	0.041(2)	0.100(3)	0.077(3)	–0.042(2)	0.005(2)	–0.017(2)
F(4)	0.043(2)	0.096(3)	0.0376(18)	–0.0121(18)	0.0127(16)	0.000(2)
F(5)	0.046(2)	0.098(3)	0.073(3)	–0.044(2)	0.002(2)	–0.013(2)
F(6)	0.0338(19)	0.082(2)	0.0363(17)	–0.0155(16)	0.0048(15)	0.0040(18)
N(1)	0.032(3)	0.025(2)	0.025(2)	–0.0012(17)	0.0062(19)	0.004(2)
N(2)	0.117(9)	0.054(5)	0.070(6)	0.000	–0.028(6)	0.000
N(3)	0.076(5)	0.094(5)	0.049(4)	0.003(3)	0.004(3)	0.014(4)
C(1)	0.030(3)	0.027(3)	0.026(3)	0.000(2)	0.003(2)	0.006(3)
C(2)	0.027(3)	0.034(3)	0.022(2)	–0.003(2)	0.001(2)	0.004(3)
C(3)	0.029(3)	0.030(2)	0.022(2)	0.000(2)	0.007(2)	–0.003(3)
C(4)	0.027(3)	0.030(3)	0.034(3)	0.001(2)	0.003(2)	0.004(3)
C(5)	0.027(3)	0.031(3)	0.034(3)	–0.003(2)	0.002(2)	–0.008(3)
C(6)	0.044(4)	0.023(2)	0.030(3)	0.003(2)	0.002(3)	0.005(3)
C(7)	0.033(3)	0.017(2)	0.036(3)	0.000(2)	0.002(2)	0.005(3)
C(8)	0.039(4)	0.023(3)	0.053(4)	0.003(3)	0.002(3)	0.004(3)
C(9)	0.037(4)	0.026(3)	0.071(4)	0.005(3)	–0.008(3)	–0.001(3)
C(10)	0.057(4)	0.032(3)	0.054(4)	–0.015(3)	–0.030(3)	0.015(3)
C(11)	0.053(4)	0.049(3)	0.042(3)	–0.010(3)	0.006(3)	0.011(3)
C(12)	0.038(3)	0.038(3)	0.034(3)	–0.007(2)	0.001(3)	–0.006(3)
C(13)	0.091(6)	0.061(4)	0.074(5)	–0.033(4)	–0.049(4)	0.020(4)
C(14)	0.099(10)	0.041(5)	0.055(6)	0.000	–0.010(7)	0.000
C(15)	0.065(8)	0.085(8)	0.083(8)	0.000	–0.012(6)	0.000
C(16)	0.076(6)	0.061(4)	0.043(4)	0.013(3)	–0.002(4)	0.004(4)
C(17)	0.070(5)	0.076(5)	0.046(4)	0.003(3)	0.008(4)	0.012(4)

Table 5. Hydrogen coordinates and isotropic displacement parameters ($Å^2$) for acb119a.

	x	y	z	U
H(1A)	0.6983	0.6523	0.6410	0.033
H(4A)	0.2689	0.7072	0.5705	0.037
H(5A)	0.3145	0.6318	0.5722	0.037
H(6A)	0.4778	0.5745	0.6666	0.039
H(6B)	0.6269	0.5814	0.6200	0.039
H(8A)	0.3185	0.5403	0.5488	0.046
H(9A)	0.2606	0.5070	0.3808	0.054
H(11A)	0.5941	0.5542	0.2370	0.057
H(12A)	0.6530	0.5884	0.4059	0.044
H(13A)	0.4645	0.4895	0.1520	0.113
H(13B)	0.3584	0.5278	0.1258	0.113
H(13C)	0.3121	0.4842	0.1915	0.113
H(15A)	–0.1005	0.7207	0.3753	0.117
H(15B)	–0.0804	0.7571	0.2790	0.117
H(15C)	–0.1069	0.7722	0.4061	0.117
H(17A)	0.8398	0.6331	0.2678	0.096
H(17B)	0.8213	0.6732	0.1813	0.096
H(17C)	0.7314	0.6296	0.1690	0.096

Table 6. Torsion angles [°] for acb119a.

C(5)–N(1)–C(1)–C(2)	−2.1(7)	C(6)–N(1)–C(1)–C(2)	179.8(4)
N(1)–C(1)–C(2)–S(1)	−176.9(3)	N(1)–C(1)–C(2)–C(3)	0.9(7)
C(2A)–S(1)–C(2)–C(1)	178.9(3)	C(2A)–S(1)–C(2)–C(3)	0.9(5)
S(1)–C(2)–C(3)–C(3A)	−0.7(3)	S(1)–C(2)–C(3)–C(4)	179.0(4)
C(1)–C(2)–C(3)–C(3A)	−178.8(3)	C(1)–C(2)–C(3)–C(4)	0.9(7)
C(2)–C(3)–C(4)–C(5)	−1.5(7)	C(3A)–C(3)–C(4)–C(5)	178.1(3)
C(1)–N(1)–C(5)–C(4)	1.5(7)	C(6)–N(1)–C(5)–C(4)	179.5(4)
C(3)–C(4)–C(5)–N(1)	0.4(7)	C(1)–N(1)–C(6)–C(7)	−123.0(5)
C(5)–N(1)–C(6)–C(7)	58.9(6)	N(1)–C(6)–C(7)–C(8)	−106.1(5)
N(1)–C(6)–C(7)–C(12)	75.8(6)	C(6)–C(7)–C(8)–C(9)	−177.9(5)
C(12)–C(7)–C(8)–C(9)	0.1(7)	C(7)–C(8)–C(9)–C(10)	−0.2(8)
C(8)–C(9)–C(10)–C(11)	0.5(8)	C(8)–C(9)–C(10)–C(13)	179.0(5)
C(9)–C(10)–C(11)–C(12)	−0.8(8)	C(13)–C(10)–C(11)–C(12)	−179.3(5)
C(6)–C(7)–C(12)–C(11)	177.7(5)	C(8)–C(7)–C(12)–C(11)	−0.4(7)
C(10)–C(11)–C(12)–C(7)	0.7(8)		

Symmetry operations for equivalent atoms
A x,–y+3/2,z

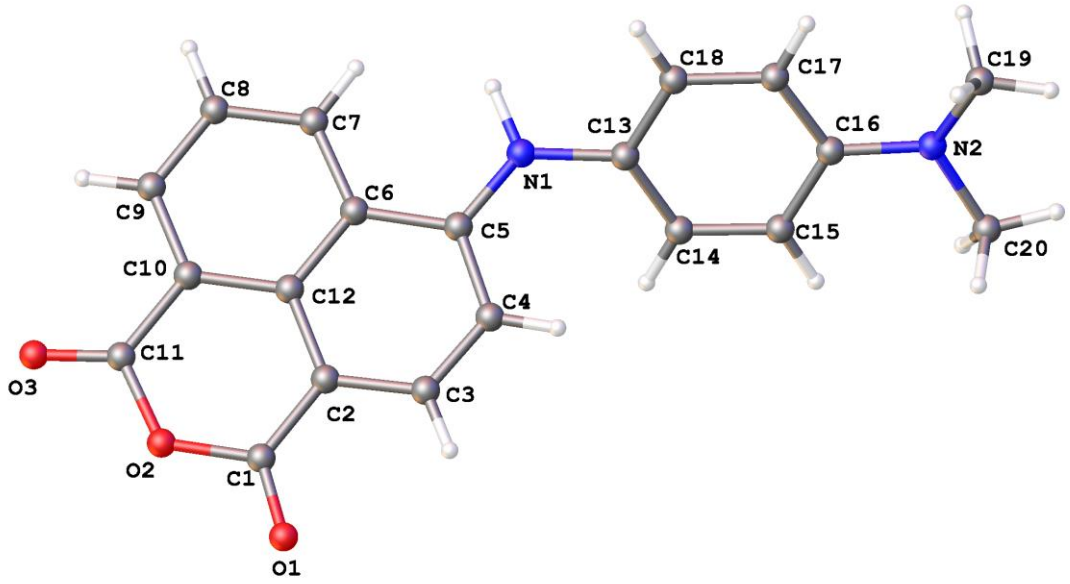
C8
C7
C9
C6
C10
C12
C11
O3
O2
C1
O1
C4
C3
C2
C5
N1
C13
C18
C17
C16
C19
N2
C15
C14
C20

Table 1. Crystal data and structure refinement for **NAP**.

Identification code	**NAP**	
Chemical formula (moiety)	$C_{20}H_{16}N_2O_3$	
Chemical formula (total)	$C_{20}H_{16}N_2O_3$	
Formula weight	332.35	
Temperature	120(2) K	
Radiation, wavelength	synchrotron, 0.68890 Å	
Crystal system, space group	orthorhombic, Pbca	
Unit cell parameters	a = 12.938(4) Å	α = 90°
	b = 8.719(3) Å	β = 90°
	c = 28.518(10) Å	γ = 90°
Cell volume	3217.0(19) Å^3	
Z	8	
Calculated density	1.372 g/cm^3	
Absorption coefficient μ	0.094 mm^{-1}	
F(000)	1392	
Crystal colour and size	red, 0.07 × 0.05 × 0.01 mm^3	
Reflections for cell refinement	4012 (θ range 3.0 to 24.0°)	
Data collection method	Rigaku	
	thick-slice ω scans	
θ range for data collection	2.8 to 24.4°	
Index ranges	h −10 to 15, k −10 to 10, l −34 to 34	
Completeness to θ = 24.4°	99.1 %	
Reflections collected	23938	
Independent reflections	2873 (R_{int} = 0.0964)	
Reflections with $F^2>2\sigma$	1875	
Absorption correction	semi-empirical from equivalents	
Min. and max. transmission	0.9935 and 0.9995	
Structure solution	direct methods	
Refinement method	Full-matrix least-squares on F^2	
Weighting parameters a, b	0.0657, 1.5391	
Data / restraints / parameters	2873 / 0 / 233	
Final R indices [$F^2>2\sigma$]	R1 = 0.0505, wR2 = 0.1222	
R indices (all data)	R1 = 0.0909, wR2 = 0.1447	
Goodness-of-fit on F^2	1.021	
Extinction coefficient	0.021(4)	
Largest and mean shift/su	0.000 and 0.000	
Largest diff. peak and hole	0.23 and −0.24 e Å^{-3}	

Table 2. Atomic coordinates and equivalent isotropic displacement parameters ($Å^2$) for acb139. U_{eq} is defined as one third of the trace of the orthogonalized U^{ij} tensor.

	x	y	z	U_{eq}
O(1)	0.39163(14)	–0.10786(19)	0.45395(6)	0.0451(5)
O(2)	0.38070(13)	–0.01316(18)	0.52545(5)	0.0405(5)
O(3)	0.37223(14)	0.0693(2)	0.59844(6)	0.0466(5)
N(1)	0.36832(16)	0.6066(2)	0.40487(7)	0.0377(5)
N(2)	0.3493(2)	0.8124(3)	0.21770(8)	0.0711(8)
C(1)	0.38352(19)	0.0078(3)	0.47703(8)	0.0373(6)
C(2)	0.37913(18)	0.1615(3)	0.45974(8)	0.0346(6)
C(3)	0.38288(19)	0.1882(3)	0.41157(8)	0.0391(6)
C(4)	0.37820(19)	0.3333(3)	0.39341(8)	0.0394(6)
C(5)	0.37104(18)	0.4627(3)	0.42241(8)	0.0340(6)
C(6)	0.36996(17)	0.4401(3)	0.47278(7)	0.0317(5)
C(7)	0.36769(17)	0.5620(3)	0.50548(8)	0.0344(6)
C(8)	0.36832(18)	0.5348(3)	0.55291(8)	0.0381(6)
C(9)	0.36927(18)	0.3857(3)	0.57025(8)	0.0371(6)
C(10)	0.37185(17)	0.2633(3)	0.53947(8)	0.0351(6)
C(11)	0.37443(18)	0.1055(3)	0.55780(8)	0.0380(6)
C(12)	0.37328(16)	0.2878(3)	0.49050(7)	0.0319(5)
C(13)	0.36464(19)	0.6507(3)	0.35674(8)	0.0387(6)
C(14)	0.2958(2)	0.5861(3)	0.32506(8)	0.0441(6)
C(15)	0.2922(2)	0.6354(3)	0.27905(9)	0.0517(7)
C(16)	0.3564(2)	0.7556(3)	0.26334(8)	0.0515(7)
C(17)	0.4248(2)	0.8188(3)	0.29563(9)	0.0466(7)
C(18)	0.4293(2)	0.7673(3)	0.34156(8)	0.0402(6)
C(19)	0.4322(3)	0.9035(5)	0.19990(12)	0.0901(13)
C(20)	0.2816(3)	0.7333(5)	0.18431(10)	0.1012(15)

Table 3. Bond lengths [Å] and angles [°] for acb139.

O(1)–C(1)	1.209(3)	O(2)–C(1)	1.393(3)
O(2)–C(11)	1.389(3)	O(3)–C(11)	1.201(3)
N(1)–C(5)	1.351(3)	N(1)–C(13)	1.426(3)
N(1)–H(1)	1.00(3)	N(2)–C(16)	1.396(3)
N(2)–C(19)	1.428(4)	N(2)–C(20)	1.466(4)
C(1)–C(2)	1.429(3)	C(2)–C(3)	1.394(3)
C(2)–C(12)	1.410(3)	C(3)–H(3A)	0.950
C(3)–C(4)	1.368(3)	C(4)–H(4A)	0.950
C(4)–C(5)	1.402(3)	C(5)–C(6)	1.450(3)
C(6)–C(7)	1.414(3)	C(6)–C(12)	1.421(3)
C(7)–H(7A)	0.950	C(7)–C(8)	1.373(3)
C(8)–H(8A)	0.950	C(8)–C(9)	1.391(3)
C(9)–H(9A)	0.950	C(9)–C(10)	1.382(3)
C(10)–C(11)	1.472(3)	C(10)–C(12)	1.413(3)
C(13)–C(14)	1.388(3)	C(13)–C(18)	1.386(3)
C(14)–H(14A)	0.950	C(14)–C(15)	1.382(3)
C(15)–H(15A)	0.950	C(15)–C(16)	1.411(4)
C(16)–C(17)	1.391(4)	C(17)–H(17A)	0.950
C(17)–C(18)	1.386(3)	C(18)–H(18A)	0.950
C(19)–H(19A)	0.980	C(19)–H(19B)	0.980
C(19)–H(19C)	0.980	C(20)–H(20A)	0.980
C(20)–H(20B)	0.980	C(20)–H(20C)	0.980

C(1)–O(2)–C(11)	124.21(19)	C(5)–N(1)–C(13)	127.4(2)
C(5)–N(1)–H(1)	117.4(15)	C(13)–N(1)–H(1)	115.0(15)
C(16)–N(2)–C(19)	118.6(3)	C(16)–N(2)–C(20)	118.6(3)
C(19)–N(2)–C(20)	118.7(3)	O(1)–C(1)–O(2)	115.6(2)
O(1)–C(1)–C(2)	126.7(2)	O(2)–C(1)–C(2)	117.6(2)
C(1)–C(2)–C(3)	119.7(2)	C(1)–C(2)–C(12)	121.3(2)
C(3)–C(2)–C(12)	119.0(2)	C(2)–C(3)–H(3A)	119.1
C(2)–C(3)–C(4)	121.7(2)	H(3A)–C(3)–C(4)	119.1
C(3)–C(4)–H(4A)	119.2	C(3)–C(4)–C(5)	121.6(2)
H(4A)–C(4)–C(5)	119.2	N(1)–C(5)–C(4)	122.1(2)
N(1)–C(5)–C(6)	119.5(2)	C(4)–C(5)–C(6)	118.4(2)
C(5)–C(6)–C(7)	123.5(2)	C(5)–C(6)–C(12)	118.61(19)
C(7)–C(6)–C(12)	117.9(2)	C(6)–C(7)–H(7A)	119.3
C(6)–C(7)–C(8)	121.3(2)	H(7A)–C(7)–C(8)	119.3
C(7)–C(8)–H(8A)	119.6	C(7)–C(8)–C(9)	120.8(2)
H(8A)–C(8)–C(9)	119.6	C(8)–C(9)–H(9A)	120.1
C(8)–C(9)–C(10)	119.7(2)	H(9A)–C(9)–C(10)	120.1
C(9)–C(10)–C(11)	119.8(2)	C(9)–C(10)–C(12)	120.7(2)
C(11)–C(10)–C(12)	119.5(2)	O(2)–C(11)–O(3)	116.5(2)
O(2)–C(11)–C(10)	117.50(19)	O(3)–C(11)–C(10)	126.0(2)
C(2)–C(12)–C(6)	120.68(19)	C(2)–C(12)–C(10)	119.8(2)
C(6)–C(12)–C(10)	119.5(2)	N(1)–C(13)–C(14)	122.6(2)
N(1)–C(13)–C(18)	118.6(2)	C(14)–C(13)–C(18)	118.8(2)
C(13)–C(14)–H(14A)	119.6	C(13)–C(14)–C(15)	120.9(2)
H(14A)–C(14)–C(15)	119.6	C(14)–C(15)–H(15A)	119.6
C(14)–C(15)–C(16)	120.9(2)	H(15A)–C(15)–C(16)	119.6
N(2)–C(16)–C(15)	121.4(3)	N(2)–C(16)–C(17)	121.3(3)
C(15)–C(16)–C(17)	117.3(2)	C(16)–C(17)–H(17A)	119.2
C(16)–C(17)–C(18)	121.6(2)	H(17A)–C(17)–C(18)	119.2
C(13)–C(18)–C(17)	120.5(2)	C(13)–C(18)–H(18A)	119.7

C(17)–C(18)–H(18A)	119.7	N(2)–C(19)–H(19A)	109.5
N(2)–C(19)–H(19B)	109.5	N(2)–C(19)–H(19C)	109.5
H(19A)–C(19)–H(19B)	109.5	H(19A)–C(19)–H(19C)	109.5
H(19B)–C(19)–H(19C)	109.5	N(2)–C(20)–H(20A)	109.5
N(2)–C(20)–H(20B)	109.5	N(2)–C(20)–H(20C)	109.5
H(20A)–C(20)–H(20B)	109.5	H(20A)–C(20)–H(20C)	109.5
H(20B)–C(20)–H(20C)	109.5		

Table 4. Anisotropic displacement parameters ($Å^2$) for acb139. The anisotropic displacement factor exponent takes the form: $-2\pi^2[h^2a^{*2}U^{11} + ...+ 2hka^*b^*U^{12}]$

	U^{11}	U^{22}	U^{33}	U^{23}	U^{13}	U^{12}
O(1)	0.0553(12)	0.0321(9)	0.0480(10)	–0.0051(8)	0.0025(8)	–0.0020(8)
O(2)	0.0466(10)	0.0350(9)	0.0400(9)	0.0026(7)	–0.0006(8)	0.0007(8)
O(3)	0.0543(12)	0.0502(11)	0.0354(10)	0.0096(8)	–0.0033(8)	–0.0042(9)
N(1)	0.0491(13)	0.0337(11)	0.0303(10)	0.0000(9)	–0.0013(9)	–0.0011(9)
N(2)	0.094(2)	0.083(2)	0.0366(13)	0.0154(13)	–0.0060(13)	–0.0174(16)
C(1)	0.0346(14)	0.0391(14)	0.0383(13)	0.0008(11)	–0.0027(11)	–0.0029(11)
C(2)	0.0368(14)	0.0323(12)	0.0348(12)	–0.0025(10)	–0.0009(10)	–0.0021(10)
C(3)	0.0435(15)	0.0388(14)	0.0351(12)	–0.0061(11)	0.0014(11)	–0.0001(11)
C(4)	0.0465(15)	0.0405(14)	0.0314(12)	0.0000(10)	0.0016(11)	–0.0017(12)
C(5)	0.0348(13)	0.0325(12)	0.0346(12)	0.0005(10)	–0.0019(10)	–0.0018(10)
C(6)	0.0305(13)	0.0329(12)	0.0316(12)	–0.0018(9)	0.0007(10)	0.0001(10)
C(7)	0.0350(14)	0.0326(12)	0.0355(12)	–0.0004(10)	0.0000(10)	–0.0003(10)
C(8)	0.0386(15)	0.0415(14)	0.0341(12)	–0.0092(10)	–0.0015(10)	–0.0007(11)
C(9)	0.0396(14)	0.0430(14)	0.0287(11)	0.0017(10)	–0.0010(10)	0.0009(11)
C(10)	0.0326(13)	0.0391(13)	0.0336(12)	0.0027(10)	–0.0007(10)	–0.0009(11)
C(11)	0.0363(14)	0.0416(14)	0.0362(13)	–0.0004(11)	–0.0029(11)	–0.0011(11)
C(12)	0.0291(13)	0.0360(12)	0.0307(12)	–0.0015(9)	–0.0015(10)	–0.0006(10)
C(13)	0.0481(15)	0.0369(13)	0.0311(12)	–0.0007(10)	0.0005(11)	0.0044(11)
C(14)	0.0496(16)	0.0450(15)	0.0378(13)	0.0001(11)	–0.0018(12)	–0.0056(13)
C(15)	0.0643(19)	0.0545(17)	0.0364(14)	0.0008(12)	–0.0069(12)	–0.0067(15)
C(16)	0.0643(18)	0.0566(17)	0.0336(13)	0.0048(12)	0.0010(12)	–0.0008(15)
C(17)	0.0544(17)	0.0438(15)	0.0414(14)	0.0057(12)	0.0036(12)	–0.0014(13)
C(18)	0.0451(16)	0.0369(13)	0.0387(13)	0.0011(11)	–0.0010(11)	–0.0006(12)
C(19)	0.088(3)	0.126(3)	0.0560(19)	0.035(2)	0.0156(18)	–0.005(2)
C(20)	0.150(4)	0.114(3)	0.0387(16)	0.0158(19)	–0.027(2)	–0.036(3)

Table 5. Hydrogen coordinates and isotropic displacement parameters ($Å^2$) for acb139.

	x	y	z	U
H(3A)	0.3889	0.1034	0.3908	0.047
H(4A)	0.3798	0.3467	0.3604	0.047
H(7A)	0.3657	0.6647	0.4944	0.041
H(8A)	0.3681	0.6188	0.5741	0.046
H(9A)	0.3682	0.3681	0.6031	0.045
H(14A)	0.2506	0.5068	0.3352	0.053
H(15A)	0.2458	0.5878	0.2577	0.062
H(17A)	0.4696	0.8992	0.2860	0.056
H(18A)	0.4771	0.8122	0.3628	0.048
H(19A)	0.4360	0.9999	0.2175	0.135
H(19B)	0.4200	0.9258	0.1667	0.135
H(19C)	0.4974	0.8474	0.2033	0.135
H(20A)	0.2122	0.7234	0.1978	0.152
H(20B)	0.3095	0.6311	0.1777	0.152
H(20C)	0.2778	0.7926	0.1552	0.152
H(1)	0.3744(19)	0.694(3)	0.4276(9)	0.056(8)

Table 6. Torsion angles [°] for acb139.

C(11)–O(2)–C(1)–O(1)	178.2(2)	C(11)–O(2)–C(1)–C(2)	–0.3(3)
O(1)–C(1)–C(2)–C(3)	0.9(4)	O(1)–C(1)–C(2)–C(12)	–177.7(2)
O(2)–C(1)–C(2)–C(3)	179.3(2)	O(2)–C(1)–C(2)–C(12)	0.7(3)
C(1)–C(2)–C(3)–C(4)	179.5(2)	C(12)–C(2)–C(3)–C(4)	–1.8(4)
C(2)–C(3)–C(4)–C(5)	1.0(4)	C(13)–N(1)–C(5)–C(4)	4.8(4)
C(13)–N(1)–C(5)–C(6)	–177.3(2)	C(3)–C(4)–C(5)–N(1)	178.7(2)
C(3)–C(4)–C(5)–C(6)	0.8(4)	N(1)–C(5)–C(6)–C(7)	–1.0(3)
N(1)–C(5)–C(6)–C(12)	–179.7(2)	C(4)–C(5)–C(6)–C(7)	177.1(2)
C(4)–C(5)–C(6)–C(12)	–1.7(3)	C(5)–C(6)–C(7)–C(8)	–179.0(2)
C(12)–C(6)–C(7)–C(8)	–0.2(3)	C(6)–C(7)–C(8)–C(9)	–1.2(4)
C(7)–C(8)–C(9)–C(10)	1.4(4)	C(8)–C(9)–C(10)–C(11)	179.1(2)
C(8)–C(9)–C(10)–C(12)	–0.2(3)	C(1)–O(2)–C(11)–O(3)	179.7(2)
C(1)–O(2)–C(11)–C(10)	–0.8(3)	C(9)–C(10)–C(11)–O(2)	–177.7(2)
C(9)–C(10)–C(11)–O(3)	1.8(4)	C(12)–C(10)–C(11)–O(2)	1.5(3)
C(12)–C(10)–C(11)–O(3)	–179.0(2)	C(1)–C(2)–C(12)–C(6)	179.4(2)
C(1)–C(2)–C(12)–C(10)	0.1(3)	C(3)–C(2)–C(12)–C(6)	0.8(3)
C(3)–C(2)–C(12)–C(10)	–178.5(2)	C(9)–C(10)–C(12)–C(2)	178.1(2)
C(9)–C(10)–C(12)–C(6)	–1.3(3)	C(11)–C(10)–C(12)–C(2)	–1.2(3)
C(11)–C(10)–C(12)–C(6)	179.5(2)	C(5)–C(6)–C(12)–C(2)	1.0(3)
C(5)–C(6)–C(12)–C(10)	–179.7(2)	C(7)–C(6)–C(12)–C(2)	–177.9(2)
C(7)–C(6)–C(12)–C(10)	1.4(3)	C(5)–N(1)–C(13)–C(14)	48.2(4)
C(5)–N(1)–C(13)–C(18)	–134.7(3)	N(1)–C(13)–C(14)–C(15)	177.8(2)
C(18)–C(13)–C(14)–C(15)	0.6(4)	C(13)–C(14)–C(15)–C(16)	–1.7(4)
C(19)–N(2)–C(16)–C(15)	–163.7(3)	C(19)–N(2)–C(16)–C(17)	18.5(5)
C(20)–N(2)–C(16)–C(15)	–6.9(5)	C(20)–N(2)–C(16)–C(17)	175.3(3)
C(14)–C(15)–C(16)–N(2)	–176.3(3)	C(14)–C(15)–C(16)–C(17)	1.6(4)
N(2)–C(16)–C(17)–C(18)	177.3(3)	C(15)–C(16)–C(17)–C(18)	–0.6(4)
N(1)–C(13)–C(18)–C(17)	–176.9(2)	C(14)–C(13)–C(18)–C(17)	0.4(4)
C(16)–C(17)–C(18)–C(13)	–0.4(4)		

Table 7. Hydrogen bonds for acb139 [Å and °].

D–H...A	d(D–H)	d(H...A)	d(D...A)	<(DHA)
N(1)–H(1)...O(1A)	1.00(3)	1.90(3)	2.872(3)	163(2)

Symmetry operations for equivalent atoms
A x,y+1,z

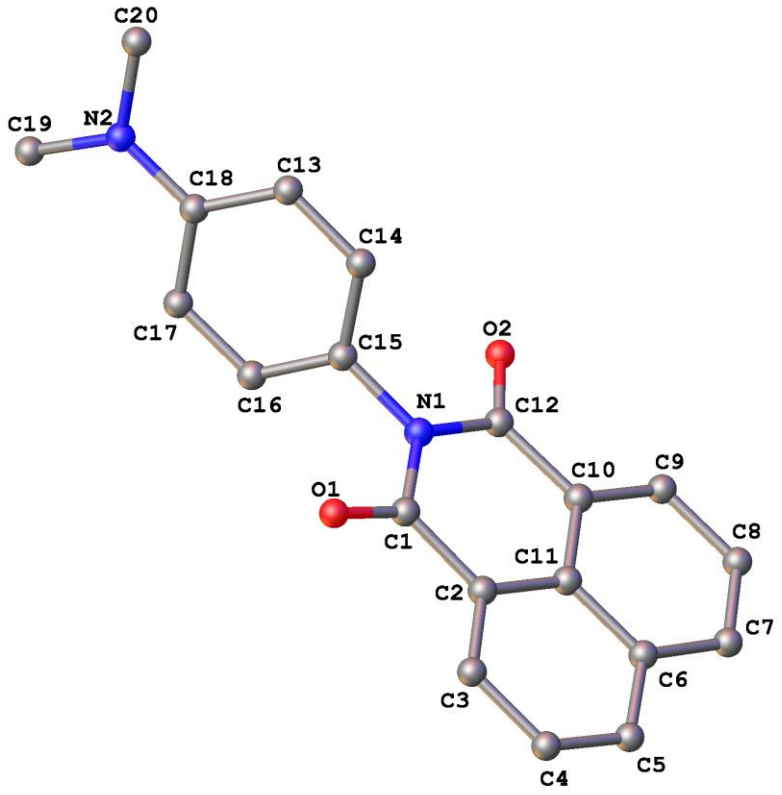
C20
C19
N2
C18
C13
C14
C17
C15
O2
C16
N1
C12
C10
C9
O1
C1
C8
C11
C2
C7
C6
C3
C5
C4

Table 1. Crystal data and structure refinement for **NAP1-G**.

Identification code	**NAP1-G**	
Chemical formula (moiety)	$C_{20}H_{16}N_2O_2$	
Chemical formula (total)	$C_{20}H_{16}N_2O_2$	
Formula weight	316.35	
Temperature	150(2) K	
Radiation, wavelength	MoKα, 0.71073 Å	
Crystal system, space group	triclinic, $P\bar{1}$	
Unit cell parameters	a = 9.4336(8) Å	α = 115.803(9)°
	b = 9.5749(8) Å	β = 97.324(7)°
	c = 9.9183(9) Å	γ = 104.839(7)°
Cell volume	749.69(11) $Å^3$	
Z	2	
Calculated density	1.401 g/cm^3	
Absorption coefficient μ	0.092 mm^{-1}	
F(000)	332	
Crystal colour and size	yellow, 0.30 × 0.20 × 0.20 mm^3	
Reflections for cell refinement	2145 (θ range 3.2 to 28.6°)	
Data collection method	Xcalibur, Atlas, Gemini ultra thick-slice ω scans	
θ range for data collection	3.2 to 28.6°	
Index ranges	h −12 to 11, k −9 to 11, l −11 to 12	
Completeness to θ = 25.0°	99.7 %	
Reflections collected	5582	
Independent reflections	3090 (R_{int} = 0.0207)	
Reflections with $F^2>2\sigma$	2403	
Absorption correction	semi-empirical from equivalents	
Min. and max. transmission	0.9730 and 0.9819	
Structure solution	direct methods	
Refinement method	Full-matrix least-squares on F^2	
Weighting parameters a, b	0.0551, 0.2663	
Data / restraints / parameters	3090 / 0 / 220	
Final R indices [$F^2>2\sigma$]	R1 = 0.0452, wR2 = 0.1115	
R indices (all data)	R1 = 0.0599, wR2 = 0.1260	
Goodness-of-fit on F^2	1.027	
Extinction coefficient	0.014(3)	
Largest and mean shift/su	0.004 and 0.000	
Largest diff. peak and hole	0.31 and −0.26 e $Å^{-3}$	

Table 2. Atomic coordinates and equivalent isotropic displacement parameters ($Å^2$) for acb166. U_{eq} is defined as one third of the trace of the orthogonalized U^{ij} tensor.

	x	y	z	U_{eq}
O(1)	0.25449(12)	0.66487(13)	0.28678(13)	0.0268(3)
O(2)	–0.15781(12)	0.24727(14)	0.22209(15)	0.0307(3)
N(1)	0.04762(13)	0.45362(15)	0.24946(14)	0.0188(3)
N(2)	–0.32148(15)	0.83405(17)	0.25520(15)	0.0259(3)
C(1)	0.20408(16)	0.52731(18)	0.27257(17)	0.0191(3)
C(2)	0.30074(16)	0.42855(18)	0.27596(17)	0.0186(3)
C(3)	0.45568(17)	0.49578(19)	0.30319(18)	0.0219(3)
C(4)	0.54888(17)	0.4018(2)	0.30141(19)	0.0249(4)
C(5)	0.48591(17)	0.2424(2)	0.27177(18)	0.0240(4)
C(6)	0.32713(17)	0.16865(19)	0.24361(17)	0.0205(3)
C(7)	0.25665(18)	0.00442(19)	0.21265(18)	0.0238(3)
C(8)	0.10269(18)	–0.06100(19)	0.18724(18)	0.0244(4)
C(9)	0.01062(17)	0.03502(19)	0.19223(17)	0.0221(3)
C(10)	0.07483(16)	0.19488(18)	0.22159(17)	0.0183(3)
C(11)	0.23351(16)	0.26514(18)	0.24727(16)	0.0177(3)
C(12)	–0.02329(16)	0.29518(18)	0.22997(17)	0.0202(3)
C(13)	–0.23733(16)	0.60489(18)	0.11433(17)	0.0201(3)
C(14)	–0.14547(16)	0.51268(18)	0.11313(17)	0.0203(3)
C(15)	–0.04811(16)	0.55044(18)	0.25048(17)	0.0186(3)
C(16)	–0.04368(17)	0.68009(19)	0.38882(18)	0.0216(3)
C(17)	–0.13422(17)	0.77372(19)	0.39169(18)	0.0216(3)
C(18)	–0.23300(16)	0.73944(18)	0.25386(17)	0.0187(3)
C(19)	–0.3324(2)	0.9573(2)	0.3993(2)	0.0311(4)
C(20)	–0.41784(19)	0.8017(2)	0.1118(2)	0.0311(4)

Table 3. Bond lengths [Å] and angles [°] for acb166.

O(1)–C(1)	1.2171(18)	O(2)–C(12)	1.2133(18)
N(1)–C(1)	1.4030(19)	N(1)–C(12)	1.4065(19)
N(1)–C(15)	1.4485(17)	N(2)–C(18)	1.3773(18)
N(2)–C(19)	1.441(2)	N(2)–C(20)	1.445(2)
C(1)–C(2)	1.479(2)	C(2)–C(3)	1.375(2)
C(2)–C(11)	1.410(2)	C(3)–H(3A)	0.950
C(3)–C(4)	1.407(2)	C(4)–H(4A)	0.950
C(4)–C(5)	1.367(2)	C(5)–H(5A)	0.950
C(5)–C(6)	1.414(2)	C(6)–C(7)	1.415(2)
C(6)–C(11)	1.425(2)	C(7)–H(7A)	0.950
C(7)–C(8)	1.367(2)	C(8)–H(8A)	0.950
C(8)–C(9)	1.408(2)	C(9)–H(9A)	0.950
C(9)–C(10)	1.374(2)	C(10)–C(11)	1.413(2)
C(10)–C(12)	1.4803(19)	C(13)–H(13A)	0.950
C(13)–C(14)	1.384(2)	C(13)–C(18)	1.408(2)
C(14)–H(14A)	0.950	C(14)–C(15)	1.383(2)
C(15)–C(16)	1.379(2)	C(16)–H(16A)	0.950
C(16)–C(17)	1.382(2)	C(17)–H(17A)	0.950
C(17)–C(18)	1.405(2)	C(19)–H(19A)	0.980
C(19)–H(19B)	0.980	C(19)–H(19C)	0.980
C(19)–H(19D)	0.980	C(19)–H(19E)	0.980
C(19)–H(19F)	0.980	C(20)–H(20A)	0.980
C(20)–H(20B)	0.980	C(20)–H(20C)	0.980
C(20)–H(20D)	0.980	C(20)–H(20E)	0.980
C(20)–H(20F)	0.980		

C(1)–N(1)–C(12)	125.33(12)	C(1)–N(1)–C(15)	117.39(12)
C(12)–N(1)–C(15)	117.25(12)	C(18)–N(2)–C(19)	121.35(13)
C(18)–N(2)–C(20)	120.72(13)	C(19)–N(2)–C(20)	117.67(13)
O(1)–C(1)–N(1)	120.42(13)	O(1)–C(1)–C(2)	122.95(13)
N(1)–C(1)–C(2)	116.63(12)	C(1)–C(2)–C(3)	119.48(13)
C(1)–C(2)–C(11)	120.05(13)	C(3)–C(2)–C(11)	120.44(13)
C(2)–C(3)–H(3A)	119.8	C(2)–C(3)–C(4)	120.34(14)
H(3A)–C(3)–C(4)	119.8	C(3)–C(4)–H(4A)	119.9
C(3)–C(4)–C(5)	120.22(14)	H(4A)–C(4)–C(5)	119.9
C(4)–C(5)–H(5A)	119.4	C(4)–C(5)–C(6)	121.26(14)
H(5A)–C(5)–C(6)	119.4	C(5)–C(6)–C(7)	123.38(14)
C(5)–C(6)–C(11)	118.25(13)	C(7)–C(6)–C(11)	118.38(13)
C(6)–C(7)–H(7A)	119.4	C(6)–C(7)–C(8)	121.21(14)
H(7A)–C(7)–C(8)	119.4	C(7)–C(8)–H(8A)	119.8
C(7)–C(8)–C(9)	120.31(14)	H(8A)–C(8)–C(9)	119.8
C(8)–C(9)–H(9A)	119.9	C(8)–C(9)–C(10)	120.18(14)
H(9A)–C(9)–C(10)	119.9	C(9)–C(10)–C(11)	120.65(13)
C(9)–C(10)–C(12)	119.40(13)	C(11)–C(10)–C(12)	119.94(13)
C(2)–C(11)–C(6)	119.48(13)	C(2)–C(11)–C(10)	121.25(13)
C(6)–C(11)–C(10)	119.27(13)	O(2)–C(12)–N(1)	120.27(13)
O(2)–C(12)–C(10)	123.24(14)	N(1)–C(12)–C(10)	116.50(12)
H(13A)–C(13)–C(14)	119.4	H(13A)–C(13)–C(18)	119.4
C(14)–C(13)–C(18)	121.19(14)	C(13)–C(14)–H(14A)	119.9
C(13)–C(14)–C(15)	120.25(14)	H(14A)–C(14)–C(15)	119.9
N(1)–C(15)–C(14)	120.30(13)	N(1)–C(15)–C(16)	120.14(13)
C(14)–C(15)–C(16)	119.56(13)	C(15)–C(16)–H(16A)	119.6
C(15)–C(16)–C(17)	120.82(14)	H(16A)–C(16)–C(17)	119.6

C(16)–C(17)–H(17A)	119.5	C(16)–C(17)–C(18)	120.90(14)
H(17A)–C(17)–C(18)	119.5	N(2)–C(18)–C(13)	121.42(13)
N(2)–C(18)–C(17)	121.31(13)	C(13)–C(18)–C(17)	117.26(13)
N(2)–C(19)–H(19A)	109.5	N(2)–C(19)–H(19B)	109.5
N(2)–C(19)–H(19C)	109.5	N(2)–C(19)–H(19D)	109.5
N(2)–C(19)–H(19E)	109.5	N(2)–C(19)–H(19F)	109.5
H(19A)–C(19)–H(19B)	109.5	H(19A)–C(19)–H(19C)	109.5
H(19A)–C(19)–H(19D)	141.1	H(19A)–C(19)–H(19E)	56.3
H(19A)–C(19)–H(19F)	56.3	H(19B)–C(19)–H(19C)	109.5
H(19B)–C(19)–H(19D)	56.3	H(19B)–C(19)–H(19E)	141.1
H(19B)–C(19)–H(19F)	56.3	H(19C)–C(19)–H(19D)	56.3
H(19C)–C(19)–H(19E)	56.3	H(19C)–C(19)–H(19F)	141.1
H(19D)–C(19)–H(19E)	109.5	H(19D)–C(19)–H(19F)	109.5
H(19E)–C(19)–H(19F)	109.5	N(2)–C(20)–H(20A)	109.5
N(2)–C(20)–H(20B)	109.5	N(2)–C(20)–H(20C)	109.5
N(2)–C(20)–H(20D)	109.5	N(2)–C(20)–H(20E)	109.5
N(2)–C(20)–H(20F)	109.5	H(20A)–C(20)–H(20B)	109.5
H(20A)–C(20)–H(20C)	109.5	H(20A)–C(20)–H(20D)	141.1
H(20A)–C(20)–H(20E)	56.3	H(20A)–C(20)–H(20F)	56.3
H(20B)–C(20)–H(20C)	109.5	H(20B)–C(20)–H(20D)	56.3
H(20B)–C(20)–H(20E)	141.1	H(20B)–C(20)–H(20F)	56.3
H(20C)–C(20)–H(20D)	56.3	H(20C)–C(20)–H(20E)	56.3
H(20C)–C(20)–H(20F)	141.1	H(20D)–C(20)–H(20E)	109.5
H(20D)–C(20)–H(20F)	109.5	H(20E)–C(20)–H(20F)	109.5

Table 4. Anisotropic displacement parameters ($Å^2$) for acb166. The anisotropic displacement factor exponent takes the form: $-2\pi^2[h^2a^{*2}U^{11} + ...+ 2hka^*b^*U^{12}]$

	U^{11}	U^{22}	U^{33}	U^{23}	U^{13}	U^{12}
O(1)	0.0242(6)	0.0200(6)	0.0399(7)	0.0166(5)	0.0108(5)	0.0089(5)
O(2)	0.0188(6)	0.0317(7)	0.0510(8)	0.0255(6)	0.0139(5)	0.0114(5)
N(1)	0.0174(6)	0.0201(7)	0.0244(7)	0.0129(5)	0.0082(5)	0.0100(5)
N(2)	0.0314(7)	0.0302(8)	0.0261(7)	0.0152(6)	0.0123(6)	0.0214(6)
C(1)	0.0184(7)	0.0196(8)	0.0197(7)	0.0098(6)	0.0058(6)	0.0067(6)
C(2)	0.0194(7)	0.0210(8)	0.0180(7)	0.0104(6)	0.0073(6)	0.0083(6)
C(3)	0.0197(7)	0.0220(8)	0.0261(8)	0.0138(7)	0.0071(6)	0.0062(6)
C(4)	0.0173(7)	0.0313(9)	0.0302(9)	0.0174(7)	0.0076(7)	0.0101(6)
C(5)	0.0215(8)	0.0298(9)	0.0294(9)	0.0177(7)	0.0100(7)	0.0150(7)
C(6)	0.0222(8)	0.0244(8)	0.0208(8)	0.0130(6)	0.0084(6)	0.0125(6)
C(7)	0.0281(8)	0.0235(8)	0.0285(8)	0.0155(7)	0.0118(7)	0.0152(7)
C(8)	0.0292(8)	0.0188(8)	0.0286(8)	0.0127(7)	0.0112(7)	0.0098(6)
C(9)	0.0206(7)	0.0215(8)	0.0239(8)	0.0115(6)	0.0068(6)	0.0059(6)
C(10)	0.0190(7)	0.0206(8)	0.0191(7)	0.0113(6)	0.0077(6)	0.0088(6)
C(11)	0.0179(7)	0.0209(8)	0.0160(7)	0.0094(6)	0.0058(6)	0.0080(6)
C(12)	0.0187(7)	0.0215(8)	0.0225(8)	0.0120(6)	0.0068(6)	0.0074(6)
C(13)	0.0184(7)	0.0217(8)	0.0219(8)	0.0120(6)	0.0051(6)	0.0071(6)
C(14)	0.0211(7)	0.0187(7)	0.0212(8)	0.0087(6)	0.0081(6)	0.0079(6)
C(15)	0.0167(7)	0.0191(7)	0.0258(8)	0.0135(6)	0.0088(6)	0.0091(6)
C(16)	0.0195(7)	0.0247(8)	0.0220(8)	0.0117(6)	0.0063(6)	0.0089(6)
C(17)	0.0216(8)	0.0205(8)	0.0218(8)	0.0082(6)	0.0080(6)	0.0087(6)
C(18)	0.0173(7)	0.0185(7)	0.0251(8)	0.0131(6)	0.0095(6)	0.0072(6)
C(19)	0.0344(9)	0.0287(9)	0.0332(9)	0.0118(7)	0.0121(8)	0.0203(7)
C(20)	0.0291(9)	0.0315(9)	0.0346(10)	0.0151(8)	0.0044(7)	0.0175(7)

Table 5. Hydrogen coordinates and isotropic displacement parameters ($Å^2$) for acb166.

	x	y	z	U
H(3A)	0.5000	0.6063	0.3233	0.026
H(4A)	0.6559	0.4492	0.3209	0.030
H(5A)	0.5500	0.1800	0.2701	0.029
H(7A)	0.3174	–0.0616	0.2095	0.029
H(8A)	0.0576	–0.1718	0.1661	0.029
H(9A)	–0.0962	–0.0109	0.1752	0.026
H(13A)	–0.3045	0.5769	0.0193	0.024
H(14A)	–0.1493	0.4231	0.0176	0.024
H(16A)	0.0224	0.7054	0.4833	0.026
H(17A)	–0.1296	0.8625	0.4882	0.026
H(19A)	–0.2413	1.0571	0.4446	0.047
H(19B)	–0.3403	0.9139	0.4721	0.047
H(19C)	–0.4232	0.9848	0.3790	0.047
H(19D)	–0.4285	0.9134	0.4192	0.047
H(19E)	–0.3296	1.0567	0.3917	0.047
H(19F)	–0.2467	0.9857	0.4848	0.047
H(20A)	–0.3584	0.7936	0.0363	0.047
H(20B)	–0.4573	0.8921	0.1324	0.047
H(20C)	–0.5032	0.6973	0.0696	0.047
H(20D)	–0.5209	0.7950	0.1225	0.047
H(20E)	–0.4220	0.6966	0.0265	0.047
H(20F)	–0.3760	0.8914	0.0893	0.047

Table 6. Torsion angles [°] for acb166.

C(12)–N(1)–C(1)–O(1)	179.28(13)	C(12)–N(1)–C(1)–C(2)	0.2(2)
C(15)–N(1)–C(1)–O(1)	−2.7(2)	C(15)–N(1)–C(1)–C(2)	178.19(12)
O(1)–C(1)–C(2)–C(3)	3.0(2)	O(1)–C(1)–C(2)–C(11)	−175.29(13)
N(1)–C(1)–C(2)–C(3)	−177.91(13)	N(1)–C(1)–C(2)–C(11)	3.8(2)
C(1)–C(2)–C(3)–C(4)	−177.75(13)	C(11)–C(2)–C(3)–C(4)	0.6(2)
C(2)–C(3)–C(4)–C(5)	0.3(2)	C(3)–C(4)–C(5)–C(6)	−0.5(2)
C(4)–C(5)–C(6)–C(7)	−179.91(15)	C(4)–C(5)–C(6)–C(11)	−0.2(2)
C(5)–C(6)–C(7)–C(8)	179.52(15)	C(11)–C(6)–C(7)–C(8)	−0.2(2)
C(6)–C(7)–C(8)–C(9)	−0.3(2)	C(7)–C(8)–C(9)–C(10)	0.5(2)
C(8)–C(9)–C(10)–C(11)	−0.1(2)	C(8)–C(9)–C(10)–C(12)	−178.60(13)
C(1)–C(2)–C(11)–C(6)	177.05(13)	C(1)–C(2)–C(11)–C(10)	−2.8(2)
C(3)–C(2)–C(11)–C(6)	−1.2(2)	C(3)–C(2)–C(11)–C(10)	178.95(13)
C(9)–C(10)–C(11)–C(2)	179.34(13)	C(9)–C(10)–C(11)–C(6)	−0.5(2)
C(12)–C(10)–C(11)–C(2)	−2.1(2)	C(12)–C(10)–C(11)–C(6)	178.06(13)
C(5)–C(6)–C(11)–C(2)	1.0(2)	C(5)–C(6)–C(11)–C(10)	−179.14(13)
C(7)–C(6)–C(11)–C(2)	−179.21(13)	C(7)–C(6)–C(11)–C(10)	0.6(2)
C(1)–N(1)–C(12)–O(2)	174.57(14)	C(1)–N(1)–C(12)–C(10)	−4.9(2)
C(15)–N(1)–C(12)–O(2)	−3.4(2)	C(15)–N(1)–C(12)–C(10)	177.15(12)
C(9)–C(10)–C(12)–O(2)	4.9(2)	C(9)–C(10)–C(12)–N(1)	−175.67(13)
C(11)–C(10)–C(12)–O(2)	−173.63(14)	C(11)–C(10)–C(12)–N(1)	5.8(2)
C(18)–C(13)–C(14)–C(15)	0.7(2)	C(13)–C(14)–C(15)–N(1)	179.75(13)
C(13)–C(14)–C(15)–C(16)	0.3(2)	C(1)–N(1)–C(15)–C(14)	106.91(16)
C(1)–N(1)–C(15)–C(16)	−73.67(18)	C(12)–N(1)–C(15)–C(14)	−74.93(17)
C(12)–N(1)–C(15)–C(16)	104.48(16)	N(1)–C(15)–C(16)–C(17)	179.94(13)
C(14)–C(15)–C(16)–C(17)	−0.6(2)	C(15)–C(16)–C(17)–C(18)	−0.1(2)
C(19)–N(2)–C(18)–C(13)	171.66(14)	C(19)–N(2)–C(18)–C(17)	−8.6(2)
C(20)–N(2)–C(18)–C(13)	−2.3(2)	C(20)–N(2)–C(18)–C(17)	177.42(14)
C(16)–C(17)–C(18)–N(2)	−178.73(14)	C(16)–C(17)–C(18)–C(13)	1.0(2)
C(14)–C(13)–C(18)–N(2)	178.42(13)	C(14)–C(13)–C(18)–C(17)	−1.3(2)

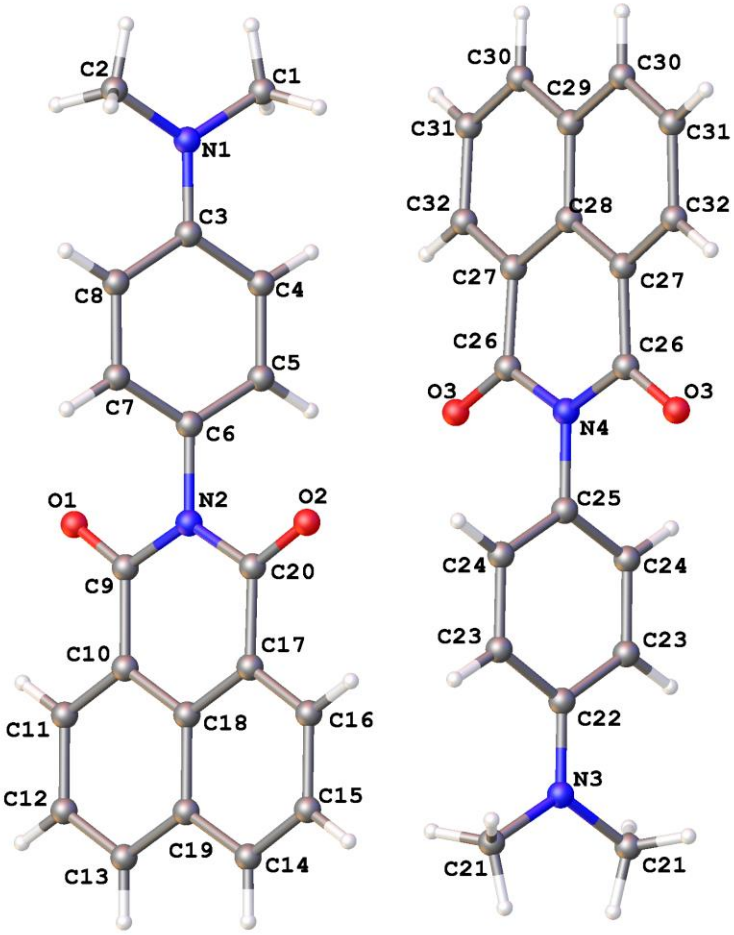
C2
C1
N1
C3
C8
C4
C5
C7
C6
O1
N2
O2
C9
C20
C10
C17
C11
C18
C16
C12
C15
C19
C13
C14
C30
C29
C30
C31
C31
C32
C28
C32
C27
C27
C26
C26
O3
O3
N4
C25
C24
C24
C23
C23
C22
N3
C21
C21

Table 1. Crystal data and structure refinement for **NAP1-O**.

Identification code	**NAP1-O**	
Chemical formula (moiety)	$C_{60}H_{48}N_6O_6$	
Chemical formula (total)	$C_{60}H_{48}N_6O_6$	
Formula weight	949.04	
Temperature	150(2) K	
Radiation, wavelength	MoKα, 0.71073 Å	
Crystal system, space group	monoclinic, C12/c1	
Unit cell parameters	a = 17.3700(9) Å	α = 90°
	b = 29.0684(13) Å	β = 94.498(4)°
	c = 8.8805(4) Å	γ = 90°
Cell volume	4470.1(4) $Å^3$	
Z	4	
Calculated density	1.410 g/cm^3	
Absorption coefficient μ	0.092 mm^{-1}	
F(000)	1992	
Crystal colour and size	orange, 0.20 × 0.08 × 0.08 mm^3	
Reflections for cell refinement	5796 (θ range 3.3 to 28.5°)	
Data collection method	Xcalibur, Atlas, Gemini ultra thick-slice ω scans	
θ range for data collection	3.3 to 28.6°	
Index ranges	h –23 to 22, k –39 to 38, l –10 to 11	
Completeness to θ = 26.0°	99.4 %	
Reflections collected	23905	
Independent reflections	5091 (R_{int} = 0.0278)	
Reflections with $F^2>2\sigma$	3685	
Absorption correction	semi-empirical from equivalents	
Min. and max. transmission	0.9818 and 0.9926	
Structure solution	direct methods	
Refinement method	Full-matrix least-squares on F^2	
Weighting parameters a, b	0.0588, 1.9423	
Data / restraints / parameters	5091 / 0 / 331	
Final R indices [$F^2>2\sigma$]	R1 = 0.0429, wR2 = 0.1098	
R indices (all data)	R1 = 0.0653, wR2 = 0.1247	
Goodness-of-fit on F^2	1.029	
Largest and mean shift/su	0.001 and 0.000	
Largest diff. peak and hole	0.19 and –0.24 e $Å^{-3}$	

Table 2. Atomic coordinates and equivalent isotropic displacement parameters ($Å^2$) for acb134. U_{eq} is defined as one third of the trace of the orthogonalized U^{ij} tensor.

	x	y	z	U_{eq}
N(1)	0.82485(7)	0.78584(4)	0.66712(12)	0.0307(3)
N(2)	0.81869(6)	0.59248(3)	0.66643(11)	0.0223(2)
N(3)	0.5000	0.45877(6)	0.7500	0.0460(5)
N(4)	0.5000	0.65253(5)	0.7500	0.0226(3)
O(1)	0.91587(6)	0.59211(3)	0.85388(10)	0.0336(2)
O(2)	0.71892(5)	0.59231(3)	0.48454(10)	0.0302(2)
O(3)	0.59340(6)	0.65259(3)	0.94404(10)	0.0358(3)
C(1)	0.76186(9)	0.81167(5)	0.72215(17)	0.0356(3)
C(2)	0.88741(9)	0.81021(4)	0.60480(18)	0.0366(3)
C(3)	0.82270(8)	0.73857(4)	0.66483(13)	0.0246(3)
C(4)	0.76043(8)	0.71441(4)	0.71834(14)	0.0268(3)
C(5)	0.75935(7)	0.66667(4)	0.71868(14)	0.0250(3)
C(6)	0.81955(7)	0.64222(4)	0.66578(13)	0.0229(3)
C(7)	0.88195(8)	0.66516(4)	0.61408(14)	0.0262(3)
C(8)	0.88366(8)	0.71284(4)	0.61313(14)	0.0270(3)
C(9)	0.87206(7)	0.57008(4)	0.76823(14)	0.0238(3)
C(10)	0.87109(7)	0.51933(4)	0.76518(14)	0.0236(3)
C(11)	0.92163(8)	0.49573(5)	0.86271(15)	0.0314(3)
C(12)	0.92097(8)	0.44738(5)	0.86685(16)	0.0330(3)
C(13)	0.86967(8)	0.42353(4)	0.77277(15)	0.0307(3)
C(14)	0.76456(9)	0.42325(5)	0.56594(15)	0.0325(3)
C(15)	0.71480(9)	0.44703(5)	0.46845(15)	0.0344(3)
C(16)	0.71487(8)	0.49552(5)	0.46845(14)	0.0297(3)
C(17)	0.76532(7)	0.51927(4)	0.56621(13)	0.0235(3)
C(18)	0.81805(7)	0.49534(4)	0.66609(13)	0.0224(3)
C(19)	0.81758(8)	0.44645(4)	0.66802(14)	0.0265(3)
C(20)	0.76434(7)	0.57004(4)	0.56611(13)	0.0224(3)
C(21)	0.44199(10)	0.43357(5)	0.82398(19)	0.0473(4)
C(22)	0.5000	0.50611(6)	0.7500	0.0300(4)
C(23)	0.55404(8)	0.53114(5)	0.67426(16)	0.0318(3)
C(24)	0.55362(8)	0.57892(4)	0.67400(15)	0.0289(3)
C(25)	0.5000	0.60258(6)	0.7500	0.0241(4)
C(26)	0.55000(7)	0.67488(4)	0.85862(13)	0.0239(3)
C(27)	0.54628(7)	0.72559(4)	0.86175(13)	0.0229(3)
C(28)	0.5000	0.74960(6)	0.7500	0.0207(4)
C(29)	0.5000	0.79842(6)	0.7500	0.0239(4)
C(30)	0.54320(8)	0.82152(4)	0.86865(14)	0.0272(3)
C(31)	0.58603(8)	0.79776(5)	0.97802(15)	0.0309(3)
C(32)	0.58881(8)	0.74936(5)	0.97344(15)	0.0286(3)

Table 3. Bond lengths [Å] and angles [°] for acb134.

N(1)–C(1)	1.4433(18)	N(1)–C(2)	1.4433(19)
N(1)–C(3)	1.3750(16)	N(2)–C(6)	1.4460(15)
N(2)–C(9)	1.4034(15)	N(2)–C(20)	1.4065(15)
N(3)–C(21)	1.4448(18)	N(3)–C(21A)	1.4449(18)
N(3)–C(22)	1.376(2)	N(4)–C(25)	1.452(2)
N(4)–C(26)	1.4054(13)	N(4)–C(26A)	1.4055(13)
O(1)–C(9)	1.2154(14)	O(2)–C(20)	1.2152(14)
O(3)–C(26)	1.2139(14)	C(1)–H(1A)	0.980
C(1)–H(1B)	0.980	C(1)–H(1C)	0.980
C(2)–H(2A)	0.980	C(2)–H(2B)	0.980
C(2)–H(2C)	0.980	C(3)–C(4)	1.4033(19)
C(3)–C(8)	1.4026(18)	C(4)–H(4A)	0.950
C(4)–C(5)	1.3881(17)	C(5)–H(5A)	0.950
C(5)–C(6)	1.3770(18)	C(6)–C(7)	1.3815(18)
C(7)–H(7A)	0.950	C(7)–C(8)	1.3862(17)
C(8)–H(8A)	0.950	C(9)–C(10)	1.4753(17)
C(10)–C(11)	1.3683(17)	C(10)–C(18)	1.4081(17)
C(11)–H(11A)	0.950	C(11)–C(12)	1.4058(18)
C(12)–H(12A)	0.950	C(12)–C(13)	1.362(2)
C(13)–H(13A)	0.950	C(13)–C(19)	1.4126(18)
C(14)–H(14A)	0.950	C(14)–C(15)	1.363(2)
C(14)–C(19)	1.4120(18)	C(15)–H(15A)	0.950
C(15)–C(16)	1.4095(19)	C(16)–H(16A)	0.950
C(16)–C(17)	1.3708(17)	C(17)–C(18)	1.4078(17)
C(17)–C(20)	1.4760(17)	C(18)–C(19)	1.4213(17)
C(21)–H(21A)	0.980	C(21)–H(21B)	0.980
C(21)–H(21C)	0.980	C(22)–C(23)	1.4007(17)
C(22)–C(23A)	1.4007(17)	C(23)–H(23A)	0.950
C(23)–C(24)	1.3889(18)	C(24)–H(24A)	0.950
C(24)–C(25)	1.3765(16)	C(25)–C(24A)	1.3765(16)
C(26)–C(27)	1.4758(17)	C(27)–C(28)	1.4118(14)
C(27)–C(32)	1.3756(17)	C(28)–C(27A)	1.4118(14)
C(28)–C(29)	1.419(2)	C(29)–C(30)	1.4143(15)
C(29)–C(30A)	1.4143(15)	C(30)–H(30A)	0.950
C(30)–C(31)	1.3640(18)	C(31)–H(31A)	0.950
C(31)–C(32)	1.4084(18)	C(32)–H(32A)	0.950

C(1)–N(1)–C(2)	119.22(11)	C(1)–N(1)–C(3)	120.29(12)
C(2)–N(1)–C(3)	120.34(11)	C(6)–N(2)–C(9)	117.39(9)
C(6)–N(2)–C(20)	117.89(9)	C(9)–N(2)–C(20)	124.71(10)
C(21)–N(3)–C(21A)	119.06(18)	C(21)–N(3)–C(22)	120.47(9)
C(21A)–N(3)–C(22)	120.47(9)	C(25)–N(4)–C(26)	117.53(7)
C(25)–N(4)–C(26A)	117.53(7)	C(26)–N(4)–C(26A)	124.94(14)
N(1)–C(1)–H(1A)	109.5	N(1)–C(1)–H(1B)	109.5
N(1)–C(1)–H(1C)	109.5	H(1A)–C(1)–H(1B)	109.5
H(1A)–C(1)–H(1C)	109.5	H(1B)–C(1)–H(1C)	109.5
N(1)–C(2)–H(2A)	109.5	N(1)–C(2)–H(2B)	109.5
N(1)–C(2)–H(2C)	109.5	H(2A)–C(2)–H(2B)	109.5
H(2A)–C(2)–H(2C)	109.5	H(2B)–C(2)–H(2C)	109.5
N(1)–C(3)–C(4)	121.05(12)	N(1)–C(3)–C(8)	121.17(12)
C(4)–C(3)–C(8)	117.76(11)	C(3)–C(4)–H(4A)	119.6
C(3)–C(4)–C(5)	120.79(12)	H(4A)–C(4)–C(5)	119.6
C(4)–C(5)–H(5A)	119.9	C(4)–C(5)–C(6)	120.29(12)

H(5A)–C(5)–C(6)	119.9	N(2)–C(6)–C(5)	120.42(11)
N(2)–C(6)–C(7)	119.51(11)	C(5)–C(6)–C(7)	120.07(12)
C(6)–C(7)–H(7A)	119.9	C(6)–C(7)–C(8)	120.15(12)
H(7A)–C(7)–C(8)	119.9	C(3)–C(8)–C(7)	120.93(12)
C(3)–C(8)–H(8A)	119.5	C(7)–C(8)–H(8A)	119.5
N(2)–C(9)–O(1)	120.54(11)	N(2)–C(9)–C(10)	116.50(10)
O(1)–C(9)–C(10)	122.96(11)	C(9)–C(10)–C(11)	118.95(11)
C(9)–C(10)–C(18)	120.84(11)	C(11)–C(10)–C(18)	120.20(12)
C(10)–C(11)–H(11A)	119.6	C(10)–C(11)–C(12)	120.78(12)
H(11A)–C(11)–C(12)	119.6	C(11)–C(12)–H(12A)	120.0
C(11)–C(12)–C(13)	119.93(12)	H(12A)–C(12)–C(13)	120.0
C(12)–C(13)–H(13A)	119.4	C(12)–C(13)–C(19)	121.21(12)
H(13A)–C(13)–C(19)	119.4	H(14A)–C(14)–C(15)	119.5
H(14A)–C(14)–C(19)	119.5	C(15)–C(14)–C(19)	120.99(12)
C(14)–C(15)–H(15A)	119.8	C(14)–C(15)–C(16)	120.45(12)
H(15A)–C(15)–C(16)	119.8	C(15)–C(16)–H(16A)	119.9
C(15)–C(16)–C(17)	120.27(12)	H(16A)–C(16)–C(17)	119.9
C(16)–C(17)–C(18)	120.14(12)	C(16)–C(17)–C(20)	119.76(11)
C(18)–C(17)–C(20)	120.09(11)	C(10)–C(18)–C(17)	120.69(11)
C(10)–C(18)–C(19)	119.46(11)	C(17)–C(18)–C(19)	119.84(11)
C(13)–C(19)–C(14)	123.33(12)	C(13)–C(19)–C(18)	118.39(11)
C(14)–C(19)–C(18)	118.28(11)	N(2)–C(20)–O(2)	120.18(11)
N(2)–C(20)–C(17)	117.14(10)	O(2)–C(20)–C(17)	122.68(11)
N(3)–C(21)–H(21A)	109.5	N(3)–C(21)–H(21B)	109.5
N(3)–C(21)–H(21C)	109.5	H(21A)–C(21)–H(21B)	109.5
H(21A)–C(21)–H(21C)	109.5	H(21B)–C(21)–H(21C)	109.5
N(3)–C(22)–C(23)	121.30(8)	N(3)–C(22)–C(23A)	121.30(8)
C(23)–C(22)–C(23A)	117.40(17)	C(22)–C(23)–H(23A)	119.4
C(22)–C(23)–C(24)	121.11(13)	H(23A)–C(23)–C(24)	119.4
C(23)–C(24)–H(24A)	119.9	C(23)–C(24)–C(25)	120.17(13)
H(24A)–C(24)–C(25)	119.9	N(4)–C(25)–C(24)	119.98(8)
N(4)–C(25)–C(24A)	119.98(8)	C(24)–C(25)–C(24A)	120.04(17)
N(4)–C(26)–O(3)	120.15(11)	N(4)–C(26)–C(27)	116.68(10)
O(3)–C(26)–C(27)	123.17(11)	C(26)–C(27)–C(28)	120.26(11)
C(26)–C(27)–C(32)	119.57(11)	C(28)–C(27)–C(32)	120.16(12)
C(27)–C(28)–C(27A)	120.73(15)	C(27)–C(28)–C(29)	119.63(8)
C(27A)–C(28)–C(29)	119.63(8)	C(28)–C(29)–C(30)	118.35(8)
C(28)–C(29)–C(30A)	118.34(8)	C(30)–C(29)–C(30A)	123.31(16)
C(29)–C(30)–H(30A)	119.4	C(29)–C(30)–C(31)	121.19(12)
H(30A)–C(30)–C(31)	119.4	C(30)–C(31)–H(31A)	119.9
C(30)–C(31)–C(32)	120.22(11)	H(31A)–C(31)–C(32)	119.9
C(27)–C(32)–C(31)	120.33(12)	C(27)–C(32)–H(32A)	119.8
C(31)–C(32)–H(32A)	119.8		

Symmetry operations for equivalent atoms
A –x+1,y,–z+3/2

Table 4. Anisotropic displacement parameters ($Å^2$) for acb134. The anisotropic displacement factor exponent takes the form: $-2\pi^2[h^2a^{*2}U^{11} + ...+ 2hka^*b^*U^{12}]$

	U^{11}	U^{22}	U^{33}	U^{23}	U^{13}	U^{12}
N(1)	0.0416(7)	0.0168(5)	0.0340(6)	–0.0007(4)	0.0041(5)	0.0026(5)
N(2)	0.0275(6)	0.0159(5)	0.0230(5)	0.0000(4)	0.0002(4)	0.0013(4)
N(3)	0.0699(14)	0.0203(9)	0.0489(11)	0.000	0.0114(10)	0.000
N(4)	0.0245(8)	0.0174(7)	0.0250(7)	0.000	–0.0033(6)	0.000
O(1)	0.0384(6)	0.0244(5)	0.0358(5)	–0.0002(4)	–0.0111(4)	–0.0027(4)
O(2)	0.0341(5)	0.0242(5)	0.0310(5)	0.0034(4)	–0.0059(4)	0.0011(4)
O(3)	0.0415(6)	0.0248(5)	0.0380(5)	0.0048(4)	–0.0162(4)	0.0008(4)
C(1)	0.0470(9)	0.0207(7)	0.0386(8)	–0.0015(6)	–0.0009(7)	0.0090(6)
C(2)	0.0403(8)	0.0184(6)	0.0501(9)	0.0022(6)	–0.0026(7)	–0.0022(6)
C(3)	0.0345(7)	0.0180(6)	0.0201(6)	–0.0010(5)	–0.0043(5)	0.0020(5)
C(4)	0.0284(7)	0.0233(6)	0.0281(6)	–0.0024(5)	–0.0005(5)	0.0049(5)
C(5)	0.0259(7)	0.0230(6)	0.0257(6)	–0.0006(5)	0.0000(5)	–0.0008(5)
C(6)	0.0295(7)	0.0170(6)	0.0216(6)	0.0005(5)	–0.0021(5)	0.0003(5)
C(7)	0.0328(7)	0.0187(6)	0.0276(6)	–0.0019(5)	0.0048(5)	0.0029(5)
C(8)	0.0325(7)	0.0217(6)	0.0271(6)	0.0003(5)	0.0044(5)	–0.0015(5)
C(9)	0.0255(7)	0.0209(6)	0.0248(6)	0.0018(5)	0.0007(5)	0.0010(5)
C(10)	0.0260(7)	0.0207(6)	0.0245(6)	0.0019(5)	0.0042(5)	0.0020(5)
C(11)	0.0308(7)	0.0259(7)	0.0369(7)	0.0026(6)	–0.0021(6)	0.0022(6)
C(12)	0.0329(8)	0.0256(7)	0.0408(8)	0.0087(6)	0.0038(6)	0.0075(6)
C(13)	0.0396(8)	0.0189(6)	0.0354(7)	0.0033(5)	0.0152(6)	0.0057(6)
C(14)	0.0499(9)	0.0183(6)	0.0308(7)	–0.0024(5)	0.0123(6)	–0.0075(6)
C(15)	0.0455(9)	0.0278(7)	0.0297(7)	–0.0049(6)	0.0022(6)	–0.0112(6)
C(16)	0.0361(8)	0.0272(7)	0.0254(6)	0.0004(5)	0.0004(5)	–0.0052(6)
C(17)	0.0289(7)	0.0211(6)	0.0211(6)	0.0001(5)	0.0060(5)	–0.0030(5)
C(18)	0.0280(7)	0.0190(6)	0.0211(6)	0.0007(5)	0.0080(5)	–0.0001(5)
C(19)	0.0359(7)	0.0201(6)	0.0253(6)	0.0003(5)	0.0124(5)	–0.0007(5)
C(20)	0.0253(7)	0.0216(6)	0.0205(6)	0.0004(5)	0.0025(5)	–0.0010(5)
C(21)	0.0605(11)	0.0237(7)	0.0547(10)	0.0075(7)	–0.0139(8)	–0.0114(7)
C(22)	0.0393(11)	0.0196(9)	0.0297(9)	0.000	–0.0056(8)	0.000
C(23)	0.0344(8)	0.0247(7)	0.0362(7)	–0.0027(6)	0.0022(6)	0.0062(6)
C(24)	0.0288(7)	0.0246(7)	0.0333(7)	0.0019(5)	0.0025(5)	–0.0001(6)
C(25)	0.0263(9)	0.0178(8)	0.0270(9)	0.000	–0.0052(7)	0.000
C(26)	0.0238(7)	0.0232(6)	0.0241(6)	0.0018(5)	–0.0018(5)	–0.0014(5)
C(27)	0.0245(7)	0.0216(6)	0.0225(6)	0.0006(5)	0.0007(5)	–0.0019(5)
C(28)	0.0221(9)	0.0201(8)	0.0202(8)	0.000	0.0031(6)	0.000
C(29)	0.0271(9)	0.0214(9)	0.0238(9)	0.000	0.0067(7)	0.000
C(30)	0.0338(7)	0.0199(6)	0.0286(7)	–0.0027(5)	0.0063(5)	–0.0052(5)
C(31)	0.0368(8)	0.0276(7)	0.0275(7)	–0.0050(5)	–0.0027(6)	–0.0082(6)
C(32)	0.0311(7)	0.0275(7)	0.0262(6)	0.0009(5)	–0.0050(5)	–0.0038(6)

Table 5. Hydrogen coordinates and isotropic displacement parameters ($Å^2$) for acb134.

	x	y	z	U
H(1A)	0.7575	0.8044	0.8289	0.053
H(1B)	0.7136	0.8035	0.6636	0.053
H(1C)	0.7717	0.8447	0.7113	0.053
H(2A)	0.8904	0.8012	0.4991	0.055
H(2B)	0.9361	0.8026	0.6626	0.055
H(2C)	0.8782	0.8434	0.6104	0.055
H(4A)	0.7185	0.7309	0.7548	0.032
H(5A)	0.7169	0.6508	0.7556	0.030
H(7A)	0.9238	0.6482	0.5791	0.031
H(8A)	0.9267	0.7283	0.5769	0.032
H(11A)	0.9576	0.5122	0.9284	0.038
H(12A)	0.9563	0.4314	0.9352	0.040
H(13A)	0.8689	0.3909	0.7777	0.037
H(14A)	0.7636	0.3906	0.5652	0.039
H(15A)	0.6798	0.4308	0.4000	0.041
H(16A)	0.6798	0.5118	0.4004	0.036
H(21A)	0.4415	0.4440	0.9288	0.071
H(21B)	0.4539	0.4006	0.8224	0.071
H(21C)	0.3912	0.4390	0.7709	0.071
H(23A)	0.5916	0.5152	0.6222	0.038
H(24A)	0.5904	0.5953	0.6212	0.035
H(30A)	0.5424	0.8542	0.8722	0.033
H(31A)	0.6141	0.8139	1.0576	0.037
H(32A)	0.6202	0.7331	1.0478	0.034

Table 6. Torsion angles [°] for acb134.

C(1)–N(1)–C(3)–C(4)	−1.28(17)	C(1)–N(1)–C(3)–C(8)	−179.39(11)
C(2)–N(1)–C(3)–C(4)	−176.92(11)	C(2)–N(1)–C(3)–C(8)	4.97(17)
N(1)–C(3)–C(4)–C(5)	−178.64(11)	C(8)–C(3)–C(4)–C(5)	−0.47(17)
C(3)–C(4)–C(5)–C(6)	−0.22(18)	C(4)–C(5)–C(6)–N(2)	179.81(10)
C(4)–C(5)–C(6)–C(7)	0.95(17)	C(9)–N(2)–C(6)–C(5)	−110.47(13)
C(9)–N(2)–C(6)–C(7)	68.40(15)	C(20)–N(2)–C(6)–C(5)	69.14(14)
C(20)–N(2)–C(6)–C(7)	−111.99(13)	N(2)–C(6)–C(7)–C(8)	−179.85(11)
C(5)–C(6)–C(7)–C(8)	−0.97(18)	C(6)–C(7)–C(8)–C(3)	0.27(18)
N(1)–C(3)–C(8)–C(7)	178.61(11)	C(4)–C(3)–C(8)–C(7)	0.44(17)
C(6)–N(2)–C(9)–O(1)	1.43(18)	C(6)–N(2)–C(9)–C(10)	−178.98(11)
C(20)–N(2)–C(9)–O(1)	−178.15(12)	C(20)–N(2)–C(9)–C(10)	1.43(17)
N(2)–C(9)–C(10)–C(11)	−179.62(11)	N(2)–C(9)–C(10)–C(18)	−0.99(17)
O(1)–C(9)–C(10)–C(11)	0.0(2)	O(1)–C(9)–C(10)–C(18)	178.59(12)
C(9)–C(10)–C(11)–C(12)	177.98(12)	C(18)–C(10)–C(11)–C(12)	−0.7(2)
C(10)–C(11)–C(12)–C(13)	0.1(2)	C(11)–C(12)–C(13)–C(19)	1.3(2)
C(19)–C(14)–C(15)–C(16)	−0.5(2)	C(14)–C(15)–C(16)–C(17)	0.3(2)
C(15)–C(16)–C(17)–C(18)	0.74(19)	C(15)–C(16)–C(17)–C(20)	−179.44(12)
C(16)–C(17)–C(18)–C(10)	178.86(12)	C(16)–C(17)–C(18)–C(19)	−1.56(18)
C(20)–C(17)–C(18)–C(10)	−0.96(18)	C(20)–C(17)–C(18)–C(19)	178.61(11)
C(9)–C(10)–C(18)–C(17)	0.81(18)	C(9)–C(10)–C(18)–C(19)	−178.77(11)
C(11)–C(10)–C(18)–C(17)	179.43(12)	C(11)–C(10)–C(18)–C(19)	−0.15(19)
C(15)–C(14)–C(19)–C(13)	179.12(13)	C(15)–C(14)–C(19)–C(18)	−0.30(19)
C(12)–C(13)–C(19)–C(14)	178.54(13)	C(12)–C(13)–C(19)–C(18)	−2.03(19)
C(10)–C(18)–C(19)–C(13)	1.46(18)	C(10)–C(18)–C(19)–C(14)	−179.09(11)
C(17)–C(18)–C(19)–C(13)	−178.12(11)	C(17)–C(18)–C(19)–C(14)	1.33(18)
C(6)–N(2)–C(20)–O(2)	−1.51(17)	C(6)–N(2)–C(20)–C(17)	178.83(10)
C(9)–N(2)–C(20)–O(2)	178.07(11)	C(9)–N(2)–C(20)–C(17)	−1.59(17)
C(16)–C(17)–C(20)–N(2)	−178.53(11)	C(16)–C(17)–C(20)–O(2)	1.81(19)
C(18)–C(17)–C(20)–N(2)	1.29(17)	C(18)–C(17)–C(20)–O(2)	−178.36(12)
C(21)–N(3)–C(22)–C(23)	−177.66(9)	C(21A)–N(3)–C(22)–C(23)	2.34(9)
C(21)–N(3)–C(22)–C(23A)	2.34(9)	C(21A)–N(3)–C(22)–C(23A)	−177.66(9)
N(3)–C(22)–C(23)–C(24)	179.72(9)	C(23A)–C(22)–C(23)–C(24)	−0.28(9)
C(22)–C(23)–C(24)–C(25)	0.56(18)	C(23)–C(24)–C(25)–N(4)	179.72(9)
C(23)–C(24)–C(25)–C(24A)	−0.28(9)	C(26)–N(4)–C(25)–C(24)	−84.85(9)
C(26A)–N(4)–C(25)–C(24)	95.15(9)	C(26)–N(4)–C(25)–C(24A)	95.15(9)
C(26A)–N(4)–C(25)–C(24A)	−84.85(9)	C(25)–N(4)–C(26)–O(3)	2.98(14)
C(25)–N(4)–C(26)–C(27)	−176.99(8)	C(26A)–N(4)–C(26)–O(3)	−177.02(14)
C(26A)–N(4)–C(26)–C(27)	3.00(8)	N(4)–C(26)–C(27)–C(28)	−6.18(16)
N(4)–C(26)–C(27)–C(32)	174.46(11)	O(3)–C(26)–C(27)–C(28)	173.85(11)
O(3)–C(26)–C(27)–C(32)	−5.5(2)	C(26)–C(27)–C(28)–C(27A)	3.16(8)
C(26)–C(27)–C(28)–C(29)	−176.84(8)	C(32)–C(27)–C(28)–C(27A)	−177.49(14)
C(32)–C(27)–C(28)–C(29)	2.51(14)	C(27)–C(28)–C(29)–C(30)	−3.83(8)
C(27)–C(28)–C(29)–C(30A)	176.17(8)	C(27A)–C(28)–C(29)–C(30A)	−3.83(8)
C(27A)–C(28)–C(29)–C(30)	176.17(8)	C(28)–C(29)–C(30)–C(31)	2.16(14)
C(30A)–C(29)–C(30)–C(31)	−177.84(14)	C(29)–C(30)–C(31)–C(32)	0.9(2)
C(26)–C(27)–C(32)–C(31)	179.92(12)	C(28)–C(27)–C(32)–C(31)	0.56(19)
C(30)–C(31)–C(32)–C(27)	−2.3(2)		

Symmetry operations for equivalent atoms
A −x+1,y,−z+3/2

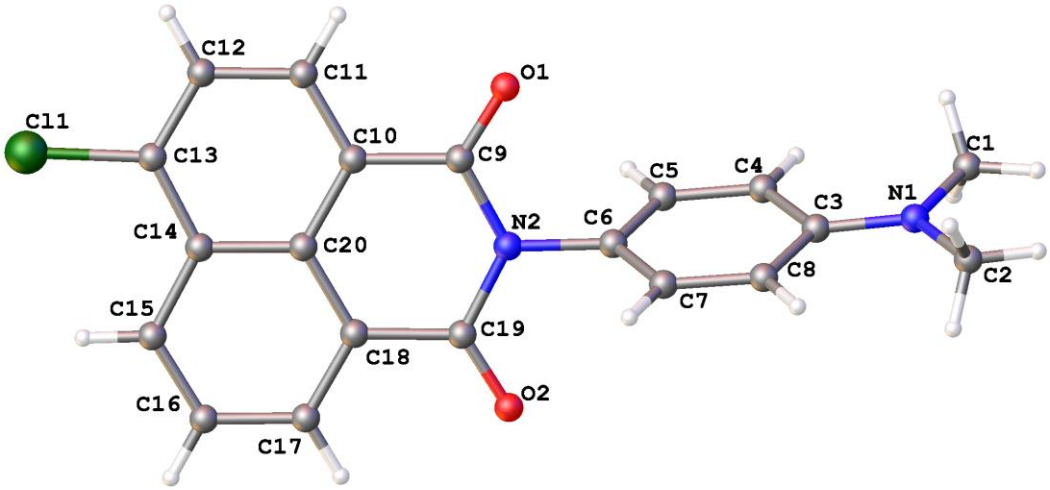
C12
C11
O1
Cl1
C10
C9
C13
C5
C4
C1
C3
N1
N2
C6
C14
C20
C8
C2
C7
C15
C19
C18
O2
C16
C17

Table 1. Crystal data and structure refinement for **NAP2**.

Identification code	**NAP2**	
Chemical formula (moiety)	$C_{20}H_{15}ClN_2O_2$	
Chemical formula (total)	$C_{20}H_{15}ClN_2O_2$	
Formula weight	350.79	
Temperature	150(2) K	
Radiation, wavelength	MoKα, 0.71073 Å	
Crystal system, space group	triclinic, $P\bar{1}$	
Unit cell parameters	a = 8.0297(10) Å	α = 98.082(8)°
	b = 8.7857(8) Å	β = 98.708(9)°
	c = 12.6909(12) Å	γ = 114.068(11)°
Cell volume	787.47(14) $Å^3$	
Z	2	
Calculated density	1.479 g/cm^3	
Absorption coefficient μ	0.259 mm^{-1}	
F(000)	364	
Reflections for cell refinement	2225 (θ range 3.3 to 28.4°)	
Data collection method	Xcalibur, Atlas, Gemini ultra thick-slice ω scans	
θ range for data collection	3.3 to 28.5°	
Index ranges	h −10 to 9, k −10 to 11, l −16 to 13	
Completeness to θ = 28.5°	83.1 %	
Reflections collected	6845	
Independent reflections	3307 (R_{int} = 0.0255)	
Reflections with $F^2>2\sigma$	2636	
Absorption correction	semi-empirical from equivalents	
Min. and max. transmission	0.89753 and 1.00000	
Structure solution	direct methods	
Refinement method	Full-matrix least-squares on F^2	
Weighting parameters a, b	0.0427, 0.2462	
Data / restraints / parameters	3307 / 0 / 241	
Final R indices [$F^2>2\sigma$]	R1 = 0.0421, wR2 = 0.0970	
R indices (all data)	R1 = 0.0575, wR2 = 0.1088	
Goodness-of-fit on F^2	1.067	
Extinction coefficient	0.004(2)	
Largest and mean shift/su	0.001 and 0.000	
Largest diff. peak and hole	0.25 and –0.25 e $Å^{-3}$	

Table 2. Atomic coordinates and equivalent isotropic displacement parameters ($Å^2$) for acb139. U_{eq} is defined as one third of the trace of the orthogonalized U^{ij} tensor.

	x	y	z	U_{eq}
Cl(1)	0.92126(7)	1.32843(6)	0.56799(4)	0.03133(18)
Cl(1A)	1.1029(7)	1.4033(6)	0.4142(5)	0.0574(18)
O(1)	0.4407(2)	0.48466(16)	0.36731(11)	0.0396(4)
O(2)	0.80973(18)	0.60568(15)	0.12321(10)	0.0328(3)
N(1)	0.2804(2)	–0.16390(18)	0.06443(13)	0.0292(4)
N(2)	0.63093(19)	0.54289(17)	0.24804(11)	0.0226(3)
C(1)	0.3191(3)	–0.2803(2)	0.12164(18)	0.0378(5)
C(2)	0.1435(3)	–0.2332(2)	–0.03850(15)	0.0314(4)
C(3)	0.3708(2)	0.0088(2)	0.10709(14)	0.0224(4)
C(4)	0.5040(2)	0.0784(2)	0.20735(15)	0.0256(4)
C(5)	0.5902(2)	0.2525(2)	0.25118(14)	0.0251(4)
C(6)	0.5471(2)	0.3621(2)	0.19748(14)	0.0228(4)
C(7)	0.4190(2)	0.2977(2)	0.09843(14)	0.0238(4)
C(8)	0.3326(2)	0.1236(2)	0.05326(14)	0.0251(4)
C(9)	0.5671(2)	0.5907(2)	0.33815(14)	0.0252(4)
C(10)	0.6596(2)	0.7728(2)	0.39447(14)	0.0217(4)
C(11)	0.6141(2)	0.8235(2)	0.48830(15)	0.0259(4)
C(12)	0.6980(2)	0.9967(2)	0.54211(15)	0.0253(4)
C(13)	0.8249(2)	1.1152(2)	0.50013(14)	0.0234(4)
C(14)	0.8812(2)	1.0705(2)	0.40455(14)	0.0221(4)
C(15)	1.0169(2)	1.1869(2)	0.36004(15)	0.0264(4)
C(16)	1.0677(2)	1.1316(2)	0.26986(15)	0.0281(4)
C(17)	0.9843(2)	0.9573(2)	0.21854(15)	0.0264(4)
C(18)	0.8494(2)	0.8401(2)	0.25819(14)	0.0221(4)
C(19)	0.7659(2)	0.6566(2)	0.20321(14)	0.0231(4)
C(20)	0.7956(2)	0.8934(2)	0.35164(13)	0.0201(4)

Table 3. Bond lengths [Å] and angles [°] for acb139.

Cl(1)–C(13)	1.7358(17)	Cl(1A)–C(15)	1.727(5)
O(1)–C(9)	1.214(2)	O(2)–C(19)	1.210(2)
N(1)–C(1)	1.439(2)	N(1)–C(2)	1.443(2)
N(1)–C(3)	1.369(2)	N(2)–C(6)	1.449(2)
N(2)–C(9)	1.402(2)	N(2)–C(19)	1.400(2)
C(1)–H(1A)	0.980	C(1)–H(1C)	0.980
C(1)–H(1B)	0.980	C(2)–H(2A)	0.980
C(2)–H(2B)	0.980	C(2)–H(2C)	0.980
C(3)–C(4)	1.404(2)	C(3)–C(8)	1.401(2)
C(4)–H(4A)	0.950	C(4)–C(5)	1.382(2)
C(5)–H(5A)	0.950	C(5)–C(6)	1.377(2)
C(6)–C(7)	1.375(2)	C(7)–H(7A)	0.950
C(7)–C(8)	1.384(2)	C(8)–H(8A)	0.950
C(9)–C(10)	1.474(2)	C(10)–C(11)	1.366(2)
C(10)–C(20)	1.417(2)	C(11)–H(11A)	0.950
C(11)–C(12)	1.403(2)	C(12)–H(12A)	0.950
C(12)–C(13)	1.363(2)	C(13)–H(13)	0.950
C(13)–C(14)	1.417(2)	C(14)–C(15)	1.411(2)
C(14)–C(20)	1.428(2)	C(15)–H(15)	0.950
C(15)–C(16)	1.364(3)	C(16)–H(16A)	0.950
C(16)–C(17)	1.403(2)	C(17)–H(17A)	0.950
C(17)–C(18)	1.374(2)	C(18)–C(19)	1.482(2)
C(18)–C(20)	1.406(2)		

C(1)–N(1)–C(2)	118.57(15)	C(1)–N(1)–C(3)	120.68(15)
C(2)–N(1)–C(3)	120.75(15)	C(6)–N(2)–C(9)	116.69(13)
C(6)–N(2)–C(19)	118.40(13)	C(9)–N(2)–C(19)	124.90(14)
N(1)–C(1)–H(1A)	109.5	N(1)–C(1)–H(1C)	109.5
N(1)–C(1)–H(1B)	109.5	H(1A)–C(1)–H(1C)	109.5
H(1A)–C(1)–H(1B)	109.5	H(1C)–C(1)–H(1B)	109.5
N(1)–C(2)–H(2A)	109.5	N(1)–C(2)–H(2B)	109.5
N(1)–C(2)–H(2C)	109.5	H(2A)–C(2)–H(2B)	109.5
H(2A)–C(2)–H(2C)	109.5	H(2B)–C(2)–H(2C)	109.5
N(1)–C(3)–C(4)	121.53(16)	N(1)–C(3)–C(8)	121.37(16)
C(4)–C(3)–C(8)	117.10(15)	C(3)–C(4)–H(4A)	119.5
C(3)–C(4)–C(5)	120.97(16)	H(4A)–C(4)–C(5)	119.5
C(4)–C(5)–H(5A)	119.7	C(4)–C(5)–C(6)	120.66(16)
H(5A)–C(5)–C(6)	119.7	N(2)–C(6)–C(5)	119.66(15)
N(2)–C(6)–C(7)	120.67(15)	C(5)–C(6)–C(7)	119.62(15)
C(6)–C(7)–H(7A)	119.8	C(6)–C(7)–C(8)	120.31(16)
H(7A)–C(7)–C(8)	119.8	C(3)–C(8)–C(7)	121.32(16)
C(3)–C(8)–H(8A)	119.3	C(7)–C(8)–H(8A)	119.3
O(1)–C(9)–N(2)	120.52(16)	O(1)–C(9)–C(10)	122.32(16)
N(2)–C(9)–C(10)	117.17(14)	C(9)–C(10)–C(11)	119.44(15)
C(9)–C(10)–C(20)	119.97(15)	C(11)–C(10)–C(20)	120.59(15)
C(10)–C(11)–H(11A)	119.8	C(10)–C(11)–C(12)	120.34(16)
H(11A)–C(11)–C(12)	119.8	C(11)–C(12)–H(12A)	120.1
C(11)–C(12)–C(13)	119.81(16)	H(12A)–C(12)–C(13)	120.1
Cl(1)–C(13)–C(12)	118.14(13)	Cl(1)–C(13)–H(13)	0.7
Cl(1)–C(13)–C(14)	119.25(13)	C(12)–C(13)–H(13)	118.7
C(12)–C(13)–C(14)	122.60(16)	H(13)–C(13)–C(14)	118.7
C(13)–C(14)–C(15)	124.91(16)	C(13)–C(14)–C(20)	116.70(15)
C(15)–C(14)–C(20)	118.38(15)	Cl(1A)–C(15)–C(14)	118.8(2)

Cl(1A)–C(15)–H(15)	5.1	Cl(1A)–C(15)–C(16)	120.0(2)
C(14)–C(15)–H(15)	119.5	C(14)–C(15)–C(16)	120.94(16)
H(15)–C(15)–C(16)	119.5	C(15)–C(16)–H(16A)	119.7
C(15)–C(16)–C(17)	120.51(16)	H(16A)–C(16)–C(17)	119.7
C(16)–C(17)–H(17A)	119.8	C(16)–C(17)–C(18)	120.41(16)
H(17A)–C(17)–C(18)	119.8	C(17)–C(18)–C(19)	119.14(15)
C(17)–C(18)–C(20)	120.29(16)	C(19)–C(18)–C(20)	120.55(15)
O(2)–C(19)–N(2)	120.92(15)	O(2)–C(19)–C(18)	122.49(15)
N(2)–C(19)–C(18)	116.59(14)	C(10)–C(20)–C(14)	119.90(15)
C(10)–C(20)–C(18)	120.64(15)	C(14)–C(20)–C(18)	119.46(15)

Table 4. Anisotropic displacement parameters ($Å^2$) for acb139. The anisotropic displacement factor exponent takes the form: $-2\pi^2[h^2a^{*2}U^{11} + ...+ 2hka^*b^*U^{12}]$

	U^{11}	U^{22}	U^{33}	U^{23}	U^{13}	U^{12}
Cl(1)	0.0360(3)	0.0183(3)	0.0345(3)	0.0001(2)	0.0028(2)	0.0106(2)
Cl(1A)	0.041(3)	0.036(3)	0.078(4)	–0.005(2)	0.006(2)	0.008(2)
O(1)	0.0447(9)	0.0229(7)	0.0373(8)	0.0021(6)	0.0185(7)	–0.0001(6)
O(2)	0.0370(8)	0.0266(7)	0.0289(7)	0.0008(5)	0.0122(6)	0.0083(6)
N(1)	0.0278(8)	0.0191(8)	0.0334(9)	0.0004(6)	–0.0018(7)	0.0079(7)
N(2)	0.0233(8)	0.0185(7)	0.0212(7)	0.0026(6)	0.0037(6)	0.0056(6)
C(1)	0.0422(12)	0.0200(10)	0.0452(12)	0.0043(8)	0.0029(10)	0.0112(9)
C(2)	0.0299(10)	0.0241(9)	0.0305(10)	–0.0035(7)	0.0022(8)	0.0072(8)
C(3)	0.0178(8)	0.0212(9)	0.0262(9)	0.0020(7)	0.0070(7)	0.0070(7)
C(4)	0.0242(9)	0.0225(9)	0.0297(10)	0.0067(7)	0.0037(8)	0.0107(8)
C(5)	0.0218(9)	0.0242(9)	0.0239(9)	0.0034(7)	–0.0006(7)	0.0076(8)
C(6)	0.0209(9)	0.0189(8)	0.0240(9)	0.0030(7)	0.0041(7)	0.0053(7)
C(7)	0.0250(9)	0.0219(9)	0.0228(9)	0.0051(7)	0.0034(7)	0.0095(8)
C(8)	0.0237(9)	0.0244(9)	0.0220(9)	0.0012(7)	0.0013(7)	0.0081(8)
C(9)	0.0243(9)	0.0228(9)	0.0238(9)	0.0059(7)	0.0041(8)	0.0062(8)
C(10)	0.0210(9)	0.0193(9)	0.0227(9)	0.0040(7)	0.0012(7)	0.0084(7)
C(11)	0.0248(9)	0.0246(9)	0.0284(10)	0.0083(7)	0.0068(8)	0.0100(8)
C(12)	0.0265(9)	0.0274(9)	0.0238(9)	0.0043(7)	0.0050(8)	0.0142(8)
C(13)	0.0227(9)	0.0195(9)	0.0250(9)	0.0018(7)	–0.0014(7)	0.0095(7)
C(14)	0.0183(8)	0.0207(9)	0.0243(9)	0.0055(7)	–0.0021(7)	0.0078(7)
C(15)	0.0247(9)	0.0196(9)	0.0295(10)	0.0055(7)	–0.0005(8)	0.0069(8)
C(16)	0.0223(9)	0.0245(9)	0.0301(10)	0.0090(7)	0.0034(8)	0.0031(8)
C(17)	0.0243(9)	0.0283(10)	0.0229(9)	0.0051(7)	0.0038(7)	0.0088(8)
C(18)	0.0188(8)	0.0216(9)	0.0214(9)	0.0042(7)	–0.0009(7)	0.0066(7)
C(19)	0.0213(9)	0.0245(9)	0.0210(9)	0.0050(7)	0.0019(7)	0.0086(8)
C(20)	0.0180(8)	0.0208(8)	0.0194(8)	0.0056(6)	–0.0004(7)	0.0079(7)

Table 5. Hydrogen coordinates and isotropic displacement parameters ($Å^2$) for acb139.

	x	y	z	U
H(1A)	0.4536	–0.2493	0.1354	0.057
H(1C)	0.2486	–0.3972	0.0770	0.057
H(1B)	0.2814	–0.2738	0.1914	0.057
H(2A)	0.1993	–0.1783	–0.0948	0.047
H(2B)	0.0350	–0.2115	–0.0308	0.047
H(2C)	0.1032	–0.3567	–0.0598	0.047
H(4A)	0.5353	0.0046	0.2456	0.031
H(5A)	0.6801	0.2971	0.3190	0.030
H(7A)	0.3898	0.3730	0.0608	0.029
H(8A)	0.2455	0.0812	–0.0156	0.030
H(11A)	0.5252	0.7410	0.5173	0.031
H(12A)	0.6666	1.0314	0.6076	0.030
H(13)	0.8776	1.2323	0.5364	–0.01(2)
H(15)	1.0736	1.3055	0.3934	0.026(6)
H(16A)	1.1604	1.2116	0.2416	0.034
H(17A)	1.0212	0.9202	0.1560	0.032

Table 6. Torsion angles [°] for acb139.

C(1)–N(1)–C(3)–C(4)	0.1(2)	C(1)–N(1)–C(3)–C(8)	−178.97(16)
C(2)–N(1)–C(3)–C(4)	179.77(15)	C(2)–N(1)–C(3)–C(8)	0.7(2)
N(1)–C(3)–C(4)–C(5)	−178.02(15)	C(8)–C(3)–C(4)–C(5)	1.1(2)
C(3)–C(4)–C(5)–C(6)	0.1(3)	C(4)–C(5)–C(6)–N(2)	176.37(15)
C(4)–C(5)–C(6)–C(7)	−1.0(2)	C(9)–N(2)–C(6)–C(5)	−71.6(2)
C(9)–N(2)–C(6)–C(7)	105.78(19)	C(19)–N(2)–C(6)–C(5)	109.44(18)
C(19)–N(2)–C(6)–C(7)	−73.2(2)	N(2)–C(6)–C(7)–C(8)	−176.78(15)
C(5)–C(6)–C(7)–C(8)	0.6(2)	C(6)–C(7)–C(8)–C(3)	0.8(3)
N(1)–C(3)–C(8)–C(7)	177.58(16)	C(4)–C(3)–C(8)–C(7)	−1.6(2)
C(6)–N(2)–C(9)–O(1)	−3.8(2)	C(6)–N(2)–C(9)–C(10)	176.30(14)
C(19)–N(2)–C(9)–O(1)	175.16(17)	C(19)–N(2)–C(9)–C(10)	−4.8(2)
O(1)–C(9)–C(10)–C(11)	5.8(3)	O(1)–C(9)–C(10)–C(20)	−174.74(17)
N(2)–C(9)–C(10)–C(11)	−174.27(16)	N(2)–C(9)–C(10)–C(20)	5.2(2)
C(9)–C(10)–C(11)–C(12)	−178.84(16)	C(20)–C(10)–C(11)–C(12)	1.7(3)
C(10)–C(11)–C(12)–C(13)	0.4(3)	C(11)–C(12)–C(13)–Cl(1)	178.67(13)
C(11)–C(12)–C(13)–C(14)	−1.8(3)	Cl(1)–C(13)–C(14)–C(15)	2.0(2)
Cl(1)–C(13)–C(14)–C(20)	−179.34(12)	C(12)–C(13)–C(14)–C(15)	−177.47(17)
C(12)–C(13)–C(14)–C(20)	1.2(3)	C(13)–C(14)–C(15)–Cl(1A)	−8.3(3)
C(13)–C(14)–C(15)–C(16)	177.45(17)	C(20)–C(14)–C(15)–Cl(1A)	173.1(2)
C(20)–C(14)–C(15)–C(16)	−1.2(3)	Cl(1A)–C(15)–C(16)–C(17)	−173.5(3)
C(14)–C(15)–C(16)–C(17)	0.7(3)	C(15)–C(16)–C(17)–C(18)	0.3(3)
C(16)–C(17)–C(18)–C(19)	−179.06(16)	C(16)–C(17)–C(18)–C(20)	−0.9(3)
C(6)–N(2)–C(19)–O(2)	1.1(2)	C(6)–N(2)–C(19)–C(18)	−179.39(14)
C(9)–N(2)–C(19)–O(2)	−177.83(16)	C(9)–N(2)–C(19)–C(18)	1.7(2)
C(17)–C(18)–C(19)–O(2)	−1.2(3)	C(17)–C(18)–C(19)–N(2)	179.24(15)
C(20)–C(18)–C(19)–O(2)	−179.40(16)	C(20)–C(18)–C(19)–N(2)	1.1(2)
C(17)–C(18)–C(20)–C(10)	−178.60(16)	C(17)–C(18)–C(20)–C(14)	0.5(2)
C(19)–C(18)–C(20)–C(10)	−0.5(2)	C(19)–C(18)–C(20)–C(14)	178.60(15)
C(9)–C(10)–C(20)–C(14)	178.22(15)	C(9)–C(10)–C(20)–C(18)	−2.7(2)
C(11)–C(10)–C(20)–C(14)	−2.3(2)	C(11)–C(10)–C(20)–C(18)	176.73(16)
C(13)–C(14)–C(20)–C(10)	0.9(2)	C(13)–C(14)–C(20)–C(18)	−178.17(15)
C(15)–C(14)–C(20)–C(10)	179.62(15)	C(15)–C(14)–C(20)–C(18)	0.6(2)

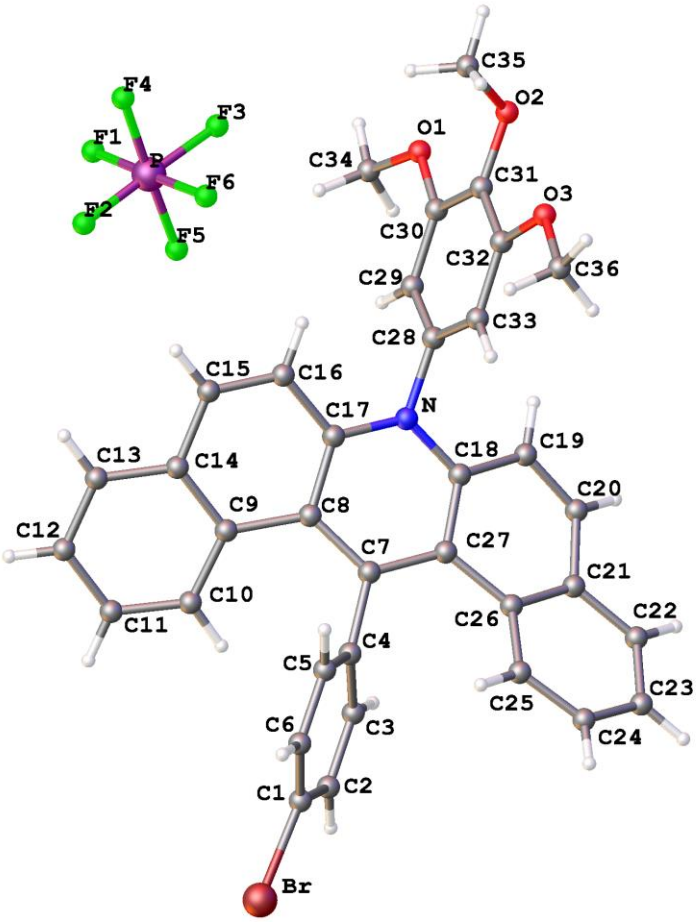
F4
F3
F1
P
F6
F2
F5
C35
O2
O1
C34
C31
O3
C30
C32
C36
C29
C33
C28
C15
C16
C17
N
C18
C19
C13
C14
C20
C9
C8
C12
C7
C27
C21
C10
C26
C22
C11
C4
C5
C23
C25
C6
C3
C24
C1
C2
Br

Table 1. Crystal data and structure refinement for **OAC**.

Identification code	**OAC**	
Chemical formula (moiety)	$C_{36}H_{27}BrF_6NO_3P$	
Chemical formula (total)	$C_{36}H_{27}BrF_6NO_3P$	
Formula weight	746.47	
Temperature	150(2) K	
Radiation, wavelength	MoKα, 0.71073 Å	
Crystal system, space group	monoclinic, $P12_1/c1$	
Unit cell parameters	a = 10.5148(4) Å	α = 90°
	b = 8.7448(3) Å	β = 93.098(3)°
	c = 34.5974(11) Å	γ = 90°
Cell volume	3176.58(19) $Å^3$	
Z	4	
Calculated density	1.561 g/cm^3	
Absorption coefficient μ	1.419 mm^{-1}	
F(000)	1512	
Crystal colour and size	yellow, 0.50 × 0.05 × 0.05 mm^3	
Reflections for cell refinement	9108 (θ range 2.9 to 28.5°)	
Data collection method	Xcalibur, Atlas, Gemini ultra thick-slice ω scans	
θ range for data collection	3.0 to 28.6°	
Index ranges	h −12 to 14, k −11 to 11, l −34 to 43	
Completeness to θ = 25.0°	99.8 %	
Reflections collected	28287	
Independent reflections	7008 (R_{int} = 0.0333)	
Reflections with $F^2>2\sigma$	5783	
Absorption correction	semi-empirical from equivalents	
Min. and max. transmission	0.5373 and 0.9324	
Structure solution	direct methods	
Refinement method	Full-matrix least-squares on F^2	
Weighting parameters a, b	0.0400, 5.1123	
Data / restraints / parameters	7008 / 0 / 436	
Final R indices [$F^2>2\sigma$]	R1 = 0.0419, wR2 = 0.0963	
R indices (all data)	R1 = 0.0556, wR2 = 0.1027	
Goodness-of-fit on F^2	1.028	
Largest and mean shift/su	0.001 and 0.000	
Largest diff. peak and hole	0.84 and −0.56 e $Å^{-3}$	

Table 2. Atomic coordinates and equivalent isotropic displacement parameters ($Å^2$) for acb196. U_{eq} is defined as one third of the trace of the orthogonalized U^{ij} tensor.

	x	y	z	U_{eq}
Br	0.29258(3)	0.27842(3)	0.173158(7)	0.02877(9)
P	0.08043(7)	1.42054(9)	0.39122(2)	0.03055(18)
F(1)	0.1310(3)	1.5810(3)	0.37775(9)	0.0833(9)
F(2)	−0.0011(3)	1.4007(3)	0.35261(6)	0.0784(8)
F(3)	0.1648(3)	1.4359(3)	0.43065(8)	0.0844(9)
F(4)	−0.03145(19)	1.5055(2)	0.41124(6)	0.0500(5)
F(5)	0.1960(2)	1.3369(3)	0.37221(8)	0.0709(8)
F(6)	0.0309(2)	1.2609(2)	0.40549(6)	0.0530(5)
O(1)	0.40049(19)	1.2156(2)	0.48904(5)	0.0291(4)
O(2)	0.27574(19)	1.0485(2)	0.53755(5)	0.0318(5)
O(3)	0.1835(2)	0.7709(2)	0.51763(5)	0.0343(5)
N	0.36097(19)	0.8077(2)	0.39225(5)	0.0171(4)
C(1)	0.3169(2)	0.3776(3)	0.22176(7)	0.0193(5)
C(2)	0.4369(2)	0.4302(3)	0.23371(7)	0.0198(5)
C(3)	0.4521(2)	0.5106(3)	0.26804(7)	0.0181(5)
C(4)	0.3478(2)	0.5377(3)	0.29020(7)	0.0166(5)
C(5)	0.2296(2)	0.4779(3)	0.27837(7)	0.0197(5)
C(6)	0.2136(2)	0.3975(3)	0.24405(7)	0.0209(5)
C(7)	0.3581(2)	0.6355(3)	0.32529(7)	0.0164(5)
C(8)	0.2916(2)	0.7761(3)	0.32534(7)	0.0157(5)
C(9)	0.2271(2)	0.8500(3)	0.29132(7)	0.0181(5)
C(10)	0.2525(2)	0.8174(3)	0.25259(7)	0.0200(5)
C(11)	0.1937(2)	0.8966(3)	0.22234(7)	0.0235(5)
C(12)	0.1059(2)	1.0112(3)	0.22902(8)	0.0254(6)
C(13)	0.0796(2)	1.0475(3)	0.26630(8)	0.0250(6)
C(14)	0.1402(2)	0.9698(3)	0.29785(7)	0.0202(5)
C(15)	0.1186(3)	1.0188(3)	0.33628(8)	0.0247(6)
C(16)	0.1883(2)	0.9652(3)	0.36712(7)	0.0230(5)
C(17)	0.2810(2)	0.8498(3)	0.36173(7)	0.0170(5)
C(18)	0.4474(2)	0.6914(3)	0.38969(7)	0.0174(5)
C(19)	0.5510(2)	0.6801(3)	0.41798(7)	0.0223(5)
C(20)	0.6367(2)	0.5676(3)	0.41475(7)	0.0243(6)
C(21)	0.6159(2)	0.4439(3)	0.38798(7)	0.0226(5)
C(22)	0.6939(3)	0.3134(3)	0.39064(8)	0.0303(6)
C(23)	0.6621(3)	0.1843(3)	0.37019(8)	0.0342(7)
C(24)	0.5494(3)	0.1822(3)	0.34684(8)	0.0305(6)
C(25)	0.4748(3)	0.3112(3)	0.34196(7)	0.0238(5)
C(26)	0.5086(2)	0.4479(3)	0.36137(7)	0.0193(5)
C(27)	0.4345(2)	0.5894(3)	0.35808(7)	0.0169(5)
C(28)	0.3436(2)	0.8736(3)	0.43052(7)	0.0192(5)
C(29)	0.3895(2)	1.0168(3)	0.43968(7)	0.0208(5)
C(30)	0.3638(2)	1.0757(3)	0.47581(7)	0.0212(5)
C(31)	0.2947(2)	0.9900(3)	0.50156(7)	0.0218(5)
C(32)	0.2501(2)	0.8454(3)	0.49101(7)	0.0228(5)
C(33)	0.2748(2)	0.7852(3)	0.45491(7)	0.0206(5)
C(34)	0.4629(3)	1.3118(3)	0.46240(9)	0.0355(7)
C(35)	0.1502(4)	1.1021(6)	0.54242(13)	0.0711(14)
C(36)	0.1263(3)	0.6292(4)	0.50604(8)	0.0399(8)

Table 3. Bond lengths [Å] and angles [°] for acb196.

Br–C(1)	1.897(2)	P–F(1)	1.580(2)
P–F(2)	1.558(2)	P–F(3)	1.592(2)
P–F(4)	1.5820(19)	P–F(5)	1.591(2)
P–F(6)	1.579(2)	O(1)–C(30)	1.355(3)
O(1)–C(34)	1.433(3)	O(2)–C(31)	1.371(3)
O(2)–C(35)	1.420(4)	O(3)–C(32)	1.354(3)
O(3)–C(36)	1.426(3)	N–C(17)	1.364(3)
N–C(18)	1.371(3)	N–C(28)	1.464(3)
C(1)–C(2)	1.385(4)	C(1)–C(6)	1.377(4)
C(2)–H(2A)	0.950	C(2)–C(3)	1.382(3)
C(3)–H(3A)	0.950	C(3)–C(4)	1.393(3)
C(4)–C(5)	1.389(3)	C(4)–C(7)	1.484(3)
C(5)–H(5A)	0.950	C(5)–C(6)	1.382(3)
C(6)–H(6A)	0.950	C(7)–C(8)	1.414(3)
C(7)–C(27)	1.413(3)	C(8)–C(9)	1.475(3)
C(8)–C(17)	1.424(3)	C(9)–C(10)	1.410(3)
C(9)–C(14)	1.417(3)	C(10)–H(10A)	0.950
C(10)–C(11)	1.374(4)	C(11)–H(11A)	0.950
C(11)–C(12)	1.390(4)	C(12)–H(12A)	0.950
C(12)–C(13)	1.371(4)	C(13)–H(13A)	0.950
C(13)–C(14)	1.408(4)	C(14)–C(15)	1.426(4)
C(15)–H(15A)	0.950	C(15)–C(16)	1.345(4)
C(16)–H(16A)	0.950	C(16)–C(17)	1.423(4)
C(18)–C(19)	1.427(3)	C(18)–C(27)	1.412(3)
C(19)–H(19A)	0.950	C(19)–C(20)	1.344(4)
C(20)–H(20A)	0.950	C(20)–C(21)	1.433(4)
C(21)–C(22)	1.405(4)	C(21)–C(26)	1.417(4)
C(22)–H(22A)	0.950	C(22)–C(23)	1.364(4)
C(23)–H(23A)	0.950	C(23)–C(24)	1.398(4)
C(24)–H(24A)	0.950	C(24)–C(25)	1.379(4)
C(25)–H(25A)	0.950	C(25)–C(26)	1.407(4)
C(26)–C(27)	1.464(3)	C(28)–C(29)	1.373(3)
C(28)–C(33)	1.378(3)	C(29)–H(29A)	0.950
C(29)–C(30)	1.392(3)	C(30)–C(31)	1.398(3)
C(31)–C(32)	1.391(4)	C(32)–C(33)	1.392(3)
C(33)–H(33A)	0.950	C(34)–H(34A)	0.980
C(34)–H(34B)	0.980	C(34)–H(34C)	0.980
C(35)–H(35A)	0.980	C(35)–H(35B)	0.980
C(35)–H(35C)	0.980	C(36)–H(36A)	0.980
C(36)–H(36B)	0.980	C(36)–H(36C)	0.980

F(1)–P–F(2)	91.38(16)	F(1)–P–F(3)	89.83(17)
F(1)–P–F(4)	89.01(12)	F(1)–P–F(5)	90.54(13)
F(1)–P–F(6)	178.94(16)	F(2)–P–F(3)	178.41(15)
F(2)–P–F(4)	92.28(14)	F(2)–P–F(5)	89.50(15)
F(2)–P–F(6)	89.66(14)	F(3)–P–F(4)	88.76(13)
F(3)–P–F(5)	89.46(15)	F(3)–P–F(6)	89.13(15)
F(4)–P–F(5)	178.17(14)	F(4)–P–F(6)	90.72(11)
F(5)–P–F(6)	89.70(12)	C(30)–O(1)–C(34)	116.4(2)
C(31)–O(2)–C(35)	114.4(2)	C(32)–O(3)–C(36)	116.9(2)
C(17)–N–C(18)	122.2(2)	C(17)–N–C(28)	119.5(2)
C(18)–N–C(28)	117.79(19)	Br–C(1)–C(2)	119.57(18)
Br–C(1)–C(6)	118.80(19)	C(2)–C(1)–C(6)	121.6(2)

C(1)–C(2)–H(2A)	120.4	C(1)–C(2)–C(3)	119.2(2)
H(2A)–C(2)–C(3)	120.4	C(2)–C(3)–H(3A)	120.0
C(2)–C(3)–C(4)	120.1(2)	H(3A)–C(3)–C(4)	120.0
C(3)–C(4)–C(5)	119.5(2)	C(3)–C(4)–C(7)	121.6(2)
C(5)–C(4)–C(7)	118.8(2)	C(4)–C(5)–H(5A)	119.7
C(4)–C(5)–C(6)	120.7(2)	H(5A)–C(5)–C(6)	119.7
C(1)–C(6)–C(5)	118.8(2)	C(1)–C(6)–H(6A)	120.6
C(5)–C(6)–H(6A)	120.6	C(4)–C(7)–C(8)	119.2(2)
C(4)–C(7)–C(27)	120.3(2)	C(8)–C(7)–C(27)	120.4(2)
C(7)–C(8)–C(9)	125.8(2)	C(7)–C(8)–C(17)	117.2(2)
C(9)–C(8)–C(17)	116.9(2)	C(8)–C(9)–C(10)	124.6(2)
C(8)–C(9)–C(14)	118.0(2)	C(10)–C(9)–C(14)	117.3(2)
C(9)–C(10)–H(10A)	119.3	C(9)–C(10)–C(11)	121.4(2)
H(10A)–C(10)–C(11)	119.3	C(10)–C(11)–H(11A)	119.6
C(10)–C(11)–C(12)	120.8(2)	H(11A)–C(11)–C(12)	119.6
C(11)–C(12)–H(12A)	120.2	C(11)–C(12)–C(13)	119.5(2)
H(12A)–C(12)–C(13)	120.2	C(12)–C(13)–H(13A)	119.6
C(12)–C(13)–C(14)	120.8(2)	H(13A)–C(13)–C(14)	119.6
C(9)–C(14)–C(13)	120.1(2)	C(9)–C(14)–C(15)	120.4(2)
C(13)–C(14)–C(15)	119.3(2)	C(14)–C(15)–H(15A)	119.1
C(14)–C(15)–C(16)	121.9(2)	H(15A)–C(15)–C(16)	119.1
C(15)–C(16)–H(16A)	120.3	C(15)–C(16)–C(17)	119.4(2)
H(16A)–C(16)–C(17)	120.3	N–C(17)–C(8)	119.2(2)
N–C(17)–C(16)	119.2(2)	C(8)–C(17)–C(16)	121.6(2)
N–C(18)–C(19)	119.4(2)	N–C(18)–C(27)	118.9(2)
C(19)–C(18)–C(27)	121.7(2)	C(18)–C(19)–H(19A)	120.5
C(18)–C(19)–C(20)	118.9(2)	H(19A)–C(19)–C(20)	120.5
C(19)–C(20)–H(20A)	119.1	C(19)–C(20)–C(21)	121.8(2)
H(20A)–C(20)–C(21)	119.1	C(20)–C(21)–C(22)	120.2(2)
C(20)–C(21)–C(26)	119.3(2)	C(22)–C(21)–C(26)	120.2(2)
C(21)–C(22)–H(22A)	119.6	C(21)–C(22)–C(23)	120.8(3)
H(22A)–C(22)–C(23)	119.6	C(22)–C(23)–H(23A)	120.4
C(22)–C(23)–C(24)	119.2(3)	H(23A)–C(23)–C(24)	120.4
C(23)–C(24)–H(24A)	119.4	C(23)–C(24)–C(25)	121.2(3)
H(24A)–C(24)–C(25)	119.4	C(24)–C(25)–H(25A)	119.7
C(24)–C(25)–C(26)	120.6(3)	H(25A)–C(25)–C(26)	119.7
C(21)–C(26)–C(25)	117.4(2)	C(21)–C(26)–C(27)	118.2(2)
C(25)–C(26)–C(27)	124.1(2)	C(7)–C(27)–C(18)	117.9(2)
C(7)–C(27)–C(26)	125.5(2)	C(18)–C(27)–C(26)	116.4(2)
N–C(28)–C(29)	120.6(2)	N–C(28)–C(33)	115.3(2)
C(29)–C(28)–C(33)	124.0(2)	C(28)–C(29)–H(29A)	121.2
C(28)–C(29)–C(30)	117.5(2)	H(29A)–C(29)–C(30)	121.2
O(1)–C(30)–C(29)	124.9(2)	O(1)–C(30)–C(31)	114.7(2)
C(29)–C(30)–C(31)	120.4(2)	O(2)–C(31)–C(30)	119.0(2)
O(2)–C(31)–C(32)	120.9(2)	C(30)–C(31)–C(32)	120.0(2)
O(3)–C(32)–C(31)	116.0(2)	O(3)–C(32)–C(33)	123.8(2)
C(31)–C(32)–C(33)	120.2(2)	C(28)–C(33)–C(32)	117.8(2)
C(28)–C(33)–H(33A)	121.1	C(32)–C(33)–H(33A)	121.1
O(1)–C(34)–H(34A)	109.5	O(1)–C(34)–H(34B)	109.5
O(1)–C(34)–H(34C)	109.5	H(34A)–C(34)–H(34B)	109.5
H(34A)–C(34)–H(34C)	109.5	H(34B)–C(34)–H(34C)	109.5
O(2)–C(35)–H(35A)	109.5	O(2)–C(35)–H(35B)	109.5
O(2)–C(35)–H(35C)	109.5	H(35A)–C(35)–H(35B)	109.5
H(35A)–C(35)–H(35C)	109.5	H(35B)–C(35)–H(35C)	109.5
O(3)–C(36)–H(36A)	109.5	O(3)–C(36)–H(36B)	109.5

O(3)–C(36)–H(36C)	109.5	H(36A)–C(36)–H(36B)	109.5
H(36A)–C(36)–H(36C)	109.5	H(36B)–C(36)–H(36C)	109.5

Table 4. Anisotropic displacement parameters ($Å^2$) for acb196. The anisotropic displacement factor exponent takes the form: $-2\pi^2[h^2a^{*2}U^{11} + ...+ 2hka^*b^*U^{12}]$

	U^{11}	U^{22}	U^{33}	U^{23}	U^{13}	U^{12}
Br	0.03754(17)	0.03113(15)	0.01747(14)	–0.00929(11)	–0.00024(10)	0.00586(12)
P	0.0311(4)	0.0346(4)	0.0268(4)	–0.0100(3)	0.0095(3)	–0.0133(3)
F(1)	0.0923(18)	0.0427(13)	0.122(2)	–0.0086(13)	0.0730(17)	–0.0282(12)
F(2)	0.103(2)	0.097(2)	0.0317(11)	–0.0045(12)	–0.0234(12)	–0.0082(16)
F(3)	0.0799(17)	0.0811(18)	0.0866(18)	–0.0468(15)	–0.0456(15)	0.0178(14)
F(4)	0.0499(12)	0.0483(12)	0.0547(12)	0.0063(9)	0.0292(10)	0.0075(9)
F(5)	0.0548(13)	0.0543(13)	0.108(2)	–0.0340(13)	0.0468(13)	–0.0160(11)
F(6)	0.0686(14)	0.0397(11)	0.0530(13)	0.0024(9)	0.0257(11)	–0.0082(10)
O(1)	0.0429(12)	0.0241(10)	0.0208(9)	–0.0093(8)	0.0080(8)	–0.0150(9)
O(2)	0.0402(11)	0.0410(12)	0.0154(9)	–0.0140(8)	0.0108(8)	–0.0161(9)
O(3)	0.0477(12)	0.0391(12)	0.0173(9)	–0.0062(8)	0.0122(9)	–0.0270(10)
N	0.0214(10)	0.0198(10)	0.0105(9)	–0.0036(7)	0.0035(8)	–0.0058(8)
C(1)	0.0271(13)	0.0179(12)	0.0125(11)	–0.0029(9)	–0.0015(10)	0.0049(10)
C(2)	0.0220(12)	0.0233(13)	0.0141(11)	0.0015(9)	0.0029(9)	0.0078(10)
C(3)	0.0160(11)	0.0219(12)	0.0161(11)	–0.0001(9)	0.0002(9)	0.0024(10)
C(4)	0.0196(12)	0.0182(12)	0.0121(11)	–0.0017(9)	0.0030(9)	0.0010(9)
C(5)	0.0179(12)	0.0235(13)	0.0181(12)	–0.0040(10)	0.0054(9)	0.0002(10)
C(6)	0.0213(12)	0.0209(13)	0.0205(12)	–0.0061(10)	–0.0001(10)	–0.0012(10)
C(7)	0.0152(11)	0.0216(12)	0.0129(11)	–0.0035(9)	0.0055(9)	–0.0058(9)
C(8)	0.0143(11)	0.0206(12)	0.0127(11)	–0.0027(9)	0.0037(9)	–0.0044(9)
C(9)	0.0163(11)	0.0194(12)	0.0187(12)	–0.0013(9)	0.0010(9)	–0.0051(9)
C(10)	0.0174(12)	0.0249(13)	0.0176(12)	–0.0014(10)	0.0008(9)	–0.0029(10)
C(11)	0.0242(13)	0.0313(14)	0.0150(12)	0.0004(10)	0.0005(10)	–0.0053(11)
C(12)	0.0225(13)	0.0284(14)	0.0246(13)	0.0047(11)	–0.0059(11)	–0.0042(11)
C(13)	0.0216(13)	0.0230(13)	0.0301(14)	0.0008(11)	–0.0011(11)	0.0008(10)
C(14)	0.0191(12)	0.0198(12)	0.0215(13)	–0.0016(10)	–0.0007(10)	–0.0041(10)
C(15)	0.0237(13)	0.0230(13)	0.0278(14)	–0.0064(11)	0.0038(11)	0.0009(11)
C(16)	0.0272(14)	0.0226(13)	0.0197(12)	–0.0074(10)	0.0053(10)	–0.0010(11)
C(17)	0.0181(12)	0.0178(12)	0.0155(11)	–0.0006(9)	0.0029(9)	–0.0057(9)
C(18)	0.0202(12)	0.0195(12)	0.0129(11)	0.0005(9)	0.0044(9)	–0.0063(9)
C(19)	0.0281(13)	0.0253(13)	0.0135(12)	–0.0009(10)	0.0006(10)	–0.0084(11)
C(20)	0.0230(13)	0.0318(14)	0.0179(12)	0.0027(10)	–0.0026(10)	–0.0055(11)
C(21)	0.0238(13)	0.0293(14)	0.0149(12)	0.0034(10)	0.0041(10)	–0.0009(11)
C(22)	0.0292(15)	0.0399(17)	0.0218(14)	0.0046(12)	0.0014(11)	0.0080(12)
C(23)	0.0433(17)	0.0330(16)	0.0269(15)	0.0025(12)	0.0064(13)	0.0147(13)
C(24)	0.0468(17)	0.0251(14)	0.0202(13)	–0.0033(11)	0.0065(12)	0.0045(12)
C(25)	0.0296(14)	0.0256(14)	0.0164(12)	–0.0011(10)	0.0036(10)	0.0007(11)
C(26)	0.0229(12)	0.0236(13)	0.0120(11)	0.0015(9)	0.0064(9)	–0.0016(10)
C(27)	0.0175(11)	0.0208(12)	0.0127(11)	–0.0004(9)	0.0042(9)	–0.0039(9)
C(28)	0.0232(12)	0.0235(13)	0.0110(11)	–0.0027(9)	0.0026(9)	–0.0034(10)
C(29)	0.0278(14)	0.0212(13)	0.0139(11)	–0.0022(9)	0.0050(10)	–0.0073(10)
C(30)	0.0264(13)	0.0198(12)	0.0172(12)	–0.0038(10)	0.0005(10)	–0.0069(10)
C(31)	0.0257(13)	0.0282(14)	0.0119(11)	–0.0059(10)	0.0037(10)	–0.0069(11)
C(32)	0.0256(13)	0.0281(14)	0.0152(12)	–0.0008(10)	0.0061(10)	–0.0109(11)
C(33)	0.0257(13)	0.0209(12)	0.0154(12)	–0.0029(10)	0.0023(10)	–0.0083(11)
C(34)	0.0534(19)	0.0247(15)	0.0287(15)	–0.0035(11)	0.0052(14)	–0.0176(13)
C(35)	0.050(2)	0.098(4)	0.067(3)	–0.052(3)	0.021(2)	–0.004(2)

C(36)	0.055(2)	0.0445(18)	0.0213(14)	–0.0020(13)	0.0103(13)	–0.0321(16)

Table 5. Hydrogen coordinates and isotropic displacement parameters ($Å^2$) for acb196.

	x	y	z	U
H(2A)	0.5078	0.4112	0.2185	0.024
H(3A)	0.5339	0.5475	0.2765	0.022
H(5A)	0.1591	0.4924	0.2940	0.024
H(6A)	0.1327	0.3568	0.2360	0.025
H(10A)	0.3116	0.7389	0.2473	0.024
H(11A)	0.2132	0.8728	0.1965	0.028
H(12A)	0.0645	1.0640	0.2079	0.030
H(13A)	0.0199	1.1261	0.2709	0.030
H(15A)	0.0532	1.0912	0.3402	0.030
H(16A)	0.1757	1.0042	0.3923	0.028
H(19A)	0.5591	0.7511	0.4388	0.027
H(20A)	0.7133	0.5700	0.4306	0.029
H(22A)	0.7697	0.3150	0.4069	0.036
H(23A)	0.7158	0.0970	0.3718	0.041
H(24A)	0.5237	0.0901	0.3341	0.037
H(25A)	0.3999	0.3077	0.3254	0.029
H(29A)	0.4371	1.0735	0.4220	0.025
H(33A)	0.2451	0.6865	0.4473	0.025
H(34A)	0.4821	1.4109	0.4746	0.053
H(34B)	0.4070	1.3271	0.4391	0.053
H(34C)	0.5423	1.2632	0.4553	0.053
H(35A)	0.1477	1.1567	0.5671	0.107
H(35B)	0.0914	1.0150	0.5424	0.107
H(35C)	0.1247	1.1715	0.5211	0.107
H(36A)	0.0730	0.5921	0.5265	0.060
H(36B)	0.1930	0.5539	0.5016	0.060
H(36C)	0.0735	0.6440	0.4821	0.060

Table 6. Torsion angles [°] for acb196.

Br–C(1)–C(2)–C(3)	176.04(18)	C(6)–C(1)–C(2)–C(3)	–2.9(4)
C(1)–C(2)–C(3)–C(4)	0.1(4)	C(2)–C(3)–C(4)–C(5)	2.7(4)
C(2)–C(3)–C(4)–C(7)	–174.3(2)	C(3)–C(4)–C(5)–C(6)	–2.8(4)
C(7)–C(4)–C(5)–C(6)	174.3(2)	Br–C(1)–C(6)–C(5)	–176.14(19)
C(2)–C(1)–C(6)–C(5)	2.8(4)	C(4)–C(5)–C(6)–C(1)	0.0(4)
C(3)–C(4)–C(7)–C(8)	113.5(3)	C(3)–C(4)–C(7)–C(27)	–65.8(3)
C(5)–C(4)–C(7)–C(8)	–63.5(3)	C(5)–C(4)–C(7)–C(27)	117.3(3)
C(4)–C(7)–C(8)–C(9)	–10.4(3)	C(4)–C(7)–C(8)–C(17)	166.6(2)
C(27)–C(7)–C(8)–C(9)	168.9(2)	C(27)–C(7)–C(8)–C(17)	–14.2(3)
C(7)–C(8)–C(9)–C(10)	–19.8(4)	C(7)–C(8)–C(9)–C(14)	165.0(2)
C(17)–C(8)–C(9)–C(10)	163.3(2)	C(17)–C(8)–C(9)–C(14)	–11.9(3)
C(8)–C(9)–C(10)–C(11)	–176.4(2)	C(14)–C(9)–C(10)–C(11)	–1.2(4)
C(9)–C(10)–C(11)–C(12)	–0.5(4)	C(10)–C(11)–C(12)–C(13)	1.2(4)
C(11)–C(12)–C(13)–C(14)	–0.2(4)	C(12)–C(13)–C(14)–C(9)	–1.6(4)
C(12)–C(13)–C(14)–C(15)	174.9(2)	C(8)–C(9)–C(14)–C(13)	177.7(2)
C(8)–C(9)–C(14)–C(15)	1.3(3)	C(10)–C(9)–C(14)–C(13)	2.2(3)
C(10)–C(9)–C(14)–C(15)	–174.2(2)	C(9)–C(14)–C(15)–C(16)	7.0(4)
C(13)–C(14)–C(15)–C(16)	–169.5(3)	C(14)–C(15)–C(16)–C(17)	–3.9(4)
C(18)–N–C(17)–C(8)	–3.3(3)	C(18)–N–C(17)–C(16)	176.2(2)
C(28)–N–C(17)–C(8)	–174.9(2)	C(28)–N–C(17)–C(16)	4.6(3)
C(15)–C(16)–C(17)–N	172.9(2)	C(15)–C(16)–C(17)–C(8)	–7.7(4)
C(7)–C(8)–C(17)–N	17.6(3)	C(7)–C(8)–C(17)–C(16)	–161.8(2)
C(9)–C(8)–C(17)–N	–165.1(2)	C(9)–C(8)–C(17)–C(16)	15.4(3)
C(17)–N–C(18)–C(19)	162.5(2)	C(17)–N–C(18)–C(27)	–14.9(3)
C(28)–N–C(18)–C(19)	–25.8(3)	C(28)–N–C(18)–C(27)	156.8(2)
N–C(18)–C(19)–C(20)	–178.6(2)	C(27)–C(18)–C(19)–C(20)	–1.3(4)
C(18)–C(19)–C(20)–C(21)	–10.9(4)	C(19)–C(20)–C(21)–C(22)	–167.2(3)
C(19)–C(20)–C(21)–C(26)	6.6(4)	C(20)–C(21)–C(22)–C(23)	168.2(3)
C(26)–C(21)–C(22)–C(23)	–5.5(4)	C(21)–C(22)–C(23)–C(24)	–1.0(4)
C(22)–C(23)–C(24)–C(25)	4.7(4)	C(23)–C(24)–C(25)–C(26)	–1.8(4)
C(24)–C(25)–C(26)–C(21)	–4.6(4)	C(24)–C(25)–C(26)–C(27)	–179.5(2)
C(20)–C(21)–C(26)–C(25)	–165.6(2)	C(20)–C(21)–C(26)–C(27)	9.6(3)
C(22)–C(21)–C(26)–C(25)	8.2(4)	C(22)–C(21)–C(26)–C(27)	–176.6(2)
N–C(18)–C(27)–C(7)	17.9(3)	N–C(18)–C(27)–C(26)	–165.7(2)
C(19)–C(18)–C(27)–C(7)	–159.4(2)	C(19)–C(18)–C(27)–C(26)	16.9(3)
C(4)–C(7)–C(27)–C(18)	175.9(2)	C(4)–C(7)–C(27)–C(26)	0.0(4)
C(8)–C(7)–C(27)–C(18)	–3.3(3)	C(8)–C(7)–C(27)–C(26)	–179.3(2)
C(21)–C(26)–C(27)–C(7)	155.3(2)	C(21)–C(26)–C(27)–C(18)	–20.7(3)
C(25)–C(26)–C(27)–C(7)	–29.8(4)	C(25)–C(26)–C(27)–C(18)	154.2(2)
C(17)–N–C(28)–C(29)	–80.6(3)	C(17)–N–C(28)–C(33)	96.7(3)
C(18)–N–C(28)–C(29)	107.5(3)	C(18)–N–C(28)–C(33)	–75.2(3)
N–C(28)–C(29)–C(30)	176.7(2)	C(33)–C(28)–C(29)–C(30)	–0.4(4)
C(34)–O(1)–C(30)–C(29)	4.3(4)	C(34)–O(1)–C(30)–C(31)	–175.3(3)
C(28)–C(29)–C(30)–O(1)	–179.0(2)	C(28)–C(29)–C(30)–C(31)	0.6(4)
C(35)–O(2)–C(31)–C(30)	105.8(3)	C(35)–O(2)–C(31)–C(32)	–76.4(4)
O(1)–C(30)–C(31)–O(2)	–3.2(4)	O(1)–C(30)–C(31)–C(32)	179.0(2)
C(29)–C(30)–C(31)–O(2)	177.2(2)	C(29)–C(30)–C(31)–C(32)	–0.6(4)
C(36)–O(3)–C(32)–C(31)	174.0(3)	C(36)–O(3)–C(32)–C(33)	–5.9(4)
O(2)–C(31)–C(32)–O(3)	2.7(4)	O(2)–C(31)–C(32)–C(33)	–177.4(2)
C(30)–C(31)–C(32)–O(3)	–179.6(2)	C(30)–C(31)–C(32)–C(33)	0.4(4)

N–C(28)–C(33)–C(32)	–177.0(2)	C(29)–C(28)–C(33)–C(32)	0.2(4)
O(3)–C(32)–C(33)–C(28)	179.8(3)	C(31)–C(32)–C(33)–C(28)	–0.2(4)

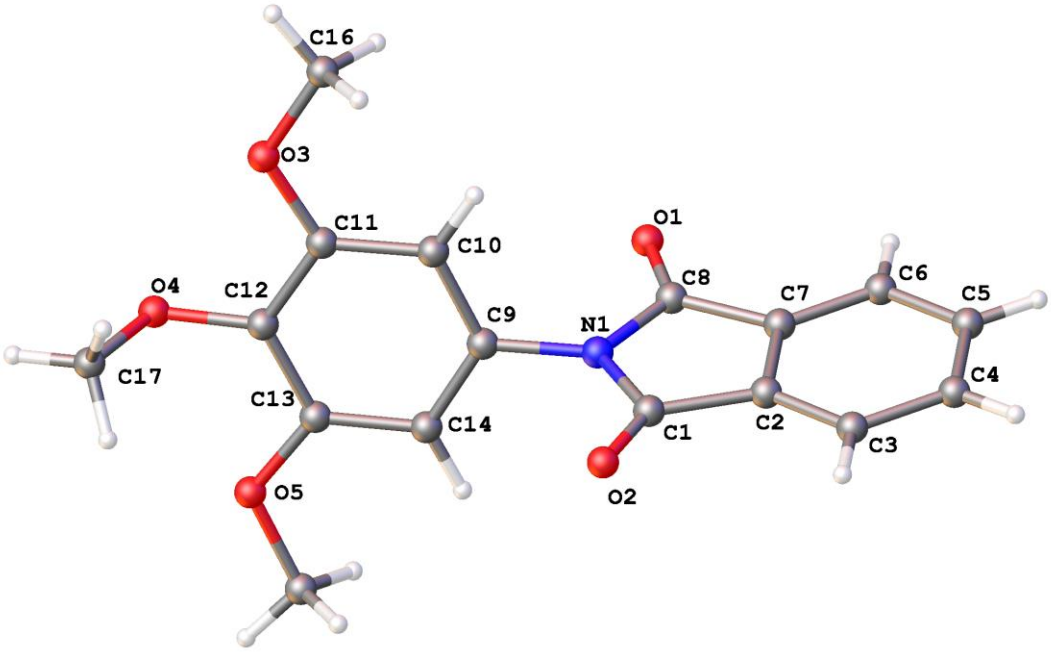
C16
O3
C11
C10
O1
C8
C6
C7
C5
O4
C12
C9
N1
C17
C13
C14
C1
C2
C4
C3
O5
O2

Table 1. Crystal data and structure refinement for **PHTH1**.

Identification code	**PHTH1**	
Chemical formula (moiety)	$C_{17}H_{15}NO_5$	
Chemical formula (total)	$C_{17}H_{15}NO_5$	
Formula weight	313.30	
Temperature	150(2) K	
Radiation, wavelength	MoKα, 0.71073 Å	
Crystal system, space group	triclinic, $P\bar{1}$	
Unit cell parameters	a = 5.2034(5) Å	α = 68.696(6)°
	b = 12.1688(8) Å	β = 78.984(7)°
	c = 12.5890(9) Å	γ = 83.613(7)°
Cell volume	728.21(10) $Å^3$	
Z	2	
Calculated density	1.429 g/cm^3	
Absorption coefficient μ	0.106 mm^{-1}	
F(000)	328	
Reflections for cell refinement	2547 (θ range 3.3 to 28.5°)	
Data collection method	Oxford Diffraction Gemini A Ultra diffractometer thick-slice ω scans	
θ range for data collection	3.3 to 28.6°	
Index ranges	h −6 to 6, k −12 to 15, l −16 to 16	
Completeness to θ = 26.0°	97.7 %	
Reflections collected	5749	
Independent reflections	3022 (R_{int} = 0.0365)	
Reflections with $F^2>2\sigma$	2200	
Absorption correction	semi-empirical from equivalents	
Min. and max. transmission	0.80972 and 1.00000	
Structure solution	direct methods	
Refinement method	Full-matrix least-squares on F^2	
Weighting parameters a, b	0.0649, 0.0000	
Data / restraints / parameters	3022 / 0 / 212	
Final R indices [$F^2>2\sigma$]	R1 = 0.0486, wR2 = 0.1140	
R indices (all data)	R1 = 0.0722, wR2 = 0.1312	
Goodness-of-fit on F^2	1.028	
Extinction coefficient	0.012(4)	
Largest and mean shift/su	0.000 and 0.000	
Largest diff. peak and hole	0.26 and –0.22 e $Å^{-3}$	

Table 2. Atomic coordinates and equivalent isotropic displacement parameters ($Å^2$) for acb127. U_{eq} is defined as one third of the trace of the orthogonalized U^{ij} tensor.

	x	y	z	U_{eq}
O(1)	0.0813(3)	0.10045(11)	0.10984(11)	0.0310(4)
O(2)	0.7704(3)	0.34374(12)	–0.01089(11)	0.0334(4)
O(3)	–0.1118(3)	0.44076(11)	0.30497(11)	0.0278(3)
O(4)	0.1447(2)	0.32532(11)	0.48194(10)	0.0249(3)
O(5)	0.5511(3)	0.17502(11)	0.46323(10)	0.0262(3)
N(1)	0.4156(3)	0.22519(13)	0.07666(12)	0.0219(4)
C(1)	0.6215(4)	0.27531(15)	–0.01284(15)	0.0223(4)
C(2)	0.6074(4)	0.22898(15)	–0.10535(15)	0.0215(4)
C(3)	0.7565(4)	0.25338(16)	–0.21356(16)	0.0273(5)
C(4)	0.6881(4)	0.20284(17)	–0.28655(16)	0.0310(5)
C(5)	0.4773(4)	0.13042(17)	–0.25063(16)	0.0319(5)
C(6)	0.3286(4)	0.10494(16)	–0.14087(16)	0.0271(4)
C(7)	0.3970(4)	0.15631(15)	–0.06941(15)	0.0215(4)
C(8)	0.2712(4)	0.15246(15)	0.04821(15)	0.0222(4)
C(9)	0.3512(4)	0.25270(15)	0.18041(15)	0.0206(4)
C(10)	0.1467(3)	0.33447(15)	0.18729(15)	0.0210(4)
C(11)	0.0836(3)	0.36148(14)	0.28777(15)	0.0213(4)
C(12)	0.2207(4)	0.30532(15)	0.37960(14)	0.0194(4)
C(13)	0.4280(4)	0.22433(15)	0.36895(15)	0.0204(4)
C(14)	0.4953(3)	0.19770(15)	0.26846(15)	0.0209(4)
C(16)	–0.2561(4)	0.49948(16)	0.21204(16)	0.0294(5)
C(17)	0.2943(4)	0.41088(17)	0.49289(17)	0.0310(5)
C(18)	0.7672(4)	0.09342(16)	0.45488(17)	0.0269(4)

Table 3. Bond lengths [Å] and angles [°] for acb127.

O(1)–C(8)	1.212(2)	O(2)–C(1)	1.208(2)
O(3)–C(11)	1.364(2)	O(3)–C(16)	1.433(2)
O(4)–C(12)	1.374(2)	O(4)–C(17)	1.426(2)
O(5)–C(13)	1.366(2)	O(5)–C(18)	1.430(2)
N(1)–C(1)	1.405(2)	N(1)–C(8)	1.399(2)
N(1)–C(9)	1.434(2)	C(1)–C(2)	1.483(2)
C(2)–C(3)	1.378(3)	C(2)–C(7)	1.386(3)
C(3)–H(3A)	0.950	C(3)–C(4)	1.391(3)
C(4)–H(4A)	0.950	C(4)–C(5)	1.386(3)
C(5)–H(5A)	0.950	C(5)–C(6)	1.392(3)
C(6)–H(6A)	0.950	C(6)–C(7)	1.381(3)
C(7)–C(8)	1.486(2)	C(9)–C(10)	1.386(3)
C(9)–C(14)	1.381(3)	C(10)–H(10A)	0.950
C(10)–C(11)	1.391(2)	C(11)–C(12)	1.395(3)
C(12)–C(13)	1.399(3)	C(13)–C(14)	1.390(2)
C(14)–H(14A)	0.950	C(16)–H(16A)	0.980
C(16)–H(16B)	0.980	C(16)–H(16C)	0.980
C(17)–H(17A)	0.980	C(17)–H(17B)	0.980
C(17)–H(17C)	0.980	C(18)–H(18A)	0.980
C(18)–H(18B)	0.980	C(18)–H(18C)	0.980

C(11)–O(3)–C(16)	116.78(14)	C(12)–O(4)–C(17)	113.43(13)
C(13)–O(5)–C(18)	116.86(14)	C(1)–N(1)–C(8)	111.68(15)
C(1)–N(1)–C(9)	123.68(14)	C(8)–N(1)–C(9)	124.49(15)
O(2)–C(1)–N(1)	124.64(16)	O(2)–C(1)–C(2)	129.52(17)
N(1)–C(1)–C(2)	105.83(15)	C(1)–C(2)–C(3)	129.93(17)
C(1)–C(2)–C(7)	108.33(15)	C(3)–C(2)–C(7)	121.65(16)
C(2)–C(3)–H(3A)	121.2	C(2)–C(3)–C(4)	117.68(18)
H(3A)–C(3)–C(4)	121.2	C(3)–C(4)–H(4A)	119.7
C(3)–C(4)–C(5)	120.63(18)	H(4A)–C(4)–C(5)	119.7
C(4)–C(5)–H(5A)	119.2	C(4)–C(5)–C(6)	121.60(18)
H(5A)–C(5)–C(6)	119.2	C(5)–C(6)–H(6A)	121.4
C(5)–C(6)–C(7)	117.28(18)	H(6A)–C(6)–C(7)	121.4
C(2)–C(7)–C(6)	121.16(17)	C(2)–C(7)–C(8)	108.35(15)
C(6)–C(7)–C(8)	130.44(17)	O(1)–C(8)–N(1)	124.65(17)
O(1)–C(8)–C(7)	129.53(17)	N(1)–C(8)–C(7)	105.81(15)
N(1)–C(9)–C(10)	118.14(16)	N(1)–C(9)–C(14)	118.98(16)
C(10)–C(9)–C(14)	122.88(16)	C(9)–C(10)–H(10A)	120.8
C(9)–C(10)–C(11)	118.34(17)	H(10A)–C(10)–C(11)	120.8
O(3)–C(11)–C(10)	124.04(16)	O(3)–C(11)–C(12)	115.66(15)
C(10)–C(11)–C(12)	120.29(16)	O(4)–C(12)–C(11)	120.10(16)
O(4)–C(12)–C(13)	120.12(16)	C(11)–C(12)–C(13)	119.71(16)
O(5)–C(13)–C(12)	115.18(15)	O(5)–C(13)–C(14)	124.24(16)
C(12)–C(13)–C(14)	120.57(16)	C(9)–C(14)–C(13)	118.17(17)
C(9)–C(14)–H(14A)	120.9	C(13)–C(14)–H(14A)	120.9
O(3)–C(16)–H(16A)	109.5	O(3)–C(16)–H(16B)	109.5
O(3)–C(16)–H(16C)	109.5	H(16A)–C(16)–H(16B)	109.5
H(16A)–C(16)–H(16C)	109.5	H(16B)–C(16)–H(16C)	109.5
O(4)–C(17)–H(17A)	109.5	O(4)–C(17)–H(17B)	109.5
O(4)–C(17)–H(17C)	109.5	H(17A)–C(17)–H(17B)	109.5
H(17A)–C(17)–H(17C)	109.5	H(17B)–C(17)–H(17C)	109.5
O(5)–C(18)–H(18A)	109.5	O(5)–C(18)–H(18B)	109.5
O(5)–C(18)–H(18C)	109.5	H(18A)–C(18)–H(18B)	109.5

H(18A)–C(18)–H(18C)	109.5	H(18B)–C(18)–H(18C)	109.5

Table 4. Anisotropic displacement parameters ($Å^2$) for acb127. The anisotropic displacement factor exponent takes the form: $-2\pi^2[h^2a^{*2}U^{11} + ...+ 2hka^*b^*U^{12}]$

	U^{11}	U^{22}	U^{33}	U^{23}	U^{13}	U^{12}
O(1)	0.0317(8)	0.0299(7)	0.0327(8)	–0.0141(6)	0.0042(6)	–0.0116(6)
O(2)	0.0340(8)	0.0372(8)	0.0311(8)	–0.0129(6)	–0.0002(6)	–0.0157(7)
O(3)	0.0265(7)	0.0267(7)	0.0296(7)	–0.0120(6)	–0.0030(6)	0.0064(6)
O(4)	0.0274(7)	0.0281(7)	0.0220(7)	–0.0135(6)	0.0016(6)	–0.0060(6)
O(5)	0.0321(8)	0.0242(7)	0.0235(7)	–0.0088(5)	–0.0092(6)	0.0043(6)
N(1)	0.0229(8)	0.0237(8)	0.0218(8)	–0.0119(6)	0.0001(7)	–0.0040(6)
C(1)	0.0236(10)	0.0204(9)	0.0222(9)	–0.0068(8)	–0.0033(8)	–0.0013(8)
C(2)	0.0225(10)	0.0213(9)	0.0192(9)	–0.0058(7)	–0.0052(8)	0.0032(7)
C(3)	0.0267(11)	0.0262(10)	0.0250(10)	–0.0064(8)	0.0008(9)	–0.0021(8)
C(4)	0.0385(12)	0.0317(11)	0.0213(10)	–0.0108(8)	–0.0001(9)	0.0016(9)
C(5)	0.0402(12)	0.0326(11)	0.0290(11)	–0.0182(9)	–0.0067(10)	0.0012(9)
C(6)	0.0303(11)	0.0239(10)	0.0289(10)	–0.0111(8)	–0.0053(9)	–0.0011(8)
C(7)	0.0233(10)	0.0186(9)	0.0224(9)	–0.0075(7)	–0.0052(8)	0.0028(7)
C(8)	0.0229(10)	0.0187(9)	0.0244(9)	–0.0072(8)	–0.0049(8)	0.0016(8)
C(9)	0.0229(10)	0.0208(9)	0.0196(9)	–0.0091(7)	–0.0008(8)	–0.0048(7)
C(10)	0.0214(10)	0.0209(9)	0.0204(9)	–0.0059(7)	–0.0038(8)	–0.0035(7)
C(11)	0.0202(9)	0.0164(9)	0.0256(10)	–0.0067(8)	0.0002(8)	–0.0034(7)
C(12)	0.0232(9)	0.0194(9)	0.0157(8)	–0.0067(7)	0.0010(8)	–0.0064(7)
C(13)	0.0225(9)	0.0172(9)	0.0207(9)	–0.0047(7)	–0.0029(8)	–0.0053(7)
C(14)	0.0215(10)	0.0169(9)	0.0244(9)	–0.0082(7)	–0.0019(8)	–0.0012(7)
C(16)	0.0248(10)	0.0242(10)	0.0312(11)	–0.0032(9)	–0.0016(9)	0.0042(8)
C(17)	0.0341(11)	0.0330(11)	0.0330(11)	–0.0205(9)	–0.0022(9)	–0.0054(9)
C(18)	0.0268(10)	0.0241(10)	0.0294(10)	–0.0077(8)	–0.0095(9)	0.0038(8)

Table 5. Hydrogen coordinates and isotropic displacement parameters ($Å^2$) for acb127.

	x	y	z	U
H(3A)	0.9009	0.3030	–0.2375	0.033
H(4A)	0.7869	0.2181	–0.3618	0.037
H(5A)	0.4332	0.0974	–0.3022	0.038
H(6A)	0.1859	0.0543	–0.1161	0.033
H(10A)	0.0520	0.3711	0.1249	0.025
H(14A)	0.6366	0.1431	0.2606	0.025
H(16A)	–0.3924	0.5528	0.2347	0.044
H(16B)	–0.3378	0.4407	0.1943	0.044
H(16C)	–0.1369	0.5450	0.1435	0.044
H(17A)	0.2385	0.4174	0.5693	0.047
H(17B)	0.2665	0.4876	0.4331	0.047
H(17C)	0.4807	0.3864	0.4838	0.047
H(18A)	0.8432	0.0663	0.5261	0.040
H(18B)	0.9004	0.1324	0.3890	0.040
H(18C)	0.7062	0.0256	0.4438	0.040

Table 6. Torsion angles [°] for acb127.

C(8)–N(1)–C(1)–O(2)	177.97(17)	C(8)–N(1)–C(1)–C(2)	–0.69(19)
C(9)–N(1)–C(1)–O(2)	2.3(3)	C(9)–N(1)–C(1)–C(2)	–176.38(15)
O(2)–C(1)–C(2)–C(3)	–1.4(3)	O(2)–C(1)–C(2)–C(7)	–177.70(19)
N(1)–C(1)–C(2)–C(3)	177.20(18)	N(1)–C(1)–C(2)–C(7)	0.87(19)
C(1)–C(2)–C(3)–C(4)	–175.62(18)	C(7)–C(2)–C(3)–C(4)	0.3(3)
C(2)–C(3)–C(4)–C(5)	–0.1(3)	C(3)–C(4)–C(5)–C(6)	–0.5(3)
C(4)–C(5)–C(6)–C(7)	1.0(3)	C(5)–C(6)–C(7)–C(2)	–0.8(3)
C(5)–C(6)–C(7)–C(8)	176.21(18)	C(1)–C(2)–C(7)–C(6)	176.89(16)
C(1)–C(2)–C(7)–C(8)	–0.72(19)	C(3)–C(2)–C(7)–C(6)	0.2(3)
C(3)–C(2)–C(7)–C(8)	–177.41(16)	C(1)–N(1)–C(8)–O(1)	–178.79(17)
C(1)–N(1)–C(8)–C(7)	0.27(19)	C(9)–N(1)–C(8)–O(1)	–3.1(3)
C(9)–N(1)–C(8)–C(7)	175.91(16)	C(2)–C(7)–C(8)–O(1)	179.30(18)
C(2)–C(7)–C(8)–N(1)	0.30(19)	C(6)–C(7)–C(8)–O(1)	2.0(3)
C(6)–C(7)–C(8)–N(1)	–177.01(19)	C(1)–N(1)–C(9)–C(10)	98.7(2)
C(1)–N(1)–C(9)–C(14)	–80.9(2)	C(8)–N(1)–C(9)–C(10)	–76.4(2)
C(8)–N(1)–C(9)–C(14)	104.0(2)	N(1)–C(9)–C(10)–C(11)	–179.97(14)
C(14)–C(9)–C(10)–C(11)	–0.4(3)	C(16)–O(3)–C(11)–C(10)	–0.7(2)
C(16)–O(3)–C(11)–C(12)	–179.85(15)	C(9)–C(10)–C(11)–O(3)	179.58(15)
C(9)–C(10)–C(11)–C(12)	–1.3(2)	C(17)–O(4)–C(12)–C(11)	–98.14(19)
C(17)–O(4)–C(12)–C(13)	84.90(19)	O(3)–C(11)–C(12)–O(4)	4.3(2)
O(3)–C(11)–C(12)–C(13)	–178.72(14)	C(10)–C(11)–C(12)–O(4)	–174.91(14)
C(10)–C(11)–C(12)–C(13)	2.1(3)	C(18)–O(5)–C(13)–C(12)	–178.86(15)
C(18)–O(5)–C(13)–C(14)	1.8(2)	O(4)–C(12)–C(13)–O(5)	–3.6(2)
O(4)–C(12)–C(13)–C(14)	175.77(14)	C(11)–C(12)–C(13)–O(5)	179.42(14)
C(11)–C(12)–C(13)–C(14)	–1.2(3)	N(1)–C(9)–C(14)–C(13)	–179.19(14)
C(10)–C(9)–C(14)–C(13)	1.2(3)	O(5)–C(13)–C(14)–C(9)	178.91(15)
C(12)–C(13)–C(14)–C(9)	–0.4(3)		

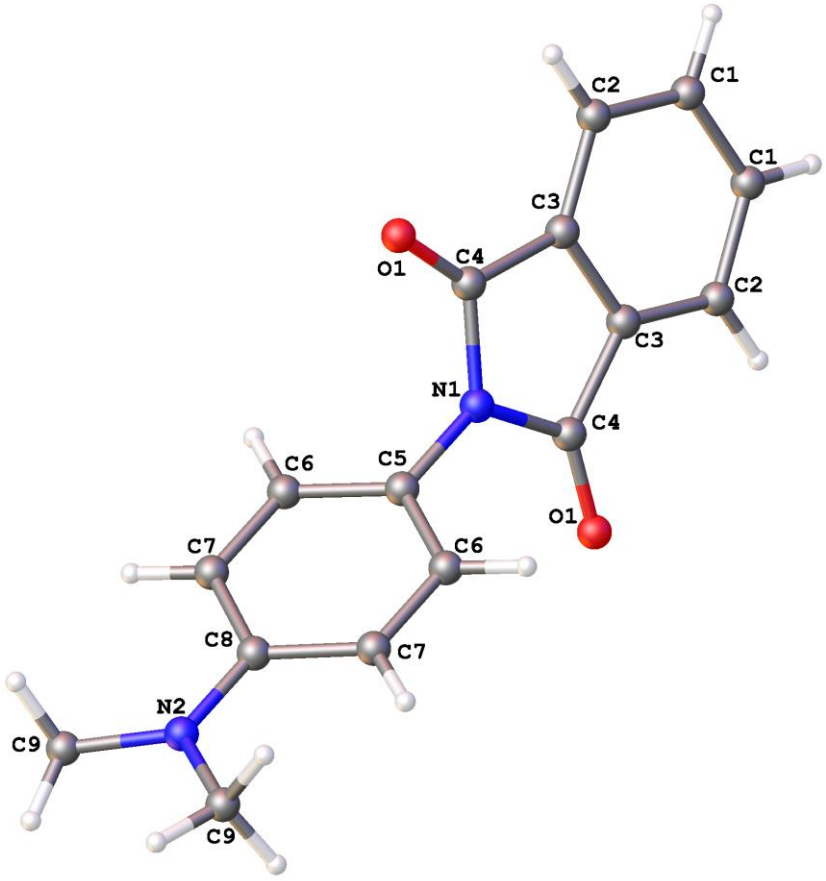
C2
C1
C1
C3
O1
C4
C2
C3
N1
C4
C6
C5
O1
C7
C6
C8
C7
N2
C9
C9

Table 1. Crystal data and structure refinement for **PHTH2**.

Identification code	**PHTH2**	
Chemical formula (moiety)	$C_{16}H_{14}N_2O_2$	
Chemical formula (total)	$C_{16}H_{14}N_2O_2$	
Formula weight	266.29	
Temperature	150(2) K	
Radiation, wavelength	CuKα, 1.54178 Å	
Crystal system, space group	orthorhombic, Pcnb	
Unit cell parameters	a = 5.5271(7) Å	α = 90°
	b = 28.565(5) Å	β = 90°
	c = 7.9350(17) Å	γ = 90°
Cell volume	1252.8(4) $Å^3$	
Z	4	
Calculated density	1.412 g/cm^3	
Absorption coefficient μ	0.767 mm^{-1}	
F(000)	560	
Reflections for cell refinement	1435 (θ range 3.1 to 62.3°)	
Data collection method	Xcalibur, Atlas, Gemini ultra thick-slice ω scans	
θ range for data collection	3.1 to 62.3°	
Index ranges	h –4 to 6, k –29 to 32, l –8 to 9	
Completeness to θ = 62.3°	98.0 %	
Reflections collected	3341	
Independent reflections	981 (R_{int} = 0.0385)	
Reflections with $F^2>2\sigma$	808	
Absorption correction	semi-empirical from equivalents	
Min. and max. transmission	0.52486 and 1.00000	
Structure solution	direct methods	
Refinement method	Full-matrix least-squares on F^2	
Weighting parameters a, b	0.0662, 0.1872	
Data / restraints / parameters	981 / 0 / 95	
Final R indices [$F^2>2\sigma$]	R1 = 0.0417, wR2 = 0.1077	
R indices (all data)	R1 = 0.0517, wR2 = 0.1180	
Goodness-of-fit on F^2	1.077	
Extinction coefficient	0.0009(4)	
Largest and mean shift/su	0.000 and 0.000	
Largest diff. peak and hole	0.17 and –0.16 e $Å^{-3}$	

Table 2. Atomic coordinates and equivalent isotropic displacement parameters ($Å^2$) for acb130. U_{eq} is defined as one third of the trace of the orthogonalized U^{ij} tensor.

	x	y	z	U_{eq}
O(1)	0.1530(2)	0.07974(4)	0.09050(15)	0.0367(4)
N(1)	0.5000	0.09266(7)	0.2500	0.0310(5)
C(8)	0.5000	0.24072(9)	0.2500	0.0349(7)
C(5)	0.5000	0.14242(8)	0.2500	0.0301(6)
C(4)	0.3229(3)	0.06481(6)	0.1700(2)	0.0302(5)
C(6)	0.3181(3)	0.16698(7)	0.3311(2)	0.0343(5)
N(2)	0.5000	0.28887(8)	0.2500	0.0507(7)
C(3)	0.3933(3)	0.01574(6)	0.2032(2)	0.0307(5)
C(9)	0.3321(4)	0.31441(7)	0.3541(3)	0.0484(6)
C(7)	0.3176(3)	0.21511(7)	0.3319(2)	0.0368(5)
C(2)	0.2840(3)	–0.02569(7)	0.1541(2)	0.0364(5)
C(1)	0.3941(4)	–0.06717(7)	0.2022(2)	0.0425(6)

Table 3. Bond lengths [Å] and angles [°] for acb130.

O(1)–C(4)	1.2088(19)	N(1)–C(5)	1.422(3)
N(1)–C(4)	1.412(2)	N(1)–C(4A)	1.412(2)
C(8)–N(2)	1.375(3)	C(8)–C(7)	1.405(2)
C(8)–C(7A)	1.405(2)	C(5)–C(6)	1.385(2)
C(5)–C(6A)	1.385(2)	C(4)–C(3)	1.478(2)
C(6)–H(6A)	0.950	C(6)–C(7)	1.375(3)
N(2)–C(9)	1.441(2)	N(2)–C(9A)	1.441(2)
C(3)–C(3A)	1.393(3)	C(3)–C(2)	1.385(3)
C(9)–H(9A)	0.980	C(9)–H(9B)	0.980
C(9)–H(9C)	0.980	C(7)–H(7A)	0.950
C(2)–H(2A)	0.950	C(2)–C(1)	1.386(3)
C(1)–C(1A)	1.395(4)	C(1)–H(1A)	0.950

C(5)–N(1)–C(4)	124.29(10)	C(5)–N(1)–C(4A)	124.29(10)
C(4)–N(1)–C(4A)	111.4(2)	N(2)–C(8)–C(7)	121.38(12)
N(2)–C(8)–C(7A)	121.38(12)	C(7)–C(8)–C(7A)	117.2(2)
N(1)–C(5)–C(6)	120.44(12)	N(1)–C(5)–C(6A)	120.44(12)
C(6)–C(5)–C(6A)	119.1(2)	O(1)–C(4)–N(1)	125.05(17)
O(1)–C(4)–C(3)	129.20(16)	N(1)–C(4)–C(3)	105.75(15)
C(5)–C(6)–H(6A)	119.7	C(5)–C(6)–C(7)	120.68(17)
H(6A)–C(6)–C(7)	119.7	C(8)–N(2)–C(9)	120.42(12)
C(8)–N(2)–C(9A)	120.41(12)	C(9)–N(2)–C(9A)	119.2(2)
C(4)–C(3)–C(3A)	108.53(10)	C(4)–C(3)–C(2)	130.18(17)
C(3A)–C(3)–C(2)	121.29(11)	N(2)–C(9)–H(9A)	109.5
N(2)–C(9)–H(9B)	109.5	N(2)–C(9)–H(9C)	109.5
H(9A)–C(9)–H(9B)	109.5	H(9A)–C(9)–H(9C)	109.5
H(9B)–C(9)–H(9C)	109.5	C(8)–C(7)–C(6)	121.13(18)
C(8)–C(7)–H(7A)	119.4	C(6)–C(7)–H(7A)	119.4
C(3)–C(2)–H(2A)	121.3	C(3)–C(2)–C(1)	117.48(18)
H(2A)–C(2)–C(1)	121.3	C(2)–C(1)–C(1A)	121.23(12)
C(2)–C(1)–H(1A)	119.4	C(1A)–C(1)–H(1A)	119.4

Symmetry operations for equivalent atoms
A –x+1,y,–z+1/2

Table 4. Anisotropic displacement parameters ($Å^2$) for acb130. The anisotropic displacement factor exponent takes the form: $-2\pi^2[h^2a^{*2}U^{11} + ...+ 2hka^*b^*U^{12}]$

	U^{11}	U^{22}	U^{33}	U^{23}	U^{13}	U^{12}
O(1)	0.0361(7)	0.0383(9)	0.0356(7)	–0.0003(6)	–0.0002(5)	0.0005(6)
N(1)	0.0338(11)	0.0267(12)	0.0327(11)	0.000	0.0005(8)	0.000
C(8)	0.0487(16)	0.0262(15)	0.0298(13)	0.000	–0.0038(11)	0.000
C(5)	0.0344(13)	0.0268(14)	0.0289(13)	0.000	–0.0011(10)	0.000
C(4)	0.0310(9)	0.0344(12)	0.0253(9)	–0.0001(8)	0.0047(7)	–0.0023(8)
C(6)	0.0357(10)	0.0323(12)	0.0349(10)	0.0010(8)	0.0034(7)	0.0003(9)
N(2)	0.0826(19)	0.0275(14)	0.0420(13)	0.000	0.0110(12)	0.000
C(3)	0.0374(9)	0.0297(10)	0.0249(9)	–0.0001(7)	0.0102(7)	–0.0015(8)
C(9)	0.0537(13)	0.0333(13)	0.0584(13)	–0.0070(10)	–0.0155(10)	0.0090(10)
C(7)	0.0410(11)	0.0327(11)	0.0367(10)	–0.0026(9)	0.0040(8)	0.0041(9)
C(2)	0.0431(10)	0.0338(12)	0.0323(10)	–0.0027(8)	0.0115(8)	–0.0068(9)
C(1)	0.0602(12)	0.0278(11)	0.0395(11)	–0.0041(9)	0.0189(9)	–0.0074(9)

Table 5. Hydrogen coordinates and isotropic displacement parameters ($Å^2$) for acb130.

	x	y	z	U
H(6A)	0.1924	0.1504	0.3868	0.041
H(9A)	0.3305	0.3009	0.4676	0.073
H(9B)	0.1696	0.3124	0.3051	0.073
H(9C)	0.3818	0.3473	0.3603	0.073
H(7A)	0.1918	0.2313	0.3889	0.044
H(2A)	0.1390	–0.0257	0.0898	0.044
H(1A)	0.3240	–0.0962	0.1696	0.051

Table 6. Torsion angles [°] for acb130.

C(4)–N(1)–C(5)–C(6)	65.59(11)	C(4A)–N(1)–C(5)–C(6)	−114.41(11)
C(4)–N(1)–C(5)–C(6A)	−114.41(11)	C(4A)–N(1)–C(5)–C(6A)	65.59(11)
C(5)–N(1)–C(4)–O(1)	1.08(19)	C(5)–N(1)–C(4)–C(3)	−179.62(7)
C(4A)–N(1)–C(4)–O(1)	−178.92(19)	C(4A)–N(1)–C(4)–C(3)	0.38(7)
N(1)–C(5)–C(6)–C(7)	179.81(12)	C(6A)–C(5)–C(6)–C(7)	−0.19(12)
C(7)–C(8)–N(2)–C(9)	8.84(12)	C(7)–C(8)–N(2)–C(9A)	−171.16(12)
C(7A)–C(8)–N(2)–C(9A)	8.84(12)	C(7A)–C(8)–N(2)–C(9)	−171.16(12)
O(1)–C(4)–C(3)–C(3A)	178.22(17)	O(1)–C(4)–C(3)–C(2)	−0.6(3)
N(1)–C(4)–C(3)–C(3A)	−1.0(2)	N(1)–C(4)–C(3)–C(2)	−179.89(15)
C(5)–C(6)–C(7)–C(8)	0.4(2)	N(2)–C(8)–C(7)–C(6)	179.81(12)
C(7A)–C(8)–C(7)–C(6)	−0.19(12)	C(4)–C(3)–C(2)–C(1)	179.05(16)
C(3A)–C(3)–C(2)–C(1)	0.3(3)	C(3)–C(2)–C(1)–C(1A)	0.5(3)

Symmetry operations for equivalent atoms
A −x+1,y,−z+1/2

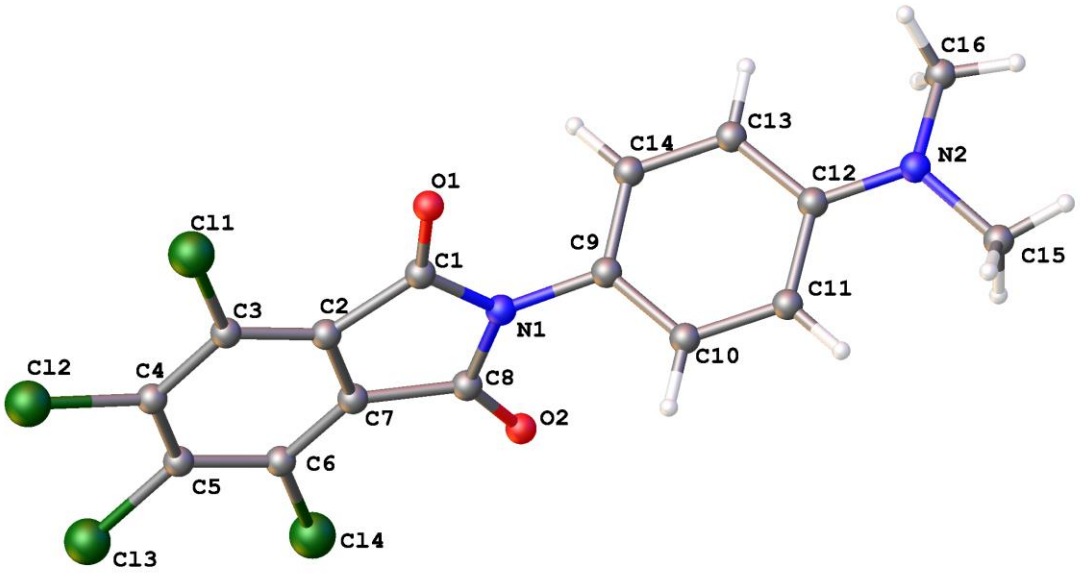
C16
C13
C14
N2
C12
O1
C15
C11
C9
C1
C11
C3
C2
N1
C4
C12
C8
C10
C7
O2
C6
C5
C14
C13

Table 1. Crystal data and structure refinement for **PHTH3**.

Identification code	**PHTH3**	
Chemical formula (moiety)	$C_{16}H_{10}Cl_4N_2O_2$	
Chemical formula (total)	$C_{16}H_{10}Cl_4N_2O_2$	
Formula weight	404.06	
Temperature	150(2) K	
Radiation, wavelength	synchrotron, 0.68890 Å	
Crystal system, space group	orthorhombic, Pbca	
Unit cell parameters	a = 16.608(3) Å	α = 90°
	b = 6.6724(14) Å	β = 90°
	c = 29.798(6) Å	γ = 90°
Cell volume	3302.1(11) Å^3	
Z	8	
Calculated density	1.626 g/cm^3	
Absorption coefficient μ	0.663 mm^{-1}	
F(000)	1632	
Crystal colour and size	yellow, 0.10 × 0.10 × 0.00 mm^3	
Reflections for cell refinement	9912 (θ range 2.7 to 27.4°)	
Data collection method	Rigaku Spider CCD diffractometer thick-slice ω scans	
θ range for data collection	1.8 to 27.4°	
Index ranges	h –15 to 21, k –8 to 8, l –39 to 39	
Completeness to θ = 27.4°	97.5 %	
Reflections collected	31172	
Independent reflections	4029 (R_{int} = 0.0517)	
Reflections with $F^2>2\sigma$	3432	
Absorption correction	semi-empirical from equivalents	
Min. and max. transmission	0.9366 and 0.9987	
Structure solution	direct methods	
Refinement method	Full-matrix least-squares on F^2	
Weighting parameters a, b	0.0412, 2.0510	
Data / restraints / parameters	4029 / 0 / 220	
Final R indices [$F^2>2\sigma$]	R1 = 0.0342, wR2 = 0.0878	
R indices (all data)	R1 = 0.0412, wR2 = 0.0914	
Goodness-of-fit on F^2	1.039	
Extinction coefficient	0.0036(7)	
Largest and mean shift/su	0.001 and 0.000	
Largest diff. peak and hole	0.32 and –0.31 e Å^{-3}	

Table 2. Atomic coordinates and equivalent isotropic displacement parameters ($Å^2$) for acb136. U_{eq} is defined as one third of the trace of the orthogonalized U^{ij} tensor.

	x	y	z	U_{eq}
Cl(1)	0.82248(3)	0.53936(6)	0.200552(14)	0.02747(12)
Cl(2)	0.72199(3)	0.58707(7)	0.112700(14)	0.03285(12)
Cl(3)	0.53521(3)	0.57746(7)	0.115780(14)	0.03701(13)
Cl(4)	0.44576(3)	0.52753(6)	0.206936(14)	0.02920(12)
O(1)	0.77627(8)	0.4841(2)	0.30281(4)	0.0333(3)
O(2)	0.50139(8)	0.5203(2)	0.30771(4)	0.0323(3)
N(1)	0.63958(8)	0.5033(2)	0.31704(5)	0.0275(3)
N(2)	0.63936(13)	0.4307(3)	0.50523(6)	0.0514(5)
C(1)	0.70814(11)	0.5026(2)	0.28976(5)	0.0261(3)
C(2)	0.67782(10)	0.5253(2)	0.24279(5)	0.0249(3)
C(3)	0.71911(11)	0.5400(2)	0.20269(5)	0.0250(3)
C(4)	0.67351(11)	0.5577(2)	0.16312(5)	0.0263(3)
C(5)	0.58984(11)	0.5553(2)	0.16442(5)	0.0271(3)
C(6)	0.54859(11)	0.5377(2)	0.20542(5)	0.0263(3)
C(7)	0.59430(10)	0.5275(2)	0.24408(5)	0.0253(3)
C(8)	0.56809(11)	0.5169(2)	0.29217(5)	0.0266(3)
C(9)	0.64155(10)	0.4858(3)	0.36520(6)	0.0287(4)
C(10)	0.61675(13)	0.6446(3)	0.39133(6)	0.0369(4)
C(11)	0.61535(13)	0.6273(3)	0.43770(6)	0.0405(5)
C(12)	0.63961(12)	0.4491(3)	0.45875(6)	0.0370(4)
C(13)	0.66578(12)	0.2914(3)	0.43132(6)	0.0374(4)
C(14)	0.66637(12)	0.3095(3)	0.38500(6)	0.0336(4)
C(15)	0.60401(16)	0.5879(4)	0.53230(7)	0.0523(6)
C(16)	0.64424(17)	0.2344(4)	0.52460(7)	0.0567(6)

Table 3. Bond lengths [Å] and angles [°] for acb136.

Cl(1)–C(3)	1.7179(18)	Cl(2)–C(4)	1.7157(17)
Cl(3)–C(5)	1.7163(17)	Cl(4)–C(6)	1.7097(18)
O(1)–C(1)	1.203(2)	O(2)–C(8)	1.201(2)
N(1)–C(1)	1.399(2)	N(1)–C(8)	1.402(2)
N(1)–C(9)	1.440(2)	N(2)–C(12)	1.390(2)
N(2)–C(15)	1.448(3)	N(2)–C(16)	1.434(3)
C(1)–C(2)	1.495(2)	C(2)–C(3)	1.381(2)
C(2)–C(7)	1.388(3)	C(3)–C(4)	1.406(2)
C(4)–C(5)	1.390(3)	C(5)–C(6)	1.406(2)
C(6)–C(7)	1.381(2)	C(7)–C(8)	1.500(2)
C(9)–C(10)	1.378(3)	C(9)–C(14)	1.380(2)
C(10)–H(10A)	0.950	C(10)–C(11)	1.387(3)
C(11)–H(11A)	0.950	C(11)–C(12)	1.403(3)
C(12)–C(13)	1.401(3)	C(13)–H(13A)	0.950
C(13)–C(14)	1.386(2)	C(14)–H(14A)	0.950
C(15)–H(15A)	0.980	C(15)–H(15B)	0.980
C(15)–H(15C)	0.980	C(16)–H(16A)	0.980
C(16)–H(16B)	0.980	C(16)–H(16C)	0.980

C(1)–N(1)–C(8)	112.47(14)	C(1)–N(1)–C(9)	124.07(14)
C(8)–N(1)–C(9)	123.43(14)	C(12)–N(2)–C(15)	119.48(19)
C(12)–N(2)–C(16)	118.80(19)	C(15)–N(2)–C(16)	117.42(19)
O(1)–C(1)–N(1)	125.32(16)	O(1)–C(1)–C(2)	129.04(16)
N(1)–C(1)–C(2)	105.63(14)	C(1)–C(2)–C(3)	130.53(16)
C(1)–C(2)–C(7)	108.17(14)	C(3)–C(2)–C(7)	121.29(15)
Cl(1)–C(3)–C(2)	121.87(13)	Cl(1)–C(3)–C(4)	120.49(13)
C(2)–C(3)–C(4)	117.64(16)	Cl(2)–C(4)–C(3)	119.40(13)
Cl(2)–C(4)–C(5)	119.67(13)	C(3)–C(4)–C(5)	120.93(15)
Cl(3)–C(5)–C(4)	120.26(13)	Cl(3)–C(5)–C(6)	118.91(14)
C(4)–C(5)–C(6)	120.83(15)	Cl(4)–C(6)–C(5)	120.88(13)
Cl(4)–C(6)–C(7)	121.66(13)	C(5)–C(6)–C(7)	117.45(16)
C(2)–C(7)–C(6)	121.80(15)	C(2)–C(7)–C(8)	108.42(15)
C(6)–C(7)–C(8)	129.78(16)	O(2)–C(8)–N(1)	125.34(15)
O(2)–C(8)–C(7)	129.45(16)	N(1)–C(8)–C(7)	105.21(14)
N(1)–C(9)–C(10)	119.63(16)	N(1)–C(9)–C(14)	120.13(16)
C(10)–C(9)–C(14)	120.23(16)	C(9)–C(10)–H(10A)	119.9
C(9)–C(10)–C(11)	120.28(18)	H(10A)–C(10)–C(11)	119.9
C(10)–C(11)–H(11A)	119.6	C(10)–C(11)–C(12)	120.74(18)
H(11A)–C(11)–C(12)	119.6	N(2)–C(12)–C(11)	121.29(18)
N(2)–C(12)–C(13)	121.03(18)	C(11)–C(12)–C(13)	117.67(17)
C(12)–C(13)–H(13A)	119.4	C(12)–C(13)–C(14)	121.21(17)
H(13A)–C(13)–C(14)	119.4	C(9)–C(14)–C(13)	119.87(17)
C(9)–C(14)–H(14A)	120.1	C(13)–C(14)–H(14A)	120.1
N(2)–C(15)–H(15A)	109.5	N(2)–C(15)–H(15B)	109.5
N(2)–C(15)–H(15C)	109.5	H(15A)–C(15)–H(15B)	109.5
H(15A)–C(15)–H(15C)	109.5	H(15B)–C(15)–H(15C)	109.5
N(2)–C(16)–H(16A)	109.5	N(2)–C(16)–H(16B)	109.5
N(2)–C(16)–H(16C)	109.5	H(16A)–C(16)–H(16B)	109.5
H(16A)–C(16)–H(16C)	109.5	H(16B)–C(16)–H(16C)	109.5

Table 4. Anisotropic displacement parameters ($Å^2$) for acb136. The anisotropic displacement factor exponent takes the form: $-2\pi^2[h^2a^{*2}U^{11} + ...+ 2hka^*b^*U^{12}]$

	U^{11}	U^{22}	U^{33}	U^{23}	U^{13}	U^{12}
Cl(1)	0.0210(2)	0.02586(19)	0.0355(2)	–0.00123(14)	0.00234(15)	–0.00028(15)
Cl(2)	0.0319(3)	0.0360(2)	0.0306(2)	0.00161(15)	0.00487(16)	–0.00142(17)
Cl(3)	0.0312(3)	0.0496(3)	0.0303(2)	0.00324(17)	–0.00412(17)	–0.00327(19)
Cl(4)	0.0206(2)	0.0328(2)	0.0342(2)	0.00047(15)	–0.00144(15)	–0.00028(15)
O(1)	0.0237(7)	0.0422(7)	0.0339(6)	–0.0022(5)	–0.0021(5)	–0.0003(5)
O(2)	0.0221(7)	0.0407(7)	0.0341(6)	0.0007(5)	0.0030(5)	0.0011(5)
N(1)	0.0212(8)	0.0327(7)	0.0286(7)	–0.0013(5)	0.0004(5)	–0.0003(6)
N(2)	0.0726(15)	0.0520(11)	0.0296(8)	0.0002(7)	0.0013(8)	0.0067(9)
C(1)	0.0223(10)	0.0249(7)	0.0310(8)	–0.0024(6)	0.0004(6)	0.0002(6)
C(2)	0.0231(9)	0.0207(7)	0.0310(8)	–0.0019(6)	–0.0004(6)	–0.0005(6)
C(3)	0.0235(9)	0.0192(7)	0.0322(8)	–0.0018(6)	0.0016(6)	–0.0007(6)
C(4)	0.0281(10)	0.0210(7)	0.0297(8)	–0.0008(6)	0.0030(6)	–0.0014(6)
C(5)	0.0286(10)	0.0238(7)	0.0290(8)	–0.0009(6)	–0.0026(6)	–0.0009(6)
C(6)	0.0239(9)	0.0238(7)	0.0313(8)	–0.0007(6)	–0.0006(6)	0.0002(6)
C(7)	0.0218(9)	0.0229(7)	0.0313(8)	–0.0017(6)	0.0008(6)	0.0000(6)
C(8)	0.0243(10)	0.0246(7)	0.0310(8)	–0.0003(6)	–0.0006(6)	0.0007(6)
C(9)	0.0229(9)	0.0359(9)	0.0274(8)	–0.0013(6)	0.0004(6)	–0.0011(7)
C(10)	0.0433(12)	0.0342(9)	0.0333(9)	0.0005(7)	0.0018(8)	0.0071(8)
C(11)	0.0507(13)	0.0365(10)	0.0343(9)	–0.0048(7)	0.0030(8)	0.0069(9)
C(12)	0.0387(12)	0.0415(10)	0.0309(9)	–0.0004(7)	–0.0007(7)	0.0005(8)
C(13)	0.0397(11)	0.0361(9)	0.0364(9)	0.0013(7)	–0.0038(8)	0.0064(8)
C(14)	0.0341(11)	0.0318(8)	0.0348(9)	–0.0037(7)	–0.0011(7)	0.0056(7)
C(15)	0.0613(15)	0.0645(15)	0.0311(9)	–0.0085(9)	0.0003(10)	0.0046(12)
C(16)	0.0748(18)	0.0613(14)	0.0340(10)	0.0100(10)	–0.0056(10)	0.0026(13)

Table 5. Hydrogen coordinates and isotropic displacement parameters ($Å^2$) for acb136.

	x	y	z	U
H(10A)	0.6005	0.7664	0.3775	0.044
H(11A)	0.5978	0.7373	0.4554	0.049
H(13A)	0.6834	0.1700	0.4447	0.045
H(14A)	0.6838	0.2006	0.3669	0.040
H(15A)	0.6325	0.7142	0.5268	0.078
H(15B)	0.6085	0.5525	0.5641	0.078
H(15C)	0.5471	0.6035	0.5243	0.078
H(16A)	0.6966	0.1748	0.5175	0.085
H(16B)	0.6012	0.1501	0.5124	0.085
H(16C)	0.6382	0.2441	0.5572	0.085

Table 6. Torsion angles [°] for acb136.

C(8)–N(1)–C(1)–O(1)	−176.85(16)	C(8)–N(1)–C(1)–C(2)	2.17(18)
C(9)–N(1)–C(1)–O(1)	1.4(3)	C(9)–N(1)–C(1)–C(2)	−179.62(15)
O(1)–C(1)–C(2)–C(3)	−3.2(3)	O(1)–C(1)–C(2)–C(7)	175.85(17)
N(1)–C(1)–C(2)–C(3)	177.79(16)	N(1)–C(1)–C(2)–C(7)	−3.11(17)
C(1)–C(2)–C(3)–Cl(1)	−1.5(2)	C(1)–C(2)–C(3)–C(4)	179.12(15)
C(7)–C(2)–C(3)–Cl(1)	179.53(12)	C(7)–C(2)–C(3)–C(4)	0.1(2)
Cl(1)–C(3)–C(4)–Cl(2)	−2.15(18)	Cl(1)–C(3)–C(4)–C(5)	178.99(12)
C(2)–C(3)–C(4)–Cl(2)	177.27(12)	C(2)–C(3)–C(4)–C(5)	−1.6(2)
Cl(2)–C(4)–C(5)–Cl(3)	1.04(19)	Cl(2)–C(4)–C(5)–C(6)	−178.00(12)
C(3)–C(4)–C(5)–Cl(3)	179.90(12)	C(3)–C(4)–C(5)–C(6)	0.9(2)
Cl(3)–C(5)–C(6)–Cl(4)	2.83(19)	Cl(3)–C(5)–C(6)–C(7)	−177.69(12)
C(4)–C(5)–C(6)–Cl(4)	−178.12(12)	C(4)–C(5)–C(6)–C(7)	1.4(2)
Cl(4)–C(6)–C(7)–C(2)	176.61(12)	Cl(4)–C(6)–C(7)–C(8)	−3.3(2)
C(5)–C(6)–C(7)–C(2)	−2.9(2)	C(5)–C(6)–C(7)–C(8)	177.27(15)
C(1)–C(2)–C(7)–C(6)	−177.02(15)	C(1)–C(2)–C(7)–C(8)	2.87(17)
C(3)–C(2)–C(7)–C(6)	2.2(2)	C(3)–C(2)–C(7)–C(8)	−177.93(14)
C(1)–N(1)–C(8)–O(2)	−179.97(16)	C(1)–N(1)–C(8)–C(7)	−0.48(18)
C(9)–N(1)–C(8)–O(2)	1.8(3)	C(9)–N(1)–C(8)–C(7)	−178.71(15)
C(2)–C(7)–C(8)–O(2)	177.90(17)	C(2)–C(7)–C(8)–N(1)	−1.57(17)
C(6)–C(7)–C(8)–O(2)	−2.2(3)	C(6)–C(7)–C(8)–N(1)	178.31(16)
C(1)–N(1)–C(9)–C(10)	114.4(2)	C(1)–N(1)–C(9)–C(14)	−67.1(2)
C(8)–N(1)–C(9)–C(10)	−67.6(2)	C(8)–N(1)–C(9)–C(14)	110.9(2)
N(1)–C(9)–C(10)–C(11)	177.50(18)	C(14)–C(9)–C(10)–C(11)	−1.0(3)
C(9)–C(10)–C(11)–C(12)	0.5(3)	C(15)–N(2)–C(12)–C(11)	7.9(3)
C(15)–N(2)–C(12)–C(13)	−173.4(2)	C(16)–N(2)–C(12)–C(11)	164.0(2)
C(16)–N(2)–C(12)–C(13)	−17.3(3)	C(10)–C(11)–C(12)–N(2)	179.3(2)
C(10)–C(11)–C(12)–C(13)	0.6(3)	N(2)–C(12)–C(13)–C(14)	−179.8(2)
C(11)–C(12)–C(13)–C(14)	−1.1(3)	N(1)–C(9)–C(14)–C(13)	−178.01(17)
C(10)–C(9)–C(14)–C(13)	0.5(3)	C(12)–C(13)–C(14)–C(9)	0.6(3)